

Yasuyuki Tezuka  
Tetsuo Deguchi *Editors*

# Topological Polymer Chemistry

Concepts and Practices

 Springer

# Topological Polymer Chemistry

Yasuyuki Tezuka · Tetsuo Deguchi  
Editors

# Topological Polymer Chemistry

Concepts and Practices

 Springer

*Editors*

Yasuyuki Tezuka  
Tokyo Institute of Technology  
Tokyo, Japan

Tetsuo Deguchi  
Ochanomizu University  
Tokyo, Japan

ISBN 978-981-16-6806-7

ISBN 978-981-16-6807-4 (eBook)

<https://doi.org/10.1007/978-981-16-6807-4>

© The Editor(s) (if applicable) and The Author(s), under exclusive license to Springer Nature Singapore Pte Ltd. 2022

This work is subject to copyright. All rights are solely and exclusively licensed by the Publisher, whether the whole or part of the material is concerned, specifically the rights of translation, reprinting, reuse of illustrations, recitation, broadcasting, reproduction on microfilms or in any other physical way, and transmission or information storage and retrieval, electronic adaptation, computer software, or by similar or dissimilar methodology now known or hereafter developed.

The use of general descriptive names, registered names, trademarks, service marks, etc. in this publication does not imply, even in the absence of a specific statement, that such names are exempt from the relevant protective laws and regulations and therefore free for general use.

The publisher, the authors and the editors are safe to assume that the advice and information in this book are believed to be true and accurate at the date of publication. Neither the publisher nor the authors or the editors give a warranty, expressed or implied, with respect to the material contained herein or for any errors or omissions that may have been made. The publisher remains neutral with regard to jurisdictional claims in published maps and institutional affiliations.

This Springer imprint is published by the registered company Springer Nature Singapore Pte Ltd.

The registered company address is: 152 Beach Road, #21-01/04 Gateway East, Singapore 189721, Singapore

*The book is dedicated to the memory of  
Nadrian C. Seeman, upon his abrupt demise  
in November 2021. He is credited with  
pioneering works on topological polymer  
chemistry by DNAs, which eventually evolved  
into the impactful DNA nanotechnology.*

# Preface

Myriad forms in nature, which are static or dynamic, identified among limitless varieties of dimensions from the scale of the universe to the subatomic ones, have been inspiring the artistic minds of humans by their precise geometric beauties with exciting fineness and marvelous diversity. Moreover, these fascinating forms in three dimensions are often crucial to bring about their astonishing properties and functions as materials. And notably, the fabrication of molecular size objects having specifically defined forms has now become an attractive and rewarding endeavor, opening the door to nanoscience and nanotechnology.

During the first two decades of this century, in particular, accessible polymer constructions have dramatically increased not only in number but also in variety beyond linear polymers or randomly branched ones, along with formidable development of synthetic polymer chemistry. A number of pivotal breakthroughs have been witnessed to produce particularly an important class of polymers having a variety of cyclic and multicyclic topologies with ultimate precision control, to provide unique opportunities in polymer materials which are designed to uncover unprecedented properties and functions as materials simply based on their *topologies*.

In retrospect, a seminal book edited by Semlyen (*Cyclic Polymers, second edition*, Kluwer, 2000), which was the following up of the first edition in 1986, pioneered to document the significant features of cyclic polymers accessible by means of emerging synthetic methodologies at the time, concurrently with those of bioresources, including DNAs, proteins/peptides, poly(or oligo)saccharides, and lipids. We have since experienced an even accelerated progress on *topological polymer chemistry* to achieve the remarkable broadening of a variety of topologically intriguing polymer entities based on cyclic topologies. And the noteworthy developments in the following decade were outlined in *Topological Polymer Chemistry: Progress of cyclic polymers in synthesis, properties and functions* (World Scientific, 2013), edited by one of the coeditors of this Book. It is remarkable, moreover, *topological polymer chemistry* has attracted due scientific interests beyond chemistry and physics expertise, and particularly on topological geometry, leading to a unique

collaboration project by the partnership among basic science disciplines. Consequently, the interdisciplinary fulfillment, *Topology of Polymers* (Springer, 2019), was published as a series content of Springer Briefs in the Mathematics of Materials.

This book is intended to offer a timely extension of these preceding works, to feature key issues in concepts and practices of *topological polymer chemistry*. The book is comprising four parts compiled with chapters by diverse expert authors, covering from topological geometry and statistical physics to synthetic polymer chemistry and polymer materials engineering. The first part describes theories and practices of multicyclic and topological polymers, to discuss comprehensively elementary issues on topological analysis, classification, physical characterization by simulation, and the eventual chemical constructions. The next part is focusing on theories and practices of the polymer folding, recognized as an emerging sector in *topological polymer chemistry*. The ongoing breakthrough by the precision AI prediction of protein folding events will inevitably pose intriguing impacts on the current topological polymer chemistry, to address a formidable challenge of the programmed polymer folding by synthetic polymers. Moreover, the following two parts cover the state of the art in both synthetic approaches with the precision designing and topology-directed properties/functions by single cyclic (ring) polymers. Chapters in these parts collectively depict a wider variety of tailored cyclic polymers accessible by means of diverse synthetic approaches and their properties and functions upon their cyclic topology effects leading to eventual applications in practice. The book will serve readers collectively to acquire beneficial insights over exciting innovations ongoing in *topological polymer chemistry*.

We thank all chapter contributors for this Book. We are also grateful to Mr. Shinichi Koizumi of Springer Japan for his continuous encouragement and support during this book project and to Mr. Rammohan Krishnamurthy for his outstanding works in the production process.

Finally, we acknowledge financial support to our collaborating project involving topological geometry, statistical physics and polymer chemistry and polymer materials engineering, which started in 2014, by JSPS KAKENHI Grant-in-Aid for Scientific Research (B) (Generative Research Fields, Grant Number JP26310206), which has evolved into the extended phase in 2017 by the MEXT KAKENHI Grant-in-Aid for Scientific Research on Innovative Areas (Research in a Proposed Research Area) (Planned Research, Grant Number JP17H06463). We also acknowledge financial support from the Japan Science and Technology Agency CREST (Grant Number JPMJCR19T4).

Tokyo, Japan  
August 2021

Yasuyuki Tezuka  
Tetsuo Deguchi

# Contents

<b>1</b>	<b>Introductory Remarks</b> .....	<b>1</b>
	Yasuyuki Tezuka	
<b>Part I Theories and Practices of Multicyclic and Topological Polymers</b>		
<b>2</b>	<b>Graph Theoretical and Knot Theoretical Analyses of Multi-cyclic Polymers</b> .....	<b>9</b>
	Kai Ishihara and Koya Shimokawa	
<b>3</b>	<b>Classification, Notation and Isomerism of Topological Polymers</b> .....	<b>23</b>
	Yasuyuki Tezuka	
<b>4</b>	<b>Exact Evaluation of the Mean Square Radius of Gyration for Gaussian Topological Polymer Chains</b> .....	<b>37</b>
	Jason Cantarella, Tetsuo Deguchi, Clayton Shonkwiler, and Erica Uehara	
<b>5</b>	<b>Fundamentals of the Theory of Chromatography of Topologically Constrained Random Walk Polymers</b> .....	<b>65</b>
	Alexei A. Gorbunov and Andrey V. Vakhrushev	
<b>6</b>	<b>Construction of Multicyclic Polymer Topologies through Electrostatic Self-assembly and Covalent Fixation (ESA-CF)</b> .....	<b>89</b>
	Yasuyuki Tezuka	
<b>Part II Theories and Practices of Polymer Folding Topologies</b>		
<b>7</b>	<b>Topological Analysis of Folded Linear Molecular Chains</b> .....	<b>105</b>
	Anatoly Golovnev and Alireza Mashaghi	
<b>8</b>	<b>DNA Knots</b> .....	<b>115</b>
	Cristian Micheletti	



<b>9</b>	<b>Cyclotides—Cyclic and Disulfide-Knotted Polypeptides</b> .....	135
	David J. Craik, Yuhui Zhang, Yan Zhou, Quentin Kaas, and Meng-Wei Kan	
<b>10</b>	<b>Construction of a Macromolecular <math>K_{3,3}</math> Graph Topology by the ESA-CF Polymer Folding</b> .....	149
	Yasuyuki Tezuka	
<b>11</b>	<b>Programmed Polymer Folding</b> .....	159
	Laurens W. H. J. Heling, Seyedeh Elnaz Banijamali, Vahid Satarifard, and Alireza Mashaghi	
<b>12</b>	<b>Spatially and Chemically Programmed Polymer Folding by the ESA-CF Protocol</b> .....	177
	Yasuyuki Tezuka	
<b>13</b>	<b>Macromolecular Rotaxanes, Catenanes and Knots</b> .....	187
	Harry W. Gibson	
<b>Part III Cyclic Polymer Innovations: Syntheses</b>		
<b>14</b>	<b>Recent Progress on the Synthesis of Cyclic Polymers</b> .....	213
	Brennan J. Curole, Ashley V. Miles, and Scott M. Grayson	
<b>15</b>	<b>Recent Progress on the Synthesis of Cyclic Polymers via Ring-Closure Methods</b> .....	243
	Qingquan Tang and Ke Zhang	
<b>16</b>	<b>Ring-Expansion Polymerization of Cycloalkenes and Linear Alkynes by Transition Metal Catalysts</b> .....	261
	Tomohiro Kubo, Rinku Yadav, and Adam S. Veige	
<b>17</b>	<b>Synthesis of Cyclic Vinyl Polymers via <i>N</i>-Heterocyclic Carbene (NHC)-Initiated Anionic Polymerization and Subsequent Ring-Closure Without Highly Dilute Conditions</b> .....	277
	Yuki Muramatsu and Akinori Takasu	
<b>18</b>	<b>Controlled Ring-Expansion Polymerization Based on Acyl-Transfer Polymerization of Thiiranes with Aromatic Heterocycles as Initiators</b> .....	293
	Atsushi Kameyama and Akira Takahashi	
<b>19</b>	<b>A Conjunctive RC and RE Polymer Cyclization with Zwitterionic Telechelic Precursors</b> .....	309
	Yasuyuki Tezuka	
<b>20</b>	<b>Cyclic Polymers Synthesized by Spontaneous Selective Cyclization Approaches</b> .....	319
	Daisuke Aoki, Hideyuki Otsuka, and Toshikazu Takata	

<b>21 Unstoichiometric Polycondensation for the Synthesis of Aromatic Cyclic Polymers</b> .....	335
Tsutomu Yokozawa, Hajime Sugita, and Yoshihiro Ohta	
<b>Part IV Cyclic Polymer Innovations: Topology Effects</b>	
<b>22 Entanglement in Solution of Non-concatenated Rings</b> .....	355
Takahiro Sakaue and Davide Michieletto	
<b>23 Dilute Solution Properties of Ring Polymers</b> .....	365
Daichi Ida	
<b>24 Cyclic Polymers for Innovative Functional Materials</b> .....	379
Takuya Yamamoto	
<b>25 Surface Functionalization with Cyclic Polymers</b> .....	395
Edmondo M. Benetti	
<b>26 Morphological Significances of Cyclic Polymers in Solution and Solid State</b> .....	409
Brian J. Ree, Takuya Isono, and Toshifumi Satoh	
<b>27 Transforming Cyclic/Linear Polymer Topologies: Emerging Techniques and Opportunities</b> .....	421
Satoshi Honda and Minami Oka	

# Chapter 1

## Introductory Remarks



Yasuyuki Tezuka

**Abstract** This Chapter outlines, firstly, the background and the current state of the art of *topological polymer chemistry*, followed by the brief summaries of each chapter of this Book, which are compiled into four parts to cover comprehensively the ongoing evolution extending toward diverse directions from theoretical to practical purposes. Finally, future perspectives of *topological polymer chemistry* are highlighted with selected goals/targets envisioned from the chapters of the Book.

During the first two decades of the new century, we have witnessed the formidable diversion in the choice of macromolecular structures from linear or randomly branched forms toward a variety of precisely controlled topologies, implemented via a number of formidable breakthroughs in the field of synthetic polymer chemistry. In particular, an important class of polymers having, in particular, a variety of cyclic and multicyclic topologies have now been obtainable through the precision structure designing attainable with the intriguing synthetic protocols demonstrated in the following chapters of the Book. These developments have subsequently offered unique opportunities to yield unprecedented properties and functions by polymer materials simply based on the form, i.e., *topology*, of polymer molecules [1–6].

This Book is aiming to gain due recognition over ongoing developments in *topological polymer chemistry* through compiled chapters contributed by authors of diverse expertise, covering from topological geometry to synthetic polymer chemistry and polymer materials engineering. The Book is composed of four parts to highlight the diverse approaches in pursuit of important objectives featured in concepts and practices of topological polymers. The Book emphasizes particularly on topological analysis approaches as a basis toward the broadly interactive subsequent studies in the areas of polymer chemistry/physics and of polymer materials involving both simulation and experimental approaches.

Thereby, the Book will be able to convey comprehensive insights evolved uniquely through mutual interactions between fundamental and practical endeavors, pushing

---

Y. Tezuka (✉)  
Tokyo Institute of Technology, Tokyo, Japan  
e-mail: [ytezukak33@gmail.com](mailto:ytezukak33@gmail.com)

forward the *topological polymer chemistry*. More specifically, topological or soft geometry analyses of randomly coiled macromolecular structures could provide key parameters dictating their principal physicochemical and/or biological properties solely based on their geometrical chain forms. Thus, the Book with chapters by prominent contributors accommodates thorough discussion over ongoing achievements and anticipating breakthroughs in *topological polymer chemistry*, to bring about conceptually insightful inspiration to readers with an emphasis on the spectacular diversion of polymer constructions.

The Book consists of four main parts, with the introductory remarks as this chapter. Part I (**Theories and Practices of Multicyclic and Topological Polymers**) focuses on topologically intriguing multicyclic polymers, where the key conception of *topological polymer chemistry* is presented by taking into account for topological geometry (soft geometry) conjectures to deal with uniquely flexible polymer chain constructions, in contrast to the relevant Euclidian geometry (hard geometry) conjectures applicable to small chemical compound structures. Thus, Chap. 2 by Ishihara and Shimokawa presents a mathematical basis with graph theoretical and knot theoretical analyses of multicyclic polymers, followed by Chap. 3 by Tezuka on their systematic classification and notation protocols and the subsequent analysis of topological polymers in light of the isomerism conception. Topological geometry and graph theory conjectures are applied to formulate the systematic classification and notation protocol for polymer molecules comprising branched and multicyclic structure units. Subsequently, a unique conception of *topological isomerism*, in addition to the conventional constitutional and stereoisomerism typically occurring in small chemical compounds, is introduced. The following Chap. 4 coauthored by Cantarella, Deguchi, Shonkwiler, and Uehara outlines the new explicit and quantitative method to investigate fundamental statistical properties in topological polymers, including the mean square radius of gyration, with topologically constrained random walks (TCRW) of the topological polymers expressed by the graph constructions. The subsequent Chap. 5 by Gorbunov et al. presents the theory of chromatography for topologically complex multicyclic polymers, by representing their structures again as a graph and by using a model of TCRW for the macromolecule. The resulting simulation chromatograms for a selected set of topological polymers are applied in practice for the characterization of experimentally obtained polymer products. And indeed, Chap. 6 by Tezuka describes the state-of-the-art synthetic polymer chemistry to construct diverse multicyclic polymers. An *electrostatic self-assembly and covalent fixation* (ESA-CF) protocol, by employing specifically designed telechelic precursors having selected cyclic ammonium salt groups, is introduced for designing unconventional polymer topologies of cyclic and multicyclic constructions. Moreover, the ESA-CF process in conjunction with recently developed effective linking chemistries, including alkyne-azide addition (*click*) and olefin metathesis (*clip*) reactions, is developed to produce complex multicyclic polymers of either *spiro*-, *bridged*- and *fused*-constructions. Such evolution in the current frontier of synthetic polymer chemistry may direct future promising research endeavors in *topological polymer chemistry*.

Part II (**Theories and Practices of Polymer Folding Topologies**) focuses on polymer chain folding as an emerging branch of *topological polymer chemistry*. The polymer chain folding in proteins, polypeptides as well as DNAs is recognized as a crucial event for biopolymers to acquire optimized properties and functions by constructing their designated structures in the 3D space. Though such chemical evolution in biopolymer systems is inspiring to synthetic polymer chemistry, the precision folding by synthetic polymers is still a formidable challenge despite their potential in practice, including single-chain nanoparticles and eventually polymer networks. Thus, Chap. 7 by Golovnev and Mashaghi presents mathematically rigorous, circuit topology approaches to describe the topology of linear folded chains as the geometry framework for biomolecular analysis and molecular engineering. The following Chap. 8 by Micheletti reviews topologically intriguing knotted DNAs observed in various organisms with the emphasis on ongoing innovations both in theoretical and experimental approaches to reveal their unique properties and biofunctions. The subsequent Chap. 9 by Craik et al reviews the topological features of naturally occurring cyclic peptides (cyclotides) identified in plants and animals. Cyclotides are characterized by a macrocyclic backbone and additional disulfide folding units to form topologically significant chain frameworks, to provide exceptional thermal stability and resistance to proteolysis, suitable for agriculture and medicine applications. And the following Chap. 10 by Tezuka presents a synthetic approach of topologically significant  $K_{33}$  graph construction, identified in a class of cyclotides shown in Chap. 9, as a showcase example. The two subsequent chapters (Chap. 11 by Mashaghi et al. and Chap. 12 by Tezuka) outline collectively the current innovation in programmed polymer folding, either focusing on engineered proteins and DNAs (Chap. 11) or on a synthetic polymer system by the extension of the ESA-CF protocol (Chap. 12), respectively. These two chapters discuss the formation of any specific folding topologies according to the kinetic control of folding processes, as well as the relationship between topology and properties. Finally, Chap. 13 by Gibson comprehensively reviews a class of topologically significant polymers, including polyrotaxanes, polycatenanes, and polymeric knots, with the description of key geometrical aspects in these topological polymers. The Chapter also emphasizes the rapid progress of this research area within the recent decade.

The following Part III (**Cyclic Polymer Innovations: Syntheses**) and Part IV (**Cyclic Polymer Innovations: Topology Effects**), respectively, focus on single cyclic (ring) polymers, in particular, outlining ongoing developments in their synthetic approaches (Part III) and in their topology effects uniquely attainable through the precision topology designing (Part IV). Chapters included in these parts collectively depict a class of cyclic polymers realizing the unique polymer properties and functions leading to their eventual applications.

Thus, Part III starts with Chap. 14 by Grayson et al. reviewing updated synthetic protocols of cyclic polymers by means of the ring closure of telechelic precursors (RC), followed by Chap. 15 by Zhang et al. with an emphasis on the effective polymer cyclization by the RC methods through alkyne-azide addition (*click*) processes, including a photoinduced and self-accelerating *click* chemistry, in particular. The subsequent three chapters, i.e., Chap. 16 by Kubo, Veige et al., Chap. 17 by

Takasu et al., and Chap. 18 by Kameyama et al., collectively highlight the remarkable innovation in the ring expansion processes (RE), an alternative of the RC counterparts, to produce cyclic polymers. Thus, Chap. 16 outlines the newly developed RE technique for cycloalkenes and linear alkynes with purposely designed transition metal catalysts. The following Chap. 17 demonstrates the RE process for selected vinyl monomers, (meth)acrylates in particular, with *N*-heterocyclic carbene (NHC) as initiators. Moreover, Chap. 18 describes the RE procedure for heterocyclic thiranes monomers via the acyl-transfer polymerization with aromatic benzothiazolones as initiators. As a further challenge to the effective and scalable means to produce cyclic polymers, Chap. 19 by Tezuka describes a conjunctive RC and RE polymer cyclization by employing the designated zwitterionic telechelic precursors, in order to join together the synthetic benefits from each of the RC and RE processes. In addition, Chap. 20 by Aoki et al. and Chap. 21 by Yokozawa presents examples of innovating synthetic approaches for cyclic polymers. Thus, Chap. 20 outlines unique processes relied upon the dynamic covalent or non-covalent chemistry, and Chap. 21 describes the nonstoichiometric polycondensation processes to produce cyclic polyamides and polyesters, respectively.

Finally, Part IV with chapters focusing on topology effects by cyclic polymers starts with Chap. 22 coauthored by Sakaue and Michieletto presenting the new approach based on the analysis of cooperative motions between entangled chains to reveal distinctive entanglement structures by linear polymers and non-concatenated ring (simple monocyclic) polymers in their concentrated solutions. The following Chap. 23 by Ida outlines theories and experiments of dilute solution properties of ring polymers. In particular, the theory on the basis of the wormlike ring model is applied by taking into account for effects of chain stiffness to give the reasonable interpretation of experimental data on ring polystyrenes. The subsequent Chap. 24 by Yamamoto reviews recent noteworthy examples of topology effects by cyclic polymers applied as innovative functional materials, with particular emphases on self-assembly state by amplifying any topological distinction, either linear or cyclic, of individual polymer chains. The following Chap. 25 by Benetti focuses on topology effects by cyclic polymers at the surface states, in particular, to bring unique wetting and lubrication properties as well as biointerface functions in reference to linear counterparts. Moreover, Chap. 26 by Satoh et al. outlines the morphological topology effects by cyclic block polymers, in particular, either in solution, in bulk, or in thin-film states revealed by high resolution X-ray analyses. Finally, Chap. 27 by Honda et al. describes the reversible conversion of polymer topologies between cyclic and linear forms by external stimuli and their applications by taking advantage of the discrete change of their properties by topology effects.

The Book including those chapters highlights the fascinating developments ongoing in *topological polymer chemistry*. Numerous future opportunities are envisaged through close interactions between the broad expertise ranging from mathematics, physics, chemistry, biology, and materials sciences. Remarkably, indeed, a variety of topologically defined and formidably complex polymers have now become accessible along with the rapid evolution of *topological polymer chemistry* during

the two decades of this current century. Notably, in particular, the recent enumeration analysis has shown the enormous diversity of polymer topologies, beyond the one simple ring, three dicyclic and 15 tricyclic constructions. Indeed, the number reaches 111 in tetracyclic and 1076 in pentacyclic constructions, respectively, and to as many as 13,870 in hexacyclic forms free of knotting. Thus, in parallel with the ongoing progress in computational simulations, one will become able to foresee the precision control of static and dynamic polymer properties relying on their topological geometries, intriguingly counterintuitive to Euclidian geometry conjectures. Thereupon, unprecedented topology effects in polymer materials will subsequently be uncovered leading to eventual applications in practice.

By witnessing ongoing innovations in *topological polymer chemistry*, we are entering into an epoch-making era of polymer science and materials engineering based on precision topology designing, which is comparable to a “Cambrian explosion period” at 550 million years ago, observed in the evolutionary history of life systems. Until then, the forms of most living species were simple and primitive with as small as dozens of varieties. Over the following short period of 10 million years, the abrupt diversification evolved with an order of magnitude yielding more than 10,000 different body plans, identified even today. *Topological polymer chemistry* will certainly contribute to opening such a new exciting paradigm in polymer science.

## References

1. K. Shimokawa, K. Ishihara, Y. Tezuka, *Topology of Polymers* (Springer, Tokyo, 2020)
2. Y. Tezuka (ed.), *Topological Polymer Chemistry: Progress of cyclic polymers in syntheses, properties and functions* (World Scientific, Singapore, 2013)
3. Y. Tezuka, *Acc. Chem. Res.* **50**, 2661 (2017)
4. Y. Tezuka, *Isr. J. Chem.* **60**, 67 (2020)
5. Y. Tezuka, *React Funct Polym.* **148**, 104489 (2020)
6. Z. Qu, S.Z.D. Cheng, W.-B. Zhang, *Trend Chem.* **3**, 402 (2021)

**Part I**  
**Theories and Practices of Multicyclic  
and Topological Polymers**



# Chapter 2

## Graph Theoretical and Knot Theoretical Analyses of Multi-cyclic Polymers



Kai Ishihara and Koya Shimokawa

**Abstract** In this chapter, we will discuss the mathematical method used in analyses of topological polymers. First, we apply graph theory to define a notation for multi-cyclic polymers. We also consider the types of polymers and study the construction method. Second, we apply knot theory to multi-cyclic polymers. We analyze topological isomers derived from knot, link, and spatial graph structure of polymers.

### 2.1 Topology of polymers

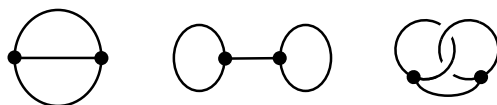
In discussing the topology of polymers, we encounter two meanings of *topology*. One is the topology of the polymer itself, which is how the components are connected. The other is the topology in the 3-dimensional space, which is how they are intertwined. The former topology is used to classify structural isomers and the latter stereoisomers. In either sense, it is useful to study topology of polymers using *graphs*, a mathematical object, consisting of vertices and edges. To distinguish two meanings, we use the terminology ‘abstract graph’ when we deal with topology in the first sense, and we use the terminology ‘spatial graph’ when we consider topology in the latter sense.

For example, the three graphs in Fig. 2.1 consist of two vertices and three edges, respectively. All three edges of the graph on the left connect the two vertices, and the two edges of the center and the right graph form rings. From this observation, it can be said that the left has a different topology from the center and the right as an abstract graph. On the other hand, the two rings on the right are entwined, while that on the center are not, so we can say that the right and the center are the same as

---

K. Ishihara  
Yamaguchi University, Yamaguchi 753-8513, Japan  
e-mail: [kishihara@yamaguchi-u.ac.jp](mailto:kishihara@yamaguchi-u.ac.jp)

K. Shimokawa (✉)  
Saitama University, Saitama 338-8570, Japan  
e-mail: [kshimoka@rimath.saitama-u.ac.jp](mailto:kshimoka@rimath.saitama-u.ac.jp)



**Fig. 2.1** The left has a different topology in itself when compared to the center and the right. The center and the right have the same topology in themselves but different topologies in the 3-dimensional space

abstract graphs, but different as spatial graphs. *Graph theory* can be used to discuss topology as an abstract graph, and *knot theory* can be used to discuss topology as a spatial graph.

## 2.2 Graph Theoretical Analyses Of polymers

In this section, we will use graph theory to analyze structures of multi-cyclic polymers see [1] for the discussion in detail.

### 2.2.1 Graphs

We will start with the definition of graphs.

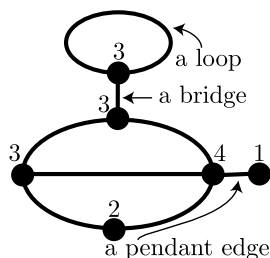
**Definition 2.1** A *graph* is an object consisting of vertices and edges. A *vertex* is a point and an *edge* is a segment with endpoints that are vertices. A graph  $G$  is represented by a pair  $(V, E)$ , where  $V$  and  $E$  are the sets of vertices and edges, respectively.

An edge is a *loop* if two endpoints coincide. The *degree* (or *valency*) of a vertex  $v$ , denoted by  $d(v)$ , is the number of parts of edges incident to  $v$ . That is the sum of non-loop edges incident to  $v$  and twice the number of loops incident to  $v$ . A degree one vertex and a unique edge incident to the vertex are called a *pendant vertex* and a *pendant edge*, respectively. An edge is called a *bridge* if its deletion increases the number of components of the graph. A bridge is called a *cut-edge*. Similarly, a vertex is called a *cut-vertex* if its deletion increases the number of components of the graph see Fig. 2.2.

The *rank*  $r(G)$  of the graph  $G$  is the rank of the 1-dimensional homology of  $G$ , which indicates how many different loops are in  $G$ . Let  $n$  and  $m$  denote the number of vertices and edges of  $G$ , respectively. Then, if  $G$  is connected,  $r(G) = m - n + 1$ .

An operation to put a vertex with degree two to the middle of an edge (a *subdivision*), and its reverse operation (a *smoothing*) do not change the rank of graphs, since they increase or decrease both the number of vertices and the number of edges by one. Moreover, they do not change the homeomorphic type of graph. Similarly, an

**Fig. 2.2** Example of a graph with a loop and a pendant edge. The rank of this graph is 3



operation to add a pendant edge/vertex (a *P-addition*) does not change the rank of graphs, and the existence of pendant edge/vertex is not essential when considering the topology of graphs in the 3-dimensional space. Thus, it is natural to consider simplified graphs that consist of vertices with degree of at least three.

There are two types of graphs used to describe the structure: molecular graph and polymer graph. A *molecular graph* has atom vertices and edges that are chemical bonds. On the other hand, in a *polymer graph* a vertex is a branched point of a polymer and an edge is a linear structure that is a chain of bonds between two branched points. We will consider polymer graphs here.

**Definition 2.2** A polymer is called a *cyclic polymer* (resp. a *multi-cyclic polymer*) if the rank of its polymer graph is one (resp. more than one). If the rank of the polymer graph is 2 (resp. 3 or 4), then it is called a *dicyclic polymer* (resp. a *tricyclic polymer* or a *tetracyclic polymer*).

For an example, a polymer in Fig. 2.2 is a tricyclic polymer.

By applying graph theory, we can classify multi-cyclic polymer graphs. For example, there are exactly 3 distinct polymer graphs with rank 2, exactly 15 distinct graphs with rank 3, exactly 111 distinct graphs with rank 4, and exactly 1075 distinct graphs with rank 5 [2] see Fig. 2.7. Dicyclic and tricyclic polymers have been already synthesized [3].

## 2.2.2 Nomenclature

In this subsection, we will review the nomenclature of multi-cyclic polymers. Let  $G = (V, E)$  be a graph with  $V = \{v_1, \dots, v_n\}$ . The *degree sequence* of  $G$  is the non-increasing sequence of degrees of vertices  $(d_1, \dots, d_n)$ , where  $d_i$  is the degree  $d(v_j)$  of some vertex  $v_j$ , where  $i, j \in \{1, \dots, n\}$ . That is, we arrange  $d(v_j)$ 's in the non-increasing sequence  $(d_1, \dots, d_n)$ . For simplicity, we will often use the notation  $(3^3)$  to mean the degree sequence  $(3, 3, 3)$ .

Now we introduce the nomenclature of graphs.

**Definition 2.3** Let  $G = (V, E)$  be a graph. Suppose the degree sequence of  $G$  is  $(d_1, \dots, d_n)$  and  $G$  has  $\ell$  loops. Then  $G$  is denoted by  $(d_1, \dots, d_n)_k^\ell$ , where  $k$  is the numbering.

See Fig. 2.4 for examples. We can calculate the rank of the graph from its nomenclature.

**Proposition 2.1** ([1]) Let  $G$  be the graph with the nomenclature  $(d_1, \dots, d_n)_k^\ell$ . Then  $r(G) = 1 - n + \frac{1}{2} \sum_{j=1}^n d_j$ .

### 2.2.3 Folding Construction of Graphs (Polymers)

In this subsection, we will consider graphs obtained from a simple linear graph by folding operations.

**Definition 2.4** A graph  $G$  is obtained from  $G'$  by a folding if  $G$  is obtained by identifying several vertices of  $G'$ . A graph  $G$  is obtained from  $G'$  by a simple folding if  $G$  is obtained by identifying pairs of vertices of  $G'$  of degree one or two.

**Definition 2.5** If  $G_1$  and  $G_2$  are obtained from a graph  $G$  by foldings and have the same number of vertices, then we say  $G_1$  and  $G_2$  are folding isomers.

A path or a cycle of a graph  $G$  is called *Eulerian* if it traverses each edge of  $G$  exactly once. A graph  $G$  is *Eulerian* if  $G$  contains an Eulerian cycle. A graph  $G$  is *semi-Eulerian* if  $G$  contains an Eulerian path. A *simple linear graph* with length  $m$  is a graph consisting of only one path with  $m$  edges and is denoted by  $L_m$ .

**Theorem 2.1** [1] A graph  $G$  is obtained from a simple linear graph  $L_m$  by a folding for some  $m$ , if and only if  $G$  is semi-Eulerian.

For example, the theta graph  $(3^2)_1$  is obtained from  $L_3$  by a folding operation.

**Theorem 2.2** [1] Let  $G$  be a connected graph with the nomenclature  $(d_1, \dots, d_n)_k^\ell$ .

1.  $G$  can be obtained from  $L_m$  by folding if and only if  $G$  is semi-Eulerian and  $\sum_{i=1}^n d_i = 2m$ .
2.  $G$  can be obtained from  $L_m$  by simple folding if and only if  $\sum_{i=1}^n d_i = 2m$  and one of the following holds:
  - a.  $(d_1, \dots, d_n) = (2^n)$  or  $(4^{n_1}, 2^{n_2})$ ,
  - b.  $(d_1, \dots, d_n) = (4^{n_1-1}, 3^2, 2^{n_2-1})$ ,
  - c.  $(d_1, \dots, d_n) = (4^{n_1-1}, 3, 2^{n_2-1}, 1)$ ,
  - d.  $(d_1, \dots, d_n) = (4^{n_1-1}, 2^{n_2-1}, 1^2)$ .

Here  $n_1$  and  $n_2$  are positive integers with  $n_1 + n_2 = n$ .

Using Theorem 2.2, we can see that  $K_{3,3} = (3^6)_1$  cannot be obtained by a folding from a simple linear graph. The three dicyclic graphs  $(3^2)_1$ ,  $(4)_1^2$ , and  $(3^2)_1^2$  can be obtained from a simple linear graph by simple folding. Tricyclic graphs  $(4^2)_1$ ,  $(4, 3^2)_1$ ,  $(5, 3^1)_1$ ,  $(4, 3^2)_1^1$ ,  $(4, 3^2)_1^2$ ,  $(4^2)_1^2$ ,  $(4, 3^2)_1^2$ ,  $(6)_1^3$ ,  $(5, 3)_1^3$ , and  $(4, 3^2)_1^3$  can be obtained from a simple linear graph by simple folding.

### 2.2.4 Types of Graphs (Polymers)

In this subsection, we will consider types of graphs. We introduce elementary dicyclic subgraphs for multi-cyclic graphs: An *8-subgraph* is a subgraph of  $G$  which is homeomorphic to the graph  $(4)_1^2$ , (i.e., isomorphic to a subdivision of  $(4)_1^2$ ). We say an 8-subgraph is *proper* if the cut-vertex of the 8-subgraph is a cut-vertex of  $G$ . A *manacle-subgraph* of  $G$  is a subgraph which is homeomorphic to the graph  $(3^2)_1^2$ , (i.e., isomorphic to a subdivision of  $(3^2)_1^2$ ). We say a manacle-subgraph is *proper* if each bridge of the manacle-subgraph is a bridge of  $G$ . A  *$\theta$ -subgraph* of  $G$  is a subgraph which is homeomorphic to the graph  $(3^2)_1$ , (i.e., isomorphic to a subdivision of  $(3^2)_1$ ) see Fig. 2.3.

Graphs can be categorized into seven types depending on the presence of proper 8-subgraphs, proper manacle-subgraphs and  $\theta$ -subgraphs.

- Definition 2.6**
1.  $G$  is of *spiro type* if  $G$  contains a proper 8-subgraph, but neither a proper manacle-subgraph nor a  $\theta$ -subgraph.
  2.  $G$  is of *bridged type* if  $G$  contains a proper manacle-subgraph, but neither a proper 8-subgraph nor a  $\theta$ -subgraph.
  3.  $G$  is of *fused type* if  $G$  contains a  $\theta$ -subgraph, but neither a proper 8-subgraph nor a proper manacle-subgraph.
  4.  $G$  is of *spiro/bridged hybrid type* if  $G$  contains a proper 8-subgraph and a proper manacle-subgraph, but not a  $\theta$ -subgraph.
  5.  $G$  is of *spiro/fused hybrid type* if  $G$  contains a proper 8-subgraph and a  $\theta$ -subgraph, but not a proper manacle-subgraph.
  6.  $G$  is of *bridged/fused hybrid type* if  $G$  contains a proper manacle-subgraph and a  $\theta$ -subgraph, but not a proper 8-subgraph.
  7.  $G$  is of *spiro/bridged/fused hybrid type* if  $G$  contains a proper 8-subgraph, a proper manacle-subgraph, and a  $\theta$ -subgraph.

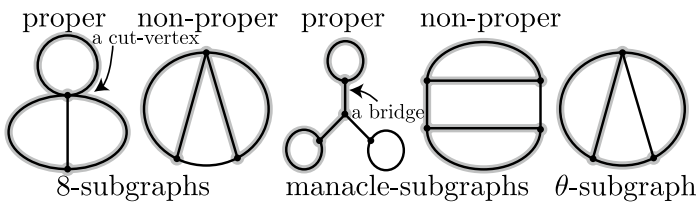
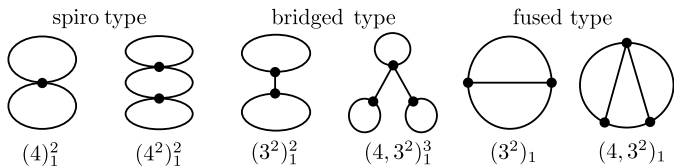
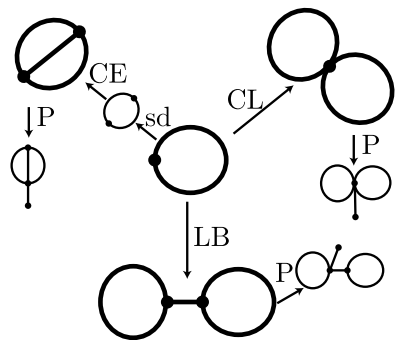


Fig. 2.3 Examples of 8-subgraphs, manacle-subgraphs and  $\theta$ -subgraph



**Fig. 2.4** Examples of spiro, bridged, and fused types of graphs

**Fig. 2.5** A construction of dicyclic graphs by some operations. A CL-addition, an LB-addition, a CE-addition, a P-addition, and a subdivision are indicated by CL, LB, CE, P, and sd, respectively



For example, the graphs  $(4)_1^2, (4^2)_1^2$  are of spiro type, the graphs  $(3^2)_1^2, (4, 3^2)_1^3$  are of bridged type, and the graphs  $(3^2)_1, (4, 3^2)_1$  are of fused type, see Fig. 2.4.

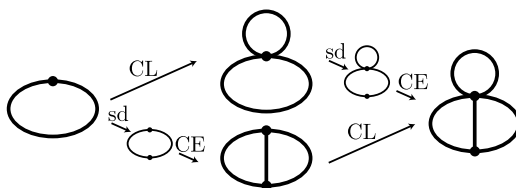
Recall that a P-addition and a subdivision were operations that did not change the rank of the graph. Here, we will introduce three operations that increase the rank of the graph by one; a *CL-addition*, an *LB-addition* and a *CE-addition*. A CL-addition is an operation to add a loop at a vertex which is contained in a cycle of the initial graph. An LB-addition is an operation to add a loop and a bridge so that the bridge connects the loop and a vertex of the initial graph. A CE-addition is an operation to add an edge at two vertices which contained in a cycle of the initial graph. Let us consider the construction of graphs by these operations. It is easy to see that any tree (resp. monocyclic graph) can be constructed from a vertex (resp. loop) by a sequence of P-additions and subdivisions. Similarly any dicyclic graphs can be obtained from the three dicyclic graphs by a sequence of P-additions and subdivisions, and the three dicyclic graphs can be constructed from a loop or a subdivision of a loop by a CL-addition, an LB-addition and a CE-addition, respectively, see Fig. 2.5.

In general, for any multi-cyclic graph, there is a construction from a loop using these operations:

**Theorem 2.3** [1] *Any multi-cyclic graph can be constructed from a loop by a sequence of CL-additions, LB-additions, CE-additions, P-additions, and subdivisions.*

The sequence of the construction from a loop in Theorem 2.3 is not uniquely determined for a given multi-cyclic graph, see Fig. 2.6. However, whether each of CL-, LB- and CE-additions is used or not in the construction is uniquely determined by the type of graph given. Namely, the following theorem holds.

**Fig. 2.6** Two sequences of a CL-addition, a CE-addition and a subdivision that produce the same tricyclic graph



### Theorem 2.4 [1]

1. A multi-cyclic graph  $G$  is of spiro type if and only if  $G$  is constructed from a loop by a sequence of CL-additions (possibly with P-additions and subdivisions).
2. A multi-cyclic graph  $G$  is of bridged type if and only if  $G$  is constructed from a loop by a sequence of LB-additions (possibly with P-additions and subdivisions).
3. A multi-cyclic graph  $G$  is of fused type if and only if  $G$  is constructed from a loop by a sequence of CE-additions (possibly with P-additions and subdivisions).
4. A multi-cyclic graph  $G$  is of spiro/bridged hybrid type if and only if  $G$  is constructed from a loop by a sequence of CL-additions and LB-additions (possibly with P-additions and subdivisions).
5. A multi-cyclic graph  $G$  is of spiro/fused hybrid type if and only if  $G$  is constructed from a loop by a sequence of CL-additions and CE-additions (possibly with P-additions and subdivisions).
6. A multi-cyclic graph  $G$  is of bridged/fused hybrid type if and only if  $G$  is constructed from a loop by a sequence of LB-additions and CE-additions (possibly with P-additions and subdivisions).
7. A multi-cyclic graph  $G$  is of spiro/bridged/fused hybrid type if and only if  $G$  is constructed from a loop by a sequence of CL-additions, LB-additions, and CE-additions (possibly with P-additions and subdivisions).

By Theorems 2.3 and 2.4, the 3 distinct dicyclic polymer graphs, 15 distinct tricyclic polymer graphs, and 111 distinct tetracyclic polymer graphs can be constructed step by step as in Fig. 2.7.

## 2.3 Knot Theoretical Analyses Of polymers

In this section, we will discuss topology of polymers induced by its spatial arrangement using knot theory. Applications of knot theory to polymers are also discussed in [4–7].

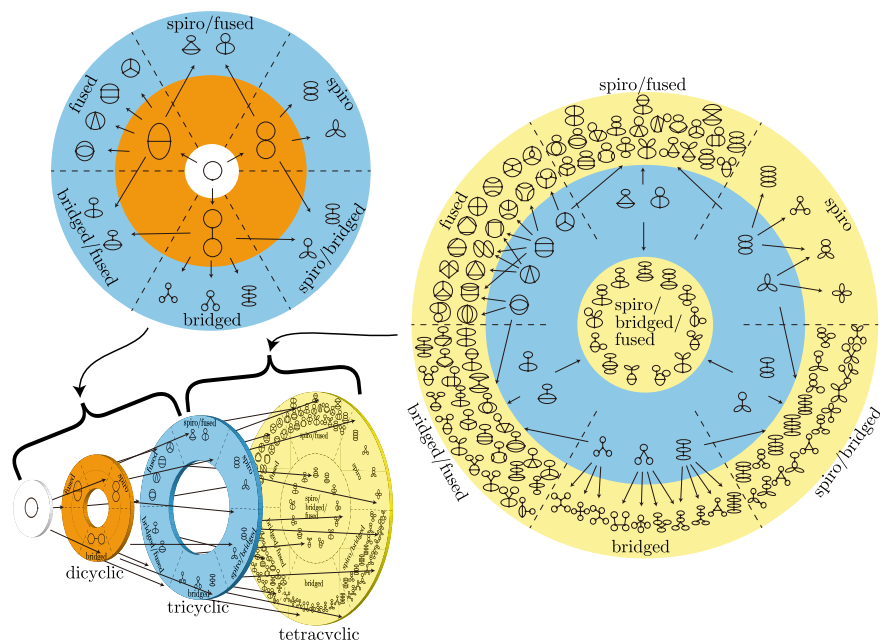


Fig. 2.7 Dicyclic, tricyclic, tetracyclic polymer graphs

### 2.3.1 Knots, Links, And spatial Graphs

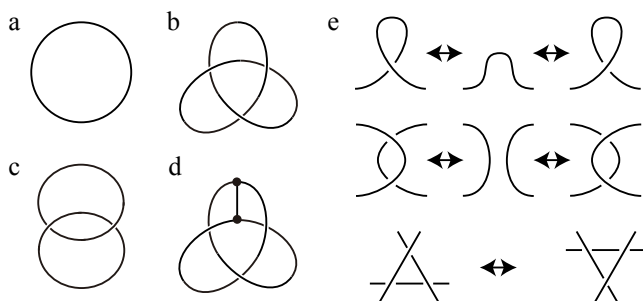
Knot theory is a branch of topology. Mathematically a *knot* is a knotted circle in 3-dimensional space. A *link* or a *catenane* is a union of entangled circles see Fig. 2.8. We often use *diagrams* of knots and links to study their properties. Using knots and links, we can discuss 3-dimensional shapes of cyclic polymers. The *trivial knot* is a knot as in Fig. 2.8a. The knot in Fig. 2.8b is called the *trefoil knot* and the link Fig. 2.8c is called the *Hopf link*.

On the other hand, we will use *spatial graphs* to discuss the spatial arrangement of multi-cyclic polymers. A spatial realization of a graph is called a *spatial graph*. Mathematically a spatial graph is an embedding of a graph into the 3-dimensional space.

Knots, links, and spatial graphs are found in structures of various kinds of polymers, such as DNA and proteins, and used to study their functions [8, 9] see also [10, 11] for reports on various examples of molecules and polymers of knotted and linked structures.

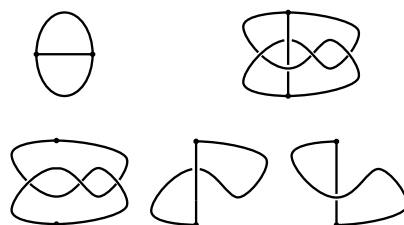
A *constituent knot* (resp. *constituent link*) is a subset of a spatial graph corresponding to a cycle (resp. disjoint cycles) in the graph. A spatial graph of the theta graph as in Fig. 2.9 is called a *theta curve*. A theta curve has three constituent knots. A theta curve is *non-trivial* if it is different from the trivial theta curve as in the top left in Fig. 2.9. If a theta curve contains a non-trivial constituent knot, then it is non-trivial.





**Fig. 2.8** **a** The trivial knot, **b** The trefoil knot, **c** The Hoph link, **d** The theta curve  $\theta_{3_1}$ , **e** Reidemeister moves I(top), II(middle) and III(bottom)

**Fig. 2.9** Top: Two theta curves. The left is a trivial theta curve and the right is  $\theta_{5_1}$ . Bottom: The theta curve  $\theta_{5_1}$  contains three constituent knots, each of which is a trivial knot

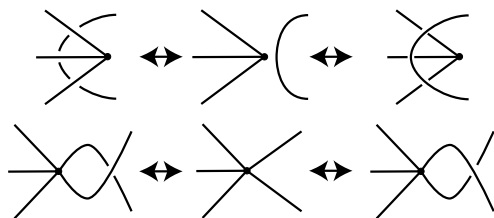


For example, the theta curve  $\theta_{3_1}$  in Fig. 2.8d is non-trivial as it contains the trefoil knot as a constituent knot. The theta curve  $\theta_{5_1}$ , which is also called Kinoshita's theta curve, is an interesting example. It is known to be non-trivial, but each constituent knot is trivial.

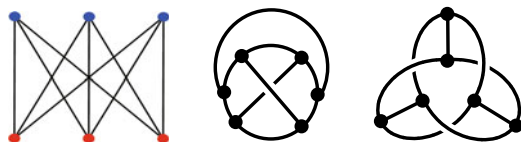
### 2.3.2 Topological Isomers

In knot theory, two knots (links, or spatial graphs) are considered as same if one knot can be changed into the other by a continuous transformation, i.e., without cutting and intersecting itself. Two diagrams of the same knot (link) can be related by a sequence of Reidemeister moves I, II, and III as in Fig. 2.8e. Two diagrams of the same spatial graph with non-rigid vertices can be related by a sequence of generalized Reidemeister moves I, II, and III as in Fig. 2.8e (same as the original Reidemeister moves) and generalized Reidemeister move IV and V for spatial graphs as in Fig. 2.10.

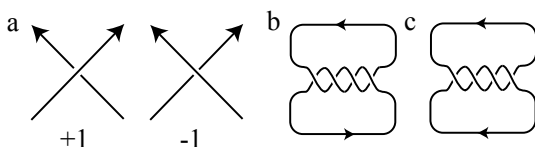
Different knots (links, or spatial graphs) will produce *topological isomers* of polymers. A topological isomer is an example of stereoisomers caused by its knot, link, or spatial graph structure. For example, polymers with the shape of spatial graphs in Fig. 2.11 are topological isomers. We can see that each cycle of the center is the trivial knot, whereas one cycle in the right is the trefoil knot. Hence they are different



**Fig. 2.10** The generalized Reidemeister moves IV(top) and V(bottom) for spatial graphs with non-rigid vertices



**Fig. 2.11** The left is the  $K_{3,3}$  graph. The center and the right are spatial graphs of  $K_{3,3}$ . Two non-equivalent spatial graphs will give topological isomers



**Fig. 2.12** **a** Signs of crossings. **b** and **c** Links with different orientations. Two oriented links are different as oriented links

spatial graphs. Knot structures in polymers change their properties. For instance, the radius of gyration becomes smaller if the polymer contains a knot structure [14].

Next, we consider the orientation of knots and links. The *orientation* of a knot, expressed by an arrow, is a direction along a knot. The orientation of a link is a union of orientations of components. A knot (link) with orientation is called an *oriented knot (link)*. Two oriented knots (links) are same if they are same knots (links) with the same orientation. For knots and links in polymers, the orientation can be defined using the sequence of monomers.

For 2-component oriented links, we can define the *linking number*. We consider a diagram of a 2-component oriented link  $L = K_1 \cup K_2$ , where  $K_1$  and  $K_2$  are components of  $L$ . For each crossing, we assign  $+1$  or  $-1$  according to the configuration of strands at the crossing see Fig. 2.12a. Then the half of the sum of the signs at the crossings of  $K_1$  and  $K_2$  is called the linking number. For example, the link in Fig. 2.12b has linking number  $-2$  and the one in c has  $+2$ . If two oriented links are same, then they have the same linking number. Hence we can conclude that two oriented links b and c in Fig. 2.12 are different as oriented links.

### 2.3.3 Topological Chirality

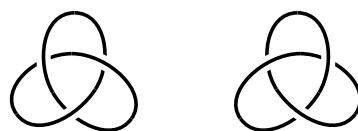
The presence of knots, links, and spatial graphs produces chiral polymers. For example, it is known that the trefoil knot is chiral, i.e., it is different from its mirror image see Fig. 2.13. Hence a polymer with the trefoil knot structure (and without its mirror image) is chiral. Each of the theta curve  $\theta_{3,1}$  in Fig. 2.8d and the right spatial graph of  $K_{3,3}$  in Fig. 2.11 contains the trefoil knot as a constituent knot and does not contain its mirror image. Hence they are chiral. This type of chirality is called *topological chirality*. We remark that there are examples of chiral spatial graphs whose constituent knots are achiral.

### 2.3.4 Rigid Vertex Versus Non-rigid Vertex

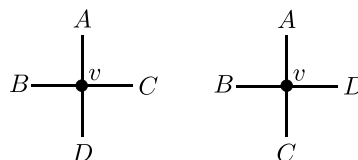
We will discuss the difference between rigid vertices and non-rigid vertices of spatial graphs. Let  $v$  be a vertex in a spatial graph with degree 4. If  $v$  is a non-rigid vertex, we allow rotations of edges incident to  $v$ . Hence we can locally change the position of edges see Fig. 2.14. On the other hand, if  $v$  is a rigid vertex, such rotations are not allowed. If  $v$  corresponds to a carbon atom, then  $v$  is a rigid vertex.

If vertices are rigid, we have more variety of spatial graphs. For example, Fig. 2.15 is an example of a non-trivial spatial graph with a rigid vertex. If we change that vertex into a non-rigid vertex, then the spatial graph will become trivial, i.e., we can eliminate two crossings of the spatial graph with a rotation at the vertex. Hence it is important to draw a distinction between spatial graphs with rigid vertices and with non-rigid vertices. For example, the multi-cyclic polymers synthesized in [12, 13] have rigid vertex structures.

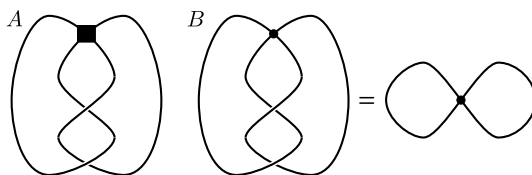
**Fig. 2.13** The trefoil knot is chiral. It is different from its mirror image



**Fig. 2.14** For a non-rigid vertex  $v$ , we can rotate two edges incident to  $v$ . One can change one conformation to the other



**Fig. 2.15** **a** Rigid vertex spatial graph. **b** Non-rigid vertex spatial graph. Two crossings can be eliminated by a rotation at the vertex



## 2.4 Summary and Perspective

In this chapter, we considered two meanings of topology of polymers.

Graph theoretical analysis reveals the structure of multi-cyclic polymers, i.e., how parts are connected. As an application, we can define a systematic nomenclature of multi-cyclic polymers. We also discussed the type of polymers. We hope the mathematical construction of multi-cyclic graphs (Theorems 2.2, 2.3, and 2.4) will give an idea for a new method of synthesis of a multi-cyclic polymer.

On the other hand, knot theoretical analysis informs us the 3-dimensional shape of polymers. A knot structure will change the property of a polymer. For multi-cyclic polymers, we can utilize spatial graph theory. Rigid vertices and non-rigid vertices give different phenomena. For example, rigid vertices give more knotted structures. It is extremely difficult to manipulate such structures of polymers, however we think such challenge will be important to obtain new function of multi-cyclic polymers in the future.

**Acknowledgements** We would like to thank Prof. Yasuyuki Tezuka and Prof. Tetsuo Deguchi for providing us the opportunity to contribute this chapter and their precious advices on this research. We also would like to express our gratitude to the referee for their helpful comments. This research is supported by JSPS KAKENHI Grant Number JP17H06463.

## References

1. K. Shimokawa, K. Ishihara, Y. Tezuka, *Topology of Polymers, SpringerBriefs in the Mathematics of Materials*, 4th edn. (Springer, Tokyo, 2020)
2. T. Haruna, T. Horiyama, K. Shimokawa, *IPSJ SIG Technical Report, 2017-AL-162* (Information Processing Society of Japan, 2017)
3. Y. Tezuka, *Acc. Chem. Res.* **50**, 2611 (2017)
4. C. Adams, *The Knot Book: An Elementary Introduction to the Mathematical Theory of Knots* (American Mathematical Society, United States, 2001)
5. E. Flapan, *When Topology Meets Chemistry: A Topological Look at Molecular Chirality* (Cambridge University Press, Cambridge, 2000)
6. E. Flapan, *Knots, Molecules, and the Universe: An Introduction to Topology* (American Mathematical Society, United States, 2016)
7. K. Murasugi, *Knot Theory and Its Applications* (Birkhäuser, Basel, 1996)
8. K. Shimokawa, K. Ishihara, I. Grainge, D.J. Sherratt, M. Vazquez, *Proc. Natl. Acad. Sci. USA* **110**, 20906–20911 (2013)
9. P. Dabrowski-Tumanski, P. Rubach, D. Goundaroulis, J. Dorier, P. Sulkowski, K.C. Millett, E.J. Rawdon, A. Stasiak, J.I. Sulkowska, *Nucleic Acids Res.* **47**, D367–D375 (2019)

10. T. Sawada, A. Saito, K. Tamiya, K. Shimokawa, Y. Hisada, M. Fujita, *Nat. Commun.* **10**, 921 (2019)
11. T. Sawada, Y. Inomata, K. Shimokawa, M. Fujita, *Nat. Commun.* **10**, 5687 (2019)
12. H. Heguri, T. Yamamoto, Y. Tezuka, *Angew. Chem., Int. Ed.* **54**, 8688–8692 (2015)
13. N. Sugai, H. Heguri, T. Yamamoto, Y. Tezuka, *J. Am. Chem. Soc.* **133**, 19694–19697 (2011)
14. E. Uehara, T. Deguchi, *J. Chem. Phys.*, **147**, 094901 (2017)

# Chapter 3

## Classification, Notation and Isomerism of Topological Polymers



Yasuyuki Tezuka

**Abstract** A systematic classification and notation procedure for non-linear polymer constructions composed of sufficiently long and thus flexible segment components, and in particular cyclic and multicyclic forms, has been formulated based on the *molecular graph* presentation adopted in organic chemistry to express the skeleton structure of alkanes and cycloalkanes. Subsequently, topological (soft) geometry properties, specifically involved in polymer substrates comprised of flexible chain components, are highlighted by focusing on their uniquely identified constitutional and stereoisomers, in comparison to Euclidian (hard) geometry basis to account for relevant isomer properties of ordinary non-polymeric chemical substances.

### 3.1 Classification of Polymer Substances by Their Topologies

Any classification protocols according to arbitrary criteria to distinguish relevant objects into divided groups, adopted typically for animals or plants, arguably provide conceptual insights into the nature of concerned substances. In this respect, a systematic classification of polymer topologies is of a fundamental significance, as the topology of polymer molecules is often a basis to control their properties and functions at static and dynamic states both in bulk and in solution [1]. Remarkably, moreover, unprecedented progress has been fulfilled within recent decades to implement novel strategies for the precision designing of versatile polymer topologies [2].

As was observed so far on such topologically unique (macro)molecules, as dendrimers [3], knots [4], catenanes [4] and rotaxanes [5], a systematic classification, which is often relevant to their terminology, has provided useful insights into their structural relationships and eventually in their rational synthesis. And specifically, the fundamental mathematical theory of knots has been applied to elucidate topological properties of such (macro)molecular substances [1, 6].

---

Y. Tezuka (✉)  
Tokyo Institute of Technology, Tokyo, Japan  
e-mail: [ytezukak33@gmail.com](mailto:ytezukak33@gmail.com)

In this chapter, a systematic classification procedure for non-linear polymer constructions, and in particular cyclic and multicyclic polymer architectures composed of sufficiently long and thus flexible segment components, is outlined [1, 7]. The process is formulated based on the geometrical presentation system applied in organic chemistry as a *molecular graph*, in which the skeletal structures of linear and branched alkanes ( $C_nH_{2n+2}$ ) as well as a series of mono- and polycycloalkanes ( $C_nH_{2n}$ ,  $C_nH_{2n-2}$ , etc.) are depicted by using the line graph presentation [7].

Thus, the total number of termini (chain ends) and of junctions (branch points) are maintained as invariant (constant) geometric parameters, together with the total number of branches at each junction and the connectivity of each junction. On the other hand, the spatial or bond distance between two adjacent junctions and that between the junction and terminus are taken as variant geometrical parameters, in contrast to Euclidian geometry, to adopt the flexible nature of the randomly coiled and constrained polymer segments. Furthermore, any line constructions having five or more branches at one junction are allowed to be included, contrary to the classical molecular graphs based on the tetravalent carbon atom.

A systematic notation protocol, which is a slightly modified version from the original one, is subsequently configured upon the hierarchical classification principles [7]. Thereupon, distinctive features uniquely identified in polymeric constitutional isomers as well as in polymeric stereoisomers are highlighted by focusing on their topological geometry properties, in comparison to Euclidian geometry basis to account for relevant isomer properties of ordinary non-polymeric chemical substances. Finally, selected examples of topologically rational experimental pathways to construct complex polymer topologies are postulated.

### 3.2 Classification of Acyclic and Monocyclic Polymer Topologies

The graph presentation of basic alkanes having generic molecular formula  $C_nH_{2n+2}$  with  $n = 3-7$  and of their corresponding topological polymer constructions are hierarchically ranked as listed in Table 3.1a. A line construction is produced both from ethane ( $C_2H_6$ ) and from propane ( $C_3H_8$ ), and the latter is presented for the sake of brevity.

Thus, two butanes of *n*- and *iso*-forms produce a linear and a three-armed star branched construction, respectively. A *neo*-pentane produces a new four-armed star construction, besides the two forms already obtained from butanes. Likewise, an H-shaped and a five-armed star construction are newly produced from hexanes, and two of a super H-shaped and a six-armed star counterparts from heptanes, respectively.

The systematic notation for a series of branched polymers is also given in Table 3.1a [1]. They are labelled as <sup>0</sup>A main class, as they are produced from alkanes free of cyclic skeletal units. A linear construction is produced from propane ( $C_3H_8$ ) and this particular topology is ubiquitously present in those from all higher alkanes.

**Table 3.1 a** Linear and branched polymer topologies produced from molecular graphs of alkanes ( $C_nH_{2n+2}$ :  $n = 3-7$ ), and **b** Monocyclic polymer topologies produced from molecular graphs of cycloalkanes ( $C_nH_{2n}$ :  $n = 3-6$ ) Adapted by permission from Springer Japan KK: [1], [COPYRIGHT (Copyright Springer Japan KK. 2019)]

Topology	$C_nH_{2n+2}$				
	$n=3$	4	5	6	7
${}^0A_3(2,0)$					
${}^0A_4(3,1)$					
${}^0A_5(4,1)$					
${}^0A_6(4,2)$					
${}^0A_6(5,1)$					
${}^0A_7(5,2)$					
${}^0A_7(6,1)$					

Topology	$C_nH_{2n}$			
	$n=3$	4	5	6
${}^1A_3(0,0)$				
${}^1A_4(1,1)$				
${}^1A_5(2,1)$				
${}^1A_5(2,2)$				
${}^1A_6(2,2)$				
${}^1A_6(3,1)$				
${}^1A_6(3,2)$				
${}^1A_6(3,3)$				

This sub-class construction is thus termed  ${}^0A_3$ , or alternatively  ${}^0A_3(2,0)$  to identify the total number of termini and of junctions, respectively, in parentheses. Likewise, sub-classes  ${}^0A_4$  (or  ${}^0A_4(3,1)$ ) and  ${}^0A_5$  (or  ${}^0A_5(4,1)$ ) are uniquely notated as seen in Table 3.1a. Furthermore, multiple constructions are included in sub-classes  ${}^0A_6$  and  ${}^0A_7$ , from hexanes and heptanes, respectively, while each component in these classes are specified by indicating the total number of termini and junctions, respectively, in parentheses as shown in Table 3.1a. Accordingly, an m-armed star polymer topology is notated as  ${}^0A_{m+1}(m,1)$ .

A series of monocyclic polymer topologies are classified in the same manner, according to the molecular graph of monocycloalkanes having a generic formula of  $C_nH_{2n}$ , and those up to  $n = 6$  are presented in Table 3.1b. A simple cyclic (ring) construction is produced from the molecular graph of cyclopropane ( $C_3H_6$ ). Methylcyclopropane and cyclobutane, having commonly the chemical formula of  $C_4H_8$  produce two constructions, namely a ring with a branch forms (tadpole) together with a simple ring counterpart, already listed from the cyclopropane. From the molecular



graphs of cyclopentane isomers,  $C_5H_{10}$ , moreover, the two constructions are newly produced, i.e., a twin-tail tadpole form having two outward branches at one common junction in the ring skeleton and a two-tail tadpole counterpart having two outward branches located at two separate junctions in the ring unit. Further, four constructions are newly identified according to the molecular graphs of cyclohexane isomers,  $C_6H_{12}$ , where one hypothetical form having five branches at one junction is included and thus shown in parentheses in Table 3.1b.

The systematic notation for a series of monocyclic constructions is shown in Table 3.1b, where each construction is classified into a  $^1A$  main class, according to monocycloalkanes. Thus, a simple ring construction from cyclopropane is designated as sub-class  $^1A_3$ , or alternatively  $^1A_3(0,0)$  to identify the total number of termini and junctions in parentheses. Likewise, a tadpole construction is notated as  $^1A_4$  or  $^1A_4(1,1)$ , from the molecular graph of  $C_4H_8$ . Further multiple constructions are appeared in the sub-classes  $^1A_5$  and  $^1A_6$ , and each of them are uniquely notated by specifying the total number of termini and junctions.








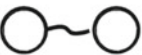
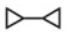































### 3.3 Classification of Dicyclic Polymer Topologies

A class of dicyclic polymer constructions are classified according to molecular graphs of bicycloalkanes, and primary members from  $C_nH_{2n-2}$  of up to  $n = 6$  are listed in Table 3.2. The three constructions are identified as basic forms without any outward branches; those are an internally linked (*fused*),  $\theta$ -form, a directly linked (*spiro*), 8-form and an internally linked (*bridged*), manacle-form, respectively.

A *fused*-dicyclic ( $\theta$ -form) construction is a primary form relevant to bicyclo[1,1,0]butane,  $C_4H_6$ . From the five molecular graphs of bicyclopentane isomers of the chemical formulae of  $C_5H_8$ , three new constructions, including a *spiro*-dicyclic (8-shaped) construction from *spiro*-[2,2]pentane are introduced. Moreover, a *bridged*-dicyclic (manacle-form) construction formed from bi(cyclopropane) is identified among eight new constructions by bicyclohexane isomers ( $C_6H_{10}$ ).

The systematic notation for a series of dicyclic polymer constructions is listed in Table 3.2, where each construction is assigned as a  $^2A$  main-class, according to dicycloalkanes. Thus, a  $\theta$ -form construction is notated as a sub-class  $^2A_4$ , or  $^2A_4(0,2)$  to identify the total number of termini and junctions, respectively, in parentheses. Three and eight constructions are subsequently appeared in the sub-classes  $^2A_5$  and  $^2A_6$ , respectively, as listed in Table 3.2. Notably, a pair of components identified in the sub-classes  $^2A_6(2,2)$  and  $^2A_6(2,3)$  are not specified simply by the total number of termini and junctions. Thus, in the brackets after the closing parenthesis, the number of not only outward branches but also internally linked branches on the ring skeleton unit is identified, and these numbers (thus 0 for the latter, and 1, 2, .. for the former) are shown by the linking with hyphens. Moreover, the positions of the two specific junctions internally linked to each other are expressed by giving superscripts (a, b,

**Table 3.2** Dicyclic polymer topologies produced from molecular graphs of bicycloalkanes ( $C_nH_{2n-2}$ :  $n = 4-6$ ). Reprinted by permission from Springer Japan KK: [1], [COPYRIGHT (Copyright Springer Japan KK. 2019)]

Topology	$C_nH_{2n-2}$			Topology	$C_nH_{2n-2}$ $n = 6$
	$n = 4$	5	6		
 ${}^2A_4(0,2)$		 	  	 ${}^2A_6(0,2)$	
 ${}^2A_5(0,1)$		 		 ${}^2A_6(1,1)$	
 ${}^2A_5(1,2)$		  	  	 ${}^2A_6(1,2)$	
 ${}^2A_5(1,3)$		   	   	 ${}^2A_6(2,2)[1^a-1^a]$	
				 ${}^2A_6(2,3)[2-0^a-0^a]$	
				 ${}^2A_6(2,3)[1^a-1-0^a]$	
				 ${}^2A_6(2,4)$	

etc.) at the relevant junction numbers. For examples, the two  ${}^2A_6(2,2)$ 's are specified each other as  ${}^2A_6(2,2)[2^a-0^a]$  and  ${}^2A_6(2,2)[1^a-1^a]$  and the two  ${}^2A_6(2,3)$ 's as  ${}^2A_6(2,3)[2-0^a-0^a]$  and  ${}^2A_6(2,3)[1^a-1-0^a]$ , respectively.

### 3.4 Tri-, Tetra- and Pentacyclic Polymer Topologies

Fifteen tricyclic constructions without any outward branches are identified, and are corresponding to the relevant molecular graphs of tricycloalkane isomers having the chemical formula of  $C_nH_{2n-4}$  with  $n = 4-10$ , as listed in Table 3.3a, where a large number of tricyclic constructions having outward branches are omitted for brevity. More specifically, the four tricyclic constructions are assigned to the *fused*-form, the two to the *spiro*-form and the three to the *bridged*-form, respectively, in addition to the six *hybrid*-form by the combination of either *fused/spiro*, *fused/bridged* or *spiro/bridged* components.

The systematic notation for a series of tricyclic polymer topologies is listed in Table 3.3a, where each construction is assigned as a  ${}^3A$  main class, according to tricycloalkanes. Thus, a doubly *fused* (internally double-linked) ring construction, which is a primary component formed from tetrahedrane, is designated as a subclass  ${}^3A_4$  or  ${}^3A_4(0,4)$  to identify the total number of termini and junctions, respectively, in parentheses. Notably, all four doubly *fused* tricyclic constructions,  ${}^3A_4(0,4)$ ,  ${}^3A_5(0,2)$ ,  ${}^3A_5(0,3)$  and  ${}^3A_6(0,4)$ , are alternatively named as  $\alpha$ ,  $\delta$ ,  $\gamma$  and  $\beta$  graph, respectively [8]. In a series of doubly *fused* constructions of  ${}^3A_4(0,4)$ ,  ${}^3A_5(0,2)$  and  ${}^3A_5(0,3)$ , moreover, the mode of the internally linked branches on the ring unit is uniquely defined as  $[0^a-0^b-0^a-0^b]$ ,  $[0^{a,b}-0^{a,b}]$  and  $[0^{a,b}-0^a-0^b]$ , respectively. Other tricyclic constructions having either *spiro*-, *bridged*-, or *hybrid*-forms listed in Table 3.3a are, on the other hand, uniquely identified simply with the total number of termini and junctions in each construction.

Finally, selected examples of topologically significant, *fused*-tetracyclic and *fused*-pentacyclic constructions, including a  $K_{3,3}$  graph, are listed in Table 3.3b. Each construction is produced accordingly from the relevant tetra- and pentacycloalkanes having the chemical formula of  $C_nH_{2n-6}$  with  $n = 6$ , and of  $C_nH_{2n-8}$  with  $n = 8$ , respectively, and thus are classified into the  ${}^4A$  and  ${}^5A$  main class, respectively. The notation of *triply* fused tetracyclic constructions is completed to uniquely identify the mode of the internally linked branches on the ring unit, namely,  ${}^4A_6(0,6)[0^a-0^b-0^c-0^a-0^b-0^c]$  for the  $K_{3,3}$  construction,  ${}^4A_6(0,3)[0^{a,c}-0^{a,b}-0^{b,c}]$  for the “unfolded tetrahedron” construction,  ${}^4A_6(0,6)[0^a-0^b-0^a-0^c-0^b-0^c]$  for the prismane construction,  ${}^4A_6(0,6)[0^a-0^a-0^b-0^c-0^c-0^b]$  for the ladder construction, and  ${}^4A_6(0,4)[0^{a,b,c}-0^a-0^b-0^c]$  for the “königsberg bridge” construction, respectively. Moreover, a quadruply *fused* pentacyclic constructions of a “shippo” form is assigned as  ${}^5A_8(0,4)[0^{b,d}-0^{a,c}-0^{b,d}-0^{a,c}]$ , as listed in Table 3.3b. Chemical construction of these complex polymer topologies is the topics in the following chapters in this book.

**Table 3.3 a** Tricyclic polymer topologies produced from molecular graphs of tricycloalkanes without outward branches ( $C_nH_{2n-4}$ :  $n = 4-10$ ), and **b** selected tetracyclic and pentacyclic polymer topologies produced from tetra- and pentacycloalkanes ( $C_nH_{2n-6}$ :  $n = 6$ , and  $C_nH_{2n-8}$ :  $n = 8$ ). Adapted by permission from Springer Japan KK: [1], [COPYRIGHT (Copyright Springer Japan KK. 2019)]

a

Topology	$C_nH_{2n-4}$				Topology	$C_7H_{10}$
	n = 4	5	6	7		
${}^3A_4(0,4)[0^a-0^b-0^a-0^b]$					${}^3A_7(0,3)$	
${}^3A_5(0,2)[0^a,b-0^a,b]$					${}^3A_7(0,4)$	
${}^3A_5(0,3)[0^a,b-0^a-0^b]$					Topology	$C_8H_{12}$
${}^3A_6(0,4)[0^a-0^a-0^b-0^b]$					${}^3A_8(0,2)$	
${}^3A_6(0,2)$					${}^3A_8(0,3)$	
${}^3A_6(0,3)$					Topology	$C_9H_{14}$
${}^3A_7(0,1)$					${}^3A_9(0,3)$	
${}^3A_7(0,2)$					${}^3A_9(0,4)$	
					Topology	$C_{10}H_{16}$
					${}^3A_{10}(0,4)$	

b

Topology	$C_6H_6$	Topology	$C_6H_6$
${}^4A_6(0,3)[0^a,c-0^a,b-0^b,c]$	Unfolded tetrahedron	${}^4A_8(0,6)[0^a-0^a-0^b-0^c-0^c-0^b]$	Ladder
${}^4A_6(0,6)[0^a-0^b-0^a-0^c-0^b-0^c]$	Prisman	${}^4A_6(0,4)[0^a,b,c-0^a-0^b-0^c]$	Koenigsberg bridge
${}^4A_6(0,6)[0^a-0^b-0^c-0^a-0^b-0^c]$	$K_{3,3}$	${}^5A_8(0,4)[0^b,d-0^a,c-0^b,d-0^a,c]$	Shippo

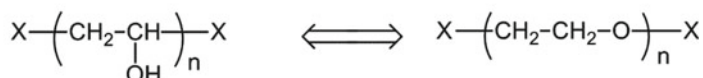
### 3.5 Topological Insights into Polymeric Constitutional Isomers

Isomer, a term derived from Greek, *isos* (equal) and *meros* (part), is defined as a set of chemical compounds with the same chemical constitution (thus molar mass) but distinctive properties. The evolution of chemical conception over the isomerism since its introduction by Berzelius [9], followed by Kekulé [10] and van 't Hoff [11] has bestowed deeper understanding in both static and dynamic structures of chemical substances.

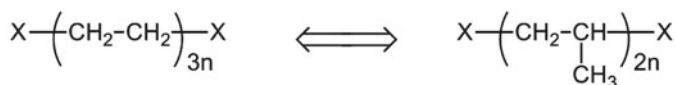
Constitutional (structural) isomers are the relevant pair of chemical compounds having distinctive *connectivity* with respect to atoms or atomic groups. Thus, the constitutional isomers of polymer compounds are firstly defined as in the relevant small chemical compound, where isomers are distinguished by using their chemical formulas and atomic groups. As a typical example, poly(vinyl alcohol) and poly(ethylene oxide) shown in Fig. 3.1 are a pair of isomers by this conventional definition, with the distinctive connectivity of atoms in their repeating units (Fig. 3.1). Another isomer pair by this definition could include polyethylene and polypropylene, comprised of a different set of atomic groups, as shown in Fig. 3.1.

On the other hand, a set of constitutional isomers are identified uniquely for polymer substances, in which their line constructions, thus without showing any chemical formulas, are sufficient to distinguish isomer structures. A pair of star polymers of the same arm numbers and of the total arm length, while having different sets of arm length composition, shown in Fig. 3.2, is a prototypical example. In such polymeric constitutional isomers with identical connectivity by different sets of chains, the total edge length of the molecular graphs corresponds to their molar masses or degree of polymerizations, while the chemical entity of junctions and terminus is identical each other. For this class of constitutional isomer pairs, the

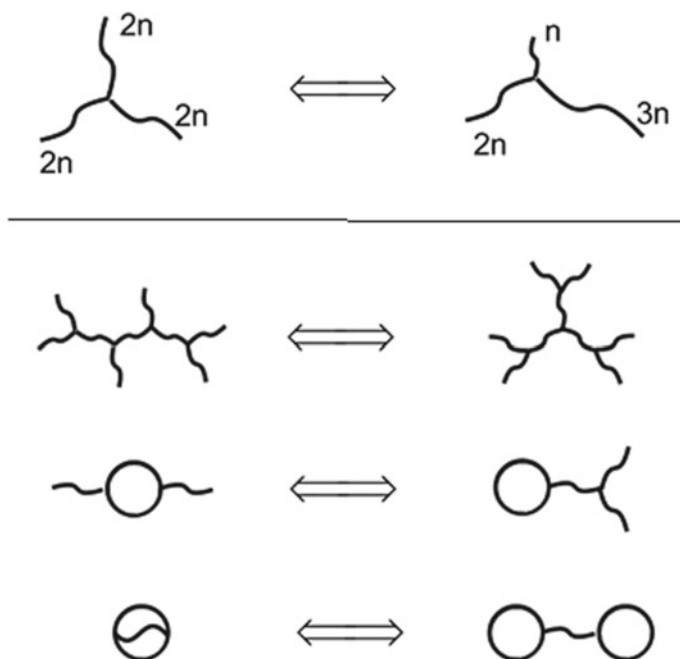
#### Different connectivity of atoms



#### Different sets of atomic groups



**Fig. 3.1** Polymeric constitutional isomers by different connectivity of atoms and by different sets of atomic groups



**Fig. 3.2** A pair of constitutional isomers of *topologically equivalent* star polymer constructions (above) and of *topologically distinctive* branched, monocyclic and dicyclic polymer constructions (below)

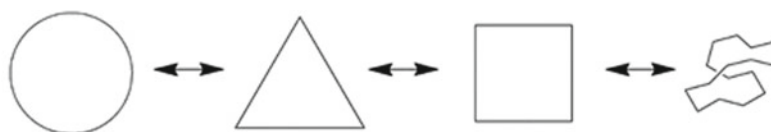
mutual interconversion of each isomer forms requires the chain-breaking with at least *two* appropriate positions, followed by the chain-recombination to average out the arm segment lengths. And importantly from topological geometry viewpoints, a pair of these isomer graphs are convertible each other through the topological transformation by the continuous deformation of the arm chain lengths but without any chain-breaking operation.

In contrast, another class of polymeric constitutional isomers is identified, including a pair of a dendritic and a comb-type branched polymers,  ${}^0A_{10}(6,4)[3-3-3-3]$  and  ${}^0A_{10}(6,4)[3-3(3)-3]$ , of a two-tail tadpole and a y-tail tadpole form polymers,  ${}^1A_5(2,2)$  and  ${}^1A_6(2,2)$ , and of a  $\theta$ - and a manacle-form polymers,  ${}^2A_4(0,2)$  and  ${}^2A_6(0,2)$ , respectively, as listed in Fig. 3.2. These isomer constructions are composed of identical sets of edges but with the different connectivity each other. In contrast to the pair of star polymer isomers shown above, the mutual interconversion of such isomer constructions requires the chain-breaking operation with at least *two* appropriate positions, followed by the chain-rearrangement and the chain-recombination. By this distinction of topological properties, these constitutional isomers are identified as *topologically distinctive* in contrast to the relevant constitutional isomers of star polymers as *topologically equivalent* (Fig. 3.2).

Interestingly, the subsequent experimental study showed that a mixture of a  $\theta$ - and a manacle-shaped constitutional isomers has been successfully produced from an identical set of the polymer precursors and the linking reagents, namely a set of three units of a linear precursor and two units of a trifunctional linking reagent, or alternatively of two units of a three-armed precursor and three units of a bifunctional linking reagent. And moreover, each polymeric isomer component is subsequently isolated in a pure form by means of a preparative chromatography technique [12].

### 3.6 Topological Insights into Polymeric Stereoisomers

The graph theory analysis has also been conducted in order to gain further topological insights into stereoisomers involving a series of topological polymers of loop constructions. Thus, a simple ring polymer is identified firstly as a *stereoisomer* of a triangle, a square or a randomly folded ring counterpart, as shown in Fig. 3.3, since



*topologically equivalent*



*topologically distinctive*



**Fig. 3.3** Polymeric stereoisomers of *topologically equivalent* and *topologically distinctive* loop constructions (above), and the interconversion of  $\theta$ -, manacle- and pretzel-form polymeric isomers (below)

they are convertible each other through the conceptual continuous chain deformation with retaining the total chain length, but without the chain-breaking operation. In contrast, a pair of a ring and a knot polymer construction are classified as a different type of isomers each other, since each construction can be interconvertible only with the chain-breaking applied with an appropriate SINGLE position and the subsequent recombination operation (Fig. 3.3).

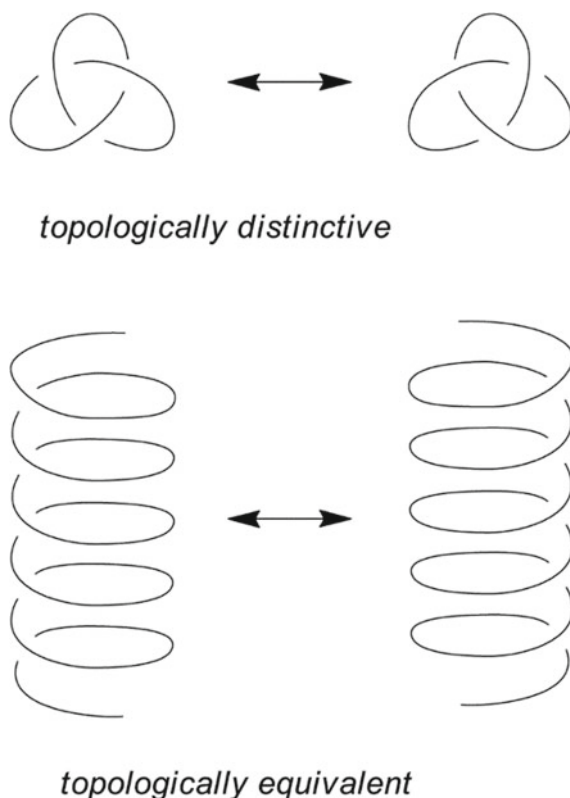
A pair of a simple ring, or a trivial knot by the topology term, and a knot (typically a trefoil knot) molecular graph are traditionally assigned as an example of stereoisomers, more specifically *topologically distinctive* stereoisomers [4], in accord with a topological geometry conjecture, where a simple ring and a knot are mutually interconvertible each other when they are placed in four-dimensional space. However, this particular operation seems hard to reconcile with an actual chemical process undergoing in the more intuitive three-dimensional space. In addition, the mutual graph transformation by the chain-breaking with a SINGLE position is intrinsically inconsistent with the conventional operation involving constitutional isomers, where the chain-breaking with at least TWO appropriate positions is required to complete the interconversion process.

In this relevance, a pair of a manacle- and a pretzel-form polymers are identified as a *topologically distinctive* stereoisomer each other, as the latter is produced through the catenation of two ring units in the former. In addition, the former is constitutional isomer of the  $\theta$ -form counterpart (Fig. 3.3). Thus, the manacle and pretzel constructions are interconvertible each other by applying the chain-breaking at an appropriate SINGLE position, as in the case of a ring and a knot.

Notably, moreover, a pair of a right- and a left-handed knot polymer are identified as *topologically distinctive* stereoisomers (enantiomers), as they are mutually convertible each other by the chain-breaking process at a SINGLE position (Fig. 3.4). In contrast, another pair of a right-handed and a left-handed helix polymers are *topologically equivalent* isomer each other, as their graphs are converted each other simply by the conceptual topological transformation, but without any chain-breaking operation (Fig. 3.4).

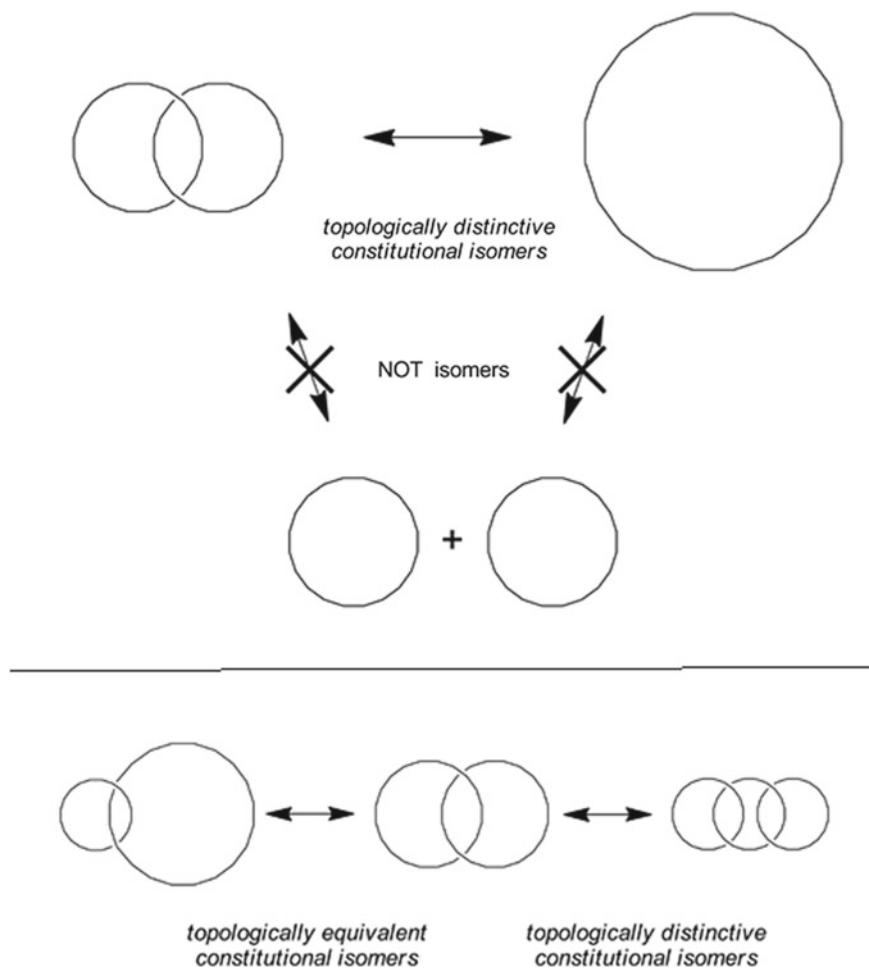
Finally, it is important to point out some limitation for the application of topological geometry conjectures to actual polymer substrate systems. This is, in particular, the case involving a set of a large single ring and a catenane (more precisely [2]-catenane, or Hopf link by topology term) polymers. They are assigned as *topologically distinctive* constitutional isomers, as they follow a criterion of the mutual conversion by applying the chain-breaking with at least appropriate TWO positions followed by the chain-rearrangement/chain-recombination (Fig. 3.5). However, the [2]-catenane polymer is NOT the isomer of the two separated ring polymers, just as a cyclohexane is not an isomer of two cyclopropanes from the chemistry prin-





**Fig. 3.4** A pair of *topologically distinctive* enantiomeric stereoisomers of trefoil knot polymers and a pair of *topologically equivalent* counterparts of helix polymers. Reprinted by permission from Springer Japan KK: [1], [COPYRIGHT ( Copyright Springer Japan KK. 2019)]

ciple. By topological geometry, on the contrary, these are regarded as equivalent constituents as they are convertible each other by applying the chain-breaking with a SINGLE position and the subsequent chain-rearrangement/chain-recombination process, which is applied for the isomerization between a ring and a knot, or dicyclic manacle- and pretzelan-form polymers (Fig. 3.5). In this connection, a pair of a [2]-catenane and a [3]-catenane are identified as *topologically distinctive* constitutional isomers, while a set of [2]-catenanes possessing different ring sizes as *topologically equivalent* constitutional isomers, as for a pair of the star polymers of different set of chain components (Fig. 3.5).



**Fig. 3.5** A pair of *topologically distinctive* constitutional isomers of a catenane and a ring construction polymers, while the two separated rings are not isomers of each substrate (above), and a set of *topologically distinctive* and *topologically equivalent* constitutional isomers of catenane polymers (below). Reprinted by permission from Springer Japan KK: [1], [COPYRIGHT ( Copyright Springer Japan KK. 2019)]

## References

1. K. Shimokawa, K. Ishihara, Y. Tezuka, *Topology of Polymers* (Springer, Tokyo, 2020)
2. Y. Tezuka (ed.), *Topological Polymer Chemistry: Progress of cyclic polymers in syntheses, properties and functions* (World Scientific, Singapore, 2013)
3. G.R. Newkome, C.N. Moorefield, F. Vögtle, *In Dendritic Molecules-Concepts, Syntheses, Perspectives* (Wiley-VCH, Weinheim, 1996), p. 37
4. J.-P. Sauvage, C. Dietrich-Buchecker (eds.), *Molecular Catenanes, Rotaxanes and Knots* (Wiley-VCH, Weinheim, 1999)

5. H.W. Gibson, M.C. Bheda, P.T. Eugen, *Prog. Polym. Sci.* **19**, 843 (1994)
6. E. Flapan, *When topology meets chemistry. A topological look at molecular chirality.* (Cambridge University Press: Cambridge, 2000)
7. Y. Tezuka, H. Oike, *J. Am. Chem. Soc.* **123**, 11570 (2001)
8. A.T. Balaban, *Chemical Application of Graph Theory*, ed. by A.T. Balaban, (Academic Press, London, 1976), p. 63.
9. J.J. Berzelius, *Pogg. Ann.* **19**, 305 (1830)
10. F.A. Kekulé, *Ann. Chem.* **106**, 129 (1858)
11. J. H. van 't Hoff, *Archives néerlandaises des sciences exactes et naturelles* **9**, 445 (1874)
12. H. Oike, H. Imaizumi, T. Mouri, Y. Yoshioka, A. Uchibori, Y. Tezuka, *J. Am. Chem. Soc.* **122**, 9592 (2000)

# Chapter 4

## Exact Evaluation of the Mean Square Radius of Gyration for Gaussian Topological Polymer Chains



Jason Cantarella, Tetsuo Deguchi, Clayton Shonkwiler, and Erica Uehara

**Abstract** Various polymers with nontrivial molecular structures expressed by graphs have recently been synthesized in experiments. We call them topological polymers for the graphs. We consider a set of Gaussian chains describing an ideal topological polymer or ideal polymer network for a given graph and call it topologically constrained random walks (TCRW) of the graph. In this chapter we show an exact evaluation of the mean square radius of gyration for the TCRW of complete graphs. We first review fundamental aspects of the novel method for constructing TCRW through the boundary operator of homology theory, as given in Ref. (Cantarella et al., Gaussian Random Embeddings of Multigraph, [5]). Then we rigorously derive the average size of the TCRW for complete graphs. By making use of the asymptotic formula (Cantarella et al., Radius of Gyration, Contraction Factors, and Subdivisions of Topological Polymers, [6]) we exactly derive the mean square radius of gyration for the subdivided topological polymers consisting of Gaussian chains or the subdivided TCRW for a given graph in the large subdivision degree limit. That is, in the limit of sending the number of subdivided segments in each branch to infinity. Throughout the chapter we emphasize the key point of the TCRW method that the probability distribution function of the edge displacements or bond vectors of the TCRW for a connected graph is directly derived from the normal distribution with unit variance. For instance, thanks to it we can rapidly generate conformations of the Gaussian network of a given graph where external forces are applied at the surfaces so that it has a nonzero finite volume in equilibrium.

---

J. Cantarella

Mathematics Department, University of Georgia, Athens, GA, USA

T. Deguchi (✉)

Department of Physics, Ochanomizu University, Tokyo 112-8610, Japan

e-mail: [deguchi@phys.ocha.ac.jp](mailto:deguchi@phys.ocha.ac.jp)

C. Shonkwiler

Department of Mathematics, Colorado State University, Fort Collins, CO, USA

E. Uehara

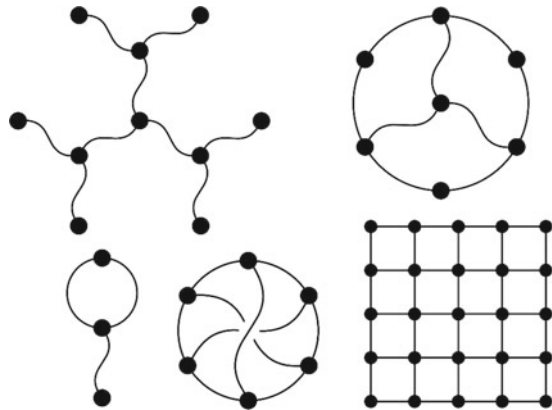
Center for Soft Matter Physics, Ochanomizu University, Tokyo 112-8610, Japan

## 4.1 Introduction

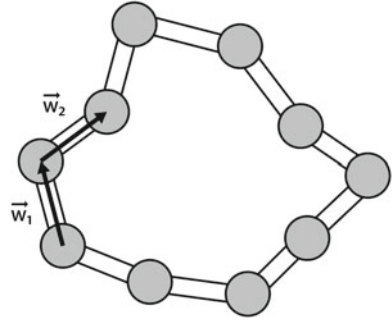
Polymer architecture is an important feature in polymeric materials. It represents the chemical connectivity among the monomers or subchains and characterizes most of the physical quantities of the polymers such as the mean square radius of gyration and the scattering functions. There are various types of polymer architecture: linear, cyclic (ring), star-branched, comb-like, randomly branched, and multi-cyclic polymers. Moreover, polymer networks have complex polymer architectures (Fig. 4.1). Recently, polymers of nontrivial architectures have been designed and synthesized in chemical experiments [1–3]. We call them topological polymers. In a given polymer network such as rubbers and gels, there exist a huge number of cross-links, each of which is connected to subchains with a fixed functionality, and all the cross-links and subchains lead to a large number of topological constraints corresponding to many loops in the polymer network. It is therefore nontrivial to calculate the statistical average of a physical quantity over all conformations of the polymer satisfying the topological constraints. Thus, it is often suggested that a straightforward theoretical or numerical study on topological polymers or polymer networks should be quite intricate and perhaps nontrivial. For polymer networks, almost all theoretical studies on the macroscopic behavior so far are performed under phenomenological assumptions such as affine deformation [4].

For an illustration, let us consider a cyclic polymer chain, which forms a cycle or loop (Fig. 4.2). It has such a constraint that the sum of all bond vectors between pairs of adjacent monomers is equal to zero. Thus, in order to construct conformations of the cyclic polymer, as a direct method we may generate randomly many sequences of bond vectors and select only conformations in which the sum of the bond vectors is given by zero. Of course, the probability of having such a set of bond vectors satisfy the constraint is very small and hence the direct method is not practically useful. Here we assume that a sequence of the position vectors of vertices or that of the bond vectors in a cyclic polymer determines a polymer conformation. There can

**Fig. 4.1** Various topological architectures: Branched tree, alpha graph, in the upper level from the left; tadpole graph,  $K_{3,3}$  bipartite graph, and square lattice network, in the lower level from the left



**Fig. 4.2** Cyclic polymer imposes on its bond vectors the loop constraint:  
 $\vec{w}_1 + \vec{w}_2 + \dots + \vec{w}_{10} = 0$ .



be many topological constraints in topological polymers with complex architectures, since their number is equal to that of independent loops. We call the constraints on the bond vectors associated with loops *topological constraints*. As the conformation of a linear polymer chain is given by a random walk, that of a topological polymer or polymer network is expressed by a complex of several random walks satisfying all the topological constraints. We call such a set of the positions of vertices connected by the bond vectors *topologically constrained random walks* (TCRW) or *Gaussian random embeddings of multigraphs* [5]. Hereafter, we call the bond vectors the edge displacements, in the manuscript.

It should be nontrivial to generate non-biased random walks satisfying all the topological constraints, i.e., TCRW: Even for a cyclic polymer, we hardly obtain it if we simply generate a random walk step by step, as argued above. However, in the present manuscript we demonstrate that by the method of Gaussian random embeddings of multigraphs [5] we can systematically evaluate the statistical average of any physical quantity for a given topological polymer or polymer network where we take into account all the topological constraints. All the topological constraints are taken into account in terms of the boundary operator in graph theory or homology theory. Furthermore, the method is practically useful even if the polymer architecture is quite complex [5, 6]. As an illustration, we evaluate the mean square radius of gyration for topological polymers of complete graphs. In this manuscript we first review the method presented in Ref. [5] and then show the applied result.

One of the most important properties in the method of TCRW (or Gaussian random embeddings of multigraphs) is that for any given topological polymer or polymer network consisting of Gaussian chains the probability distribution function of the edge displacements is directly constructed from the normal distributions with unit variance [5]. By taking advantage of this key property, we can easily generate non-biased random walks satisfying all the topological constraints, i.e., TCRW. Most importantly, we can generate many samples of conformations for the polymer by making use of it. Thus, the method is practically useful in evaluating statistical expectation values by taking the average over generated samples.

The key property is consistent with physical requirements in statistical physics. A polymer in solution or melt is exposed to incessant thermal collisions due to solvent molecules or monomers and changes its conformation in time evolution. We can show

that the statistical ensemble derived in the method of TCRW is consistent with the Rouse dynamics of the polymer in solution or melt. Furthermore, we can also show that the normal distributions of the edge displacements (i.e., the bond vectors) are transformed into the Boltzmann distributions of the position vectors of vertices where the elastic potentials are assigned on them and the center of mass in each network conformation is always located at the origin. We thus obtain a special regularized version of the Gaussian phantom networks [7–10]. In the standard regularization of the phantom networks, however, the position vectors of selected vertices in the networks are fixed [7–12]. Hereafter, if the center of mass is located at the origin in a polymer conformation, we call it *centered*. Thus, if we regard TCRW as a model of polymer networks, the normal distributions of the edge displacements due to thermal noises correspond to the Boltzmann distributions of the centered network conformations (i.e., the sets of vertex position vectors with the center of mass fixed at the origin). In fact, most of the polymer networks are of bulk size, so that the center of mass does not fluctuate thermally.

There are two different methods for deriving statistical properties of TCRWs: one method is that we generate a large number of independent TCRWs, and numerically evaluate the average of some physical quantity over them; another method is that we derive an explicit form of the probability distribution of TCRWs and analytically evaluate the expectation value of some physical quantity. In this article, we employ the second method.

Here we present an introductory review on fundamental aspects of the method of TCRW [5, 6]. In particular, we elaborate the key property of TCRW found recently and addressed in Ref. [5] in Sects. 4.2 and 4.3. As an application of the method of TCRW we show an exact evaluation of the mean square radius of gyration for TCRW of topological polymers associated with an  $n$ -subdivided complete graph of a finite number of vertices in Sects. 4.4 and 4.5. Here, the  $n$ -subdivided complete graph is derived from a complete graph by replacing each edge (or branch) in the graph with a linear chain of  $n$  edges (or  $n$  bonds). It should be a realistic model of topological polymers synthesized in experiments, since each branch is given by a linear polymer chain consisting of a sequence of monomers for most of the topological polymers.

## 4.2 Elements of Graph Theory

We express the architecture of a polymer by a graph. Let us introduce useful tools in graph theory. A graph consists of a set of vertices also called nodes and a set of edges also called links or lines. An edge has a pair of vertices at the ends called the endpoints, i.e., it links its two endpoints. A graph represents the way that some objects denoted as vertices or nodes are connected to each other with edges or lines. For an illustration, let us consider a railway map. It is a graph in which a vertex corresponds to a station. Distances between vertices are not always proportional to those of corresponding stations, and the shapes of railway tracks are simplified to straight lines since a passenger often desires just to find which train to take for

transfer. For a polymer, a graph represents the structure of the chemical connectivity. A subchain (or a Kuhn segment in polymer physics, i.e., a subchain with the Kuhn length (see Ref. [4])) corresponds to an edge in the graph, while a chemical cross-link or an end point of the Kuhn segment to a vertex.

### 4.2.1 Boundary Matrix

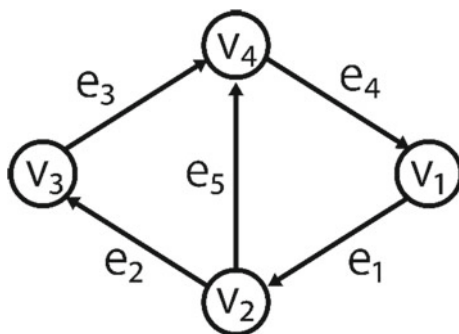
We express the set of vertices of a graph  $G$  by  $\{v_1, v_2, \dots, v_{\mathcal{V}}\}$  where the number of the vertices is denoted as  $\mathcal{V}(G)$  or simply by  $\mathcal{V}$ , and the set of edges by  $\{e_1, e_2, \dots, e_{\mathcal{E}}\}$  where the number of the edges is denoted as  $\mathcal{E}(G)$  or  $\mathcal{E}$ . The number of edges which link to vertex  $v_i$ , namely, the vertex degree or the valence of vertex  $v_i$  is denoted by  $d_i$ . Here we remark that the sum is equal to  $2\mathcal{E}$ . If there are plural edges between a pair of vertices, they are called multiple edges or a multi-edge. If an edge links a vertex to itself, it is called a loop. If vertices  $v_i$  and  $v_j$  are connected by a finite sequence of edges, we say that there is a path between the pair of the vertices or the two vertices are connected. If all pairs of vertices in a graph are connected, we say that the graph is connected.

Let us consider graphs with directions, i.e., directed graphs. A directed graph is exhibited in Fig. 4.3. All edges in the graph have directions: edge  $e_1$  is a directed edge from  $v_1$  to  $v_2$ . A graph is said to be directed if all the edges have directions. In a polymer graph, the directions do not have any chemical meaning. They are simply an organizational device and can be assigned in any way which is convenient.

The boundary matrix  $B$  of a directed graph shows both the connectivity at the vertices and the directions of the edges in the graph. We define the  $(i, j)$  entry of  $B$  by

$$B_{ij} = \begin{cases} +1 & \text{if } v_i \text{ is the head vertex of } e_j, \\ -1 & \text{if } v_i \text{ is the tail vertex of } e_j, \\ 0 & \text{otherwise.} \end{cases} \quad (4.1)$$

**Fig. 4.3** A directed graph with four vertices and five edges





For example, the boundary matrix of the graph of Fig. 4.3 is given by the following matrix:

$$B = \begin{pmatrix} -1 & 0 & 0 & 1 & 0 \\ 1 & -1 & 0 & 0 & -1 \\ 0 & 1 & -1 & 0 & 0 \\ 0 & 0 & 1 & -1 & 1 \end{pmatrix}. \quad (4.2)$$

Here the nonzero matrix elements of the  $j$ -th column of matrix  $B$  correspond to the endpoints of the  $j$ -th edge.

## 4.2.2 The Space of Paths

Let us introduce the space of paths for a given graph. We assume that edges  $\{e_1, e_2, \dots, e_\epsilon\}$  in the graph correspond to the standard basis vectors  $\vec{e}_j$  for  $j = 1, 2, \dots, \epsilon$ , in the  $\epsilon$ -dimensional Euclidean space  $R^\epsilon$ , respectively. We call it the space of paths in the graph. Any path in the graph can be expressed as a linear combination of the basis vectors. For instance, the path from vertex  $v_1$  to  $v_3$  via  $v_2$  shown in Fig. 4.3 is given by  $\vec{e}_1 + \vec{e}_2$ .

The boundary matrix acts on the vector space of paths  $R^\epsilon$ . If we apply it to a path  $p$ , the product  $Bp$  leads to the difference of the two endpoints of the path  $p$ . For instance, we have  $B(\vec{e}_1 + \vec{e}_2) = \vec{v}_3 - \vec{v}_1$ . Here we recall that the boundary matrix acting on an edge leads to the difference of the two endpoints of the edge. We have  $B\vec{e}_1 = \vec{v}_2 - \vec{v}_1$ .

The boundary matrix  $B$  of a graph characterizes the topological constraints associated with loops in the graph: it annihilates any loop in the graph, and hence every loop in the graph is an element of  $\ker B$ . For instance, it is easy to show that we have  $B(\vec{e}_1 + \vec{e}_4 + \vec{e}_5) = 0$ , where path  $\vec{e}_1 + \vec{e}_4 + \vec{e}_5$  gives a loop in the graph of Fig. 4.3. Here we recall that the symbol  $\ker B$  denotes such a subspace of  $R^\epsilon$  on which the action of  $B$  vanishes, i.e., the null space.

Similarly for edges, we introduce the space of vertices in a given graph by assuming that vertices in  $\{v_1, v_2, \dots, v_\nu\}$  correspond to the standard basis vectors  $\vec{v}_j$  for  $j = 1, 2, \dots, \nu$  in the  $\nu$ -dimensional Euclidean space  $R^\nu$ . Therefore, the boundary matrix  $B$  is a linear map from the space of paths  $R^\epsilon$  to the space of vertices  $R^\nu$ .

We define the graph Laplacian  $L$  for a given graph by the product between the boundary matrix  $B$  and its transpose  $B^T$ :

$$L = BB^T. \quad (4.3)$$

For instance, the graph Laplacian of the graph in Fig. 4.3 is given as follows:

$$L = \begin{pmatrix} 2 & -1 & 0 & -1 \\ -1 & 3 & -1 & -1 \\ 0 & -1 & 2 & -1 \\ -1 & -1 & -1 & 3 \end{pmatrix}.$$

The diagonals of  $L$  are positive integer numbers since  $B$  is an integer matrix. Off-diagonal element  $L_{ij}$  is the product of  $-1$  and the number of the edges that link  $v_i$  and  $v_j$ . If there are neither multiple edges nor loop edges, we have

$$L_{ij} = \begin{cases} d_i & \text{if } i = j, \\ -1 & \text{if } i \text{ and } j \text{ are adjacent,} \\ 0 & \text{otherwise.} \end{cases} \quad (4.4)$$

We remark that the sum of all elements in each row of  $L$  is given by zero. The sum of all the elements of a row of  $L$  is equal to the product of the row with the vector in which all components are equal to 1:

$$\vec{1} = (1, 1, \dots, 1)^T. \quad (4.5)$$

Therefore, the vector  $\vec{1}$  is in the kernel of  $L$ .

### 4.2.3 Singular Value Decomposition of Boundary Matrix $B$

We first recall that the boundary matrix  $B$  is a linear map from the space of paths  $R^{\mathcal{E}}$  to that of vertices  $R^{\mathcal{V}}$ . We can express it in terms of singular value decomposition as follows.

$$B = USV^T. \quad (4.6)$$

Here the matrix  $S$  is pseudo-diagonal where all off-diagonal matrix elements are equal to zero, and the matrices  $U$  and  $V$  are  $\mathcal{V}$ -dimensional and  $\mathcal{E}$ -dimensional orthogonal matrices, respectively. We recall that  $V^T$  denotes the transpose of the matrix  $V$ .

Since the graph Laplacian  $L$  is real and symmetric, we can diagonalize it by an orthogonal matrix  $U$ :

$$L = U\Lambda U^T. \quad (4.7)$$

Here the diagonal matrix  $\Lambda$  is given by  $\Lambda = SS^T$ . We denote the eigenvalues of the graph Laplacian  $L$  by  $\lambda_j$  for  $j = 1, 2, \dots, \mathcal{V}$ . We remark that the orthogonal matrix  $U$  has appeared in the singular value decomposition of boundary matrix  $B$  of Eq. (4.6).

Let us introduce the Moore–Penrose inverse  $A^+$  for a given square or rectangular matrix  $A$ . It satisfies the defining relations.

$$\begin{aligned} AA^+A &= A, & A^+AA^+ &= A^+, \\ (A^+A)^T &= A^+A, & (AA^+)^T &= AA^+. \end{aligned} \tag{4.8}$$

Here the symbol  $A^T$  denotes the transpose of the matrix  $A$ . It is associated with the inner products in the vector spaces as the domain or the range of the linear transformation  $A$ . We can show the following properties.

$$(A^+)^+ = A, \quad (A^T)^+ = (A^+)^T.$$

Hereafter we call the Moore–Penrose inverse also the pseudo-inverse of the matrix  $A$ .

It is now easy to show that the pseudo-inverse of the boundary matrix  $B$  is given by

$$B^+ = (USV^T)^+ = VS^+U^T. \tag{4.9}$$

We remark that for an  $m \times n$  pseudo-diagonal matrix  $S$  its pseudo-inverse  $S^+$  is given by an  $n \times m$  matrix in which each nonzero diagonal element is given by the reciprocal of the corresponding nonzero diagonal element of  $S$  and all other matrix elements are given by zero.

### 4.3 Graph Embeddings

We now explain the method for embedding a graph in space [5]. We assign a set of values to the  $x$ -,  $y$ -, or  $z$ -coordinates of the vertices in a connected graph  $G$ . Let the symbol  $x_i$  denote the  $x$ -coordinate of vertex  $v_i$  for each  $i$  and  $w_i$  that of the edge displacement (i.e., the bond vector) of edge  $e_i$  for each  $i$ . The vector  $\vec{x}$  denotes the collection of the coordinates  $x_i$  for all vertices of graph  $G$ , and the vector  $\vec{w}$  the collection of the edge displacements  $w_i$  for all edges of  $G$ .

#### 4.3.1 Direct Sum Decomposition of the Space of Paths

We first recall that the boundary matrix  $B$  is a linear map from the space of paths  $R^{\mathcal{E}}$  to the space of the  $x$ -coordinates of vertices  $R^{\mathcal{V}}$  in the graph  $G$ . We decompose the space of paths as a direct sum as follows (see, Definition 4 in Ref. [5]).

$$R^{\mathcal{E}} = \ker B \oplus \operatorname{im} B^T. \tag{4.10}$$

The space  $\text{im}B^T$  is the orthogonal complement of  $\ker B$ , and hence it gives the configuration space of paths under all the loop constraints:  $\text{im}B^T = R^{\mathcal{E}}/\ker B$ . Here we have introduced equivalence classes under  $\ker B$ : If given two paths are different only with respect to some additional loops, we say that they are equivalent to each other. We expect that by generating random configurations of paths uniformly in the space  $\text{im}B^T$  we can numerically evaluate the statistical average of any physical quantity for the polymer with a given nontrivial architecture.

In order to generate Gaussian random numbers uniformly in the space  $\text{im}B^T$ , we take an orthonormal basis for the  $(\mathcal{V}-1)$ -dimensional space  $\text{im}B^T$  :  $\vec{V}_1, \vec{V}_2, \dots, \vec{V}_{\mathcal{V}-1}$ . Since the number of independent loops is given by  $\mathcal{E} - \mathcal{V} + 1$ , the space  $\ker B$  has  $\mathcal{E} - \mathcal{V} + 1$  dimensions. Therefore,  $\text{im}B^T$  has  $\mathcal{V} - 1$  dimensions:  $\mathcal{E} - (\mathcal{E} - \mathcal{V} + 1) = \mathcal{V} - 1$ . Here we can construct the basis of the space  $\text{im}B^T$  by applying the Gram–Schmidt orthogonalization to the row vectors of the matrix  $B^T$ . Let us denote by  $\vec{\alpha}$  a sequence of  $\mathcal{V} - 1$  random numbers which follow the normal distributions with unit variance. Thus, we construct the vector  $\vec{w}$  of edge displacements (the x-coordinates of the bond vectors) by

$$\vec{w} = \sum_{j=1}^{\mathcal{V}-1} \vec{V}_j \alpha_j . \quad (4.11)$$

We have called it the key property in introduction. It gives explicitly edge displacements  $\vec{w}$ .

We can show that the vector  $\vec{x}$  of the x-coordinates of vertices  $v_j$  is related to the vector  $\vec{w}$  of edge displacements by the following:

$$\vec{w} = B^T \vec{x} . \quad (4.12)$$

Let us derive Eq. (4.12). First, we note that there are only two nonzero matrix elements 1 and -1 in each column of boundary matrix  $B$ , as shown in Eq. (4.2) for the graph of Fig. 4.3. It follows that each  $j$ -th entry of  $B^T \vec{x}$  is given by the difference between the x-coordinates of the two end points of the  $j$ -th edge, which is equal to the  $j$ -th edge displacement  $w_j$ . We thus obtain Eq. (4.12).

### 4.3.2 Centered Conformations

Let us now consider only centered conformations for the polymer. Hereafter we assume that the center of mass is always located at the origin for them. Or, we may assume that after all the displacements are given, we shift all the vertices in space together so that the center of mass is equal to zero.

For the centered conformations, by making use of the singular value decomposition of boundary matrix  $B$  in Eqs. (4.6) and (4.9), we express the vector  $\vec{x}$  of the  $x$ -coordinates of vertices  $v_j$  in terms of the vector  $\vec{w}$  of edge displacements from Eq. (4.12) as follows.

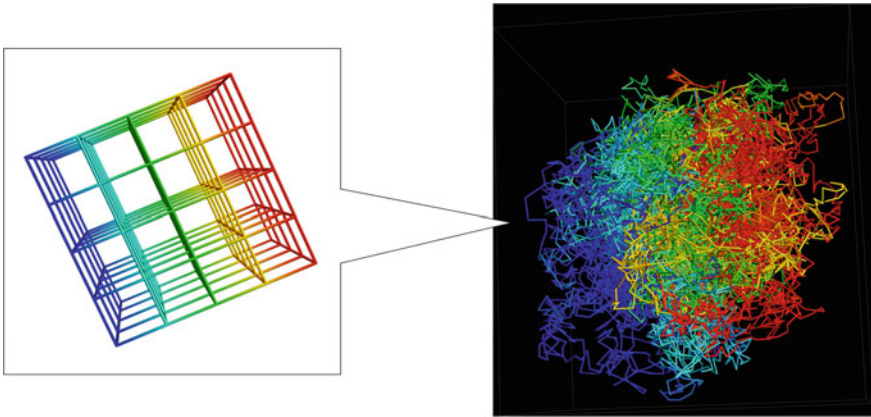
$$\vec{x} = B^T + \vec{w}. \quad (4.13)$$

It is easy to show that the probability distribution function of  $\vec{x}$  for centered conformations is given by the following Gaussian form:

$$P(\vec{x}) \propto \exp\left[-\frac{1}{2}\vec{x}^T L \vec{x}\right] \delta(x_1 + \dots + x_\nu). \quad (4.14)$$

Thus, the probability distribution of the coordinates  $\vec{x}$  is given by the Boltzmann distribution for the Gaussian polymer network. Here we remark that the delta functional factor in Eq. (4.14) corresponds to the constraint that the center of mass is fixed at the origin. The probability distribution for three-dimensional conformations is given by the product of the three one-dimensional distributions with respect to the  $x$ -,  $y$ -, and  $z$ -coordinates, respectively, since in the phantom chains the  $x$ -,  $y$ -, and  $z$ -coordinates are independent of each other.

In order to illustrate the practical usefulness of the key property in the distribution of edge displacements, i.e., Eq. (4.11), let us consider the Gaussian network of a cubic lattice. In Fig. 4.4 each lattice edge of the cubic lattice consists of five bridges (or subchains) between cross-linking vertices (or cross-links), where each bridge has fifty edges or bonds. By applying external forces on the three opposite pairs



**Fig. 4.4** The network of the  $5 \times 5 \times 5$  cubic lattice where each branch has 50 edges in the left-hand side has three-dimensional conformations such as depicted in the right-hand side where external forces are applied at the vertices in the opposite pairs of surfaces in the opposite directions for the three directions. The corresponding edges are depicted with the same colors in the left-hand side and the right-hand side

of surfaces of the cubic lattice in the opposite directions, respectively, such as with respect to the  $x$ -,  $y$ -, and  $z$ -axis, we keep the volume of the network nonzero and finite even in equilibrium. We have generated conformations of the Gaussian network of the  $5 \times 5 \times 5$  cubic lattice by making use of the key property of the TCRW method: We have first constructed an ensemble of the edge displacements by applying the normal distribution with unit variance to them through Eq. (4.11) and then derived the coordinates by Eq. (4.13). Such an ensemble of random conformations of the Gaussian network should be useful when we study statistical properties of the polymer network by evaluating the expectation values of a physical quantity in interest.

### 4.3.3 Diagonalization of the Graph Laplacian in Terms of Eigenmodes

The graph Laplacian  $L$  is real and symmetric, and we can diagonalize it by an orthogonal matrix  $U$ :  $L = U \Lambda U^T$ . Here we recall that  $U$  is given by the same matrix that has appeared in the singular value decomposition of matrix  $B$ :  $B = U S V^T$ , if we arrange the order of the basis vectors. Thus, through the transformation:  $\vec{X} \equiv U^T \vec{x}$ , we express the probability distribution function of the  $x$ -coordinates in terms of normal mode coordinates  $X_i$  as follows.

$$\begin{aligned} \exp\left[-\frac{1}{2}\vec{x}^T U \Lambda U^T \vec{x}\right] \delta(x_1 + \dots + x_\nu) &\propto \exp\left[-\frac{1}{2}\vec{X}^T \Lambda \vec{X}\right] \delta(X_\nu) \\ &= \delta(X_\nu) \prod_i^{\nu-1} \exp\left[-\frac{1}{2}\lambda_i X_i^2\right]. \end{aligned} \quad (4.15)$$

Here we remark that the diagonal matrix  $\Lambda$  has a zero eigenvalue. i.e., a zero mode. We thus arrange the eigenvalues of  $\Lambda$  in descending order, so that the last eigenvalue  $\lambda_\nu$  is given by the zero eigenvalue:

$$\Lambda = \text{diag}(\lambda_1, \dots, \lambda_{\nu-1}, 0). \quad (4.16)$$

We now calculate the Moore–Penrose inverse  $L^+$  of the graph Laplacian  $L$ . Here we recall that  $L$  is not invertible. By making use of Eqs. (4.3), (4.6), and (4.9) we have

$$L^+ = (B B^T)^+ = (B^+)^T B^+ = U S^+ V^T V S^+ U^T = U \Lambda^+ U^T. \quad (4.17)$$

We also recall that the pseudo-inverse of a diagonal matrix is given by such a diagonal matrix in which each of the nonzero element of the former is reciprocal to the corresponding nonzero diagonal element of the latter and all other elements are given by zero (see also Eq. 4.9).

$$\Lambda^+ = \text{diag}(1/\lambda_1, 1/\lambda_2, \dots, 1/\lambda_{\nu-1}, 0). \quad (4.18)$$

The normal mode coordinates  $\{X_1, X_2, \dots, X_{\nu-1}\}$  are independent of each other as random variables, since the probability distribution function is diagonalized with respect to them, as shown in Eq. (4.15). Making use of the distribution function in Eq. (4.15) we can show

$$\langle x_i x_j \rangle = \left\langle \sum_{k=1}^{\nu-1} U_{ik} X_k \sum_{l=1}^{\nu-1} U_{jl} X_l \right\rangle = \sum_{k=1}^{\nu-1} \sum_{l=1}^{\nu-1} U_{ik} U_{jl} \langle X_k X_l \rangle = \sum_{k=1}^{\nu} \sum_{l=1}^{\nu} U_{ik} U_{jl} \Lambda_{kl}^+ = L_{ij}^+. \quad (4.19)$$

We have thus shown that the two-point correlation functions for the position coordinates of a given pair of vertices are given by the corresponding matrix elements of the pseudo-inverse matrix  $L^+$  of the graph Laplacian.

### 4.3.4 Mean Square Radius of Gyration

By making use of Eq. (4.19) we derive the following relations.

$$\langle (x_i - x_j)^2 \rangle = \langle x_i^2 \rangle - 2\langle x_i x_j \rangle + \langle x_j^2 \rangle = L_{ii}^+ - 2L_{ij}^+ + L_{jj}^+. \quad (4.20)$$

That is, the mean square of the difference between the coordinates of a given pair of vertices is expressed in terms of the corresponding matrix elements of the pseudo-inverse of the graph Laplacian. As shown in Ref. [5], it follows from Eq. (4.20) that the mean square radius of gyration for any given connected (multi-)graph is calculated as follows.

$$R_g^2 = \frac{1}{2\nu^2} \sum_{i,j} (r_i - r_j)^2 = \frac{1}{2\nu^2} \sum_{i,j} (L_{ii}^+ - 2L_{ij}^+ + L_{jj}^+) = \frac{1}{2\nu} \left( 2\text{tr}L^+ - \frac{2}{\nu} \sum_{i,j} L_{ij}^+ \right). \quad (4.21)$$

We thus obtain the following formula.

$$R_g^2 = \frac{1}{\nu} \text{tr}L^+. \quad (4.22)$$

Here we have made use of the fact that  $L$  is symmetric and hence the following equations hold.

$$\sum_{i=1}^{\nu} L_{ij}^+ = 0. \quad (4.23)$$

**Table 4.1** Exact values of the mean square radius of gyration of a ring TCRW for small values of  $\mathcal{V}$  and the estimates of formula  $\mathcal{V}/12$

$\mathcal{V}$	$\text{tr } L + / \mathcal{V}$	$\mathcal{V}/12$
4	$5/16 = 0.3125$	0.3333...
8	$21/32 = 0.65625$	0.6666...
12	$143/144 = 0.993056$	1
16	$85/64 = 1.32813$	1.333...
20	$133/80 = 1.6625$	1.666...
24	$575/288 = 1.99653$	2
28	$261/112 = 2.33036$	2.333...
32	$341/128 = 2.66406$	2.666...

In order to derive Eq. (4.23), we remark that the kernel space of  $L$  coincides with that of  $L^+$ , since the graph Laplacian  $L$  is a symmetric matrix. Therefore, if an element is in  $\ker L$ , then it is also in  $\ker L^+$ :  $\vec{1} \in \ker L = \ker L^+$  (see also Eqs. 4.28 and 4.29 in Sect. 4.4).

We can evaluate the mean square radius of gyration for TCRW with any given connected graph rigorously by making use of Eq. (4.22), as we shall explicitly demonstrate in Sect. 4.4 for some graphs such as a subdivided theta graph and subdivided complete graphs. For an illustration, the exact values of the mean square radius of gyration for the ring TCRW with some small values of the number of vertices  $\mathcal{V}$  are listed in Table 4.1.

We can show that the mean square radius of gyration for the ring TCRW with the number of vertices  $\mathcal{V}$  is exactly given by  $(\mathcal{V}^2 - 1)/(12\mathcal{V})$ . For instance, it is shown in Ref. [5]. Thus, the well-known approximation  $\mathcal{V}/12$  as the mean square radius of gyration for the ring polymer becomes close to the exact value as the number of vertices  $\mathcal{V}$  increases.

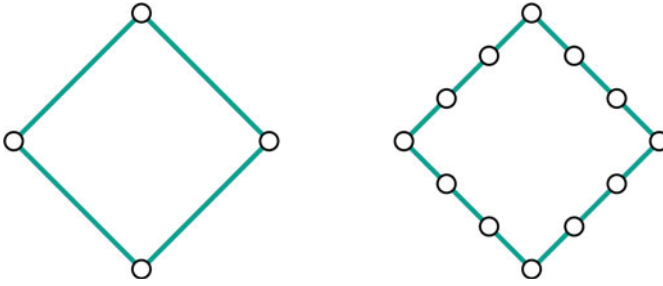
We remark that the mean square radius of gyration has explicitly been evaluated for several topological polymers such as those associated with double-ring chain, cyclic multiple-ring chains, and long chain branch polymer chains [13, 14].

## 4.4 Exact Dependence of the Mean Square Radius of Gyration on Polymerization Degree

### 4.4.1 Subdivision

When we study the topological polymer of a given graph synthesized in experiments, it is often important to evaluate the mean square radius of gyration for the TCRW of such a graph that is obtained by replacing each edge of the original graph with  $n$  edges or  $n$  monomers for some large  $n$ . Here we remark that the number  $n$  is proportional to the degree of polymerization. We thus consider subdividing a graph  $G$  by replacing





**Fig. 4.5** Graph in the right-hand side is the 3-subdivided graph of the left one

each edge with  $n$  edges, as shown in Fig. 4.5. The subdivided graph is denoted by  $G_n$ . We call each sequence of  $n$  edges in  $G_n$ , i.e., each subdivided edge, a branch, or an arc of  $G_n$ , if it corresponds to an edge of  $G$ .

We shall derive the exact formula of the mean square radius of gyration as a function of the number of all vertices  $\mathcal{V}$  for the topological polymer of an  $n$ -subdivided complete graph for an arbitrary integer  $n$ .

### 4.4.2 Resistance Distances in Electrical Circuits

Let us regard a graph as an electric circuit where each edge is a  $1 \Omega$  resistor. Then, the resistance between a given pair of vertices  $v_i$  and  $v_j$  in the circuit is denoted by  $r_{ij}$ . We also call  $r_{ij}$  the resistance distance. Suppose that the electric potential denoted by  $\vec{\phi}_{ij}$  appears in the electric circuit when the unit electric current flows in at the vertex  $v_i$  and flows out at the vertex  $v_j$ . The resistance distance  $r_{ij}$  is equal to the difference between the value of the electric potential  $\vec{\phi}_{ij}$  at  $v_i$  and that of  $v_j$ . Here we remark that the  $k$ -th component of vector  $\vec{\phi}_{ij}$  denotes the value of the electric potential at the  $k$ -th vertex  $v_k$  for each  $k$ .

In order to derive the electric potential  $\vec{\phi}_{ij}$  we introduce vector  $\vec{\phi}$ . Then, the  $k$ -th component of product  $B^T \vec{\phi}$  is given by the difference between the electric potentials at the two ends of edge  $e_k$ , respectively, for each  $k$ . It is equal to the current  $J_k$  flowing via edge  $e_k$  if the resistance of edge  $e_k$  is equal to 1. The current denoted as  $\vec{J}$  is therefore given by

$$B^T \vec{\phi} = B^T \begin{pmatrix} \phi_1 \\ \phi_2 \\ \vdots \\ \phi_v \end{pmatrix} = \vec{J}. \tag{4.24}$$

The  $j$ -th component of product  $B \vec{J}$  is equal to the sum of electric currents flowing in at the  $j$ -th vertex  $v_j$ . We therefore have

$$B \vec{J} = L \vec{\phi}. \quad (4.25)$$

Thus, the electric potential in the case when the unit electric current flows in at  $v_i$  and flows out at  $v_j$  is derived from the system of equations expressed by  $L$  as follows.

$$L \vec{\phi}_{ij} = \vec{v}_i - \vec{v}_j = \begin{pmatrix} \vdots \\ 0 \\ 1(i) \\ 0 \\ \vdots \\ 0 \\ -1(j) \\ 0 \\ \vdots \end{pmatrix}. \quad (4.26)$$

Here we recall that  $\vec{v}_i$  denotes the unit vector in which the  $i$ -th component is given by 1 and the other components by zero.

We apply the pseudo-inverse  $L^+$  to the above equation. Then, we have

$$L^+ L \vec{\phi}_{ij} = L^+ (\vec{v}_i - \vec{v}_j). \quad (4.27)$$

Here we remark that we have

$$\begin{aligned} L^+ L &= U \Lambda^+ U^T U \Lambda U^T = U \Lambda^+ \Lambda U^T = U \text{diag}(1, \dots, 1, 0) U^T \\ &= U (I - E_{\mathcal{V}\mathcal{V}}) U^T \equiv I - P_0. \end{aligned} \quad (4.28)$$

where  $E_{\mathcal{V}\mathcal{V}}$  denotes the unit matrix whose only nonzero element 1 is located at entry  $(\mathcal{V}, \mathcal{V})$  and  $P_0$  denotes the projection operator as follows.

$$U E_{\mathcal{V}\mathcal{V}} U^T = (\vec{U}_1, \dots, \vec{U}_{\mathcal{V}}) \text{diag}(0, \dots, 0, 1) \begin{pmatrix} \vec{U}_1^T \\ \vdots \\ \vec{U}_{\mathcal{V}}^T \end{pmatrix} = \frac{1}{\mathcal{V}} \vec{1} \vec{1}^T \equiv P_0. \quad (4.29)$$

We now choose the zero point of potential  $\vec{\phi}$  so that we have  $(I - P_0) \vec{\phi} = \vec{\phi}$ . We thus solve the above equation as follows:

$$\vec{\phi}_{ij} = L^+(\vec{v}_i - \vec{v}_j). \quad (4.30)$$

Since the electric potential  $\vec{\phi}_{ij}$  at vertex  $v_j$  denoted as  $\vec{\phi}_{ij}(\vec{v}_j)$  is given by

$$\vec{\phi}_{ij}(\vec{v}_j) = \vec{v}_j^T \vec{\phi}_{ij}.$$

we obtain the expression of resistance distance in terms of the pseudo-inverse of the graph Laplacian as follows.

$$r_{ij} = \vec{\phi}_{ij}(\vec{v}_i) - \vec{\phi}_{ij}(\vec{v}_j) = (\vec{v}_i - \vec{v}_j)^T L^+(\vec{v}_i - \vec{v}_j) = L_{ii}^+ + L_{jj}^+ - 2L_{ij}^+. \quad (4.31)$$

Therefore, resistance distance  $r_{ij}$  is equal to the mean squared difference between the  $x$ -coordinates of vertices  $v_i$  and  $v_j$ .

$$r_{ij} = \langle (x_i - x_j)^2 \rangle. \quad (4.32)$$

#### 4.4.3 Derivation of an Exact Formula for the $n$ -subdivided Theta Graph

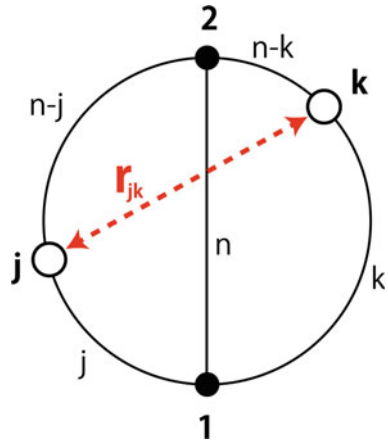
We now calculate the mean square radius of gyration for an  $n$ -subdivided connected graph. It is given by the sum of the resistance distances between two vertices in the subdivided graph over all the pairs of vertices. We take advantage of the analogy to electric circuits. We remark that the resistance of  $n$  unit resistances in a series circuit is equal to  $n$ . We also recall that the resistance distance is inversely proportional to the matrix elements of the graph Laplacian.

For a given graph  $G$  and its subdivided graph  $G_n$  we introduce a reduced graph and its weighted reduced graph Laplacian. We remark that its matrix size is much smaller than that of the subdivided graph Laplacian  $L(G_n)$ . We define the weighted reduced graph Laplacian as follows. Suppose that  $\rho_{ij}$  denotes the resistance between a given pair of vertices  $v_i$  and  $v_j$  in  $G_n$ . We assign the value  $-1/\rho_{ij}$  to the off-diagonal matrix element  $L_{ij}$  of the weighted reduced graph Laplacian:  $L_{ij} = -1/\rho_{ij}$ , while we assign the value  $L_{ii} = -\sum_{j \neq i} L_{ij}$  to each diagonal element  $L_{ii}$  in the weighted reduced graph Laplacian.

Here we remark that replacing an edge of unit resistance in the graph  $G$  with a set of  $\rho_{ij}$  consecutive edges of unit resistance in the subdivided graph  $G_n$  should correspond to replacing it with an edge of resistance  $\rho_{ij}$  in the reduced graph.

We distinguish interior and exterior vertices in the subdivided graph  $G_n$ . We call the vertices added by subdivision *interior* and the original vertices before subdivision *exterior*. Here we remark that the number of interior vertices is given by  $\mathcal{E}(G)(n - 1)$ .

**Fig. 4.6** Reduced graph with weights on edges for calculating the resistance distance between the type-(i) pair vertex  $j$  and vertex  $k$



We consider the following four cases among all the pairs of vertices in the subdivided graph  $G_n$ : (i) pairs between interior–interior vertices on different branches; (ii) pairs between interior–interior vertices on the same branch, (iii) pairs between exterior–interior vertices, (iv) pairs between exterior–exterior vertices.

For an illustration, we consider the  $n$ -subdivided theta graph. We give numbers 1, 2, and 3 to the three branches, respectively. The two branching points (or vertices) in the original theta graph before subdivision are denoted by 1 and 2, respectively, in Fig. 4.6.

(i) Interior–interior vertex pairs on different branches.

Let us consider the resistance distance  $r_{jk}$  between the  $k$ -th vertex of branch 1 and the  $j$ -th vertex of branch 2. We replace branch 1 by the two edges with weights  $k$  and  $n - k$ , respectively, and add a new vertex called vertex  $k$ ; we replace branch 2 by the two edges with weights  $j$  and  $n - j$ , respectively, and add a new vertex called vertex  $j$ ; we replace branch 3 by an edge of weight  $n$ , as shown in Fig. 4.6. Here we remark that integers  $k, j$ , and  $n$  satisfy  $0 < k, j < n$ .

Let  $G(n, 1, k, 2, j)$  denotes the reduced graph in Fig. 4.6, with vertices  $k$  and  $j$  in branches 1 and 2, respectively. It has four vertices 1,  $k$ , 2, and  $j$  counterclockwise along the outer circle from vertex 1, and five edges: edges with weights  $k$  and  $n-k$  on branch 1, those of weights  $n-j$  and  $j$  on branch 2, and the vertical edge of weight  $n$  which connects vertices 1 and 2.

We derive the weighted reduced graph Laplacian of  $G(n, 1, k, 2, j)$  as follows:

$$L(G(n, 1, k, 2, j)) = \begin{pmatrix} \frac{1}{n} + \frac{1}{k} + \frac{1}{j} & -\frac{1}{n} & -\frac{1}{k} & -\frac{1}{j} \\ -\frac{1}{n} & \frac{1}{n} + \frac{1}{n-k} + \frac{1}{n-j} & -\frac{1}{n-k} & -\frac{1}{n-j} \\ -\frac{1}{k} & -\frac{1}{n-k} & \frac{1}{k} + \frac{1}{n-k} & 0 \\ -\frac{1}{j} & -\frac{1}{n-j} & 0 & \frac{1}{j} + \frac{1}{n-j} \end{pmatrix}.$$

Here we have assumed that the vertex  $1, 2, k, j$  of the reduced graph  $G(n, 1, k, 2, j)$  correspond to the vertex  $1, 2, 3$  and  $4$  in  $L(G(n, 1, k, 2, j))$ : The third column and row correspond to vertex  $k$  and the 4-th ones to vertex  $j$ , where the matrix elements of  $(3,4)$  and  $(4,3)$  are given by zero since there is no edge between vertices  $j$  and  $k$ . The resistance distance between vertices  $k$  and  $j$  is derived from the pseudo-inverse matrix  $L^+(G(n, 1, k, 2, j))$ .

We make use of the Bapat–Gutman–Xiao theorem to calculate the resistance distance [15]:

$$r_{ij} = \frac{\text{Det } L(i, j)}{\text{Det } L(i)}. \tag{4.33}$$

where  $L(i, j)$  denotes the partial matrix obtained from  $L$  by deleting the  $i$ -th and  $j$ -th columns and the  $i$ -th and  $j$ -th rows, and  $L(i)$  that of deleting the  $i$ -th column and the  $i$ -th row. We thus avoid calculating the pseudo-inverse matrix directly. Here we remark that it might take a long computational time to calculate a matrix element of the pseudo-inverse matrix.

Thus, we obtain the resistance distance between vertices  $k$  and  $j$  as follows:

$$r_{kj} = \frac{1}{3n} (2j^2 + 2k^2 + 2jk - 3jn - 3kn).$$

The contribution from the type-(i) pairs between branches 1 and 2 to the mean square radius of gyration is therefore given by

$$\text{RII}_{12} = \sum_{k=1}^{n-1} \sum_{j=1}^{n-1} r_{kj} = \frac{7n^3 - 10n^2 - n + 4}{18}. \tag{4.34}$$

We have the same contribution from the type-(i) pairs between branches 2 and 3 and that of the type-(i) pairs between branches 1 and 3. It is because the theta graph is symmetric with respect to the three branches 1, 2, and 3.

Here we remark that according to Ref. [16] the same formula as Bapat’s formula is addressed in the Ph.D. thesis of den Nijs (1979) (see, e.g., Eq. (4.34) of Ref. [16]).

(ii) Interior–interior vertex pairs on a branch

We consider the resistance distance between the  $j$ -th and  $j + k$ -th vertices on branch 1, where integers  $j, k$  and  $n$  satisfy  $0 < j, k < n$ . We replace branch 1 by three edges with weights  $j, k, n - j - k$ , respectively, and add vertices  $j$  and  $k$ , and replace branches 2 and 3 by two parallel edges of weight  $n$ . The reduced graph is denoted by  $G(n, 1, j, 1, k)$ . We obtain the graph Laplacian of  $G(n, 1, j, 1, k)$  as follows:

$$L(G(n, 1, j, 1, k)) = \begin{pmatrix} \frac{2}{n} + \frac{1}{j} & -\frac{2}{n} & -\frac{1}{j} & 0 \\ -\frac{2}{n} & \frac{2}{n} + \frac{1}{n-j-k} & 0 & -\frac{1}{n-j-k} \\ -\frac{1}{j} & 0 & \frac{1}{j} + \frac{1}{k} & -\frac{1}{k} \\ 0 & -\frac{1}{n-j-k} & -\frac{1}{k} & \frac{1}{k} + \frac{1}{n-j-k} \end{pmatrix}.$$

Note that the third column and row correspond to vertex  $j$ , and the 4-th ones to vertex  $k$ . We obtain the resistance distance by making use of the Bapat formula:

$$r_{kj} = k - \frac{2k^2}{3n}.$$

The contribution of the type-(ii) pairs on branch 1 to the mean square radius of gyration is given by

$$RII_1 = \sum_{j=1}^{n-2} \sum_{k=1}^{n-j-1} r_{kj} = \frac{1}{18}(2n^3 - 5n^2 + n + 2). \tag{4.35}$$

We remark that the contributions from branches 2 and 3 are the same as  $RII_1$ .

(iii) Exterior–interior vertex pairs

We consider the resistance distance between the  $k$ -th vertex on branch 1 and an exterior vertex, i.e., a vertex of the original graph  $G$ . We replace branch 1 by two edges with weights  $k$  and  $n - k$ , respectively, and add a new vertex called vertex  $k$ , and replace branches 2 and 3 by two edges of weight  $n$ . Here we recall  $0 < k < n$ . The reduced graph is denoted as  $G(n, 1, k)$ . We obtain the graph Laplacian of  $G(n, 1, k)$  as follows:

$$L(G(n, 1, k)) = \begin{pmatrix} \frac{2}{n} + \frac{1}{n-k} & -\frac{2}{n} & -\frac{1}{n-k} \\ -\frac{2}{n} & \frac{2}{n} + \frac{1}{k} & -\frac{1}{k} \\ -\frac{1}{n-k} & -\frac{1}{k} & \frac{1}{k} + \frac{1}{n-k} \end{pmatrix}.$$

The resistance distance between vertices 1 and  $k$  is given by

$$r_{1k} = \frac{(n - k)(n + 2k)}{3n}.$$

The contribution from all the pairs between vertex 1 and interior vertices on edge 1 is

$$REI_1 = \sum_{k=1}^{n-1} r_{1k} = \frac{1}{18}(5n^2 - 3n - 2). \tag{4.36}$$

The total contribution from all the branches and the original vertices are equal to  $6 \text{REI}_1$ .

(iv) Exterior–exterior vertex pair

The theta graph has an exterior–exterior pair, i.e., vertices 1 and 2, and the three branches are replaced with three edges of weight  $n$ . We have the weighted reduced graph Laplacian

$$L(G) = \begin{pmatrix} \frac{3}{n} & -\frac{3}{n} \\ -\frac{3}{n} & \frac{3}{n} \end{pmatrix}.$$

and the contribution of the type-(iv) pairs is given by

$$\text{REE}_{12} = \frac{1}{\text{Det} \frac{3}{n}} = \frac{n}{3}. \tag{4.37}$$

We now take the sum of the contributions from all the pairs such as Eqs. (4.34), (4.35), (4.36), and (4.37), and divide it by the square of the number of vertices

$$\mathcal{V}^2(G_n) = (\mathcal{V}(G) + (n - 1)\mathcal{E}(G))^2 = (3n - 1)^2. \tag{4.38}$$

and we have

$$\begin{aligned} \frac{3 \text{RII}_{12} + 3 \text{RII}_1 + 6 \text{REI}_1 + \text{REE}_{12}}{(3n - 1)^2} &= \frac{9n^3 - 5n^2 - 4n + 2}{6(3n - 1)^2} \\ &= \frac{3\mathcal{V}^3 + 4\mathcal{V}^2 - 13\mathcal{V} + 4}{54\mathcal{V}^2}. \end{aligned} \tag{4.39}$$

Thus, we obtain an exact expression of the mean square radius of the  $n$ -subdivided theta graph expressed as a function of the total number of vertices  $\mathcal{V} = \mathcal{V}(G_n)$  as follows:

$$\langle R_g^2 \rangle = \frac{3\mathcal{V}^3 + 4\mathcal{V}^2 - 13\mathcal{V} + 4}{54\mathcal{V}^2}. \tag{4.40}$$

If the number of vertices  $\mathcal{V}$  is very large, we have the following approximation

$$\langle R_g^2 \rangle \cong \frac{\mathcal{V}}{18}. \tag{4.41}$$

It should be emphasized that the expression of Eq. (4.40) gives the exact value of the mean square radius of gyration for the  $n$ -subdivided theta graph in terms of the total number of vertices  $\mathcal{V}(G_n)$ . It can also be expressed in terms of the degree  $n$  of subdivision, since we have  $\mathcal{V}(G_n) = 3n - 1$ , as seen in Eq. (4.38). There is

no approximation made. The expression of Eq. (4.41) gives its asymptotic value for  $\mathcal{V} \gg 1$ . When  $n$  is large, the number  $\mathcal{V}$  of all the vertices in the  $n$ -subdivided theta graph is approximately equal to  $3n$ . We therefore have the asymptotic value of the mean square radius of gyration for the  $n$ -subdivided theta graph as follows:

$$\langle R_g^2 \rangle \cong \frac{\mathcal{V}}{18} = \frac{n}{6}. \quad (4.42)$$

Thus, the mean square radius of gyration is the same as that of the corresponding linear chain with the same number of vertices as that of each branch of the  $n$ -subdivided theta graph [17].

#### 4.4.4 Exact Expressions of the Mean Square Radius of Gyration for the $n$ -subdivided Complete Graphs

In the TCRW of the  $n$ -subdivided complete graphs with the number of exterior vertices (cross-links)  $m$  for  $m = 3, 4, 5$ , and 6, and that of the  $n$ -subdivided bipartite complete graph with  $m + m = 3 + 3$  exterior vertices (cross-links) (i.e.,  $m = 3$ ) we present the exact expressions of the mean square radius of gyration as a function of the total number of vertices  $\mathcal{V}$ . They are listed in Table 4.2.

We emphasize that the expressions are exact and valid for the TCRW with any finite number of vertices  $\mathcal{V}(G_n)$ . Here we recall  $\mathcal{V}(G_n) = \mathcal{V}(G) + (n - 1)\mathcal{E}(G)$ . For complete graphs we have  $\mathcal{V}(G_n) = m + (n - 1)m(m - 1)/2$ . Here and hereafter, we abbreviate  $\mathcal{V}(G_n)$  by  $\mathcal{V}$  for simplicity. We remark that in the  $n$ -subdivided graphs we also call exterior vertices cross-links, at which some subchains with length  $n$  are connected in the polymer.

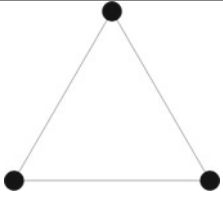
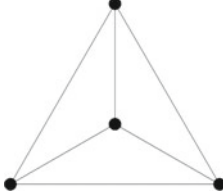
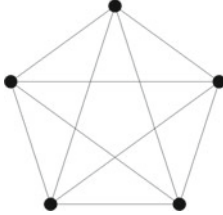
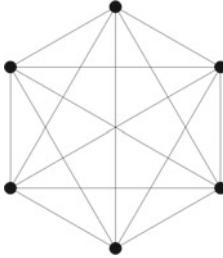
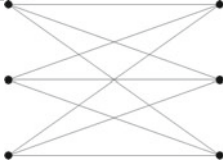
It is straightforward to calculate the mean square radius of gyration for the Gaussian topological polymer simply associated with complete graph  $K_m$ . That is, we consider the case of  $n = 1$ . The graph Laplacian is given by  $L = m(I - \frac{1}{m}\vec{1}\vec{1}^T)$ , where the symbol  $\vec{1}$  denotes the vector with  $m$  elements where all of them are equal to 1, as shown in Eq. (4.5). Since its pseudo-inverse is given by  $L^+ = m^{-1}(I - \frac{1}{m}\vec{1}\vec{1}^T)$ , it follows from Eq. (4.22) that the mean square radius of gyration of TCRW with complete graph  $K_m$  is given by

$$\langle R_g^2 \rangle = m^{-1}(1 - m^{-1}). \quad (4.43)$$

Here we have considered only the one-dimensional contribution to the mean square radius of gyration. The expression (4.43) is much simpler than any expression listed in Table 4.2.



**Table 4.2** Exact expressions of the mean square radius of gyration for TCRW of  $n$ -subdivided complete graphs and an  $n$ -subdivided bipartite graph with a finite number of vertices  $\mathcal{V}$ 

G	$\langle R_g^2(\mathcal{V}) \rangle$	Note
	$-\frac{1}{12\mathcal{V}} + \frac{\mathcal{V}}{12}$	Complete graph K3 (Circle)
	$\frac{5}{48} + \frac{4}{27\mathcal{V}^2} - \frac{7}{18\mathcal{V}} + \frac{37\mathcal{V}}{864}$	Complete graph K4 6 edges 4 vertices
	$\frac{67}{400} + \frac{5}{16\mathcal{V}^2} - \frac{35}{48\mathcal{V}} + \frac{151\mathcal{V}}{6000}$	Complete graph K5 10 edges 5 vertices
	$\frac{31}{150} + \frac{12}{25\mathcal{V}^2} - \frac{161}{150\mathcal{V}} + \frac{11\mathcal{V}}{675}$	Complete graph K6 15 edges 6 vertices
	$\frac{10}{81} + \frac{2}{9\mathcal{V}^2} - \frac{29}{54\mathcal{V}} + \frac{17\mathcal{V}}{486}$	Complete bipartite graph K3,3 9 edges 3 + 3 vertices

Thus, we conclude that the mean square radius of gyration for the Gaussian topological polymers associated with the  $n$ -subdivided complete graph of  $K_m$  is quite different from that of complete graph  $K_m$ . The former is much more complex than the latter. However, one can probably synthesize topological polymers of  $n$ -subdivided graphs more often in experiments.

### 4.5 Asymptotic Value of the Mean Square Radius of Gyration for an Arbitrary Complete Graph

Let us recall that in the study of a topological polymer with a graph synthesized in experiments, it is often significant to evaluate the mean square radius of gyration for the polymer of an  $n$ -subdivided graph with large  $n$ . Here we remark that a method for reducing the graph Laplacian of the Gaussian topological polymer of an  $n$ -subdivided graph for large  $n$  has been derived [18]. Furthermore, we can derive even the exact asymptotic value of the mean square radius of gyration for TCRW of the  $n$ -subdivided graph in the large  $n$  limit [6].

It has been rigorously shown in Ref. [6] that the ratio between the mean square radius of gyration and the number of vertices in the subdivided graph is given by the following formula.

$$\lim_{n \rightarrow \infty} \frac{\langle R_g^2(G_n) \rangle}{\mathcal{V}(G_n)} = \frac{1}{2\mathcal{E}^2(G)} \left( \text{tr} \mathcal{L}^+(G) + \frac{1}{3} \text{Loops}(G) - \frac{1}{6} \right). \tag{4.44}$$

Here  $\mathcal{L}$  denotes the normalized graph Laplacian. It is defined as follows:

$$\mathcal{L}_{ij} = \begin{cases} 1 & \text{if } i = j, \\ -1/\sqrt{d_i d_j} & \text{if } i \text{ and } j \text{ are adjacent,} \\ 0 & \text{otherwise.} \end{cases}$$

For example, the normalized graph Laplacian and its pseudo-inverse for the 3-complete graph, i.e., a ring, is given by

$$\mathcal{L} = \begin{pmatrix} 1 & -1/2 & -1/2 \\ -1/2 & 1 & -1/2 \\ -1/2 & -1/2 & 1 \end{pmatrix}, \quad \mathcal{L}^+ = \frac{1}{9} \begin{pmatrix} 4 & -2 & -2 \\ -2 & 4 & -2 \\ -2 & -2 & 4 \end{pmatrix}.$$

Thus, we confirm by taking the trace of  $\mathcal{L}^+$  that the asymptotic value of the ratio of the mean square radius of gyration to the number of vertices for a ring is given by  $1/12$ .

(i) Complete graph.

For the complete graph with  $m$  exterior vertices (cross-links), the normalized graph Laplacian is given by

$$\mathcal{L} = \begin{pmatrix} 1 & -1/(m-1) & -1/(m-1) & \dots \\ -1/(m-1) & 1 & -1/(m-1) & \dots \\ -1/(m-1) & -1/(m-1) & 1 & \dots \\ \vdots & \vdots & \vdots & \ddots \end{pmatrix} = \frac{1}{m-1} \left( mI - \vec{1} \vec{1}^T \right).$$

and its pseudo-inverse matrix is given by

$$\mathcal{L}^+ = \begin{pmatrix} (m-1)^2/m^2 & -(m-1)/m^2 & \dots \\ -(m-1)/m^2 & (m-1)^2/m^2 & \\ -(m-1)/m^2 & -(m-1)/m^2 & \\ \vdots & \vdots & \end{pmatrix} = \frac{m-1}{m^2} \left( mI - \vec{1}\vec{1}^T \right).$$

We recall  $\vec{1}\vec{1}^T$  denotes such a matrix in which all the matrix elements are given by 1. We remark that its square is given by  $m$  times itself:  $(\vec{1}\vec{1}^T)^2 = m\vec{1}\vec{1}^T$ . We confirm that it leads to the pseudo-inverse of  $\mathcal{L}$ :

$$\begin{aligned} \mathcal{L}\mathcal{L}^+\mathcal{L} &= \frac{1}{m-1} \left( mI - \vec{1}\vec{1}^T \right) \frac{m-1}{m^2} \left( mI - \vec{1}\vec{1}^T \right) \frac{1}{m-1} \left( mI - \vec{1}\vec{1}^T \right) \\ &= \frac{1}{m(m-1)} \left( m^2I - m\vec{1}\vec{1}^T \right) = \mathcal{L}. \end{aligned}$$

We obtain from Eq. (4.44) the asymptotic value of the mean square radius of gyration by calculating the trace:  $\text{tr}\mathcal{L}^+ = (m-1)^2/m$ , the number of edges  $\mathcal{E}(G) = m(m-1)/2$  and the number of loops  $\text{Loop}(G) = \mathcal{E}(G) - \nu(G) + 1 = m(m-1)/2 - m + 1$  as follows:

$$\begin{aligned} &\frac{1}{2\mathcal{E}^2(G)} \left( \text{tr}\mathcal{L}^+(G) + \frac{1}{3}\text{Loops}(G) - \frac{1}{6} \right) \\ &= \frac{2}{m^2(m-1)^2} \left( \frac{(m-1)^2}{m} + \frac{1}{3} \left( \frac{m(m-1)}{2} - m + 1 \right) - \frac{1}{6} \right) \\ &= \frac{6 - 11m + 3m^2 + m^3}{3(m-1)^2m^3}. \end{aligned}$$

Thus, the average size of an  $n$ -subdivided complete graph with  $m$  exterior vertices (cross-links) is much smaller than that of the corresponding linear chain with the same number of vertices. Furthermore, if  $m$  is large enough, the ratio of the sizes is approximately given by  $1/3m^2$ . Here we remark that the ratio is different from that of the case of  $n = 1$ .

(ii) Complete bipartite graph.

The normalized graph Laplacian and its pseudo-inverse of the complete bipartite graph with  $m+m$  exterior vertices (cross-links), respectively, are expressed in terms of block matrices as follows:

$$\mathcal{L} = \begin{pmatrix} I & -\frac{\vec{1}\vec{1}^T}{m} \\ -\frac{\vec{1}\vec{1}^T}{m} & I \end{pmatrix}, \quad \mathcal{L}^+ = \frac{1}{4m} \begin{pmatrix} 4mI - 3\vec{1}\vec{1}^T & -\vec{1}\vec{1}^T \\ -\vec{1}\vec{1}^T & 4mI - 3\vec{1}\vec{1}^T \end{pmatrix}.$$

We thus obtain from Eq. (4.44) the asymptotic value of the mean square radius of gyration by calculating the trace of the pseudo-inverse of the normalized graph Laplacian as  $\text{tr}\mathcal{L}^+ = (4m - 3)/2$ , the number of the edges  $\mathcal{E}(G) = m^2$  and the number of the loops:  $\text{Loop}(G) = \mathcal{E}(G) - \mathcal{V}(G) + 1 = m^2 - 2m + 1$ , as follows:

$$\begin{aligned} \frac{1}{2\mathcal{E}^2(G)} \left( \text{tr}\mathcal{L}^+(G) + \frac{1}{3}\text{Loops}(G) - \frac{1}{6} \right) &= \frac{1}{2m^4} \left( \frac{4m - 3}{2} + \frac{1}{3}(m^2 - 2m + 1) - \frac{1}{6} \right) \\ &= \frac{m^2 + 4m - 4}{6m^4}. \end{aligned}$$

The average size of an  $n$ -subdivided complete bipartite graph with  $m + m$  exterior vertices (cross-links) is much smaller than that of the corresponding linear chain with the same number of vertices. Furthermore, if the number of cross-links  $m$  is large enough, the ratio of the sizes is approximately given by  $1/6m^2$ . Here we also remark that the ratio is different from that of the case of  $n = 1$ .

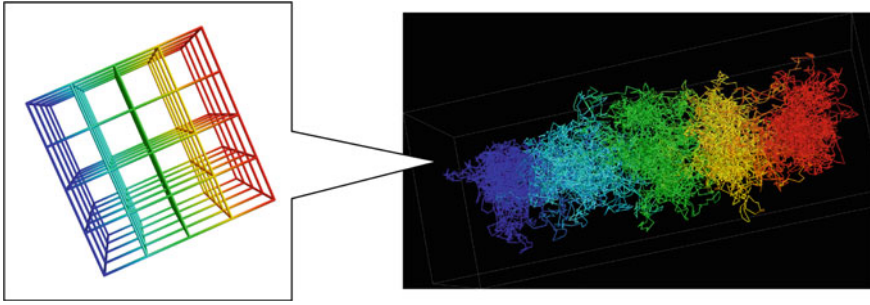
## 4.6 Perspectives on Gaussian Networks

There are two important physical aspects in polymer networks: The molecular size of a polymer network is very large, and the volume of the region in space occupied by the polymer network is nonzero and finite valued. Thus, the polymer network has a finite density. Furthermore, the center of mass of the network is fixed at the origin since the mass of the network is of a bulk quantity and hence is asymptotically large such as Avogadro's number.

In the method for constructing TCRW, we can make the volume of the system nonzero finite by applying external forces at the vertices located on the surfaces of the network. Let us consider the cubic lattice network depicted in Fig. 4.7. By adding external forces at the opposite or antipodal faces of the cubic lattice in opposite directions, respectively, we can keep the volume of the network nonzero finite in equilibrium. Here we remark that in the phantom network model, it is often assumed that the vertices on the surface of the network are fixed at some points of the boundary walls or containers.

We recall the Gaussian TCRW for the  $5 \times 5 \times 5$  cubic lattice depicted in Fig. 4.7. Here each lattice edge of the cubic lattice consists of five branches while each branch has fifty edges or bond vectors. When we elongate the network in one direction, we increase the external forces acting on the two opposite faces of the cubic lattice network in opposite directions which are parallel to the elongation direction, while we decrease the corresponding forces in two other directions properly, so that the total volume of the network is kept constant under elongation of the network.

Furthermore, we can easily generate conformations of the Gaussian network elongated due to an external force. Here we make use of the construction of the edge displacements through the normal distribution with unit variance again.



**Fig. 4.7** The  $5 \times 5 \times 5$  cubic lattice where each branch has 50 edges is elongated by 5 times in one direction due to the force applied at the opposite faces in opposite directions as shown in the three-dimensional conformation in the right-hand side. It is compressed by about  $\sqrt{5}$  times in other two directions perpendicular to it. The corresponding edges in the network are depicted by the same colors

## 4.7 Concluding Remarks

By making use of the method of TCRW we can derive exact expressions for most of the statistical quantities of TCRW with any given graph.

We have presented the exact expressions of the mean square radius of gyration for Gaussian topological polymers with the  $n$ -subdivided complete graphs in Table 4.2. They are valid for any given finite number of vertices. We have also derived the exact asymptotic values for the mean square radius of gyration for the Gaussian topological polymers of the  $n$ -subdivided complete graphs. The result should be useful in future researches on topological polymers in experiments.

Through the method of TCRW we can investigate systematically statistical properties of Gaussian polymer networks. In order to assign the bulk behavior of the Gaussian network of a given graph, i.e., in order to let the TCRW of the graph have some finite volume, we can apply external fields on the surface vertices of the network, as was briefly shown in Sect. 4.6. The results of the systematic study will be reported in subsequent publications.

Making use of the key property shown in Eq. (4.11) we can explicitly and exactly evaluate almost any physical quantities of the Gaussian networks such as the shear modulus elasticity without making any macroscopic assumptions. In particular, we do not assume the affine deformation of cross-linking chains under network deformation. Details will be reported elsewhere.

The simple method for generating edge displacements, i.e., the key property shown in Eq. (4.11), plays a central role in constructing the topologically constrained random walks (TCRW). This viewpoint can be extended and then applied not only to the Gaussian topological polymers with elastic potentials but also to almost arbitrary polymer models with general potentials on edge displacements [19]. Details will be presented in subsequent reports.

We expect that by making use of the method of TCRW many fundamental aspects on the statistical properties of topological polymers and polymer networks will be explicitly and quantitatively studied. Therefore, we expect that they should indeed be clarified in the near future.

**Acknowledgements** The authors would like to acknowledge many friends and colleagues whose helpful discussions and generous explanations shaped this work. In addition, we are grateful for the support of the Simons Foundation (#524120 to Cantarella, #354225 and #709150 to Shonkwiler), the Japan Science and Technology Agency (CREST Grant Number JPMJCR19T4), and the Japan Society for the Promotion of Science (KAKENHI Grant Number JP17H06463).

## References

1. T. Suzuki, T. Yamamoto, Y. Tezuka, *J. Am. Chem. Soc.* **136**(28), 10148–10155 (2014)
2. Y. Tezuka, *Acc. Chem. Res.* **50**(11), 2661–2672 (2017)
3. Y. Mato, K. Honda, B.J. Ree, K. Tajima, T. Yamamoto, T. Deguchi, T. Isono, T. Satoh, *Commun. Chem.* **3**, 97 (2020)
4. M. Rubinstein, R.H. Colby, *Polymer Physics* (Oxford Univ. Press, New York, 2003)
5. J. Cantarella, T. Deguchi, C. Shonkwiler, E. Uehara, Gaussian Random Embeddings of Multigraph. [arXiv:2001.11709](https://arxiv.org/abs/2001.11709) [cond-mat.stat-mech]
6. J. Cantarella, T. Deguchi, C. Shonkwiler, E. Uehara, Radius of Gyration, Contraction Factors, and Subdivisions of Topological Polymers. [arXiv:2004.06199](https://arxiv.org/abs/2004.06199) [cond-mat.stat-mech]
7. H.M. James, E. Guth, *J. Chem. Phys.* **11**, 455–481 (1943)
8. H.M. James, *J. Chem. Phys.* **15**, 651–668 (1947)
9. R. Kubo, *J. Phys. Soc. Jpn.* **2**, 51–56 (1947)
10. P.J. Flory, *Proc. R. Soc. Lond. A.* **351**, 351–380 (1976)
11. B.E. Eichinger, *Macromolecules* **5**, 496–505 (1972)
12. B.E. Eichinger, *Macromolecules* **13**, 1–11 (1980)
13. Y. Yang, *Macromol. Theory Simul.* **7**, 521–549 (1998)
14. D. Bonchev, E.J. Markel, A.H. Dekmezian, *Polymer* **43**, 203–222 (2002)
15. R.B. Bapat, I. Gutman, W. Xiao, *Z. Naturforsch.* **58a**, 494–498 (2003)
16. F.Y. Wu, *Rev. Mod. Phys.* **54**, 235–268 (1982)
17. E. Uehara and T. Deguchi, *J. Phys. A: Math. Gen.* **51**, 134001 (2018)
18. B.E. Eichinger, J.E. Martin, *J. Chem. Phys.* **69**, 4595 (1978)
19. J. Cantarella, T. Deguchi, C. Shonkwiler, E. Uehara, Random graph embeddings with general edge potentials, in preparation

# Chapter 5

## Fundamentals of the Theory of Chromatography of Topologically Constrained Random Walk Polymers



Alexei A. Gorbunov and Andrey V. Vakhrushev

**Abstract** Molecular topology-dependent phenomena involving complex polymers, such as their adsorption and behavior in porous media, can be used to separate and analyze topological polymers by chromatography. To describe theoretically the chromatographic behavior, we consider partitioning of a flexible macromolecule between a slit-like pore with impenetrable interacting walls and an external reservoir. In the Gaussian chain approximation, exact solutions to this problem are known for linear and ring macromolecules, as well as for a number of particular more complex structures. To cover a variety of topological polymers, we extend this approach by representing a complex macromolecule as a graph, and by using a model of topologically constrained random walks for the macromolecule. We have obtained a unified equation for the partition coefficient that numerically reproduces all previous theoretical results for specific polymer structures and can also be used for more complex topologies. This approach allows describing the theoretical behavior of both chemically homogeneous and heterogeneous topological polymers (e.g., complex block copolymers) in various chromatographic modes such as size-exclusion and interactive chromatography. To illustrate the use of the novel approach, we simulate and discuss chromatographic separations of both previously studied and unexplored topological polymers. The scope of this approach, its ability to describe real polymers, and comparison of theory and experiments on chromatography of cyclic polymers are discussed. Prospects for further development of the theory of chromatography of topologically complex polymers are outlined.

### 5.1 Introduction

Since the topological structure of macromolecules significantly influences their solution and bulk behaviors, as well as properties of polymeric materials [1–3], in recent years, great progress has been achieved in the synthesis of topologically complex macrocyclic polymers [4, 5].

---

A. A. Gorbunov (✉) · A. V. Vakhrushev  
Institute for Highly Pure Biopreparations, St. Petersburg, Russian Federation  
e-mail: [alexeigorbunov@hotmail.com](mailto:alexeigorbunov@hotmail.com)

In particular, molecular topology affects the chromatographic behavior of polymers. This allows chromatography to be used both for the separation of polymers and for the analysis of their molecular structure and chemical composition [6–9].

In chromatography, the main characteristic is the elution volume,  $V_e = V_i + V_p K$ , where  $V_i$  and  $V_p$  are the chromatographic column parameters, while  $K$  is the partition coefficient that depends both on the molecular structure of the polymer and on the pore size, as well as on the strength of the adsorption interaction of the polymer with the column porous material.

The basis of the molecular-statistical theory of polymer chromatography was laid by Casassa [10, 11]. Using a continuum random walk (RW) model for a flexible polymer molecule (also known as a Gaussian or an ideal chain), Casassa considered the equilibrium distribution of macromolecules between the macroscopic solution phase and neutral (non-adsorbing) pores, and obtained accurate formulae for the partition coefficient of linear and star-shaped polymers in size-exclusion chromatography (SEC). According to [10, 11], in SEC,  $K$  depends on the ratio of the molecular and pore sizes and decreases from 1 to 0 with increasing molecular weight.

A more general theory for the partition coefficient of a linear polymer and a slit-like pore, taking into account adsorption interactions, was developed by Gorbunov and Skvortsov [12–14]. Along with SEC, this theory also allowed describing the behavior of linear polymers in adsorption chromatography (AC), where  $K$  exponentially increases with molecular weight. The theory [12, 13] also established for linear RW polymers the presence of a special chromatography mode intermediate between SEC and AC (the so-called chromatography under critical interaction conditions), where  $K = 1$  and does not depend on molecular weight and pore size. Such critical conditions have been experimentally discovered by Tennikov et al. [15] and Belenky et al. [16], and subsequently were realized by hundreds of other researchers. The principles of the method of chromatography under critical conditions and its possible applications were discussed [17].

Based on the continuum RW model, theories have been developed describing the chromatography of certain types of chemically inhomogeneous polymers, such as macromolecules containing special (functional) groups that may differ considerably from the repeating ones in the aspect of adsorption interaction [18–21], as well as two-component linear and star-shaped block copolymers [22]. The main results of the theories [17–22] have gained experimental confirmation and are widely used for the efficient separation of linear polymers by the number of functional groups and for the analysis of block copolymers [6–8, 23, 24].

Taking into account both geometric and topological constrains, it turned out possible to construct similar partition coefficient theories for several particular types of cyclic macromolecules, such as ring—[14, 25, 26], eight—[27], theta—[28], tadpole—, and manacle-shaped [29] ones, as well as for cyclic polymers with functional groups [18, 30] and for ring-shaped block copolymers [31]. However, there was no general approach for studying theoretically the chromatographic behavior of an enormous variety of other topological polymers.

We present a new approach that uses both a basic model of a macromolecule in a slit-like pore and a graph representation of topological polymers. Within the

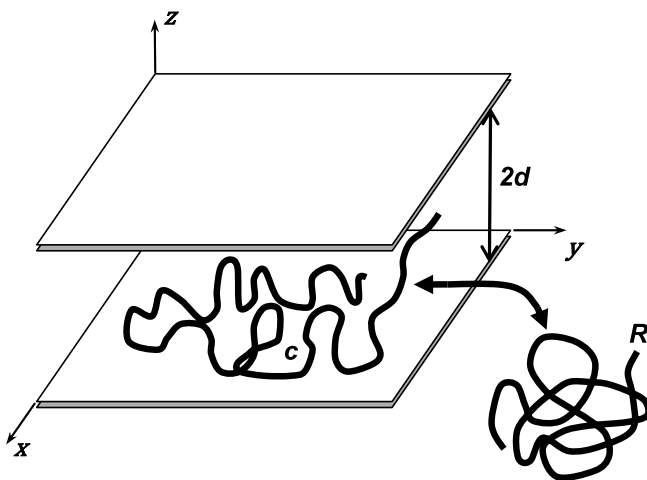


framework of the topologically constrained random walk (TCRW) model, a unified formula for the partition coefficient of topological polymers is obtained, suitable for numerical calculations. This formula is valid for any TCRW polymer and is especially convenient for theoretical simulation of chromatographic separations of topological polymers, since it does not require separate theory for every polymer.

The underlying model and equations are given in Sect. 5.2, while the new unified numerical approach and its use for the simulation of chromatographic separations in Sect. 5.3. In Sect. 5.4, we turn to specific chromatographic applications and give a brief overview of previously obtained theoretical results, as well as provide examples of the use of the new approach to the theoretical description and modeling of chromatography of previously unexplored complex polymers. We also briefly discuss the accordance of theory with experiments on chromatography of topological polymers. Section 5.5 outlines the prospects for further development of the theory of chromatography of topologically complex polymers. The appendix contains mathematical details and explains the main steps in deriving the unified formula for the partition coefficient of a complex polymer.

## 5.2 Basic Model and Equations

The basic model [12] is shown in Fig. 5.1. A slit with impenetrable interacting (attractive or repulsive) walls, infinite in the  $x$ -,  $y$ -directions and having a width of  $2d$ , serves as a pore model, and an equilibrium partitioning of a macromolecule between



**Fig. 5.1** A continuum random walk model describing the partitioning of a flexible macromolecule between mobile and stationary chromatographic phases. The model parameters:  $R$  is the radius of gyration of an unconfined macromolecule,  $2d$  is the width of a slit-like pore, and  $c$  is the adsorption interaction parameter

this pore and a large external reservoir is considered. We consider partitioning of a single macromolecule, thus assuming diluted situations in both chromatographic mobile and stationary phases.

A continuum RW model, which is analogous to describing the motion of a Brownian particle, serves as a model of a linear flexible macromolecule. As an alternative, the well-known lattice RW model [32, 33] can be used, which is qualitatively equivalent to the continual description [34–36]. However, we prefer to use the continuum RW model, where the parameters are related only to large-scale spatial properties, and which is largely universal and independent of the microscopic structure of a surface and the details of the adsorption interaction potential.

According to [10], the partition coefficient  $K$  is the ratio of the partition functions  $Z^{(slit)}$  and  $Z^{(0)}$  for a polymer within a pore and in an unrestricted space of the same volume:

$$K = \frac{Z^{(slit)}}{Z^{(0)}} \quad (5.1)$$

The partition functions  $Z^{(slit)}$  and  $Z^{(0)}$  are expressible in terms of the corresponding Green functions  $G^{(slit)}$  and  $G^{(0)}$  describing the statistical probabilities of finding the chain ends at the coordinates  $x', y', z'$  and  $x'', y'', z''$ .

In a slit-like pore model, only the direction  $z$  normal to the walls ( $z = 0$  and  $z = 2d$ ) is of interest, since the motion in the  $x$ - $y$  plane parallel to the pore walls is free and is described by the usual Gaussian functions. For a chain of contour length  $n \cdot b$  (where  $b$  is the Kuhn length) the Green functions satisfy the diffusion equation [37]

$$\frac{\partial G}{\partial n} - \frac{b^2}{6} \frac{\partial^2 G}{\partial z^2} = 0 \quad (5.2)$$

The interaction with the walls of the slit is described through the de Gennes' boundary condition [38]

$$G^{-1} \frac{\partial G}{\partial z} \Big|_{\text{on walls}} = -c \quad (5.3)$$

Negative values of  $c$  correspond to effective repulsive forces. The point  $c = 0$ , at which an adsorption of an infinitely long chain on the plane starts, is referred to as a critical adsorption point (CAP). Positive  $c$  corresponds to the adsorption and therefore  $c$  may be considered as the adsorption interaction parameter. The parameter  $c$  has the dimension of inverse length. Its inverse  $c^{-1}$  has the meaning of an average thickness of the layer formed by an adsorbed macromolecule on the surface.

So, there are three parameters in the basic model: the radius of gyration of an unconfined macromolecule,  $R$ , the pore size parameter,  $d$ , and the adsorption interaction parameter,  $c$ . A macromolecule is assumed flexible ( $b$  much less than  $R$ ,  $d$ , and  $c^{-1}$ ).

Both  $G^{(slit)}$  and  $G^{(0)}$  can be written as

$$G = G_{xy}(x', x'', y', y'') \cdot G_z(z', z'') \quad (5.4)$$

with the same  $G_{xy} = \frac{1}{4\pi R^2} \exp\left[-\frac{(x'-x'')^2 + (y'-y'')^2}{4R^2}\right]$ , while the functions  $G_z^{(slit)}$  and  $G_z^{(0)}$  are different.

The function  $G_z^{(0)}$  for a linear unrestricted chain of  $n$  units has a form of a Gaussian distribution:

$$G_z^{(0)}(z', z'') = \frac{1}{2\sqrt{\pi}R} \exp\left[-\frac{(z' - z'')^2}{4R^2}\right] \quad (5.5)$$

where  $R = b\sqrt{n/6}$  is the radius of gyration of a free linear RW chain of  $n$  chain units.

In a slit-like pore,  $G_z^{(slit)}(z', z'')$  has a form: [14]

$$G_z^{(slit)}(z', z'') = \frac{1}{d} \sum_{k=0}^{\infty} \frac{\cos[\alpha_k \zeta'] \cdot \cos[\alpha_k \zeta'' - k\pi/2]}{1 + \lambda/(\alpha_k^2 + \lambda^2)} \exp[-(g\alpha_k)^2] \quad (5.6)$$

where  $\zeta' = (z' - d)/d$  and  $\zeta'' = (z'' - d)/d$  are reduced distances between chain ends and the middle of the slit;  $g = R/d$  is the molecule-to-pore size ratio;  $\lambda = -cd$  is a dimensionless parameter of a polymer-wall interaction; and  $\alpha_k$  are eigenvalues, which are the roots of the equation:

$$\alpha_k = \arctg\left(\frac{\lambda}{\alpha_k}\right) + k\frac{\pi}{2}, k = 0, 1, 2, \dots \quad (5.7)$$

The properties of these eigenvalues were discussed previously [12, 25].

Using these basic equations, the theory of the partition coefficient has been constructed [12], describing the chromatographic behavior of linear RW macromolecules at all  $R$ ,  $d$ , and  $c$ . Both an equation in the form of eigenfunction expansion, suitable for numerical calculations, and simple approximate formulae that are convenient for analysis were obtained.

### 5.3 Unified Approach for Calculating the Partition Coefficient of an Arbitrary TCRW Polymer

#### 5.3.1 Generalized Model and Common Parameters for a Complex TCRW Polymer Interacting with Walls of a Slit-Like Pore

In the generalized model, the slit-like pore is the same as in Fig. 5.1, but now we deal with an arbitrary complex TCRW macromolecule. We consider a complex macromolecule consisting of  $m$  connected chain sections. Chain sections connecting nodes in a complex polymer generally can possess of different number of chain units,  $n_i$ , and therefore can be of different contour length  $n_i b$ .

In a TCRW macromolecule consisting of  $m$  sections, the size of each section is characterized by its radius of gyration in an unrestricted space,  $R_i$  (for an ideal chain  $R_i = b\sqrt{n_i}/6$ ). Hence, a complex macromolecule will be characterized by  $m$  size parameters  $R_i (i = 1, 2, \dots, m)$ . We also have the pore width characterizing parameter  $d$ . However, as we shall see later, only  $m$  dimensionless ratios  $g_i = R_i/d$  will enter the final equations.

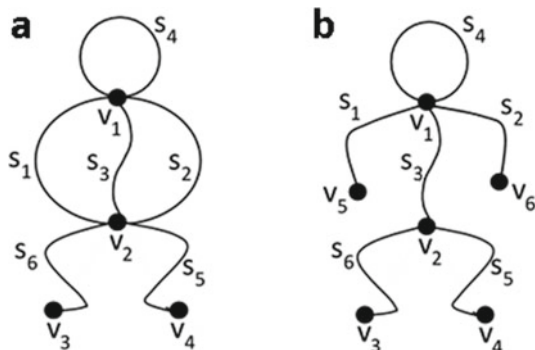
For topological polymers, we define the parameter  $R = \sqrt{\sum_{i=1}^m R_i^2}$ , which has the meaning of the radius of gyration of a reference linear macromolecule having the same chain length (the same molar mass) as a considered TCRW polymer. The corresponding ratio  $g = R/d$  will be used to compare different polymers of the same molar mass.

Like in the theory [12–14] for a linear RW chain, the interaction of polymer chain units with pore walls is accounted for by the interaction parameter  $c$ . For a complex macromolecule with chemically identical units, we have a single interaction parameter  $c$ . In a more general case, for a block copolymer of  $m$  chemically different chain sections, there are  $m$  interaction parameters  $c_i (i = 1, 2, \dots, m)$ . It is convenient to introduce dimensionless interaction parameters  $\lambda_i = -c_i d$ , which will enter the final equations. In terms of  $\lambda$ , negative values of  $\lambda$  will correspond to the adsorption.

#### 5.3.2 Graph Representation of a Complex Macromolecule

In addition to the common parameters, in order to fully characterize the architecture and topology of a complex macromolecule, it is necessary to take into account how the sections are connected to each other. The type of the sections connection is conveniently represented by a graph. Employing the concepts, and the definitions of the graph theory [39, 40], we shall use the following terminologies. Formally, such graph is a pair of sets  $(V, S)$ , where  $V$  is the set of nodes (nodes are also often called as vertices), and  $S$  is the set of chain sections (often called as edges) connecting either pairs of nodes, or one node (pairs are not ordered). Let some complex polymer has

**Fig. 5.2** The graph representation of two complex macromolecules with marked nodes and chain sections



$h$  nodes, and  $m$  sections. We will designate the nodes as  $v_1, v_2, \dots, v_h$ , the sections will be designated as  $s_1, s_2, \dots, s_m$ . So,  $V = \{v_1, v_2, \dots, v_h\}$ ,  $S = \{s_1, s_2, \dots, s_m\}$ . For each chain section, we will indicate its end nodes ( $v_k, v_j$ ). A section of the form  $(v_j, v_j)$  is a loop; sections having the same pair of the end nodes will be called parallel. The degree of the node  $v_j$ , denoted as  $f_j$ , is the number of sections with  $v_j$  as an end node (a loop is counted twice and parallel sections contribute separately). A pendant node is a node whose degree is 1; a section with a pendant node is a pendant section. Since every section has two end nodes,  $\sum_{j=1}^h f_j = 2m$ .

Some connected graphs can be made disconnected by removing one node, which is called the junction point. The parts of the graph together with its junction points are its blocks.

In the framework of the TCRW-model, the topology of a macromolecule is uniquely identified by its graph  $(V, S)$ .

In the example of Fig. 5.2a,  $h = 4$ , and  $m = 6$ . Here we have  $V = \{v_1, v_2, v_3, v_4\}$  for the nodes, and  $S = \{s_1, s_2, s_3, s_4, s_5, s_6\} = \{(v_1, v_2), (v_1, v_2), (v_1, v_2), (v_1, v_1), (v_2, v_4), (v_2, v_3)\}$  for the sections. There is a loop here ( $s_4$ ), three parallel sections ( $s_1, s_2, s_3$ ), and two pendant sections ( $s_5, s_6$ );  $f_3 = f_4 = 1$ ,  $f_1 = f_2 = 5$ . In this example,  $v_1$ , and  $v_2$  are the junction points, while  $(v_1, s_4)$ ,  $(\{v_1, v_2\}, \{s_1, s_2, s_3\})$ ,  $(\{v_2, v_4\}, s_5)$ , and  $(\{v_2, v_3\}, s_6)$  are the blocks. In the structure of Fig. 5.2b,  $h = 6$ ,  $m = 6$ ;  $f_3 = f_4 = f_5 = f_6 = 1$ ,  $f_1 = 5$ ,  $f_2 = 3$ .

### 5.3.3 Partition Coefficient

Using Eqs. (5.1), (5.4)–(5.7), we write for  $Z^{(slit)}$ , and  $Z^{(0)}$ :  $Z^{(slit)} = I_{xy} \cdot I_z^{(slit)}$ ;  $Z^{(0)} = I_{xy} \cdot I_z^{(0)}$ . Since  $I_{xy}$  is the same integral,

$$K = \frac{I_z^{(slit)}}{I_z^{(0)}} \quad (5.8)$$

where

$$I_z^{(slit)} = \int_{z_1, \dots, z_h=0}^{2d} dz_1 dz_2 \cdots dz_h \cdot \prod_{i=1}^m G_{z,i}^{(slit)}(z'_i, z''_i) \quad (5.9)$$

$$I_z^{(0)} = 2d \cdot \int_{z_1, \dots, z_{h-1}=-\infty}^{\infty} dz_1 dz_2 \cdots dz_{h-1} \cdot \prod_{i=1}^m G_{z,i}^{(0)}(z'_i, z''_i) \quad (5.10)$$

In Eq. (5.9), the integration goes over the  $z$ -coordinates of all  $h$  nodes, while in Formula (5.10), the integration variables are  $z$ -coordinates of  $h - 1$  nodes (the integral over  $z_h$  gives  $2d$ ).

As explained in the appendix, these integrations can be completed for any graph representing a TCRW macromolecule. In the result, a unified formula for the partition coefficient (Eq. 5.17 of the Appendix) is obtained, where all integrals are taken. Formula (5.17) represents a fully defined algorithm for calculating the partition coefficient of a TCRW polymer. It contains the model parameters  $g_i = R_i/d$  and  $\lambda_i = -c_i d$  (together with the corresponding eigenvalues  $\alpha_{k_i}$ ), as well as some other parameter values that are uniquely determined by the topological structure of the graph. Therefore, using Formula (5.17), one can compute  $K$ , if the model parameters and the graph structure are known.

In principle, this approach can be applied to an arbitrary complex TCRW polymer. However, the more complex the polymer, the longer it takes to calculate  $K$ : the computation time increases with decreasing  $g$  and strongly depends on  $m$ . In practice, when using an ordinary PC or laptop of medium performance, the dependences  $K(g)$  in the entire range of  $g$  can be obtained so far only at  $m \leq 6$ .

We made sure that all previous theoretical results for the partition coefficient of both simple and more complex TCRW polymers are numerically reproduced by using formula (5.17).

The unified approach described above in this section is especially convenient for theoretical simulating chromatographic separations of mixtures of heterogeneous complex polymers, since it does not require preliminary construction of a theory for each component of the simulated mixture.

### 5.3.4 A Theoretical Chromatograph

Topological polymers generally possess multi-dimensional heterogeneity: every polymeric chain section can be heterogeneous in molar mass and have a different chemical structure. Moreover, polymer samples can contain both target and by-product macromolecules of various topologies. One typical problem in topological polymer chemistry is to separate heterogeneous polymers by topology.

In order to investigate this problem theoretically and to visualize expected separations, we use the virtual chromatography technique [41]. The virtual chromatograph is previously developed software tool, where the simulation procedures are based on the theoretical equations. A polydisperse linear polymer represents an ensemble of individual macromolecules of different chain length (molar mass). A heterogeneous topological polymer represents a more complex ensemble in which molar masses of all sections can be different. Since the chromatographic elution volume  $V_e = V_i + V_p K$  is determined by the partition coefficient  $K$ , by calculating  $K$  values for the members of a given ensemble of macromolecules one can construct a theoretical chromatogram for a heterogeneous complex polymer [20, 22, 27–31].

A similar procedure, modified in a straightforward way, is used to simulate two-dimensional chromatograms [42–44]. This procedure includes calculation of pairs of values  $K_1$  and  $K_2$  for the macromolecules of an ensemble. In order to account for different chromatographic conditions in two dimensions,  $K_1$  and  $K_2$  are calculated at different values of pore size  $d$  and interaction parameter  $c$ , which correspond to the first and the second dimensions.

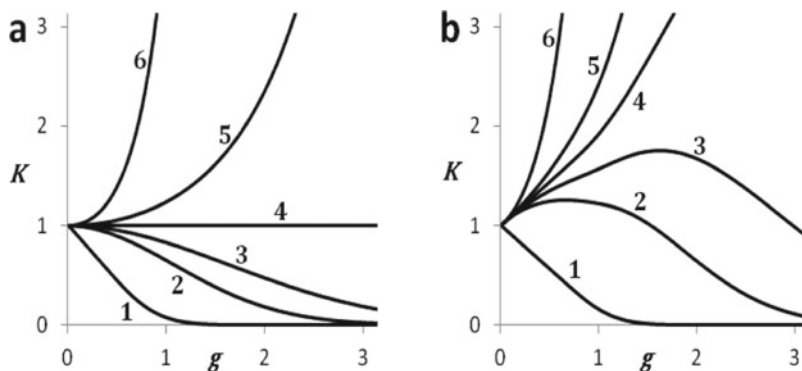
With Eq. (5.17) incorporated into the virtual chromatography software, we now can simulate one- and two-dimensional separations of a variety of heterogeneous topological polymers in order to clarify the conditions under which their separation by topology is possible. Examples of calculated theoretical chromatograms will be provided in the next section.

## 5.4 Theory in Chromatographic Applications

### 5.4.1 Chromatographic Separation of Linear and Ring Polymers

A ring macromolecule is the simplest representative of topological polymers. Theory [25, 26] has predicted significant differences in the chromatographic behavior of ring and linear polymers. Figure 5.3 (modified from [26]) visualizes these differences.

Figure 5.3 shows the theoretical dependences of the partition coefficient  $K$  for linear and ring macromolecules on the parameter  $g = R/d$  at various values of the adsorption interaction parameter  $\lambda$ . Large positive  $\lambda$  values correspond to the SEC conditions, and under such conditions the  $K(g)$  dependences for linear and ring polymers are qualitatively similar (lines 1 in Fig. 5.3). In both cases, at small  $g$ ,  $K$  decreases linearly with increasing  $g$ , while the slopes are different due to different sizes of linear and ring macromolecules. At negative  $\lambda$  (corresponding to the AC conditions), the  $K(g)$  dependences in Fig. 5.3a and b are also qualitatively similar, in both cases  $K$  increases nearly exponentially with the chain length (Fig. 5.3, lines 5 and 6). According to the theory for a linear RW polymer, at the critical adsorption point  $c = 0$ ,  $K_{lin} = 1$ , regardless of  $g$  (Fig. 5.3a, line 4), which means that linear polymers of all molecular weights will co-elute at the CAP. The analogous theory



**Fig. 5.3** Dependences of the partition coefficient  $K$  of linear **a** and ring **b** macromolecules on the parameter  $g = R/d$  at various values of the interaction parameter  $\lambda = -cd$ :  $\lambda = 100$  (1), 0.5 (2), 0.2 (3), 0 (4),  $-0.2$  (5),  $-1$  (6)

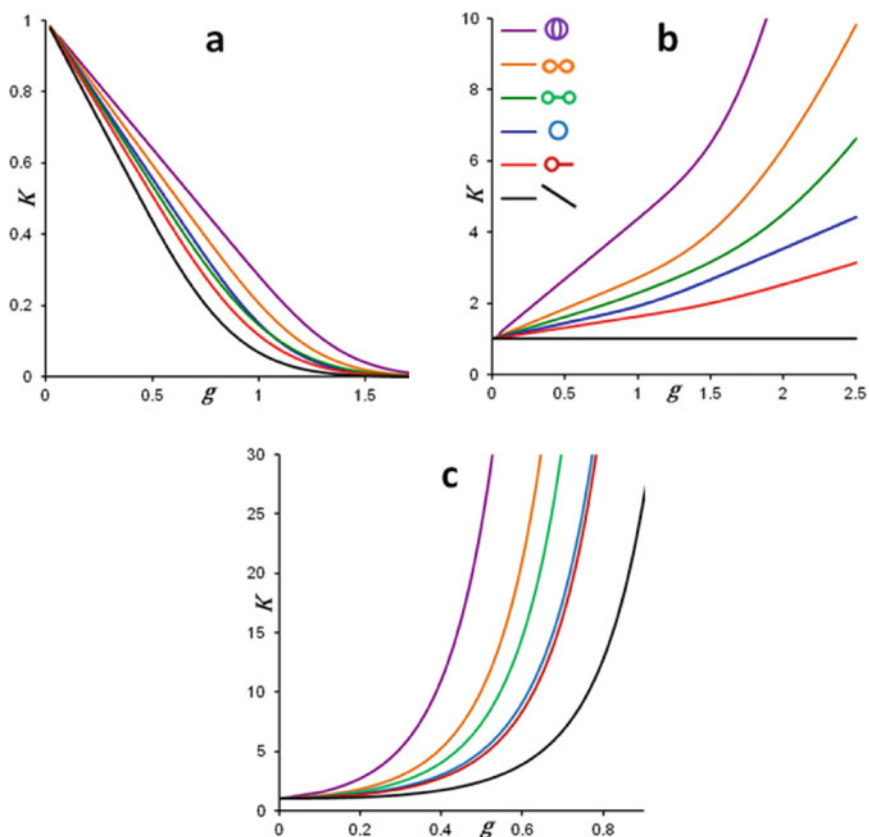
for a ring polymer [26] at  $c = 0$  has predicted an increase in  $K$  with  $g$ : at  $g < 1$ ,  $K_{Ring} \approx 1 + \frac{\sqrt{\pi}}{2}g$  (Fig. 5.3b, line 4). According to [26], there is no co-elution of rings at  $c = 0$ . Moreover, for a ring polymer there are no conditions under which co-elution would occur in a wide range of the parameter  $g$ , that is, at all molecular weights—Fig. 5.3b. Note that under pre-critical conditions, intermediate between the SEC and CAP conditions, the  $K_{ring}(g)$  dependences are non-monotonic and have a maximum. As can be seen in Fig. 5.3b (lines 2, 3), the position of the maximum,  $g^*$ , depends on the interaction parameter  $\lambda$  ( $g^* \approx \frac{\sqrt{\pi}}{8\lambda}$ , at  $g < 1$  [26]). Although absolute co-elution of the rings does not occur, one can speak of seeming co-elution in a narrow interval around  $g^*$ , that is, within the corresponding range of  $M$ . In the pre-critical mode, depending on the interaction parameter and the range of  $M$ , many conditions can exist for seeming co-elution of rings. At such conditions, the elution order of the linear polymers should be SEC-similar—Fig. 5.3a (lines 2, 3). Based on the theory, Gorbunov and Skvortsov concluded [26] that good topological separation of linear and ring polymers heterogeneous in molar mass can be expected under both critical and pre-critical interaction conditions.

### 5.4.2 More Complex Topological Polymers

Theoretical data on the partition coefficient of several topological polymers are shown in Fig. 5.4 (modified from [44]). These data, originally obtained using the corresponding complete theories, have already been published, but now we present these results obtained using a new unified numerical approach (all previous results are accurately reproduced).

Figure 5.4a shows the theoretical dependences of the partition coefficient  $K$  at the SEC condition on the ratio  $R/d$  for polymers of different topology, Fig. 5.4b





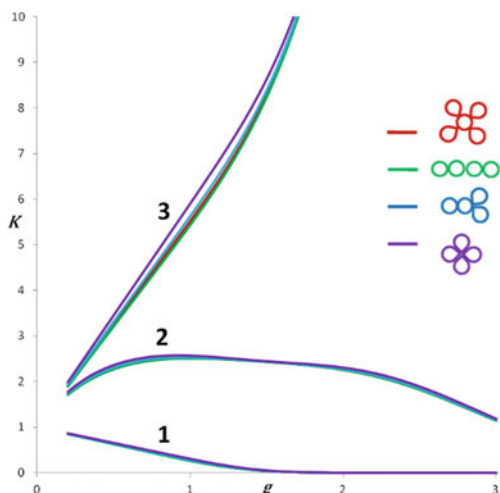
**Fig. 5.4** Theoretical dependences of  $K$  on  $g = R/d$  for different types of polymers in **a** SEC, **b** critical, and **c** adsorption modes of chromatography. The lines are color-coded as in **b**

visualizes the theoretical results at the critical interaction point  $c = 0$ , while Fig. 5.4c shows the results at the conditions of adsorption chromatography. As explained in Sect. 5.3.1, for complex polymers,  $R$  denotes the radius of gyration of a referent linear macromolecule, which has the same chain length (and therefore molar mass) as the given complex polymer. This means that the separation of topologically different polymers of the same molar mass can be analyzed by comparing  $K$  values at the same  $g$ , while each dependence  $K(g)$  characterizes the separation of the corresponding polymer by molar mass.

As it follows from Fig. 5.4a–c, a topological separation of polymers with the same average molar mass and with the narrow molar-mass distributions, in principle, can be achieved by using various modes of chromatography.

Note the trend seen in Fig. 5.4: at the same molecular weight,  $K$  increases with increasing the number of cycles.

**Fig. 5.5** The dependences  $K(g)$  for four topological polymers at different interaction conditions: (1)  $\lambda = 1000$  (SEC), (2)  $\lambda = 0.5$  (pre-critical interaction), and (3)  $\lambda = 0$  (CAP)



Let us now consider topologically different macromolecules with the same number of cycles. Figure 5.5 shows the calculated dependences  $K(g)$  for four macromolecules consisting of the same number of identical cycles and differing in nothing except the way of connecting the cycles.

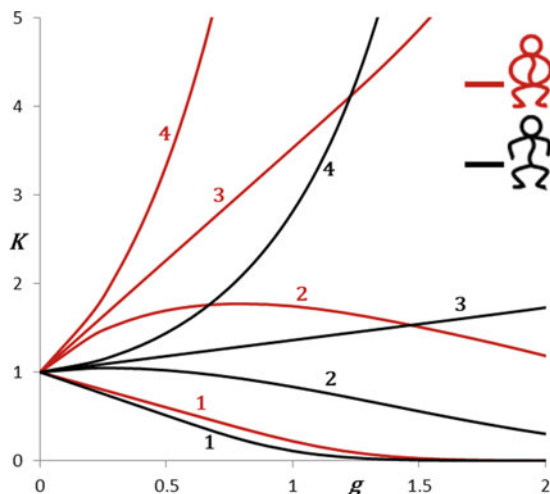
As seen in Fig. 5.5, curves  $K(g)$  practically coincide for these polymers: at all  $\lambda$  and  $g$ , their partition coefficients differ only slightly. Therefore, one can expect that such polymers cannot be separated from each other by means of chromatography.

### 5.4.3 *Simulating Chromatographic Separations of Heterogeneous Topological Polymers and Copolymers*

It is especially difficult to separate topological polymers that are inhomogeneous in molar mass, because of the possible co-elution of molecules with different molar mass and topology. In such cases, the use of interactive chromatography often leads to success, while theory and modeling can help to select the conditions that provide good separation of specific complex polymers.

As an example, imagine you want to separate two complex polymers, having the structures shown in Fig. 5.2. The dependences  $K(g)$  calculated for these polymers are shown in Fig. 5.6. According to the results of Fig. 5.6, there are principal possibilities to separate these two polymers from each other by using both SEC and interactive chromatography modes. However, if these polymers are inhomogeneous in molecular mass, then they may not separate from each other.

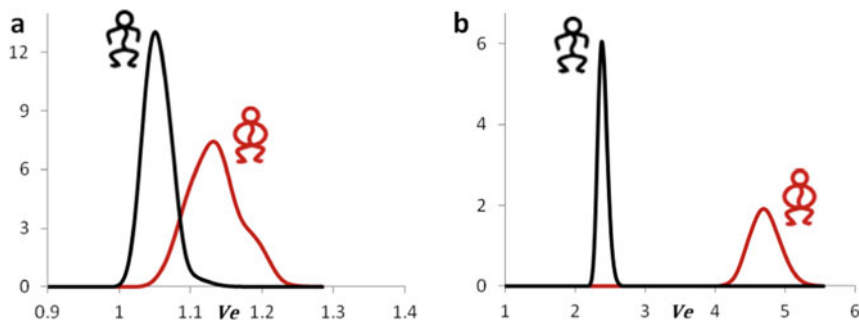
**Fig. 5.6** The dependences  $K(g)$  for two topologically different polymers at various interaction conditions (1) SEC, (2) pre-critical interaction, (3) CAP, and (4) weak adsorption



Let us assume that each of these polymers is inhomogeneous in molecular mass, with all sections having the same average contour length (that is the same average molar mass) and the same heterogeneity index of  $M_w/M_n = 1.1$ .

Figure 5.7a, b show simulated chromatograms for these two inhomogeneous polymers. As can be seen in Fig. 5.7a, in the SEC mode peaks are poorly separated. Better separations can be expected by using interactive chromatography modes, in particular, the chromatography at the CAP (Fig. 5.7b).

As was explained in Sect. 5.3, the new unified numerical approach can also be applied to simulate chromatograms of topological block copolymers. Here we give just one example. Let us consider three different block copolymers of ABA type, where blocks A and B are chemically different. In this example, the middle block B is linear, while the blocks A are either linear or cyclic. We assume that each of these copolymers is inhomogeneous in molecular weight, with all blocks having the



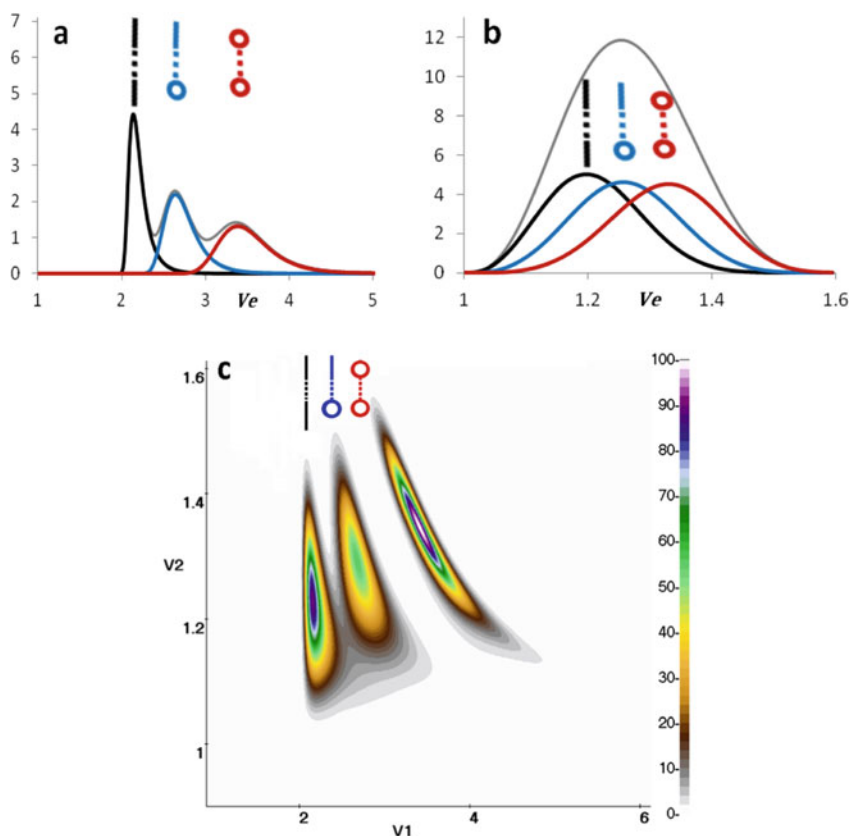
**Fig. 5.7** Chromatograms for two heterogeneous complex polymers simulated at interaction conditions of **a** SEC, and **b** CAP

same average molecular weight and the same heterogeneity index of  $M_w/M_n = 1.25$ . Figure 5.8 shows theoretical chromatograms obtained for a mixture of these copolymers.

Figure 5.8b shows the simulated chromatogram at the SEC condition for both A and B, while in Fig. 5.8a the chromatogram is shown that corresponds to the CAP condition for A, and weak adsorption for B. The two-dimensional chromatogram for this hypothetical sample (Fig. 5.8c) is simulated at the conditions of Fig. 5.8a in the first dimension and of Fig. 5.8b—in the second.

The one-dimensional chromatograms of Fig. 5.8a, b show rather poor topological separation of these three copolymers. Much better separation is expected using 2D technique (Fig. 5.8c).

As follows from the simulations, two chromatographic approaches are expected to be especially promising for separating heterogeneous complex polymers by their



**Fig. 5.8** Topologically different block copolymers ABA: simulated one- and two-dimensional chromatograms. The middle blocks B in the structures are shown as dotted lines. Interaction conditions: **a** CAP for A-blocks, weak adsorption for B, **b** SEC for both A and B, **c** first dimension as in **a**, second dimension as in **b**

topology: the first one is the chromatography at optimized (critical or near-critical) interaction conditions; the second one consists in combining different chromatographic modes, which allows obtaining a separation by both topology and molar mass in a 2D chromatogram.

#### 5.4.4 Comparison of Theory and Experiment

Size-exclusion chromatography, which separates macromolecules by their sizes, is one of the main instruments for polymer analysis and characterization. Casassa's SEC theory [10, 11, 45], and its extensions for describing SEC of topological polymers [14, 27–29, 46] have predicted universal SEC behavior at  $g < 1$  (see, for example, [27–29]), if a theoretical SEC-radius is used as the size of a macromolecule. According to Casassa [45] (see also Wang et al. [46]), the theoretical SEC-radius equals half the average span of a macromolecule. The theoretical SEC radii have been calculated for a number of cyclic and multicyclic macromolecules [27–29, 46]. To the other hand, the effective SEC radii can be obtained experimentally and compared with the theoretical ones. Such comparisons based on the available experimental data showed a good qualitative correlation between theoretical and experimental SEC radii [28, 47]. However, there was no exact quantitative agreement: it seems that generally real macrocyclic polymers are more expanded than can be expected from the TCRW model-based theory [28].

In interaction chromatography, adsorption effects play a very important role. In experiments, adsorption interactions are usually varied by varying temperature or mixed solvent composition, and the relationships between the experimental conditions and the interaction parameter  $c$  can be obtained [41, 48, 49], which allows the comparison of theory and experiment.

The theoretically predicted [14, 26] chromatographic separation of linear and ring polymers at the CAP has been implemented by many groups, and now the method of liquid chromatography at the CAP conditions has become a recognized technique in the separation and characterization of macrocycles (see, for example, [28, 50, 51] and references therein).

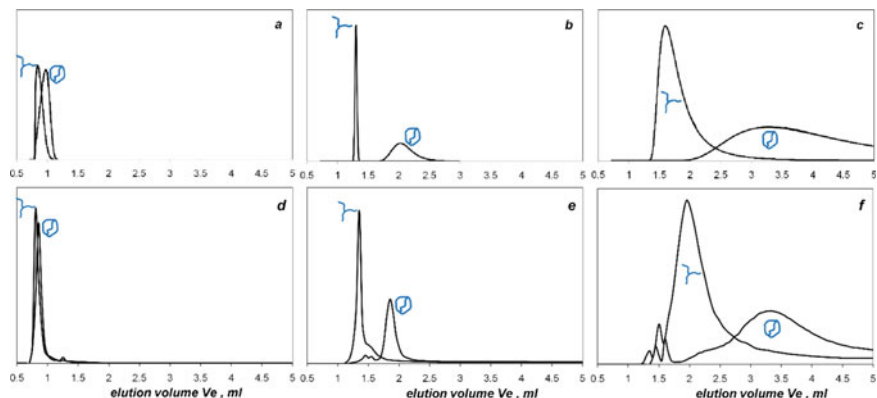
A number of reported studies have attempted to compare theoretical results with experimental data on the chromatographic behavior of cyclic polymers. Lee et al. [50] performed a detailed investigation of the retention of ring polystyrenes at the chromatographic condition, which was estimated as being close to the CAP. Reversed phase columns of various pore size were examined, and retentions of nine different molecular weight ring polystyrenes were measured for each pore-sized column. Within a wide-pore regime ( $R/d < 1$ ), the experimental partition coefficient of ring PS plotted against  $R/d$  showed a nice universal dependence regardless of column pore size, in excellent qualitative agreement with theoretical predictions. However, significant deviations from the ideal-chain theory were observed in the narrow-pore regime ( $R/d > 1$ ).

Ziebarth et al. [51], in the experimental part of their work, used four pairs of linear and ring polystyrenes in the range of  $M$  (16–90) kg/mol (in each pair, linear and ring polymers were of the same molar mass). In the examined  $M$  range, they found both CAP and a condition for seeming co-elution of rings (somewhat shifted from the CAP toward the SEC condition), and studied the elution of linear and ring polymers at these two conditions. These experimental data show good qualitative agreement with the theoretical predictions [26], visualized in Fig. 5.3.

The chromatographic behavior of theta-shaped polymers in comparison with their star-shaped analogues was studied experimentally by Tezuka and co-workers [52], and the agreement between their experimental data and theory was discussed [28, 44]. Simulated and real chromatograms obtained for these heterogeneous theta and star polymers in SEC and interactive chromatography modes are shown in Fig. 5.9 (modified from [44]).

In all studied chromatographic modes, simulated chromatograms look very similar to real ones. In the SEC mode, although the peak positions are somewhat different, peaks overlap considerably—Fig. 5.9a and d. In the AC mode (Fig. 5.9c and f) peak maxima are separated considerably, but there is a huge peak broadening due to the molar-mass heterogeneity; this results in rather poor separation of these two polymers. As can be seen in Fig. 5.9b and e, the separation pattern becomes quite good at the interaction corresponding to the CAP.

Thus, in the wide-pore situations, there is a qualitative agreement between the TCRW-based theory and available experimental data on the chromatography of cyclic polymers of particular topological structures. The theoretical predictions for more complex polymers still need experimental verification.



**Fig. 5.9** Comparison of simulated **a–c** and real **d–f** chromatograms of heterogeneous ( $M_w/M_n = 1.24$ ) star- and theta-shaped polyTHFs of  $M_w = 9600$  under the condition of **a, d** SEC, **b, e** CAP, and **c, f** more strong adsorption. Simulated interaction conditions: **a**  $c = -5000$ , **b**  $c = 0$ , and **c**  $c = 0.17$ . Experimental conditions: TSK ODS-80TS column at eluent compositions of THF/acetonitrile of **d** 100/0, **e** 52/48, and **f** 48/52 (Data from [28])

Unfortunately, not many systematic experimental studies of the chromatographic behavior of complex cyclic polymers have been reported. For comparison with theory, experiments are needed in which fully characterized topological polymers with a reliably identified structure are used and the adsorption interaction conditions are determined. It should be noted that it is especially difficult to obtain reliable experimental data when studying high molecular weight polymers in narrow pores under conditions close to the CAP, where even minor shifts in experimental conditions (temperature, solvent composition) can lead to dramatic changes in chromatographic retention.

We believe that the TCRW-based theory and the new TCRW-based unified numerical approach can qualitatively describe chromatography of real macrocyclic polymers in situations, where molecules are less than pores.

## 5.5 Concluding Remarks and Prospects for Further Development of the Theory of Chromatography of Topologically Complex Polymers

The TCRW model permits intersections of chain units, which of course cannot happen in real macromolecules, and therefore, this model does not account for the excluded-volume effects. It takes into account the interactions of the chain units with the pore walls, but does not take into consideration the interactions between the chain units. The latter interactions, in particular, may influence the chromatographic behavior of block copolymers. When applied to complex macrocyclic polymers, the TCRW model takes into account how chain sections are connected to each other, but obviously cannot account for knotting, since self-intersections are allowed in this model.

Uehara and Deguchi have studied the effect of excluded volume on the mean-square radius of gyration [53] and that of the scattering profile [54] for some topological polymers. In particular, it was suggested in [53] that the order among different ideal-chain topological polymers is the same as that of real chains with respect to the mean-square radius of gyration. If it is the case, one could expect that the separation of real topological polymers should be practically similar to that of their ideal-chain analogues. In our opinion, it would be interesting to perform similar studies with respect to the average span dimensions of topological polymers, which determine their behavior in size-exclusion chromatography.

Despite some unrealistic features of the model, nowadays the TCRW-based theory is the only one available to describe analytically chromatography of complex polymers. However, such theories have been developed only for a number of particular types of topological polymers. The new TCRW-based approach, which uses a graph representation of the macromolecular topological structure, provides a unified algorithm for obtaining accurate theoretical results for a variety of topologically complex polymers.

Within the framework of the TCRW model-based approach, we think that the following extensions and further studies would be interesting and useful.

It would be helpful to develop a mathematical formalism and create a computational algorithm that will converge quickly at small  $g$ , based on alternative formulas for the Green's functions of this problem. This would greatly speed up the calculation of the partition coefficients, using, depending on  $g$ , one or another fast computational algorithm.

Another challenge is obtaining a theoretical solution for an analogous model with TCRW macromolecules and cylindrical pores.

Further systematic theoretical studies and modeling of the chromatographic behavior of chemically heterogeneous topological polymers, for example, complex block copolymers and macrocyclic polymers containing chemically specific groups, are required. As already mentioned, to date, such studies have been performed only for several types of topological polymers of particular graph structures.

It should also be noted that along with the partition coefficient  $K$ , which is mainly related to chromatography, there are other thermodynamic and structural characteristics of interest that can also be obtained using the unified approach of Sect. 5.3. In particular, after  $K$ , the free energy change  $\Delta F/(k_B T) = -\ln K$  (where  $k_B$  is the Boltzmann's constant, and  $T$  is the absolute temperature) can be immediately calculated. With a slight modification of the calculation final part, one can also compute the compressibility factor  $\kappa = PV/(k_B T)$  [55], where  $V$  is the volume, and  $P = -\frac{\partial(\Delta F)}{\partial V}|_T$  is the pressure. Since for a chain confined by the slit with the interacting walls  $\kappa = d\frac{\partial(\ln K)}{\partial d}|_c$ , the derivative can be calculated numerically, and hence the compressibility factor for a complex polymer can be computed. It seems also possible to calculate some structural characteristics of a complex polymer within a pore, such as the adsorbed chain unit fractions.

Further comparisons of theoretical results with experiments will be very important. Such studies will require well-characterized topological polymers and specially designed accurate experiments.

Finally, we think that the Monte-Carlo modeling with due regard for excluded-volume effects and topological constraints would be of primary importance. Extending the previous studies on linear [56, 57] and more complex polymers [58, 59], such modeling will provide a better understanding of the chromatographic behavior of real topological polymers. We hope that the theoretical results based on the TCRW model may serve as useful reference cases for more sophisticated studies that employ more realistic physical assumptions.

**Acknowledgements** We are grateful to Prof. Yasuyuki Tezuka for stimulating and fruitful discussions on the topological chemistry of polymers.



## Appendix

### Derivation of the Generalized Equation for the Partition Coefficient of a TCRW Polymer

Let us consider the integral  $I_z^{(0)}$  of Eq. (5.10) for an unrestricted space.

$$I_z^{(0)} = 2d \cdot \int_{z_1, \dots, z_{h-1} = -\infty}^{\infty} dz_1 dz_2 \cdots dz_{h-1} \cdot \prod_{i=1}^m \frac{1}{2\sqrt{\pi} R_i} \exp \left[ -\frac{(z_i' - z_i'')^2}{4R_i^2} \right]$$

By changing the variables  $\zeta_i = \frac{z_i}{2d}$ ,  $d\zeta_i = \frac{dz_i}{2d}$ , and using dimensionless parameters  $g_i = R_i/d$ , we obtain

$$I_z^{(0)} = \frac{d^{h-m}}{2^{m-h} (\sqrt{\pi})^m} \prod_{i=1}^m g_i^{-1} \int_{\zeta_1, \dots, \zeta_{h-1} = -\infty}^{\infty} d\zeta_1 d\zeta_2 \cdots d\zeta_{h-1} \cdot \exp \left[ -\sum_{i=1}^m \frac{(\zeta_i' - \zeta_i'')^2}{g_i^2} \right] \quad (5.11)$$

For every complex polymer, represented by its graph  $(V, S)$ , one can write down the corresponding quadratic form in the exponent of Eq. (5.11). This quadratic form can be brought to the canonical form by the Lagrange method, and after that the integral  $\int_{-\infty}^{\infty} d\zeta_1 \dots d\zeta_{h-1} \exp \left[ -\sum_{i=1}^m \frac{(\zeta_i' - \zeta_i'')^2}{g_i^2} \right]$  can be taken by successive integration with respect to each variable, this procedure reduces to integrals of the form  $\int_{-\infty}^{\infty} \exp[-(av)^2] dv = \sqrt{\pi}/a$ . This results in

$$\int_{-\infty}^{\infty} d\zeta_1 \dots d\zeta_{h-1} \exp \left[ -\sum_{i=1}^m \frac{(\zeta_i' - \zeta_i'')^2}{g_i^2} \right] = \sqrt{\pi}^{h-1} \prod_{j=1}^{h-1} a_j^{-1}$$



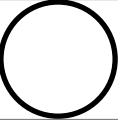
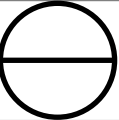

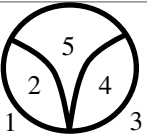
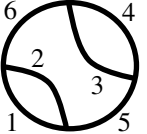
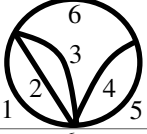
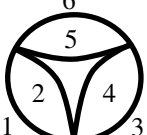
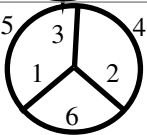
where  $a_j = a_j(g_1, \dots, g_m)$  are the diagonal elements in the Lagrange transform matrix. We thus obtain  $I_z^{(0)}$  in the form:

$$I_z^{(0)} = \frac{d^{h-m}}{2^{m-h} (\sqrt{\pi})^{m-h+1}} Q^{-1} \quad (5.12)$$

wherein  $Q = Q_{(V,S)}(g_1, \dots, g_m) = \prod_{i=1}^m g_i \cdot \prod_{j=1}^{h-1} a_j$  is a graph-dependent function of  $\{g_1, \dots, g_m\}$ .

By using this general procedure, one can construct the function  $Q$  for any complex polymer.

**Table 5.1** Explicit expressions of  $Q^2$  for some polymer chain topologies

Polymer	$Q^2$
1: Linear 	1
2: Branched structures without loops 	1
3: Ring 	$g^2$
4: Theta-(Bunch $m = 3$ ) 	$g_1^2 g_2^2 + g_2^2 g_3^2 + g_3^2 g_1^2$
5: Bunch of $m$ sections 	$\sum_{l=1}^m \prod_{i=1}^m g_i^2$ $i \neq l$
6: 	$g_1^2 g_2^2 (g_3^2 + g_4^2) + g_3^2 g_4^2 (g_1^2 + g_2^2) + g_5^2 (g_1^2 + g_2^2) (g_3^2 + g_4^2)$
7: 	$g_1^2 g_2^2 (g_3^2 + g_4^2) + g_3^2 g_4^2 (g_1^2 + g_2^2) + (g_5^2 + g_6^2) (g_1^2 + g_2^2) (g_3^2 + g_4^2)$
8: 	$g_1^2 g_2^2 g_3^2 (g_4^2 + g_5^2) + (g_1^2 g_2^2 + g_2^2 g_3^2 + g_3^2 g_1^2) \times (g_4^2 g_5^2 + g_5^2 g_6^2 + g_6^2 g_4^2)$
9: 	$g_1^2 g_2^2 (g_3^2 + g_4^2) (g_5^2 + g_6^2) + g_3^2 g_4^2 (g_1^2 + g_2^2) (g_5^2 + g_6^2) + g_5^2 g_6^2 (g_1^2 + g_2^2) (g_3^2 + g_4^2)$
10: 	$(g_1^2 g_2^2 + g_1^2 g_3^2 + g_2^2 g_3^2) (g_4^2 + g_5^2 + g_6^2) + g_1^2 g_4^2 (g_5^2 + g_6^2) + g_2^2 g_5^2 (g_4^2 + g_6^2) + g_3^2 g_6^2 (g_4^2 + g_5^2) + g_4^2 g_5^2 g_6^2$

In Table 5.1 we list  $Q^2$  for some particular topologically different polymers. Where necessary, the sections are numbered.

It follows from the Eqs. (5.11), (5.12) that the function  $Q$  of a complex polymer consisting of  $i_b$  blocks is equal to the product of such functions of all blocks:

$$Q_{(V,S)} = \prod_{i=1}^{i_b} Q_{(V_i,S_i)} \quad (5.13)$$

Knowing  $Q$  for the blocks, and using Eq. (5.13), one can construct  $Q$  for a more complex polymer. For example, using Formula (5.13), and the data for ring, theta, and linear structures listed in Table 5.1, for the polymer shown in Fig. 5.2b we have  $Q = g_4$ , while for the structure of Fig. 5.2a.

$$\begin{aligned} Q &= Q_{(v_1,s_4)} \cdot Q_{(\{v_1,v_2\},\{s_1,s_2,s_3\})} \cdot Q_{(\{v_2,v_4\},s_5)} \cdot Q_{(\{v_2,v_3\},s_6)} \\ &= g_4 \sqrt{g_1^2 g_2^2 + g_2^2 g_3^2 + g_3^2 g_1^2} \end{aligned}$$

Note that  $g$ -parameters of the linear blocks (for which  $Q_i = 1$ ) do not contribute to  $Q$ . In general, since  $Q_i = 1$  for all linear and branched structures,  $Q$  will only include the parameters of the cycle-containing blocks.

Using Eq. (5.13), and the data of Table 5.1, one can easily construct  $Q$  for a variety of complex polymers, in particular, for all polymers represented by graphs of  $m \leq 6$ .

Let us now proceed with  $I_z^{(slit)}$  having a form of the integral of Eq. (5.9). We substitute the functions  $G_z^{(slit)}$  of Eq. (5.6) into Eq. (5.9), and replace the variables  $\zeta = (z - d)/d$ ;  $d\zeta = dz/d$ . For brevity, we will use the notations:

$$\Lambda_{i,k_i} = \frac{\lambda_i^2 + \alpha_{k_i}^2}{\lambda_i + \lambda_i^2 + \alpha_{k_i}^2}; \quad \cos\left(\alpha_{k_i} \zeta - k_i \frac{\pi}{2}\right) = \text{cs}(\alpha_{k_i} \zeta) = \begin{cases} \cos(\alpha_{k_i} \zeta) & k \text{ even} \\ \sin(\alpha_{k_i} \zeta) & k \text{ odd} \end{cases}$$

With these replacements, and after algebraic transformations, Eq. (5.9) takes the form:

$$\begin{aligned} I_z^{(slit)} &= d^{h-m} \int_{\zeta_1, \dots, \zeta_h = -1}^1 d\zeta_1 \cdots d\zeta_h \prod_{i=1}^m \sum_{k_i=0}^{\infty} \Lambda_{i,k_i} \cdot \text{cs}(\alpha_{k_i} \zeta_i') \text{cs}(\alpha_{k_i} \zeta_i'') \cdot \exp(-g_i^2 \alpha_{k_i}^2) \\ &= d^{h-m} \sum_{k_1, \dots, k_m=0}^{\infty} \left\{ \exp\left(-\sum_{i=1}^m g_i^2 \alpha_{k_i}^2\right) \cdot \prod_{i=1}^m \Lambda_{i,k_i} \right. \\ &\quad \left. \cdot \int_{-1}^1 d\zeta_1 \cdots d\zeta_h \prod_{i=1}^m \text{cs}(\alpha_{k_i} \zeta_i') \text{cs}(\alpha_{k_i} \zeta_i'') \right\} \end{aligned}$$

Then, using the graph representation of the complex polymer under consideration, we group by nodes  $cs$ -functions in the  $2^m$ -member product and replace the  $h$ -fold integral with the product of  $h$  integrals over each  $\zeta$ . This will result in:

$$I_z^{(slit)} = d^{h-m} \sum_{k_1 \cdots k_m=0}^{\infty} \left\{ \exp\left(-\sum_{i=1}^m g_i^2 \alpha_{k_i}^2\right) \cdot \prod_{i=1}^m \Lambda_{i,k_i} \cdot \prod_{j=1}^h \int_{-1}^1 d\zeta_j \prod_{l=1}^{f_j} cs(\alpha_{k_{j_l}} \zeta_j) \right\} \quad (5.14)$$

Consider an integral that differs only by a factor from that in the Eq. (5.14):

$$I_j = 2^{f_j-1} \int_{-1}^1 d\zeta_j \prod_{l=1}^{f_j} cs(\alpha_{k_{j_l}} \zeta_j)$$

This integral corresponds to the  $j$ th node of the degree  $f_j$ ;  $k_{j_1}, k_{j_2}, \dots, k_{j_{f_j}}$  being the set of the numbers of the corresponding eigenvalues. The integral equals zero, if there are odd number of sines in the product (this happens at  $\sum_{l=1}^{f_j} k_{j_l}$  odd). Otherwise, at  $\sum_{l=1}^{f_j} k_{j_l}$  even,  $\int_{-1}^1 = 2 \int_0^1$ . At  $\sum_{l=1}^{f_j} k_{j_l}$  even, using the trigonometric formulae  $2\sin(x)\sin(y) = \cos(x-y) - \cos(x+y)$ ,  $2\cos(x)\cos(y) = \cos(x-y) + \cos(x+y)$ , the product of the  $cs$ -functions can be transformed into the sum of cosines:

$$2^{f_j} \prod_{l=1}^{f_j} cs(\alpha_{k_{j_l}} \zeta_j) = \sum_{\sigma_{j_l}=\pm 1} (-1)^{\left( \begin{matrix} \sum_{l=1}^{f_j} \sigma_{j_l}/2 \\ k_{j_l} \text{ odd} \end{matrix} \right)} \cdot \cos\left(\zeta_j \sum_{l=1}^{f_j} \sigma_{j_l} \alpha_{k_{j_l}}\right)$$

where all  $\sigma_{j_l}$  are the signs (+1, or -1), and  $\sum_{\sigma_{j_l}=\pm 1}$  is a sum over all combinations of signs  $\sigma_{j_l}$  (this sum consists of  $2^{f_j}$  terms).

By integrating, we have

$$I_j = \begin{cases} 0, & \sum_{l=1}^{f_j} k_{j_l} \text{ odd} \\ \sum_{\sigma_{j_l}=\pm 1} (-1)^{\left( \sum_{k_{j_l} \text{ odd}} \sigma_{j_l}/2 \right)} \frac{\sin\left(\sum_{l=1}^{f_j} \sigma_{j_l} \alpha_{k_{j_l}}\right)}{\sum_{l=1}^{f_j} \sigma_{j_l} \alpha_{k_{j_l}}}, & \sum_{l=1}^{f_j} k_{j_l} \text{ even} \end{cases} \quad (5.15)$$

Taking into account that  $\prod_{j=1}^h 2^{f_j-1} = 2^{2m-h}$ , we obtain  $I_z^{(slit)}$  as the following:

$$I_z^{(slit)} = \frac{d^{h-m}}{2^{2m-h}} \sum_{k_1 \cdots k_m=0}^{\infty} \left\{ \prod_{i=1}^m \frac{\lambda_i^2 + \alpha_{k_i}^2}{\lambda_i + \lambda_i^2 + \alpha_{k_i}^2} \exp(-g_i^2 \alpha_{k_i}^2) \cdot \prod_{j=1}^h I_j \right\} \quad (5.16)$$

where  $I_j$  is given by Eq. (5.15).

Now, when all the integrations are completed, we can write down the resulting formula. Substituting Eqs. (5.12) and (5.16) into Eq. (5.8), we finally obtain the following formula for the partition coefficient of a complex polymer:

$$K = \frac{(\sqrt{\pi})^{m-h+1} Q}{2^m} \sum_{k_1 \dots k_m=0}^{\infty} \left\{ \prod_{i=1}^m \frac{\lambda_i^2 + \alpha_{k_i}^2}{\lambda_i + \lambda_i^2 + \alpha_{k_i}^2} \exp(-g_i^2 \alpha_{k_i}^2) \cdot \prod_{j=1}^h I_j \right\} \quad (5.17)$$

Formula (5.17) provides a universal algorithm for calculating the partition coefficient of a TCRW polymer. It contains the parameters  $g_i$  and  $\lambda_i$ , and for each  $\lambda_i$  there is its own set of eigenvalues  $\alpha_{k_i}$ , given by Eq. (5.7). Formula (5.17) also includes  $Q$  and  $I_j$  values that are uniquely determined by the graph topological structure. Therefore, using Formula (5.17), one can compute  $K$ , if the model parameters and the graph structure are known.

It should be noted that at positive  $\lambda$  all  $\alpha_k$  are real and positive. For negative  $\lambda$ ,  $\alpha_0$  is a pure imaginary number (if  $\lambda < -1$ ,  $\alpha_1$  is also imaginary). However,  $K$  given by Eqs. (5.15), (5.17) is always real.

When programming the Formula (5.17), one should keep in mind that uncertainties of the form 0/0 appear in this formula at some values of  $\lambda$ . These uncertainties are eliminated by calculating the limits in both the numerator and denominator.

Note that the convergence of the  $m$ -fold series in Formula (5.17) slows down with decreasing  $g_i$ , therefore, it is necessary to take many terms in the series to accurately calculate  $K$  at small  $g_i$  values.

## References

1. K. Matyjaszewski, Y. Gnanou, L. Leibler (eds.), *Macromolecular Engineering: Precise Synthesis, Materials Properties, Applications* (Wiley-VCH, Weinheim, 2007)
2. N. Hadjichristidis, M. Pitsikalis, S. Pispas, H. Iatrou, *Chem. Rev.* **101**, 3747 (2001)
3. T. Yamamoto, Y. Tezuka, Cyclic and multicyclic topological polymers, in *Complex Macromolecular Architectures: Synthesis, Characterization, and Self-assembly*, ed. by N. Hadjichristidis, A. Hirao, Y. Tezuka, F. Du Prez (Wiley (Asia), Singapore, 2011), p. 3.
4. T. Yamamoto, Y. Tezuka, *Polym. Chem.* **2**, 1930 (2011)
5. Y. Tezuka, *React. Funct. Polym.* **148**, 104489 (2020).
6. H. Pasch, B. Trathnigg, *HPLC of polymers* (Springer, Berlin, Heidelberg/NY, 1997)
7. T. Chang, *Adv. Polym. Sci.* **163**, 1 (2003)
8. W. Radke, *J. Chromatogr. A* **1335**, 62 (2014)
9. P. Kiltz, W. Radke, *Anal. Bioanal. Chem.* **407**, 193 (2015)
10. E.F. Casassa, *J. Polym. Sci. Part B* **5**, 773 (1967)
11. E.F. Casassa, Y. Tagami, *Macromolecules* **2**, 14 (1969)
12. A.A. Gorbunov, A.M. Skvortsov, *Polym. Sci. U.S.S.R.* **28**, 2412 (1986)
13. A.M. Skvortsov, A.A. Gorbunov, *J. Chromatogr. A* **358**, 77 (1986)
14. A.A. Gorbunov, A.M. Skvortsov, *Adv. Colloid Interf. Sci.* **62**, 31 (1995)
15. M.B. Tennikov, P.P. Nefedov, M.A. Lazareva, and S.Ya. Frenkel, *Polym.Sci. U.S.S.R.* **19**, 764 (1977).

16. B.G. Belenky, E.S. Gankina, M.B. Tennikov, L.Z. Vilenchik, *J. Chromatogr. A* **147**, 99 (1978)
17. A.M. Skvortsov, A.A. Gorbunov, *J. Chromatogr. A* **507**, 487 (1990)
18. A. Gorbunov, B. Trathnigg, *J. Chromatogr. A* **955**, 9 (2002)
19. A.M. Skvortsov, G.J. Fleer, *Macromolecules* **35**, 8609 (2002)
20. A.A. Gorbunov, A.V. Vakhrushev, *Polymer* **45**, 7303 (2004)
21. W. Radke, K. Rode, A.V. Gorshkov, T. Biela, *Polymer* **46**, 5456 (2005)
22. A.A. Gorbunov, A.V. Vakhrushev, *J. Chromatogr. A* **1064**, 169 (2005)
23. S.G. Entelis, V.V. Evreinov, A.V. Gorshkov, *Adv. Polym. Sci.* **76**, 129 (1986)
24. A.V. Gorshkov, H. Much, H. Becker, H. Pasch, V.V. Evreinov, S.G. Entelis, *J. Chromatogr. A* **523**, 91 (1990)
25. A.A. Gorbunov, A.M. Skvortsov, *Polym. Sci. U.S.S.R.* **28**, 2722 (1986)
26. A.A. Gorbunov, A.M. Skvortsov, *Polym. Sci. U.S.S.R.* **29**, 1025 (1987)
27. A.A. Gorbunov, A.V. Vakhrushev, *Polymer* **45**, 6761 (2004)
28. A.V. Vakhrushev, A.A. Gorbunov, Y. Tezuka, A. Tsuchitani, H. Oike, *Anal. Chem.* **80**, 8153 (2008)
29. A.V. Vakhrushev, A.A. Gorbunov, *J. Chromatogr. A* **1433**, 56 (2016)
30. A.A. Gorbunov, A.V. Vakhrushev, *J. Chromatogr. A* **1456**, 162 (2016)
31. A.A. Gorbunov, A.V. Vakhrushev, *Polymer* **51**, 3285 (2010)
32. E.A. DiMarzio, R.J. Rubin, *J. Chem. Phys.* **55**, 4318 (1971)
33. G.J. Fleer, M.A. Cohen Stuart, J.M.H.M. Scheutjens, T. Cosgrove, B. Vincent, *Polymers at Interfaces* (Chapman and Hall, London, 1993)
34. P.G. de Gennes, *Scaling Concepts in Polymer Physics* (Cornell University Press, Ithaca, NY, 1979)
35. E. Eisenriegler, K. Kremer, K. Binder, *J. Chem. Phys.* **77**, 6296 (1982)
36. A.A. Gorbunov, A.M. Skvortsov, J. van Male, G.J. Fleer, *J. Chem. Phys.* **114**, 5366 (2001)
37. S. Chandrasekhar, *Rev. Mod. Phys.* **15**, 1 (1943)
38. P.G. de Gennes, *Rept. Progr. Phys.* **32**, 187 (1969)
39. R. Diestel, *Graph Theory*. Graduate Texts in Mathematics, vol. 173, 5th edn. (Springer, Heidelberg, 2016)
40. F. Harary, *Graph Theory* (Addison-Wesley Publishing Company, Reading, MA, 1969)
41. B. Trathnigg, A. Gorbunov, A. Skvortsov, *J. Chromatogr. A* **890**, 195 (2000)
42. A.A. Gorbunov, A.V. Vakhrushev, *J. Chromatogr. A* **1217**, 4825 (2010)
43. A.A. Gorbunov, A.V. Vakhrushev, *Polymer* **50**, 2727 (2009)
44. A.A. Gorbunov, A.V. Vakhrushev, *Proc. Chem.* **2**, 140 (2010)
45. E.F. Casassa, *Macromolecules* **9**, 182 (1976)
46. Y. Wang, I. Teraoka, F.Y. Hansen, G.H. Peters, O. Hassager, *Macromolecules* **44**, 403 (2011)
47. L. Zhu, X. Wang, J. Li, Y. Wang, *Macromol. Theory Simul.* **25**, 482 (2016)
48. A.A. Gorbunov, L.Y. Solovyova, A.M. Skvortsov, *Polymer* **39**, 697 (1998)
49. A.A. Gorbunov, A.V. Vakhrushev, B. Trathnigg, *J. Chromatogr. A* **1216**, 8883 (2009)
50. W. Lee, H. Lee, H.C. Lee, D. Cho, T. Chang, A.A. Gorbunov, J. Roovers, *Macromolecules* **35**, 529 (2002)
51. J.D. Ziebarth, A.A. Gardiner, Y. Wang, Y. Jeong, J. Ahn, Y. Jin, T. Chang, *Macromolecules* **49**, 8780 (2016)
52. Y. Tezuka, A. Tsuchitani, Y. Yoshioka, H. Oike, *Macromolecules* **36**, 65 (2003)
53. E. Uehara, T. Deguchi, *J. Chem. Phys.* **145**, 164905 (2016)
54. E. Uehara, T. Deguchi, *J. Phys. A: Math. Theor.* **51**, 134001 (2018)
55. K.F. Freed, J. Dudowicz, E.B. Stukalin, J.F. Douglas, *J. Chem. Phys.* **133**, 094901 (2010)
56. P. Cifra, T. Bleha, *Polymer* **41**, 1003 (2000)
57. Y. Wang, D. Howard, Y. Gong, *Polymer* **45**, 313 (2004)
58. C.R.A. Abreu, A.E. Escobedo, *Macromolecules* **38**, 8532 (2005)
59. Y. Wang, Theory and principles of interaction chromatography, in *Recent Progress in Separation of Macromolecules and Particulates*, ed. by Y. Wang, W. Gao, S. Orski, X.M. Liu. ACS Symposium Series, vol. 1281 (2018), p. 19. <https://doi.org/10.1021/bk-2018-1281.ch002>

# Chapter 6

## Construction of Multicyclic Polymer Topologies through Electrostatic Self-assembly and Covalent Fixation (ESA-CF)



Yasuyuki Tezuka

**Abstract** An *electrostatic self-assembly and covalent fixation* (ESA-CF) protocol has been developed for the precision designing of complex macromolecular chain architectures, including, in particular, a class of cyclic and multicyclic topologies, by employing a series of designated linear and branched telechelic precursors having prescribed cyclic ammonium salt end groups accompanying carboxylate counteranions. The ESA-CF process has been extended to prepare a variety of *kyklo*-telechelics, i.e., (multi)cyclic polymer precursors having such a pair of complementary reactive groups, as alkyne and azide units for an addition (*click*) reaction, as well as two olefin units for metathesis condensation (*clip*) reaction, at the prescribed location of cyclic polymer frameworks. A wide variety of multicyclic polymer topologies of either *spiro*-, *bridged*-, *fused*- as well as their *hybrid*-form has been subsequently constructed by means of the orthogonal techniques based on the ESA-CF protocol in conjunction with the *click* and the *clip* processes.

### 6.1 Introduction

Topologically intriguing polymer chain architectures have continuously attracted enormous research efforts as a catchily inspiring subject, since the seminal discovery of knotted and catenated circular DNAs configured purposely in nature with topoisomerase enzymes [1]. From the relevant topological (soft) geometry viewpoint, cyclic and multicyclic polymers are inherently unique by the absence of chain termini in contrast to linear and branched counterparts [2]. Additional feature of the topological geometry of polymer chain architectures is apparently the randomly coiled flexible nature of skeletal chain segments between junctions and between junction-terminus to allow the dynamic conformational transformation in a 3D space [3].

As presented in Part III of this book, a number of effective means for *single*-cyclic (or simple ring) polymers have been developed in the last decades, either

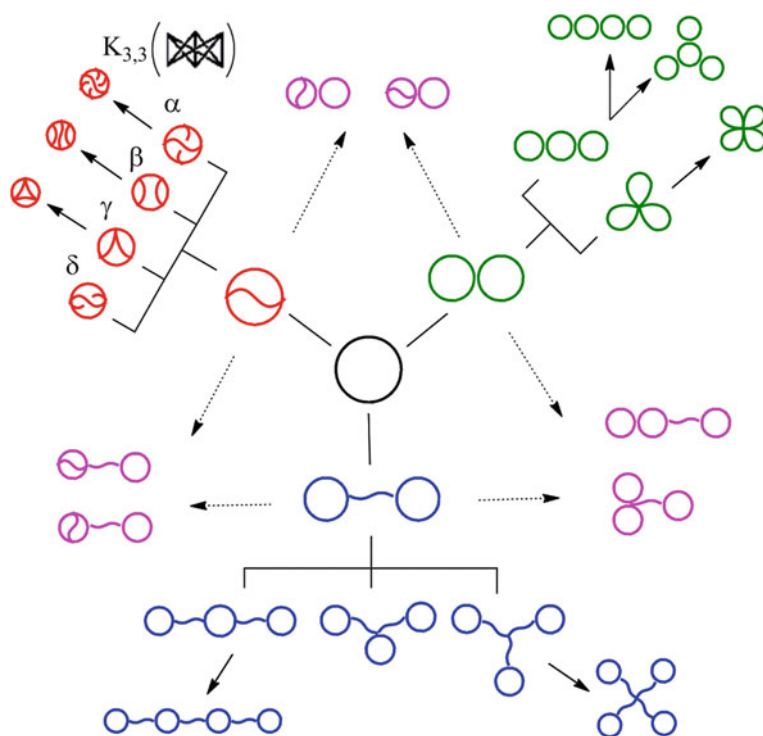
---

Y. Tezuka (✉)  
Tokyo Institute of Technology, Tokyo, Japan  
e-mail: [ytezukak33@gmail.com](mailto:ytezukak33@gmail.com)

by an end-to-end prepolymer linking process or alternatively by a ring-expansion polymerization technique. And remarkable topology effects arisen from their cyclic forms have now been unequivocally demonstrated by making use of diverse cyclic polymers having prescribed chemical structures [4, 5].

Notably, on the other hand, the synthesis of a class of topological polymers comprised of *multiple* cyclic units, i.e., multicyclic polymers, has been a formidable challenge until recently, despite their significant potential to polymer materials designing since the topology of polymer molecules is often a basis to control their properties and functions at static and dynamic states both in bulk and in solution. During recent decades of this century, nevertheless, a remarkable strategy has been introduced for the precision designing of versatile polymer topologies, given in Fig. 6.1 as a *ring family tree*, where mono-, di- and tricyclic forms and selected tetracyclic counterparts are listed hierarchically [6].

Thus, a versatile protocol based on an *electrostatic self-assembly and covalent fixation* (ESA-CF) procedure has been successfully developed to construct nearly all of multicyclic topologies shown in Fig. 6.1 and some others beyond [6]. For the



**Fig. 6.1** A ring family diagram from monocylic, shown in black, to tricyclic and selected tetracyclic constructions, where *spiro*-, *bridged*-, *fused*- and their *hybrid*-constructions are shown in green, in blue, in red and in pink, respectively. Reprinted with permission from [6]. Copyright 2017 American Chemical Society



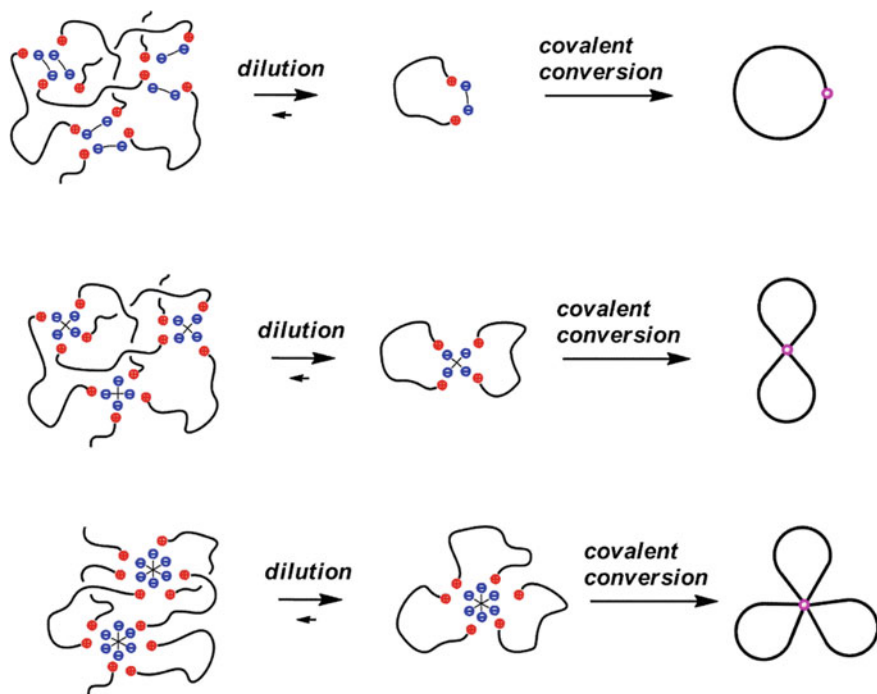
ESA-CF process, a variety of prescribed linear and/or branched telechelic precursors having designated cyclic ammonium salt end groups accompanying pluricarboxylate counteranions has been introduced. Moreover, the ESA-CF protocol has been applied to produce *kyklo*-telechelics, i.e., monocyclic and multicyclic polymer precursors with complementary reactive groups at the prescribed positions in their polymer segment scaffolds. A series of multicyclic polymers having either *spiro*-, *bridged*- and *fused*- and their *hybrid*-forms have subsequently been constructed by the extended ESA-CF protocol in conjunction with alkyne-azide addition (*click*) and olefin metathesis (*clip*) reactions.

## 6.2 Electrostatic Self-assembly and Covalent Fixation by Telechelic Polymers

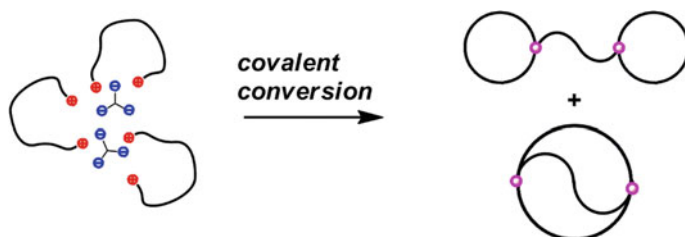
A class of *ionomers*, i.e., hydrophobic polymers modified with a small content of ionic groups, has been employed in practice due to their unique properties both in bulk and in solution [7]. Through the Coulombic interaction between ionic species along hydrophobic polymer backbone, they incline to produce aggregates (self-assembly) in nonpolar organic solutions as well as in bulk. Thus, a class of telechelic polymers possessing ionic groups exclusively located at their chain ends are considered a prototypical model of *ionomers*, in which the location, in addition to the content, of ionic species directs their aggregation/self-assembly behaviors [8]. Notably, they tend to form prescribed self-assemblies under dilution, which consist of a smallest number of polymer precursor units, with balancing the charges of cationic and anionic components. Thus, a linear telechelic precursor possessing two ionic end groups carrying either two monofunctional or one difunctional counterions tends to form, in each case, an electrostatic self-assembly comprising a single polymer component (Fig. 6.2). On the other hand, the relevant self-assemblies with a tetra- and a hexafunctional counterion are apparently comprised of two and three polymer components, respectively, to maintain the smallest number of the polymer units in the self-assemblies by keeping the balance of the charges between the cations and anions (Fig. 6.2).

The ESA-CF procedure has evolved further by taking advantage of the unique feature of equilibrated (temporal) electrostatic polymer self-assemblies formed in nonpolar media. Specifically, the new synthetic process has been introduced by making use of telechelic polymer precursors having moderately strained cyclic onium salt groups, which allows to cause the following covalent conversion reaction to produce eventually robust polymer products of topologically unique architectures (Fig. 6.2) [6, 9].

Interestingly, moreover, an electrostatic self-assembly with a linear difunctional precursor and trifunctional counteranion tend to accommodate the three polymer units and the two tricarboxylate counteranions units to balance the charges between cations and anions. Thus eventually, a pair of polymeric isomers, i.e., a *bridged*-dicyclic, manacle-form and a *fused*-dicyclic,  $\theta$ -form, are produced (Fig. 6.3) [9]. The relevant



**Fig. 6.2** Electrostatic self-assembly and the subsequent covalent conversion products with a telechelic polymer precursor having ionic groups with di-, tetra-, and hexafunctional counteranions. Reprinted with permission from [6]. Copyright 2017 American Chemical Society



**Fig. 6.3** An electrostatic self-assembly and the subsequent covalent conversion products of a manacle- and a  $\theta$ -form isomer pair, with a telechelic polymer precursor having two ionic groups with trifunctional counteranions. Reprinted with permission from [6]. Copyright 2017 American Chemical Society

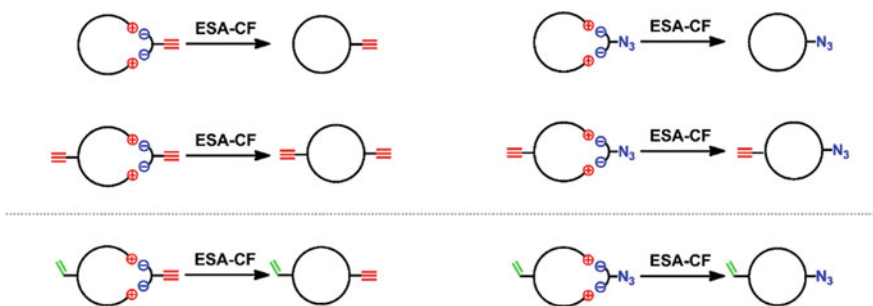
electrostatic self-assembly and thus the isomer pair is produced alternatively by the combination of the two units of a trifunctional star polymer precursor and three units of bifunctional carboxylate counteranions [10].

The covalent conversion of ionic linkages in polymer self-assemblies by the telechelic precursor components has been completed through the nucleophilic ring-opening reaction of cyclic ammonium or sulfonium groups by carboxylate counteranions [3, 6]. The ring-opening reaction of a series of 3-, 4-, and 5-membered cyclic oxonium, sulfonium, and ammonium salts by a class of carboxylates has so far been studied extensively as a basic synthetic route to produce a variety of ether ester, thioether ester, and amino ester compounds [11]. For the ESA-CF protocol, in particular, the 5-membered ring, *N*-phenylpyrrolidinium salt group has been selected purposely for the chain end units of diverse polymers, as it is stable with carboxylate counteranions at ambient condition but the selective and quantitative ring-opening esterification proceeds at an elevated temperature around 70 °C to complete the covalent transformation in practice [9].

### 6.3 Preparation of *kyklo*-Telechelics by the ESA-CF Protocol

A class of *kyklo*-telechelics (a Greek, *kyklos*, means cyclic), referring to monocyclic or multicyclic polymer precursors with reactive groups at the prescribed positions, has been utilized routinely as versatile building blocks to construct complex macromolecular topologies including cyclic segment components [12]. A series of *kyklo*-telechelics have been successfully prepared by means of the ESA-CF method, in which the relevant linear or branched telechelic precursors, having additional functional groups at any prescribed positions within the polymer segment, are subjected to the efficient polymer cyclization with carboxylate counteranion components optionally having designated functional groups. Thus, a range of available *kyklo*-telechelics covers not only simple monocyclic polymer derivatives having one specific or multiple (identical or different) functional groups, including cyclic macromonomers having a polymerizable group, but also tadpole polymers having functional groups at the designated positions within a *ring with a branch* framework, as well as multicyclic polymers having functional groups at the prescribed positions within their loop topologies [3].

In order to adopt, in particular, the alkyne-azide *click* reaction, a series of mono- and difunctional *kyklo*-telechelic precursors having either an alkyne or an azide group, as well as those having either two alkyne groups at the opposite positions, or a pair of an alkyne and an azide group at the opposite positions, have been introduced (Fig. 6.4) [13]. The ESA-CF process has been extended further by making use of a *kentro*-telechelic precursor having *N*-phenylpyrrolidinium salt end groups and having an olefinic group at the center position of the polymer chain, with a dicarboxylate counteranion having either an alkyne or an azide group. Subsequently, a series of *homo*- and *hetero*difunctional *kyklo*-telechelic polymers having an olefinic group in



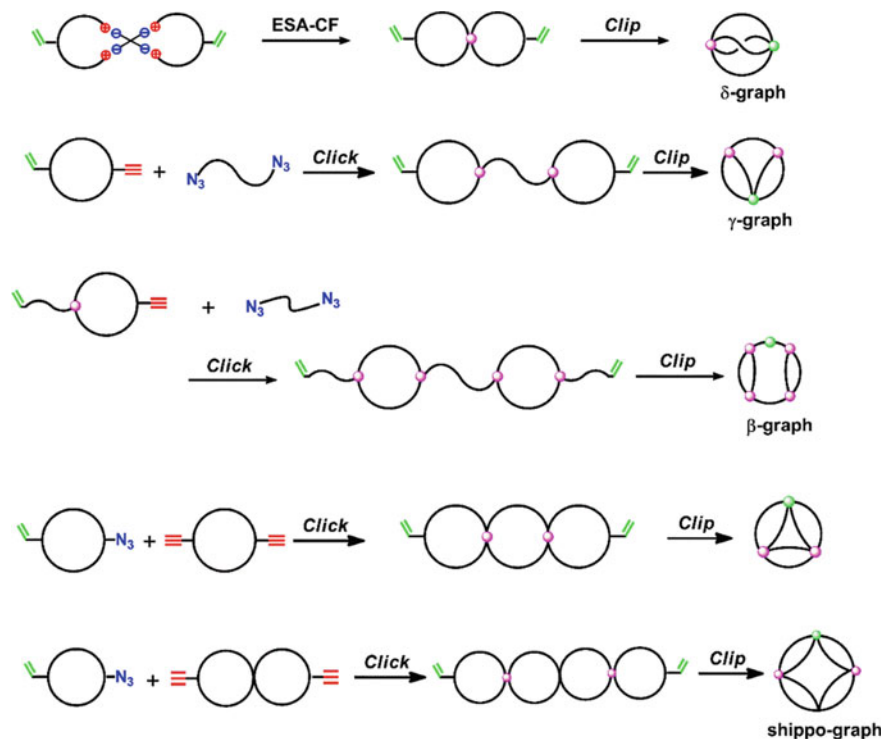
**Fig. 6.4** A series of mono- and difunctional *kyklo*-telechelics of homo- and hetero-functionalities either with alkyne, azide, or olefinic groups obtained through the ESA-CF protocol

addition to an alkyne or an azide group have been introduced [14]. The obtained *kyklo*-telechelic polymers have eventually been employed for the alkyne-azide addition (*click*) and the metathesis condensation (*clip*) reactions, as detailed in the following sections (Fig. 6.4) [6].

## 6.4 Construction of *fused*-Multicyclic Polymer Topologies

A singly *fused* dicyclic,  $\theta$ -form polymer was selectively obtained through the ESA-CF protocol by employing a three-armed, star telechelic precursor carrying a tricarboxylate counteranion [6, 9]. The  $\theta$ -shaped polymer was produced alternatively together with its manacle-form isomer through the relevant ESA-CF process, or by the metathesis *clip* reaction by the relevant precursors having olefinic end groups [3].

The four members of doubly *fused* tricyclic polymer topologies, notated as  $\alpha$ -,  $\beta$ -,  $\gamma$ , and  $\delta$ -graph constructions, are shown in Fig. 6.1. The ESA-CF process has been applied to construct these topological polymers in conjunction with the *click* and *clip* protocols [15, 16]. Thus, a  $\delta$ -graph polymer was synthesized from the relevant 8-shaped polymer precursor having two allyl groups at the opposite positions in the 8-shaped skeletal unit. The ESA-CF process with two units of a *kyklo*-telechelic precursor having an additional allyl group at the center position of the polymer segment and having a tetrafunctional carboxylate counteranion was employed to produce the 8-shaped polymer precursor (Fig. 6.5) [15]. The subsequent metathesis *clip* condensation under dilution in the presence of the Grubbs catalyst afforded the targeted  $\delta$ -graph polymer in good yield (Fig. 6.5) [15]. In addition,  $\gamma$ -graph and  $\beta$ -graph polymers both having the doubly *fused* tricyclic topology were produced from the corresponding *kyklo*-telechelic precursors prepared through the tandem ESA-CF, *click* coupling, and the subsequent olefin metathesis *clip* folding processes (Fig. 6.5) [16]. Thus, a *bridged*-dicyclic (manacle-form) *kyklo*-telechelic precursor



**Fig. 6.5** A series of *fused*-multicyclic polymer graphs constructed through the ESA-CF in conjunction with the *click* and *clip* processes by employing *kyklo*-telechelic precursors having either olefinic, alkyne or azide groups. Reprinted with permission from [6]. Copyright 2017 American Chemical Society

for the former, and another having additional two emanating linear segments for the latter, in which two allyloxy groups were commonly introduced either at the opposite positions of the ring units or at the emanating chain ends, were prepared through the ESA-CF method in conjunction with the *click* process. The  $\gamma$ -graph and  $\beta$ -graph polymer products were subsequently obtained through the intramolecular *clip* reaction under dilution in the presence of the Grubbs catalyst, and were isolated by means of the preparative SEC fractionation technique (Fig. 6.5) [16].

A class of triply *fused* tetracyclic topologies include an unfolded tetrahedron graph, named also as a  $D_4$  graph having a  $p4m$  symmetry (Fig. 6.5) [14]. Another notable member in this class, i.e., the  $K_{3,3}$  graph will be discussed in detail in Chap. 10. As the remarkable extension, moreover, a homologous member of a “shippo” graph, frequently encountered in traditional design arts in Japan, is highlighted in quadruply *fused* pentacyclic topologies [17]. These significant polymer topologies were constructed by exploiting the ESA-CF protocol in conjunction with

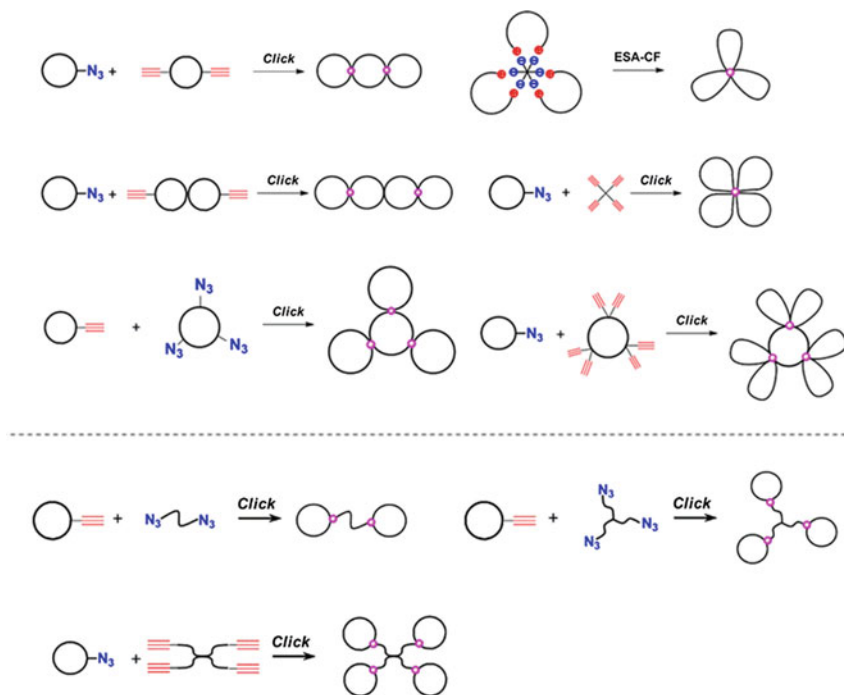
the relevant *click* and *clip* processes (Fig. 6.5) [14, 17]. Specifically, tandemly linked *spiro*-tricyclic and *spiro*-tetracyclic polymer precursors, in which two allyloxy groups are introduced commonly at the opposite positions of the triply cyclic and quadruply cyclic polymer units, respectively, were prepared for the eventual *clip* folding to proceed. And these tricyclic and tetracyclic precursors were produced via the *click* linking between the two units of *hetero*-bifunctional single-cyclic precursor having an allyloxy and an azide group and one unit of either monocyclic or dicyclic *kyklo*-telechelics having two alkyne groups at the opposite positions of cyclic and dicyclic 8-form units, both obtainable by the ESA-CF procedure. The subsequent polymer folding by means of the intramolecular olefin metathesis (*clip*) reaction was conducted under dilution by repeated addition of the Grubbs catalyst, to construct a respective triply *fused* tetracyclic and a quadruply *fused* pentacyclic polymer topology (Fig. 6.5) [14, 17]. These topological polymers were unequivocally characterized by means of  $^1\text{H-NMR}$ , MALDI-TOF mass and SEC techniques, after the isolation with the preparative SEC fractionation [14, 17].

## 6.5 Construction of *spiro*-, *bridged*-, and *hybrid*-Multicyclic Polymer Constructions

As shown previously in Fig. 6.2, a dicyclic *spiro*-form, i.e., 8-shaped, polymer was obtainable directly with the ESA-CF process by employing the two units of linear telechelic precursor accompanying one unit of tetrafunctional carboxylate counteranion. In the relevant manner, a tricyclic *spiro*-form polymer having a trefoil topology was produced with the three units of the linear telechelic precursor carrying one unit of a hexacarboxylate counteranion [9]. Alternatively, a double-metathesis condensation (*clip*) was adopted to prepare the 8-shaped polymer product, in which a four-armed star-shaped prepolymer having allyloxy end groups was employed [18]. In addition, a twin-tailed tadpole polymer precursor having two allyloxy groups at the tail-end positions, as well as a ring polymer precursor having two allyloxy groups at opposite positions in the ring polymer unit, were subjected to the *clip* reaction to give the 8-shaped polymer product [19].

A class of tandem *spiro*-form topologies linking either three or four ring polymer units was constructed through the *click* linking of a complementary pair of *kyklo*-telechelic polymer precursors accessible via the ESA-CF technique, involving one having two alkyne groups at the opposite positions of either the monocyclic or dicyclic 8-shaped unit and another monocyclic counterpart having an azide group [13].

Another class of *spiro*-tetracyclic polymer topology of a quatrefoil form was effectively constructed through the *click* linking of a monocyclic precursor having an azide group, obtained through the ESA-CF process, and a complementary reactive small coupling reagent, such as a pentaerythritol derivative having four alkyne units



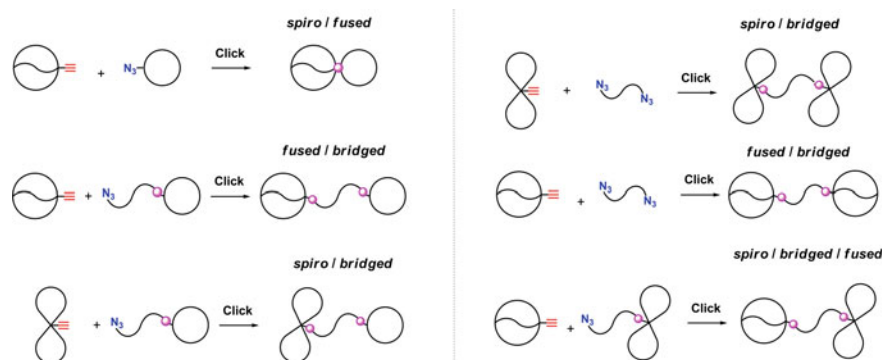
**Fig. 6.6** A series of *spiro*- and *bridged*-multicyclic polymer graphs constructed through the ESA-CF in conjunction with the *click* process by employing *kyklo*-telechelic precursors having either alkyne or azide groups. Adapted with permission from [6]. Copyright 2017 American Chemical Society

(Fig. 6.6) [20]. Moreover, *spiro*-pentacyclic and *spiro*-heptacyclic polymer topologies were constructed by the *click* reaction with *kyklo*-telechelic polymer precursors having multiple azide or alkyne groups, both obtained via an iterative polymer chain extension and the subsequent polymer cyclization also by making use of the *click* reaction (Fig. 6.6) [21].

A *bridged*-dicyclic, manacle-form polymer was obtained together with its  $\theta$ -form isomer through the relevant ESA-CF process, where the polymer self-assembly composed of three units of a linear difunctional polymer precursor carrying two units of trifunctional carboxylate counteranions, or another comprised of two units of a star-shaped trifunctional polymer precursor carrying three units of bifunctional carboxylate counteranions were involved (Fig. 6.3) [3, 9]. On the other hand, the selective construction of a manacle-form polymer was achieved through the *click* coupling of a *kyklo*-telechelic precursor having an alkyne unit, accessible through the ESA-CF protocol, with a difunctional linear precursor having azide groups (Fig. 6.6) [13].

Moreover, the relevant *click* coupling reaction between a star-shaped trifunctional precursor having azide groups with a *kyklo*-telechelic counterpart having an alkyne groups could produce a *bridged*-tricyclic, three-way paddle-form polymer product, as shown in Fig. 6.6 [13]. In the relevant manner, a *bridged*-tetracyclic, quaterefoil-form polymer topology was constructed by the *click* linking of a *kyklo*-telechelic precursor having an azide group with a complementary reactive, four-armed star polymer counterpart having four alkyne end groups [20]. Moreover, a class of topological block copolymers comprised of alternating cyclic/linear or cyclic/star components were obtained by the *click* polyaddition reaction between a difunctional *kyklo*-telechelic precursor having two alkyne groups and either a linear or a star polymer counterpart having azide end groups [13].

A unique class of *hybrid-multicyclic* polymer topologies are included among the tricyclic constructions and beyond as shown in Fig. 6.1, to combine any distinctive constructions from the subclass of dicyclic *spiro*, *bridged*, and *fused* forms. The ESA-CF protocol in conjunction with the *click* polymer linking was again adopted to produce such topologically remarkable polymers by employing a complementary reactive pair of *kyklo*-telechelic polymer precursors having either an alkyne or an azide group at the designated positions (Fig. 6.7) [22, 23]. Thus, an unprecedented *hybrid*-tetracyclic topology combined with all three elementary dicyclic units of  $\theta$ -, 8-, and *manacle*-forms, in addition to a variety of *hybrid*-tricyclic polymer topologies composed of a dicyclic ( $\theta$ - or 8-shaped) and a monocyclic (simple ring or tadpole-shaped) unit, was constructed through the effective *click* linking of complementarily reactive *kyklo*-telechelic precursors (Fig. 6.7) [22, 23]. Furthermore, a tetracyclic and a hexacyclic *spiro/bridged* hybrid polymer topologies, having a double-8 and a double-*trefoil* forms, respectively, were constructed by the alkyne-azide



**Fig. 6.7** A series of *hybrid-multicyclic* polymer graphs constructed through the ESA-CF in conjunction with the *click* process by employing *kyklo*-telechelic precursors having either alkyne or azide groups. Reprinted with permission from [6]. Copyright 2017 American Chemical Society



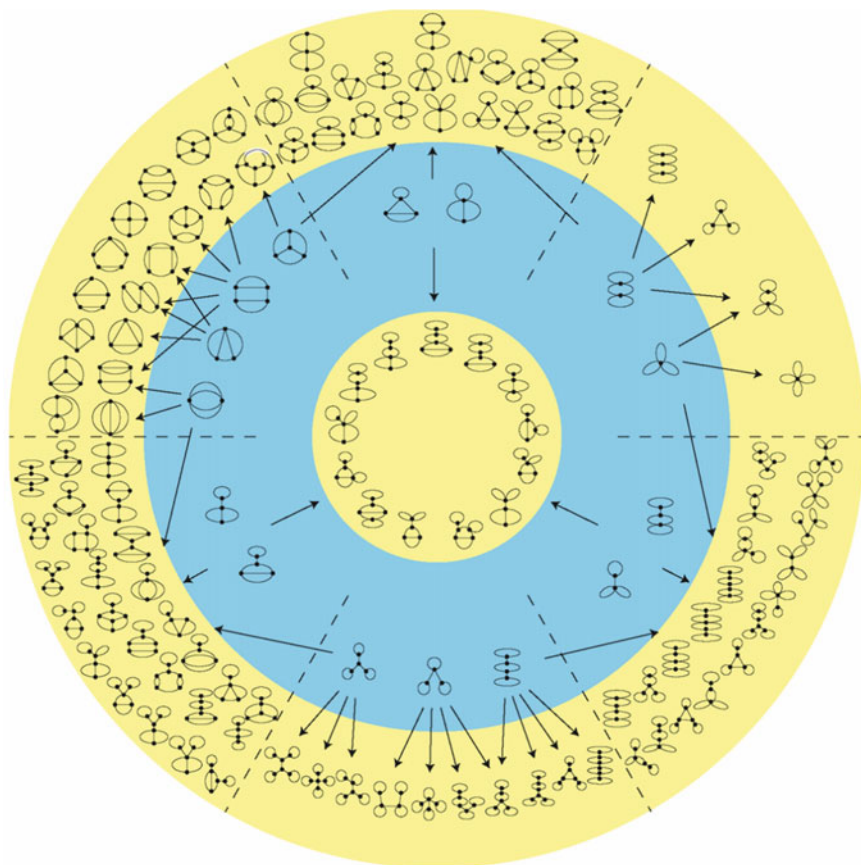
*click* polymer linking between the complementary reactive *kyklo*-telechelic precursors, where the kinetic suppression possibly caused by sterically crowded polymer reagents and by lowered concentration of reactive groups at the polymer chain ends was apparently mitigated [22].

## 6.6 Future Perspectives on the Construction of Complex Polymer Topologies

The ESA-CF protocol has been demonstrated as a versatile means for *topological polymer chemistry*, to afford not only three dicyclic constructions having either 8 (*spiro*), manacle (*bridged*) or  $\theta$  (*fused*) forms, but also a tricyclic trefoil (*spiro*) construction, and beyond [6]. Furthermore, the ESA-CF protocol has been extended in conjunction with tandem *click* and *clip* reactions to construct a variety of complex macromolecular architectures of multicyclic forms, in particular. Those include three doubly *fused* tricyclic ( $\beta$ -,  $\gamma$ -, and  $\delta$ -graph), and a triply *fused* tetracyclic and a quadruply *fused* pentacyclic polymer topology, as well as a series of tri-, tetra- and even hexacyclic *spiro*- and *bridged*-counterparts, and *hybrid*-constructions comprised of three subclasses of *spiro*, *bridged* and *fused*-multicyclic units.

Now, it is joyfully surprising to confirm nearly all polymer topologies listed in Fig. 6.1 have become accessible during the starting decades of this century. The ongoing rapid evolution of *topological polymer chemistry* will push forward further the fascinating exploration of polymer topologies, as the enormously diverse feature of polymer topologies is demonstrated along with the cyclic rank, thus from 15 tricyclic constructions to 111 tetracyclic counterparts, shown totally in Fig. 6.8 [24, 25], and continues further to the higher ranks of the discrete 1076 pentacyclic and as many as 13,870 hexacyclic constructions free of knotting, respectively, according to the mathematical enumeration [2, 26].

Thus, it is tempting to assume that the discipline of polymer science is now entering into an exciting era based on the precision designing of polymer topologies, which is alike a “Cambrian explosion period” experienced in the evolution of life systems at 550 million years ago [24, 25]. Until that time, the forms of most living species were limited and simple, covered by as small as dozens of varieties, but the explosion of diversification followed by an order of magnitude over the following 10 million years, to produce more than 10,000 different categories maintained even today. *Topological polymer chemistry* will certainly contribute to open such a new exciting paradigm in polymer science.



**Fig. 6.8** An extended ring family tree showing 15 tricyclic and 111 tetracyclic constructions. Reprinted from [24], Copyright 2020, with permission from Elsevier

## References

1. E.M. Shekhtman, S.A. Wasserman, N.R. Cozzarelli, M.J. Solomon, *New J. Chem.* **17**, 757 (1993)
2. K. Shimokawa, K. Ishihara, Y. Tezuka, *Topology of Polymers* (Springer, Tokyo, 2020)
3. Y. Tezuka (ed.), *Topological Polymer Chemistry: Progress of cyclic polymers in syntheses, properties and functions* (World Scientific, Singapore, 2013)
4. F.M. Haque, S.M. Grayson, *Nature Chem.* **12**, 433 (2020)
5. T. Yamamoto, Y. Tezuka, *Soft Matter* **11**, 7458 (2015)
6. Y. Tezuka, *Acc. Chem. Res.* **50**, 2661 (2017)
7. A. Eisenberg, J.-S. Kim, *Introduction to Ionomers* (Wiley, New York, 1998)
8. E.J. Goethals, *Telechelic Polymers: Synthesis and Applications* (CRC Press, Boca Raton, 1989)
9. H. Oike, H. Imaizumi, T. Mouri, Y. Yshioka, A. Uchibori, Y. Tezuka, *J. Am. Chem. Soc.* **122**, 9592 (2000)
10. Y. Tezuka, A. Tsuchitani, H. Oike, *Macromol. Rapid Commun.* **25**, 1531 (2004)
11. Y. Tezuka, *Prog. Polym. Sci.* **17**, 471 (1992)

12. H. Oike, S. Kobayashi, T. Mouri, Y. Tezuka, *Macromolecules* **34**, 2742 (2001)
13. N. Sugai, H. Heguri, K. Ohta, Q. Meng, T. Yamamoto, Y. Tezuka, *J. Am. Chem. Soc.* **132**, 14790 (2010)
14. N. Sugai, H. Heguri, T. Yamamoto, Y. Tezuka, *J. Am. Chem. Soc.* **133**, 19694 (2011)
15. Y. Tezuka, K. Fujiyama, *J. Am. Chem. Soc.* **127**, 6266 (2005)
16. M. Igari, H. Heguri, T. Yamamoto, Y. Tezuka, *Macromolecules* **46**, 7303 (2013)
17. H. Heguri, T. Yamamoto, Y. Tezuka, *Angew. Chem., Int. Ed.*, **54**, 8688 (2015)
18. S. Hayashi, K. Adachi, Y. Tezuka, *Polym. J.* **40**, 572 (2008)
19. Y. Tezuka, R. Komiya, M. Washizuka, *Macromolecules* **36**, 12 (2003)
20. Y.S. Ko, T. Yamamoto, Y. Tezuka, *Macromol. Rapid Commun.* **35**, 412 (2014)
21. Md.H. Hossain, Z. Jia, M.J. Monteiro, *Macromolecules* **47**, 4955 (2014)
22. Y. Tomikawa, T. Yamamoto, Y. Tezuka, *Macromolecules* **49**, 4076 (2016)
23. Y. Tomikawa, H. Fukata, Y.S. Ko, T. Yamamoto, Y. Tezuka, *Macromolecules* **47**, 8214 (2014)
24. Y. Tezuka, *React Funct Polym.*, **148**, 104489 (2020)
25. Y. Tezuka, *Isr. J. Chem.* **60**, 67 (2020)
26. T. Haruna, T. Horiyama, K. Shimokawa, *IP SJ SIG Technical Report*, **2017-AL-162**, 1 (2017)

**Part II**  
**Theories and Practices of Polymer Folding**  
**Topologies**

# Chapter 7

## Topological Analysis of Folded Linear Molecular Chains



Anatoly Golovnev and Alireza Mashaghi

**Abstract** The topology of folded linear polymers such as proteins and nucleic acids is a key aspect of their structure. Circuit topology is a mathematically rigorous way of describing the topology of a folded molecular chain and is emerging as the preferred topology framework for modelling biomolecular folds. Here, we discuss the notion of circuit topology and how it can be used to formalize the arrangements of intra-chain contacts and entanglement in a folded linear chain.

### Main Text

Molecular chains possess several levels of structural complexity. The so-called primary structure describes their chemical composition. In case of small molecules, it would be the end of the story. However, properties of long chains cannot be described based on their chemical composition only. Two chemically identical protein chains can have strikingly different biological characteristics, depending on higher levels of structural organization. A molecular chain can form regular local patterns, the so-called secondary structure. In case of proteins, they are alpha-helices and beta-sheets. A global 3D shape of a molecular chain is called the tertiary structure. To attain its tertiary structure, the chain has to fold. Even minor mistakes during folding, i.e., misfolding, can have a severe effect on the chain biological function. In order to function properly, a biological molecule has to take a very specific tertiary structure. However, one cannot speak of the molecule's geometry as such, because the molecule is not rigid and still can change its shape to some extent. The topology of the molecule has to be discussed instead because it can grasp the tertiary structure without being sensitive to irrelevant details of geometry.

In this chapter, we discuss circuit topology, a recently developed approach that is emerging as the preferred topology framework for biomolecular analysis and molecular fold engineering.

---

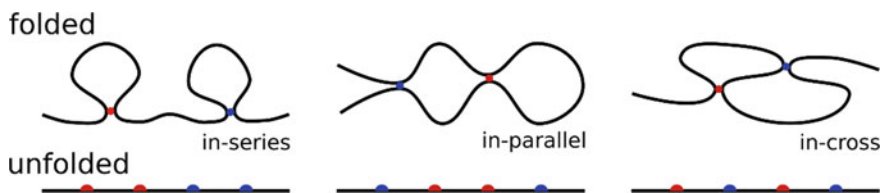
A. Golovnev · A. Mashaghi (✉)  
Faculty of Science, Leiden University, Einsteinweg 55, 2333CC Leiden, The Netherlands  
e-mail: [a.mashaghi.tabari@lacr.leidenuniv.nl](mailto:a.mashaghi.tabari@lacr.leidenuniv.nl)

## 7.1 Circuit Topology of Folded Chains

Linear chains are a commonly used model employed to describe various systems. An obvious example of such a system is proteins which are long rope-like molecules. More broadly, linear polymer molecules, such as natural or synthetic proteins, DNAs and RNAs, are commonly modeled as chains [1]. A less obvious example is an abstract chain where a sequence of events can be formally mapped to a linear chain of sorted objects. One can think of a cascade of chemical reactions where products of one reaction are utilized as reactants in the proceeding reactions. Each reaction is viewed as a link at an abstract chain. However, there could be that products of one reaction participate in several other reactions which occur a way later along the cascade. It offers a shortcut connecting distant segments of the chain. Such shortcuts are called intra-chain contacts. In case of proteins, intra-chain contacts are realized by chemical bonds or interactions (e.g., H-bonds or disulfide bonds) and crucial to ensure protein's structural stability. By connecting different segments of proteins to each other, proteins fold and form the tertiary structure. Circuit topology was first developed in order to describe and categorize intra-chain contacts in linear chains, including folded linear molecular chains.

### 7.1.1 Principles of Circuit Topology

Let us consider the simplest folded chain, i.e., a chain which has one contact. A contact forms a loop composed of a chain segment locked between the contact sites. Altogether, the chain consists of three parts: two tails and one loop. To form a second contact, we may grab one of the tails and connect it to another segment of the chain. There are only three parts of the chain, hence there are only three possibilities shown in Fig. 7.1. The tail can be forwarded to itself, forming two consecutive loops. Or this tail can go to another tail, forming a loop containing the first loop. The last possibility is when the tail connects to the first loop, whereby forming two closely connected loops. These three kinds of arrangements are called in-series (S), in-parallel (P), and in-cross (X), correspondingly, and are the only possible configurations of two loops.



**Fig. 7.1** All possible configurations of two loops. Contacts are depicted with colored balls. Contact sites at unfolded chains are shown with correspondingly colored hemispheres

Note that if we were to form the second loop by manipulating the first loop, not the tail as we did, then we would end up with P and X configurations.

Let us formulate the above construction by using the formal language of set theory [2]. A chain with  $n$  contacts has  $2n$  contact sites counted along the chain starting from one of the chain ends. Let  $C_{ij}$  denote the contact connecting  $i$ th and  $j$ th contact sites, where  $i$  and  $j$  are natural numbers changing from 1 to  $2n$ ,  $i$  not equal  $j$ . The S, P, X configurations are

$$\begin{aligned} \text{Series: } & C_{i,j}\mathbf{S}C_{r,s} \Leftrightarrow [i, j] \cap [r, s] \subset \{i, j, r, s\} \\ \text{Parallel: } & C_{i,j}\mathbf{P}C_{r,s} \Leftrightarrow [i, j] \subset [r, s] \\ \text{Cross: } & C_{i,j}\mathbf{X}C_{r,s} \Leftrightarrow [i, j] \cap [r, s] \notin \{[i, j], [r, s]\} \cup \mathcal{P}(\{i, j, r, s\}) \end{aligned}$$

Mathematically, it means that two intervals,  $i$  to  $j$  and  $r$  to  $s$ , are either not overlapping, or partly overlapping, or one is entirely inside of another.  $\mathcal{P}$  denotes the powerset, i.e., all subsets of a set including the null set ( $\emptyset$ ). Note that the P configuration gives rise to a hierarchy of contacts because one contact is completely within other contacts. When this hierarchy should be specified, it is marked as  $P^{-1}$  configuration.

To formally prove that these and only these three configurations are possible, we show that if two contacts are not in-parallel, then they must be either in-series or in-cross,

$$\begin{aligned} C_{i,j} \sim \mathbf{P}C_{r,s} \wedge C_{r,s} \sim \mathbf{P}C_{i,j} &\Rightarrow [i, j] \not\subset [r, s] \wedge [r, s] \not\subset [i, j] \\ &\Rightarrow [i, j] \cap [r, s] \notin \{[r, s], [i, j]\} \\ [i, j] \cap [r, s] \subset \{i, j, r, s\} &\Rightarrow C_{i,j}\mathbf{S}C_{r,s} \\ [i, j] \cap [r, s] \not\subset \{i, j, r, s\} &\Rightarrow [i, j] \cap [r, s] \notin \{[i, j], [r, s]\} \cup \mathcal{P}(\{i, j, r, s\}) \\ &\Rightarrow C_{i,j}\mathbf{X}C_{r,s} \end{aligned}$$

where  $\sim$  is the logical NOT,  $\wedge$  is the logical AND. The logical OR is denoted by  $\vee$  and will be used below.

Notice that other contacts, the ones apart from  $C_{ij}$  and  $C_{r,s}$ , are irrelevant in this formulation. In over words, a pair-wise consideration of contacts is sufficient. Indeed, if in Fig. 7.1 we form a third contact, i.e., another loop, it will not change the relation between the first two contacts. Therefore, circuit topology considers only pairs of contacts.

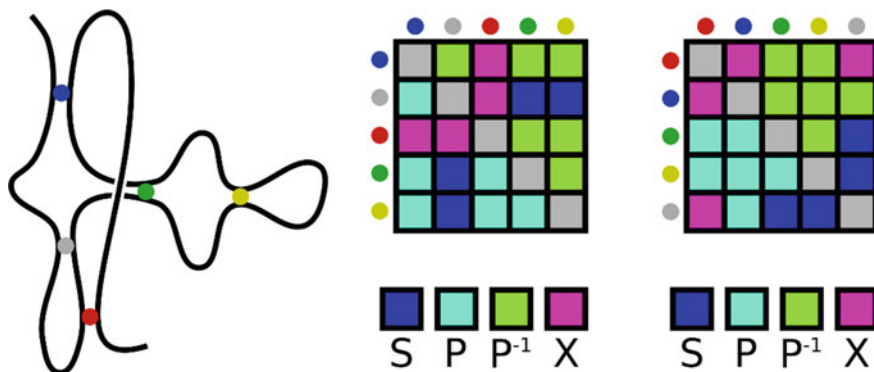
One remark concerning practical applications should be made. In experiments, it is not always possible to distinguish between  $j$ th and  $r$ th contact sites due to limited resolution of the experimental approach. In this case, it is not clear whether the intervals from  $i$  to  $j$  and from  $r$  to  $s$  overlap or separated, i.e., whether the contacts  $C_{ij}$  and  $C_{r,s}$  are in-cross or in-series. Similarly, if external ends of intervals coalesce, i.e.,  $j$  and  $s$  or  $i$  and  $r$ , then it is not clear whether the intervals partially or completely overlap, i.e., whether the contacts  $C_{ij}$  and  $C_{r,s}$  are in-cross or in-parallel. In these situations, one should decide against cross configurations for consistency and, as will

be seen later, for convenience. The corresponding configurations are called concerted series (CS) and concerted parallel (CP). One can then redefine S, P, X relations and include CS and CP as a separate relation from S and P:

$$\begin{aligned}
 C_{i,j}\mathbf{SC}_{r,s} &\Leftrightarrow [i, j] \cap [r, s] = \emptyset \\
 C_{i,j}\mathbf{PC}_{r,s} &\Leftrightarrow [i, j] \subset (r, s) \\
 C_{i,j}\mathbf{XC}_{r,s} &\Leftrightarrow [i, j] \cap [r, s] \notin \{[i, j], [r, s]\} \cup \mathcal{P}(\{i, j, r, s\}) \\
 C_{i,j}\mathbf{CSC}_{r,s} &\Leftrightarrow (([i, j] \cap [r, s] = \{i\}) \vee ([i, j] \cap [r, s] = \{j\})) \\
 C_{i,j}\mathbf{CPC}_{r,s} &\Leftrightarrow (([i, j] \subset [r, s]) \wedge (i = r \vee j = s))
 \end{aligned}$$

### 7.1.2 Topology Rules and Their Inference

Since circuit topology considers all pairs of contacts occurring on a linear chain, one should find a convenient way to write it down and visualize. It can be done by a CT matrix, where CT stands for Circuit Topology. Let us consider an example from Fig. 7.2 which shows a model of a hammerhead ribosome. Its intra-chain contacts are color coded. Each row and column of the CT matrix correspond to a contact, while each cell color codes the kind of relation between the chosen contacts. By definition, a CT matrix is symmetric (up to P vs.  $P^{-1}$  relations). The contacts, and hence the rows and columns, are listed in the sequence they appear along the chain while following the chain from one end to another. Since each chain has two ends, there are two directions along the chain (forth and back), and hence there could be two CT matrices describing the same chain. However, they are not independent and biomolecules usually possess directionality which specifies the choice of the CT matrix.



**Fig. 7.2** A schematic of a hammerhead ribozyme and its two CT matrices with contact numeration performed in both directions



**Table 7.1** Properties of P, S, and X relations, when any given contact site contributes to one contact only, and thus no two contacts share a contact site

Relation	Reflexive	Symmetric	Transitive
In-series (S)	No	Yes	No
In-parallel (P)	Yes	No	Yes
In-cross (X)	No	Yes	No

Another property of a CT matrix to keep in mind is that not all combinations of colors of cells allowed by combinatorics are allowed by circuit topology. In other words, not every symmetric matrix can be a CT matrix. It arises from the properties of topological relations summarized in Table 7.1. For instance, in the example with a hammerhead ribosome, the green contact is  $P^{-1}$  relation to the yellow contact, and P relation to the blue contact. Hence, the blue contact must be  $P^{-1}$  relation to the yellow contact. In this context, the concerted relations, CS and CP, can be viewed as a specific case of S and P relations, following the same symmetry rules as in Table 7.1, though without preserving the attribute of concertedness (e.g., 3 contacts can all be in S relation, but not in CS relation).

So far, our narration of circuit topology has been quite descriptive, while any theory should bear a predictive power. So, is it potentially useful to proceed developing this theory? It turned out that protein circuit topology is a very good predictor of protein folding rate [1]. Furthermore, topology of a protein may inform on its function. Let us consider two proteins: alpha enolase and gamma crystallin D. They perform a similar biological function, however have a negligible sequence overlap and structural similarity [1]. What makes these two very different proteins so similar in function? Circuit topology analysis shows that the two are very similar topologically, namely the fractions of S, P, X configurations are nearly matching. Several other examples show the same trend. One can speculate that topological similarity is related to functional similarity. In fact, the problem of the relation of protein spatial structure, or protein shape, to protein function is very old. Protein topology should be able to reflect the relevant characteristics of a spatial structure and relate them to a protein function.

### 7.1.3 Coding Circuit Topology

Though a CT matrix contains all the information about a topological arrangement of intra-chain contacts and appears as a convenient visualization tool, it might not be an optimal representation of CT for calculations or particular applications. Here, we will introduce two other ways of presenting, or coding, topological properties of folded linear chains. They all contain the same information and one can always translate one to another. However, different representations are fit for different tasks.

A CT matrix lists intra-chain contacts as rows and columns of the matrix. A so-called connectivity matrix lists contact sites in the same manner. Connectivity matrix elements are either 0 or 1, signifying whether contact sites are connected or not. In

case of two contacts S, P, and X relations, connectivity matrices are

$$S = \begin{pmatrix} 0 & 1 & 0 & 0 \\ 1 & 0 & 0 & 0 \\ 0 & 0 & 0 & 1 \\ 0 & 0 & 1 & 0 \end{pmatrix}; \quad P = \begin{pmatrix} 0 & 0 & 0 & 1 \\ 0 & 0 & 1 & 0 \\ 0 & 1 & 0 & 1 \\ 1 & 0 & 0 & 0 \end{pmatrix}; \quad X = \begin{pmatrix} 0 & 0 & 1 & 0 \\ 0 & 0 & 0 & 1 \\ 1 & 0 & 0 & 0 \\ 0 & 1 & 0 & 0 \end{pmatrix}$$

This connectivity matrix representation is a convenient algebraic description of common molecular operations such as formation and elimination of contacts, or merging of molecules. The operations can be viewed as linear matrix operators acting on the connectivity matrix [3].

Another way to code the information contained in a CT matrix is the string notation, where contact sites are listed as a string of letters [4]. Each contact is given a name, for example, “contact A” or “contact color-coded green”, etc. Contact names appear on the string each time we encounter this contact site while scanning along the chain. A chain with only one contact looks like AA. Series, parallel, and cross configurations are AABB, ABBA, and ABAB, see unfolded chains in Fig. 7.1. Notice that these three are the only possible permutations of two letters, up to the choice of contact names (AABB and BBAA are considered equivalent). It is another proof that only these three configurations are possible. Though very simple, this proof formally employs combinatorics. It highlights one of the advantages of this notation which allows one to implement combinatorial analysis on topological properties of a linear chain.

In the string notation, sites of concerted contacts are marked with parenthesis; A(AB)B for concerted series and AB(BA), or (AB)BA, for concerted parallel.

## 7.2 Generalized Circuit Topology

There are two important parameters defining a spatial structure of folded linear chains such as proteins: intra-chain contacts discussed above, and chain entanglement owing to chain impenetrability. Both parameters restrict the motion of the chain segments. Entanglement is conventionally described by means of knot theory which is a very powerful mathematical approach. On the other hand, it might be convenient to be able to describe intra-chain contacts and entanglement in a similar manner via the same approach and mathematical apparatus because, after all, they both lead to the same effect of restriction of motion of a molecular chain. Circuit topology in its generalized form offers such a possibility. The core idea is to code a chain entanglement in terms of some basic structural units called contacts. If these fictitious contacts resemble in some way actual intra-chain contacts, then entanglement can be treated by circuit topology. To make a clear distinction between intra-chain contacts and fictitious contacts describing entanglement, the former will be called hard contacts or h-contacts, while the latter is called soft contacts or s-contacts. Hard means that

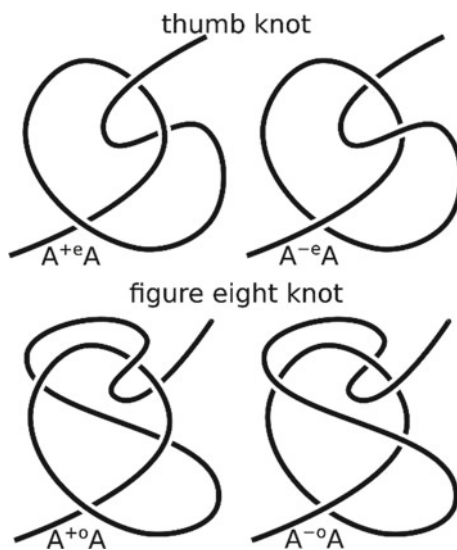
contact sites are fixed and cannot be changed, while soft highlights the ability of an entangled chain to move, not completely free but to some extent.

### 7.2.1 Entanglement Expressed via Soft Contacts

Due to thermal fluctuations, an entangled chain is not completely immobilized; yet one may identify simple but steady structures which cannot be untied easily. Strictly speaking, if a chain has been intertwined and twisted into a messy blob, it can always be untied by reversing all the moves, implying that no knotted structure is absolutely stable. However, such a reversion might be very complicated and unlikely to occur on its own on realistic timescales. We are looking for such meta-stable structures. A simple loop, which is one twist of a chain, is not stable at all. However, if a chain is threaded through a loop, the resulting structure gains a lot in stability. A loop can be threaded in only two directions, either up or down, see Fig. 7.3, which lead to thumb knot or to figure eight knot, correspondingly. These two knots are the simplest, most basic structures we are looking for. They are s-contacts.

Let us formalize and count s-contacts [4]. Loops can be either positive or negative, according to the sign of the crossing which appears due to the loop formation. This property is called chirality. The sign is defined by the right-hand rule, i.e., if the chain at the crossing shifts as a helix of a right-hand screw, then the loop is positive, otherwise negative. If the chain threads the loop in the direction the chain shifts at the crossing, such s-contact is called even. If the chain threads the loop in another direction, the resulting s-contact is called odd. Hence, there are 4 s-contacts:  $A^{+e}A$ ,  $A^{+o}A$ ,  $A^{-o}A$ ,  $A^{-e}A$ —positive even, positive odd, negative odd, negative even. Note that these are

Fig. 7.3 A list of s-contacts



3D structures. Crossings appear only when we draw them as 2D projections, while the above definition is 3D.

Let us consider  $A^{+e}A$ . Its string notation is similar to that of h-contacts, though the kind of s-contact (“+e”) has to be specified. S-contacts are symmetric, i.e., they look the same regardless in which direction we move along the chain. Indeed, while threading the chain through the loop, we form another loop, see Fig. 7.3. In other words, each s-contact consists of two interlocking loops. One can show that their chirality must coincide. Hence, s-contacts, as well as h-contacts, are topologically symmetric (except for concerted parallel contacts). The notation  $A^{+e}A$  implies that this s-contact has two contact sites. Its sites are located where the chain is circled by the loop while threading through this loop. These locations are not exact and will change whenever the chain is deformed. Therefore, s-contacts are called “soft”. This softness is important for grasping topological properties of the chain, while ignoring the exact positions of each segment of the chain. This is quite typical in statistical physics, when we have to lose excessive information (exact segment positions) in order to gain clarity on the remaining, relevant information (topological properties).

## 7.2.2 Beyond Soft Contacts: Completeness of Generalized Circuit Topology

One of the basic ideas of circuit topology is that a restriction of motion of the chain is described via the notion of contacts, be they due to chemical bonds or chain entanglement. Above, we considered these two effects separately. Now, we will consider them simultaneously. Figure 7.4 shows a chain with h-contacts which give rise to two loops. However, the loops are interlocked, which poses additional restrictions on a chain motion. This interlocking does not lead to a formation of s-contacts, which can be easily visualized by breaking the h-contacts and making sure that the chain will untie. Thus, there is a sort of entanglement but a complete s-contact is not formed. In such cases, subscripts are used, which can be viewed as a half of s-contact. The string notation of this chain is  $A_B A B_A B$ . Indeed, if we scan the

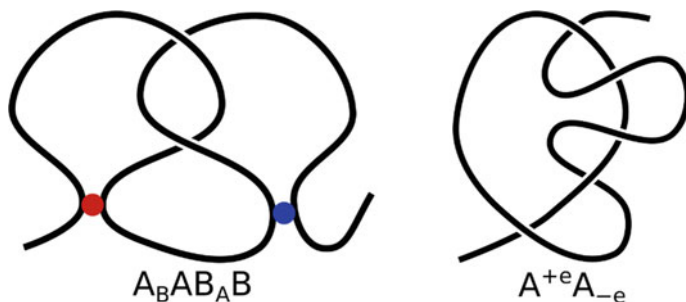


Fig. 7.4 Entanglement of h-contacts (left panel) and slipknots (right panel)

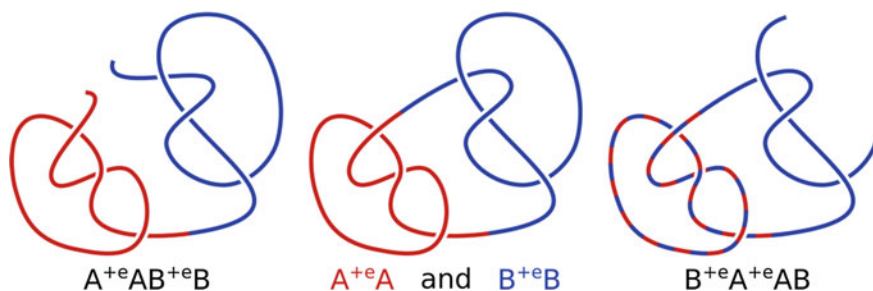
chain from one end to another, first we pass at contact A, then we go through the loop due to contact B, which is marked as a subscript on the string, then we pass at contact A again, then we have the same experience with contact B. Circuit topology states that h-contacts, s-contacts, and subscripts all together can describe any interplay of chain entanglement and intra-chain contacts.

An important case occurs when the chain passes through an s-contact. Normally, it would simply lead to a formation of another s-contact in-cross with the first one. But in the case shown in Fig. 7.4 it does not. Indeed, if we pull the ends of the chain, it will untie, so this configuration is unstable. Its string is  $A^{+e}A_{-e}$  which is a code for a slip-knot. The sign in the subscript is needed because s-contacts (unlike h-contacts) have chirality. Slip-knots are common in proteins. They are less stable than s-contacts along, but still significantly stable. As we mentioned above, circuit topology has a hierarchy of stability and is able to deal with such meta-stable conformations.

### 7.2.3 Circuit Topology and Knot Theory

Circuit topology was originally designed to describe intra-chain contacts. Generalized circuit topology extended to the territory of knot theory which has been for a long time successfully employed to describe entanglement [5]. What extra information can circuit topology bring to the table? Mathematical knots are different from the knots as we understand them in everyday life. Mathematical knots are closed structures. To turn a tangled chain into a knot, one has to merge its ends together. It leads to an issue of a non-unique representation. Figure 7.5 shows two very different chains which correspond to the same mathematical knot and hence are identical in terms of knot theory. Yet, these chains are distinguished between in terms of circuit topology. Namely, they are in-series and in-parallel configurations of two s-contacts.

An important element of folded molecular chains which is typically not included in knot theoretic analysis are the h-contacts. This is a major strength of circuit topology. Recently, knot theory has been extended to include h-contacts seen in biomolecules.



**Fig. 7.5** Two folded chains with distinct circuit topology (right and left) give rise to identical knot representations (middle)

To do this, knot theory was extended to singular knot theory, in which h-contacts appear as singularities [6]. Reidemeister move set has also been extended to allow features present in folded molecular chains, including h-contacts. In this knot theoretic framework, projections of 3D folded chains are represented using Gauss codes, or strings of numbers and letters. Algebraic structure of quandles can then be used to distinguish the topologies of folded chains. However, the approach is limited in resolution as compared to circuit topology and apparently distinct topologies may end up having the same number of quandle colorings.

### 7.2.4 *Circuit Topology and Network Topology*

A complementary approach to circuit topology in describing the topology of folded chains comes from graph theory [7]. A folded molecular chain can be considered as a spatial graph, where chain segments are the nodes and the graph edges represent the connections between different segments. Such connections appear when the distance between the chain atoms does not exceed a certain cutoff radius. Thereby, spatial graphs account for intra-chain contacts. This can be visualized in the form of a contact map, where nodes are left in the 3D positions of the corresponding chain segments, or as a wheel diagram, where the 3D coordinates are not retained but the nodes are placed in a circle.

This approach allows one to utilize some statistical descriptions applicable to graphs. The most prominent ones are the shortest path between two random nodes, the average path length, the clustering coefficient [8]. They are helpful for understanding the interactions within molecular chains and the topology of a folded chain. We note that folded chains with distinct circuit topologies may have identical average path length, and identical clustering coefficient, thus the resolving power of network topology is limited [2].

## References

1. B. Scalvini, V. Sheikhhassani, J. Woodard, J. Aupic, R.T. Dame, R. Jerala, A. Mashaghi, *Trends Chem.* **2**(7), 609–622 (2020)
2. A. Mashaghi, R.J. van Wijk, S.J. Tans, *Structure* **22**, 1227–1237 (2014)
3. O. Schullian, J. Woodard, A. Tirandaz, A. Mashaghi, *Front. Phys.* **8**, 5–15 (2020)
4. A. Golovnev, A. Mashaghi, *iScience* **23**, 101492 (2020)
5. E. Flapan, A. He, H. Wong, *PNAS* **116**(19), 9360–9369 (2019)
6. C. Adams, J. Devadoss, M. Elhamedi, A. Mashaghi, *J. Math. Chem.* **58**, 1711–1736 (2020)
7. S.K. Verovšek, A. Mashaghi, *Front. Appl. Math. Stat.*, **31**(2), 6 (2016)
8. L. Paola, M. Ruvo, P. Paci, D. Santoni, A. Giuliani, *Chem. Rev.* **113**, 1598–1613 (2013)

# Chapter 8

## DNA Knots



Cristian Micheletti

**Abstract** Knotting is statistically inevitable in long polymer chains, especially under spatial confinement, and tightly packed genomic DNA filaments are no exception. Over several decades, ever more powerful experimental techniques have demonstrated the occurrence of knots and other forms of entanglements in DNA extracted from viruses, bacteria, and eukaryotes. The data have in turn prompted a broad range of theoretical and computational studies of the abundance and complexity of DNA knots, and especially: (i) how it depends on the length and degree of confinement of the filaments (ii) whether it can be used to infer the multiscale spatial organization of genomic DNA, and (iii) its impact on biological processes in vivo. Here, we present an overview and a personal perspective of such theoretical and experimental efforts, from the equilibrium knotting of DNA in bulk to the one observed in various organisms, and concluding with a comparison with RNAs and their entanglement properties.

### 8.1 Introduction

We are all familiar with the inconveniences posed by knots and other entanglements that arise in long cables that have been carelessly stored away.

We also know how challenging it is to arrange a ribbon or a rope in a desired knotted shape for decorative or functional purposes, a task for which we usually necessitate step-by-step guidance from a good knot book [1].

Our intricate relationship with macroscopic knots occurs between these two extremes: preventing or fighting against the statistical incidence of knots and creating or designing knots for specific functions.

A similar balancing act is continuously taking place at a molecular level in all organisms, from viruses to bacterial and eukaryotic cells, where active (enzyme

---

C. Micheletti (✉)  
SISSA, Via Bonomea 265, 34136 Trieste, Italy  
e-mail: [michelet@sisssa.it](mailto:michelet@sisssa.it)

mediated) and passive (physics mediated) mechanisms control the entanglement of different types of biopolymers in vivo.

Nucleic acid filaments offer, perhaps, the best illustration of biomolecular entanglement. In all organisms, genomic DNA filaments are confined in regions much smaller than their contour length, a situation that already makes them prone to spontaneous entanglement. In addition to this, the incessant DNA processing during transcription, replication, and recombination accumulates DNA entanglements that can be lethal for the cell and, thus, must be efficiently removed by specialized enzymes [2–4].

At the other extreme we have RNAs, where no physical knots have been discovered yet [5, 6]. Unlike double-stranded DNA, which can be often modelled as a fluctuating filament, naturally occurring RNAs have definite folds that, though physically unknotted, can still be intricate. In this case, too, RNA entanglement appears to be instrumental for specific biological functions, such as inducing ribosomal frameshifting [7–10] or stalling the action of degrading enzymes [11–17].

Our understanding of these manifestations of physical entanglement in nucleic acids has increased immensely in recent years, thanks to parallel theoretical and experimental advancements [18–21]. Thanks to these interdisciplinary and still ongoing efforts we have gained much insight into the general mechanisms that control knot abundance, size, and complexity in these biomolecules, and clarified the functional implications, too.

Here, we present an overview and personal perspective of such theoretical and experimental findings starting from DNA knotting in bulk, then moving to the knotting of genomic DNA in various organisms, and finally discussing on RNA entanglement.

## 8.2 Spontaneous Knotting of DNA in Solution

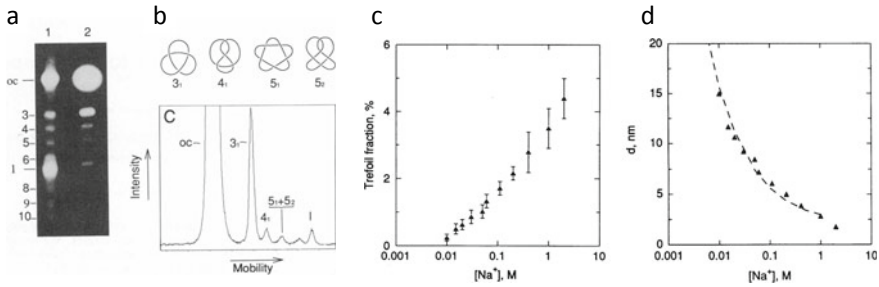
### 8.2.1 *Experimental Results*

A natural starting point is the entanglement of DNA filaments that fluctuate freely in solution. A landmark study was carried out by Rybenkov et al. who considered 10kb-long DNA filaments from P4 viral particles [22]. The DNA of these bacteriophages is double-stranded except for the two termini, which are single-stranded and have complementary sequences. Thus, when the two termini come in contact, they can anneal and turn the DNA from linear to circular.

Such stochastic cyclization events make it possible to turn the transient physical entanglement of fluctuating linear DNA filaments into proper knotted states of the circularized DNA [23].

The abundance and complexity of knots in cyclized DNA were then established using gel electrophoresis. The gel matrix constitutes an array of obstacles that the DNA rings have to negotiate when drawn through the gel by an electric field. The





**Fig. 8.1** **a, b** Gel-electrophoretic separation of DNA knots. **c** Fraction of cyclized DNA rings with trefoil knot topology as a function of the concentration of monovalent counterions in solution. **d** Effective DNA diameter, theoretical-inferred from the observed knotting probability, as a function of counterion concentration. Reproduced with permission from Ref. [22]. Copyright (1993) National Academy of Sciences, U.S.A

DNA rings' capability to slide through or past the obstacles depends on their topological state [24–28]. Accordingly, DNA rings with different knot types acquire different electrophoretic velocities and form distinct gel bands. The bands' intensities can then be used to quantify the relative abundance of the various types of knots; see Fig. 8.1a, b. Similar electrophoretic principles are conventionally used to separate DNA molecules by length or degree of supercoiling, as these properties too are coupled to gel mobility [29]. For this reason, electrophoretic topological profiling requires DNA rings to be of the same length and free of torsional stress, which is the case for the doubly nicked P4 DNA rings.

Using this technique, Rybenkov et al. were able to profile the type and abundance of DNA knots at different monovalent salt concentrations [22]. At these chain lengths, the most abundant type of non-trivial knots is the trefoil one, whose incidence as a function of the solution ionic strength is shown in Fig. 8.1c.

Two notable features emerge from the experimental results. First, the knot spectrum is dominated by trefoil knots, the simplest knot type, with only traces of more complex topologies. Second, the unknotting probability, which is the probability of unknotted DNA rings, decreases rapidly with the solution's ionic strength.

### 8.2.2 Theoretical Modelling and Interpretation

The results can be qualitatively rationalized in terms of the electrostatic screening operated by dissolved counterions.

Salt concentration controls both the effective DNA charge density via counterion condensation and the Debye screening length. To a first approximation, the DNA screened self-repulsion can be treated as an effective increase in DNA diameter. By increasing the solution's ionic strength, the Debye screening length and hence the

effective DNA thickness decrease. Because the DNA contour length is unchanged, a diameter reduction induces an enhanced knotting probability.

These qualitative considerations were turned into quantitative ones using stochastic simulations on a coarse-grained DNA model [22]. Circularized P4 DNA rings were modelled as a semi-flexible ring of cylinders of length  $l$  and diameter  $\Delta$ . The cylinders' length was set to be  $l = 10$  nm, a fraction of the nominal DNA persistence length  $l_p \sim 50$  nm. The latter was accounted for by a bending energy term for consecutive (hinged) cylinders. At the same time, excluded volume interactions were enforced by preventing non-consecutive cylinders from overlapping.

A Monte Carlo scheme was next employed to sample the equilibrium ensemble of the model rings. The Monte Carlo evolution involved the use of crankshaft moves to rotate a portion of the rings. The moves do not disconnect the chain but can alter the ring topology. The two conformations before and after the move must be self-avoiding to be part of the Monte Carlo trajectory. However, the continuous deformation bridging the two states can still involve “unphysical crossings” of the cylinders. The Monte Carlo evolution can, thus, introduce or remove knots, which can be detected by computing topological invariants.

The ensemble generated by such Monte Carlo scheme is often referred to as “topologically unrestricted ensemble”, and sampled conformations are expectedly equivalent to those obtained by circularisation in equilibrium.

The Monte Carlo sampling of this ensemble was used to reproduce and interpret the experimental knotting data from P4 cyclization [22]. Specifically, the topological spectrum was computed by keeping fixed the contour and persistence length of the model DNA rings and varying the cylinders' diameter. Finally, for each ionic strength condition, it was determined which diameter gave the best match between the computed and experimental knot spectra.

This strategy allowed for inferring the effective thickness of DNA from experimental data on equilibrium knotting probabilities; see Fig. 8.1d. The recovered functional dependence of DNA diameter on salt concentration was in good agreement with polyelectrolytes theory. The results confirm a posteriori the theoretical framework's viability to correctly reproduce the physical properties of fluctuating DNA filaments, knotting included.

To summarize, the seminal study of Rybenkov et al. allowed for establishing the following results and concepts.

First, fluctuating filaments of dsDNA even as short as 10kb can present detectable levels of spontaneous knotting. Second, these knots were detected after being trapped by DNA circularization, but clearly, they pre-existed as “physical knots”, or knots in open chains. Third, the experimental DNA knotting probability and topological spectrum are well accounted for by coarse-grained models, making them an essential ally to experiments. Modelling and simulations can provide quantitative physical interpretations of experimental data. When used predictively, they can help design or pre-condition experimental setups and discover emergent phenomena verifiable in the lab.

The coarse-grained model used in Ref. [22] has provided the bases for many later studies. Its physical appeal rests in the fact that it is informed by three physical length scales only. These are the DNA thickness, persistence length, and contour

length. In fact, we note the choice of the cylinders' length is immaterial as long as it is sufficiently smaller than the persistence length [22]. Thus, it is presently more common to use chains of beads in place of chains of cylinders.

The interplay of all these lengthscales and their effect on knotting has been systematically addressed in a large number of studies where contour length [30–34], chain diameter [35–37], and persistence length [38–41] were systematically varied. Though we still lack a general theory of polymer entanglement, these length scales are recognized as central to knotting and are used in scaling approaches for recapitulating knotting properties across various contexts and models [42, 43].

## 8.3 Native Knotting of Genomic DNA

### 8.3.1 *Viral DNA*

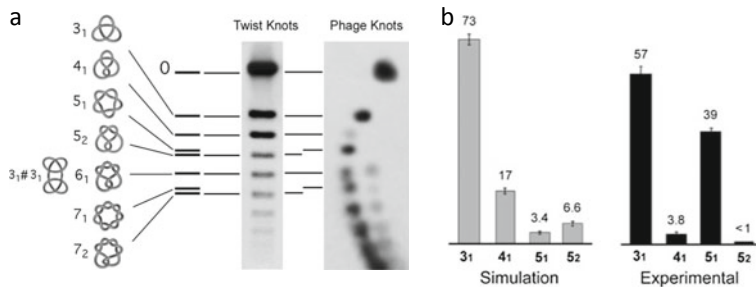
The sizeable knotting found in the 10kb-long P4 genome in solution prompts the question of how much more entangled the same viral DNA filaments can become inside the P4 capsid, where it is stored at high packing densities.

This point was quantitatively addressed by Roca et al. in a series of experiments on P4 mutants [44–46]. Unlike the wild-type P4, where one of the DNA ends is secured to the virus tail, the genome of these mutants is fully loaded inside the capsid. As in the bulk experiments of Rybenkov et al., the annealing of the two ends can, thus, trap any entanglement of the packaged DNA as proper knotted states of the cyclized genome [44]. The circularized DNA extracted from an ensemble of viral particles can then be topologically profiled using gel electrophoresis.

The resulting topological spectrum highlighted three main features. First, the extracted DNA was knotted in more than 95% of the cases [44]. Second, the spectrum contained knots with large crossing numbers, a standard measure of knot complexity [44]. Finally, torus knots were significantly over-represented in the topological spectrum [45]; see Fig. 8.2.

These features provide important clues about the organization of DNA inside viral particles. The varied topological spectrum, covering different knot types, directly proves that DNA packing inside viral capsids is structurally heterogeneous. Instead, the over-representation of torus knots in the spectrum indicates an overall spool-like arrangement of the packed DNA.

Above all, the pervasive amount of knotting was particularly surprising and also perplexing considering the expected obstacle it could pose to viral genome delivery. In fact, it posed a conundrum: how is it possible that the knotted DNA can be ejected through the exit channel that is too narrow to allow for the simultaneous occupation by multiple DNA strands [47, 48]?



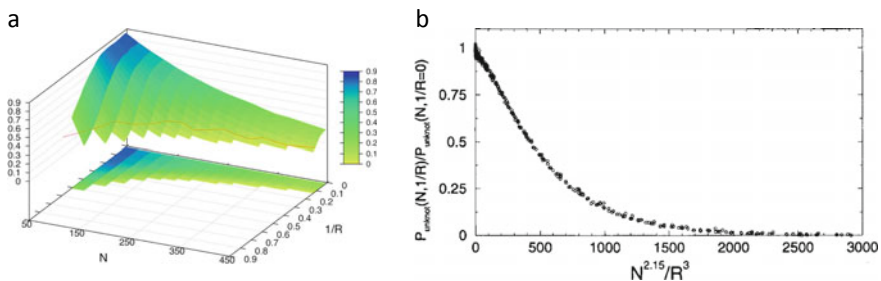
**Fig. 8.2** **a** Gel-electrophoretic separation of different knot types established by 10kb-long DNA inside P4 viral capsid. **b** Comparison of the relative (percentage) incidence of the four simplest knot types in experiments and in a general model of confined polymer. The DNA bias towards forming torus knots inside capsids is apparent from experimental data. Reproduced with permission from Ref. [45]. Copyright (2005) National Academy of Sciences, U.S.A

### 8.3.2 Theoretical Modelling and Interpretation

Coarse-grained models have proved very valuable to gain insight in all the above aspects [48, 49] and helped unveil the surprising physical mechanisms underpinning them.

From a qualitative point of view, the high overall incidence of viral DNA knotting is well accounted for by the high level of confinement. Various studies have addressed the knotting of equilibrated rings in three-dimensional confinement with molecular dynamics and the Monte Carlo simulations.

The first such study was arguably carried out by Michels and Wiegel, who profiled the knot spectrum of infinitely thin and fully flexible equilateral rings inside spherical cavities and observed that the knotting probability increased rapidly with the packing fraction [51]. More precisely, the incidence of unknots, that is, of rings with the trivial



**Fig. 8.3** **a** Manifold of the unknotting probability inside spheres of radius  $R$ . Data are for rings of  $50 \leq N \leq 450$  edges. **b** The same data points collapse on a single curve when plotted as a function of  $N^{2.15}/R^3$ . Reproduced with permission from Ref. [50]

(unknotted) circular topology, was not controlled by the mere packing density,  $N/R^3$ , but by a different scaling parameter,  $N^\alpha/R^3$  with  $\alpha \sim 2.2$  [50, 52]; see Fig. 8.3.

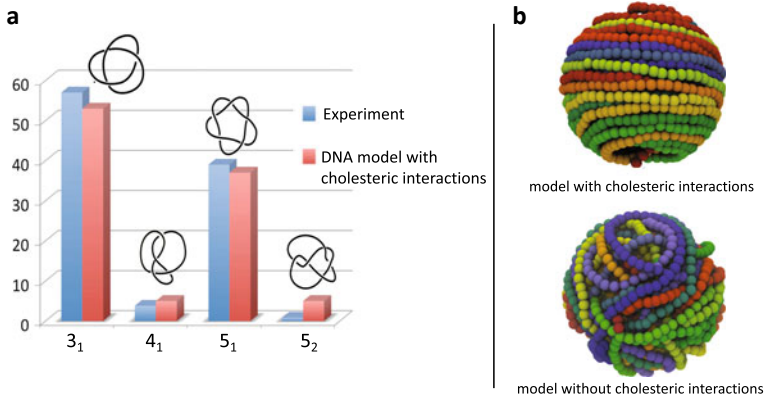
These results, thus, help rationalize the overall high abundance of knots found inside viral capsids, as fully flexible equilateral rings can be taken as a crude model of circularized DNA, with the bond length corresponding to the Kuhn length. Incidentally, we note that thermal fluctuations that establish canonical equilibrium are essential to introduce knotting in the confined rings. In fact, DNA packing models at zero temperature, i.e. energy-minimizing configurations, yield ordered spools that are virtually knot-free [53].

Though the overall high incidence of DNA knots is accounted for by general models of confined polymers [50, 54], the same models fail to reproduce the key features of the knot spectrum, such as the characteristic over-representation of torus knots.

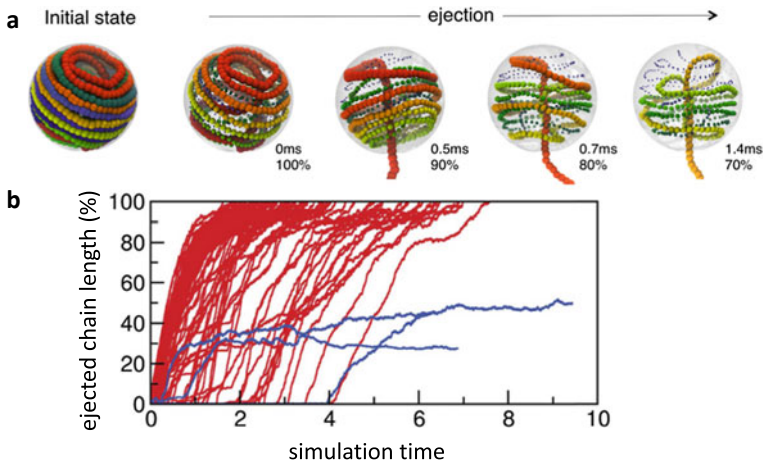
This is well illustrated by the relative abundance of  $5_1$  and  $5_2$  knots, which have the same nominal complexity (5 crossings in their simplest diagrammatic representation) but one belongs to the torus knots family and the other to the twist knot family. At all levels of spatial confinement of infinitely thin rings, the population of  $5_2$  knots is usually twice as abundant as the  $5_1$  knot, see e.g. simulation data in Fig. 8.2b. The result holds more in general, as it applies to other common models of rings, such as semi-flexible rings of cylinders or semi-flexible chains of beads, and, thus, reflects the larger configurational entropy of  $5_2$  knots compared to  $5_1$  ones [49, 50, 54, 55]. However, the opposite bias is observed in viral DNA, see experimental data in Fig. 8.2b. One, thus, concludes that the strong bias towards torus knots observed experimentally is due to specific properties of DNA packing that are not captured by general polymer models.

The conundrum was clarified in the study of Ref. [49], which noted that the DNA packing density inside viral capsids is sufficiently high to cause a local cholesteric ordering of contacting DNA strands. This cholesteric ordering follows from the double-helical nature of DNA, which causes contacting strands to juxtapose at a preferred angle. The study then showed that when propensities for local cholesteric ordering are included in DNA models, the knot spectrum acquires the correct bias towards torus knots, and even a quantitative agreement with experimental data can be reached; see Fig. 8.4a.

The good match of the topological spectra from theory and experiment is an appealing result per se but has broader implications, too. It validates a posteriori the coarse-grained model and, thus, gives confidence for using it to capture the DNA structural organization under spatial confinement. Typical model DNA configurations inside spherical cavities, an approximation to viral capsids, are shown in Fig. 8.4b, where they can be contrasted with those obtained without the cholesteric interaction term. The differences in arrangement are very noticeable, with the refined model showing an enhanced ordering of the DNA in layered shells. The order, however, is not perfect as regions at large sequence separation can be stacked one upon the other (as denoted by the different colours of the juxtaposed regions), and the winding directionality is not necessarily constant.



**Fig. 8.4** **a** Accounting for DNA cholesteric interactions allows to reproduce the experimental topological spectrum of DNA inside capsids. **b** Including or excluding cholesteric interactions significantly affects the arrangement of the confined model DNA. Reproduced with permission from Ref. [49]



**Fig. 8.5** **a** Snapshots from simulations where knotted DNA ejects from a model spherical capsids. **b** Time evolution of the ejected chain fractions over the independent realization of the process. In only a small fraction of the trajectories, the presence of the knot hinders the translocation process. Reproduced with permission from Ref. [48]

The same model was subsequently used to study the ejection process and solve the puzzle of how the viral DNA could exit from the capsid through a narrow pore despite being highly knotted [48].

Inspection of the trajectories clarified the underlying physical mechanism. The high degree of confinement causes the knot to be delocalized over most of the DNA contour. Because the knot is widely spread, the continuous rearrangements of the chain facilitate the strand passages leading to a progressive untying of the DNA as

more of it is ejected from the pore. In practice, knot complexity diminishes in parallel with the length of the chain inside the capsid; see Fig. 8.5.

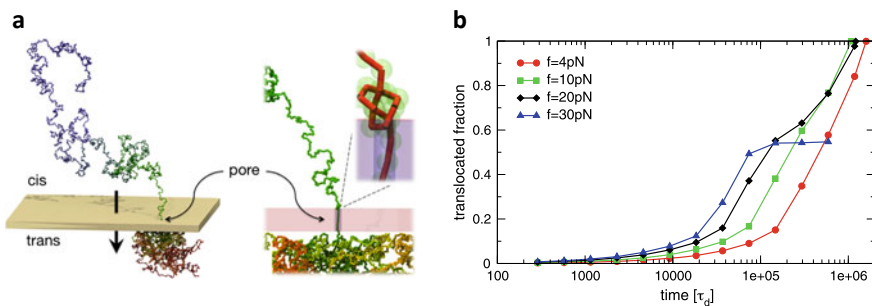
This simplification would not be possible if the knot were tight, a condition that is prevented by confinement. The results, thus, highlight a dual effect of capsid confinement on DNA: it boosts the entanglement of the packaged DNA but, because it causes knot delocalization, it also facilitates the smooth ejection of knotted DNA.

### 8.3.2.1 Pore Translocation of Tightly Knotted Filaments

The results discussed above leave unanswered a more general issue: how is polymer translocation affected by tight physical knots? The question is relevant in the many contexts where pore translocation is used to profile the physical properties of polymers [56–61] and in applicative contexts too, such as the sequencing of single-stranded DNA [9, 62–64, 64–68, 68–73]. In the latter setups, an electric field applied along the pore axis is used to drive through the pore the DNA strand along with ions in solution. The temporal modulation of the ionic current through the pore can then be used to infer the chemical identity of the nucleotides as they pass through the pore.

The pore translocation of (unknotted) polymer chains is a classic problem in polymer physics, which is now relatively well understood [56, 58, 61, 74–76]. The translocation response is dictated by the tension propagating from inside the pore, where the driving force is applied, to the rest of the chain.

The simulations of Ref. [77] showed that the propagating tension causes the tightening of the knots in the translocating chain. The tightened knots eventually reach the pore where they are pulled even more tightly against the outer surface of the pore.



**Fig. 8.6** **a** Initial stages of the driven translocation of a knotted chain through a narrow pore. The chain is modelled as a fully flexible string of beads. **b** Temporal traces of the translocated chain fraction. The presence of the tight knot at the pore entrance can stall translocation only at sufficiently large driving forces. Reproduced with permission from Ref. [77]

Our everyday experience with macroscopic ropes suggests that the translocation of a knotted rope should stall when the knot reaches the pore entrance in a tight form due to the significant friction developed in the knotted region.

However, the results of Ref. [77] demonstrated that this intuitive picture is not necessarily applicable to microscopic situations.

In fact, it was observed that tight knots do not per se prevent translocation of chains of beads, as illustrated in Fig. 8.6. In this context, unlike the macroscopic case, thermal fluctuations allow the beads in the knotted portions to overcome the barriers of the corrugated potential created by the tightly contacting portions of the knot that slide relative to each other. Thermal fluctuations, thus, allow the knot to “breathe” and overcome these microscopic realizations of friction and, thus, slide along the knotted chain contour.

Thanks to this mechanism, chains can slide and translocate through narrow pores even when they accommodate tight knots. However, applying sufficiently high driving forces eventually causes such a tight interdigitation of the beads that thermal fluctuations cannot compete with frictional effects anymore [77]. When this happens, one recovers the intuitive stalling of translocation in knotted macroscopic ropes.

Since it has been first reported, this mechanism has been found in other contexts too and, for instance, has been argued to be relevant in connection to protein degradation by the proteasome [78–83].

### 8.3.3 *Bacterial DNA*

Knots have long been known to occur in bacterial DNA too, which is organized in circular form [84, 85]. Unlike the case of viral DNA knotting, which occurs inside the capsid, the knotting of bacterial DNA is created by the action of enzymes during, e.g. transcription or replication [2, 86–88].

The entanglement that is inevitably created during these processes is continuously relieved by topoisomerase enzymes, which come in two types or classes [89]. Type I topoisomerases act by cutting only one strand of the DNA double helix and allowing it to swivel around the other strand. This mechanism does not alter the topology of DNA plasmids or circular chromosomes. It is instrumental for achieving the torsional relaxation of the chain and for controlling its degree of supercoiling, that is, the level of over or underwinding (bacterial DNA is kept at around 0.05 negative supercoiling density).

Type II topoisomerases cut both strands and, by assisting the passage of another DNA strand through the cut, can alter DNA topology [84, 90, 91]. The action of type II topoisomerases is, thus, crucial to eliminate detrimental forms of DNA entanglement [88, 92, 93]. For instance, newly replicated plasmids are catenated and must be unlinked via suitable strand passages for correct subdivision into daughter cell to proceed [94, 95]. Similarly, topoisomerases must efficiently remove DNA knots, such as those created by concurrent replication and transcription activities, and whose accumulation would be detrimental and even lethal for the bacterial cell [91, 93, 96].



Many efforts have been spent to rationalize how these enzymes, which are too small to “sense” the global DNA topology, can recognize and perform the correct strand passages leading to knot simplification. Random passages would yield the “equilibrium” knotting observed in random cyclization, and topoisomerases can bring knotting much below this equilibrium level.

Several elegant and physically appealing suggestions have been made over the years to reconcile the local action of topoisomerases with the resulting global simplification of DNA topology.

These suggestions include the recognition by topoisomerases of local geometrical features that are over-represented in knotted DNA rings. These notably include so-called hooked juxtapositions of DNA strands, which corresponds to DNA strands that are contacting so tightly that they establish a clasp [97–100]. These clasps are distinctive of essential crossings in tight knots, but they occur in delocalized knots too. Numerical simulations on various models have verified that strand passages at hooked juxtapositions can indeed take the knotting probability well below the equilibrium values. Interestingly, recent modelling work by Ziraldo et al. [101] has shown that clasp condition can be relaxed and that topological simplification can be achieved by performing crossings in correspondence of juxtapositions where one strand is bent around the other. Other invoked mechanisms involve the actual localization of the knot itself, for instance by accumulated supercoiling [102–105].

The simultaneous presence of DNA knotting and supercoiling is particularly interesting as it combines geometrical and topological entanglement. How exactly the two affect DNA conformational dynamics is a particularly relevant issue for bacterial DNA, and it was recently tackled in Ref. [106] with molecular dynamics simulations of 2kb-long DNA rings with supercoiling and/or 5-crossing knots. The rings’ length and topology were chosen to approximate those reported experimentally [2, 84].

Analysis of trajectories showed that when either supercoiling or knotting were individually present, DNA rings retained substantial conformational freedom. The rings could, in fact, interconvert between states with different numbers of plectonemes or localized and delocalized knot states [106], see Fig. 8.7.

However, when both knotting and supercoiling were present, the reconfiguration dynamics was dramatically slowed down. The location of the essential crossings of the knotted region and of plectonemes remained locked over timescales at least an order of magnitude longer than when either knots and supercoiling alone are present. In fact, the location of plectonemes and knot crossings persisted for the entire simulated trajectories; see Fig. 8.7.

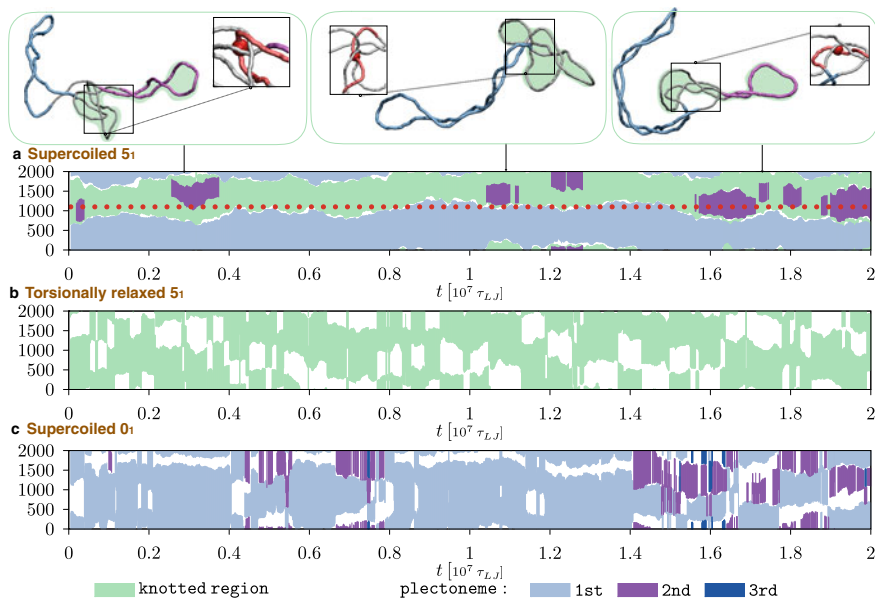
The slowed conformational dynamics is an unexpected emergent property of knotted and supercoiled rings that can illuminate a thus far underexplored aspect of DNA topological simplification. A pre-requisite for topoisomerases to detect and remove essential crossings is that the distinctive local geometry of the latter persists long enough to be recognized.

This temporal element, which had been envisioned in Ref. [107], is still beyond the reach of current experimental probing techniques, and numerical simulations and modelling are currently our best source of insight into this fascinating subject.

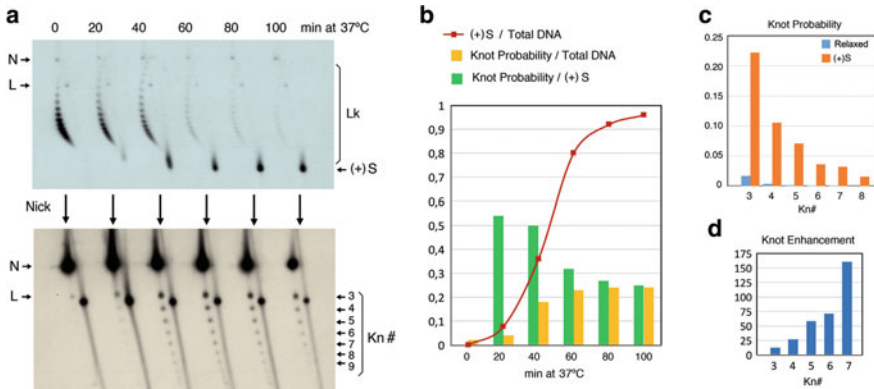
### 8.3.4 Eukaryotic DNA

It is only recently that experimental breakthroughs have allowed for probing the knotting properties of eukaryotic DNA. This feat was recently accomplished by Roca's lab with a series of studies on the in vivo topological entanglement of YRp4 yeast minichromosomes [108, 109].

These circular minichromosomes are 4.4kb long, involve  $\sim 25$  nucleosomal units, and are typically maintained at a negative level of supercoiling. Using gel electrophoresis, it was established that the typical in vivo level of knotting was about 2% [108]. The result is noteworthy in several respects. First, it gave a first demonstration that even very short eukaryotic DNA is knotted in vivo. Second, the observed knotting is substantially different from the one of DNA rings of similar length that circularize in solution. Additionally, the knot spectrum is biased in favour of left-handed knots, again differently from the case of random circularisation in solution [108]. These topological differences, thus, follow from the specific spatial arrangement of eukaryotic DNA, including its torsional stress associated with wrapping around nucleosomes and the overall degree of supercoiling.



**Fig. 8.7** Kymplots showing the position of the plectonemes and/or the knotted region in a model 2kb-long DNA ring. The first kymplot is for the supercoiled unknotted chain, the second is for a knotted but torsionally relaxed chain, and the third is for a knotted supercoiled chain. The persistence of plectonemes and knot boundaries in the latter is apparent. Reproduced with permission from Ref. [106]



**Fig. 8.8** Electrophoretic traces and measurements showing the increasing incidence of knots and positive supercoiling, (+S), accumulated during transcription of yeast minichromosome YRp4. Reproduced with permission from Ref. [109]

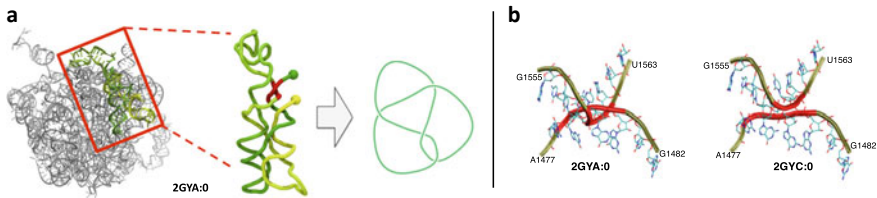
A subsequent study succeeded at probing the amount of knotting that is generated during transcription/replication [109]. When the two DNA strands are pulled apart, negative and positive supercoiling is generated, respectively, behind and ahead of the transcribing machinery. The ensuing torsional stress and entanglement are relaxed by the action of both type I and type II topoisomerases; the latter, we recall, can alter DNA topology.

The topological profiling at different transcription stages gave remarkable results. During transcription, knotting was boosted up to an approximately 25-fold increase of the baseline level, which is about 2% for YRp4. The enhancement of knots was accompanied by a concomitant increase of the positive supercoiling [109], see Fig. 8.8.

The experiments, thus, gave a striking demonstration that, in the course of removing torsional stress, topoisomerases can transiently increase DNA knotting much above the homeostatic level, before eventually re-establishing the baseline entanglement.

Coarse-grained models based on strings and beads (used to model nucleosomes and linkers) were also used to rationalize the high level of transient knotting. The Monte Carlo simulations of the model YRp4 chromatin showed that the observed boost of knotting probability is compatible with a fivefold increase of compactification (i.e. decrease of gyration volume) of the chromosome [109], which is expectedly induced by the local accumulation of supercoiling during transcription.

The results open entirely new perspectives on the entanglement of eukaryotic genomes and prompt numerous questions. What amount of homeostatic knotting is actually present in much longer chromosomes than YRp4? How much can it increase during transcription and other enzymatic processing of DNA? Does chromatin entanglement play any role in structuring chromatin in vivo [109–111]? We expect that



**Fig. 8.9** **a** RNA conformation of PDB entry 2GYA:0 presents a physical knot, arising from the highlighted interlocking of two helices. **b** Comparison with a higher resolution homolog (PDB entry 2GYC:0), where the interlocking is not present, suggests the artefactual nature of the physical knot. Reproduced with permission from Ref. [5]

significant breakthroughs will be achieved in all these avenues with a synergistic effort of experiments, models, and simulations.

## 8.4 RNA (un)Knotting

We conclude this overview of knots in nucleic acids by extending considerations from DNA to RNA.

RNA filaments are flexible, their persistence length being about 1 nm, and their length can range from a few nucleotides to thousands of them, as for ribosomal units.

One might expect that RNA knotting properties are not different from those of other flexible biopolymers such as proteins. Regarding the latter, we recall that a few percent of protein PDB entries are physically knotted [112–115].

A first systematic survey of RNA knotting was carried out in Ref. [5] and gave a surprisingly negative outcome.

Out of the thousands of RNA entries present in the protein data bank at that time, only three putative knotted RNA structures were found, all solved by cryo-em. For two of them, there were available homolog structures solved by X-ray crystallography, which were unknotted. A detailed comparison of the cryo-em and X-ray versions revealed that the former featured interlocked RNA helices, which were instead well-separated and disentangled in the higher resolution X-ray counterpart; see, e.g. Fig. 8.9. The third knotted structure presented other issues, too, such as atypical bends of the RNA virtual backbone (P-trace). It was, thus, deemed that the crossings responsible for the putative knotted states of the three RNA entries were most likely artefactual [5].

The analysis, thus, gave the unexpected result that no knotted RNA entries existed among the thousands deposited in the PDB. The conclusion remained unchanged in a later survey on a larger dataset [6].

The result prompted several considerations and speculations too. The fact that knots have a much lower incidence in natural RNAs (where none has been found so far) compared to proteins suggests the possibility that the folding kinetics or

thermodynamics of naturally occurring RNAs has been co-opted by evolution to minimize the incidence of knots. For instance, secondary elements established during co-transcriptional folding of nascent RNAs may already decrease the knotting probability. Compared to an unstructured filament, it would be more difficult for a structured RNA to establish the loops and threadings conducive to knots. In addition, the RNA sequence itself may have evolved so that the native folded state can be established by accretion or modularly, which also would make RNA less prone to form knots [5].

It cannot be ruled out that genuinely knotted RNA structures can be found in the future with the growing size of the database. An indication that this is possible, or even likely, comes from the groundbreaking work of Seeman et al. [116] who, as early as 1996, succeeded at designing and synthesizing RNA strands of about 100 nucleotides that adopted knotted folds. As a matter of fact, there already exists circumstantial evidence pointing at the knotted state of certain natural RNAs [6]. However, a positive confirmation of their entanglement from direct structural determination is still pending.

While the quest for physically knotted RNAs is still open, it is appropriate to recall that RNAs are rich in other forms of entanglement or structural complexities termed pseudoknots. These structures are particularly common in viral RNAs where they serve different functional purposes such as causing ribosomal frameshifting [7–10] or resisting degradation by cellular defence mechanisms [11–17, 117]. Interestingly, in both cases, their functional role is to hinder RNA translocation through the lumen of enzymes, presenting, thus, qualitative analogies with translocating knotted chains.

It appears, thus, likely that further work on the properties of RNA secondary and tertiary elements can advance our understanding of the functional implications of entanglement in biomolecules.

## 8.5 Conclusions

Knots have been found in genomic DNA filaments of all organisms: from viruses to bacteria to eukaryotes. What we know today about the ubiquity of DNA entanglement *in vivo* and its quantification is the result of a long series of experimental breakthroughs, from trapping the transient DNA entanglement in robust topological states [23] to detecting the abundance of different knot types and their chirality too [26, 108] and to extending knot detection techniques to DNA strands of increasing lengths [118, 119].

The chase between new challenges and breakthroughs is not over yet, and theoretical models and numerical simulations play an essential part in it. Models with different levels of structural detail are indispensable to interpret experimental data and obtain the direct microscopic and dynamical insight that is often beyond the reach of experiments and are increasingly used to predict DNA entanglement properties. More than the complex biological contexts, such theoretical predictions are typically directed at nano-manipulation contexts, such as mechanical stretching and

translocation [77, 120], microfluidics [121–123], and confinement inside nanochannels, slits, and cavities [124–132]. These are all instances where the insight afforded by such approaches is advancing our understanding of the role of how the static and dynamics of polymers are affected by topology. This rapidly evolving field will undoubtedly expose many surprising and counter-intuitive results, most likely in the context of inter-molecular DNA entanglement.

**Acknowledgements** The material presented in this overview intersects the work of many colleagues and research groups that I had the pleasure to interact with during collaborations, visits, and exchanges and at conferences. For the topics touched here, I wish to recall, in particular, Lucia Coronel, Tetsuo Deguchi, Giovanni Dietler, Marco Di Stefano, Massimiliano Di Ventra, Alexander Grosberg, Davide Marenduzzo, Ken Millet, Henri Orland, Enzo Orlandini, Eric Rawdon, Joaquim Roca, Angelo Rosa, Andrzej Stasiak, Antonio Suma, De Witt Summers, Erica Uehara, Yasuyuki Tezuka, and Luca Tubiana. I am indebted to many of them not only for having enriched me scientifically but also personally. I am also grateful to Prof. Yasuyuki Tezuka and Prof. Tetsuo Deguchi for the editing of this contribution.

## References

1. D. Pawson, *Knot craft* (Adlard Coles Nautical, 2009)
2. L. Olavarrieta, P. Hernandez, D.B. Krimer, J.B. Schwartzman, *J. Mol. Biol.* **322**(1), 1 (2002)
3. R.W. Deibler, J.K. Mann, L.S. De Witt, L. Zechiedrich, *BMC Mol. Biol.* **8**(1), 44 (2007)
4. J. Portugal, A. Rodriguez-Campos, *Nucleic Acids Res.* **24**, 4890 (1996)
5. C. Micheletti, M. Di Stefano, H. Orland, *Proc. Natl. Acad. Sci.* **112**(7), 2052 (2015)
6. A.S. Burton, M. Di Stefano, N. Lehman, H. Orland, C. Micheletti, *RNA Biol.* **13**(2), 134 (2016)
7. D.P. Giedroc, P.V. Cornish, *Virus Res.* **139**(2), 193 (2009)
8. D.P. Giedroc, C.A. Theimer, P.L. Nixon, *J. Mol. Biol.* **298**(2), 167 (2000)
9. G. Chen, K.Y. Chang, M.Y. Chou, C. Bustamante, I. Tinoco, *Proc. Natl. Acad. Sci. U.S.A.* **106**(31), 12706 (2009)
10. S.Y. Le, B.A. Shapiro, J.H. Chen, R. Nussinov, J.V. Maizel, *Gen. Anal.: Biomol. Eng.* **8**(7), 191 (1991)
11. G.P. Pijlman, A. Funk, N. Kondratieva, J. Leung, S. Torres, L. Van der Aa, W.J. Liu, A.C. Palmenberg, P.Y. Shi, R.A. Hall, A.A. Khromykh, *Cell Host Microbe* **4**(6), 579 (2008)
12. E.G. Chapman, D.A. Costantino, J.L. Rabe, S.L. Moon, J. Wilusz, J.C. Nix, J.S. Kieft, *Science* **344**(6181), 307 (2014)
13. B.M. Akiyama, H.M. Laurence, A.R. Massey, D.A. Costantino, X. Xie, Y. Yang, P.Y. Shi, J.C. Nix, J.D. Beckham, J.S. Kieft, *Science* **354**(6316), 1148 (2016)
14. A. Slonchak, A.A. Khromykh, *Antivir. Res.* (2018)
15. A. MacFadden, Z. O'Donoghue, P.A. Silva, E.G. Chapman, R.C. Olsthoorn, M.G. Sterken, G.P. Pijlman, P.J. Bredenbeek, J.S. Kieft, *Nat. Commun.* **9**(1), 119 (2018)
16. W.C. Ng, R. Soto-Acosta, S.S. Bradrick, M.A. Garcia-Blanco, E.E. Ooi, *Viruses* **9**(6), 137 (2017)
17. A. Suma, L. Coronel, G. Bussi, C. Micheletti, *Nat. Commun.* **11**(1), 1 (2020)
18. D. Marenduzzo, C. Micheletti, E. Orlandini, *J. Phys.: Condens. Matter* **22**, 283102 (2010)
19. D. Meluzzi, D.E. Smith, G. Arya, *Annu. Rev. Biophys.* **39**, 349 (2010)
20. C. Micheletti, D. Marenduzzo, E. Orlandini, *Phys. Rep.* **504**, 1 (2011)
21. L. Dai, C.B. Renner, P.S. Doyle, *Adv. Coll. Interface. Sci.* **232**, 80 (2016)
22. V.V. Rybenkov, N.R. Cozzarelli, A.V. Vologodskii, *Proc. Natl. Acad. Sci. U.S.A.* **90**, 5307 (1993)

23. J.C.W.S.Y. Shaw, *Science* **260**, 533 (1993)
24. A. Stasiak, V. Katritch, J. Bednar, D. Michoud, J. Dubochet, *Nature* **384**(6605), 122 (1996)
25. J. Cebrián, M.J. Kadomatsu-Hermosa, A. Castán, V. Martínez, C. Parra, M.J. Fernández-Nestosa, C. Schaerer, M.L. Martínez-Robles, P. Hernández, D.B. Krimer, A. Stasiak, J.B. Schwartzman, *Nucleic Acids Res.* **43**(4), e24 (2015)
26. S. Trigueros, J. Arsuaga, M.E. Vazquez, D. Sumners, J. Roca, *Nucleic Acids Res.* **29**(13), E67 (2001)
27. C. Weber, A. Stasiak, P. De Los Rios, G. Dietler, *Biophys. J.* **90**(9), 3100 (2006)
28. D. Michieletto, D. Marenduzzo, E. Orlandini, *Proc. Natl. Acad. Sci.* **112**(40), E5471 (2015)
29. R.N. Irobalieva, J.M. Fogg, D.J. Catanese, T. Sutthitbutpong, M. Chen, A.K. Barker, S.J. Ludtke, S.A. Harris, M.F. Schmid, W. Chiu et al., *Nat. Commun.* **6**(1), 1 (2015)
30. T. Deguchi, K. Tsurusaki, *Lectures at Knots*, vol. 96 (World Scientific, Singapore, 1997), pp. 95–122
31. E. Rawdon, A. Dobay, J.C. Kern, K.C. Millett, M. Piatek, P. Plunkett, A. Stasiak, *Macromolecules* **41**(12), 4444 (2008)
32. P. Virnau, Y. Kantor, M. Kardar, *J. Am. Chem. Soc.* **127**, 15102 (2005)
33. B. Marcone, E. Orlandini, A.L. Stella, F. Zonta, *J. Phys. A: Math. Gen.* **38**, L15 (2005)
34. L. Tubiana, A. Rosa, F. Fragiaco, C. Micheletti, *Macromolecules* **46**, 3669 (2013)
35. M.K. Shimamura, T. Deguchi, *Phys. Lett. A* **274**, 184 (2000)
36. M.K. Shimamura, T. Deguchi, *Phys. Rev. E* **64**, 020801 (2001)
37. M.K. Shimamura, T. Deguchi, *Phys. Rev. E* **65**, 051802 (2002)
38. E. Orlandini, M.C. Tesi, S.G. Whittington, *J. Phys. A: Math. Gen.* **38**, L795 (2005)
39. P. Virnau, F.C. Rieger, D. Reith, *Biochem. Soc. Trans.* **41**, 528 (2013)
40. L. Coronel, E. Orlandini, C. Micheletti, *Soft Matter* **13**, 4260 (2017)
41. L. Lu, H. Zhu, Y. Lu, L. An, L. Dai, *Macromolecules* **53**(21), 9443 (2020)
42. L. Dai, P.S. Doyle, *Macromolecules* **51**(16), 6327 (2018)
43. E. Uehara, L. Coronel, C. Micheletti, T. Deguchi, *React. Funct. Poly.* **134**, 141 (2019)
44. J. Arsuaga, M. Vázquez, S. Trigueros, D.W. Sumners, J. Roca, *Proc. Natl. Acad. Sci. U.S.A.* **99**, 5373 (2002)
45. J. Arsuaga, M. Vázquez, P. McGuirk, S. Trigueros, D.W. Sumners, J. Roca, *Proc. Natl. Acad. Sci. U.S.A.* **102**, 9165 (2005)
46. S. Trigueros, J. Roca, *BMC Biotechnol.* **7**, 94 (2007)
47. R. Matthews, A.A. Louis, J.M. Yeomans, *Phys. Rev. Lett.* **102**, 088101 (2009)
48. D. Marenduzzo, C. Micheletti, E. Orlandini, D.W. Sumners, *Proc. Natl. Acad. Sci. U.S.A.* **110**(50), 20081 (2013)
49. D. Marenduzzo, E. Orlandini, A. Stasiak, D.W. Sumners, L. Tubiana, C. Micheletti, *Proc. Natl. Acad. Sci. U.S.A.* **106**(52), 22269 (2009)
50. C. Micheletti, D. Marenduzzo, E. Orlandini, D.W. Sumners, *J. Chem. Phys.* **124**, 064903 (2006)
51. F.W.W.J.P.J. Michels, *J. Phys. A: Math. Gen.* **22**, 2393 (1989)
52. J.P.J. Michels, F.W. Wiegel, *Proc. R. Soc. Lond.* **A403**, 269 (1986)
53. J. Arsuaga, R.K. Tan, M. Vazquez, D.W. Sumners, S.C. Harvey, *Biophys. Chem.* **101–102**, 475 (2002)
54. C. Micheletti, D. Marenduzzo, E. Orlandini, D.W. Sumners, *Biophys. J.* **95**, 3591 (2008)
55. V. Katritch, W.K. Olson, A. Vologodskii, J. Dubochet, A. Stasiak, *Phys. Rev. E* **61**, 5545 (2000)
56. Y. Kantor, M. Kardar, *Phys. Rev. E* **69**(2), 021806 (2004)
57. M. Muthukumar, *Annu. Rev. Biophys. Biomol. Struct.* **36**, 435 (2007)
58. P. Rowghanian, A.Y. Grosberg, *Phys. Rev. E* **86**(1), 011803 (2012)
59. T. Ikonen, A. Bhattacharya, T. Ala-Nissila, W. Sung, *Phys. Rev. E* **85**(5), 051803 (2012)
60. V.V. Palyulin, T. Ala-Nissila, R. Metzler, *Soft Matter* **10**(45), 9016 (2014)
61. J. Sarabadani, T. Ala-Nissila, *J. Phys.: Condens. Matter* **30**(27), 274002 (2018)
62. A. Meller, L. Nivon, D. Branton, *Phys. Rev. Lett.* **86**(15), 3435 (2001)
63. E.H. Trepagnier, A. Radenovic, D. Sivak, P. Geissler, J. Liphardt, *Nano Lett.* **7**(9), 2824 (2007)

64. J. Comer, V. Dimitrov, Q. Zhao, G. Timp, A. Aksimentiev, *Biophys. J.* **96**(2), 593 (2009)
65. R.Y. Henley, S. Carson, M. Wanunu, in *Progress in Molecular Biology and Translational Science*, vol. 139 (Elsevier, Amsterdam, 2016), pp. 73–99
66. M. Zwolak, M. Di Ventra, *Rev. Mod. Phys.* **80**(1), 141 (2008)
67. D. Branton, D.W. Deamer, A. Marziali, H. Bayley, S.A. Benner, T. Butler, M. Di Ventra, S. Garaj, A. Hibbs, X. Huang, S.B. Jovanovich, P.S. Krstic, S. Lindsay, X.S. Ling, C.H. Mastrangelo, A. Meller, J.S. Oliver, Y.V. Pershin, J.M. Ramsey, R. Riehn, G.V. Soni, V. Tabard-Cossa, M. Wanunu, M. Wiggin, J.A. Schloss, *Nat. Biotechnol.* **26**(10), 1146 (2008)
68. C. Cao, M.Y. Li, N. Cirauqui, Y.Q. Wang, M. Dal Peraro, H. Tian, Y.T. Long, *Nat. Commun.* **9**(1), 1 (2018)
69. P. Bandarkar, H. Yang, R.Y. Henley, M. Wanunu, P.C. Whitford, *Biophys. J.* (2020)
70. K. Luo, T. Ala-Nissila, S.C. Ying, A. Bhattacharya, *Phys. Rev. Lett.* **100**(5), 058101 (2008)
71. C. Plesa, D. Verschuere, S. Pud, J. van der Torre, J.W. Ruitenber, M.J. Witteveen, M.P. Jonsson, A.Y. Grosberg, Y. Rabin, C. Dekker, *Nat. Nanotechnol.* **11**(12), 1093 (2016)
72. C.A. Merchant, K. Healy, M. Wanunu, V. Ray, N. Peterman, J. Bartel, M.D. Fischbein, K. Venta, Z. Luo, A.C. Johnson et al., *Nano Lett.* **10**(8), 2915 (2010)
73. T. Kubota, K. Lloyd, N. Sakashita, S. Minato, K. Ishida, T. Mitsui, *Polymers* **11**(1), 84 (2019)
74. J. Chuang, Y. Kantor, M. Kardar, *Phys. Rev. E* **65**(1), 011802 (2001)
75. A. Bhattacharya, W.H. Morrison, K. Luo, T. Ala-Nissila, S.C. Ying, A. Milchev, K. Binder, *Eur. Phys. J. E* **29**(4), 423 (2009)
76. M. Wanunu, W. Morrison, Y. Rabin, A.Y. Grosberg, A. Meller, *Nat. Nanotechnol.* **5**(2), 160 (2010)
77. A. Rosa, M. Di Ventra, C. Micheletti, *Phys. Rev. Lett.* **109**, 118301 (2012)
78. P. Szymczak, *Eur. Phys. J. Spec. Topics* **223**(9), 1805 (2014)
79. P. Szymczak, *Sci. Rep.* **6**(1), 1 (2016)
80. M. Wojciechowski, A. Gómez-Sicilia, M. Carrión-Vázquez, M. Cieplak, *Mol. BioSyst.* **12**(9), 2700 (2016)
81. Á. San Martín, P. Rodríguez-Aliaga, J.A. Molina, A. Martín, C. Bustamante, M. Baez, *Proc. Natl. Acad. Sci.* **114**, 9864 (2017)
82. M.K. Sriramoju, Y. Chen, Y.T.C. Lee, S.T.D. Hsu, *Sci. Rep.* **8**(1), 7076 (2018)
83. S.E. Jackson, *Topol. Geometry Biopoly.* **746**, 129 (2020)
84. K. Sishido, N. Komiyama, S. Ikawa, *J. Mol. Biol.* **195**(1), 215 (1987)
85. K. Sishido, S. Ishii, N. Komiyama, *Nucleic Acids Res.* **17**, 9749 (1989)
86. S.A. Wasserman, J.M. Dungan, N.R. Cozzarelli, *Science* **229**, 171 (1985)
87. J.M. Sogo, A. Stasiak, M.L. Martínez-Robles, D.B. Krimer, P. Hernandez, J.B. Schwartzman, *J. Mol. Biol.* **286**, 637 (1999)
88. V. López, M.L. Martínez-Robles, P. Hernández, D.B. Krimer, J.B. Schwartzman, *Nucleic Acids Res.* **40**, 3563 (2011)
89. J.C. Wang, *Annu. Rev. Biochem.* **65**, 635 (1996)
90. V. López, M.L. Martínez-Robles, P. Hernández, D.B. Krimer, J.B. Schwartzman, *Nucleic Acids Res.* **40**(8), 3563 (2012)
91. L.F. Liu, C.C. Liu, B.M. Alberts, *Cell* **19**, 697 (1980)
92. V. Rybenkov, C. Ullsperger, A.V. Vologodskii, N.R. Cozzarelli, *Science* **277**, 690 (1997)
93. R.W. Deibler, S. Rahmati, E.L. Zechiedrich, *Genes Dev.* **15**, 748 (2001)
94. D.E. Adams, E.M. Shekhtman, E.L. Zechiedrich, M.B. Schmid, N.R. Cozzarelli, *Cell* **71**, 277 (1992)
95. Z. Liu, R.W. Deibler, H.S. Chan, L. Zechiedrich, *Nucleic Acids Res.* **37**(3), 661 (2009)
96. T. Goto, J.C. Wang, *J. Biol. Chem.* **257**, 5866 (1982)
97. G.L. Randall, B.M. Pettitt, G.R. Buck, E.L. Zechiedrich, *J. Phys.: Condens. Matter* **18**, S173 (2006)
98. Z. Liu, J.K. Mann, E.L. Zechiedrich, H.S. Chan, *J. Mol. Biol.* **361**, 268 (2006)
99. Z. Liu, L. Zechiedrich, H.S. Chan, *J. Mol. Biol.* **400**(5), 963 (2010)
100. Z. Liu, H.S. Chan, *J. Phys.: Condens. Matter* **27**, 354103 (2015)
101. R. Ziraldo, A. Hanke, S.D. Levene, *Nucleic Acids Res.* **47**(1), 69 (2019)



102. G. Witz, A. Stasiak, *Nucleic Acids Res.* **38**, 2119 (2009)
103. G. Witz, G. Dietler, A. Stasiak, *Proc. Natl. Acad. Sci. U.S.A.* **108**, 3608 (2011)
104. D. Racko, F. Benedetti, J. Dorier, Y. Burnier, A. Stasiak, *Nucleic Acids Res.* **43**, 7229 (2015)
105. E.J. Rawdon, J. Dorier, D. Racko, K.C. Millett, A. Stasiak, *Nucleic Acids Res.* **44**, 4528 (2016)
106. L. Coronel, A. Suma, C. Micheletti, *Nucleic Acids Res.* **46**(15), 7533 (2018)
107. G.R. Buck, E.L. Zechiedrich, *J. Mol. Biol.* **340**(5), 933 (2004)
108. A. Valdés, J. Segura, S. Dyson, B. Martínez-García, J. Roca, *Nucleic Acids Res.* **46**(2), 650 (2018)
109. A. Valdés, L. Coronel, B. Martínez-García, J. Segura, S. Dyson, O. Díaz-Ingelmo, C. Micheletti, J. Roca, *Nucleic Acids Res.* **47**(13), 6946 (2019)
110. J.T. Siebert, A.N. Kivel, L.P. Atkinson, T.J. Stevens, E.D. Laue, P. Virnau, *Polymers* **9**(8), 317 (2017)
111. A. Rosa, M.D. Stefano, C. Micheletti, *Front. Mol. Biosci.* **6**, 127 (2019)
112. M.L. Mansfield, *Nat. Struct. Biol.* **1**(4), 213 (1994)
113. P. Virnau, A. Mallam, S. Jackson, *J. Phys.: Condens. Matter* **23**(3), 033101 (2011)
114. P. Dabrowski-Tumanski, J.I. Sulkowska, *Polymers* **9**(9), 454 (2017)
115. S.E. Jackson, A. Suma, C. Micheletti, *Curr. Opin. Struct. Biol.* **42**, 6 (2017)
116. H. Wang, R.J. Di Gate, N.C. Seeman, *Proc. Natl. Acad. Sci.* **93**(18), 9477 (1996)
117. M. Becchi, P. Chiarantoni, A. Suma, C. Micheletti, *J. Phys. Chem. B* **125**(4), 1098 (2021)
118. C. Plesa, D. Verschueren, S. Pud, J. van der Torre, J.W. Ruitenber, M.J. Witteveen, M.P. Jonsson, A.Y. Grosberg, Y. Rabin, C. Dekker, *Nat. Nanotechnol.* **11**(12), 1093 (2016)
119. A. Suma, C. Micheletti, *Proc. Natl. Acad. Sci. USA* **114**(15), E2991 (2017)
120. A. Suma, A. Rosa, C. Micheletti, *ACS Macro Lett.* **4**(12), 1420 (2015)
121. C.B. Renner, P.S. Doyle, *ACS Macro Lett.* **3**, 963 (2014)
122. A.R. Klotz, V. Narsimhan, B.W. Soh, P.S. Doyle, *Macromolecules* **50**(10), 4074 (2017)
123. A.R. Klotz, B.W. Soh, P.S. Doyle, *Phys. Rev. Lett.* **120**, 188003 (2018)
124. R. Metzler, W. Reisner, R. Riehn, R. Austin, J.O. Tegenfeldt, I.M. Sokolov, *Europhys. Lett.* **76**(4), 696 (2006)
125. W. Mobius, E. Frey, U. Gerland, *Nano Lett.* pp. 4518–4522 (2008)
126. R. Matthews, A.A. Louis, J.M. Yeomans, *Mol. Phys.* **109**(7–10), 1289 (2011)
127. L. Tubiana, E. Orlandini, C. Micheletti, *Phys. Rev. Lett.* **107**, 188302 (2011)
128. C. Micheletti, E. Orlandini, *Macromolecules* **45**, 2113 (2012)
129. C. Micheletti, E. Orlandini, *Soft Matter* **8**, 10959 (2012)
130. P.K. Lin, C.C. Hsieh, Y.L. Chen, C.F. Chou, *Macromolecules* **45**, 2920 (2012)
131. E. Orlandini, C. Micheletti, *J. Biol. Phys.* **39**, 267 (2013)
132. S. Amin, A. Khorshid, L. Zeng, P. Zimny, W. Reisner, *Nat. Commun.* **9**(1), 1 (2018)

# Chapter 9

## Cyclotides—Cyclic and Disulfide-Knotted Polypeptides



David J. Craik, Yuhui Zhang, Yan Zhou, Quentin Kaas, and Meng-Wei Kan

**Abstract** In this chapter we describe the topological features of selected ribosomally synthesized cyclic peptides from plants and animals. These peptides are characterised by their exceptional thermal stability and resistance to proteolysis due to their macrocyclic backbone. Many of these peptides additionally have stabilising disulfide bonds. They represent a class of topologically complex peptides that have applications in agriculture and medicine. After an introduction to several classes of these cyclic peptides we focus on one family, the cyclotides, which are characterised by a macrocyclic backbone and a cystine knot motif.

### 9.1 Introduction

All classes of naturally occurring cyclic peptides and proteins are biosynthesised as topologically linear chains of amino acids initially. Some peptides and proteins are subsequently post-translationally modified to produce alternative topologies other than the conventional linear chain of amino acids. Once chain assembled, proteins are typically folded into complex three-dimensional shapes or topographies that typically dictate their biological functions. Peptides on the other hand can have somewhat flexible structures, unless stabilised by additional topological features. One class of topological modification is cyclisation of the peptide chain and another is the addition of disulfide bonds to cross-brace peptide structures and thereby stabilise them.

In nature, the post-translational cyclisation process is invariably driven enzymatically, whether the original peptide chain is synthesised ribosomally, i.e., genetically encoded and sequentially chain assembled on the ribosome or non-ribosomally, being assembled by a consortium of enzymes. Disulfide bond formation is likewise facilitated by auxiliary proteins known as protein disulfide isomerases. In any case, the resultant topologically complex peptides or proteins tend to be more stable than their

---

D. J. Craik (✉) · Y. Zhang · Y. Zhou · Q. Kaas · M.-W. Kan  
Institute for Molecular Bioscience, Australian Research Council Centre of Excellence for Innovations in Peptide and Protein Science, The University of Queensland, Brisbane, QLD 4072, Australia  
e-mail: [d.craik@imb.uq.edu.au](mailto:d.craik@imb.uq.edu.au)

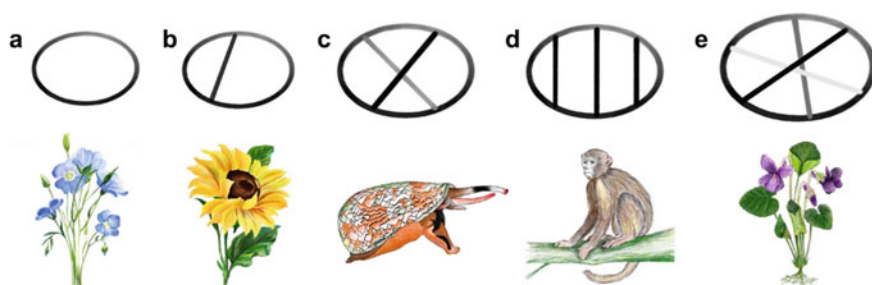
linear counterparts, making them interesting for a wide range of applications in drug design, agriculture, and biotechnology [1, 2]. Our laboratory focuses on such topologically complex peptides, and mainly on those that include both disulfide bonds and a cyclic backbone [3, 4]. Topological aspects of larger proteins are covered in other recent articles [5, 6].

Figure 9.1 summarises the classes of the complex peptides that we will describe here and schematically illustrates the organisms from which they are derived. We include this set of peptides for discussion as they represent a series of molecules of increasing complexity, ranging from cyclic peptides of just 8–10 amino acids and containing no disulfide bonds (the orbitides in Fig. 9.1a) through to the cyclotides (Fig. 9.1e) of around 30 amino acids with three intertwined disulfide bonds forming a structural motif known as a cystine knot.

Such cyclic peptides, and a host of other synthetically made examples, have become attractive therapeutic modalities due to their favourable properties such as high binding affinity, targeted selectivity and low toxicity [7]. In what follows, we describe each of these classes of molecules in more detail.

The orbitides [8], Fig. 9.1a, also called cyclolinopeptides, are a class of plant-derived cyclic peptides featuring an amino terminus to carboxy terminus linked circular structure without disulfide bonds, i.e., they do not contain internal cystine crosslinking. They were originally isolated from flax (*Linum usitatissimum*) seeds [9] and have a range of applications as industrial products and in food science. Topologically, they are the simplest of the examples we describe here, being a circle.

SFTI-1 (Fig. 9.1b) is a cyclic peptide of 14 amino acid residues that was originated from the seeds of the sunflower *Helianthus annuus* [10, 11] and functions as a potent inhibitor of trypsin. It possesses a cyclic backbone which is cross-braced by a single disulfide bridge. It also contains an extensive internal hydrogen bond network to form a well-defined structure. Topologically, it is a circle augmented by an internal covalent link.



**Fig. 9.1** Overview of five different classes of cyclic peptides. **a** An orbitide from flaxseed *Linum usitatissimum*. **b** A sunflower cyclic peptide from *Helianthus annuus*. **c** An artificially cyclised conopeptide from the cone snail *Conus victoriae*; in that case the natural peptide is a linear peptide of 16 amino acids that has been chemically cyclised by the addition of a 6-amino acid linker between its N- and C-termini. **d** A cyclic antimicrobial peptide from Rhesus monkey *Macaca mulatta*. **e** A cyclotide from the violet *Viola odorata*

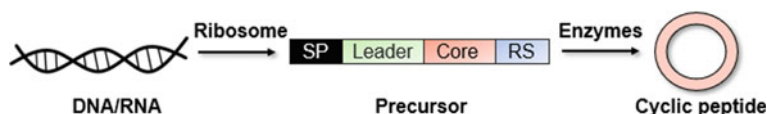
Cyclic Vc1.1 (Fig. 9.1c) is a synthetic peptide adapted from a naturally occurring linear peptide called Vc1.1 from the cone snail, *Conus victoriae* [12]. The artificially cyclised peptide comprises 22 amino acids stabilized by two disulfide bonds. It has potent analgesic properties as it is a selective inhibitor of  $\alpha 9\alpha 10$  nicotinic acetylcholine receptors (nAChRs) and also blocks high voltage-activated  $\text{Ca}^+$  channels through a GABA<sub>B</sub> receptor mediated mechanism [13]. Topologically, it is a circle with two internal links.

The cyclic antimicrobial peptide Rhesus theta defensin-1 (RTD-1) from the Rhesus monkey *Macaca mulatta* is composed of 18 amino acids (Fig. 9.1d), stabilized by three disulfide bonds and is backbone cyclized making it structurally distinct from other mammalian defensins [14]. It has antimicrobial activity against both Gram-positive and Gram-negative bacteria as well as fungi at micromolar concentrations and has a well-defined 3D structure comprising three disulfide bonds in a ladder arrangement [15]. Topologically it is a circle with three internal links.

Cycloviolacin O2 is a cyclotide from *Viola odorata* containing 30 amino acid residues. Along with kalata B1 it is one of the most extensively studied cyclotides [16] and is of particular interest for its antitumour activity [17]. It is characterised by a head-to-tail macrocyclic backbone with three conserved disulfide bonds arranged in a cystine knot motif, whereby two disulfide bonds and their linking backbone segments form an embedded ring which is penetrated by a third disulfide bond. These features define the cyclic cystine knot (CCK) motif [18] that confers cyclotides high thermal stability and remarkable resistance against proteolysis. Topologically the CCK motif is a circle with three internal links that form a knot. While cystine knots are common in many linear proteins, cyclotides are the only proteins having a cyclic cystine knot.

## 9.2 Biosynthesis

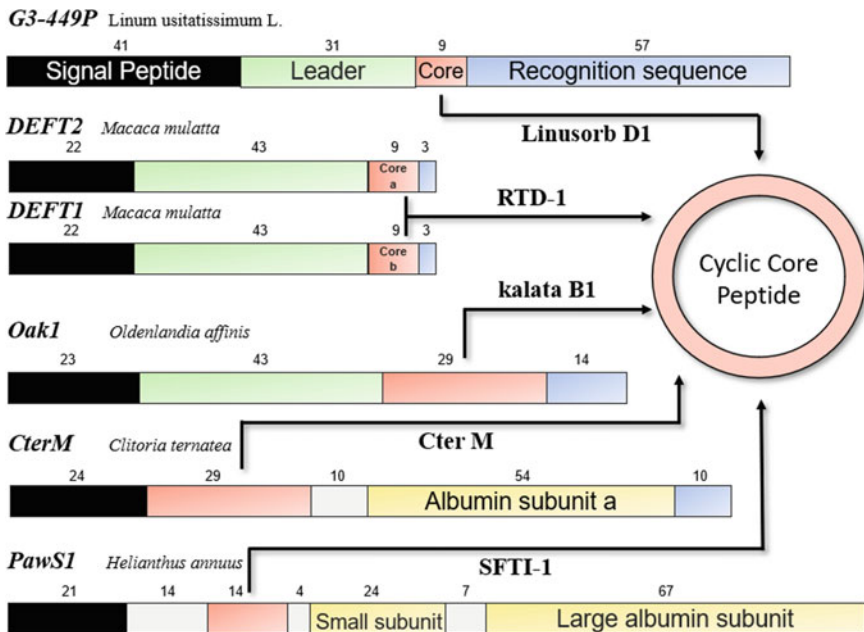
All of the ribosomally synthesised cyclic peptides shown in Fig. 9.1 are biosynthetically encoded by a gene which is then transcribed and translated to a precursor protein that is subsequently post-translationally processed to produce the cyclic disulfide rich peptide [19]. Figure 9.2 schematically illustrates this process.



**Fig. 9.2** Biosynthesis step of cyclic peptides. The DNA encoding the cyclic peptide is transcribed to RNA and then translated to a precursor protein. Precursor proteins for these ribosomal cyclic peptides contain four domains in general, i.e., a signal peptide (SP), leader sequence, core domain (i.e., the region corresponding to the cyclic peptide product) and recognition sequence (RS)

It is interesting to note that nature has evolved multiple different and independent mechanisms for making these cyclic peptides in terms of the architectures of the encoding genes and resultant precursor proteins. These alternative genetic solutions are summarised in Fig. 9.3 [20].

Generally, the precursor proteins for cyclic peptides include four motifs: a signal peptide (sometimes referred to as an endoplasmic reticulum, ER, signal sequence), leader (N-terminal repeat sequence), core peptide (corresponding to the cyclic peptide sequence) and recognition sequence (sometimes referred to as a C-terminal repeat, CTR, sequence). The cyclic peptides linusorb D1 [9], RTD-1 [14], kalata B1 [21] follow the structure mentioned above but RTD-1 is quite unique as it has two genes that each synthesise half of its core peptide, respectively. However, there are other cyclic peptides not following this structure, for example, the core sequence of the cyclotide Cter M [20] is flanked by an ER signal sequence and an albumin subunit, and also has a recognition sequence at the end. The structure of SFTI-1 [22] is similar to Cter M but it has two albumin subunits after the core sequence and no



**Fig. 9.3** Gene architecture of cyclic peptides from different species. Signal peptides are coloured in black and leader sequences in green. The core sequences that form cyclic peptides are coloured in pink. The recognition sequences are coloured in blue and subunits coloured in gold. The names of cyclic core peptides are located above or under the arrows. The names of the genes and the species are above the bars where genes are bolded and species are italicised. The number of amino acids in each domain is indicated above the sequence, e.g., the core sequence of linusorb D1 is 9 amino acids long

recognition sequence. In effect, these cases are examples where ancestral albumin genes have been hijacked to make cyclic peptides.

This biosynthetic information is useful to help understand how the linear precursor chains of these cyclic peptides originate. However, as the focus of this article is on the topologies of cyclic peptides rather than their biosynthesis we will not comment further here. For the remainder of this article will focus on just one of these classes of proteins, namely the cyclotides, which are the most topologically complex in the series.

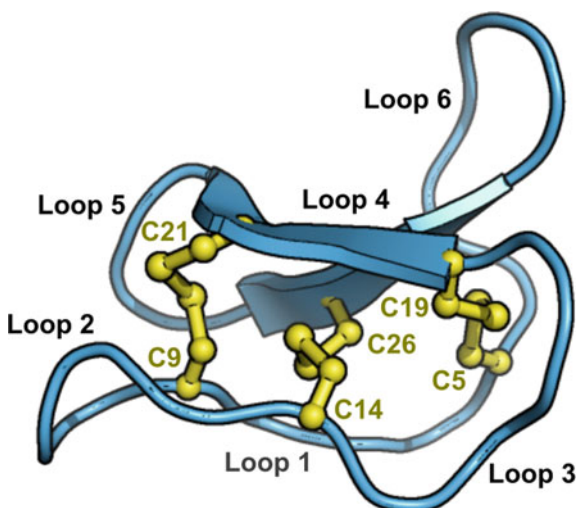
### 9.3 Cyclotides

Cyclotides are disulfide rich macrocyclic peptides from plants that were first defined as a peptide family in 1999 [18] when just a few members had been discovered. CyBase ([www.cybase.org.au](http://www.cybase.org.au)) is a database dedicated to curation of cyclotides, including their sequences, biological activities and distribution in the plant kingdom. Cyclotides have so far been found in plants from five major families [23], including the Violaceae, Rubiaceae, Cucurbitaceae, Solanaceae and Fabaceae. These families are commonly known as the violet, coffee, gourd, tomato, and legume family, respectively.

Cyclotides are ubiquitous in the Violaceae plant family [24], i.e., so far, every examined Violaceae plant has been found to contain cyclotides. By contrast cyclotides are only sparsely distributed in the other plant families, for example occurring only in a small percentage of members of the Fabaceae [25] and the Rubiaceae [26]. The reasons for this diverse distribution remain unknown, and while of great academic interest, are beyond the scope of the current review.

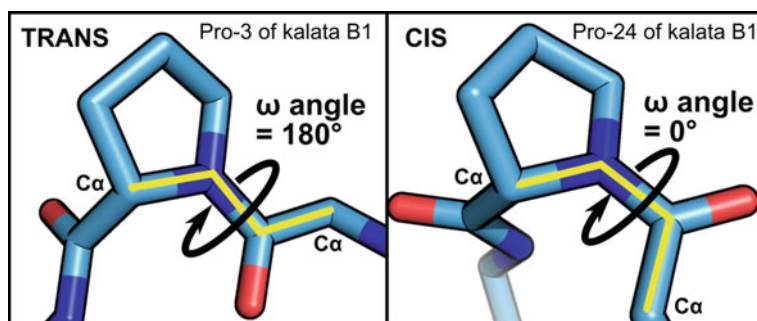
Figure 9.4 shows a schematic representation of the 3D structure of the prototypical cyclotide, kalata B1, highlighting the fact that it contains a cyclic backbone and six conserved cysteines residues that are connected in a I–IV, II–V, III–VI connectivity [27, 28]. In three dimensions this results in a knotted structure which will return to later but for now we focus on the topology and introduce relevant nomenclature. The backbone regions between the conserved cysteine residues are referred to as loops and given that there are six cysteine residues in the sequence [18], there are six loops in cyclotide structures. These loop regions are the focus of medical applications of cyclotides, and are often substituted, or ‘grafted’ to introduce a desired new therapeutic functionality.

Cyclotides are divided into three subfamilies, referred to as the *bracelet* cyclotides, which are the most common form, the *Möbius* cyclotides, and the *trypsin inhibitor* cyclotides [29]. Bracelet cyclotides are so named because they comprise a simple bracelet of amino acids. The Möbius cyclotides are so named because they contain a proline residue in loop 5 that is preceded by a cis amide bond. This cis bond effectively produces a conceptual 180° twist in the backbone ribbon and hence the definition of the molecule as a Möbius strip. Of course, this is a conceptual idea because the backbone of a peptide chain contains three variable angles, the  $\varphi$  the  $\psi$  and the  $\omega$



**Fig. 9.4** Structure of kalata B1 (PDB ID: 1NB1) showing the cyclic backbone, three knotted disulfide bonds and six backbone loops between the conserved Cys residues. The disulfide bonds are shown in yellow and for each the positions in the amino acid sequence of kalata B1 of the Cys residues are indicated

angles, with the  $\varphi$  and  $\psi$  angles being highly variable in the conformational space that they can occupy. By contrast the  $\omega$  angle is either zero (cis) or  $180^\circ$  (trans), and that is the basis on which the Möbius strip definition is made. Figure 9.5 shows the cis/trans geometry of two Xaa-Pro bonds in kalata B1, one in the cis form and one in the trans form. Trypsin inhibitor subfamily cyclotides are generally only distantly related in sequence to the Möbius or bracelet subfamily members and are so named because of their biological activity of inhibiting trypsin [30, 31].



**Fig. 9.5** Schematic illustration of trans or cis Xaa-Pro geometries. The main chain  $\omega$ -angle adopts either a  $180^\circ$  or  $0^\circ$  for the trans and cis isomers. The trans and cis conformations are illustrated with the three-dimensional structures of Pro-3 and Pro-24 of cyclotide kalata B1 in the NMR solution structure with PDB identifier 1nb1

The natural function of cyclotides is as defence peptides in plants, but they potentially have a wide range of applications in agriculture and medicine. For example, in agriculture, kalata B1 [32], kalata B2 [29] and Cter M [20] are active against *Helicoverpa punctigera* larvae, i.e. the cotton bollworm. In medicine, kalata B1, kalata B2 [33] and the cycloviolacins [34, 35] have anthelmintic activity; varv A, varv F, and cycloviolacin O2 are also reported to have anti-cancer activity [36].

Since cyclotides have many applications, artificial synthesis methods have been developed to produce adequate quantities cyclotides for these applications. These include chemical synthesis via Boc and Fmoc [37] chemistry, or by recombinant expression technology [38] or chemoenzymatic synthesis [39].

## 9.4 Topology

Figure 9.6 summarises the increasing complexity in going from a linear precursor sequence to a cyclic peptide, crossed-linked cyclic peptide, and folded cyclic peptide, which may either have a Möbius or bracelet-style cyclic backbone.

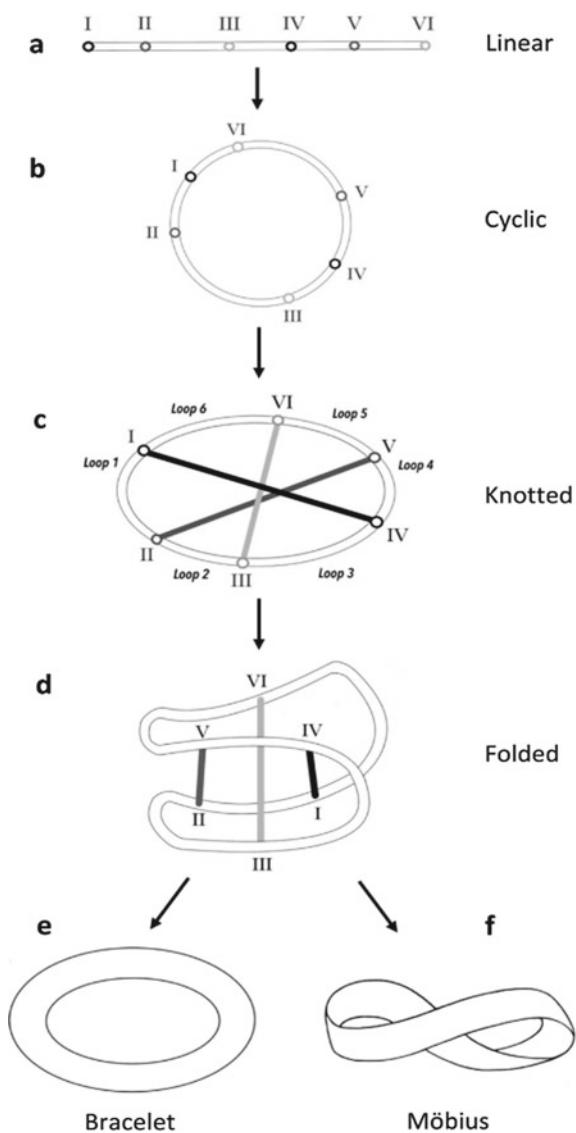
NMR has been the predominant method for determining NMR structures of cyclotides, with so far more than 30 structures deposited in the Protein Data Bank (PDB). Table 9.1 lists a selection of these deposited structures, illustrating the diversity of primary sequences that lead to the same CCK structure. An analysis of the PDB structures highlights the above topological features.

The native cyclotides are sequences found naturally in plants. The synthetic cyclotides refer to molecules with residue substitutions, disulfide bond deletions or other protein engineering changes such as chain opening or the inclusion of D-amino acids to study structure–activity relationships.

What topological lessons can we learn from this repository of structures? The first lesson is that all these structures incorporate a cystine knot motif and have a knotted arrangement of disulfide bonds. With regard to lessons from the backbone geometries of the peptide chain, we noted above that the  $\omega$ -angle is used in the definition of Möbius and bracelet cyclotides. Figure 9.7 shows an analysis of the  $\omega$ -angles for all residues in the deposited structures for the native cyclotides in Table 9.1 and confirms that these angles are either cis ( $0^\circ$ ) for the Möbius cyclotides, i.e., kalata B1, B2, B7 and B12, Rivi 3, Cter M, vhl-2 and cycloviolacin O12, or trans ( $180^\circ$ ) for the other (i.e., bracelet) cyclotides in the table. By contrast, the other two backbone angles,  $\varphi$  and  $\psi$  are more variable, although they do cluster in defined regions of conformational space, as would be expected based on Ramachandran regions of allowed space seen generally across protein structures.

Another lesson apparent from Table 9.1 is that it is indeed possible to add another layer of topological complexity by making a cyclotide with all D-amino acids, thereby making a mirror image form of the cyclotide. This was first done for kalata B1 [66] and the mirror image form used to probe membrane binding of cyclotides [67] and to assist in the X-ray structure determination of cyclotides using racemic crystallography [70].





**Fig. 9.6** Schematic illustration of topological features of the cyclotide family. **a** A linear precursor sequence. **b** A cyclic peptide. **c** A cross-linked cyclic peptide. **d** A folded cyclic peptide. **e** A Möbius-style cyclic backbone. **f** A bracelet-style cyclic backbone

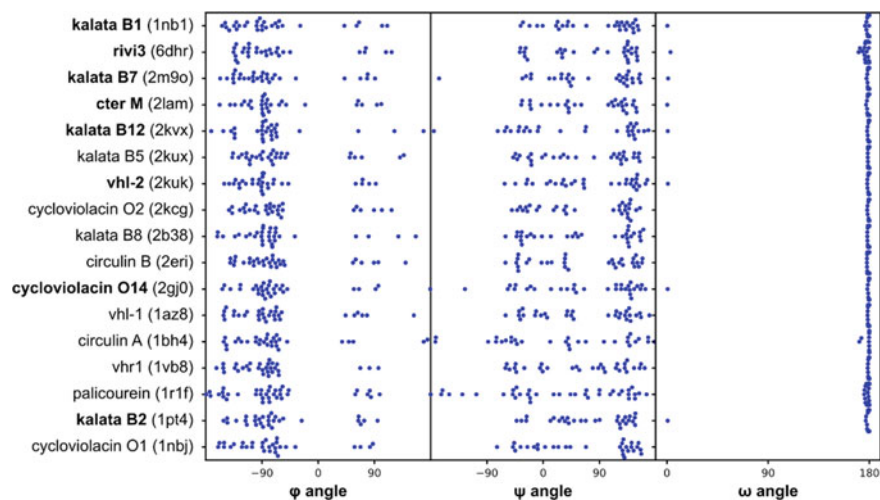
**Table 9.1** Sequences of cyclotides and synthetic derivatives in the PDB

Name of peptide	Sequence	PDB ID	ref
<b>Plant-derived native cyclotides</b>			
Kalata B1	GLPV--CGET-----CVGGT-CNTPG---CTCSWPFV---CTRN	1NB1, IZNU	[28] [40]
Kalata B2	GLPV--CGET-----CFGGT-CNTPG---CSCTWPI---CTRD	IPT4, 2KCH	[29] [41]
Kalata B5	GTP--CGES-----CVYIP-CISGVIG-CSCTDKV---CYLN	2KUX	[42]
Kalata B7	GLPV--CGET-----CTLGT-CYTQG---CTCSWPI---CKRN	2JWM, 2M9O	[43] [44]
Kalata B8	GSVLN-CGET-----CLLGT-CYTTG---CTCNKYRV---CTKD	2B38	[45]
Kalata B12	GSL---CGDT-----CFVLG-CNDSS---CSCNYPI---CVKD	2KVX	[46]
Circulin A	GIP--CGES-----CWVIP-CISAALG-CSCKNKV---CYRN	1BH4	[47]
Circulin B	GVIP--CGES-----CVPIP-CISTLLG-CSCKNKV---CYRN	2ERI	[48]
Varv F	GVPI--CGET-----CTLGT-CYTAG---CSCSWPFV---CTRN	3E4H, 2K7G	[49] [49]
Vhr-1	GIP---CAES-----CVWIP-CTVTALLGCSCSNKV---CYN	1VB8	[50]
Vhl-1	SIS---CGES-----CAMISFCFTEVIG-CSCKNKV---CYLN	1ZA8	[51]
Vhl-2	GLPV--CGET-----CFTGT-CYTNG---CTCDFWPV---CTRN	2KUK	[52]
CyO1	GIP---CAES-----CVYIP-CTVTALLGCSCSNRV---CYN	1NB1, 1DF6	[28] [18]
CyO2	GIP--CGES-----CVWIP-CISSAIG-CSCKSKV---CYRN	2KNM, 2KCG	[53] [41]
[E6E <sup>OMe</sup> ]CyO2 <sup>e</sup>	GIP---CGXS-----CVWIP-CISSAIG-CSCKSKV---CYRN	2KNN	[53]
CyO14	GSIPA-CGES-----CFKFK-CYTPG---CSCSKYPL---CAKN	2GJO	[54]
Violacin A	SAIS--CGET-----CFKFK-CYTPR---CSCSYPV---CK	2FQA	[55]
Tricyclon A	GGTIFDCGES-----CFLGT-CYTKG---CSCGEWKL---CYGTN	1YP8	[56]
Cter M	GLPT--CGET-----CTLGT-CYVPD---CSCSWPI---CMKN	2LAM	[20]
Palicouren	GLPTF-CGET-----CRVIVPVCYSAALGCTCDDRSDDLCKRN	1R1F	[57]
MCoTI-I	GGV---CPKILQR--CRRSDCPGA---CICRNGY--CGSGSD	5WOV	[58]
MCoTI-II	GGV---CPKILKK--CRRSDCPGA---CICRNGY--CGSGSD	1IB9, 1HA9	[59] [60]
MCoTI-V	QRA---CPRI LKK--CRRSDCPGE---CICKNGY--CG	2LJS	[61]
Riv3	GLPI--CGET-----CLLKG-CYTPG---CSCRRPV---CYKN	6DHR	[62]
<b>Synthetic cyclotides</b>			
[Ala 1,15]kB1	GLPV--AGET-----CVGGT-CNTPG---ATCSWPFV---CTRN	1NIU	[63]
[Δ23-28]kB1	V-----CGET-----CVGGT-CNTPG---CTCSWPFV---CT	1ORX	[64]
[P20D,V21K]kB1	GLPV--CGET-----CVGGT-CNTPG---CTCSWDK---CTRN	2F21	[65]
[W19K, P20D,V21K]kB1	GLPV--CGET-----CVGGT-CNTPG---CTCSKDK---CTRN	2F2J	[65]
All-D kalata B1	GLPV--CGET-----CVGGT-CNTPG---CTCSWPFV---CTRN	2JUE	[66]
Linear kalata B1	GLPV--CGET-----CVGGT-CNTPG---CTCSWPFV---CTRN	2KHB	[67]
[W23WW]kB1	GLPV--CGET-----CVGGT-CNTPG---CTCSWPFV---CTRN	2MN1	[68]
[GGG]kB1[GGT]	GLPV <sup>B</sup> -CGET-----CVGGT-CNTPG---CTCSWPFV---CTRN	2MH1	[69]
D/L Kalata B1	GLPV--CGET-----CVGGT-CNTPG---CTCSWPFV---CTRN	4TTM	[70]
[G6A]kalata B1	GLPV--CAET-----CVGGT-CNTPG---CTCSWPFV---CTRN	4TTN	[70]
[V25A]kalata B1	GLPV--CGET-----CVGGT-CNTPG---CTCSWPA---CTRN	4TTO	[70]
[Y15S]kalata B7	GLPV--CGET-----CTLGT-CSTQG---CTCSWPI---CKRN	2MW0	[71]
[ΔSS]MCoTI-II	GGV---CPKILKK--CRRSDCPGA---CICRNGY--CGSGSD	2PO8	[72]
Linear MCoTI-II	GGV---CPKILKK--CRRSDCPGA---CICRNGY--CGSGSD	2IT8	[73]
MTab13	PFAR--CEAIYAAPKRRSDCPGA---CICRNGY--CZ	2MT8	[74]
kB1[ghrw;23-28]	RWGV--CGET-----CVGGT-CNTPG---CTCSWPFV---CGHF	2LUR	[75]

X=E<sup>OMe</sup> B=GGTGGG Z=GEAIYAA

## 9.5 Concluding Remarks and Outlook

Cyclotides were first recognised as a peptide family in 1999 [18] and in the two decades since have been widely applied in drug design and agriculture. They are ribosomally synthesised as linear precursor proteins that are processed by enzymes to achieve their cyclic backbone and knotted trio of disulfide bonds. Cyclotides present a fascinating case study for protein topology, combining a cyclic backbone with knotted cross-linking and, additionally, they mimic molecular Möbius strips in



**Fig. 9.7** Analysis of backbone angles for cyclotide structures deposited in the PDB. The main three panels from left to right show the series of  $\phi$ ,  $\psi$ , and  $\omega$  angles for each residue of all wild-type cyclotides structures that have been studied experimentally. The Protein Data Bank identifier is given between brackets. The names of the Möbius cyclotides are in bold. In contrast to bracelet cyclotides, all Möbius cyclotides display one residue in a cis-conformation (right panel), corresponding to a Pro residue in Loop 5

some cases. Indeed, cyclotides are the only peptide family known to combine all these features into one molecule. The CCK motif occurs in cyclotides and no other family of proteins yet known.

With the ability to readily synthesize cyclotides and make ‘designer’ modifications to them we anticipate that cyclotides may in future be used as stable scaffolds for exploring yet more aspects of protein topology. This might include for example, exploring covalent multimerization of cyclotides. The circular topology of cyclotides is ‘never ending’, and it seems that their potential for interesting studies is also never ending!

**Acknowledgements** DJC is an Australian Research Council (ARC) Australian Laureate Fellow (FL150100146). Work in his laboratory is supported by the ARC Centre of Excellence for Innovations in Peptide and Protein Science (CE200100012).

## References

1. D.J. Craik, D.P. Fairlie, S. Liras, D. Price, *Chem. Biol. Drug Des.* **81**, 136–147 (2013)
2. C.K. Wang, D.J. Craik, *Nat. Chem. Biol.* **14**, 417–427 (2018)
3. D.J. Craik, M. Čemažar, N.L. Daly, *Curr. Opin. Drug Discov. Devel.* **9**, 251–260 (2006)
4. S.J. de Veer, M.-W. Kan, D.J. Craik, *Chem. Rev.* **119**, 12375–12421 (2019)
5. X.W. Wang, W.B. Zhang, *Trends Biochem. Sci.* **43**, 806–817 (2018)
6. J.I. Sulkowska, *Curr. Opin. Struct. Biol.* **60**, 131–141 (2020)
7. A. Zorzi, K. Deyle, C. Heinis, *Curr. Opin. Chem. Biol.* **38**, 24–29 (2017)
8. P.G. Arnison, M.J. Bibb, G. Bierbaum, A.A. Bowers, T.S. Bugni, G. Bulaj, J.A. Camarero, D.J. Campopiano, G.L. Challis, J. Clardy, P.D. Cotter, D.J. Craik, M. Dawson, E. Dittmann, S. Donadio, P.C. Dorrestein, K.D. Entian, M.A. Fischbach, J.S. Garavelli, U. Göransson, C.W. Gruber, D.H. Haft, T.K. Hemscheidt, C. Hertweck, C. Hill, A.R. Horswill, M. Jaspars, W.L. Kelly, J.P. Klinman, O.P. Kuipers, A.J. Link, W. Liu, M.A. Marahiel, D.A. Mitchell, G.N. Moll, B.S. Moore, R. Müller, S.K. Nair, I.F. Nes, G.E. Norris, B.M. Olivera, H. Onaka, M.L. Patchett, J. Piel, M.J. Reaney, S. Rebuffat, R.P. Ross, H.G. Sahl, E.W. Schmidt, M.E. Selsted, K. Severinov, B. Shen, K. Sivonen, L. Smith, T. Stein, R.D. Süßmuth, J.R. Tagg, G.L. Tang, A.W. Truman, J.C. Vederas, C.T. Walsh, J.D. Walton, S.C. Wenzel, J.M. Willey, W.A. van der Donk, *Nat. Prod. Rep.* **30**, 108–160 (2013)
9. Y.Y. Shim, Z. Song, P.D. Jadhav, M.J. Reaney, *Trends Food Sci. Technol.* **93**, 197–211 (2019)
10. M.L. Korsinczky, H.J. Schirra, D.J. Craik, *Curr. Protein Pept. Sci.* **5**, 351–364 (2004)
11. S. Luckett, R.S. Garcia, J.J. Barker, A.V. Konarev, P.R. Shewry, A.R. Clarke, R.L. Brady, *J. Mol. Biol.* **290**, 525–533 (1999)
12. R.J. Clark, J. Jensen, S.T. Nevin, B.P. Callaghan, D.J. Adams, D.J. Craik, *Angew. Chem. Int. Ed.* **49**, 6545–6548 (2010)
13. A.-H. Jin, M. Muttenthaler, S. Dutertre, S.W.A. Himaya, Q. Kaas, D.J. Craik, R.J. Lewis, P.F. Alewood, *Chem. Rev.* **119**, 11510–11549 (2019)
14. Y.Q. Tang, J. Yuan, G. Osapay, K. Osapay, D. Tran, C.J. Miller, A.J. Ouellette, M.E. Selsted, *Science* **286**, 498–502 (1999)
15. M. Trabi, H.J. Schirra, D.J. Craik, *Biochemistry* **40**, 4211–4221 (2001)
16. T. Leta Aboye, R.J. Clark, D.J. Craik, U. Göransson, *ChemBioChem* **9**, 103–113 (2008)
17. R. Burman, E. Svedlund, J. Felth, S. Hassan, A. Herrmann, R.J. Clark, D.J. Craik, L. Bohlin, P. Claeson, U. Göransson, J. Gullbo, *Biopolym. Pept. Sci.* **94**, 626–634 (2010)
18. D.J. Craik, N.L. Daly, T. Bond, C. Waine, *J. Mol. Biol.* **294**, 1327–1336 (1999)
19. D.J. Craik, U. Malik, *Curr. Opin. Chem. Biol.* **17**, 546–554 (2013)
20. A.G. Poth, M.L. Colgrave, R.E. Lyons, N.L. Daly, D.J. Craik, *Proc. Natl. Acad. Sci. U. S. A.* **108**, 10127–10132 (2011)
21. B.F. Conlan, A.D. Gillon, B.L. Barbata, M.A. Anderson, *Am. J. Bot.* **98**, 2018–2026 (2011)
22. S.J. de Veer, A.M. White, D.J. Craik, *Angew. Chem. Int. Ed.* (2020). <https://doi.org/10.1002/anie.202006919>
23. S.L. Gerlach, U. Göransson, Q. Kaas, D.J. Craik, D. Mondal, C.W. Gruber, *Biopolymers* **100**, 433–437 (2013)
24. R. Burman, M.Y. Yeshak, S. Larsson, D.J. Craik, K.J. Rosengren, U. Göransson, *Front. Plant Sci.* **6**, 855 (2015)
25. A.G. Poth, M.L. Colgrave, R. Philip, B. Kerenga, N.L. Daly, M.A. Anderson, D.J. Craik, *A.C.S. Chem. Biol.* **6**, 345–355 (2011)
26. C.W. Gruber, A.G. Elliott, D.C. Ireland, P.G. Delprete, S. Dessen, U. Göransson, M. Trabi, C.K. Wang, A.B. Kinghorn, E. Robbrecht, D.J. Craik, *Plant Cell* **20**, 2471–2483 (2008)
27. O. Saether, D.J. Craik, I.D. Campbell, K. Sletten, J. Juul, D.G. Norman, *Biochemistry* **34**, 4147–4158 (1995)
28. K.J. Rosengren, N.L. Daly, M.R. Plan, C. Waine, D.J. Craik, *J. Biol. Chem.* **278**, 8606–8616 (2003)
29. C.V. Jennings, K.J. Rosengren, N.L. Daly, M. Plan, J. Stevens, M.J. Scanlon, C. Waine, D.G. Norman, M.A. Anderson, D.J. Craik, *Biochemistry* **44**, 851–860 (2005)

30. P. Thongyoo, A.M. Jaulent, E.W. Tate, R.J. Leatherbarrow, *ChemBioChem* **8**, 1107–1109 (2007)
31. P. Thongyoo, N. Roqué-Rosell, R.J. Leatherbarrow, E.W. Tate, *Org. Biomol. Chem.* **6**, 1462–1470 (2008)
32. C. Jennings, J. West, C. Waive, D. Craik, M. Anderson, *Proc. Natl. Acad. Sci. U. S. A.* **98**, 10614–10619 (2001)
33. M.L. Colgrave, A.C. Kotze, Y.H. Huang, J. O’Grady, S.M. Simonsen, D.J. Craik, *Biochemistry* **47**, 5581–5589 (2008)
34. M.L. Colgrave, A.C. Kotze, S. Kopp, J.S. McCarthy, G.T. Coleman, D.J. Craik, *Acta Trop.* **109**, 163–166 (2009)
35. M.L. Colgrave, A.C. Kotze, D.C. Ireland, C.K. Wang, D.J. Craik, *ChemBioChem* **9**, 1939–1945 (2008)
36. P. Lindholm, U. Göransson, S. Johansson, P. Claeson, J. Gulbo, R. Larsson, L. Bohlin, A. Backlund, *Mol. Cancer Ther.* **1**, 365–369 (2002)
37. H. Qu, B.J. Smithies, T. Durek, D.J. Craik, *Aust. J. Chem.* **70**, 152–161 (2017)
38. K. Jagadish, A. Gould, R. Borra, S. Majumder, Z. Mushtaq, A. Shekhtman, J.A. Camarero, *Angew. Chem. Int. Ed.* **54**, 8390–8394 (2015)
39. F.B.H. Rehm, M.A. Jackson, E. De Geyter, K. Yap, E.K. Gilding, T. Durek, D.J. Craik, *Proc. Natl. Acad. Sci. U. S. A.* **116**, 7831–7836 (2019)
40. Z.O. Shenkarev, K.D. Nadezhdin, V.A. Sobol, A.G. Sobol, L. Skjeldal, A.S. Arseniev, *FEBS J.* **273**, 2658–2672 (2006)
41. C.K. Wang, M.L. Colgrave, D.C. Ireland, Q. Kaas, D.J. Craik, *Biophys. J.* **97**, 1471–1481 (2009)
42. M.R. Plan, K.J. Rosengren, L. Sando, N.L. Daly, D.J. Craik, *Biopolymers* **94**, 647–658 (2010)
43. Z.O. Shenkarev, K.D. Nadezhdin, E.N. Lyukmanova, V.A. Sobol, L. Skjeldal, A.S. Arseniev, *J. Inorg. Biochem.* **102**, 1246–1256 (2008)
44. J. Koebach, M. O’Brien, M. Muttenthaler, M. Miazzo, M. Akcan, A.G. Elliott, N.L. Daly, P.J. Harvey, S. Arrowsmith, S. Gunasekera, T.J. Smith, S. Wray, U. Göransson, P.E. Dawson, D.J. Craik, M. Freissmuth, C.W. Gruber, *Proc. Natl. Acad. Sci. U. S. A.* **110**, 21183–21188 (2013)
45. N.L. Daly, R.J. Clark, M.R. Plan, D.J. Craik, *Biochem. J.* **393**, 619–626 (2006)
46. C.K. Wang, R.J. Clark, P.J. Harvey, K.J. Rosengren, M. Cemazar, D.J. Craik, *Biochemistry* **50**, 4077–4086 (2011)
47. N.L. Daly, A. Koltay, K.R. Gustafson, M.R. Boyd, J.R. Casas-Finet, D.J. Craik, *J. Mol. Biol.* **285**, 333–345 (1999)
48. A. Koltay, N.L. Daly, K.R. Gustafson, D.J. Craik, *Int. J. Pept. Res. Ther.* **11**, 99–106 (2005)
49. C.K. Wang, S.-H. Hu, J.L. Martin, T. Sjögren, J. Hajdu, L. Bohlin, P. Claeson, U. Göransson, K.J. Rosengren, J. Tang, *J. Biol. Chem.* **284**, 10672–10683 (2009)
50. M. Trabi, D.J. Craik, *Plant Cell* **16**, 2204–2216 (2004)
51. B. Chen, M.L. Colgrave, N.L. Daly, K.J. Rosengren, K.R. Gustafson, D.J. Craik, *J. Biol. Chem.* **280**, 22395–22405 (2005)
52. N.L. Daly, B. Chen, P. Nguyencong, D.J. Craik, *Aust. J. Chem.* **63**, 771–778 (2010)
53. U. Göransson, A. Herrmann, R. Burman, L.M. Haugaard-Jönsson, K.J. Rosengren, *ChemBioChem* **10**, 2354–2360 (2009)
54. D.C. Ireland, M.L. Colgrave, D.J. Craik, *Biochem. J.* **400**, 1–12 (2006)
55. D.C. Ireland, M.L. Colgrave, P. Nguyencong, N.L. Daly, D.J. Craik, *J. Mol. Biol.* **357**, 1522–1535 (2006)
56. J.P. Mulvenna, L. Sando, D.J. Craik, *Structure* **13**, 691–701 (2005)
57. D.G. Barry, N.L. Daly, H.R. Bokesch, K.R. Gustafson, D.J. Craik, *Structure* **12**, 85–94 (2004)
58. S. Kwon, J.N. Duarte, Z. Li, J.J. Ling, O. Cheneval, T. Durek, C.I. Schroeder, D.J. Craik, H.L. Ploegh, *A.C.S. Chem. Biol.* **13**, 2973–2980 (2018)
59. M.E. Felizmenio-Quimio, N.L. Daly, D.J. Craik, *J. Biol. Chem.* **276**, 22875–22882 (2001)
60. A. Heitz, J.-F. Hernandez, J. Gagnon, T.T. Hong, T.T.C. Pham, T.M. Nguyen, D. Le-Nguyen, L. Chiche, *Biochemistry* **40**, 7973–7983 (2001)

61. J.S. Mylne, L.Y. Chan, A.H. Chanson, N.L. Daly, H. Schaefer, T.L. Bailey, P. Nguyencong, L. Cascales, D.J. Craik, *Plant Cell* **24**, 2765–2778 (2012)
62. P. Niyomploy, L.Y. Chan, P.J. Harvey, A.G. Poth, M.L. Colgrave, D.J. Craik, *J. Nat. Prod.* **81**, 2512–2520 (2018)
63. N.L. Daly, R.J. Clark, D.J. Craik, *J. Biol. Chem.* **278**, 6314–6322 (2003)
64. D.G. Barry, N.L. Daly, R.J. Clark, L. Sando, D.J. Craik, *Biochemistry* **42**, 6688–6695 (2003)
65. R.J. Clark, N.L. Daly, D.J. Craik, *Biochem. J.* **394**, 85–93 (2006)
66. L. Sando, S.T. Henriques, F. Foley, S.M. Simonsen, N.L. Daly, K.N. Hall, K.R. Gustafson, M.I. Aguilar, D.J. Craik, *ChemBioChem* **12**, 2456–2462 (2011)
67. C.K. Wang, H.P. Wacklin, D.J. Craik, *J. Biol. Chem.* **287**, 43884–43898 (2012)
68. S.T. Henriques, Y.H. Huang, S. Chaousis, C.K. Wang, D.J. Craik, *ChemBioChem* **15**, 1956–1965 (2014)
69. X. Jia, S. Kwon, C.I. Wang, Y.H. Huang, L.Y. Chan, C.C. Tan, K.J. Rosengren, J.P. Mulvenna, C.I. Schroeder, D.J. Craik, *J. Biol. Chem.* **289**, 6627–6638 (2014)
70. C.K. Wang, G.J. King, S.E. Northfield, P.G. Ojeda, D.J. Craik, *Angew. Chem. Int. Ed. Engl.* **53**, 11236–11241 (2014)
71. A.A. Strömstedt, P.E. Kristiansen, S. Gunasekera, N. Grob, L. Skjeldal, U. Göransson, *Biochim. Biophys. Acta* **1858**, 1317–1327 (2016)
72. M. Čemažar, A. Joshi, N.L. Daly, A.E. Mark, D.J. Craik, *Structure* **16**, 842–851 (2008)
73. A. Heitz, O. Avrutina, D. Le-Nguyen, U. Diederichsen, J. F. Hernandez, J. Gracy, H. Kolmar, L. Chiche, *BMC Struct. Biol.* **8**, 54 (2008)
74. Y.H. Huang, S.T. Henriques, C.K. Wang, L. Thorstholm, N.L. Daly, Q. Kaas, D.J. Craik, *Sci. Rep.* **5**, 12974 (2015)
75. R. Eliassen, N.L. Daly, B.S. Wulff, T.L. Andresen, K.W. Conde-Frieboes, D.J. Craik, *J. Biol. Chem.* **287**, 40493–40501 (2012)

# Chapter 10

## Construction of a Macromolecular $K_{3,3}$ Graph Topology by the ESA-CF Polymer Folding



Yasuyuki Tezuka

**Abstract** The chemical construction of a macromolecular  $K_{3,3}$  graph, a renowned triply-fused tetracyclic, non-planar construction with various inspiring topological properties, has been undertaken by the ESA-CF protocol. Remarkably, an equivalent topology has been identified in naturally occurring cyclic polypeptides (cyclotides) of unusual bioactivities and thermal stabilities. A uniform-size dendritic polymer precursor having six cyclic ammonium salt end groups, accompanying the two units of a trifunctional carboxylate counteranion, was prepared to balance the charges. The subsequent covalent conversion was completed under dilution to produce the target  $K_{3,3}$  graph product, together with a constitutional isomer having a tetracyclic ladder form. The  $K_{3,3}$  graph polymer product was finally isolated by means of a preparative recycling SEC fractionation technique due to its significantly contracted hydrodynamic volume.

### 10.1 Introduction

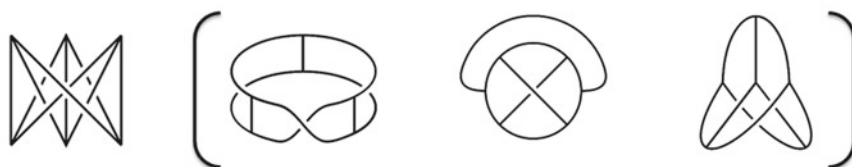
Organic and polymer molecules of appealing structures from Euclidian as well as topological geometry conjectures have continuously been attractive and inspiring synthetic targets in chemistry [1–3]. A class of multicyclic polymers has thus regarded as a bonanza of such endeavor [4], as described in detail in Chap. 6 of this book. And during the course of our pursuit toward the precision designing of multicyclic polymers, we have encountered a particularly intriguing geometrical structure, i.e., a  $K_{3,3}$  graph construction [5].

The  $K_{3,3}$  graph is a triply-fused tetracyclic construction of 6 vertices and 9 edges. Typical line presentations of the  $K_{3,3}$  graph together with its Laplacian matrix expression are shown in Fig. 10.1 [6]. The construction is known as a prototypical non-planar graph, which cannot be embedded in the plane in such a way that its edges intersect only at their endpoints. This geometrical non-planarity is also relevant to a Hopf link (2-catenane) with the inherent crossing number of two and a trefoil knot with the

---

Y. Tezuka (✉)  
Tokyo Institute of Technology, Tokyo, Japan  
e-mail: [ytezukak33@gmail.com](mailto:ytezukak33@gmail.com)

## Laplacian matrix



$$\begin{pmatrix} 3 & 0 & 0 & -1 & -1 & -1 \\ 0 & 3 & 0 & -1 & -1 & -1 \\ 0 & 0 & 3 & -1 & -1 & -1 \\ -1 & -1 & -1 & 3 & 0 & 0 \\ -1 & -1 & -1 & 0 & 3 & 0 \\ -1 & -1 & -1 & 0 & 0 & 3 \end{pmatrix}$$

For  $K_{3,3}$  Graph

vs



$$\begin{pmatrix} 3 & -1 & 0 & -2 & 0 & 0 \\ -1 & 3 & -1 & 0 & -1 & 0 \\ 0 & -1 & 3 & 0 & 0 & -2 \\ -2 & 0 & 0 & 3 & -1 & 0 \\ 0 & -1 & 0 & -1 & 3 & -1 \\ 0 & 0 & -2 & 0 & -1 & 3 \end{pmatrix}$$

For Ladder Graph

**Fig. 10.1** Typical line presentation of a  $K_{3,3}$  and its isomeric ladder graph constructions with their Laplacian matrix expressions. Reprinted from [12], Copyright 2020, with permission from Elsevier

crossing number of three. Therefore, the  $K_{3,3}$  graph having the crossing number of one is considered as a primary member in a class of non-planar graph constructions. Interestingly, moreover, the  $K_{3,3}$  graph is known to be drawn on the torus surface by avoiding such intersection of the edges [6].

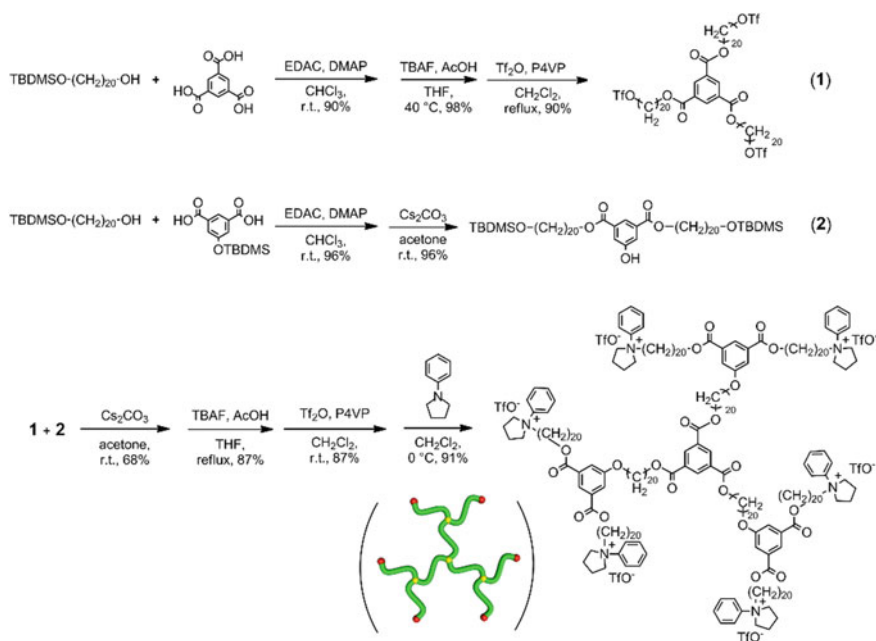
It is, therefore, inspiring to pursue experimentally how such unique topological properties in basic graph theories can direct any fundamental characteristics of flexible polymer molecules. Notably, moreover, the relevant topology has been identified in a class of cyclic peptides having *fused*-multicyclic structures, *cyclotides*, from diverse origins, to achieve the extraordinary stability and bioactivity. In nature, a class of cyclotide topologies is formed enzymatically through the folding of linear polypeptide precursor with the intramolecular S–S bridging between cysteine residues [7, 8]. Thus, in this chapter, the construction of a macromolecular  $K_{3,3}$  graph having uniform-size edge components of eicosanediol ( $C_{20}$ ) segments, is presented as a successful first step challenge [5].



## 10.2 Preparation of a Dendritic Precursor for the Construction of a $K_{3,3}$ Graph Topology

The chemical construction of a macromolecular  $K_{3,3}$  graph has been undertaken by means of the ESA-CF polymer folding with a uniform-size dendritic polymer precursor prepared according to the procedure shown in Scheme 10.1 [5]. Thus firstly, a uniform-size dendritic polymer precursor having six hydroxyl end groups was prepared by the coupling reaction of one unit of a three-armed star-shaped precursor having triflate ester end groups with three units of a linear counterpart having a phenolic group at the center position, both of which comprise the alkyl chain sequence of 1,20-eicosanediol. The coupling reaction of the two precursors was found to proceed in the presence of  $\text{Cs}_2\text{CO}_3$  in acetone.

The six hydroxyl end groups of the obtained dendritic polymer precursor were subsequently converted into trifluoromethanesulfonate (triflate) ester groups by treatment with triflic anhydride in the presence of poly(4-vinyl pyridine), followed by the quaternization treatment with *N*-phenylpyrrolidine to give a uniform-size dendritic polymer precursor with eicosanediol ( $\text{C}_{20}$ ) segments having six *N*-phenylpyrrolidinium salt end groups. The  $^1\text{H}$  and  $^{13}\text{C}$  NMR spectroscopic and



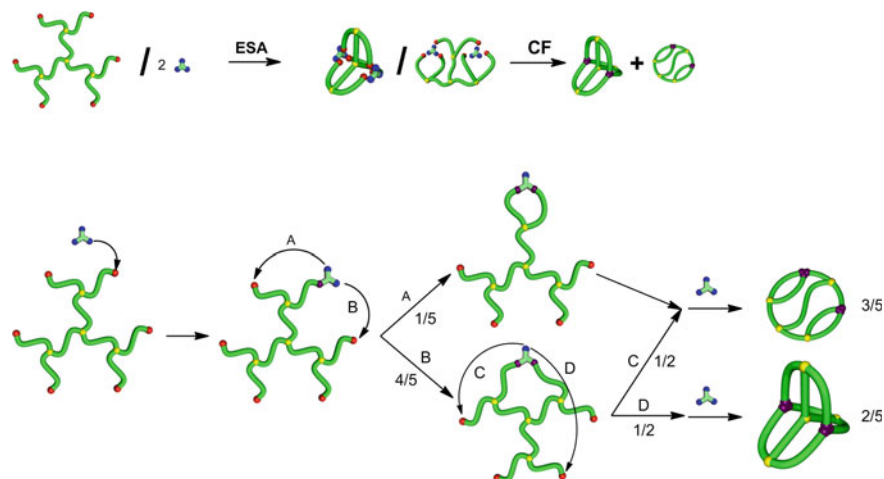
**Scheme 10.1** Synthesis of a dendritic precursor for the construction of a macromolecular  $K_{3,3}$  graph. Adapted with permission from [5]. Copyright 2014 American Chemical Society (ACS AuthorChoice)

MALDI-TOF mass analyses of each step products, and the MALDI-TOF mass analyses conducted, in particular, for the covalently converted derivative obtained by the treatment with tetrabutylammonium benzoate to cause the ring-opening reaction of the *N*-phenylpyrrolidinium salt groups, were carried out to unequivocally confirm the structure of the prescribed dendritic precursor product.

### 10.3 Constructing a Macromolecular $K_{3,3}$ Graph by the ESA-CF Protocol

The obtained dendritic precursor accompanies initially six triflate counteranions at each cyclic ammonium end groups, which were subsequently replaced by two units of trifunctional carboxylate, 1,3,5-tris(4-carboxylatephenyl)benzene (Fig. 10.2, top), by the precipitation treatment of a THF solution of the precursor into an ice-cooled aqueous solution containing a large excess of the tricarboxylate as the  $\text{Na}^+$  salt form. The ion-exchange product, in which the anions and the cations balance the charges by the smallest combination number between the components, was recovered with deliberately retaining a trace amount of water in order to avoid uncontrolled ring-opening reaction.

The subsequent covalent conversion was completed by the ring-opening reaction of cyclic ammonium salt groups at an elevated temperature under dilution [9]. Thus, the intermediate ion-pair precursor was subjected to the heat treatment by refluxing in THF/ $\text{CH}_3\text{OH}$  (vol./vol. = 9/1) at a concentration of 0.1 g/L for 12 h, to cause



**Fig. 10.2** The ESA-CF construction of triply-*fused* tetracyclic polymer topologies with a dendritic precursor carrying two trifunctional counteranions, through the random chain folding of the end groups. Adapted with permission from [5]. Copyright 2014 American Chemical Society (ACS AuthorChoice)

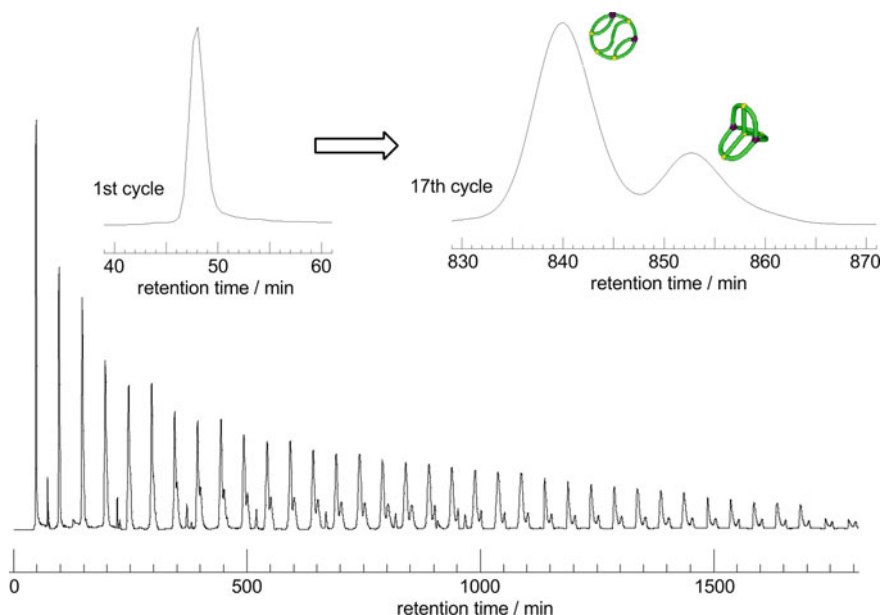
the ring-opening of the cyclic ammonium salt groups by carboxylate species. The soluble product was isolated in 17% yield after the reprecipitation into water and subsequent silica-gel column ( $\text{CH}_2\text{Cl}_2$ ) work-up. The  $^1\text{H}$  NMR spectroscopic analysis of the product showed the new multiplet signal due to the ester-methylene protons at 4.18–4.47 ppm, replacing those for the methylene protons adjacent to *N*-phenyl groups visible at 3.60–3.73 ppm. By the MALDI-TOF mass analysis, moreover, the covalent conversion product showed a peak at  $m/z = 5024.29$ , corresponding to the most abundant mass of the product possessing the expected chemical structure of  $\text{C}_{327}\text{H}_{480}\text{N}_6\text{O}_{33}$  plus  $\text{H}^+$  as 5023.63, which is expected from the presence of multiple basic amine functionalities in the macromolecule and from the use of a mildly acidic matrix.

Notably, a pair of constitutional isomer products, i.e., a  $K_{3,3}$  graph structure and another ladder-shaped counterpart, are expected during the covalent conversion, corresponding to the two distinctive linking mode by the two units of a trifunctional reagent at the six chain-ends of the dendritic precursor. And the isomer composition ratio of 2:3 is hypothesized with the  $K_{3,3}$  graph product as a minor component when the random combination takes place during the chain folding by the end groups (Fig. 10.2, bottom).

By means of a preparative recycling SEC technique, these two constitutional isomers of the  $K_{3,3}$  graph construction and the concurrent tetracyclic ladder form were successfully resolved as their hydrodynamic volumes are distinctive each other (Fig. 10.3). The presence of the two components became apparent after repeated recycling, despite the eventual resolution was not obvious at the first cycle. From the SEC peak area analysis, the isomer ratio was estimated to be 7:3, with the minor component assignable to the  $K_{3,3}$  graph fraction having the smaller hydrodynamic volume. While the observed isomer ratio was comparable to the statistic value of 6:4, the formation of the ladder isomer was appeared to be slightly favored. This result is in agreement to the model study [10], showing the spatial distance between the linking positions in the linear polymer precursor as a key parameter directing the polymer folding process. Thus, the ladder isomer product is formed through the initial smaller ring formation path by the linking of the chain ends positioned at the shorter spatial distance in the dendritic polymer framework (Fig. 10.2). The resolved two components having the larger and smaller elution volumes were subsequently isolated by a stepwise fractionation after the 17th cycle (Fig. 10.3).

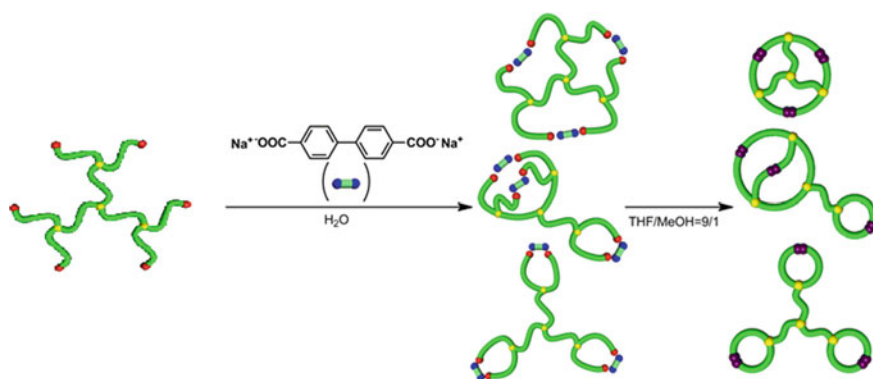
The isolated two fractions exhibited undistinguished  $^1\text{H}$  NMR and MALDI-TOF mass spectra. On the other hand, the analytical SEC measurements, using the calibration by polystyrene standards as a quantitative measure for their hydrodynamic volumes in solution, showed that their peak molecular weights ( $M_p$ ) were distinctive from each other, i.e., 3440 and 2990, respectively. And the ratio of their hydrodynamic volumes, i.e.,  $2900/3440 = 0.84$ , was in close agreement with the relevant ratio of the square of the radius of gyration ( $R_g^2$ ), i.e.,  $0.43/0.50 = 0.86$ , estimated by the simulation study [11]. Upon these results, the minor fraction having the smaller 3D size was unequivocally assigned as the  $K_{3,3}$  graph product.

The ESA-CF polymer folding with the dendric polymer precursor was further extended by employing a difunctional carboxylate, 4,4'-biphenyl dicarboxylate, in

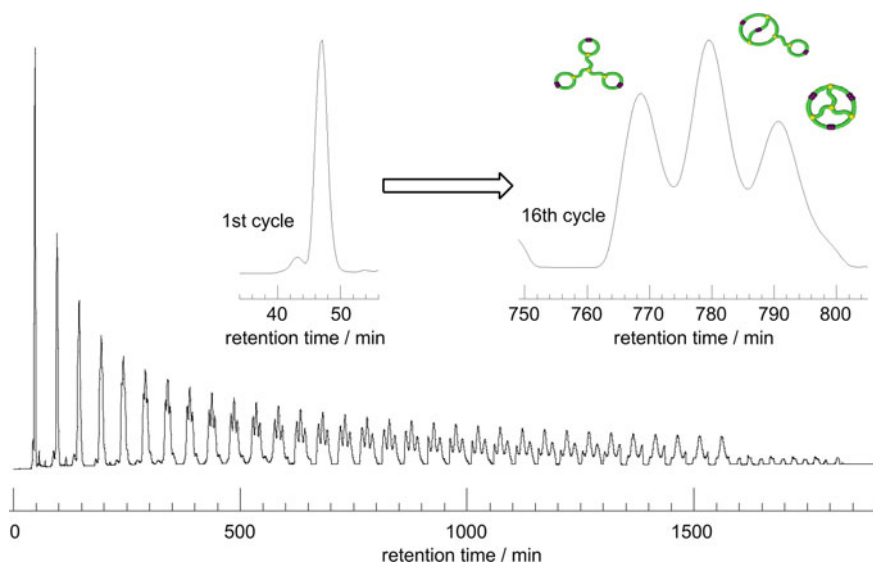


**Fig. 10.3** The resolution/isolation of the  $K_{3,3}$  graph product by means of the recycling SEC technique (the first and the 17th cycle charts are shown in insets). Adapted with permission from [5]. Copyright 2014 American Chemical Society (ACS AuthorChoice)

place of a trifunctional counterpart for the  $K_{3,3}$  graph construction (Fig. 10.4). By this process, the isomeric mixture of three types of tricyclic macromolecular topologies, including a *fused*-type  $\alpha$ -graph topology and a *bridged*-type three-way paddle-form, were expected to be produced (Fig. 10.4).



**Fig. 10.4** The ESA-CF construction of doubly-*fused* tricyclic polymer topologies with a dendritic precursor carrying three difunctional counteranions. Adapted with permission from [5]. Copyright 2014 American Chemical Society (ACS AuthorChoice)



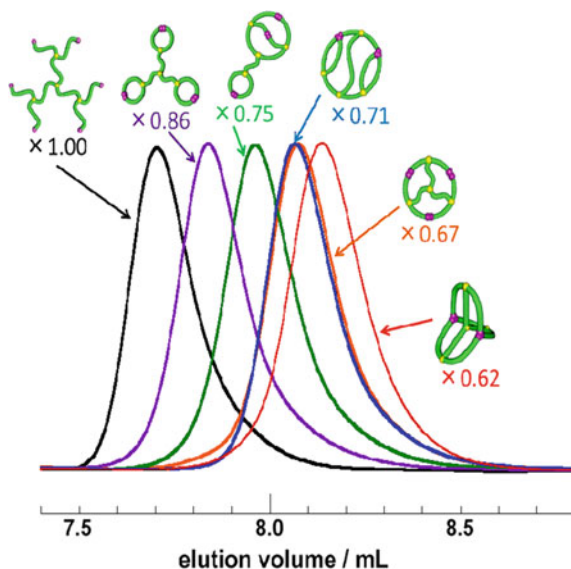
**Fig. 10.5** The resolution/isolation of the three tricyclic polymeric isomers by means of the recycling SEC technique (the first and the 16th cycle charts are shown in insets). Adapted with permission from [5]. Copyright 2014 American Chemical Society (ACS AuthorChoice)

The preparative recycling SEC technique was again successfully applied, to resolve three components after repeated recycling (Fig. 10.5). The three isomer components were subsequently isolated by first collecting the larger and smaller elution volume components with stepwise fractionation after 16th cycle (Fig. 10.5). The  $^1\text{H}$  NMR and MALDI-TOF spectra of the three isolated fractions were practically identical each other to confirm the expected chemical structures for all three constitutional isomers.

From the SEC peak area analysis, the isomer ratio was estimated to be 3:4:3, in which the smallest hydrodynamic volume fraction is assignable to a doubly-fused tricyclic  $\alpha$ -graph product, and the largest counterpart as a three-paddle form isomer, respectively, according to the simulation study applied before [11]. The observed isomer ratio was noticeably different from the statistical ratio of 1:6:8, which is again accounted for by the model study [10], showing the spatial distance between the linking positions in the linear polymer precursor as a key parameter directing the polymer folding process. Thus, the three-paddle form isomer product is formed through the initial smaller ring formation path by the linking of the chain ends positioned at the shorter spatial distance in the dendritic polymer framework (Fig. 10.4).

Finally, by making use of a variety of tricyclic and tetracyclic polymer products of defined topologies, including the  $K_{3,3}$  graph construction, their relative 3D sizes in reference to the starting dendritic precursor were compared systematically by

**Fig. 10.6** Analytical SEC charts of a series of tricyclic and tetracyclic polymers with relative hydrodynamic volumes with reference to the dendritic precursor. Reprinted with permission from [5]. Copyright 2014 American Chemical Society (ACS AuthorChoice)

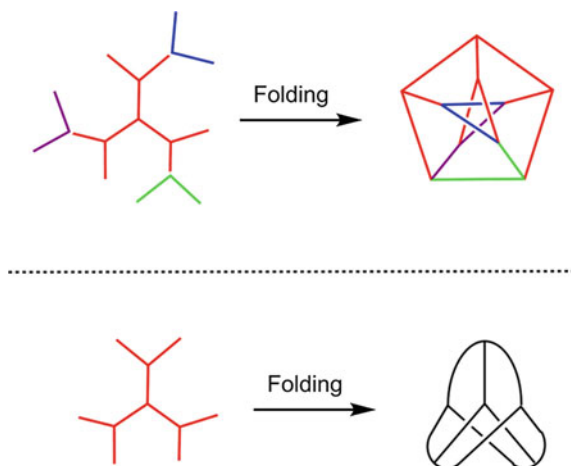


means of the analytical SEC technique (Fig. 10.6). It is clearly shown that the triply-fused tetracyclic  $K_{3,3}$  graph polymer is exceptionally contracted in its 3D size, in comparison with the starting dendritic precursor and with other *spiro*- and *bridged*-multicyclic counterparts. Indeed, by the SEC peak molecular weight analysis, the  $K_{3,3}$  graph polymer ( $M_p = 2990$ ) is significantly contracted in its hydrodynamic volume against the dendritic precursor ( $M_p = 4840$ ) by the ratio of 0.62. Thereby, one could assume that a class of cyclotides having a folded structure equivalent to the  $K_{3,3}$  graph topology has self-evolved into an extremely compact 3D conformation through the chain folding with S–S bridges, to achieve exceptionally thermostable bioactivities. Further, this work will provide new insights in polymer materials design by chain-folding, to modulate the conformational stability of randomly coiled flexible polymer segments.

## 10.4 Perspectives Toward Elusive Polymer Topologies

The ESA-CF polymer folding with a dendritic precursor is arguably a versatile means for the precision construction of complex and intriguing polymer topologies, such as a  $K_{3,3}$  graph shown in this chapter. Another attractive challenge in *topological polymer chemistry* undoubtedly includes an elusive Petersen graph polymer construction, shown in Fig. 10.7. The graph is comprised of 10 vertices and 15 edges, and is a non-planer graph as the  $K_{3,3}$  counterpart having 6 vertices and 9 edges [6]. The graph has been recognized as a useful example or a counterexample for many problems in graph theory. In particular, the Petersen graph polymer is intriguing by considering its

**Fig. 10.7** Folding construction of a Petersen graph topology (above) as the extension of a  $K_{3,3}$  counterpart (below). Reprinted from [12], Copyright 2020, with permission from Elsevier



coloring properties, as the graph has chromatic number 3, meaning that its vertices can be colored with three colors—but not with two—such that no edge connects vertices of the same color, and the graph has chromatic index 4; coloring the edges requires four colors—but not with three.

Remarkably, the Petersen graph polymer is accessible, in principle, through a direct extension of the chemical construction process of a macromolecular  $K_{3,3}$  graph, achieved by the ESA-CF folding process shown in Fig. 10.7 (bottom) [12, 13]. Thus, the relevant polymer folding using a specifically designed dendritic polymer precursor having nine end groups and with the three units of a three-way linker component eventually constitutes the Petersen graph topology as shown in Fig. 10.7 (top). The open question is to address how to translate this geometrical operation into any applicable chemical reaction processes. Such efforts greatly deserve creating important steps toward the programmed but non-enzymatic polymer folding with synthetic polymer systems [12, 13].

## References

1. E. Flapan, *When topology meets chemistry. A topological look at molecular chirality* (Cambridge University Press, Cambridge, 2000)
2. D.M. Walba, *Tetrahedron* **41**, 3161 (1985)
3. J.C. Chambron, C. Dietrich-Buchecker, J.P. Sauvage, *Topics Curr. Chem.* **165**, 131 (1993)
4. Y. Tezuka, *Acc. Chem. Res.* **50**, 2661 (2017)
5. T. Suzuki, T. Yamamoto, Y. Tezuka, *J. Am. Chem. Soc.* **136**, 10148 (2014)
6. K. Shimokawa, K. Ishihara, Y. Tezuka, *Topology of Polymers* (Springer, Tokyo, 2020)
7. D.J. Craik, *Science* **311**, 1563 (2006)
8. D.J. Craik, *Trends Plant Sci.* **14**, 328 (2009)
9. H. Oike, H. Imaizumi, T. Mouri, Y. Yoshioka, A. Uchibori, Y. Tezuka, *J. Am. Chem. Soc.* **122**, 9592 (2000)

10. K. Kyoda, T. Yamamoto, Y. Tezuka, *J. Am. Chem. Soc.* **141**, 7526 (2019)
11. E. Uehara, T. Deguchi, *J. Chem. Phys.* **145**, 164905 (2016)
12. Y. Tezuka, *React Funct Polym.* **148**, 104489 (2020)
13. Y. Tezuka, *Isr. J. Chem.* **60**, 67 (2020)



# Chapter 11

## Programmed Polymer Folding



Laurens W. H. J. Heling, Seyedeh Elnaz Banijamali, Vahid Satarifard,  
and Alireza Mashaghi

**Abstract** In this chapter, we discuss emerging concepts and tools for engineering molecular folds. We focus on linear polymers including engineered proteins and DNA as well as polymers of non-biological origins. We outline the implications of fold topology for the kinetics of folding reactions and the stability of the synthesized fold. The relation between topology and molecular properties including mechanical response to external forces will be discussed. For the desired topology, we will examine monomer chemistry options and available synthesis protocols. The chapter will end with a perspective of future challenges and possibilities in programmed polymer folding.

### 11.1 Introduction

Polymers are an important class of chemicals that exist with a wide variety of properties in natural and synthetic forms. They hold important and ubiquitous roles in nature and are the basis of important industrial goods. Polynucleotides, for instance, carry genetic information in living organisms while polypeptides, more commonly known as proteins, carry enzymatic and structural functions. On the other hand, synthetic polymers such as plastics (polyethylene, polypropylene, etc.) are vastly used in our everyday life. The chemical nature of polymers is the basis for their properties, but the geometry and topology (shape properties that are not affected by continuous deformation, and it should not be confused with geometry or configuration [1]) are

---

L. W. H. J. Heling · V. Satarifard · A. Mashaghi (✉)  
Faculty of Science, Leiden University, Einsteinweg 55, 2333CC Leiden, The Netherlands  
e-mail: [a.mashaghi.tabari@lacdr.leidenuniv.nl](mailto:a.mashaghi.tabari@lacdr.leidenuniv.nl)

S. E. Banijamali  
Department of Medical Biochemistry and Biophysics, Karolinska Institute, Biomedicum,  
Solnavägen 9, 17177 Stockholm, Sweden

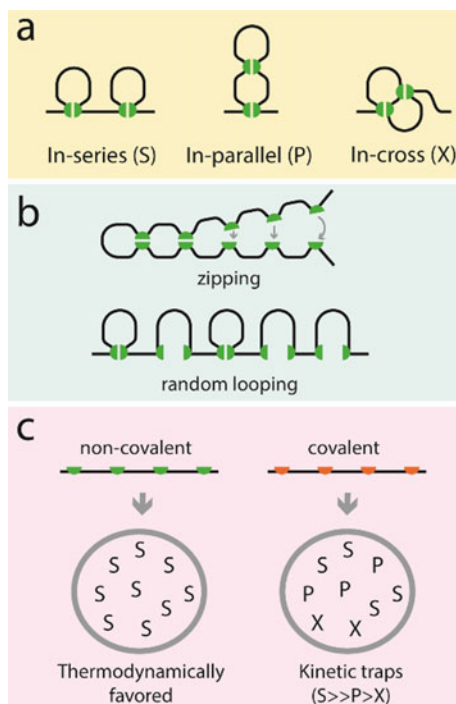
V. Satarifard  
Department of Theory and Biosystems, Max Planck Institute of Colloids and Interfaces, 14424  
Potsdam, Germany

equally important. The latter is a less explored aspect in the field of polymer science and technology. This is particularly true in the case of linear polymers.

While nature learned how to make linear polymers with various topologies, the field of topological polymer synthesis has been primarily focused on non-linear polymers. Chemists have long recognized that a lot can be done with topology and folded polymers [2], however, the lack of appropriate conceptual framework and complexity of the folding process hindered the development of folded polymer synthesis. Understanding how nature makes such polymers is not only important to understand biology and diseases but can also be used to develop bioinspired protocols for polymer synthesis.

Every folded biopolymer exists as a linear chain of subunits belonging to a limited set of chemistries, yet they create the most astonishing structural complexity and variety when folded. A chain of nucleotides that is 2 m of genomic DNA, tightly folds into a globular structure (via protein bridges) that fits within the microscopic nucleus of every human cell, while a chain of RNA folds according to their downstream function. All proteins, also called the primary machinery of life, from ATPases to channel pores and motor proteins are built up from different sequences of a set of 20 amino acids. Two topological frameworks developed to describe the structural diversity in linear biomolecules are knot theory and circuit topology (CT) [3–5]. Entanglements or knots appear in proteins and nucleic acid chains (RNA [6], viral and cellular DNA [7–10]), even though the folding kinetics of knotted chains is often significantly slower than for unknotted ones [11]. Structural analysis indicates strict evolutionary conservation which implies important physiological and structural roles for the knots [12, 13]. Knots present at important functional regions in proteins, potentially providing structural contacts and thermal stability of active sites [13]. Knot theory appears to be a strong method to characterize these structures. A downside of knot theory is that knots only appear in approximately 0.77% of all known proteins [14]. Additionally, knot theory defines knots as closed rings, which is an uncommon structure in biomolecules. For protein structure, a generalization of knot theory, knotoids—which describes open curves in three-dimensional (3D) space [15], has gained traction to define entanglement [16]. Finally, despite many applications, knot theory and knotoids ignore intrachain contacts.

Recently, the concept of CT has emerged as a powerful modern framework well suited to formally describe intramolecular interactions. These interactions, such as electrostatic interactions, hydrogen bonds, Van der Waals, or covalent bonds, manifest themselves in the form of physical contacts with non-neighboring monomers that can be obtained from structure determination techniques (most commonly X-ray crystallography, nuclear magnetic resonance spectroscopy, and electron microscopy), or extracted from single-molecule force spectroscopy experiments. For a pair of binary contacts only three arrangements are topologically distinct: series (S), parallel (P), and cross (X) (Fig. 11.1). This classification can cover all the possible arrangements of contact pairs in single-chain polymers. The concept of CT has recently been extended to include entanglements of chains (knotting and slipknots), which makes CT uniquely suited toward the engineering of molecules [17].



**Fig. 11.1** Circuit topology and its implications for folding. **a** Circuit topology categorizes pairwise arrangements of intrachain contacts into three categories, series (S), parallel (P), and cross (X). **b** Formation of two loops might happen independently (e.g., for contacts in Series) or cooperatively (e.g., zipping events), depending on the topological relation of contacts. **c** The types of bonds affect their dominant arrangements. When bonds are non-covalent, the system reaches a topology with the lowest conformational free energy. If the 4 contact sites are identical and equally spaced long enough apart, series topology will have the lowest free energy and thus all chains in an ensemble will eventually fold into series topology. When covalent bond formation is induced by adding a chemical inducer or by UV illumination, conformations will be trapped kinetically in certain topologies, where one would expect to obtain significant amounts of parallel and cross arrangements, mixed with chains with series topology

In this chapter, we discuss these topological concepts and the knowledge that has emerged from biological studies and we propose design principles to synthesize topologically diverse chains. To design a folded chain, we first need to rationally choose a topology. This is important because: (1) the topology has implications for the properties of the molecule, including its mechanical properties and stability; (2) some topologies can spontaneously form, while others need to be facilitated externally; (3) some topologies are hard to synthesize, purify, and characterize.

## 11.2 Topology and Folding Landscape

To be able to program a folding process, one must first understand folding pathways available to a given topology and their kinetics. Folding kinetics are important mainly because slow folders are prone to aggregation, which leads to lower yield. If multiple topologies provide a given desired property, the topology with better folding kinetics would be a preferred design. Kinetic control can be introduced during the folding process to promote the desired topology. The folding of polymers is a very dynamic process often with several intermediate structures which occurs when intrachain contacts are established, creating pairwise or higher-order connections, depending on the free energy barrier. The information provided by the CT framework can be used towards the design of a novel polymer chain. An engineered folded polymer should typically contain three core properties: (1) the right structure to be able to do the desired function; (2) have a good yield, established by high folding rates and low aggregation rate; and (3) to be stable under mechanical and chemical stress. The topological features of a certain structure can be used to predict the folding and unfolding dynamics, complementing the information from energetic and geometric measurements. Studies using theoretical models [18] showed that the topological arrangement of intrachain contacts affect the folding kinetics; cross and parallel relations increase the folding rate compared to series relations under certain geometric conditions. Including sequences in the polymer that will establish parallel and cross relations can possibly lead to a good yield.

Folded structures mediated by non-covalent bonds are dynamic in nature and formed by continuous breaking and formation of new contacts. Meanwhile, external factors such as temperature, ionic strength, or mechanical forces, can change this balance toward unfolded conformations. An important property of polymeric materials is their response to introduced mechanical forces. One useful example is the presence of sacrificial bonds of biomaterials and how the circuit topology affects the mechanical properties of the polymeric matrix [19, 20]. Topology has implications for unfolding [21]; thus, to have a polymer with a given desired response to mechanical stretching, certain topological designs must be considered. The likeliness of unfolding for a polymer is partly determined by the number of unfolding pathways and the inherent efficiency of the applied unfolding mechanism. Fold topology, the arrangement and number of the “non-breakable” bonds affect the unfolding process. Mechanical stretching can be applied with several methods: (1) by pulling on either end of the polymer; (2) by threading the polymer through a nanopore, or (3) by pulling and threading a polymer through a nanopore at the same time [22, 23]. Contacts that are nested inside other contacts will only break when the covering contacts are broken. Consequently, the number of unfolding pathways decreases by increasing the number of parallel relations. It should be noted that in the pulling and threading method, the distance between the end of the chain and the pore is an important factor since this will indicate the number of series and cross relations and the corresponding unfolding pathways. Thus, both topology and geometry are important determinants of polymer unfolding dynamics. Contact energy is a key player

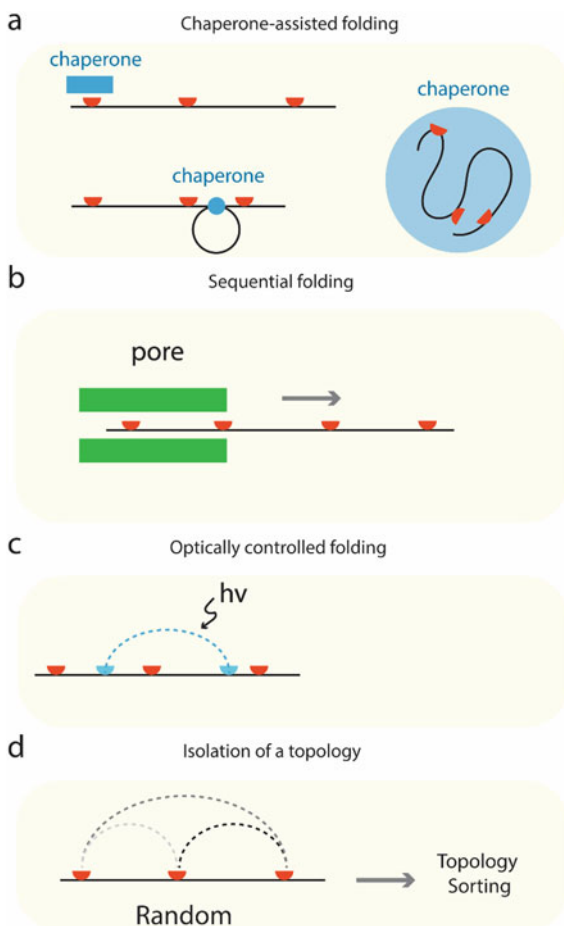
as well. Introducing an “unbreakable” contact in the chain will affect the efficiency of unfolding. It is worth noting that whenever a chain contains only cross relations, regardless of contact position, unfolding efficiency is the lowest under all pulling methods [21].

### 11.3 Guided Folding and Folding Catalysts

When programming a folding process, the ability of transiently tuning folding pathways is of significant importance. In some cases, one can readily design the primary sequence of a polymer, and subsequent folding to the desired topology occurs spontaneously with a desired kinetics and yield (Fig. 11.1c, left). However, in other cases, the desired topology might not be accessible spontaneously, or competing undesired folding processes may affect the yield significantly. One way to modulate this, is to guide the folding pathway via transient, non-native contacts that confine the chain configuration and change the searching space and kinetics of folding. Biology provides us with several different scenarios of guided polymer folding. Nascent polypeptide chains mostly follow Anfinsen’s principle [24] and can fold into their native structures spontaneously, while the rest need the help of other molecules (i.e., chaperones) to fold correctly. Chaperones can promote the correct folding of protein chains by altering the folding kinetics and facilitating the formation of native contacts. Moreover, chaperones can prevent irreversible protein aggregation by shielding the hydrophobic cores of intermediate structures [25]. Chaperones introduce various forms of confinements, thereby guide the folding process: (1) they may transiently shield a contact site; (2) they may bridge two regions of the polymer, thus introduce transient non-native contacts (so-called internal confinement); (3) they may enclose the whole polymer or a polymer segment by forming a cavity around it (external geometrical confinement) (Fig. 11.2a) [26, 27]. Bioinspired chaperone-like molecules may be designed and used in the engineering of *de novo* polymers, where certain topological designs are desired.

Constraints can be introduced to a folding chain to guide its folding within the circuit topology landscape. For example, the chain can be confined either partly or entirely in an enclosing cavity. Confinement alters the structural dynamics and stability of molecules, as well as their topological arrangements. Under different confinement scenarios, e.g., confining spheres with smaller or larger radii, certain topological conformations will be promoted while others will be suppressed [27]. For instance, under strong confinement, more entangled cross and parallel topologies are expected to have an equal or higher probability of formation compared to independent series topology which can form easily in response to entropic forces. Molecular dynamics simulations suggest that in linear chains under weak confinements, the probability of cross and parallel topological arrangements is low compared to the series counterpart. If the confinement gets stronger, the collision probability of more distant contacts is growing, which leads to an increase in parallel and cross topology

**Fig. 11.2** Guided Folding Methodologies. Guided folding can be applied by using chaperones (a) or nanopores (b), by altering the backbone chemistry with reactive groups (c), or using sorting methodologies to isolate the desired topology (d)



relations while series topology relations are sporadic. To select a certain topology, folding blockers or folding catalysts are two techniques that can be used.

For programming large folds, biology often utilizes a sequential folding strategy that allows folding of the chain from one of its ends. In cells, protein folding starts during translation, which is important especially for large proteins, since it can prevent misfolding and/or protein aggregation [28, 29]. In topology engineering, this methodology can offer additional control over the folding process and promote certain topology arrangements. In an experimental setting, a nanopore can do a similar function to ribosome exit tunnel, allowing a section of the chain to fold without interference from other chain sections, effectively selecting one topology over another (Fig. 11.2b).

## 11.4 Bond and Backbone Chemistry

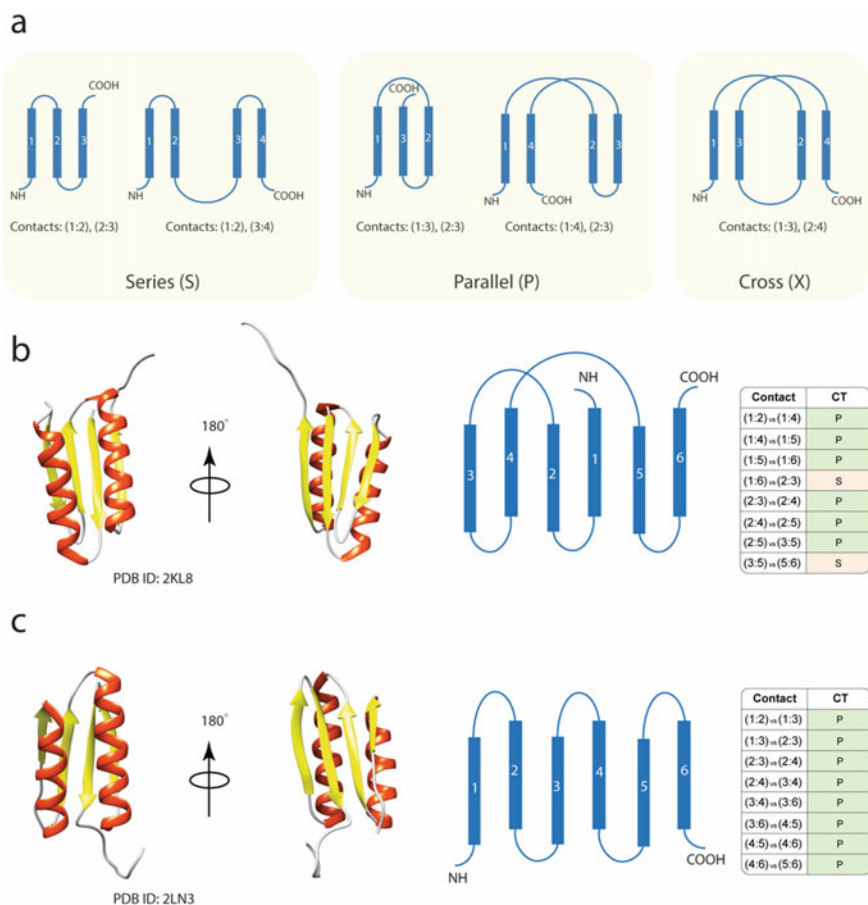
In previous sections, we outlined the implications of topology for folding/unfolding pathways, and how the guided folding process can alter the probability of topological arrangements. In this section, we discuss how these fundamental concepts can be put into practice and what practical challenges are on the way.

After choosing the desired fold topology, one must decide on appropriate backbone chemistry, type of contact sites, and develop a synthesis protocol. Depending on the chemistry, one may use chaperone-like molecules to guide folding or use other external modulators such as light in the case of photo-inducible linkages (Fig. 11.2c). *In silico* approaches tremendously help in this regard. Computational simulation techniques can be used to optimize polymer engineering by predicting folding/unfolding pathways and the structural stability of the desired folded state.

### 11.4.1 Designing New Proteins

In polypeptides, there is a vast structural and topological variety that has been developed through billions of years of evolution. The genome encodes for 20 amino acids, and considering that proteins typically are about 100 amino acids long, there are over  $20^{100}$  possible amino acid combinations, which is significantly more than what we see in nature. This means there is a vast number of possible, non-native, sequences, and structures that can be designed and used for different applications ranging from novel therapeutics to materials science. In the last few decades, advancements in computational approaches have had a great impact on bioengineering. Computational approaches can be used to generate *de novo* polypeptides with novel fold topologies, showing new functions, optimal binding affinities, and stability [30]. Current protein folding design, primarily relies on sequence engineering; the engineered sequence then spontaneously folds into secondary and tertiary structures that consistently favor the desired folded configuration. The Baker group is one of the leading groups in *de novo* proteins engineering. They have developed software packages for molecular modeling and protein structure analysis, such as Rosetta [31], and introduced a novel protocol for protein engineering based on sequence-independent backbone modeling of secondary structure elements. In their protocol, the length and orientation of each secondary structure element are selected in a way that native structure (which is the desired structure) will be more favored than other non-native intermediate states. After all, by using computational simulation techniques (i.e., Monte Carlo simulated annealing) the best amino acid sequence that can make the desired structure more stable will be selected [32]. Therefore, the incorporation of favorable secondary structure configurations is allowed, while the competing alternatives are limited by applying the ideal amino acids selection for the backbone to create chosen tertiary structures. Through these principles, one can systemically design naturally

occurring folds (such as Rossmann and ferredoxin-like) with extreme accuracy and high thermostability due to the optimization of the sequence. Their method is also applicable for designing more complex structures by combining different protein domains [33, 34]. This approach can be adapted to design proteins with a wide range of circuit topologies, that feature  $\alpha/\alpha$ ,  $\beta/\beta$ , or  $\alpha/\beta$  contacts in desired arrangements (Fig. 11.3). Circuit topology, on the other hand, provides a coarse-grained representation of the chain that speeds up in silico modeling of the folding process. For



**Fig. 11.3** Secondary structure arrangement based on CT. **a** Schematic views of three main CT arrangements: series (S), parallel (P), and cross (X). Each rectangle represents a secondary structure element, either  $\alpha$ -helix or  $\beta$ -strand. **b** and **c** show tertiary structure (on the left) and the arrangement of secondary structures (schematic view on the right) of two different proteins with the same number of secondary structures, but different arrangements. Here, two secondary structure elements are considered connected when they have at least 10 contact points within 4.5 Å as cutoff distance. The topology of connected pairs, based on the CT framework, is represented in the charts on the far right

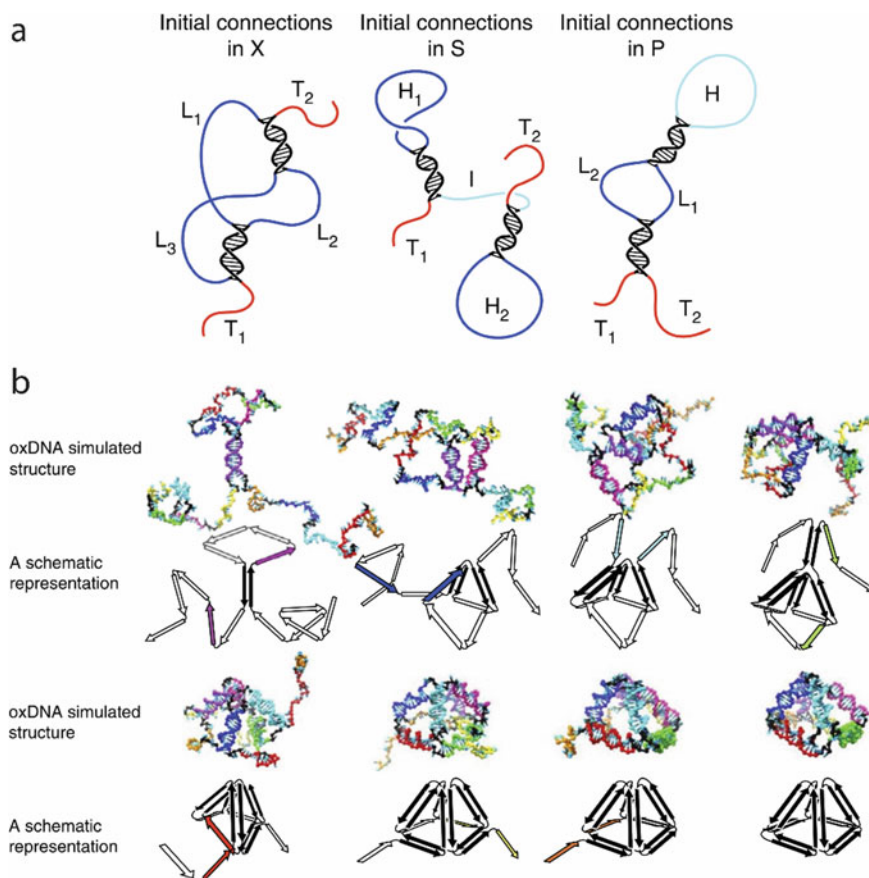


instance, two structurally similar proteins with different topologies can be easily identified when the arrangement of their secondary structure elements is simplified with CT (Fig. 11.3b, c).

### ***11.4.2 Designing DNA-Based Folded and Knotted Chains***

Chromosome folding is another important example in nature that can inspire programmed polymer folding. Human genomic DNA is folded locally via histone proteins into nucleosomes, and forms higher-order chromatin structures with the help of natural “crosslinkers”, like cohesin and CCCTC-binding factor (CTCF) [35, 36]. These structures are further organized in topologically associated domains (TADs) [37], since they can mediate genome expression, any disruption in TADs and TAD boundaries can cause a wide range of diseases such as skeletal anomalies [38], neurological diseases [38], and cancer [39]. Like other folded bio-macromolecules, folding of genomic DNA has a dynamic nature and alternates between highly packed DNA–protein complexes and exposed DNA. Recent molecular simulation studies, modeled the crosslinking of chromatin to form loops with multivalent linkers using simple string and binder switch, indicating the correlation between the concentration of the binder units and the contact probability [40]. Similar to the biological examples, several binder molecules can be employed at once to increase the probability of forming more complex folded structures. Using multiple types of crosslinker binding units, different topological relations such as series and parallel can be engineered, possibly to be controlled by external stimulations such as pH and temperature. This is an important consideration for the programmed folding of large synthetic polynucleotides into complex 3D shapes.

Lately, polynucleotide chains have attracted molecular engineers due to their high programmability. The polynucleotide chains are less complex than other biopolymers such as proteins, they can be produced in-cell or in-vitro, with high yield and fidelity, and more importantly, their folded structure is more predictable, due to a limited number of possible canonical and non-canonical base-pairing [41]. However, there are some limitations in folding polynucleotide chains into tightly knotted complexes [42], which requires the molecule to follow the correct order of folding steps [43]. Recently, the Jerala group introduced a set of design principles to efficiently fold single-stranded DNA into various circuit topologies [44]. To do this, they implemented new terminologies (i.e., terminus (T), hairpin (H), loop (L), and internal (I)) into CT, by which they achieved designing folding steps in a way that single-stranded DNA isothermally folds into a complex topology (Fig. 11.4).

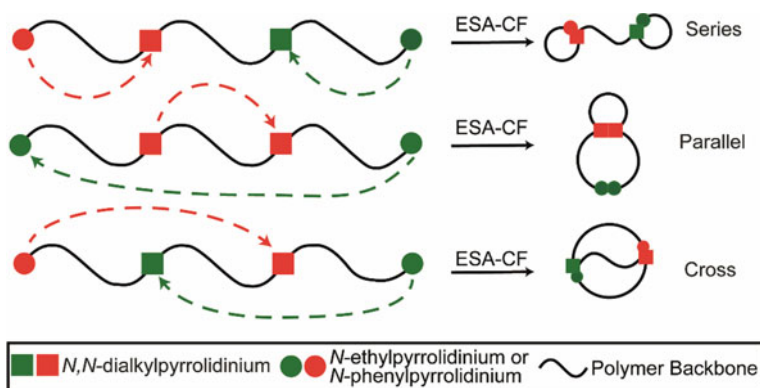


**Fig. 11.4** Effective folding of DNA into the highly knotted nanostructures. **a** Classification of the remaining segments for each basic CT arrangement. **b** Structural simulation of a coarse-grained oxDNA model folding steps and the related schematic representation. Black arrows indicate correct connections, colored arrows indicate the next folding step in the designed folding process. This figure is adapted from Kočar et al. [44] with permission

### 11.4.3 *Folded Single-Chain Polymers of Non-biological Origin*

Methods have emerged to introduce contact sites in organic linear polymers to program a fold. The Tezuka group has been at the forefront of synthesizing topologically diverse multicyclic polymers. To this end, they have developed several intriguing methods, such as the electrostatic self-assembly and covalent fixation protocol (ESA-CF) [45], “Click and Clip” [46], and using periodically positioned tetrafunctional, linear telechelic poly(THF)s [47]. ESA-CF makes use of a selection

of linear or branched telechelic precursors with 5- or 6-membered cyclic ammonium salt groups accompanied by short sequences containing carboxylates anions. Slight elevations in temperature subsequently convert the ionic bond into a permanent covalent interaction. This process can be used as an innovative way to link polymers [45]. The “Click and Clip” system consists of a tandem of alkyne-azide addition (i.e., “Click”) and an olefin metathesis condensation (i.e., “Clip”) and is a highly effective linking process that is uniquely suited toward making cyclic polymer products [46]. Recently Kyoda et al. [47] designed a protocol to direct the folding of a synthetic linear polymer system using four periodically spaced linking units, tetrafunctional telechelic poly(THF)s, two *N*-ethylpyrrolidinium or *N*-phenylpyrrolidinium groups at the end of the molecule, and two *N,N*-dialkylpyrrolidinium groups within. Polymer folding to create covalent bonds was promoted by the ESA-CF protocol. Spatial distance and reactivity of the linking units direct the folding of the linear polymer into several isomers with circuit topologies (Fig. 11.5). If all groups are equally reactive the folding is not directed in a particular way and it is to be expected that series, parallel, and cross topologies are created based on the entropically favorable states if random folding is allowed, and the series topology would be more dominant if the spatially closest points are promoted to make a contact. If the two end groups are more reactive, *N*-phenylpyrrolidinium, than the other groups it is expected they would form a contact first, encapsulating the internal points and forcing a parallel topology. If the counter anions can bind the most reactive groups first, the folding



**Fig. 11.5** Schematic construction of topological circuits using periodically spaced linking groups. Tetrafunctional telechelic poly(THF)s chain (black line) with 5-membered cyclic ammonium salt groups such as *N*-ethylpyrrolidinium or *N*-phenylpyrrolidinium groups (depicted by the colored spheres) at the chain ends, and *N,N*-dialkylpyrrolidinium groups (colored squares) at interior positions. The linking groups can either be similarly reactive to each other (*N*-ethylpyrrolidinium) or have a pair of more reactive groups (*N*-phenylpyrrolidinium). Introducing a pair of counter anions (biphenyldicarboxylate) through ion-exchange and the electrostatic self-assembly and covalent fixation process (ESA-CF) will complete the covalent conversion reactions to create contacts. Alternating the chemical reactivity of the linking groups and directing the folding process, one can select for series, parallel, or cross circuit topology relations. Figure adapted from Kyoda et al. [47] with permission

will result in a more predominant series and cross topologies. By positioning and alternating the reactive groups one can select for the topological relations that form (Fig. 11.5).

Another innovative way to induce folding of linear polymer chains into complex spiro-multicyclic topologies was recently presented by Mato et al. [48], which offers a straightforward synthesis and versatile controls over the number and size of the cyclic units. They previously reported a strategy for constructing a variety of multi-cyclic cage topologies using intramolecular ring-opening metathesis oligomerization (ROMO) [49], by attaching norbornenyl groups as polymerizable termini groups of linear chains and the addition of an excess of 3rd generation Grubbs' catalyst. Extending upon this method, the inclusion of norbornenyl along the chain can force folding into different topologies. This way they have been able to create a polymer that folds in series topology.

Leigh et al. [50] demonstrated the use of metal ion binding regions in a synthetic organic polymer chain as a way to fold a linear chain into different knots. This was achieved by including five metal complexation units in the strand. Two bidentate 1,10-diphenylphenanthroline (dpp) units bind  $\text{Cu}^+$  ions and three tridentate 2,6-pyridine dicarboxamide (pdc) are coordinated by  $\text{Lu}^{3+}$  ions. The outcome of folding was dependent on the sequence of ion introduction indicating kinetic traps. For instance, if  $\text{Lu}^{3+}$  was introduced before  $\text{Cu}^+$ , an insoluble precipitate would form. Introducing both ions at the same time resulted in a modest amount of a three-twist knot as well as a similar precipitate. Only when  $\text{Cu}^+$  was introduced before  $\text{Lu}^{3+}$  resulted in the three-fold knot as the predominant species that could covalently be transformed by ring-closing olefin metathesis. Emitting  $\text{Cu}^+$  leads to a trefoil knot [50]. This allows control over the chirality and stereochemistry of the loops of the polymer, bringing more ways to tune the properties of the molecule. By including the metal-binding regions in different regions of the linear sequence, or different sequences of the binding units, a chain can be folded in different topological arrangements.

#### ***11.4.4 Enzyme Inspired Design of Polymeric Catalysts***

While nature designed enzymes that can efficiently catalyze biological reactions in a complex organic environment, contemporary human-made catalysts often display considerable disadvantages including low catalytic activities or due to difficulties in isolating them from the final product. As such, there is an ongoing need to further develop and improve catalytic systems, possibly inspired by how nature designs its enzymes. Some initial steps have been taken. For example, inspired by metalloenzymes, chemists have synthesized folded chains with enclosed polymeric pockets, featuring metal-ions as catalytic active elements. The desired fold topology would allow the diffusion of both starting material and products freely in and out of the catalytic site [51]. Compact fold topologies may slow down this process and lead to low catalytic activity. Certain practical limitations should be considered here. For example, the minimum loop size is determined by the persistence length of the

polymer backbone; the maximum ring size is determined by the diffusion of contact sites during the folding reaction [51].

The use of folded polymer chains is however justified as it entails the advantage of being readily adjustable in terms of their solubility, size, or stability, achievable by varying the monomer type, chain composition, or chain length. This flexibility provides us with a broad applicational scope, covering practically any required chemical reaction and condition. Both covalent and non-covalent linkages can be employed to produce folded molecular chains (Fig. 11.1c). On one hand, the use of non-covalent contacts leads to adaptive molecular folds, which can respond to different stimuli. On the other hand, covalent bonds give rise to robust topologies with enhanced stability against temperature, acidity, and sonication.

Current protocols for the synthesis of folded single chains (commonly referred to as single-chain nanoparticles or SCNPs) lead to an ensemble of topologies with significant variations in composition and length [52]. The placement of contact sites is mostly statistical. This is unlike natural cellular enzymes, which typically exhibit no dispersity in topology and geometry. This is because the primary sequence of a given enzyme is replicated in each protein copy precisely, a level of accuracy that is unprecedented in polymer chemistry.

### ***11.4.5 Optically Controlled Folding Polymers***

Photochemical reactions may be employed to facilitate precision polymer design. Contact sites can be designed and coupled by light induction directly or indirectly through a bridging molecule, the so-called external crosslinkers. Direct coupling can be performed between two identical (homocoupling) or distinct (heterocoupling) contact sites [53]. Various moieties have been used including cinnamoyl moieties, coumarin moieties, pendant anthracene units, styrylpyrene units, stilbene units, among others [53]. When a pair of contact sites are designed into a polymer, photoactivation with the appropriate wavelength will lead to one primary conformation. When more than two sites are available, various conformations can be generated [53].

There are many challenges on the way. Polymer chemists are not able to insert contact sites at the desired locations. Current protocols lead to random insertion of contact sites into the polymer with their average number being under control. Thus, we are not able to program the contact order, nor guide a chain through a folding pathway and avoid other pathways using various light wavelengths (most reactions happen in the Blue/UV region) or chemical methods. In principle, one can use linkages with different timescales of bond formation or introduce different linkages that are induced by different wavelengths. These technologies could expectedly be applied to design a given circuit topology with a small number of contacts, but for a larger number of contacts, the spectral overlaps of illuminations will introduce limitations.

Note that the final product would be a mixture of different topologies when the design includes more than two contact sites. Furthermore, light induction of coupling

may lead to unwanted side reactions. This includes disruption of polymer backbone or undesired coupling between sites within a chain, or even between chains.

## 11.5 Purification and Characterization

When the final design of a folded molecular chain is realized and synthesized, the purification and characterization of the chains are key. Bulk purification of polymers has been able to sort according to their size, charge, binding affinity, or solubility using chromatography. However, two folded linear polymers similar in size may have very dissimilar topologies, so a method to sort and characterize folded polymers based on the topological arrangements is a much-needed experimental method.

Only recently, and as a breakthrough in the field of single-chain nanoparticle synthesis, accessing the compaction of discrete linear polymer chains becomes possible for the first time [54, 55]. The group of Christopher Barner-Kowollik used size exclusion chromatography and mass spectrometry to directly correlate chemical linkage formation with changes in molecular morphology associated with the compaction. By establishing a calibration between the retention time and the hydrodynamic radius, ion chromatograms of individual chains can be directly applied to measure the reduction in hydrodynamic radius accompanying each crosslinking event.

Moreover, nanopore technology provides a versatile tool that has been used in single-molecule studies and biosensing. Great advances have been made in the production of nanopores, which can be classified into three classes: (1) biological nanopores, (2) synthetic nanopores, or (3) a combination of biological and synthetic nanopores [56]. Both biological and synthetic nanopores offer certain favorable features: reproductivity and channel size (biological pores) as well as pore stability and supporting structure (synthetic pores). A recent study of a simple folded chain by Nikoofard et al. revealed how nanopore technology can distinguish between fold topologies and allow for the enrichment of a certain topology [57]. Experimentally, one can measure how many monomers have passed the pore by pulling using optical tweezers or similar force spectroscopy methods, and the number of monomers that are in the pore by the ion current fluctuations. The study modeled the passage time of a chain with two contacts through a nanopore under different applied forces [57]. When the contacts are breakable (given the range of applied force and the designed range of contact energy), the chain unfolds as it goes through the pore. Here, one can read the topology of chains, if force is carefully chosen; applying very high forces will hide the effect of topology on passage profiles, while moderate forces reveal pauses corresponding to bond breakage (distinct for different circuit topologies). When very weak forces are applied, the entropic effects become significant and again hide the effect of topology on the translocation time. The approach can be extended to chains with larger number of contacts [57]. Note that one can also characterize the topology of chains that are folded via practically unbreakable bonds using nanopores (see below).

The size of the pore and force range must be properly designed for topology sorting (Fig. 11.2d). To sort or enrich a fold topology, the desired topology should be kept intact during the process. To design an enrichment protocol, a study of a simple folded chain with two “unbreakable” contacts has been conducted by Nikoofard et al. [57]. When the applied force is strong enough, a shoulder is observed in the average number of passed monomers versus time for the cross and parallel topologies, while the series topology is clearly different with two shoulders. Useful information can be extracted from the average number of monomers inside the nanopore versus time. Here, two distinct peaks are observed for the series topology, while only one peak is seen for the cross and the parallel topologies. The results show that it is possible to distinguish the series and parallel from cross using nanopores with applying appropriate forces. The time profiles of the number of passed monomers, the number of monomers inside the nanopore, and, the maximum passage time under a given force can be used to sort the three topologies.

The sorting/enrichment approach can be extended to more complex chain topologies with higher number of contacts. Here, one can count the contact pairs that are in series, cross, or parallel arrangements, as a first-order measure of the circuit topology of a chain. Imagine that a mixture of randomly folded polymers with 5 contacts are subjected to the sorting process. Using a simple modeling approach, one can show that chains that pass the nanopore are enriched in series, while chains that do not pass are enriched in parallel regardless of the pore diameter [57]. Interestingly, the internal pore diameter changes the likelihood of chains rich in parallel contacts. If the pore size is smaller than four times the monomer size, we will see a reduced amount of parallel-rich chains in the flow through. To sum up, in an experimental setting, nanopores serve as a method for purification and enrichment. It is expected that, under appropriate conditions, a mixture that would be allowed to flow through, i.e., through hydrodynamic force or electrophoresis, would be enriched with series topology, while the mixture that failed to pass would predominantly contain parallel-rich and cross-rich chains. A series of nanopores with different internal diameters could therefore potentially purify polymer chains based on their topology. Furthermore, the model suggested that knotted proteins have extremely long passing times, allowing for a quick purification step between knotted and unknotted polymers. Nanopores thus have the potential to offer a robust method for the topological characterization and purification of polymers.

## 11.6 Concluding Remarks and Outlooks

To be able to design the desired topology, new methods of rigorous sequence control and precise placement of single functional monomer units at multiple positions along the polymer backbone are required [58]. These developments are expected to occur in the next few years as new combinations of topology modeling [17, 59], synthesis, and characterization techniques become available [60, 61]. These developments will

presumably lead to precise control of the molecular fold topology and hence to highly accurate structure–property relationships [58].

Predicting how the contact sites must be arranged and rearranged to tune the properties of a molecule is therefore of high scientific significance to polymer engineering. Circuit topology offers a unique framework to overcome this. A formal mathematical framework has been developed that can predict the topological properties outcome of molecular operations [62]. The topology states and the changes to the states by additions, eliminations, duplications, and permutations of structures are represented by matrices (thus amenable to efficient *in silico* modeling). This can be used to analyze the structural relationship between biopolymers through evolution and biological processes but also offers unique guidance for engineering synthetic polymers and generating complex polymer structures. One promising approach in engineering polymer folding would be to employ tools from machine learning such as deep learning to map the polymer sequence into its circuit topology state, a similar approach to the one employed very recently in AlphaFold [63] to map protein sequence into its 3D structure. One practical aspect of such a trained network would be to design fine-tuned artificial polymeric structures based on a circuit topology paradigm that can mimic the antigen-binding site to neutralize pathogens invasion [64–66].

## References

1. M. Francl, *Nat. Chem.* **1**, 334–335 (2009)
2. L. Pauling, *Nature* **248**, 769–771 (1974)
3. A. Mashaghi, R.J. Van Wijk, S.J. Tans, *Structure* **22**, 1227–1237 (2014)
4. B. Scalvini, V. Sheikhhassani, J. Woodard, J. Aupič, R.T. Dame, R. Jerala, A. Mashaghi, *Trends Chem.* **2**, 609–622 (2020)
5. A. Mashaghi, *Not. Am. Math. Soc.* **68**, 420–423 (2021)
6. D.P. Giedroc, P.V. Cornish, *Virus Res.* **139**, 193–208 (2009)
7. S.Y. Shaw, J.C. Wang, *Science* **260**, 533–536 (1993)
8. A. Valdés, J. Segura, S. Dyson, B. Martínez-García, J. Roca, *Nucleic Acids Res.* **46**, 650–660 (2018)
9. J.T. Siebert, A.N. Kivel, L.P. Atkinson, T.J. Stevens, E.D. Laue, P. Virnau, *Polymers* **9**, 317 (2017)
10. L.F. Liu, L. Perkocha, R. Calendar, J.C. Wang, *Proc. Natl. Acad. Sci. U. S. A.* **78**, 5498–5502 (1981)
11. M.C. Prentiss, D.J. Wales, P.G. Wolynes, *PLoS Comput. Biol.* **6**, e1000835 (2010)
12. J.I. Sułkowska, E.J. Rawdon, K.C. Millett, J.N. Onuchic, A. Stasiak, *Proc. Natl. Acad. Sci. U. S. A.* **109**, E1715 LP-E1723 (2012)
13. P. Virnau, L.A. Mirny, M. Kardar, *PLoS Comput. Biol.* **2**, e122 (2006).
14. K. Alexander, A.J. Taylor, M.R. Dennis, *Sci. Rep.* **7**, 42300 (2017)
15. V. Turaev, *Osaka J. Math.* **49**, 195–223 (2012)
16. D. Goundaroulis, J. Dorier, F. Benedetti, A. Stasiak, *Sci. Rep.* **7**, 6309 (2017)
17. A. Golovnev and A. Mashaghi, *iScience* **23**, 1–17 (2020).
18. A. Mugler, S.J. Tans, A. Mashaghi, *Phys. Chem. Chem. Phys.* **16**, 22537–22544 (2014)
19. S. Soran Nabavi, M.J. Harrington, O. Paris, P. Fratzl, M.A. Hartmann, *New J. Phys.* **16**, 013003 (2014)



20. X. Zhou, B. Guo, L. Zhang, G.H. Hu, *Chem. Soc. Rev.* **46**, 6301–6329 (2017)
21. N. Nikoofard, A. Mashaghi, *J. Phys. Chem. B.* **122**, 9703–9712 (2018)
22. T. Haslberger, A. Zdanowicz, I. Brand, J. Kirstein, K. Turgay, A. Mogk, B. Bukau, *Nat. Struct. Mol. Biol.* **15**, 641–650 (2008)
23. R. Rosenzweig, S. Moradi, A. Zarrine-Afsar, J.R. Glover, L.E. Kay, *Science* **339**, 1080–1083 (2013)
24. C.B. Anfinsen, *Science* **181**, 223–230 (1973)
25. F.U. Hartl, A. Bracher, M. Hayer-Hartl, *Nature* **475**, 324–332 (2011)
26. M. Heidari, V. Satarifard, S.J. Tans, M.R. Ejtehadi, S. Mashaghi, A. Mashaghi, *Phys. Chem. Chem. Phys.* **19**, 18389–18393 (2017)
27. V. Satarifard, M. Heidari, S. Mashaghi, S.J. Tans, M.R. Ejtehadi, A. Mashaghi, *Nanoscale* **9**, 12170–12177 (2017)
28. A. Bitran, W.M. Jacobs, X. Zhai, E. Shakhnovich, *Proc. Natl. Acad. Sci. U. S. A.* **117**, 1485–1495 (2020)
29. R.J. Ellis, *Trends Biochem. Sci.* **26**, 597–604 (2001)
30. W. Zhou, T. Šmidlehner, R. Jerala, *FEBS Lett.* **594**, 2199–2212 (2020)
31. K.T. Simons, R. Bonneau, I. Ruczinski, D. Baker, *Proteins Struct. Funct. Bioinforma.* **37**, 171–176 (1999)
32. N. Koga, R. Tatsumi-Koga, G. Liu, R. Xiao, T.B. Acton, G.T. Montelione, D. Baker, *Nature* **491**, 222–227 (2012)
33. P.S. Huang, K. Feldmeier, F. Parmegianni, D.A.F. Velasco, B. Hocker, D. Baker, *Nat. Chem. Biol.* **12**, 29–34 (2016)
34. E. Marcos, T.M. Chidyausiku, A.C. McShan, T. Evangelidis, S. Nerli, L. Carter, L.G. Nivón, A. Davis, G. Oberdorfer, K. Tripsianes, N.G. Sgourakis, D. Baker, *Nat. Struct. Mol. Biol.* **25**, 1028–1034 (2018)
35. J. Dekker, T. Misteli, *Cold Spring Harb. Perspect. Biol.* **7**, a019356 (2015)
36. C. Cubeñas-Potts, V.G. Corces, *FEBS Lett.* **589**, 2923–2930 (2015)
37. A. Pombo, N. Dillon, *Nat. Rev. Mol. Cell Biol.* **16**, 245–257 (2015)
38. M. Spielmann, D.G. Lupiáñez, S. Mundlos, *Nat. Rev. Genet.* **19**, 453–467 (2018)
39. A.L. Valton, J. Dekker, *Curr. Opin. Genet. Dev.* **36**, 34–40 (2016)
40. M. Barbieri, M. Cholalia, J. Fraser, L.M. Lavitas, J. Dostie, A. Pombo, M. Nicodemi, *Proc. Natl. Acad. Sci.* **109**, 16173–16178 (2012)
41. A. Mashaghi and A. Katan, *De Physicus* **24e** **3**, 59–61 (2013)
42. N.C. Seeman, *DNA Cell Biol.* **10**, 475–486 (1991)
43. A. Bucka, A. Stasiak, *Nucleic Acids Res.* **30**, e24–e24 (2002)
44. V. Kočar, J.S. Schreck, S. Čeru, H. Gradišar, N. Bašić, T. Pisanki, J.P.K. Doye, R. Jerala, *Nat. Commun.* **7**, 1–8 (2016)
45. H. Oike, H. Imaizumi, T. Mouri, Y. Yoshioka, A. Uchibori, Y. Tezuka, *J. Am. Chem. Soc.* **122**, 9592–9599 (2000)
46. N. Sugai, H. Heguri, T. Yamamoto, Y. Tezuka, *J. Am. Chem. Soc.* **133**, 19694–19697 (2011)
47. K. Kyoda, T. Yamamoto, Y. Tezuka, *J. Am. Chem. Soc.* **141**, 7526–7536 (2019)
48. Y. Mato, K. Honda, B.J. Ree, K. Tajima, T. Yamamoto, T. Deguchi, T. Isono, T. Satoh, *Commun. Chem.* **3**, 97 (2020)
49. Y. Mato, K. Honda, K. Tajima, T. Yamamoto, T. Isono, T. Satoh, *Chem. Sci.* **10**, 440–446 (2019)
50. D.A. Leigh, F. Schaufelberger, L. Pirvu, J.H. Stenlid, D.P. August, J. Segard, *Nature* **584**, 562–569 (2020)
51. I. Perez-Baena, F. Barroso-Bujans, U. Gasser, A. Arbe, A.J. Moreno, J. Colmenero, J.A. Pomposo, *ACS Macro Lett.* **2**, 775–779 (2013)
52. H. Rothfuss, N.D. Knöfel, P.W. Roesky, C. Barner-Kowollik, *J. Am. Chem. Soc.* **140**, 5875–5881 (2018)
53. E. Verde-Sesto, A. Blázquez-Martín, J.A. Pomposo, *Polymers* **11**, 1903 (2019)
54. T. Nitsche, J. Steinkoenig, K. De Bruycker, F.R. Bloesser, S.J. Blanksby, J.P. Blinco, C. Barner-Kowollik, *Macromolecules* **52**, 2597–2606 (2019)

55. J. Engelke, J. Brandt, C. Barner-Kowollik, A. Lederer, *Polym. Chem.* **10**, 3410–3425 (2019)
56. F. Haque, J. Li, H.C. Wu, X.J. Liang, P. Guo, *Nano Today* **8**, 56–74 (2013)
57. N. Nikoofard, A. Mashaghi, *Nanoscale* **8**, 4643–4649 (2016)
58. E. Verde-Sesto, A. Arbe, A.J. Moreno, D. Cangialosi, A. Alegría, J. Colmenero, J.A. Pomposo, *Mater. Horizons* **7**, 2292–2313 (2020)
59. M. Heidari, H. Schiessel, A. Mashaghi, *A.C.S. Cent. Sci.* **6**, 839–847 (2020)
60. J. Steinkoenig, H. Rothfuss, A. Lauer, B.T. Tuten, C. Barner-Kowollik, *J. Am. Chem. Soc.* **139**, 51–54 (2017)
61. R. Upadhyaya, N.S. Murthy, C.L. Hoop, S. Kosuri, V. Nanda, J. Kohn, J. Baum, A.J. Gormley, *Macromolecules* **52**, 8295–8304 (2019)
62. O. Schullian, J. Woodard, A. Tirandaz, A. Mashaghi, *Front. Phys.* **8**, 1–10 (2020)
63. A.W. Senior, R. Evans, J. Jumper, J. Kirkpatrick, L. Sifre, T. Green, C. Qin, A. Židek, A.W. Nelson, A. Bridgland, H. Penedones, *Nature* **577**, 706–710 (2020)
64. Y. Hoshino, H. Koide, T. Urakami, H. Kanazawa, T. Kodama, N. Oku, K.J. Shea, *J. Am. Chem. Soc.* **132**, 6644–6645 (2010)
65. Z. Zeng, Y. Hoshino, A. Rodriguez, H. Yoo, K.J. Shea, *ACS Nano* **4**, 199–204 (2010)
66. M. Mourez, R.S. Kane, J. Mogridge, S. Metallo, P. Deschatelets, B.R. Sellman, G.M. Whitesides, R.J. Collier, *Nat. Biotechnol.* **19**, 958–961 (2001)

# Chapter 12

## Spatially and Chemically Programmed Polymer Folding by the ESA-CF Protocol



Yasuyuki Tezuka

**Abstract** A programmed polymer folding of synthetic linear polymer precursors has been investigated experimentally, leading eventually to the tailored production of single polymer nanoparticles as well as crosslinked network polymers. The ESA-CF protocol has been applied by using linear telechelic precursors having a pair of cationic/anionic units positioned periodically at both chain ends and at two interior positions, to complete the polymer folding under dilution. A set of three polymeric constitutional isomers of either manacle-, 8- or  $\theta$ -form were formed, and their respective compositional ratios were determined by means of the SEC deconvolution technique. Thereby, it has been shown that the polymer folding process is directed by the spatial distance between the four nodal units of identical chemical reactivity, rather than a random combination of the mutually reactive groups introduced in the linear telechelic precursor.

### 12.1 Programmed Polymer Folding

The programmed folding by polymer molecules has been recognized as an essential event in diverse living processes, including DNA packaging/folding [1] and protein 3D structure formation [2], established along with the prolonged chemical evolution. Notably, the application of artificial intelligence (AI) has recently shown important insights in biology's long-standing challenge to predict and to eventually control the folding process of linear chains of amino acids into the defined 3D constructions [3, 4]. Moreover, a class of *fused*-multicyclic peptides, *cyclotides*, typically formed through the intramolecular S–S linking between the designated cysteine residues, has shown to bring about extraordinary stability and bioactivity [5]. Specifically, a triply *fused* tetracyclic and topologically intriguing non-planar  $K_{3,3}$  graph construction has been identified in cyclotides from diverse origins [6, 7].

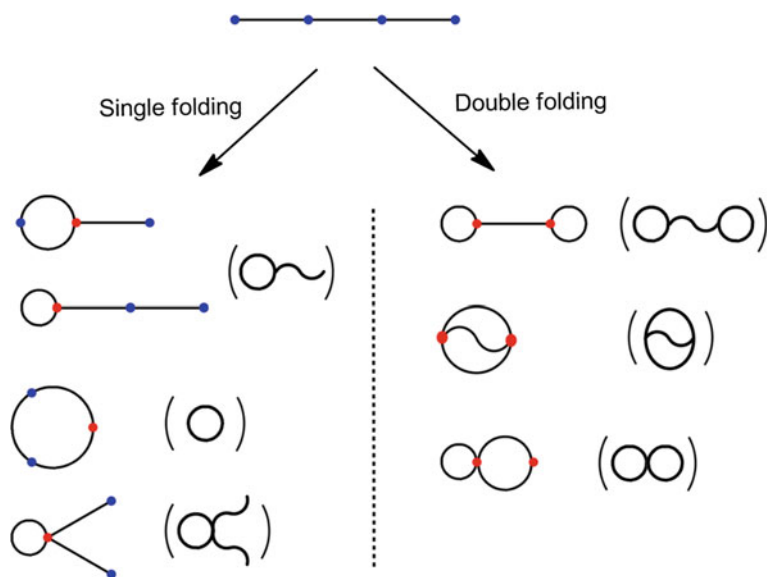
In contrast, the relevant precision control over the polymer folding process by *synthetic* macromolecules to afford the designated multicyclic graph construction

---

Y. Tezuka (✉)  
Tokyo Institute of Technology, Tokyo, Japan  
e-mail: [ytezukak33@gmail.com](mailto:ytezukak33@gmail.com)

has yet been a formidable challenge, to execute the intramolecular crosslinking reaction between the reactive groups introduced along the linear prepolymer backbone [8]. Importantly, moreover, the programmed/controlled polymer folding is crucial for the structure designing and the property tuning of such important polymer materials as single-chain polymer nanoparticles and polymer networks, [8, 9], attracting growing research interest by such broad application potential as catalyst carriers, sensor supports and biomedical scaffolds [10].

This chapter presents an attempt to experimentally elucidate the key parameters directing the non-enzymatic polymer folding processes, by employing synthetic linear polymer precursors including prescribed nodal point units [11]. Thus, a pair of linear polymer precursors having four periodic nodal units at both chain ends and additionally at two interior positions has been introduced for the subsequent covalent polymer folding by means of the ESA-CF protocol [11]. The three polymeric constitutional isomer products of either manacle-, 8- or  $\theta$ -form were obtained as shown in Fig. 12.1, and the subsequent SEC deconvolution analysis has shown that the polymer folding process is directed either by the spatial distance between the functional points, or by the chemical reactivity of the functional points in the telechelic precursor. This is apparently refuting to the frequent assumption of the hypothetical random combination between the reactive groups located along the linear polymer segment during the production of single polymer nanoparticles [10], as well as of polymer network products [9] involving polymer folding processes.

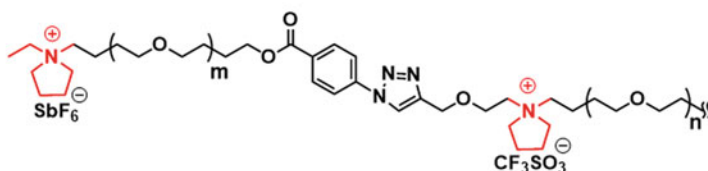
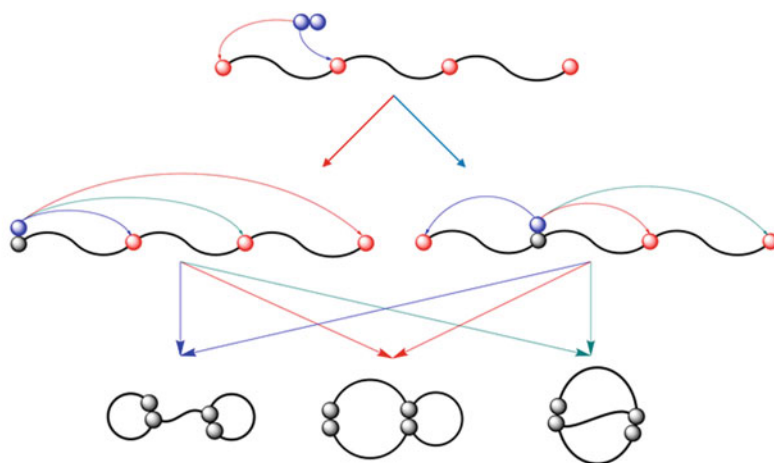


**Fig. 12.1** Single- (left) and double- (right) polymer folding with a linear polymer precursor having four nodal units (two blue nodal points are linking together to form a red nodal point by the polymer folding). Reprinted from [18]. Copyright 2020, with permission from Elsevier

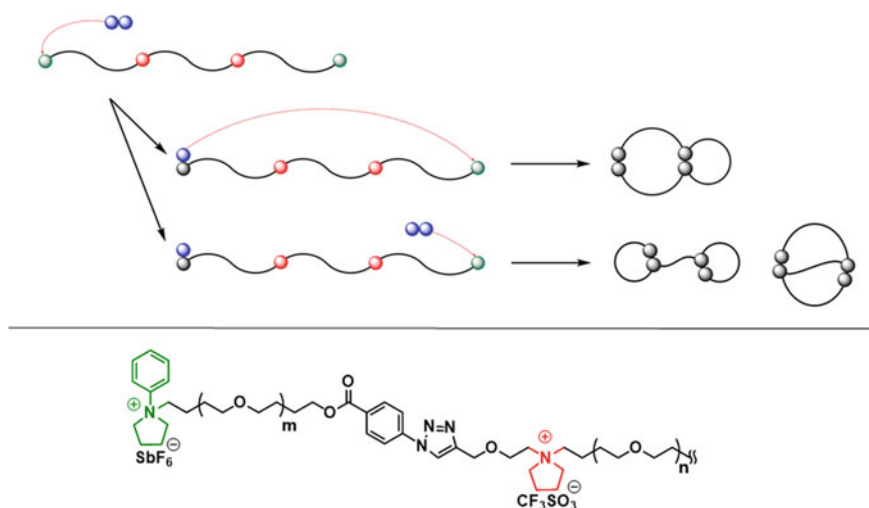
## 12.2 A Pair of Telechelic Precursors for the Programmed Polymer Folding

A pair of designated telechelic precursors was purposely prepared in order to conduct the ESA-CF polymer folding [11–13]. Those are one having four periodic nodal units of *N,N*-dialkylpyrrolidinium group of the equivalent chemical reactivity of each other (Fig. 12.2), and another having a more reactive pair of *N*-phenylpyrrolidinium groups at both chain ends, in place of *N*-ethylpyrrolidinium counterparts in the former, respectively (Fig. 12.3).

A pair of the precursors were prepared accordingly by making use of the click linking reaction, employing a telechelic poly(THF) having alkyne-modified *N,N*-dialkylpyrrolidinium salt groups and another telechelic poly(THF) having commonly an azide group and additionally either an *N*-ethyl or *N*-phenylpyrrolidinium salt group. Each of the latter *hetero*-telechelic precursors was prepared by the end-capping of a living poly(THF), initiated with an azido-benzoyl chloride/silver hexafluoroantimonate ( $\text{AgSbF}_6$ ), with either *N*-ethylpyrrolidine or *N*-phenylpyrrolidine. Subsequently, one unit of the bifunctional alkyne-ended precursor and two units of the



**Fig. 12.2** The programmed polymer folding with a poly(THF) precursor having four periodic nodal units of *N,N*-dialkylpyrrolidinium groups. Adapted with permission from [11]. Copyright 2019 American Chemical Society



**Fig. 12.3** The programmed polymer folding with a poly(THF) precursor having two *N,N*-dialkylpyrrolidinium units at the interior positions and two *N*-phenylpyrrolidinium units at both chain ends. Adapted with permission from [11]. Copyright 2019 American Chemical Society

azide-ended *hetero*-telechelic counterpart were subjected to the click linking reaction in the presence of copper sulfate hydrate and sodium ascorbate in THF/water (4/1 in vol/vol). The obtained pair of telechelic poly(THF)s having four periodic nodal units, comprising the prescribed 5-membered cyclic ammonium salt groups at both chain ends and at the interior positions (Figs. 12.2 and 12.3), were finally applied to undergo the covalent conversion through the ring-opening reaction of either *N*-ethylpyrrolidinium groups by benzoate anion at 110 °C, i.e., under reflux in toluene, or *N*-phenylpyrrolidinium counterparts of the enhanced reactivity at 70 °C also in toluene [13, 14].

The SEC of the covalently converted products showed the peak molecular weights being 9800 for the former and 9500 for the latter, respectively, and the subsequent MALDI TOF mass analyses were completed to characterize these telechelic precursors.

Upon the polymer folding by the statistical and random combination of the four nodal units of the polymer precursor, the polymeric constitutional isomers of three types, i.e., manacle-, 8- and  $\theta$ -forms, are produced in an equal molar ratio (Fig. 12.1). In contrast, the manacle-form isomer should become a predominant component, in case the linking between the spatially closer units proceeds preferentially (Fig. 12.2). On the other hand, the 8-shaped isomer should be produced predominantly with the telechelic precursor having the two *N*-phenylpyrrolidinium end groups, to promote the mutual combination in the initial step due to their higher reactivity than the interior *N*-ethylpyrrolidinium counterparts (Fig. 12.3). It is notable, nevertheless, that the manacle- and  $\theta$ -shaped counterparts could be formed concurrently, when each of the

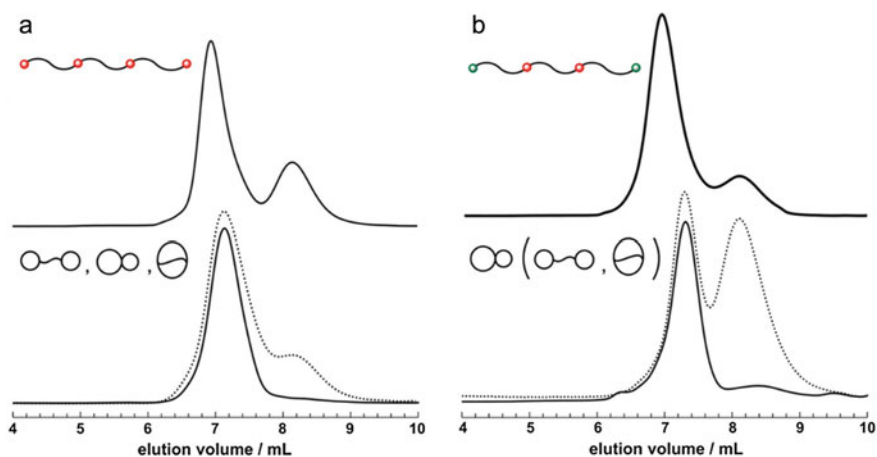
two dicarboxylate counteranions is fixed to each of *N*-phenylpyrrolidinium end units prior to the intramolecular polymer folding or cyclization process (Fig. 12.3).

### 12.3 The Programmed Polymer Folding of Telechelic Precursors Having Periodic Nodal Units

A pair of prototypical telechelic precursors, one having four periodic nodal units of *N,N*-dialkylpyrrolidinium groups with the equivalent chemical reactivity at the two interior and the two chain end positions, and another having two interior units of *N,N*-dialkylpyrrolidinium groups and two chain end units of more reactive *N*-phenylpyrrolidinium groups, was deliberately prepared in order to perform the ESA-CF polymer folding. Thus, two units of a dicarboxylate counteranion, specifically a biphenyldicarboxylate, were introduced to balance the charges against the four quaternary ammonium groups. The acetone solution of the telechelic polymer precursor having quaternary ammonium groups was repeatedly precipitated into a precooled aqueous solution containing an excess amount of disodium biphenyl dicarboxylate to replace the counteranion species of the initial  $\text{CF}_3\text{SO}_3^-$  or  $\text{PF}_6^-$ .

The subsequent ESA-CF polymer folding of the former telechelics having four periodic nodal units of the equivalent chemical reactivity was conducted by heating to reflux in toluene (110 °C) at the dilution of 0.2 g/L for 6 h, to complete the ring-opening reaction both at the *N*-ethylpyrrolidinium and at the *N,N*-dialkylpyrrolidinium units by carboxylate anions. Alternatively, the two-step ESA-CF procedure was applied for the latter telechelics having two sets of periodic nodal units of distinct ring-opening reactivities. Thus in the first step, the quantitative ring-opening reaction of the *N*-phenylpyrrolidinium end groups was allowed to proceed by heating at 70 °C in toluene at the dilution of 0.2 g/L for 3 h, followed by the second step to complete the relevant covalent conversion of the remaining interior *N,N*-dialkylpyrrolidinium units within the telechelic precursor at the higher temperature of 110 °C for 6 h.

The SEC technique was adopted to monitor the polymer folding process. As shown in Fig. 12.4 (bottom, **A** and **B**, respectively), the apparent peak molecular weights, corresponding to their 3D sizes (hydrodynamic volume), of the products were noticeably shifted to the higher elution sides along with the polymer folding. Specifically, the SEC peak molecular weight of the folding product from the former telechelic precursor was 7900, corresponding to 0.81 times of that of the starting precursor analogue (9800), and that from the latter telechelic precursor was 7300, corresponding to 0.76 times of that of the starting precursor (9500), respectively. The polymer folding products were fully characterized by means of the subsequent MALDI TOF mass measurements with their pure forms, isolated by the preparative SEC technique to remove lower molecular weight fractions (Fig. 12.4, (bottom), solid lines).



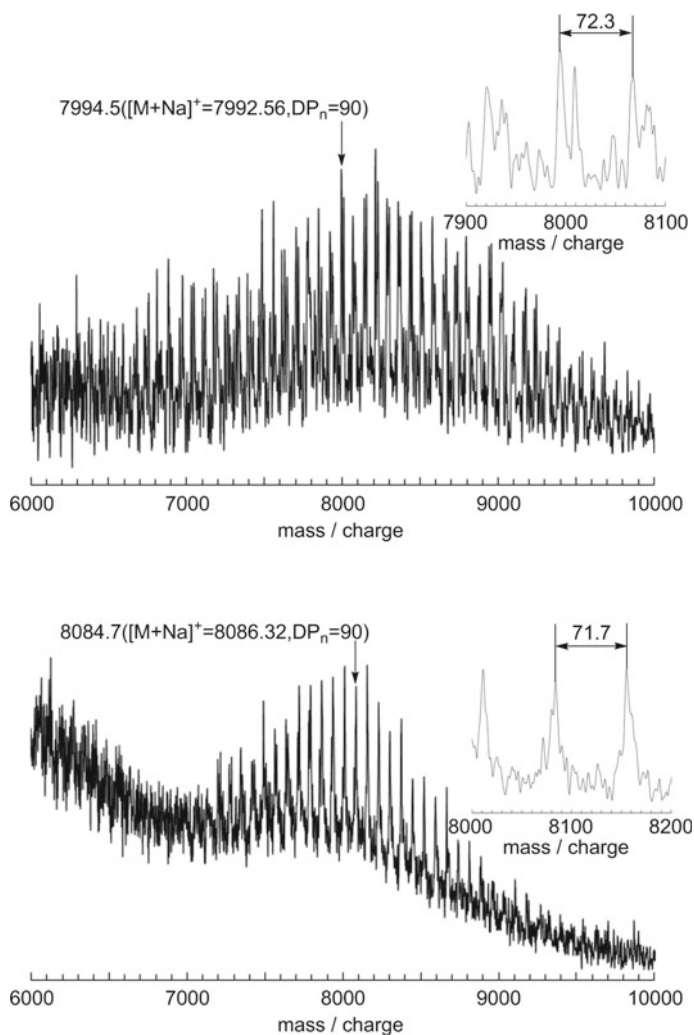
**Fig. 12.4** SEC traces of **a** the telechelic precursor with four nodal units of the equivalent chemical reactivity (top) and the folding product therefrom (bottom) before (dotted line) and after (solid line) the SEC fractionation, and of **b** the telechelic precursor with two sets of nodal units of the different chemical reactivities (top) and the folding product therefrom (bottom) before (dotted line) and after (solid line) the SEC fractionation. (THF as an eluent, 1.0 mL/min.) Reprinted with permission from [11]. Copyright 2019 American Chemical Society

MALDI-TOF mass spectra of the isolated polymer folding products (Fig. 12.5, top and bottom, respectively) showed the resolved peaks, where the peak at  $m/z = 7994.5$ , and at  $m/z = 8084.7$ , assumed to be the adduct with  $\text{Na}^+$ , correspond to the respective products, possessing the expected chemical structure with a  $\text{DP}_n$  of 90;  $(\text{C}_4\text{H}_8\text{O}) \times 90 + \text{C}_{84}\text{H}_{104}\text{N}_{10}\text{O}_{14}$  plus  $\text{Na}^+$  equals 7992.56, for the former and with a  $\text{DP}_n$  of 90;  $(\text{C}_4\text{H}_8\text{O}) \times 90 + \text{C}_{92}\text{H}_{104}\text{N}_{10}\text{O}_{14}$  plus  $\text{Na}^+$  equals 8086.32, for the latter, respectively.

## 12.4 SEC Deconvolution Analysis of the Polymer Folding Products from the Linear Precursor Having Periodic Nodal Units

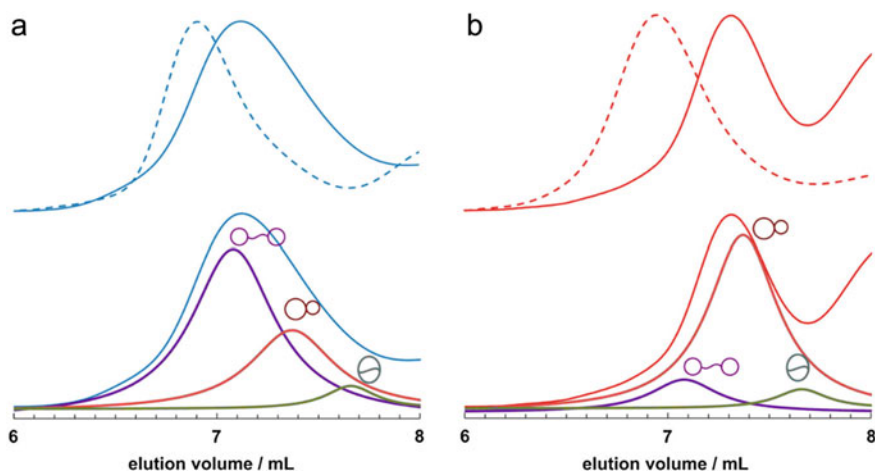
The polymer folding products obtained so far by this process are arguably comprised of three dicyclic constitutional isomers of either manacle-, 8- or  $\theta$ -form, and they are distinctive from each other by their hydrodynamic volumes or 3D sizes. Notably, the relative 3D sizes of these three polymeric constitutional isomers in reference to the linear standard were reportedly estimated by the SEC peak molecular weight analysis, and are 0.89 for the manacle-, 0.69 for the 8- and 0.57 for the  $\theta$ -form, respectively [12]. The SEC peak molecular weight comparison of the current polymer folding products with their respective linear precursors showed that the extent of the 3D size contraction along with the double polymer folding were 0.81 for the





**Fig. 12.5** MALDI-TOF MS spectra of (top) the polymer folding products from the precursor of the four nodal units of the identical chemical reactivity and (bottom) the polymer folding products from the precursor of the two sets of nodal units of the different chemical reactivities (Linear mode, matrix: dithranol with sodium trifluoroacetate.  $DP_n$  denotes the number of monomer units in the product.) Reprinted with permission from [11]. Copyright 2019 American Chemical Society

former and 0.76 for the latter, respectively, to accord with the polymer cyclization to proceed (Fig. 12.6, **a** and **b**, top). Remarkably, moreover, the quantitatively measured contraction along with the polymer folding was 19% for the polymer folding products from the former telechelic precursor, which was marginally less than that of another (24%) for the latter counterpart. In addition, the SEC peak trace profile for the former was noticeably broader in comparison with that for the latter (Fig. 12.6, **a** and **b**, top).



**Fig. 12.6** SEC traces of (a, top) the linear precursor having the four nodal units of the identical chemical reactivity (broken line) and the polymer folding product therefrom (solid line), and (b, top) the linear precursor having the two sets of nodal units of the different chemical reactivities (broken line) and the polymer folding product therefrom (solid line), and the SEC peak deconvolution (a and b, bottom) into three isomeric components in the respective products (manacle-isomer in violet, 8-isomer in red and  $\theta$ -isomer in green, respectively). Reprinted with permission from [11]. Copyright 2019 American Chemical Society

It is presumed, therefrom, that the manacle-form isomer is a major component in the polymer folding product from the former precursor, with marginal contents of the two other isomers. On the other hand, the 8-form isomer is supposedly a predominant component from the latter counterpart. In order to obtain more quantitative insights into these polymer folding processes, the relative composition of the three isomer fractions were subsequently deduced through the SEC deconvolution analysis based on the relative hydrodynamic volume of each three polymeric isomers against the linear counterpart [11, 12].

The relative ratio of the three polymeric isomer fractions of either manacle-, the 8- or the  $\theta$ -form was determined to be 60:33:7 for the polymer folding product from the former telechelic precursor (Fig. 12.6 (a, bottom)). The observed isomer ratio is apparently inconsistent with the equal isomer ratio of 33:33:33, which is hypothesized by the random and statistical combination of the linking units in the linear precursor. Instead, the obtained compositional ratio tends to substantiate an alternative polymer folding procedure, in which the linking between the two adjacent and spatially closer positions takes place preferentially for the telechelic precursor having identical chemical reactivity. Notably, indeed, the previous kinetic study on polymer cyclization reactions [15–17], by means of the photo-quenching of pyrene-ended polymers of different chain lengths, has shown the equation of  $K = N^{-d}$ ,  $d = 1.0\text{--}1.5$ , where  $K$  is the rate constant and  $N$  is the chain length of the polymer precursor.

The manacle-form isomer is anticipated as the predominant product upon the polymer folding process directed by the spatial distance between the nodal units. More specifically, when the dicarboxylate is fixed at either of the chain ends in the first step, the subsequent linking of the neighboring nodal units gives the manacle-form isomer, as schematically shown in Fig. 12.2. Moreover, even when the dicarboxylate is initially fixed at either of the interior nodal units, the manacle-form isomer is finally produced in the equal ratio of the concurrent 8-form isomer. On the other hand, the  $\theta$ -form isomer obtainable by the linking of the non-adjacent and spatially prolonged nodal units is reluctant to be formed.

In contrast, the convoluted ratio for the three polymeric isomers of the respective manacle-, 8- and  $\theta$ -forms was 11:84:5 for the polymer folding product with the linear precursor of the two sets of nodal units of the different chemical reactivities (Fig. 12.6 (b, bottom)) [11]. The 8-form isomer was observed predominantly in accordance with the promoted covalent linking of the two *N*-phenylpyrrolidinium end units with a single dicarboxylate in the first step, and the subsequent covalent conversion of the remaining two interior *N,N*-dialkylpyrrolidinium units with a second dicarboxylate, to follow the order of the chemical reactivity of the nodal pyrrolidinium units (Fig. 12.3).

The SEC deconvolution showed, moreover, the concurrent formation of the minor portions of the manacle-form (11%) and the  $\theta$ -form (5%) isomers besides the major 8-form counterpart [11]. These minor isomer pairs are produced presumably when the two separate biphenyl dicarboxylate are fixed to each of *N*-phenylpyrrolidinium ends of the telechelic precursor in the first step, followed by the covalent linking of the interior *N,N*-dialkylpyrrolidinium units (Fig. 12.3). The predominant formation of the manacle-form isomer over the  $\theta$ -form counterpart is accounted for by the promoted covalent linking by spatially closer nodal units operating in the polymer folding process.

To conclude, the SEC peak deconvolution analysis of the polymer folding products from the designated telechelic polymer precursors allowed the quantitative estimation of the relative ratio of the three polymeric constitutional isomers. Consequently, it has been shown for the first time that the polymer folding process is directed either by the spatial distance between the nodal units, to promote the manacle-form isomer over the 8- and  $\theta$ -form counterparts, or by the chemical reactivity to afford the 8-form isomer in case of the telechelic precursor having the two end groups of higher reactivity than the two interior ones [11]. The further developments in the programmed but non-enzymatic polymer folding with synthetic polymer systems are now anticipated along with the key structural/chemical parameters to be accessible in a quantitative manner, eventually leading to the precision polymer folding to allow the tailored designing of novel polymer materials, beyond single-polymer nanoparticles as well as crosslinked polymer networks.

## References

1. N.C. Seeman, *Annu. Rev. Biochem.* **56**, 65 (2010)
2. C.B. Anfinsen, *Science* **181**, 223 (1973)
3. E. Callaway, *Nature* **588**, 203 (2020)
4. R. F. Service, *Science* **370**, 1144 (2020)
5. S.J. de Veer, J. Weidmann, D. Craik, *Acc. Chem. Res.* **50**, 1557 (2017)
6. D.J. Craik, *Science* **311**, 1563 (2006)
7. T. Suzuki, T. Yamamoto, Y. Tezuka, *J. Am. Chem. Soc.* **136**, 10148 (2014)
8. S. Mavila, O. Eivgi, I. Berkovich, N.G. Lemcoff, *Chem. Rev.* **116**, 878 (2016)
9. J. Wang, T.-S. Lin, Y. Gu, R. Wang, B.D. Olsen, J.A. Johnson, *ACS Macro Lett.* **7**, 244 (2018)
10. R. Chen, E.B. Berda, *ACS Macro Lett.* **9**, 1836 (2020)
11. K. Kyoda, T. Yamamoto, Y. Tezuka, *J. Am. Chem. Soc.* **141**, 7526 (2019)
12. H. Oike, H. Imaizumi, T. Mouri, Y. Yoshioka, A. Uchibori, Y. Tezuka, *J. Am. Chem. Soc.* **122**, 9592 (2000)
13. Y. Tezuka, *Acc. Chem. Res.* **50**, 2661 (2017)
14. Y. Tezuka (ed.), *Topological Polymer Chemistry: Progress of cyclic polymers in syntheses, properties and functions* (World Scientific, Singapore, 2013)
15. I. Mita, K. Horie, *J. Macromol. Sci.-Rev. Macromol. Chem. Phys.* **C27**, 91 (1987)
16. J.E. Martin, B.E. Eichinger, *Macromolecules* **16**, 1345 (1983)
17. J.E. Martin, B.E. Eichinger, *Macromolecules* **16**, 1350 (1983)
18. Y. Tezuka, *React Funct Polym.* **148**, 104489 (2020)

# Chapter 13

## Macromolecular Rotaxanes, Catenanes and Knots



Harry W. Gibson

**Abstract** This chapter is a review of recent advances in the expanding fields of polyrotaxanes, polycatenanes and polymeric knots with emphasis on the period from 2010 to the end of 2020. A prospectus is provided for needed future efforts.

### 13.1 Introduction

This chapter is a review of polyrotaxanes, polycatenanes and polymeric knots—polymeric species bound by mechanical linkages. It is timely because of the rapid advances and increasing interest in these subfields of supramolecular polymer science.

First, some formal definitions are given. In Fig. 13.1, polyrotaxanes and polypseudorotaxanes are schematically represented; *note that neither supramolecular polymers assembled from small molecule building blocks nor related “daisy chain” polymers are included here.* Figure 13.2 contains cartoon representations of various types of polycatenanes. Figure 13.3 contains representations of polymeric knots. *This brief review does not address coordination polymers.*

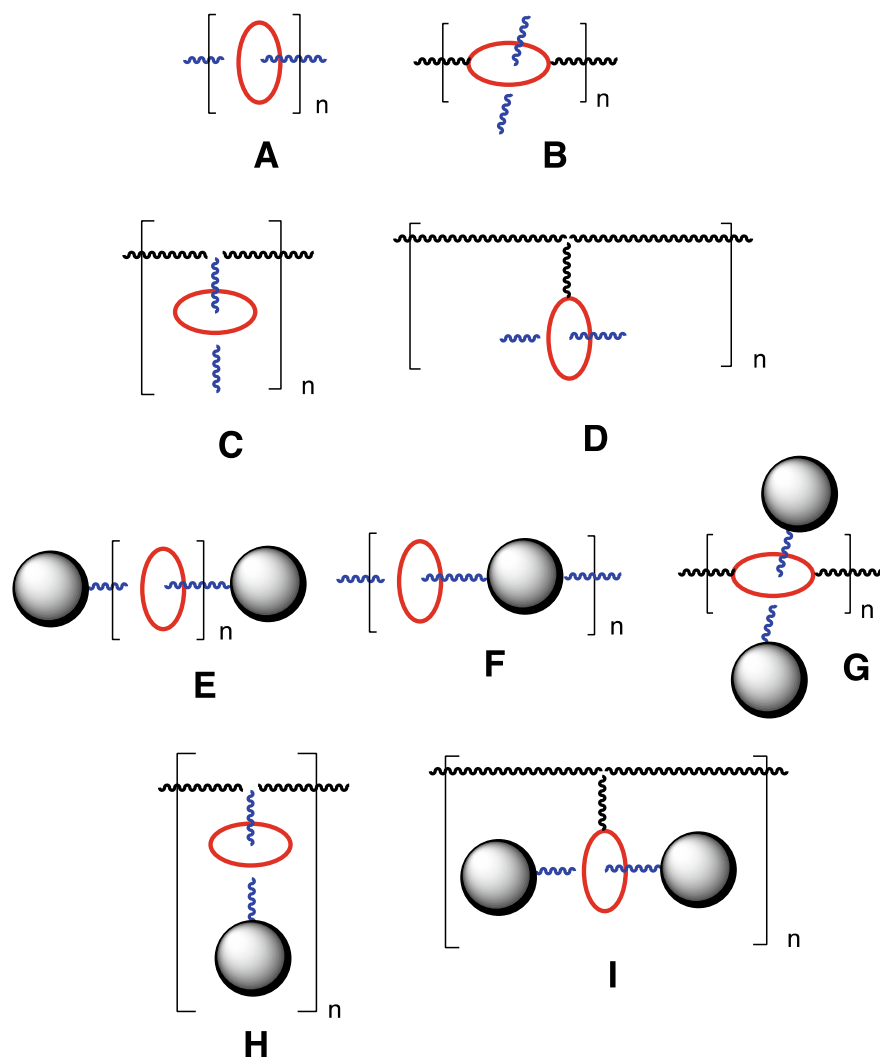
The fields of polyrotaxanes, polycatenanes and polymeric knots can be traced to their origins in the 1950s when small-molecule analogs were conceived and pursued, [5–9] although the possibility of such mechanically linked structures was mentioned more than a century ago [10]. Low molar mass rotaxanes were synthesized (with difficulty!) and examined theoretically in the 1960s [11–14]. The first oligo- or polyrotaxanes were claimed in the 1970s [15–18]. In 1961, the first low molar mass catenane was reported to have been synthesized in a painstaking statistical, multi-step manner [11]. The first polycatenanes of the interpenetrating network type (insoluble) were reported in 1975 [19]. However, “poly[2]catenanes”, in which a [2] catenane is incorporated (i.e., Type B,  $x = 1$ , Fig. 13.2) into a polymer backbone were reported only in 1999, 25 years later, [20] notwithstanding Stoddart et al.’s impressive synthesis

---

H. W. Gibson (✉)

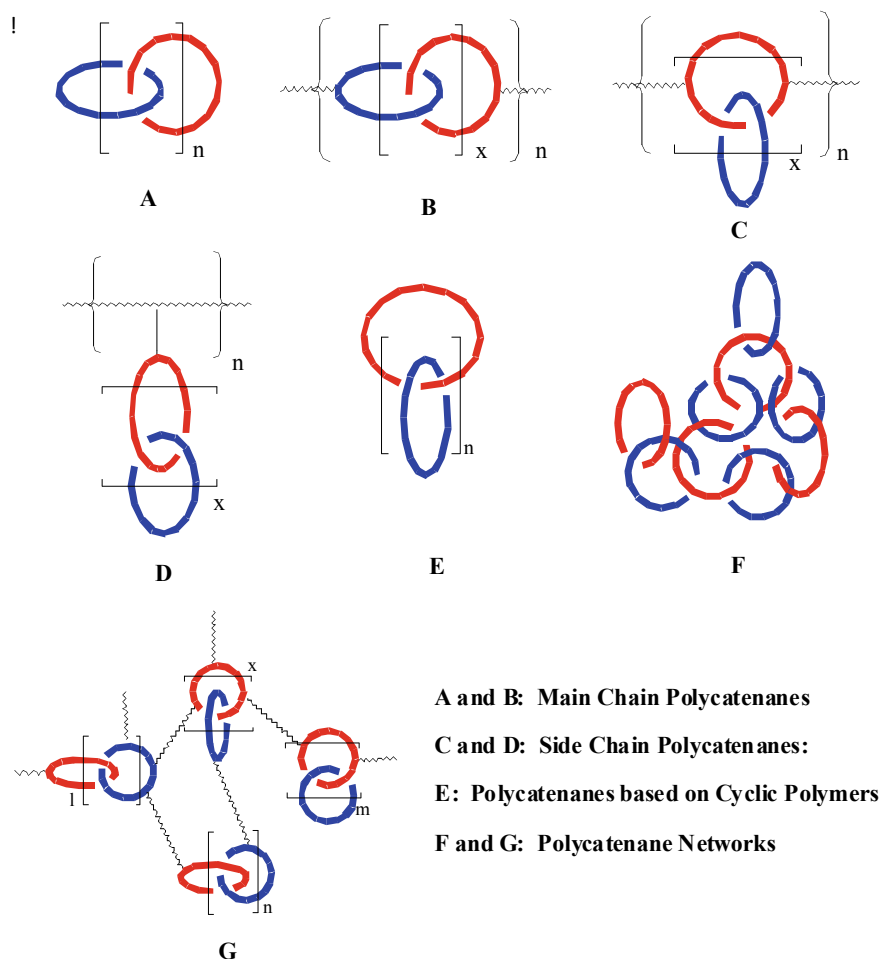
Department of Chemistry, Virginia Polytechnic Institute and State University, Blacksburg, VA 24060, USA

e-mail: [hwgibson@vt.edu](mailto:hwgibson@vt.edu)



**Fig. 13.1** Classes of polypseudorotaxanes (A–D) and polyrotaxanes (E–I). Both main chain (A, B, E, F and G) and side chain (C, D, H and I) systems are represented. The filled black circles represent bulky “blocking groups” or “stoppers” that prevent dethreading. The red ellipses represent the macrocycles. Used with permission from Ref. [1]. Copyright© Elsevier, 2005

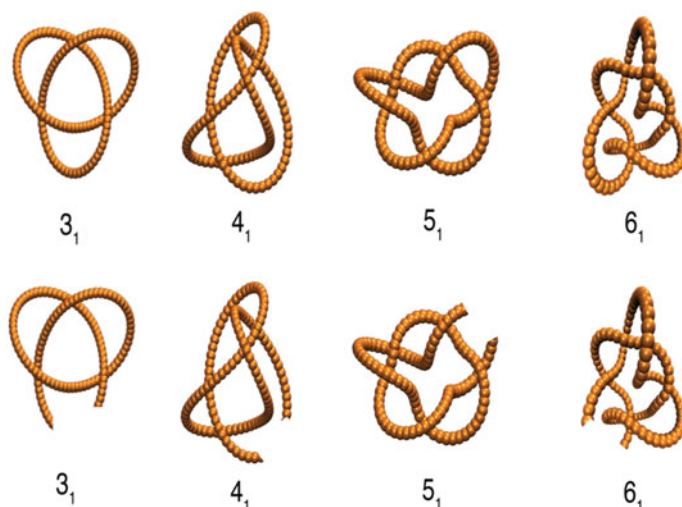
of a linear [7] catenane in 1994 [21]. The first “true” or poly[n]catenanes (Type A, Fig. 13.2, large n, in some cases with accompanying Type F structures) have only been produced recently [22–24]. The first mention of polymeric knots seems to have been made in 1960 in a preprint [25] and then subsequently in a journal article; [11] later, other chemists became interested in the possibility of knots in proteins [26] and



**Fig. 13.2** Classes of polycatenanes. The blue ring may be identical to the red ring.  $x, m, l \geq 1$ .  $n = \text{large, e.g.,} > 50$ . Reprinted with permission from Ref. [2]. Copyright© American Chemical Society, 2010

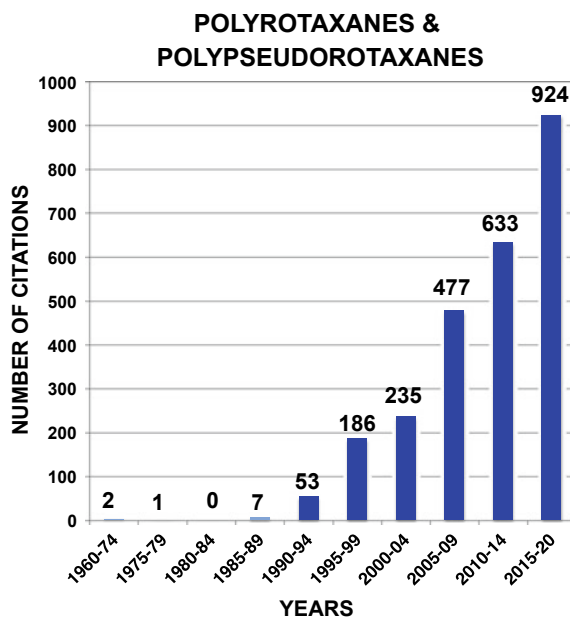
DNA, [27] and convincing evidence of knots in DNA by way of electron microscopy appeared in 1976 [28].

As can be seen in Fig. 13.4, growth in the polyrotaxane literature has accelerated exponentially in the last 15 years. Since 1960, there have been 2515 citations, including 187 abstracts/preprints, 271 reviews/books and 560 patents. Likewise, but at a more modest level (405 citations during 1960–2020 including 58 abstracts/preprints, 89 reviews and books and 20 patents), as Fig. 13.5 shows, interest in polycatenanes has increased exponentially. Polymeric knot publications have also increased exponentially, but more slowly (Fig. 13.6), amassing ~384 total citations during 1960–2020, including 3 patents, 115 abstracts/preprints and 37 reviews.



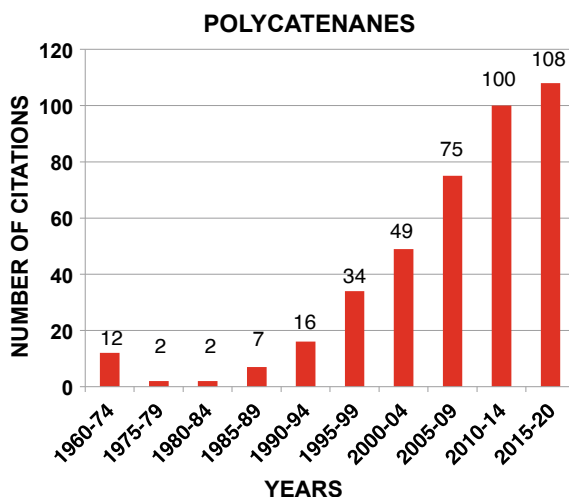
**Fig. 13.3** Representative images for some ideal or “canonical” knotted polymeric structures from a cyclic polymer (top row) and an analogous linear polymer (bottom row). The main number is the minimal crossing number  $m$  and the subscript is an arbitrary number specifying sub-classes of knots having the same  $m$  [3]. Knots having a subscript equal to unity are usually referred to “prime” knots and tend to be relatively “symmetric” in shape as a class. Adapted with permission from Ref. [4]. Copyright© Springer Nature Ltd., 2017

**Fig. 13.4** Literature citations for “polyrotaxanes, polypseudorotaxanes or pseudopolyrotaxanes” since 1960 via ScifFinder©

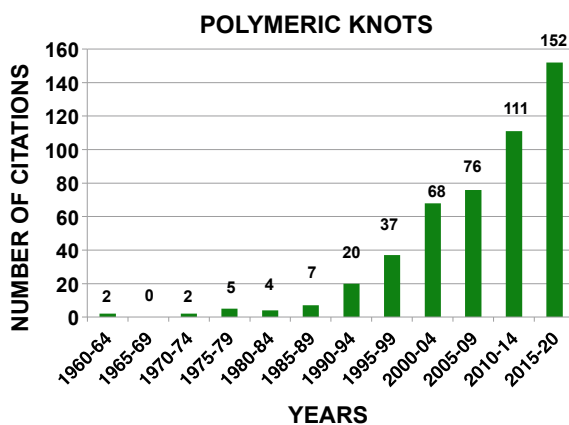




**Fig. 13.5** Literature citations for “polycatenanes or polymeric catenanes” since 1960 via SciFinder®



**Fig. 13.6** Literature citations for “polymeric knots or knotted polymers, not fiber” since 1960 via SciFinder®



Indeed, the totals are daunting in terms of attempting to review this area. The tactical approach taken for this task was to cover the subtopics in rough proportion to their numbers: polyrotaxanes (including polypseudorotaxanes and the wrongly named pseudopolyrotaxanes, 76%) > polymeric knots (>12%) > polycatenanes (<12%) and focus on the last 10 years of research. Four strategies were then applied: (1) provide citations of appropriate reviews, (2) focus mainly on synthesis and properties of real materials, (3) discuss particular work that in the opinion of the author is most noteworthy and (4) finally, try to emphasize approaches that can move the field forward both from fundamental as well as practical aspects.

## 13.2 Polyrotaxanes and Polypseudorotaxanes

Between 2010 and the end of 2020, a total of about 1557 literature reports were published on these topics according to SciFinder®. Of these papers, the great majority (999, 64%) involved systems containing cyclodextrins [CDs] as the cyclic or “wheel” component. One reason for this dominance by CDs is their commercial availability. Another reason is the fact that these macrocycles are derived from a sugar and, therefore, are biologically benign, leading to targeted applications in human health. Crown ether cyclic components were employed in 115 (7%) of the citations. The recently discovered pillararene class of cyclics was involved in 25 (~2%) of the publications. Recent reviews are noted in Table 13.1.

### 13.2.1 Cyclodextrin-Based Polyrotaxanes and Pseudorotaxanes

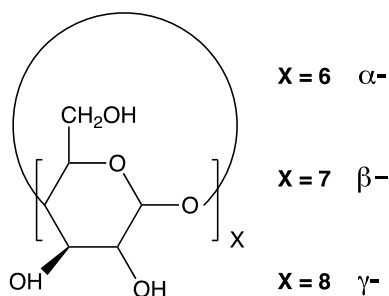
Cyclodextrins are cyclic anhydroamyloses; in the refinement of sugar, commercially three cyclodextrins are produced:  $\alpha$ -,  $\beta$ - and  $\gamma$ -, which differ in ring size (Fig. 13.7). All have cup-like structures with primary hydroxyls on the narrow port and secondary hydroxyls on the larger port; the cavity is apolar. The diameters of the openings range from 5.7 to 7.8 to 9.5 Å for the three macrocycles.

Complexes form from cyclodextrins (or partially alkylated analogs) and suitable guests in aqueous environments. The associations are typically entropically driven by the expulsion of water molecules from the cavities of the CDs upon occupation by the guests. Typical guests, therefore, are water-soluble but retain some degree of

**Table 13.1** Recent reviews of polyrotaxanes and polypseudorotaxanes

Topic	References
General	[1]
General	[29]
General	[30]
CD-based systems in biological applications	[31]
General	[32]
CD-based systems and “slide rings”	[33]
Crown ether-based systems	[34]
CD-based systems	[35]
CD-based systems	[36]
General	[37]
Cucurbituril-based systems	[38]
CD-based systems in drug delivery	[39]
Conducting Polyrotaxanes	[40]

**Fig. 13.7** Chemical structures of cyclodextrins



hydrophobicity that attracts them to the cavities. Polypseudorotaxanes and thence polyrotaxanes are typically constructed from poly(ethylene oxide) (PEO) itself, its block co-polymers (typically those with poly(propylene oxide) (PPO), called Pluronics®), PPO itself or polymers that contain oligo(ethyleneoxy) units (OEO), such as polyamides and polyesters.

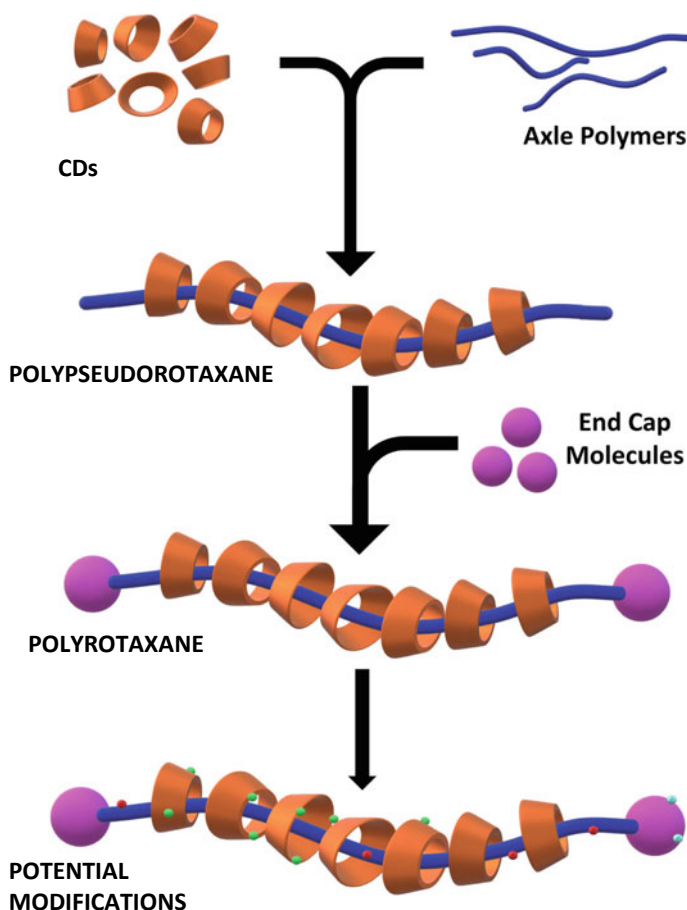
Because of their ready availability commercially and their biological inertness, CD-based polyrotaxanes have primarily been investigated in terms of applications in medicine. The reviews by Yui and Tamura [31] and Wankar et al. [39] summarize in detail the progress that has been made in these endeavors.

Cancer, as the second leading cause of death, killed 9.6 million people worldwide in 2018 [41] and, therefore, still presents a threat to humans and our economies. Thus, it is not surprising that suppression of cancerous tumors is a goal of many researchers worldwide, including many who have chosen to employ polyrotaxanes to deliver drugs to cancer cells. Several approaches have been evaluated. One method is to attach known anticancer drugs to the ends of polyrotaxanes using acid-labile bonds, which degrade to release the drug in the acidic tumor environment. Another approach is to attach the drugs to the threaded cyclodextrins again via such labile bonds with the same or another bulky end group, so that an increased load of the drug is delivered [42–44]. Another approach is to use a hydrogel formed from the polyrotaxane or polypseudorotaxane to entrap the anticancer agent; [45] here, the anticancer drug is not complexed with the CD. Recently a targeted delivery system involving an antibody attached covalently to the threaded CDs has been reported to be very effective, apparently by providing greater ability to penetrate the cancer cell membranes [46].

Another approach to disease control is gene therapy. Polyrotaxanes are also under investigation in this area. A polyethyleneimine- $\alpha$ -CD polypseudorotaxane exhibited better transfection efficiency than the polyethyleneimine system itself [47]. In another approach, an oligo(ethylene oxide) (DP = 9)- $\beta$ -CD rotaxane was reacted to attach polyethyleneimine, guanidinium and arginine moieties sequentially to the cyclodextrins, yielding a series of cationically functionalized polyrotaxanes with reproducible structures; all of these products were inferior to the parent oligorotaxane in terms of transfection efficiency at higher nitrogen to phosphorus ratios (N/P = cation/P from DNA), but the PEI functionalized rotaxane system was superior at low N/P ratios [48]. Moreover, the synthetic process allows for further optimization. A more recent

publication reports the use of an oligo(ethylene oxide) polyester scaffold and  $\alpha$ -CD; the rotaxane was treated to attach dimethylaminoethylamide units as the required cationic sites; with siRNA, the systems with varying molecular weights revealed transfection to HeLa cells with efficiencies comparable to a commercial vector [49].

Increasingly, CD-based polyrotaxanes are being explored as tissue engineering scaffolds wherein they display the ability to alter cellular functions and form complexes with growth factors and peptides by functionalizing various sites on the polyrotaxane, as shown in Fig. 13.8 [50].



**Fig. 13.8** Assembly of cyclodextrins with guest polymers to make polypseudorotaxanes, thence polyrotaxanes by attachment of bulky end group “stoppers”. Chemically modifiable locations for introduction of payloads, directing vectors, etc., are indicated by the colored dots. Adapted from Ref. [50] under the Creative Commons Attribution 4.0 International License; see <http://creativecommons.org/licenses/by/4.0/>

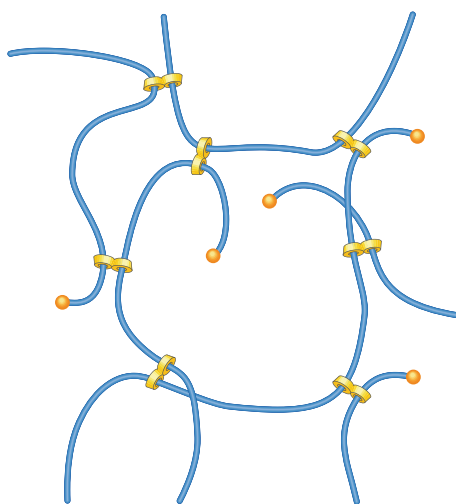
Another important health-related technical issue is contrast enhancement in magnetic resonance imaging (MRI); currently used reagents have several flaws including but not limited to low relaxivities, rapid clearance from the body and diffusion to adjacent tissues, thus reducing the resolution of tumors, etc. CD-based rotaxanes have been employed to address these deficiencies. In a recent study, triblock co-polymeric PEO-PPO-PEO- $\beta$ -CD rotaxanes of several molecular weights were fitted with various loadings of CDs with attached 1,4,7,10-tetraazacyclododecane 1,4,7,10-tetraacetic acid (DOTA) units, which complex gadolinium ions ( $Gd^{3+}$ ), known proton relaxivity agents used in commercial contrast agents [51]. Compared to a commercial agent, these polyrotaxane constructs exhibited higher contrast and extended circulation times.

Besides biological applications, CD-based polyrotaxanes are being examined to provide enhanced performance in traditional polymer applications. Good examples are the so-called “slide ring” crosslinks, portrayed in Fig. 13.9, in hydrogels and solid materials to provide improved mechanical properties [33] and introduce self-healing, [33, 35] and stimuli-responsive [52] features, including shape memory [53]. It has been shown that unlike conventionally crosslinked materials, slide rings allow toughness and stiffness to be increased simultaneously in gels [54]. Moreover, in elastomers, again unlike conventional materials slide ring crosslinks allow mechanical strength and extensibility to be increased at the same time [55–57].

Facile syntheses of some slide ring gels have been developed [59–61]. Theorists have developed models that explain and predict the unusual and beneficial properties of such crosslinked systems [62–64].

Additionally, the hydroxyl groups on CD-polyrotaxanes have been used to crosslink poly(methyl methacrylate) via reactive blending with a compatibilizing polymer-bearing maleic anhydride moieties; the resulting systems possess greatly improved tensile strength, impact strength and toughness [65].

**Fig. 13.9** Slide ring crosslinked system. Note that the bis-CDs are indicated to be linked with short tethers, but long tethers are also possible and have been employed. From Ref. [58] with permission. Copyright© IOPublishing, 2005

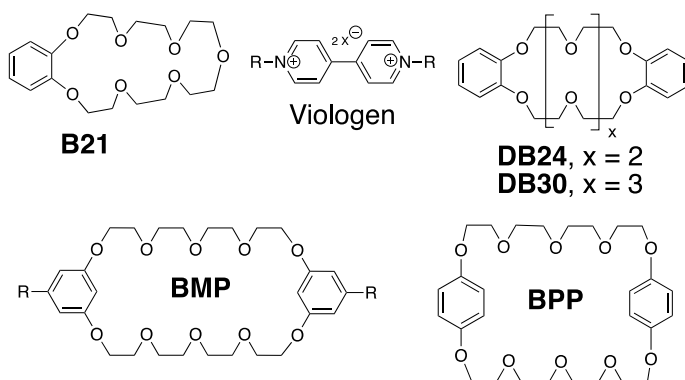


The complexation of hydrophobic guests in aqueous media by  $\beta$ -CD and derivatives has been cleverly utilized by Wenz et al. to produce water-soluble polyisoprene-containing bulky co-monomer units via an emulsion-like polymerization [66]. Subsequently, this group utilized RAFT polymerization to produce triblock copolyrotaxanes of isoprene and partially methylated  $\beta$ -CD with molecular weight and sequence control [67]. More recently, Ito, Wenz et al. utilized this RAFT protocol to prepare poly(methyl methacrylate)-based polyrotaxanes with  $\gamma$ -CD [68].

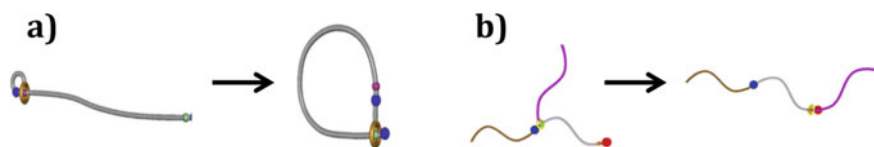
### 13.2.2 Crown Ether-Based Polyrotaxanes and Polypseudorotaxanes

Historically, the first polyrotaxanes were prepared using crown ethers [15]. For many years, it was believed that the minimum ring size required for a macrocycle to be threaded was 24 atoms [69, 70]. Now, it has been demonstrated that the minimum ring size for threading by a linear molecule containing methylene and ether linkages is 21 atoms [71, 72]. Indeed, this motif (benzo-21-crown-7, **B21**, Fig. 13.10) has been employed with secondary ammonium salts to prepare slide ring gels as described above with CDs [71, 73]. So now any crown ether larger than 21 atoms is a candidate to form polyrotaxanes.

There are basically two protocols for synthesizing crown ether-based (or any) polyrotaxanes: statistical threading and host-guest threading. Larger crown ethers are better for statistical threading. However, for host-guest complexation the tighter the fit between the two components, the higher the binding constant, so that the optimal ring size depends on the guest. However, host-guest complexation is mostly used now. Popular guests for aromatic crown ethers are secondary ammonium salts and N,N'-dialkyl-4,4'-bipyridinium salts (viologens, Fig. 13.10). With secondary



**Fig. 13.10** Crown ethers and viologens used to make polyrotaxanes



**Fig. 13.11** Topological transformations of polyrotaxanes by control of the nature of the guest binding sites: (a, left) quasi-linear to cyclic; (b, right) star to linear. Adapted from Ref. [34] with permission. Copyright© Elsevier, 2017

ammonium guest moieties, smaller crowns (21- and 24-) are best, while the viologens complex better with larger crowns (>30-).

Dibenzo-24-crown-8 (**DB24**, Fig. 13.10) is popular, partially because it is commercially available, though expensive. Recently, it has been reported that dibenzo crown ethers can be prepared in very high yields by templation with  $K^+$  in the form of the very soluble  $KPF_6$  [74–76].

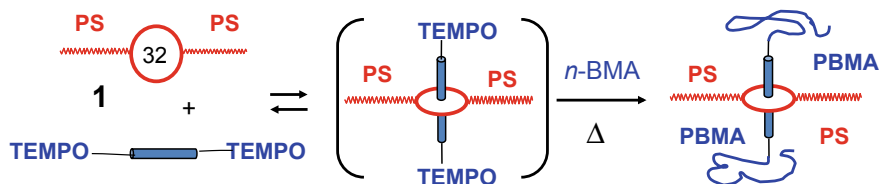
Takata et al. pursued the use of **DB24** in polyrotaxanes in their extensive work [34]. One of the most interesting results from that laboratory is controlled topological transformations of polyrotaxanes. Examples comprise the linear to cyclic [77] and star to linear transformations [78] illustrated in cartoon form in Fig. 13.11.

Again, using the **DB24**/ammonium motif Takata et al. investigated the effects of rotaxane crosslinks on physical properties and demonstrated that the mobility of the macrocycle and its range along the chain greatly influence the mechanical properties (toughness, fracture parameters) [79].

Larger crown ethers are generally not commercially available and, therefore, utilized much less frequently. However, now dibenzo-30-crown-10 (**DB30**, Fig. 13.10) can be synthesized in a high yield [75]. **DB30** blended with an oligomeric polyviologen improved the room temperature ionic conductivity by a factor of 100; this is attributed to the formation of a non-ion paired complex, partially of the rotaxane type [80].

Bis(*m*-phenylene)-32-crown-10 derivatives (**BMP**, Fig. 13.10) have been incorporated into polymer backbones for the formation of polyrotaxanes of **Types B** and **G** (Fig. 13.1) [81]. And the isomeric bis(*p*-phenylene)-34-crown-10 (**BPP**, Fig. 13.10) has been used as the cyclic component in polyurethanes with viologen units in the backbone of **Types A, E** and **F** (Fig. 13.1), which reveal shuttling of the macrocycles between urethane and viologen moieties in solution [82]. Earlier, the polyurethane of **Type A** was reported to possess a higher modulus and extension at break than the model polyurethane without the macrocycle [83].

The utility of host–guest complexation in the synthesis of different architectures is demonstrated by the conversion of a polystyrene with a **BMP** central unit to a four-armed star polymer by first complexing it with a viologen derivative bearing TEMPO-type initiator moieties and then polymerizing *n*-butyl methacrylate, as shown schematically in Fig. 13.12 [84].

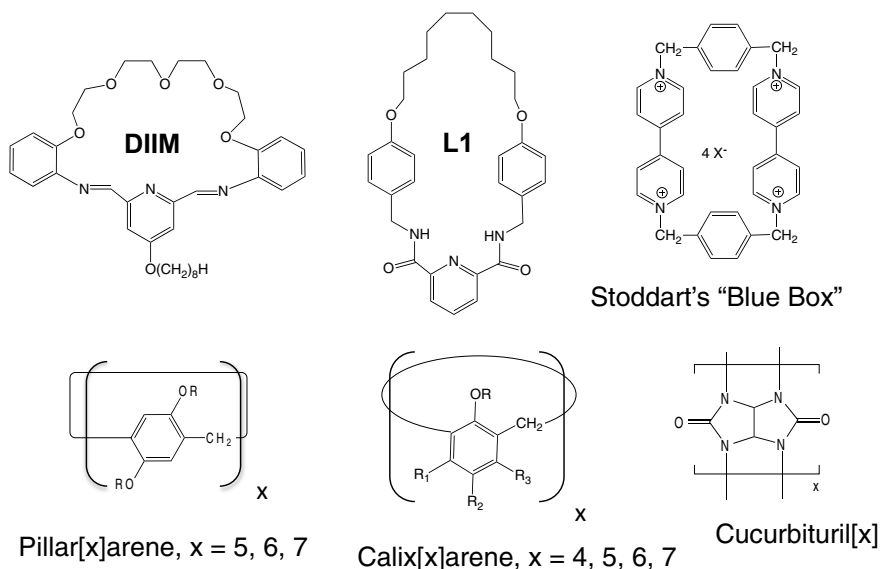


**Fig. 13.12** Formation of a miktoarm star polymer by complexation of a **BMP**-centered polystyrene with a viologen fitted with two TEMPO units, followed by nitroxide-mediated polymerization of *n*-butyl methacrylate. Taken from Ref. [84] with permission. Copyright© American Chemical Society, 2020

### 13.2.3 Polyrotaxanes and Polypseudorotaxanes Based on Other Macrocycles

The formation of a crown-like di-imino macrocycle by dynamic covalent chemistry from the pyridine-2,6-dicarboxaldehyde and tetra(ethylene glycol) bis(2-aminophenyl)ether (i.e., **DIIM**, Fig. 13.13) was used by Stoddart et al. to prepare polyrotaxanes of **Type E** in essentially quantitative yields from oligo(dibenzyl ammonium) salts with up to 11 repeat units fitted with bulky end groups [85].

A template approach using a preformed oligomeric dumbbell containing 14 atoms and end stoppers with pyridyl groups was employed to thread a macrocycle containing amide ligands (**L1**, Fig. 13.13) using Pd coordination [86]. Removal of



**Fig. 13.13** Di-imine, macrocyclic ligand **L1**, the "blue box", pillararenes, calixarenes, and cucurbiturils [8]



the Pd with cyanide freed the macrocycle and the process was repeated to position up to four macrocycles on the relatively short dumbbell. Presumably, this protocol could be extended to properly designed polymeric systems.

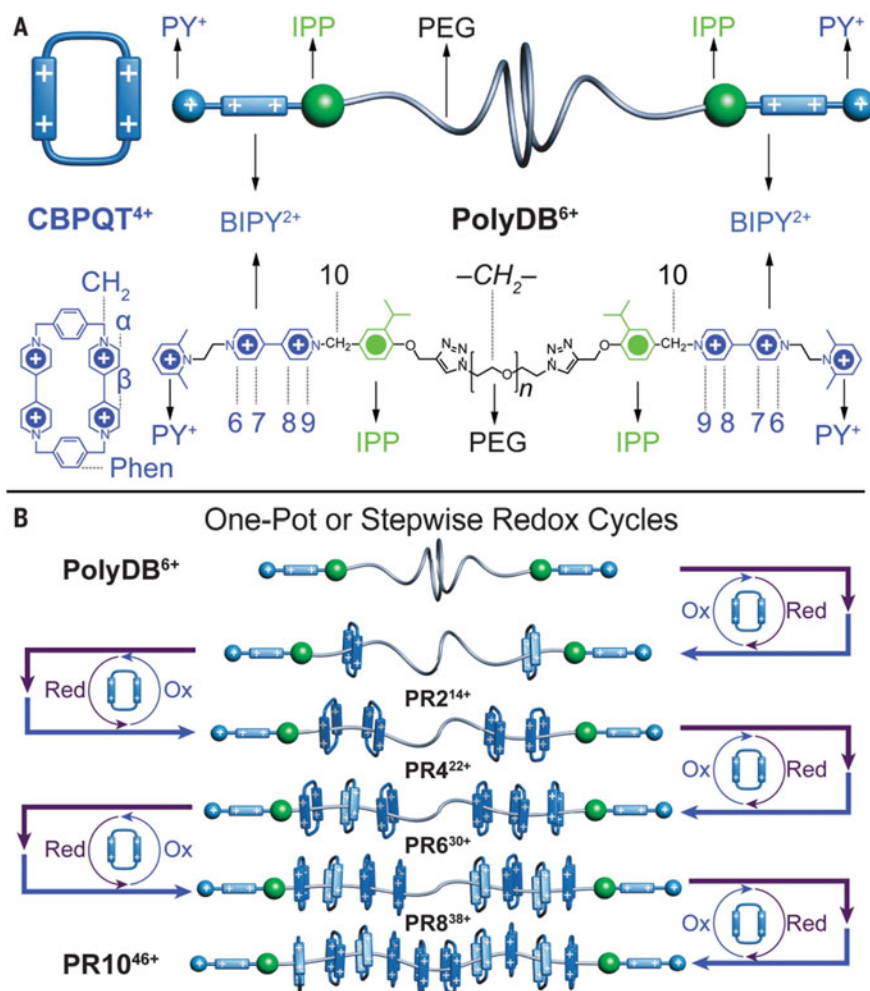
There are a few reports of calixarene-based (Fig. 13.13) polyrotaxanes, but none in the last decade. Closely related triptycene hosts, though well studied, [87] have not been employed in polyrotaxanes.

Pillararenes (Fig. 13.13) are being actively studied as host species in polypseudorotaxanes and polyrotaxanes. These studies include main chain systems of **Type A**, [88–90] **Type E** [91, 92] and side chain systems of **Type D** [93–95].

The venerable “blue box” [cyclobis(paraquat-*p*-phenylene)] (Fig. 13.13) [96] continues to yield new secrets and uses to the creativity of Fraser Stoddart and his co-workers. It was used as the cyclic host in the preparation of polyrotaxanes of **Type E** (Fig. 13.1) based on polymers with 1,5-dioxynaphthalene guest units [97]. The unexpected discovery that once a viologen is reduced by one electron to the radical cation, the latter forms a stable complex with the blue box [98], led to the controlled step-wise synthesis of polyrotaxanes (Fig. 13.14). Poly(ethylene glycol) ( $M_n \sim 2$  kDa) was fitted with terminal pyridinium moieties linked to viologens and then isopropyl-*p*-phenylene units as end groups; reduction of the viologen end units prompted complexation, i.e., capture, of the blue boxes from solution and subsequent reduction forced the captives away from the cationic ends over the steric barrier to the middle of the chain. Repetition of the redox processes led up to 10 blue boxes per linear molecule [99].

The water-soluble cucurbiturils (Fig. 13.13) possess very high binding constants with viologens (e.g.,  $>10^7$  M<sup>-1</sup> for R = CH<sub>3</sub> with **CB7**) [100] and the larger ones are able to include two guests in their cavities in some cases, e.g., **CB8** [101]. Using these host–guest complexations, side chain polypseudorotaxanes of **Type C** (Fig. 13.1) with **CB6**, [102–104] **CB7** [105–107] and both CDs and **CB7** [108] have been reported. Dendrimers [109] and 4-arm star polymers with pseudorotaxane terminal **CB7**/viologen units [110] have been prepared and characterized. Scherman et al. explored side chain polypseudorotaxanes and rotaxane crosslinks using **CB7** and **CB8** for adhesive applications [111] and hydrogels with side chain pseudorotaxane moieties and rotaxane crosslinks, based on both polyacrylamides and hydroxyethylcellulose, using **CB7** and **CB8** [112].

In terms of main chain systems, polypseudorotaxanes of **Type A** (Fig. 13.1) based on conjugated polyfluorene-co-(mono- and bis-) thiophenes with **CB7** have been developed [113–115] and in one case display improved quantum yields for luminescence [114]. Farcas et al. prepared oligomeric poly(ethylene oxide)-based polypseudorotaxanes (**Type A**, Fig. 13.1) and polyrotaxanes (**Type E**, Fig. 13.1) with an  $\alpha$ -CD derivative and **CB7** [116]. A poly(L-lysine)-**CB7** polypseudorotaxane was evaluated as a tunable antibacterial coating [117]. A novel method of bacterial inhibition utilized an oligoviologen polypseudorotaxane (**Type A**, Fig. 13.1) with a **CB6** macrocycle decorated with a sugar, mannose [118].



**Fig. 13.14** Synthesis of polyrotaxanes via redox chemistry. Used with permission from Ref. [99]. Copyright© American Association for the Advancement of Science, 2020

### 13.3 Polymeric Knots or Knotted Polymers

Between 2010 and the end of 2020, a total of about 489 literature reports were published on these topics according to SciFinder®. Screening for “not fiber” and “not root-knot” reduced the number to 367. Inspection of the remaining entries eliminated 96 irrelevant citations, leaving 271 “hits”. Of these, 22 citations are synthetically oriented and many, indeed most, of these are meeting abstracts/preprints; another ca. 15 deal with experimental studies, primarily on DNA systems. Thus, the majority of reports (ca. 236) deal with theoretical treatments. Recent reviews are noted in Table 13.2.

**Table 13.2** Recent reviews of polymeric knots or knotted polymers

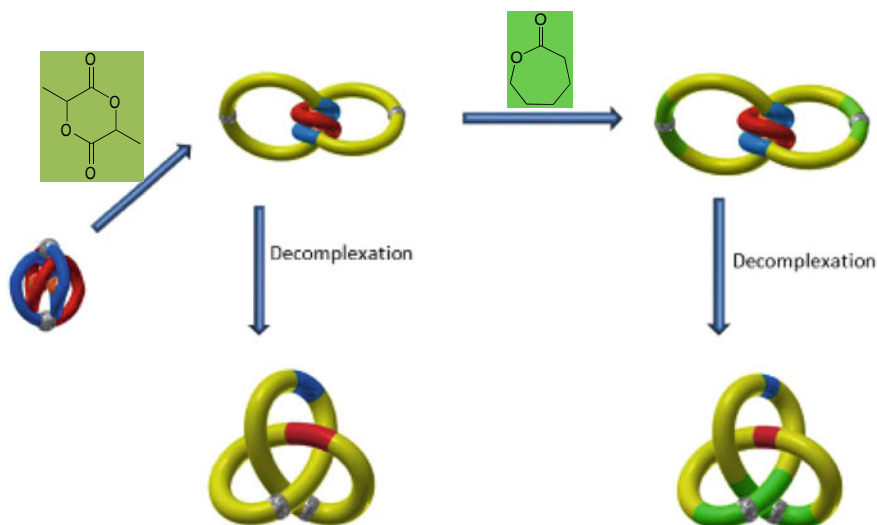
Topic	References
Nanomaterials based on DNA	[119]
Templated synthesis	[120]
Knots in chemistry and biology	[121]
Knotted proteins	[122]
Knot theory in chemistry	[123]
Statistics and dynamics, theory	[124]
Ring polymer knots, electrophoresis	[125]
Statics and dynamics of DNA, theory	[126]

Theoretical treatments include Monte Carlo simulations, [127–130] molecular dynamic simulations, [131–133] worm-like chain models, [134] Flory–Huggins theory, [135] circuit topology theories [136] and neural networks [137]. Most of the theoretical effort has been expended on single molecules, both linear and cyclic, while only a few of these studies [e.g., 125, 138] addressed knot formation in systems with more than one molecule that is closer to the reality of commercial polymeric materials, but requires much more complex treatments.

Biochemists devised several methods of producing and rearranging knots in DNA, RNA and proteins. First of all, because of its great length (up to one meter in humans), some forms of natural DNA already possess knots, [126] as do RNA and proteins [122, 139]. One approach involves the application of topoisomerases, which in Nature remove knots in a chemical manner, but under certain conditions can convert one type of knot to another [126, 140, 141] or, indeed, produce a knot [28, 121]. Physical approaches for inducing knots in these macromolecules include using (1) optical or magnetic tweezers to stretch and twist the anchored macromolecules, [126, 142] (2) microfluidic devices containing narrow channels that under pressure force folding and consequent knotting [126, 143] and (3) electrohydrodynamically stretching first in a field, then collapsing the molecule to a globule by removal of the electric field and finally reapplying a field to restretch the molecule [144]. Knotted samples formed in these ways have then been studied in terms of knotting probabilities depending on conditions, molecular mobility in solution, their tensile strengths, knot size dependences, interaction of knots on a given molecule, mobilities of knots along the macromolecule and un-knotting processes *inter alia* [125, 144–149].

Taken from the perspective of what is now known about these natural macromolecules, the science of *synthetic* knotted molecules is in its infancy, even in terms of methodologies. Indeed even in the small molecule domain, there has been progress over the last several decades, but while immensely impressive in their sophistication, synthetic protocols using metal templates are at this point limited to the preparation of relatively simple knots [120, 121, 150–154].

Only in the last few years have chemists tried to design and prepare knotted synthetic *macromolecules*. An early approach involved the polymerization of divinyl



**Fig. 13.15** Cartoon representation of conversion of a copper-phenanthroline templated trefoil knotted bis(tin) initiator to a poly(L-lactide)-based trefoil knot by insertion polymerization of L-lactide and conversion of the same initiator to a block co-polymeric trefoil knot by sequential addition of L-lactide and then caprolactone. Copper ions were removed by treatment with KCN. Adapted from reference [157] with permission. Copyright© American Chemical Society, 2017

monomers to linear oligomeric systems with pendant vinyl moieties that subsequently underwent intramolecular cyclization; the resultant loops became threaded by other parts of the growing polymer, yielding narrow dispersity “single-chain cyclized/knotted polymeric nanoparticles” at relatively low monomer conversions, i.e., < 33% [155].

In another (more controlled) approach, Advincula et al. cleverly applied copper templation of a phenanthroline-based trefoil knotted bis(tin lactide) initiator to ring expansion polymerization of L-lactide to form a trefoil knotted polymer and also sequentially to L-lactide and caprolactone, leading to an interlocked pair of cyclic block co-polymers. Removal of the copper templates led to the trefoil knotted homo- and co-polymers with polydispersities of about 1.5 (Fig. 13.15) [156].

## 13.4 Polycatenanes

Between 2010 and the end of 2020 according to SciFinder, there were 208 citations for “polycatenane or polymeric catenane”. However, about 121 of these were irrelevant, mainly dealing with coordination polymers. Of the remainder, ca. 52 citations were deemed relevant. It can be concluded that while polycatenanes are of interest, there are few examples of actual polycatenanes to date. As noted in the cited reviews (Table

**Table 13.3** Recent reviews of polycatenanes

Topic	References
General	[157]
General	[2]
Templated synthesis	[158]

13.3), this is a reflection of the fundamental difficulties associated with the synthesis of such materials.

In 2010, Stoddart and co-workers reported the synthesis of a side chain polycatenane of **Type D**,  $x = 1$  (Fig. 13.2) using the “blue box” as the initial pendant ring to template the formation of a dinaphtho-crown ether [159].

In 2015, Meijer et al. reported that Ring Opening Metathesis Polymerization (ROMP) of a copper/phenanthroline complex bearing two cyclic olefins led to a variety of oligocatenanes of up to seven macrocycles, including knots [22].

One reason for the pursuit of poly[n]catenanes has been the belief that the catenane linkages would endow the polymers with excellent stress relaxation because of the abilities of the rings to rotate through each other. A necessary corollary is that the catenane mechanical bonds must be as strong as the covalent bonds of the backbone. The important work of Craig et al. addressed this issue; [160] using sonomechanochemistry on a polymer with  $\sim 5\%$  content of [2] catenane units prepared by ROMP, it was demonstrated that the mechanical bonds of the catenane linkages were as strong or stronger than the covalent bonds of the backbone.

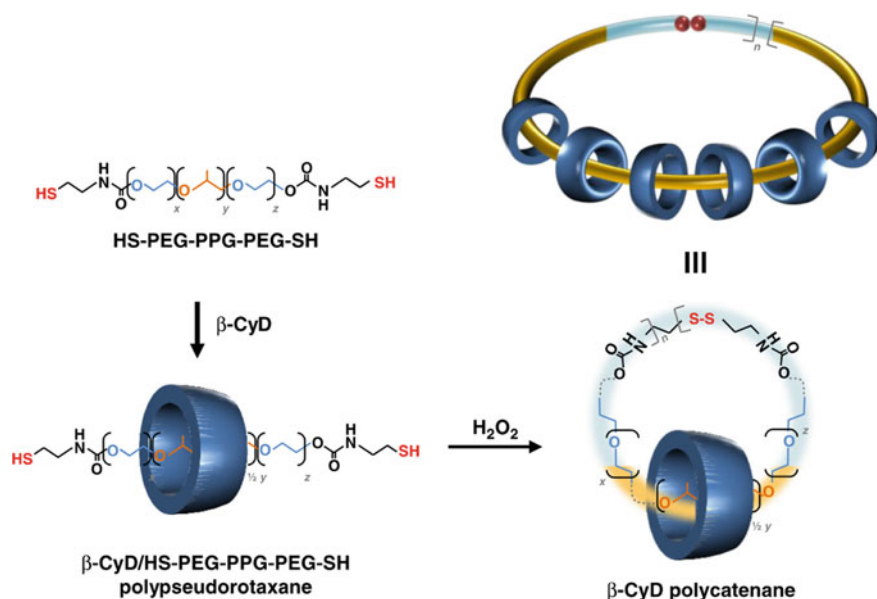
Molecular dynamic simulations of poly[n]catenanes have been carried out to assess mechanical properties (and Rouse mode analysis), [161, 162] solution properties, [163] melt dynamics [164] and thermodynamics and structure of melts [165].

It has been postulated that UV-initiated polymerization of thiol terminated oligo-disulfides produces polycatenane structures, but the insolubility of the product prevented proof of their presence [166].

Oxidative ring closure of  $\beta$ -CD- and  $\gamma$ -CD-based polypseudorotaxanes with PEG-PPG-PEG (Pluronic P123) backbones ( $M_n = 5.8$  kDa) and thiol end groups led to radial polycatenanes of **Type E**, (Figs. 13.2 and 13.16) [24]. Some chain extension occurred prior to cyclization, yielding a family of polycatenanes; the resultant mono- and di-macrocycles were cleanly resolved as narrow peaks ( $PDI < 1.1$ ) by GPC, but larger ones were not.

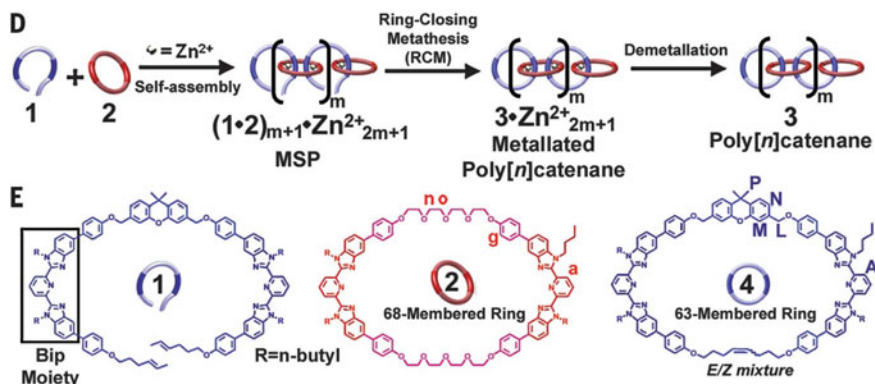
DNA-based polycatenanes of **Type A** (Fig. 13.2) have been used as effective drug carriers for cancer chemotherapy [167].

Advincula et al. cleverly utilized the copper/phenanthroline templated [2] catenane bis(tin initiator) of Fig. 13.15 to prepare a [2] catenane in which the rings are both polymeric [168]. Specifically, caprolactone underwent ring insertion polymerization to form a copper template [2] catenane, and subsequent removal of the copper by KCN treatment afforded the free [2] catenane in 73% yield. NMR indicated that each of the two rings had  $DP = 33$  for a total  $M_n$  of 9.3 kDa.



**Fig. 13.16** Formation of a radial polycatenane from a  $\beta$ -CD-based PEG-PPO-PEG polypseudorotaxane by oxidative coupling of thiol end groups. Taken from Ref. [24] with permission. Copyright© Royal Society of Chemistry, 2019

In what can only be called a true breakthrough in this field, Rowan and co-workers produced poly[n]catenanes using zinc ions to template a closed bisimidazole ring with an open bisimidazole ring, thus forming a metallosupramolecular polymer; they next carried out ring-closing metathesis on the terminal vinyl moieties of the initially open ring and finally removed the zinc template (Fig. 13.17) [23]. The overall GPC trace of the product (obtained in 75% yield) indicated  $M_n = 21.4$  kDa and PDI = 1.44. However, the signal was composed of four narrow dispersity fractions (1.11–1.18) attributed to a low molecular weight (DP ~ 9) linear/cyclic mixture, a higher molecular weight (DP ~ 11) linear/cyclic mixture, a branched fraction (DP ~ 25) and a highly branched fraction (DP ~ 55). These fractions were isolated by preparative GPC. Multiple angle light scattering results and mass spectrometric analysis showed that up to 130 rings existed in the highest molecular weight samples. Grouping the branched samples, the data indicated the relative yields of linear, cyclic and branched poly[n]catenanes were 60%, 14% and 26%. With these poly[n]catenanes in hand, it is now possible to begin exploring their properties experimentally. Furthermore, it is possible that the methodology can be improved to produce linear poly[n]catenanes of higher degrees of polymerization more selectively.



**Fig. 13.17** Synthesis of poly[n]catenane via a metallosupramolecular polymer (MSP), ring-closing metathesis (RCM) and demetallation. Adapted from reference [23] with permission. Copyright© American Association of Science, 2017

### 13.5 Summary and Prospectus

The subfield of polyrotaxanes and polypseudorotaxanes is very active presently along two fronts. On the practical or applications side, cyclodextrin-based systems have been studied in depth and seem to be in the process of being adapted for commercial purposes. On the other hand, polyrotaxanes and polypseudorotaxanes derived from other hosts or cyclic species are still being studied from a more basic perspective. It appears that these latter materials may offer polymer science the means to introduce new materials with unusual or unique properties; however, improvements in synthetic methods and building blocks are needed. More controlled syntheses and a broader range of host–guest interactions will enable more possibilities for applications; many of the guest species for the non-CD hosts are cationic in nature; it would be advantageous if neutral guests with high binding constants could be developed.

In the area of polymeric knots, much is known about the manipulation of natural polymers (DNA, RNA and proteins) to form knots and both theoretical and experimental studies of their properties have been executed. However, these studies have almost exclusively been devoted to single molecules; here, extension to multiple molecules and their abilities to form more complex knots will improve our understanding of more realistic situations. As noted above in terms of knots in synthetic polymers, knowledge lags far behind, both in terms of our ability to make such materials and fundamental understanding of the effects of knots on physical and chemical properties. Development of effective synthetic protocols for the preparation of knotted polymer and experimental studies like the ones carried out on natural polymers are needed to extend our knowledge into the broader applications realm.

Like the polymeric knot arena, the polycatenane arena is in its infancy. Only recently have systems approaching linear poly[n]catenanes of **Type A** (Fig. 13.2)

been achieved. This breakthrough paves the way for experimental studies to determine their unique or unusual physical and chemical properties. More refined synthetic techniques are required to produce totally linear poly[n]catenanes with narrow molecular weight distributions.

All three of these topological classes of materials are of increasing interest to scientists; thus, it is expected that in the next decade our understanding of these systems will expand, and applications will be uncovered to bring them into the service of humanity.

## References

1. F. Huang, H.W. Gibson, *Prog. Polym. Sci.* **30**, 982 (2005)
2. Z. Niu, H.W. Gibson, *Chem. Rev.* **109**, 6024 (2009)
3. J.W. Alexander, G.B. Briggs, *Ann. Math.* **28**, 562 (1926). <http://www.jstor.org/stable/1968399>
4. Vargas-Lara, A.M. Hassan, M.L. Mansfield, J.F. Douglas, *Nat. Sci. Rep.*, **7**, 1 (2017)
5. H. Lüttringhaus, F. Cramer, H. Prinzbach, F. Henglein, *Ann. Chem.* **613**, 185 (1958)
6. G. Schill, Ph.D. Dissertation, University of Friburg (1959)
7. H.L. Frisch, I. Martin, H. Mark, *Monatsh.* **84**, 250 (1953)
8. F. Patat, P. Derst, *Angew. Chem.* **71**, 105 (1959)
9. E. Wasserman, *J. Am. Chem. Soc.* **82**, 4433 (1960)
10. R. Willstätter, Seminar in Zurich, between 1906 and 1912; see footnote 5 in reference 9.
11. H.L. Frisch, E. Wasserman, *J. Am. Chem. Soc.* **83**, 3789 (1961)
12. G. Schill, H. Zöllenkopf, *Nachr. Chem. Tech.* **79**, 149 (1967)
13. G. Schill, H. Zöllenkopf, *J. Liebigs Ann. Chem.* **721**, 53 (1969)
14. I.T. Harrison, S. Harrison, *J. Am. Chem. Soc.* **89**, 5723 (1967)
15. G. Agam, D. Gravier, A. Zilkha, *J. Am. Chem. Soc.* **98**, 5206 (1976)
16. N. Ogata, K. Sanui, J. Wada, *J. Polym. Sci. Polym. Lett. Ed.* **14**, 459 (1976)
17. M. Maciejewski, A. Gwizdowski, P. Peczek, A. Pietrak, *J. Macromol. Sci., Chem.* **A13**, 87 (1979)
18. M. Maciejewski, *J. Macromol. Sci., Chem.* **A18**, 77 (1979)
19. D. Callahan, H.L. Frisch, *Polym. Eng. Sci.* **15**, 70 (1975)
20. D. Muscat, W. Köhler, H.J. Räder, K. Martin, S. Mullins, B. Müller, K. Müllen, Y. Geerts, *Macromolecules* **32**, 1737 (1999)
21. D.B. Amabilino, P.R. Ashton, A.S. Reder, N. Spencer, J.F. Stoddart, *Angew. Chem, Int. Ed. Engl.* **33**, 1286 (1994)
22. J.A. Berrocal, L.M. Pitet, M.M.L. Nieuwenhuizen, L. Mandolini, E.W. Meijer, S. Di Stefano, *Macromolecules* **48**, 1358–1363 (2015)
23. Q. Wu, P.M. Rauscher, X. Lang, R.J. Wojtecki, J.J.A. de Pablo, S.J. Rowan, *Science* **358**, 1434 (2017)
24. T. Higashi, K. Morita, X. Song, J. Zhu, A. Tamura, N. Yui, K. Motoyama, H. Arima, J. Li, *Nat. Commun.* **2**, 78 (2019)
25. H.L. Frisch, E. Wasserman, *Polymer Preprints (American Chemical Society, Division of Polymer Chemistry* **1 (No. 2)**, 93 (1960)
26. G.M. Crippen, *J. Theoret. Biol.* **45**, 327 (1974)
27. M.D. Frank-Kamenetskii, A.V. Lukashin, A.V. Vologodskii, *Nature* **258**, 398 (1975)
28. L.F. Liu, R.E. Depew, J.C. Wang, *J. Mol. Biol.* **106**, 439 (1976)
29. L. Fang, M.A. Olson, D. Ben´tez, E. Tkatchouk, W.A. Goddard III, J.F. Stoddart, *Chem. Soc. Rev.* **39**, 17 (2010)
30. M. Arunachalam, H.W. Gibson, *Progr. Polym. Sci.* **39**, 1043 (2014)



31. A. Tamura, N. Yui, *Chem. Comm.* **50**, 13433 (2014)
32. A. Harada, A. Hashidzume, H. Yamaguchi, Y. Takashima, *Encyclopedia of Polymer Science and Technology* (4th edn.), H. F. Mark, ed., **11**, 119 (2014)
33. K. Mayumi, K. Ito, K. Kato, *Polyrotaxane and Slide-Ring Materials* (Royal Society of Chemistry, London, 2016). ISBN 978-1-84973-933-7
34. T. Aoki, Takata. *Polymer* **128**, 276 (2017)
35. Y. Takashima, A. Harada, *J. Incl. Phenom. Macrocycl. Chem.* **88**, 85 (2017)
36. A. Hashidzume, H. Yamaguchi, A. Harada, *Eur. J. Org. Chem.* **21**, 3344 (2019)
37. S. Mena-Hernando, E.M. Perez, *Chem. Soc. Rev.* **48**, 5016 (2019)
38. N. Basílio, U. Pischel, in *Cucubituril-based Functional Materials*, D. Tuncel, ed. (Royal Society of Chemistry, London, 2020), ISBN 978-1-78801-488-5, pp. 56-94
39. J. Wankar, N.G. Kotla, S. Gera, S. Rasala, A. Pandit, Y.A. Rochev, *Adv. Funct. Mater.* **30**, 1909049 (2020)
40. J. Royakkers, H. Bronstein, *Macromolecules* **54**, 1083 (2021)
41. World Health Organization, <https://who.int>
42. S. Bai, X. Zhang, X. Ma, J. Chen, Q. Chen, X. Shi, M. Hou, P. Xue, Y. Kang, Z. Xu, *Biomater. Sci.* **6**, 3126 (2018)
43. T. Kim, S. Y. Park, M.-H. Lee, D.-H. Kim, I. Chung, *J. Bioactive Compat. Polym.* **34**, 25 (2019)
44. Y. Zhang, Q. Zhou, S. Jia, K. Lin, G. Fan, J. Yuan, S. Yu, J. Shi, *A.C.S. Appl. Mater. Interfaces* **11**, 46427 (2019)
45. X. Song, Z. Zhang, J. Zhu, Y. Wen, F. Zhao, L. Lei, N. Phan-Thien, B.C. Khoo, J. Li, *Bio-macromolecules* **21**, 1516 (2020)
46. K. Nishida, A. Tamura, T.W. Kang, H. Masuda, N. Yui, *J. Mater. Chem. B* **8**, 6975 (2020)
47. L.-Z. Hu, N. Wan, X.-X. Ma, Z.-W. Jing, Y.-X. Zhang, C. Li, S.-Y. Zhou, B.-L. Zhang, *Nanotechnology* **28** 125102 (2017)
48. R. Ardeleanu, A.I. Dascalu, A. Neamtu, D. Peptanariu, C.M. Uritu, S.S. Maier, A. Nicolescu, B.C. Simionescu, M. Barboiu, M. Pinteala, *Polym. Chem.* **9**, 845 (2018)
49. S.B. Ghodke, J.N. Parkar, A.R. Deshpande, P.P. Dandekar, R.D. Jain, *A.C.S. Appl. Bio Mater.* **3**, 7500 (2020)
50. A.K. Rajendan, Y. Arisaka, N. Yui, S. Iseki, *Inflamm. Regen.* **40**, 27 (2020)
51. Y.A. Mondjinou, B.P. Loren, C.J. Collins, S.-H. Hyun, A. Demoret, J. Skulsky, C. Chaplain, V. Badwaik, D.H. Thompson, *Bioconj. Chem.* **29**, 3550 (2018)
52. Y. Lu, D. Aoki, J. Sawada, T. Kosuge, H. Sogawa, H. Otsuka, T. Takata, *Chem. Commun.* **56**, 3361 (2020)
53. R. Wu, J. Lai, Y. Pan, Z. Zheng, X. Ding, *Soft Matter* **14**, 4558 (2018)
54. C. Liu, H. Kadono, K. Mayumi, K. Kato, H. Yokoyama, K. Ito, *ACS Macro Lett.* **6**, 1409 (2017)
55. A.B. Imran, K. Esaki, H. Gotoh, T. Seki, K. Ito, Y. Sakai, Y. Takeoka, *Nat. Commun.* **5**, 5124 (2014)
56. C.-Y. Shi, Q. Zhang, C.-Y.C. Zhao, Y. Domon, Y. Okumura, S. Okabe, M. Shibayama, K. Ito, *J. Phys.: Condens. Matter* **17**, S2841 (2005)
57. S.-J. Yu, S. Rao, H. Yang, D.-H. Tian, Qu, *Adv. Mater.* **32**, 2000345 (2020)
58. C. Zhao, Y. Domon, Y. Okumura, S. Okabe, M. Shibayama, K. Ito, *J. Phys.: Condens. Matter* **17**, S2841 (2005)
59. S. Tan, A. Blencowe, K. Ladewig, G.G. Qiao, *Soft Matter* **9**, 5239 (2013)
60. T. Murakami, B.V.K.J. Schmidt, H.R. Brown, C.J. Hawker, *Macromolecules* **48**, 7774 (2015)
61. T. Murakami, B.V.K.J. Schmidt, H.R. Brown, C.J. Hawker, *J. Polym. Sci., Part A: Polym. Chem.* **55**, 1156 (2017)
62. Z. Zhang, G. Hou, J. Shen, J. Liu, Y. Gao, X. Zhao, L. Zhang, *Polymers* **10**, 964 (2018)
63. Y. Yasuda, T. Masumoto, K. Mayumi, M. Toda, H. Yokoyama, H. Morita, K. Ito, *ACS Macro Lett.* **9**, 1280 (2020)
64. F.J. Vernerey, S. Lamont, *J. Mech. Phys. Solids* **146**, 104212 (2021)
65. A. Ishigami, K. Watanabe, T. Kurose, H. Ito, *Polymers* **12**, 1790 (2020)

66. J. Hilschmann, G. Kali, G. Wenz, *Macromolecules* **50**, 1312 (2017)
67. J. Hilschmann, G. Wenz, G. Kali, *Beilstein J. Org. Chem.* **13**, 1310 (2017)
68. Y.-C. Wang, R. Maeda, G. Kali, H. Yokoyama, G. Wenz, K. Ito, *ACS Macro Lett.* **9**, 1853 (2020)
69. I.T. Harrison, *J. Chem. Soc. Perkin Trans. I*, 301 (1974)
70. I.T. Harrison, *J. Chem. Soc. Chem. Commun.* 384 (1977)
71. C. Zhang, S. Li, J. Zhang, K. Zhu, N. Li, F. Huang, *Org. Lett.* **9**, 5553 (2007)
72. C. Zhang, K. Zhu, S. Li, J. Zhang, F. Wang, M. Liu, N. Li, F. Huang, *Tet. Lett.* **49**, 6917 (2008)
73. X. Ji, K. Jie, S.C. Zimmerman, F. Huang, *Polym. Chem.* **6**, 1912 (2015)
74. H.W. Gibson, H. Wang, K. Bonrad, J.W. Jones, C. Slebodnick, B. Habenicht, P. Lobue, *Org. Biomol. Chem.* **3**, 2114 (2005)
75. H.R. Wessels, H.W. Gibson, *Tetrahedron* **72**, 396 (2016)
76. A.M.P. Pederson, T.L. Price Jr., C. Slebodnick, D.V. Schoonover, H.W. Gibson, *J. Org. Chem.* **82**, 8489 (2017)
77. T. Ogawa, K. Nakazono, D. Aoki, S. Uchida, T. Takata, *ACS Macro Lett.* **4**, 343 (2015)
78. D. Aoki, S. Uchida, T. Takata, *Angew. Chem. Int. Ed.* **54**, 6770 (2015)
79. J. Sawad a, D. Aoki, H. Otsuka, T. Takata, *Angew. Chem., Int. Ed.* **58**, 2765 (2019)
80. M. Lee, H.W. Gibson, R.H. Colby, U.H. Choi, *Macromolecules* **52**, 4240 (2019)
81. H.W. Gibson, D.S. Nagvekar, N. Yamaguchi, Y. Delaviz, J.W. Jones, P. Balanda, A. Prasad, H. Marand, *Polymer* **142**, 256 (2018)
82. H.W. Gibson, Y.X. Shen, M.C. Bheda, C. Gong, *Polymer* **55**, 3202 (2014)
83. D. Loveday, G.L. Wilkes, M.C. Bheda, Y.X. Shen, H.W. Gibson, *J. Macromol. Sci., A-Chem.* **A32**, 1(1995)
84. M. Lee, D.V. Schoonover, Z. Niu, M.A. Rouser, H.W. Gibson, *Macromolecules* **53**, 5399 (2020)
85. J. Wu, K.C.-F. Leung, J.F. Stoddart, *Proced. Nat. Acad. Sci., USA* **104**, 17266 (2020)
86. A.M. Fuller, D.A. Leigh, P.J. Lusby, *Angew. Chem. Int. Ed.* **46**, 5015 (2007)
87. C.-F. Chen, *Chem. Commun.* **47**, 1674 (2011)
88. T. Ogoshi, Y. Nishida, T. Yamagishi, Y. Nakamoto, *Macromolecules* **43**, 3145 (2010)
89. T. Ogoshi, Y. Hasegawa, T. Aoki, Y. Ishimori, S. Inagi, T. Yamagishi, *Macromolecules* **44**, 7639 (2011)
90. T. Ogoshi, H. Kayama, T. Aoki, T.-A. Yamagishi, R. Ohashi, M. Mizuno, *Polymer J.* **46**, 77 (2014)
91. T. Ogoshi, Y. Nishida, T. Yamagishi, Y. Nakamoto, *Macromolecules* **43**, 7068 (2010)
92. T. Ogoshi, T. Aoki, S. Ueda, Y. Tamura, T.-A. Yamagishi, *Chem. Commun.* **50**, 6607 (2014)
93. X. Chi, X. Ji, D. Xia, F. Huang, *J. Am. Chem. Soc.* **137**, 1440 (2015)
94. W. Cui, H. Tang, L. Xu, L. Wang, H. Meier, D. Cao, *Macromol. Rapid Commun.* **38**, 1700161 (2017)
95. Boominathan, J. Kiruthika, M. Arunachalam, *J. Polym. Sci., Part A: Polym. Chem.* **57**, 1508 (2019)
96. P.R. Ashton, B. Odell, M.V. Reddington, A.M.Z. Slawin, J.F. Stoddart, D.J. Williams, *Angew. Chem.* **100**, 1608 (1988)
97. W. Zhang, W.R. Dichtel, A.Z. Stieg, D. Beni´tez, J.K. Gimzewski, J.R. Heath, J.F. Stoddart, *Proced. Nat. Acad. Sci. USA* **105**, 6514 (2008)
98. A. Trabolsi, N. Khashab, A.C. Fahrenbach, D.C. Friedman, M.T. Colvin, K.K. Cot´, D. Beni´tez, E. Tkatchouk, J.-C. Olsen, M.E. Belowich, R. Carmielli, H.A. Khatib, W.A. Goddard, III, M.R. Wasielewski, J. F. Stoddart, *Nat. Chem.* **2**, 42 (2009)
99. Y. Qiu, B. Song, C. Pezzato, D. Shen, W. Liu, L. Zhang, Y. Feng, Q.-H. Guo, K. Cai, W. Li, H. Chen, M.T. Nguyen, Y. Shi, C. Cheng, R.D. Astumian, X. Li, J.F. Stoddart, *Science* **368**, 1247 (2020)
100. S. Liu, C. Ruspic, P. Mukhopadhyay, S. Chakrabarti, P.Y. Zavalij, L. Isaacs, *J. Am. Chem. Soc.* **127**, 15959 (2005)
101. Y. Cui, Z. Zhao, R. Wang, W. Zhu, D. Zou, *Chinese. J. Org. Chem.* **34**, 1183 (2014)
102. Z. Hou, Y. Tan, Q. Zhou, *Polymer* **47**, 5267 (2006)

103. H. Wang, Y. Zhu, X. Ren, M. Wang, Y. Tan, Iran. Polym. J. **21**, 783 (2012)
104. Q. Ma, H. Yang, K. Kim, Y.-B. Tan, Chinese J. Polym. Sci. **30**, 578 (2012)
105. H. Yang, Y. Tan, J. Hao, H. Yang, F. Liu, J. Polym. Sci. Part A: Polym. Chem. **48**, 2135 (2010)
106. H. Yang, J. Hao, Y. Tan, J. Polym. Sci. Part A: Polym. Chem. **49**, 2138 (2011)
107. H. Chen, H. Ma, Y. Yuan Chieng, S. Hou, X. Li, Y. Tan, RSC Adv. **5**, 20684 (2015)
108. T. Ogoshi, K. Masuda, T.-A. Yamagishi, Y. Nakamoto, Macromolecules **42**, 8003 (2009)
109. J.W. Lee, Y.-H. Ko, S.H. Park, K. Yamaguchi, K., Kim, Angew. Chem. Int. Ed. **40**, 746 (2001)
110. H. Yang, C. Song, H. Chen, W. Xu, Y. Tan, Supramol. Chem. **24**, 833 (2012)
111. J. Liu, C.S.Y. Tan, O.A. Scherman, Angew. Chem. Int. Ed. **57**, 8854 (2018)
112. C.S.Y. Tan, J. Liu, A.S. Groombridge, S.J. Barrow, C.A. Dreiss, O.A. Scherman, Adv. Funct. Mater. **28**, 1702994 (2018)
113. A. Farcas, P.-H. Aubert, J. Mohanty, A.I. Lazar, S. Cantin, W.M. Nau, Eur. Polym. J. **62**, 124 (2015)
114. M. Idris, M. Bazzar, B. Guzelturk, H.V. Demir, D. Tuncel, RSC Adv. **6**, 98109 (2016)
115. T. Erdem, M. Idris, H.V. Demir, D. Tuncel, Macromol. Mater. Eng. **302**, 1700290 (2017)
116. A.-M. Resmerita, K.I. Assaf, A.I. Lazar, W.M. Nau, A. Farcas, Eur. Polym. J. **93**, 323 (2017)
117. Z. Huang, H. Zhang, H. Bai, Y. Bai, S. Wang, X. Zhang, ACS Macro Lett. **5**, 1109 (2016)
118. J. Kim, Y. Ahn, K.M. Park, D.-W. Lee, K. Kim, Chem. Eur. J. **16**, 12168 (2010)
119. N.C. Seeman, Annu. Rev. Biochem. **79**, 65 (2010)
120. J.F. Ayme, J.E. Beves, C.J. Campbell, D.A. Leigh, Chem. Soc. Rev. **42**, 1700 (2013)
121. N.C.H. Lim, S.E. Jackson, J. Phys.: Condens. Matter **27** 354101 (2015)
122. P.F.N. Faísca, Comput. Struct. Biotechn. J. **13**, 459 (2015)
123. K.E. Horner, M.A. Miller, J.W. Steed, P.M. Sutcliffe, Chem. Soc. Rev. **45**, 6432 (2016)
124. T. Deguchi, E. Uehara, Polymers **9**, 252 (2017)
125. D. Michieletto, M. Marenduzzo, E. Orlandini, M.S. Turner, Polymers **9**, 349 (2017)
126. E. Orlandini, J. Phys. A: Math. Theor. **51**, 053001 (2018)
127. J. Polson, J.M.; C.G. Hastie, Phys. Rev. E **102**, 052502 (2020)
128. J.M. Polson, C. Hastie, Cameron, Condensed Matter (2020)
129. L. Luwei, H. Zhu, Y. Lu, L. An, L. Dai, Macromolecules **53**, 9443 (2020)
130. L. Dai, Phys. Rev. Res. **2**, 022014 (2020)
131. F. Guo, K. Li, J. Wu, L. He, L. Zhang, Polymers **12**, 2659 (2020)
132. M. Caraglio, B. Marcone, F. Baldovin, E. Orlandini, A.L. Stella, Polymers **12**, 2580 (2020)
133. B.W. Soh, A.R. Klotz, P.S. Doyle, Macromolecules **53**, 7389 (2020)
134. J. Zhang, H. Meyer, P. Virnau, D. Daoulas, C. Kostas, Macromolecules **53**, 10475 (2020)
135. E.J.J. van Rensburg, J. Phys. A: Math. Theor. **53**, 015002 (2020)
136. Golovnev, A. Mashaghi, iScience **23**, 101492 (2020)
137. O. Vandans, Olafs, K. Yang, Z. Wu, L. Dai, Phys. Rev. E **101**, 022502 (2020)
138. F. Guo, K. Li, J. Wu, L. He, L. Zha, Polymers **12**, 2659 (2020)
139. C. Liang, K. Mislow, J. Am. Chem. Soc. **116**, 1118 (1994)
140. T. Goto, J.C. Wang, J. Biol. Chem. **257**, 5866 (1982)
141. J.C. Wang, Annu. Rev. Biochem. **65**, 635 (1996)
142. Y. Arai, R. Yasuda, K. Akashi, Y. Harada, H. Miyata, T. Kinoshita, H. Itoh, Nature **399**, 446 (1999)
143. R. Metzler, W. Reisner, R. Riehn, R. Austinm, J.O. Tegenfeldt, I.M. Sokolov, Eur. Phys. Lett. **76**, 696 (2006)
144. A.R. Klotz, B.W. Soh, P.S. Doyle, Eur. Phys. Lett. **129**, 68001 (2020)
145. T.C. Sayre, T.M. Lee, N.P. King, T.O. Yeates, Protein Eng. Design Sel. **24**, 627 (2011)
146. B.W. Soh, V. Narsimhan, A.R. Klotz, P.S. Doyle, Soft Matter **14**, 1689 (2018)
147. R.K. Sharma, I. Agrawal, L. Dai, P.S. Doyle, S. Garaj, Nat. Commun. **10**, 4473 (2019)
148. M. Nakata, Y. Nakamura, Y. Maki, T. Dobashi, Polymer **178**, 121541 (2019)
149. Z. Ma, K.D. Dorfman, Macromolecules **53**, 6461 (2020)
150. R.S. Forgan, J.-P. Sauvage, J.F. Stoddart, Chem. Rev. **111**, 5434 (2011)
151. J.E. Beves, B.A. Blight, C.J. Campbell, D.A. Leigh, R.T. Burney, Angew. Chem. Int. Ed. **50**, 9260 (2011)

152. J.E. Beves, *CHIMIA. Int. J. Chem.* **66**, 170 (2012)
153. D.A. Leigh, F. Schaufelberger, L. Pirvu, J.H. Stenlid, D.P. August, J. Segard, *Nature* **584**, 562 (2020)
154. D.A. Leigh, J.J. Danon, S.D.P. Fielden, J.-F. Lemonnier, G.F.S. Whitehead, S.L. Woltering, *Nat. Chem.* **13**, 117 (2020)
155. Y. Gao, D. Zhou, T. Zhao, X. Wei, S. McMahon, J.O’K. Ahern, W. Wang, U. Greiser, B.J. Rodriguez, W. Wang, *Macromolecules* **48**, 6882 (2015)
156. P.-F. Cao, L.-H. Rong, J.D. Mangadlao, R.C. Advincula, *Macromolecules* **50**, 1473 (2017)
157. L. Raehm, D.G. Hamilton, J.K.M. Sanders, *Synlett* **11**, 1743 (2002)
158. J.-F. Ayme, J.E. Beves, C.J. Campbella, D.A. Leigh, *Chem. Soc. Rev.* **2**, 1700 (2013)
159. M.A. Olson, A. Coskun, L. Fang, A.N. Basuray, J.F. Stoddart, *Angew. Chem. Int. Ed.* **49**, 3151 (2010)
160. B. Lee, Z. Niu, S.L. Craig, *Angew. Chem. Int. Ed.* **55**, 13086 (2016)
161. Z.-T. Wu, J.-J. Zhou, *Chinese. J. Polym. Sci.* **37**, 1298 (2019)
162. P.M. Rauscher, S.J. Rowan, J.J. de Pablo, *ACS Macro Lett.* **7**, 938 (2018)
163. Z.A. Dehaghani, I. Chubak, C.N. Likos, M.R. Ejtehadi, *Soft Matter* **16**, 3029 (2020)
164. P.M. Rauscher, K.S. Schweizer, S.J. Rowan, J.J. de Pablo, *J. Chem. Phys.* **152**, 214901 (2020)
165. P.M. Rauscher, K.S. Schweizer, S.J. Rowan, J.J. de Pablo, *Macromolecules* **53**, 3390 (2020)
166. A. Chemtob, N. Feillé, C. Vaulot, C. Ley, D. Le Nouen, *ACS Omega* **4**, 5722 (2019)
167. S. Yu, Y. Wang, Y. Li, L.-P. Jiang, S. Bi, J.-J. Zhu, *Adv. Funct. Mater.* **29**, 1905659 (2019)
168. P.-F. Cao, A. Bunha, J. Mangadlao, M.J. Felipe, K.I. Mongcopa, R. Advincula, *Chem. Commun.* **48**, 12094 (2012)

**Part III**  
**Cyclic Polymer Innovations: Syntheses**

# Chapter 14

## Recent Progress on the Synthesis of Cyclic Polymers



Brennan J. Curole, Ashley V. Miles, and Scott M. Grayson

**Abstract** Polymer architectures are very diverse and include linear polymers, star polymers, polymer brushes, ladder polymers, dendrimers, network polymers, and hyperbranched polymers. However, one critical topology that has become apparent in the last 50 years is cyclic polymers. Designing facile methods to create interesting polymer architectures continues to be a goal for polymer chemist. Depending on the polymer architecture, the physical properties can be affected considerably, and they include glass transition temperatures ( $T_g$ ), melt transitions temperatures ( $T_m$ ), crystallization temperatures ( $T_c$ ), thermostabilities, intrinsic and melt viscosities, rheological properties, solubilities, etc. [1]. Polymers with chain ends tend to have different properties compared to cyclic polymers which include a smaller hydrodynamic volume, a lower viscosity, a difference in crystallization temperature, and a change in glass transition temperature [3–5]. Due to these alterations in properties, cyclic polymers have been widely studied compared to their linear polymer counterparts. Throughout the years, cyclic polymers have encountered synthetic challenges such as linear impurities, low yields, and the inability to scale up to kilograms [6, 7]. As a result, many synthetic methods have been developed to overcome such limitations which include high-dilution reaction conditions for CuAAC and SPAAC catalyzed cyclic polymer synthesis. In addition many synthetic strategies have been combined to synthesize complex cyclic polymer topologies such as using ESA-CF and “click” chemistry to develop hybrid tricyclic polymers 8 and cyclic graft polymers [9].

### 14.1 Introduction

Small organic molecules were the first examples to use high-dilution reaction conditions to cyclize them. Under these conditions, complementary functional groups on the same molecule would be effectively be “in high concentration” and, as a result,

---

B. J. Curole · A. V. Miles · S. M. Grayson (✉)  
Department of Chemistry, Tulane University, 2015 Percival Stern Hall, New Orleans, LA 70118,  
USA  
e-mail: [sgrayson@tulane.edu](mailto:sgrayson@tulane.edu)

intramolecular coupling between chain ends are favored due to their proximity [10, 11]. The thermal dynamics become favorable or unfavorable depending on the length of these two coupling units. Baeyer (angle) strain is unfavorable when it comes to rings which yield three to four covalent bonds and Pitzer (transannular) strain is also unfavorable for cyclic rings with seven to thirteen bonds. Although most of these rings could be formed in low yields, five and six membered rings were substantially favored due to limited ring strain. The above-mentioned ring sizes demonstrated that enthalpy (ring strain) becomes less important with ring sizes greater than 15. It was predicted that macrocyclic polymers have a high entropic penalty, however, in the 1950's cyclic DNA was discovered; therefore new synthetic strategies were created for cyclic polymers, specifically cyclic polystyrene [12].

There are two main methods used to prepare cyclic polymers: (1) Ring-closure techniques and (2) ring-expansion techniques. Ring-closure involves a linear precursor with compatible end groups that couple together while ring-expansion mainly involves the insertion of a cyclic monomer into a cyclic initiator or catalyst. The former can be further categorized into different synthetic methods which are the bimolecular approach, the homofunctional unimolecular approach, and the heterofunctional unimolecular approach. This chapter describes the recent advances in both ring-closure and ring-expansion techniques.

## 14.2 Bimolecular Ring-Closure

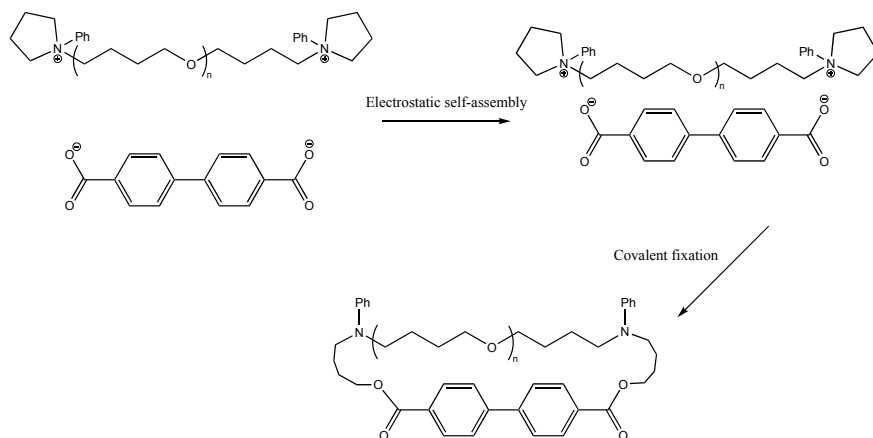
Bimolecular ring-closure approach is the coupling of a linear bisfunctional polymer with a linker that has compatible difunctional chain ends. It is difficult to prevent impurities with this approach because the reaction conditions either favor the first reactive step that involves intermolecular coupling with the linear polymer and linker (very high concentration) or the intramolecular coupling of the second step between the compatible chain ends on the same polymer (much lower concentration) [1]. The stoichiometry between the polymer and the linker must be exactly one to one for these reasons bimolecular ring-closure reactions. These typically produce impurities and is not widely used as a synthetic strategy [1, 2]. To overcome these challenges, three techniques were developed: (1) Electrostatic self-assemble and covalent fixation (ESA-CF), (2) self-accelerating "click" reactions (3) and radical trap-assisted atom transfer radical coupling (RTA-ATRC).

Electrostatic self-assembly and covalent fixation for cyclic polymer synthesis was developed by Tezuka and coworkers. ESA-CF involves electrostatic interactions between a dianionic (e.g., dicarboxylic acid) coupling agent and a polymer with two cationic chain ends (e.g., diammonium salt) that preassemble under low concentration, and upon heating, the pairs form a stable covalent bond [13]. This bimolecular method permits both inter- and intra-molecular coupling to occur under dilute conditions which increases the amount of pure cyclic products. Under dilute conditions the first coupling is achieved with ESA-CF due to the pre-assembled salt

and the second intramolecular coupling is favorable due to these highly dilute conditions. An example of this synthesis uses telechelic poly(tetrahydrofuran) with two *N*-phenylpyrrolidinium cation groups at each chain end that link ionically, and then covalently, with a sodium dicarboxylate to form a cyclic polymer. ESA-CF has been as a synthetic technique for polyTHF [14–16], quadruply fused pentacyclic polymers [17], and other cyclic polymer topologies [9, 18–26] (Fig. 14.1).

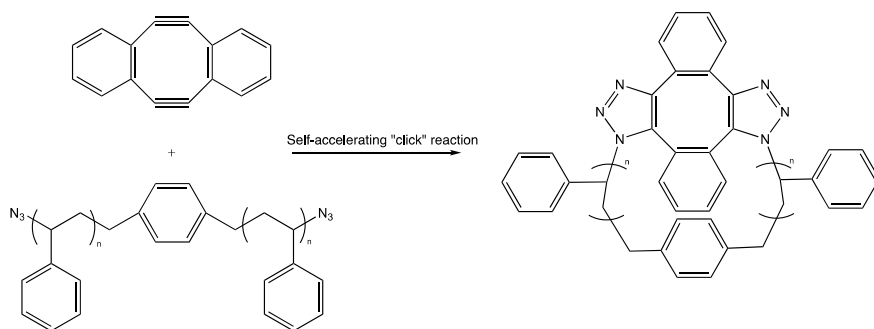
Self-accelerating click is a strained-promoted double alkyne-azide cycloaddition (SPAAC) that is catalyst free. This technique was first used to modify biomolecules [27, 28], and then, Sun et al. adapted this method as a ring-closure technique [29]. SPAAC overcomes the challenge of using an exact one to one stoichiometric amount of linear precursor to linker. For SPAAC, the excess of linker increases the rate of intermolecular coupling between the linear polymer and linker and the second reaction between the linker is an order of magnitude larger than the first reaction. Since the rate of the first coupling is increased, the ring-closure reaction is more efficient. Self-accelerating “click” involves a linear polymer with two azide end groups. Then a strained cyclodicyne, e.g., dibenzocycloocta-4a,6a-diene-5,11-diyne (DBA), can catalyze not one reaction (on one side) but two to yield the cyclic polymer. Cycloaddition to the first azide to alkyne increases ring strain of DBA and as a result the second cycloaddition is faster than the first by stimulating the second alkyne [29]. As a result, SPAAC has also been used for polyacrylate [30], polynorbornenes [31], poly(vinyl acetate) [32], poly(*N*-vinylcarbazole) [33], poly(lactic acid) [34], and other cyclic topologies [35] (Fig. 14.2).

The next method for ring-closure is cyclic polystyrene by Carnicom and Tillman through radical trap-assisted atom transfer radical coupling (RTA-ATRC) [36]. First  $\alpha,\omega$ -dibromo-polystyrene was synthesized by ATRP using a bifunctional initiator, benzal bromide. Then the reaction mixture was in pseudo-high dilute conditions with THF and the radical trap, 2-methyl-2-nitrosopropane dimer (MNP) along with



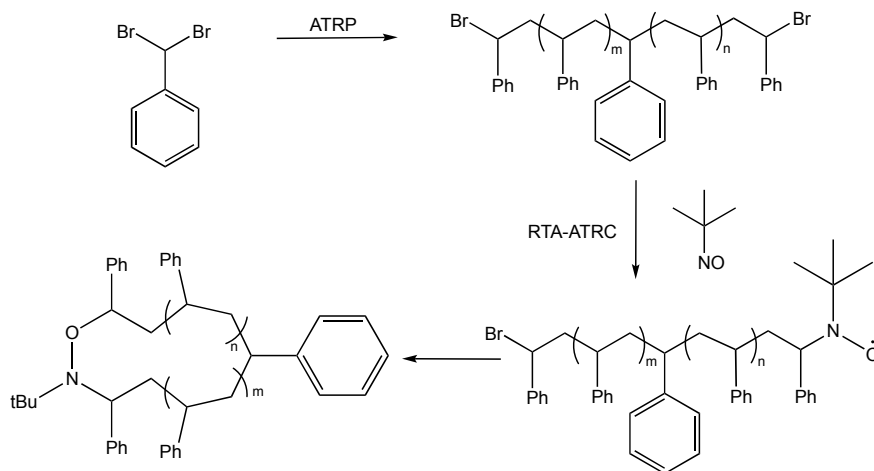
**Fig. 14.1** The synthesis of cyclic polymers via ESA-CF by Oike et al. [13]





**Fig. 14.2** The synthesis of macrocyclic polystyrene via self-accelerating “click” reaction by Sun et al. [29]

copper(I) bromide ( $\text{CuBr}$ ) and copper metal ( $\text{Cu}^0$ ) were added to the reaction flask. A solution of pentamethyldiethylene triamine (PMDETA) was then added via syringe to initiate the reaction. The radical carbon on one chain end reacts with the radical trap, MNP to form a nitroxide radical. Next, the radicals on each chain end react to form the cyclic polystyrene. The cyclic polystyrene was confirmed by GPC and NMR spectroscopy. RTA-ATRC has also been used to cyclize polystyrene [37–39], poly(methyl methacrylate) [40], and other cyclic topologies such as a tadpole polymer [41] (Fig. 14.3).



**Fig. 14.3** Cyclization of polystyrene by RTA-ATRC by Carnicom and Tillman [40]

### 14.3 Unimolecular Ring-Closure

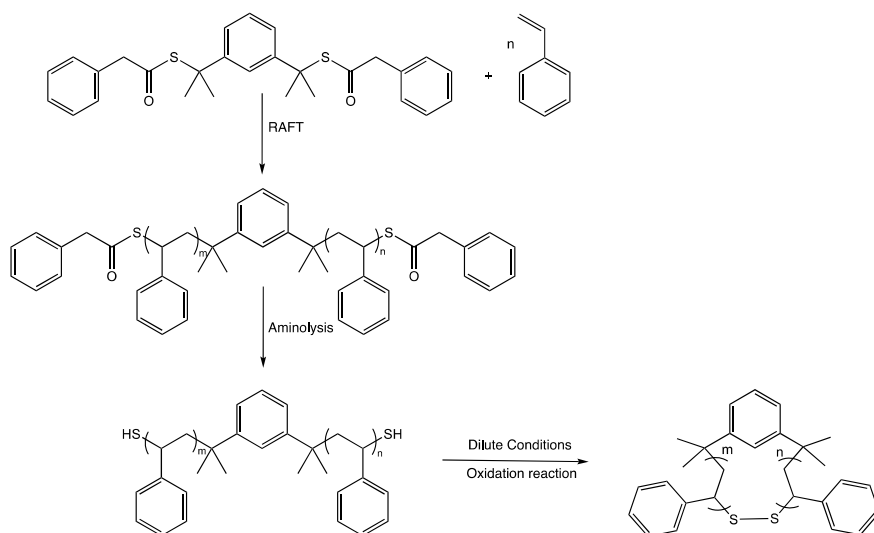
Unimolecular ring-closure is the coupling of the end groups on the same linear polymer chain. Compared to the bimolecular approach, there are advantages to using this method which include not requiring exact stoichiometric amounts and reactions entail intramolecular coupling only. In addition, versatile polymerization techniques such as RAFT, ATRP, and ROP are used to control the molecular weight and provide efficient methods to produce linear precursors with compatible chain ends. Since the reactive units are on opposite ends of the same polymer chain, intramolecular coupling is favorable by using high-dilution reaction conditions. In these conditions, the linear precursor is first diluted and added dropwise via syringe to the catalyst dissolved in a solvent which results in a high purity cyclic polymer. This strategy can be divided into two approaches based on the end groups of linear polymers which include (1) unimolecular homodifunctional ring-closure and (2) unimolecular heterodifunctional ring-closure. In the following paragraphs both methods are described, and examples of each approach have been highlighted.

### 14.4 Homodifunctional Ring-Closure

Unimolecular homofunctional polymers have the same functional groups on both of the terminal ends of a linear polymer. The precursor polymer can be synthesized directly with identical functional groups on each end, or the polymer can undergo a post-functionalization for the resulting precursor polymer. A disadvantage to using homodifunctional linear polymer is the modest number of reactions available to couple the chain ends compared to the many versatile reactions that can be used for the heterodifunctional method. Even though there are limited reactions, this approach synthesizes high purity cyclic polymers and below are a few recent examples.

The first example of a  $\alpha,\omega$ -dithiol that undergoes an oxidation to form a disulfide bond was done by Whittaker and coworkers [42]. A cyclic polymer was synthesized by first reacting a telechelic polystyrene through reversible addition fragmentation chain transfer (RAFT). RAFT is a living free radical polymerization that incorporates multiple monomers with a chain transfer agent (CTA). For this particular free radical polymerization, the CTA was 1,3-bis(2-thiobenzylthio)prop-2-yl)benzene (BTBTPB) and formed a RAFT functional group on both chain ends e.g., (S = C(Ph)S-). Next, the end groups (S = C(Ph)S-) undergo an aminolysis in a dilute solution to form an  $\alpha,\omega$ -thiol polystyrene, and the cyclic polymer is formed by an oxidation reaction under dilute conditions to form a disulfide bond (Fig. 14.4).

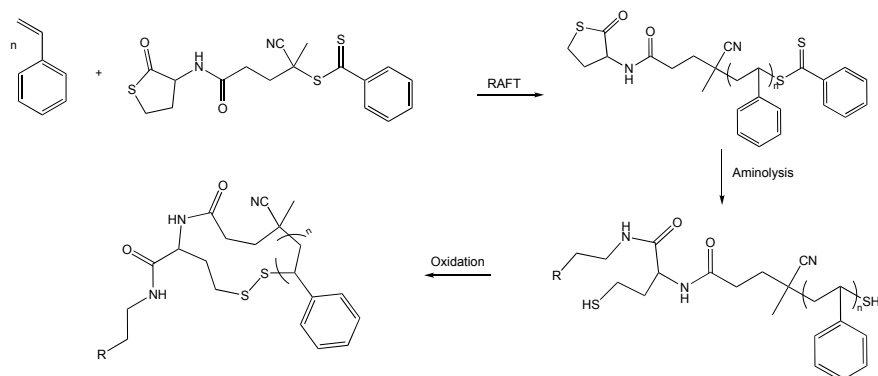
Stemanović et al. has another example of homodifunctional cyclization of a disulfide oxidative linkage from dithiol end-groups. Linear polystyrene is first synthesized by RAFT with the designed chain transfer agent  $\alpha$ -thiolactone. The resulting linear polystyrene with a thiolactone on one chain end and dithiobenzoate on the other chain end is then post-functionalized with an amine to generate  $\alpha,\omega$ -dithiol end groups.



**Fig. 14.4** Homofunctional disulfide cyclic polymer synthesis by an oxidation reaction by Whittaker et al. [42]

Under high dilution conditions, an oxidative disulfide linkage synthesized a cyclic polystyrene that was characterized by GPC and other characterization methods. This method has also been used for cyclic peptides [43] (Fig. 14.5).

The next example is Glaser coupling, which converts a  $\alpha,\omega$ -dialkyne to a 1,3-diyne with a new carbon–carbon single bond. McKeown et al. reported Glaser coupling in combination with a living catalyst-transfer polymerization (CTP) and to cyclize poly(3-hexylthiophene) (P3HT), a conjugated macrocycle, in 2017 [44]. CTP allows definite control over the chain length and conversion of end group functionalities by end capping the polymer with desired functional groups. P3HT was synthesized



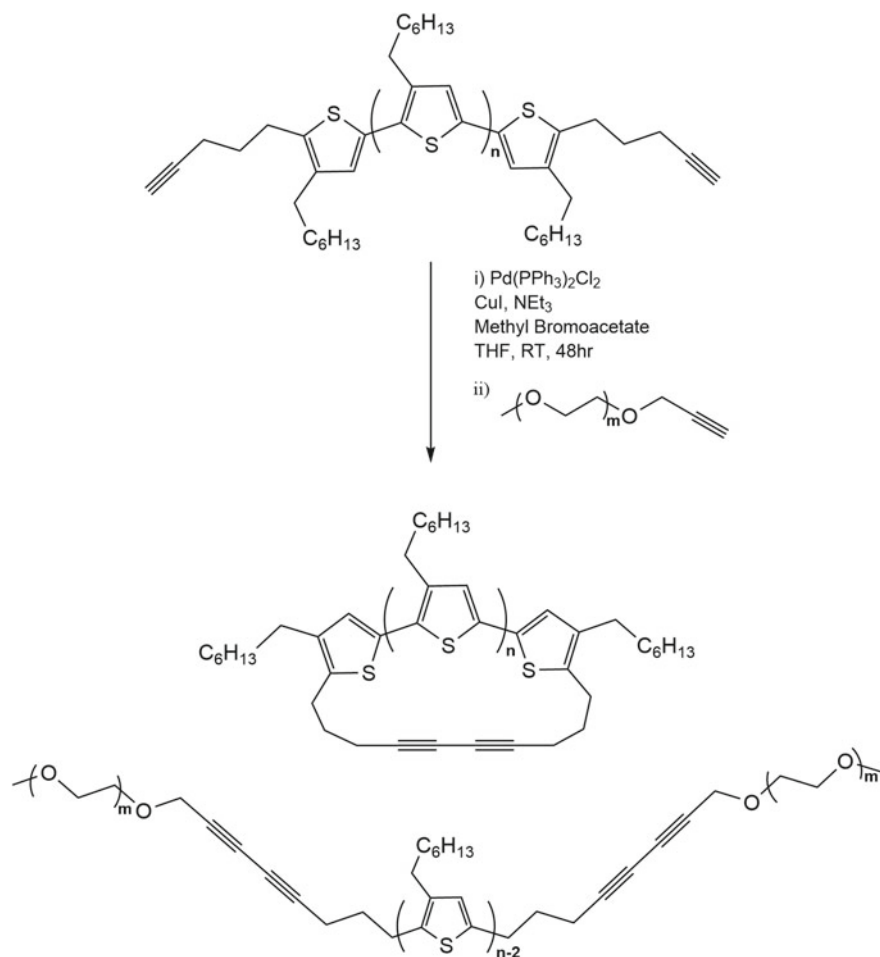
**Fig. 14.5** Cyclization of  $\alpha,\omega$ -disulfide polystyrene via oxidation by Stemanović et al. [43]

by CTP and end-capped with trimethylsilyl protected 4-pentynyl groups that were then deprotected for the desired  $\alpha,\omega$ -dialkyne end groups. Then the P3HT linear precursor with pentynyl chain ends were coupled by adding the linear polymer dropwise to a highly dilute THF solution with a copper and palladium catalyst. Before completing the reaction, a purification method was also developed to remove unreacted linear precursors. To isolate the macrocyclic polymer, an alkyne terminated PEG (5000  $M_n$ ) was added to the reaction mixture. The majority of these Glaser couplings were cyclic; however, the PEG (5000  $M_n$ ) forms a block co-polymer with the linear P3HT. Next, the reaction mixture was precipitated in methanol, filtered, then dissolved in chloroform, and passed through a silica gel column. The desired macrocyclic polymer will elute while the linear block co-polymer remains on the column. The cyclic product was confirmed through MALDI-TOF MS, NMR, and GPC. This method is beneficial due to the simplicity of converting the terminal ends and mild reaction conditions for cyclization. Glaser coupling has also been used for macrocyclic poly(ethylene oxide) [45], poly(glycidyl phenyl ether) [46], and other cyclic topologies which include triblock cyclic polymers [47], cyclic oligomers [48], and tadpole shaped polymers [49–54] (Fig. 14.6).

He et al. synthesized cyclic polystyrene by anionic polymerization, silicone chloride linking chemistry, and ring-closure metathesis (RCM) [55]. Linear polystyrene was first synthesized by alkyllithium anionic living polymerization with 4-pentenylolithium as the initiator to form 4-pentenylpoly(styryl)lithium. A primary alkyllithium initiated polymerization was used because of the ability to control molecular weights, produce narrow molecular weight distributions, and chain end functionalization. Then two linear  $\alpha$ -lithium functionalized polymers are then coupled with dimethyldichlorosilane to form a larger linear polymer. The polymer chains that did not couple were terminated with ethylene oxide and the desired linear precursor,  $\alpha,\omega$ -bis(4-pentenyl)polystyrene, was purified by silica gel column chromatography. To synthesize the macrocycle,  $\alpha,\omega$ -bis(4-pentenyl)polystyrene and the Grubbs catalyst, bis(tricyclohexylphosphine)benzylidene ruthenium(IV) chloride was refluxed in dichloromethane. The residual catalyst was removed from the cyclic polystyrene through SEC fractionations, and the cyclic polymer was confirmed by GPC, MALDI-TOF MS, and NMR. RCM has also been used for other cyclic topologies [56–62] including tadpole shaped [63] and figure-eight-shaped polystyrene [64] (Fig. 14.7).

## 14.5 Heterodifunctional

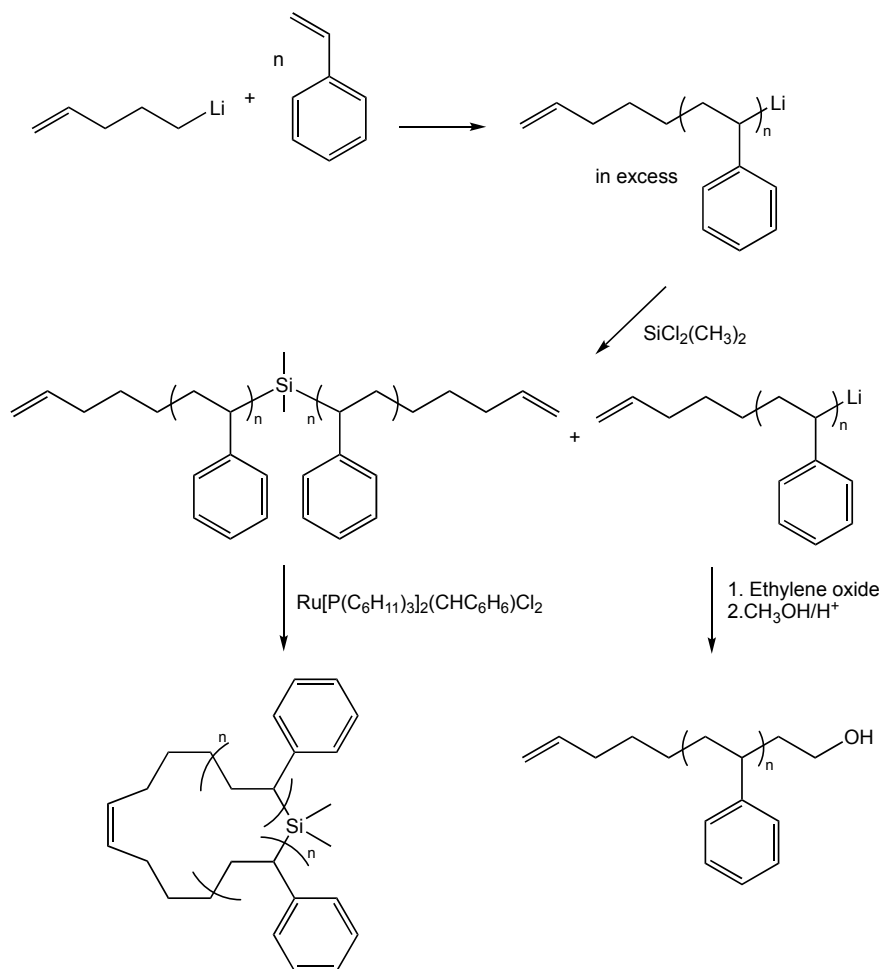
The unimolecular heterodifunctional approach synthesizes cyclic polymers with a linear precursor with two different complementary functional groups on each chain end. The increased number of synthetic steps for an  $\alpha,\omega$  heterodifunctional linear polymer is a disadvantage to this approach compared to the homodifunctional approach. Even though this approach is more time intensive, heterodifunctional linear precursors generate cyclic polymers with reasonable purity compared



**Fig. 14.6** The synthesis of cyclic poly(3-hexylthiophene) McKeown et al. [44]

to other ring-closure approaches. This reaction occurs under highly dilute conditions and the chances of coupling intramolecularly with complimentary chain ends increases while the likelihood of forming linear oligomers decreases greatly. The largest difference and advantage of utilizing this method over the homodifunctional approach is the diverse reactions that can be used to couple reactive end groups. In the following paragraphs a few examples are described.

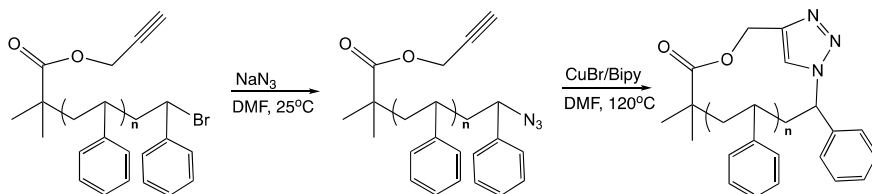
One of the most widely used strategies for the heterodifunctional ring-closure approach is copper-catalyzed azide-alkyne cycloaddition (CuAAC) which is a “click” reaction. This method is versatile, and different polymer synthesis techniques (e.g., ring opening polymerization, ATRP, RAFT, etc.) can be used to develop the linear precursor. Also, the linear polymer can be initiated and post-functionalized with



**Fig. 14.7** Cyclization synthesis of  $\alpha,\omega$ -bis(4-pentenyl)polystyrene by He et al. [55]

diverse azide and alkyne derivatives. This method is known to reduce oligomerization significantly and synthesize cyclic polymers with low polydispersity. Laurent and Grayson developed this synthesis with cyclic polystyrene [65]. The linear precursor was synthesized by atom transfer radical polymerization (ATRP) with propargyl 2-bromoisobutyrate as the  $\alpha$ -initiator. Next, the terminal  $\omega$ -bromine on one chain end was converted to an azide and were coupled to the  $\alpha$ -alkyne by CuAAC in a dilute solution. This method has also been used to cyclize poly(ethylene imine) [66], poly(caprolactone) [67–76], poly(2-alkyl-2-oxazoline) [77–80], and other cyclic polymers and topologies [81–88] (Fig. 14.8).

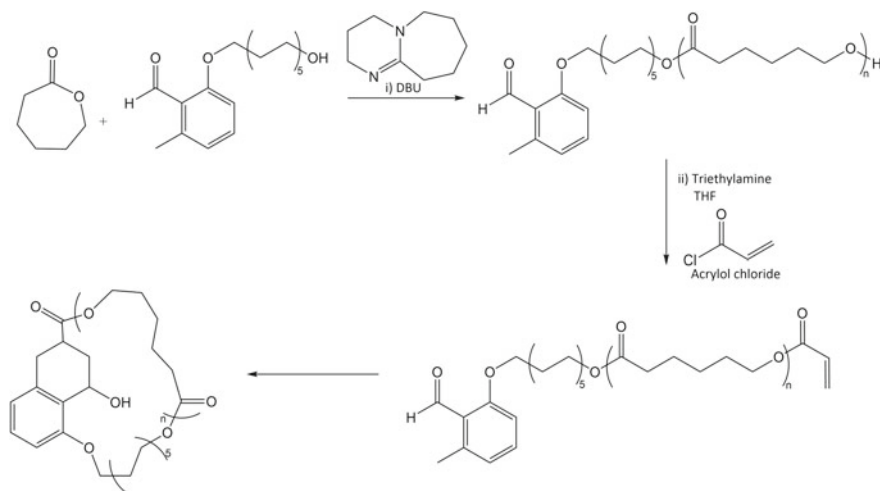
Josse et al. prepared cyclic aliphatic polyesters via a photoinduced Diels–Alder reaction in 2014 [89]. This strategy involved a linear poly(L-lactide) (PLLA) and



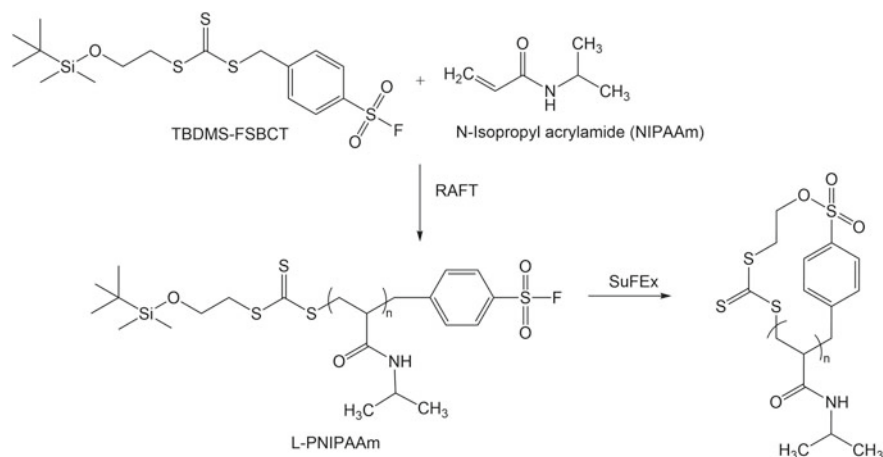
**Fig. 14.8** Cyclization of polystyrene via CuAAC “click” by Laurent and Grayson [65]

poly( $\epsilon$ -caprolactone) (PCL) which were prepared by ring opening polymerization with an organocatalysts TBD and DBU, respectively, and 2-((hydroxyundecyl)oxy)-6-methylbenzaldehyde as the initiator. Next, the hydroxyl end group was converted to an acrylate through an esterification with acryloyl chloride to give a heterodifunctional linear polymer that was cyclized by a Diels–Alder reaction catalyzed by UV irradiation in an acetonitrile solution at room temperature. The cyclic PCL and PLLA were collected through evaporation, and then cyclized product was compared and characterized through GPC which demonstrated a lower hydrodynamic volume by displaying a longer retention time than the linear precursor (Fig. 14.9).

The next synthetic example by Liu et al. is using sulfur(VI)-fluoride exchange click reaction (SuFEx) to synthesize poly(*N*-isopropylacrylamide) (PNIPAAm) (Fig. 14.10) and poly(*N*-vinylpyrrolidone) (PVP) [90]. *N*-Isopropylacrylamide with heterodifunctional end groups, *tert*-butyldimethylsilyl ether and sulfonyl fluoride, is polymerized through RAFT with a newly designed trithiocarbonate RAFT agent, 2-((*tert*-butyldimethylsilyl)oxy)ethyl(4-fluorosulfonyl)benzyl carbonotrithioate (TBDMS-FSBCT). The PNIPAAm is then cyclized through an



**Fig. 14.9** Synthesis of cyclized block poly(*L*-lactide) (PLLA) and poly( $\epsilon$ -caprolactone) (PCL) via Diels–Alder “click” by Josse et al. [89]



**Fig. 14.10** Sulfur(VI)-fluoride exchange click reaction (SuFEx) between *tert*-butyldimethylsilyl ether and sulfonyl fluoride end groups on PNIPAAm by Liu et al. [90]

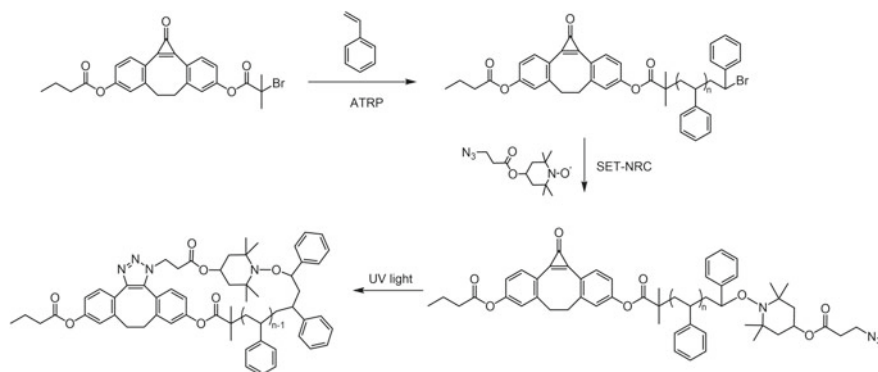
intramolecular ring-closure between the  $\alpha,\omega$ -heterodifunctional polymer in dilute conditions, at ambient temperatures with 1,5,7-triazabicyclo[4.4.0]dec-5-ene (TBD) as the catalyst. The resulting cyclic PNIPAAm was purified through dialysis with water and confirmed with a lower retention time on the GPC, MALDI-TOF MS analysis, and  $^1\text{H}$  NMR spectroscopy.

UV induced strain promoted azide-alkyne cycloaddition (SPAAC) has also been used as a heterodifunctional ring-closure method [91]. First, the heterodifunctional polystyrene with dibenzocyclooctyne and bromo end groups was synthesized by ATRP with a cyclopropanone masked dibenzocyclooctyne initiator. The bromo end group is reacted through single electron transfer-nitroxide radical coupling (SET-NRC) to produce an azide functional group. Under UV radiation in dilute conditions, the  $\alpha,\omega$ -heterodifunctional polystyrene undergoes an intramolecular ring-closure. UV induced SPAAC has also been used to synthesize poly(vinyl acetate) [92] and a tadpole-shaped polymer [93] (Fig. 14.11).

## 14.6 Ring-Expansion Polymerization

Ring-expansion polymerization (REP) is an alternative way to synthesize cyclic polymers while avoiding many of the problems that present themselves with ring-closing polymerizations. Unlike ring-closing polymerization, where linear polymers are cyclized through end-group coupling, in ring-expansion polymerization the cyclic polymer is initiated from a monomer with the help of a cyclic initiator or activated species. Monomers can then be continuously integrated into the ring, generating



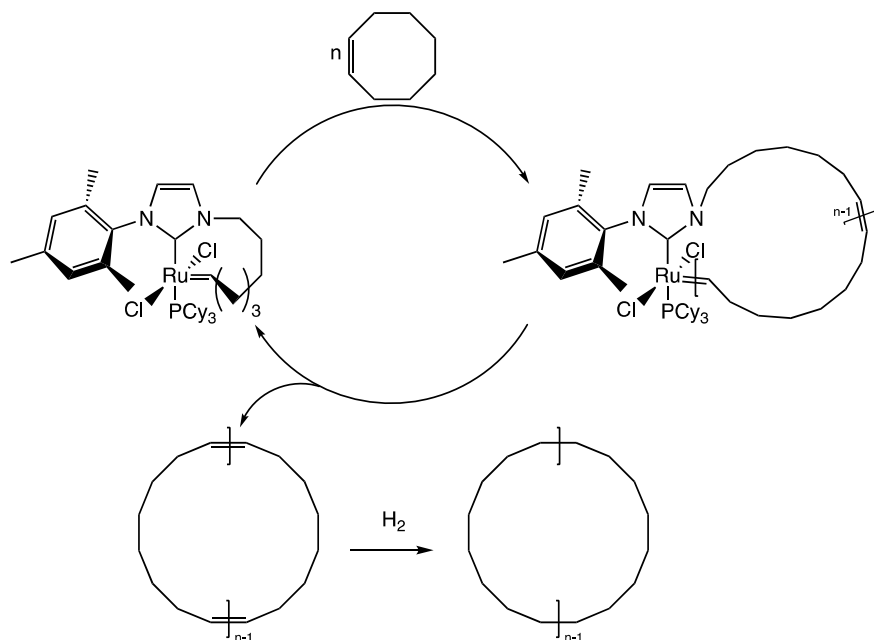


**Fig. 14.11** Polystyrene synthesized by SPAAC by Sun et al. [91]

larger cyclic polymers with minimal linear impurities. This technique is particularly useful due to the fact that ring-expansion does not suffer the same entropic penalty of ring-closing techniques. Additionally, ring-expansion polymerization does not require high dilutions like its ring-closing counterpart, and therefore, can be used in the synthesis of very high-molecular-weight cyclic polymers. The two main drawbacks of this technique include minimal control over parameters like molecular weight and dispersity and a lack of compatible monomers when compared to ring-closing techniques. Monomers are typically limited to strained lactones and cyclic olefins; however, in recent years this list has been expanded to contain alkynes, thiiranes, and vinyl ethers [94–104].

Early work from Kricheldorf and co-workers identified ring-expansion as a viable technique for the synthesis of polymer macrocycles from lactone monomers with stannous-based initiators [105, 106]. The initiator, 2,2-dibutyl-5,5-dimethyl-1,3-dioxo-2-stannane, was used to repeatedly insert strained lactones ( $\beta$ -D,L-butyrrolactone and  $\epsilon$ -caprolactone) at the Sn–O position of the cyclic initiators. Early attempts of polymerizing  $\beta$ -D,L-butyrrolactone through REP lead to an  $M_n$  value of  $\sim 19$  kDa and a dispersity of 1.7, and the use of  $\epsilon$ -caprolactone as a monomer produced cyclic polymers with  $M_n$  values between 2.6 and 114 kDa with dispersity ranging from 1.42 to 1.55. While this technique can be used to synthesize a variety of cyclic polyesters, the labile tin-alkoxide bond was still present in the cyclic product. This results in a product that was prone to bond cleavage leaving a linear polymer from a ring scission at either of the Sn–O bonds.

A solution to remove these weak linkages was developed by Grubbs and co-workers in the form of ring-expansion metathesis polymerization (REMP) [107, 108]. A cyclic Ru-based catalyst/initiator was used to polymerize strained cyclic olefins (1-octene) into cyclic poly(octenamers). Following polymerization, an intramolecular cross metathesis “backbiting” event released the original Ru-based catalyst (or small n-mers) and produce a cyclic polyolefin with no labile bonds with  $M_n$  values up to 1200 kDa and dispersity around 2. These cyclic poly(octenamers) were then reduced through hydrogenation to produce analogous cyclic poly(ethylenes) (Fig. 14.12).



**Fig. 14.12** REMP of cyclooctene to produce a cyclic poly(ethylene) by Bielawski et al. [107]

In 2007, Waymouth and co-workers pioneered work in zwitterionic ring-opening polymerizations (ZROP) by polymerizing lactide and  $\beta$ -butyrolactone with 1,3-dimesitylimidazol-2-ylidene and 1,3-dimesitylimidazolin-2-ylidene, respectively [109, 110]. With regards to the lactide polymerization the *N*-heterocyclic carbene (NHC), 1,3-dimesitylimidazol-2-ylidene, was used as an organocatalyst to produce cyclic polymers with  $M_n$  values from 7.3 to 26 kDa and dispersity values from 1.15 to 1.35 [109]. Later studies from Jeong et al. report the proposed mechanism as a nucleophilic attack of the NHC initiator to the carbonyl carbon, forming the zwitterion intermediate, successive addition of the monomer via an anionic ring-opening polymerization, and final release of the NHC initiator [111]. In 2009, Guo and Zhang employed a similar technique to produce cyclic poly( $\alpha$ -peptoid)s by using bis(2,6-diisopropylphenyl)imidazol-2-ylidene as an NHC initiator [112].

## 14.7 Ring-Expansion Polymerization of Lactones

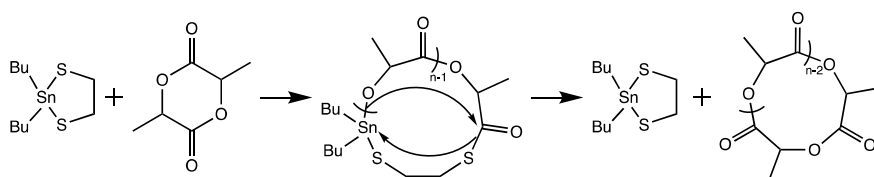
Since initial work in 1995, Kricheldorf has continued to innovator tin-based catalysts for use in ring-expansion polymerization. In 2017, Kricheldorf et al. reported a ring-expansion polymerization for the production of cyclic poly(L-lactides) catalyzed by 2,2-dibutyl-2-stanna-1,3-dithiolane [113]. This particular catalyst differs from

Kricheldorf and Lee's original work by making use of more stable Sn–S bonds rather than their prior catalysts which found monomer insertion at Sn–O bonds. This was due to tin (IV) mercaptides favoring the production of cyclic poly(L-lactides) without racemization. When 2,2-dibutyl-2-stanna-1,3-dithiolane was used as a catalyst, crude samples of L-lactide produced macrocycles with  $M_n$  values up to 21 kDa; however, after the L-lactide monomers were recrystallized twice,  $M_n$  values increased to 33 kDa with dispersity values ranging from 2.4 to 5.5. When comparing lactide to catalyst ratios, it was discovered that  $M_w$  values were nearly constant even though the lactide to catalyst ratios were varied by a factor of 8 in some cases. Kricheldorf suggests that the 2,2-dibutyl-2-stanna-1,3-dithiolane acts as what he calls a “true” catalyst and not as an initiator. This means that the catalyst is reformed after the polymerization and not incorporated into the final product as an initiator would (Fig. 14.13).

Later that same year, Kricheldorf et al. reported another tin based catalyst, dibutyltin 4-*tert*-butylcatechol, for the synthesis of cyclic poly(L-lactide) via ring-expansion polymerization [114]. When using this catalyst, cyclic poly(L-lactides) were reported with  $M_n$  values from 7.5 to 14 kDa. This new catalyst allowed for rapid polymerization of cyclic poly(L-lactide) at temperatures of 160 °C or lower without racemization. (This temperature being lower than the standard conditions used in the technical production of linear poly(L-lactide)s when using  $\text{SnOct}_2$  as a catalyst.)

In 2018, Kricheldorf and Weidner reported the polymerization of meso-lactide via a collection of dibutyltin derivatives as catalysts [115]. It was discovered that the architectures of the resulting polymers were highly dependent on the structures of the catalyst and temperature of the reactions with 2,2'-dihydroxy-1,1'-binaphthyl yielding even-numbered cyclic polymers at 100 °C and various dibutyltin derivatives of substituted catechols yielding primarily odd-numbered cyclic polymers with  $M_n$  values up to 12.5 kDa and dispersity values as low as 1.7. It was suspected that an intermolecular transesterification was responsible for the formation of the odd-numbered cyclic polymers.

Kricheldorf and co-workers have vastly contributed to the area of ring-expansion polymerization catalysis by expanding the list of catalysts for various poly(lactides) to include cyclic dibutyltin bisphenoxides, spirocyclic bisphenoxides of Ge, Zr, and Sn, cyclic tin(II) bisphenoxides, and 4-*tert*-butylcatechol in conjunction with tin(II)-2-ethylhexanoate [116–119]. In addition to Kricheldorf's expansive study of tin based



**Fig. 14.13** Ring-expansion polymerization of L-lactides via a 2,2-dibutyl-2-stanna-1,3-dithiolane initiator by Kricheldorf et al. [113]

initiators and catalyst, Phomphrai and co-workers, and Gao et al. have also reported syntheses of cyclic poly(lactides) and cyclic poly(esters) from various tin based catalysts [120–124]. Additional cyclic poly(lactides) and poly(esters) have been reported by employing both iron based [125] and aluminum based [126, 127] catalysts.

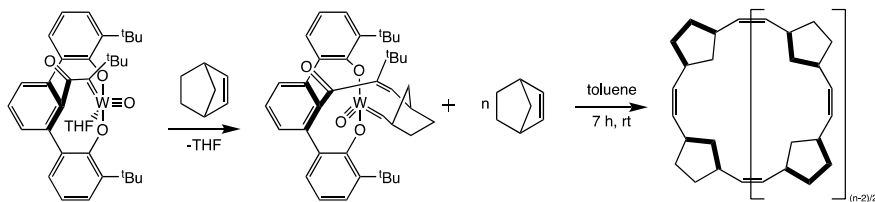
## 14.8 Ring-Expansion Metathesis Polymerization

As stated before, ring-expansion metathesis polymerization was pioneered by Bielawski, Benitez, and Grubbs [107]. In ring-expansion metathesis polymerization, catalysts contain short, tethered hydrocarbon linkages that are able to make metallocycles by joining with the present alkenes. Cyclic monomers containing these alkenes go through a ring-expansion reaction creating larger and larger metallocycles. A chain transfer event to the alkene nearest to the linking point allows for regeneration of the initial metal catalyst and the release of the cyclic polymer. However, if a chain transfer happens with any other alkene in the metallocycle, the polymer can pinch off releasing a smaller cyclic polymer and a larger metallocycle which may continue to polymerize again [108].

In 2012, Zhang and Tew reported a novel synthesis for cyclic bottle brush polymers by combining REMP and the “grafting from” technique [128]. This technique relieves the concern for steric hinderance, and tedious purifications often associated with both the “grafting to” and “grafting through” techniques. A cyclic ruthenium-alkylidene catalyst, UC-6, was synthesized along with an *exo*-norbornene-based monomer made from the condensation of *cis*-5-norbornene-*exo*-2,3-dicarboxylic anhydride with 8-amino-1-octanol. With UC-6 as a catalyst, a cyclic poly(norbornene) was produced and confirmed via  $^1\text{H-NMR}$  by the disappearance of the  $-\text{CH}=\text{CH}-$  peak (6.30 ppm) found in the monomer and the appearance of a broad  $-\text{CH}=\text{CH}-$  peak (5.35–5.75 ppm) found in the polymer. The cyclic poly(norbornene) was designed to have alcohol pendant groups to act as initiators to polymerize various cyclic ester monomers via the “grafting from” technique. Using TBD as an initiator and  $\delta$ -valerolactone (VL), L-lactide (LLA), and  $\epsilon$ -caprolactone (CL) as monomers, cyclic bottle brush polymers with  $M_n$  values from 576 to 1063 kDa, PDI values from 1.28 to 1.50, and grafting densities up to 84% were synthesized.

In 2013 Tew and co-workers expanded on this work by adding a metal-chelating terpyridine functionality to each repeat unit [129]. These pendant groups on the cyclic poly(norbornene) backbone can easily coordinate to metal complexes which have an inorganic metal with a second terpyridine group. These allowed the production of free-standing metallo-supramolecular gels when transition-metal ions, in this case  $\text{Fe}^{2+}$  or  $\text{Ni}^{2+}$ , were added to the polymer solution.

In 2013, Blencowe and Qiao reported poly(cyclooctenes) similar to the ones produced by Grubbs and co-workers; however, these were catalyzed by a second generation Hoveyda–Grubbs catalyst [107, 108, 130]. Another difference was that Blencowe and Qiao produced functionalized derivatives of their poly(cyclooctenes)



**Fig. 14.14** Ring-expansion polymerization of norbornene via a tethered tungsten-oxo alkylidene catalyst to produce highly *cis* and syndiotactic cyclic polynorbornene by Gonsales et al. [131]

that included pendant acetyl and hydroxy groups that could then be further functionalized.

In 2016, Gonsales et al. reported a highly tactic poly(norbornene) via a new tethered tungsten-alkylidene catalyst [131]. This new catalyst employs a tethered metal–carbon double bond to a substitutionally inert ancillary ligand and a tungsten-oxo alkylidene fragment to promote REMP. This combination led to a catalyst that promotes stereo-controlled REMP yielding *cis*-syndiotactic cyclic poly(norbornene) (Fig. 14.14).

When using the tungsten-alkylidene catalyst cyclic polynorbornenes were produced with high stereochemical selectivity, up to 98% *cis*, with  $M_n$  values ranging from 126 to 578 kDa and dispersity values from 1.21 to 1.29.

In 2016 Nadif et al. reported yet another highly tactic cyclic polynorbornene; however, a tungsten alkylidyne catalyst was used as an initiator to polymerize the cyclic polymer via “ynene” metathesis [132]. While multiple reports of “enene” metathesis, the reaction of an alkylidene and an alkyne have been published, at the time only one example of “ynene” metathesis, the reaction between alkylidynes and alkenes, had existed. When this tungsten alkylidyne catalyst was used as an initiator, cyclic polynorbornenes were produced with high stereoregularity, >99% *cis* and >95% syndiotactic, with  $M_n$  values ranging from 91.5 to 425 kDa and dispersity values from 1.22 to 1.45.

Later that same year, Roland et al. reported conjugated cyclic polymers from alkynes by making use of a new tungsten alkylidyne catalyst [99]. At a 10,000:1 phenylacetylene-to-catalyst ratio in 2 ml of toluene, the new catalyst averaged  $9.00 \times 10^6 \text{ g mol}^{-1} \text{ h}^{-1}$  and achieved complete conversion after only 22 min with a turnover number of roughly 10,000. The catalyst was also able to tolerate a number of functionalized acetylenes including ethers, halides and disubstituted acetylenes. While these substituents effected the polymerization activity and molecular masses, cyclic phenylacetylenes were produced in a range from 8 to 130 kDa with dispersity values as low as 1.28. The catalytic abilities were not hindered by the presence of styrene or the radical trap TEMPO (2,2,6,6-tetramethyl-1-piperidinyloxy), thus ruling out a radical mechanism. The proposed mechanism is initiated with the dissociation of THF from the tungsten center followed by the coordination of an alkyne. The coordinated alkyne is then inserted into one of the M–C bonds that are part of

the metallacyclopropene resulting in a metallacyclopentadiene. Once the metallacyclopentadiene is formed, the tungsten complex continues to coordinate and insert alkynes into the metallocycle. A chain-transfer step undergoes reductive elimination to separate the conjugated cyclic polymer and metal center, thus reforming the catalyst and allowing the initiation and propagation of another cyclic polymer. Most recently, Miao et al. reported a cyclic poly(4-methyl-1-pentene) by employing the same ruthenium-based catalyst as Roland et al. [99, 133]

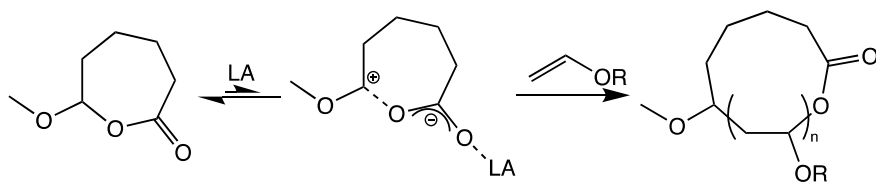
In 2017, Li et al. reported the synthesis of macrocyclic poly(methylvinylsiloxane)s from 1,3,5,7-tetramethyl-1,3,5,7-tetravinylcyclotetrasiloxane with water catalyzed by anhydrous iron(III) chloride [134]. The 1,3,5,7-tetramethyl-1,3,5,7-tetravinylcyclotetrasiloxane was combined with 0.2 equivalents of FeCl<sub>3</sub>, 1 equivalent of water, and 1 mL of acetone and was refluxed for a total of 20 h. After further work up, the reaction was confirmed via IR, <sup>1</sup>H-NMR, and <sup>29</sup>Si-NMR to ensure that only fully condensed, cyclic siloxane chains were produced. Additionally, the macrocycles were treated with dimethoxydimethylsilane in the presence of dibutyltin dilaurate. If there were terminal Si–OH groups on the macrocycles, higher molecular weight products would be observed; however, GPC curves before and after the addition of dimethoxydimethylsilane did not change. The M<sub>w</sub> values ranged from 36 to 222 kDa with dispersity values from 1.68 to 2.51.

In 2018, Lidster et al. reported fully conjugated, macrocyclic poly(*p*-phenylenevinylenes) via a ring-expansion metathesis polymerization [135]. Using a cyclic ruthenium alkylidene complex as a catalyst and cyclophanedienes (R = *n*-octyl or *O*-2-(*R/S*)-ethylhexyl) as monomers, the cyclic poly(*p*-phenylenevinylenes) exhibited M<sub>n</sub> values >13 kDa and dispersity values around 1.8. Additional work in REMP includes Imada et al. REMP to produce cyclic poly(nitrones) by using *p*-toluenesulfonic acid as a catalyst [136].

## 14.9 Zwitterionic Ring-Opening Polymerization

There are three types of zwitterionic ring-opening polymerizations. These being nucleophilic ZROP, Lewis pair-mediated ZROP, and electrophilic ZROP. Each are characterized by the species that interacts with the monomer thus creating the zwitterion. In recent years, Waymouth and co-workers continued to expand on ZROP by employing NHC initiators to include cyclic poly(carbosiloxanes) from 2,2,5,5-tetramethyl-2,5-disila-1-oxacyclopentane, cyclic poly(esters) from  $\delta$ -valerolactone and  $\epsilon$ -caprolactone, cyclic poly(alkylene phosphates) from 2-isopropoxy-2-oxo-1,3,2-dioxaphospholane, cyclic poly(carbonates) from various *N*-benzyl-substituted eight-membered cyclic carbonates, and poly(lactides) mediated by 1,8-diazabicyclo[5.4.0]undec-7-ene [137–144].

In 2013, Kammiyada et al. started work on Lewis acid-assisted “ring-expansion” living cationic polymerization of vinyl ethers [145]. They synthesized a hemiacetal ester cyclic initiator from a cyclohexanone with a vicinal methoxy group via a Baeyer–Villiger oxidation. The hemiacetal ester could then be reversibly activated



**Fig. 14.15** Living ring-expansion cationic polymerization of vinyl ethers from a cyclic initiator by Kammiyada et al. [145]

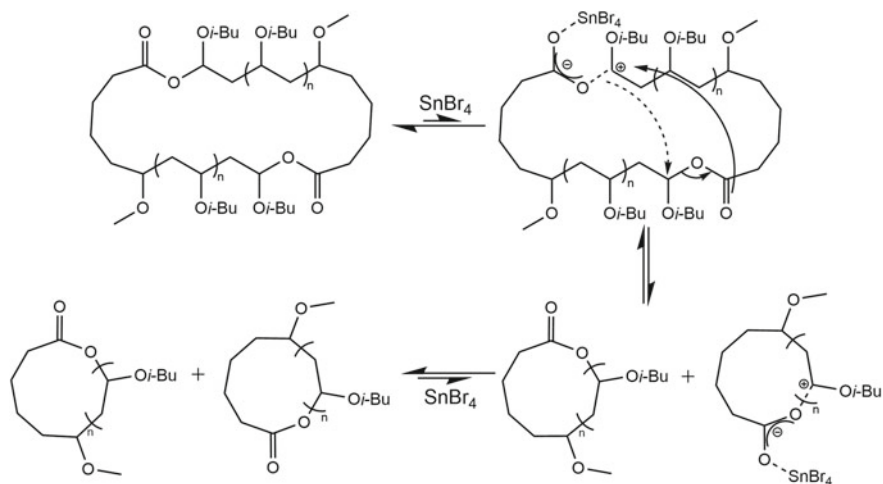
with the help of a Lewis acid catalyst,  $\text{SnBr}_4$ , creating a carbocation allowing for the insertion of various vinyl ether monomers into the polymer macrocycle. This reaction scheme produced cyclic polymers with  $M_n$  values ranging from 3.7 to 12.4 kDa with dispersity values from 1.40 to 1.67 (Fig. 14.15).

At high conversions, multiple unquenched living polymers tended to fuse with each other due to counterion exchange events with other polymer chains close by. This resulted in a cyclic polymer that contains an increased dispersity caused by numerous hemiacetal ester linkages. Gel Permeation Chromatography (GPC) data after hydrolytic cleavage of the hemiacetal bonds to the linear polymer supported this idea. When the large, fused cyclic polymers were hydrolytically cleaved, they were also broken down into their linear constituents.

In 2015 Kammiyada et al. improved upon this work by optimizing conditions to decrease the yield of fused cyclic polymers along with the ability to produce cyclic block copolymers with the first reported ring-expansion cationic block copolymerization [146]. A cyclic isobutyl vinyl ether polymer was doped with an ethyl vinyl ether monomer. Changes in GPC curves and NMR of the products after the addition of ethyl vinyl ether monomer were used to confirm the insertion of the second monomer into the cyclic block-copolymer.

In 2016 Kammiyada et al. demonstrated the ability to convert their fused oligomeric polymer rings back into the original mono-hemiacetal ester cyclic counterparts [147]. The concentration of hemiacetal ester groups in solution post-polymerization was lowered to 0.25 mM from 5.0 mM.  $\text{SnBr}_4$  was added to re-activate the hemiacetal ester to allow bond cleavage, and the polymer/Lewis acid solution was stirred for 38 h at  $-40^\circ\text{C}$ . GPC data confirmed the fission of rings back into predominantly mono-hemiacetal ester containing cyclic polymers, reaching 90% conversion. At zero hours (after diluted conditions), while there are still fused rings, the  $M_n$  and dispersity values measured 17.2 kDa and 3.18, respectively. After 38 h of stirring at diluted conditions,  $M_n$  and dispersity values measured 8 kDa and 1.19 respectively (Fig. 14.16).

In 2017, Kammiyada et al. expanded their library of monomers able to participate in their Lewis acid-assisted “ring-expansion” living cationic polymerizations to include the vinyl ethers with a sidechain of cyclohexyl, benzyl, 8-vinyloxytricyclo[5.2.1.0<sup>2,6</sup>]decane, dodecyl, and butyl 2-bromo-2-methylpropanoate [104]. Additionally, the cross-linker ethylene glycol divinyl ethers were incorporated into cyclic polymers containing a single hemiacetal ester during the end of the living



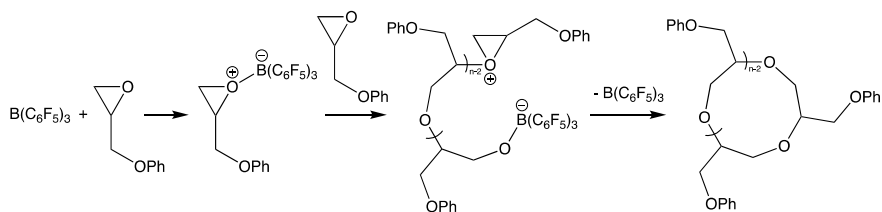
**Fig. 14.16** Proposed ring fission of cyclic poly (vinyl ethers) with multiple hemiacetal ester linkages by Kammiyada et al. [147]

polymerization. This allowed for the synthesis of microgel core-star polymers with cyclic arms by linking together the unincorporated olefins of the ethylene glycol divinyl ethers. In the case of the fused rings, the multiple hemiacetal ester linkages led to numerous additions of cross-linker to the macrocycle resulting in ring-based microgels. These structures were confirmed via GPC curves taken before and after acidolysis.

Most recently, Kubota et al. synthesized a cyclic cyclopolymer by employing the same technique used for the previously mentioned cyclic polymers, but instead of polymerizing a vinyl ether Kubota et al. used a divinyl ether with a geminal dimethyl group on the spacer [148]. At high monomer concentrations (400 mM) the GPC traces were very broad, with dispersity values from 1.3 to 1.7, and contained a high molecular weight shoulder. This is expected to be the result of frequent cross-linking between polymer macrocycles. However, at lower monomer concentrations (50 mM) much narrower GPC curves, with dispersity values from 1.2 to 1.3, were observed with only a small, high-molecular-weight shoulder. This can be attributed to a decrease in intermolecular cross-linking of the macrocycles. Furthermore, sequential addition of monomer to the reaction solution (40 eq. compared to initiator) allowed for the formation of higher molecular weight species. This can be seen from the initial cyclic polymer having molecular weight and dispersity values of 4.6 kDa and 1.13, respectively, to the final cyclic polymer having molecular weight and dispersity values of 17.4 kDa and 1.16, respectively.

In 2014, Asenjo-Sanz et al. reported cyclic poly(ethers) via the zwitterionic ring-opening polymerization of glycidyl monomers using  $\text{B}(\text{C}_6\text{F}_5)_3$  as a catalyst [149]. In the mechanism of the reaction, the  $\text{B}(\text{C}_6\text{F}_5)_3$  and glycidyl phenyl ether (GPE)





**Fig. 14.17** Mechanism of the zwitterionic ring-opening polymerization of and glycidyl phenyl ether monomer with a  $B(C_6F_5)_3$  catalyst by Asenjo-Sanz et al. [149]

monomer react directly and produce a zwitterionic GPE-borane intermediate. Nucleophilic attack from other GPE monomers to the intermediate propagates the reaction forming a macro-zwitterion. The final step is a nucleophilic attack from the oxygen that is coordinated to the borane to the electron-deficient  $\alpha$ -carbon of the oxonium ion. This results in cyclization and the regeneration of the  $B(C_6F_5)_3$  catalyst/initiator. This reaction produced cyclic poly(ethers) with  $M_n$  values up to 12 kDa with a 93% cyclic to linear ratio. In 2015, Asenjo-Sanz et al. described a method to copolymers between the GPE monomers and tetrahydrofuran, through the same ring-expansion technique [150] (Fig. 14.17).

In 2017, Haque et al. reported a technique to purify cyclic poly(ethers) that had been formed through zwitterionic ring-opening polymerization [6]. The technique deemed “click-scavenging” was used to remove linear products with two terminal alcohols that were initiated by water and “tadpoles” with one terminal alcohol that result from dimerization and hemi-cyclization of the propagating chain. Terminal alcohols in these impurities were functionalized with propargyl bromide, and the resulting alkynes were reacted with an azide functionalized Merrifield resin under copper-catalyzed azide—alkyne cycloaddition (CuAAC) reaction conditions. Afterward, the resin was removed by a simple filtration, resulting in a highly pure sample of cyclic poly(ethers).

Haque et al. expanded on Asenjo-Sanz and coworker’s 2014 work in 2019 by studying the effects that other substituents like 4-chlorophenyl glycidyl ether and styrene oxide, and their effects on macrocycle and topological impurity formation [151].

Most recently, Wu et al. reported a catalyst free, zwitterionic ring-opening copolymerization between carbonyl sulfide and 2-methyl aziridine to produce recyclable poly(thiourethanes) with cyclic structures [152]. This was achieved by reacting the two monomers at room temperature to produce a cyclic copolymer. This reaction produced cyclic poly(thiourethanes) with  $M_n$  values up to 15.2 kDa and dispersity values ranging from 1.11 to 2.30.

Additional works in zwitterionic ring-opening polymerizations include: Piedra-Aroni et al. reporting cyclic poly(esters) via  $Zn(C_6F_5)_2$  based Lewis pairs, Zhang and coworkers reporting cyclic poly(*N*-butyl glycines) from a number of NHC initiators and 1,8-diazabicycloundec-7-ene, Wang et al. reporting cyclic poly(esters) from *N*-heterocyclic olefins in conjunction with  $Al(C_6F_5)_3$ , McGraw et al. reporting

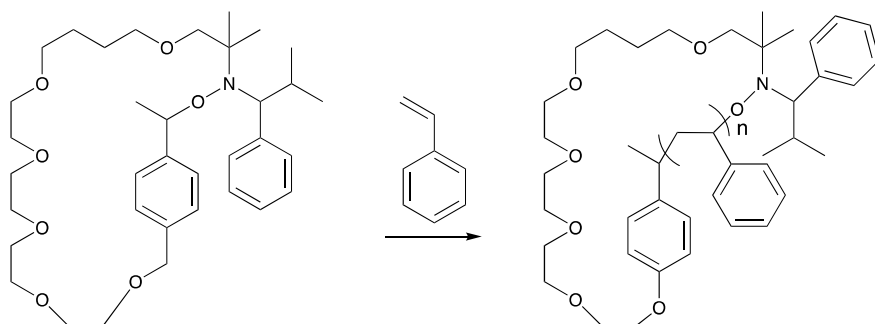
well-defined cyclic block copolymers from acrylate and methacrylate comonomer mixtures, Prasad and co-workers reporting the synthesis for cyclic poly(lactones) and cyclic poly(lactides) via NHC initiators, Coulembier et al. reporting sparteine-initiated cyclic poly(lactides), and later work in 2018 by Zhang et al., producing cyclic poly(peptides) using a variety of NHCs [153–161].

### 14.9.1 Nitroxide-Mediated Radical Polymerization

In 2016, Narumi et al. reported a vinyl ring-expansion polymerization of styrene via a nitroxide-mediated controlled radical polymerization with the help of a tetra(oxyethylene) tethered cyclic initiator [162] (Fig. 14.18).

The cyclic initiator was tethered with tetra(oxyethylene) via a ring-closing metathesis reaction and hydrogenated to produce the cyclic initiator. The addition of the tetra(oxyethylene) linker to the cyclic initiator also allowed for a high degree of solubility in common organic solvents and liquids, such as styrene. From here, ring-expansion polymerizations were carried out in bulk under nitroxide-mediated controlled radical polymerization conditions at various monomer to initiator ratios and durations. These polymerizations produced cyclic polystyrenes with  $M_n$  values ranging from 5.2 to 12 kDa and dispersity values from 1.59 to 2.05. It was suspected that a radical crossover reaction occurred producing higher molecular weights of polymer than initially expected. This ring-expansion radical crossover reaction allows for cyclic polymers with one initiator to fuse together with another initiator to produce larger macrocycles with multiple initiators in their backbone.

In 2018, Narumi et al. followed up on their previous work by expressing control over the ring-expansion and ring-contraction radical crossover reactions [163]. This control included the ability to purposely polymerize and depolymerize the tetra(oxyethylene) tethered cyclic initiators. It was discovered that by heating the cyclic alkoxyamine initiator in bulk to 115°C for 3 h, the cyclic initiator polymerized



**Fig. 14.18** Vinyl ring-expansion polymerization of styrene via nitroxide-mediated controlled radical polymerization by Narumi et al. [162]

into a large cyclic polymer with  $M_w$  values ranging from 10.3 to 38.6 kDa and dispersity values between 6.11 and 24.8. Afterward, the recently polymerized product was diluted in 1,3-dichlorobenzene and heated to 115 °C for 9 h. This resulted in a much smaller cyclic polymer with an  $M_w$  of 690 and dispersity value of 1.87 showing that the large multi-initiated macrocycle had reduced in size significantly.

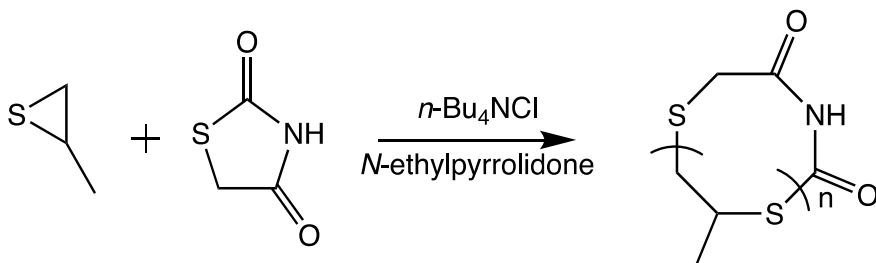
In 2019 Narumi et al. polymerized styrene and 4-vinylbenzyl alcohol in bulk, under conventional nitroxide-mediated radical polymerization conditions, to produce a di-block co-polymer macroinitiator for the polymerization of  $\epsilon$ -caprolactone off of the 4-vinylbenzyl alcohol block [164]. After the addition of the polycaprolactone side chains, atomic force microscopy was used to measure the polymer macrocycles and determine their degrees of polymerization and molecular weights.

### ***14.9.2 Thermally Induced Radical Ring-Expansion Polymerization***

In 2020, Takashima et al. reported a thermally induced radical ring-expansion polymerization that required no catalyst, atmosphere requirement, or the absence of water. Bis(2,2,6,6-tetramethylpiperidin-1-yl)disulfide (BiTEMPS) typically has a stable covalent, disulfide bond at room temperature. These bonds can cleave at temperatures above 80 °C and subsequently reform when heat is removed. Macrocylic monomers with singular BiTEMPS linkers were polymerized into larger macrocycles when heat (100 °C) was applied [63]. Linear precursors to the macrocylic monomers were synthesized via a Michael addition between BiTEMPS-diacrylate and dithiol monomers. Cyclization of the linear precursors occurs via the addition of 1,4-dioxane and produced the macrocylic monomers. Once these macrocylic monomers were heated in the presence of additional 1,4-dioxane the BiTEMPS linkers disassociate into 2,2,6,6-tetramethylpiperidine-1-sulfanyl (TEMPS) radicals. The re-association of the thiyl radicals with a separate macrocylic monomer's thiyl radical leads to the eventual macrocylic polymerization.

### ***14.9.3 Ring-Expansion Polymerization of Thiiranes***

The ring-expansion polymerization of thiiranes is a popular technique that allows for the production of well-defined cyclic polymer with low dispersity values [96]. Early work from Nishikubo and co-workers identified the feasibility of both cyclic dithioesters and thiourethane heterocycles for use in ring-expansion polymerizations of thiirane monomers [165, 166]. Schuetz et al. expanded on this work by employing thiazolidine-2,4-dione as a cyclic initiator to homopolymerize both propylene sulfide and 2-(phenoxyethyl)thiirane with values of  $M_n$  reaching from 7.4 and 50.2 kDa respectively and dispersity as low as 1.17 and 1.11, respectively [94] (Fig. 14.19).



**Fig. 14.19** Ring-expansion polymerization of 2-(phenoxymethyl)thiirane via a thiazolidine-2,4-dione catalyst to produce cyclic polysulfides by Schuetz et al. [94]

Kudo and Takeshi followed up with two different cyclic tetrathioesters (CTE) with thioester moieties at the ortho and meta positions to polymerize (phenoxymethyl)thiirane [95]. The polymerization of (phenoxymethyl)thiirane with *o*-CTE as an initiator produced cyclic polymers with  $M_n$  values ranging from 33 to 54 kDa. Further investigation led to the conclusion that the  $M_n$ 's of the polysulfides were independent of the feed ratios of (phenoxymethyl)thiirane to *o*-CTE and were difficult to manage; however, when *m*-CTE was used as an initiator, the molecular weights were able to be controlled via feed ratios and produced cyclic polymers with  $M_n$  values ranging from 46 to 107 kDa and dispersity values from 1.78 to 2.48. Takeshi et al. used 3H-benzothiazol-2-one, a cyclic, aromatic thiourethane initiator, to polymerize (phenoxymethyl)thiirane [96]. This technique produced a polysulfide polymer with a narrow dispersity of 1.1. The poly(3-phenoxypropylene sulfide) was then used as a macro-initiator for the ring-expansion polymerization of 3-butoxypropylene sulfide to produce a block copolymer of the two monomers. Recently, Zhang et al. reported a ring-expansion polymerization of various thiiranes by using rhodamine-based initiators, producing cyclic polymers with  $M_n$  values up to 71.5 kDa and dispersity values as low as 1.23 [167].

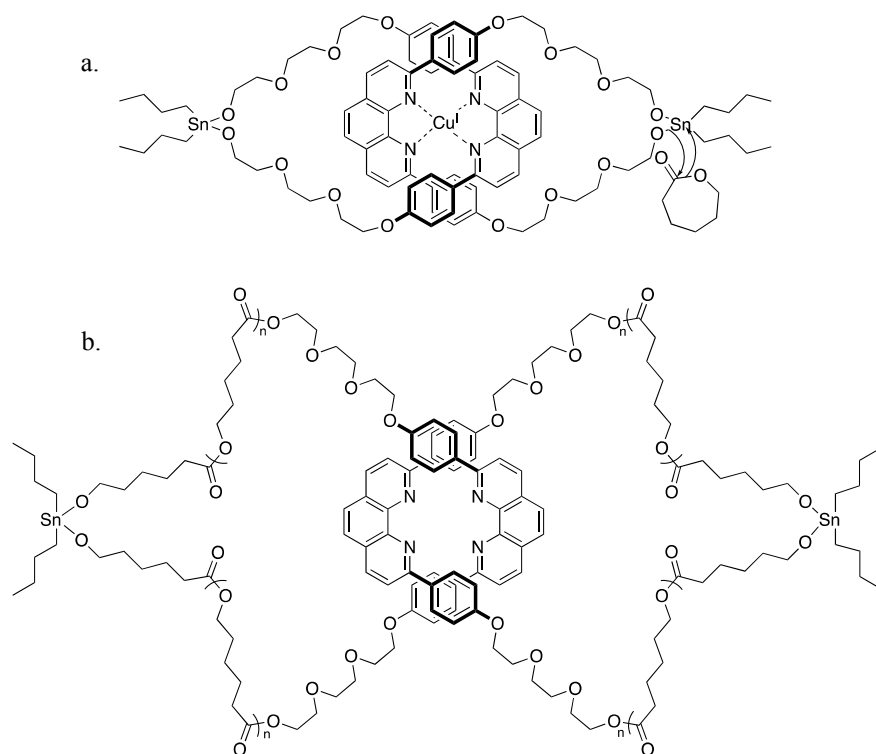
In 2020, Kudo and co-workers reported a living ring-expansion polymerization between phenoxypropylenesulfide with a cyclic monocarbamothioate, thiazolidine-2,4-dione, and tetrabutylammonium chloride as a catalyst [98]. The resulting polysulfides showed  $M_n$  values from 1.8 to 33.2 kDa and relatively narrow dispersity values from 1.07 to 1.26.

#### 14.9.4 Catenanes and Knotted Polymers via the Ring-Expansion Polymerization of Lactones

Catenanes are defined as compounds composed of two or more interlocking rings. These topologically complex macromolecules have been a source of interest over the years; however, low yield and inefficient purification techniques have plagued the study of these compounds. Consequentially, the employment of ring-expansion

polymerization has led to the ability to create catenated and knotted cyclic polymers at both high mass and yield. Advincula and co-workers were the first to report this type of synthesis using ring-expansion polymerization [168, 169]. Caprolactone was polymerized with the help of a cyclic phenanthroline-based catenane initiator. The bi-cyclic initiator was synthesized by using copper (I) ions to lock the two phenanthroline-based ligands into their respective positions. The ligands were then ring-closed with dibutyl tin (Fig. 14.20).

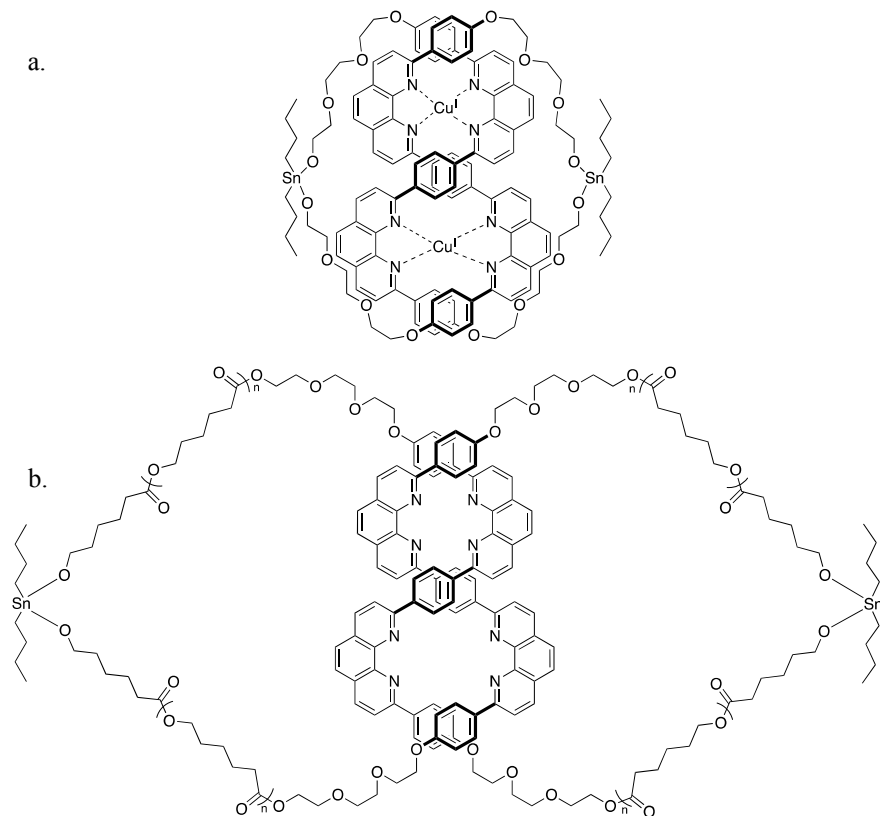
This created a catenane initiator which contained the same Sn–O bonds as observed from prior work with Kricheldorf. Once the catenane polymer was completed, the copper (I) was able to be removed by stirring the solution with 10 equivalents of potassium cyanate. Observations from GPC showed that the polymers preserved their interlocked structures even after copper decomplexation. This reaction led to an 83% population of catenated polymers and 73% yield after purification with a  $M_n$  of 4.6 kDa and dispersity of 1.89. It was later discovered that by modifying the ratios of monomer to initiator, catenated poly( $\epsilon$ -caprolactone) could be made with varying degrees of polymerization, 43.2–179.8, with monomer conversion exceeding 87%. Catenated poly(L-lactide) was also reported [168, 169].



**Fig. 14.20** **a** Cyclic phenanthroline-based catenane initiator **b** Ring-expansion polymerization of catenated initiator with poly( $\epsilon$ -caprolactone) by Cao et al. [168]

In addition to catenated polymers, Advincula and co-workers were the first to report the synthesis of trefoil knotted polymers by employing ring-expansion polymerization [170, 171]. A separate phenanthroline-based Cu(I)-templated trefoil precursor was synthesized via a ring-closing reaction with dibutyldimethoxytin (Fig. 14.21).

$\epsilon$ -Caprolactone was used as a monomer to polymerize with a yield of 65% and an  $M_n$  value of 21.3 kDa. Later work led to the synthesis of a trefoil knotted poly( $\epsilon$ -caprolactone)-*block*-poly(L-lactide) polymer [170, 171].



**Fig. 14.21** **a** Phenanthroline-based trefoil knot initiator. **b** Ring-expansion polymerization trefoil knot initiator with poly( $\epsilon$ -caprolactone) by Cao et al. [170]

## 14.9.5 Conclusion

The synthesis and topological characterization of cyclic polymers continues to be an area of significance due to their interesting physical properties along with the difficulty associated with synthesizing these macrocycles. While ring-closing approaches have dominated in the past, ring-expansion approaches have recently come forward to greatly contribute to the field of cyclic polymers. In recent years, strides have been made with both approaches in terms of the simplicity of synthesis and the complexity of polymers produced. Not only can extremely pure cyclic polymers be produced by both ring-closing and ring-expansion approaches, intricate topologies such as figure-of-eight, catenates, and knotted polymers have also been reported.

## References

1. B.A. Laurent, S.M. Grayson, *Chem. Soc. Rev.* **38**, 2202 (2009)
2. F.M. Haque, S.M. Grayson, *Nat. Chem.* **12**, 433 (2020)
3. T. Yamamoto, *Polym. J.* **45**, 711 (2013)
4. M.E. Córdova, A.T. Lorenzo, A.J. Müller, J.N. Hoskins, S.M. Grayson, *Macromolecules* **44**, 1742 (2011)
5. H.R. Kricheldorf, *J. Polym. Sci. Part Polym. Chem.* **48**, 251 (2010)
6. F.M. Haque, A. Alegria, S.M. Grayson, F. Barroso-Bujans, *Macromolecules* **50**, 1870 (2017)
7. J.D. Halverson, G.S. Grest, A.Y. Grosberg, K. Kremer, *Phys. Rev. Lett.* **108**, 38301 (2012)
8. Y. Tomikawa, T. Yamamoto, Y. Tezuka, *Macromolecules* **49**, 4076 (2016)
9. Y. Tezuka, *Acc. Chem. Res.* **50**, 2661 (2017)
10. P. Ruggli, *Justus Liebig's Ann. Chem.* **392**, 92 (1912)
11. K. Ziegler, H. Eberle, H. Ohlinger, *Justus Liebig's Ann. Chem.* **504**, 94 (1933)
12. F. Jacob, E.L. Wollman, *Symp. Soc. Exp. Biol.* **12**, 75 (1958)
13. H. Oike, H. Imaizumi, T. Mouri, Y. Yoshioka, A. Uchibori, Y. Tezuka, *J. Am. Chem. Soc.* **122**, 9592 (2000)
14. H. Wada, T. Yamamoto, Y. Tezuka, *Macromolecules* **48**, 6077 (2015)
15. S. Honda, K. Adachi, T. Yamamoto, Y. Tezuka, *Macromolecules* **50**, 5325 (2017)
16. S. Fujiwara, T. Yamamoto, Y. Tezuka, S. Habuchi, *React. Funct. Polym.* **80**, 3 (2014)
17. H. Heguri, T. Yamamoto, Y. Tezuka, *Angew. Chem. Int. Ed.* **54**, 8688 (2015)
18. S. Zhang, Y. Tezuka, Z. Zhang, N. Li, W. Zhang, X. Zhu, *Polym. Chem.* **9**, 677 (2018)
19. A. Kimura, T. Hasegawa, T. Yamamoto, H. Matsumoto, Y. Tezuka, *Macromolecules* **49**, 5831 (2016)
20. Y. Tomikawa, H. Fukata, Y.S. Ko, T. Yamamoto, Y. Tezuka, *Macromolecules* **47**, 8214 (2014)
21. Y.S. Ko, T. Yamamoto, Y. Tezuka, *Macromol. Rapid Commun.* **35**, 412 (2014)
22. M. Igari, H. Heguri, T. Yamamoto, Y. Tezuka, *Macromolecules* **46**, 7303 (2013)
23. F. Hatakeyama, T. Yamamoto, Y. Tezuka, *ACS Macro Lett.* **2**, 427 (2013)
24. A. Kimura, S. Takahashi, S. Kawauchi, T. Yamamoto, Y. Tezuka, *J. Org. Chem.* **78**, 3086 (2013)
25. Y. Tezuka, *Polym. J.* **44**, 1159 (2012)
26. N. Sugai, H. Heguri, T. Yamamoto, Y. Tezuka, *J. Am. Chem. Soc.* **133**, 19694 (2011)
27. I. Kii, A. Shiraishi, T. Hiramatsu, T. Matsushita, H. Uekusa, S. Yoshida, M. Yamamoto, A. Kudo, M. Hagiwara, T. Hosoya, *Org. Biomol. Chem.* **8**, 4051 (2010)
28. L. Wang, C. Dai, W. Chen, S.L. Wang, B. Wang, *Chem. Commun.* **47**, 10377 (2011)
29. P. Sun, J. Chen, J. Liu, K. Zhang, *Macromolecules* **50**, 1463 (2017)

30. L. Qu, P. Sun, Y. Wu, K. Zhang, Z. Liu, *Macromol. Rapid Commun.* **38**, 1700121 (2017)
31. M. Zhang, Y. Wu, Z. Liu, J. Li, L. Huang, K. Zhang, *Macromol. Rapid Commun.* **41**, 1900598 (2020)
32. Z. Li, L. Qu, W. Zhu, J. Liu, J.Q. Chen, P. Sun, Y. Wu, Z. Liu, K. Zhang, *Polymer* **137**, 54 (2018)
33. X. Liu, J.Q. Chen, M. Zhang, Y. Wu, M. Yang, K. Zhang, *J. Polym. Sci. Part Polym. Chem.* **57**, 1811 (2019)
34. L. Zhang, Y. Wu, S. Li, Y. Zhang, K. Zhang, *Macromolecules* **53**, 8621 (2020)
35. C. Liu, Y.Y. Fei, H.L. Zhang, C.Y. Pan, C.Y. Hong, *Macromolecules* **52**, 176 (2019)
36. E.M. Carnicom, E.S. Tillman, *React. Funct. Polym.* **80**, 9 (2014)
37. M.M. Arce, C.W. Pan, M.M. Thursby, J.P. Wu, E.M. Carnicom, E.S. Tillman, *Macromolecules* **49**, 7804 (2016)
38. C.W. Pan, K. Xia, S.A. Parker, E.S. Tillman, *Polymers* **10**, 844 (2018)
39. C. Pan, E. Tillman, *Polymers* **10**, 80 (2018)
40. S.C. Blackburn, K.D. Myers, E.S. Tillman, *Polymer* **68**, 284 (2015)
41. X. Xue, Y. Chen, K. Liang, W. Huang, H. Yang, L. Jiang, Q. Jiang, B. Jiang, H. Pu, *Polym. Chem.* **11**, 6529 (2020)
42. M.R. Whittaker, Y.K. Goh, H. Gemici, T.M. Legge, S. Perrier, M.J. Monteiro, *Macromolecules* **39**, 9028 (2006)
43. M.M. Stamenović, P. Espeel, E. Baba, T. Yamamoto, Y. Tezuka, F.E. Du Prez, *Polym. Chem.* **4**, 184 (2013)
44. G.R. McKeown, Y. Fang, N.K. Obhi, J.G. Manion, D.F. Perepichka, D.S. Seferos, *ACS Macro Lett.* **5**, 1075 (2016)
45. H. Shen, G. Wang, *Polym. Chem.* **8**, 5554 (2017)
46. J. Ochs, A. Alegría, E. González de San Román, S.M. Grayson, F. Barroso-Bujans, *Macromolecules* **53**, 10005 (2020)
47. G. Polymeropoulos, P. Bilalis, N. Hadjichristidis, *ACS Macro Lett.* **5**, 1242 (2016)
48. X. Jiang, J. Lu, F. Zhou, Z. Zhang, X. Pan, W. Zhang, Y. Wang, N. Zhou, X. Zhu, *Polym. Chem.* **7**, 2645 (2016)
49. G. Polymeropoulos, P. Bilalis, X. Feng, E.L. Thomas, Y. Gnanou, N. Hadjichristidis, *Macromolecules* **52**, 5583 (2019)
50. N. Alkayal, Z. Zhang, P. Bilalis, Y. Gnanou, N. Hadjichristidis, *Macromol. Chem. Phys.* **218**, 1600568 (2017)
51. X. Fan, T. Tang, K. Huang, G. Wang, J. Huang, *J. Polym. Sci. Part Polym. Chem.* **50**, 3095 (2012)
52. X. Fan, B. Huang, G. Wang, J. Huang, *Polymer* **53**, 2890 (2012)
53. B. Huang, X. Fan, G. Wang, Y. Zhang, J. Huang, *J. Polym. Sci. Part Polym. Chem.* **50**, 2444 (2012)
54. G. Wang, B. Hu, X. Fan, Y. Zhang, J. Huang, *J. Polym. Sci. Part Polym. Chem.* **50**, 2227 (2012)
55. Q. He, A.M. Yol, S.F. Wang, H. Ma, K. Guo, F. Zhang, C. Wesdemiotis, R.P. Quirk, M.D. Foster, *Polym. Chem.* **7**, 5840 (2016)
56. R.P. Quirk, S.F. Wang, M.D. Foster, C. Wesdemiotis, A.M. Yol, *Macromolecules* **44**, 7538 (2011)
57. E. Baba, T. Yatsunami, Y. Tezuka, T. Yamamoto, *Langmuir* **32**, 10344 (2016)
58. E. Baba, T. Yatsunami, T. Yamamoto, Y. Tezuka, *Polym. J.* **47**, 408 (2015)
59. S. Honda, T. Yamamoto, Y. Tezuka, *Nat. Commun.* **4**, 1574 (2013)
60. N. Sugai, T. Yamamoto, Y. Tezuka, *ACS Macro Lett.* **1**, 902 (2012)
61. E. Baba, S. Honda, T. Yamamoto, Y. Tezuka, *Polym. Chem.* **3**, 1903 (2012)
62. S. Honda, H. Sugimoto, *J. Polym. Sci. Part Polym. Chem.* **54**, 3336 (2016)
63. F. Zhang, R.P. Quirk, S. Gerislioglu, C. Wesdemiotis, S. Bekele, M. Tsige, Y.P. Koh, S.L. Simon, M.D. Foster, *Macromolecules* **51**, 9509 (2018)
64. Q. He, J. Mao, C. Wesdemiotis, R.P. Quirk, M.D. Foster, *Macromolecules* **50**, 5779 (2017)
65. B.A. Laurent, S.M. Grayson, *J. Am. Chem. Soc.* **128**, 4238 (2006)



66. M.A. Cortez, W.T. Godbey, Y. Fang, M.E. Payne, B.J. Cafferty, K.A. Kosakowska, S.M. Grayson, *J. Am. Chem. Soc.* **137**, 6541 (2015)
67. H.H. Su, H.L. Chen, A. Díaz, M.T. Casas, J. Puiggalfí, J.N. Hoskins, S.M. Grayson, R.A. Pérez, A.J. Müller, *Polymer* **54**, 846 (2013)
68. J.V. López, R.A. Pérez-Camargo, B. Zhang, S.M. Grayson, A.J. Müller, *RSC Adv.* **6**, 48049 (2016)
69. L. Xiang, W. Ryu, H. Kim, M. Ree, *Polymers* **10**, 577 (2018)
70. K. Schäler, E. Ostas, K. Schröter, T. Thurn-Albrecht, W.H. Binder, K. Saalwächter, *Macromolecules* **44**, 2743 (2011)
71. R.A. Pérez, J.V. López, J.N. Hoskins, B. Zhang, S.M. Grayson, M.T. Casas, J. Puiggalfí, A.J. Müller, *Macromolecules* **47**, 3553 (2014)
72. J. Wang, Z. Li, R.A. Pérez, A.J. Müller, B. Zhang, S.M. Grayson, W. Hu, *Polymer* **63**, 34 (2015)
73. G.M. Kelly, F.M. Haque, S.M. Grayson, J.N.L. Albert, *Macromolecules* **50**, 9852 (2017)
74. A. Shinya, R. Ono, H. Atarashi, S. Yamazaki, K. Kimura, *Polymer* **202**, 122660 (2020)
75. Z. Li, J. Wang, R.A. Pérez-Camargo, A.J. Müller, B. Zhang, S.M. Grayson, W. Hu, *Polym. Int.* **65**, 1074 (2016)
76. R.A. Pérez, M.E. Córdova, J.V. López, J.N. Hoskins, B. Zhang, S.M. Grayson, A.J. Müller, *React. Funct. Polym.* **80**, 71 (2014)
77. M. Divandari, L. Trachsel, W. Yan, J.G. Rosenboom, N.D. Spencer, M. Zenobi-Wong, G. Morgese, S.N. Ramakrishna, E.M. Benetti, *ACS Macro Lett.* **7**, 1455 (2018)
78. L. Trachsel, M. Romio, B. Grob, M. Zenobi-Wong, N.D. Spencer, S.N. Ramakrishna, E.M. Benetti, *ACS Nano* **14**, 10054 (2020)
79. S.N. Ramakrishna, G. Morgese, M. Zenobi-Wong, E.M. Benetti, *Macromolecules* **52**, 1632 (2019)
80. G. Morgese, E. Cavalli, J.G. Rosenboom, M. Zenobi-Wong, E.M. Benetti, *Angew. Chem. - Int. Ed.* **57**, 1621 (2018)
81. Y. Yang, G. Tang, M. Hu, L. Shao, J. Li, Y. Bi, *Polymer* **68**, 213 (2015)
82. Y. Wang, S. Zhang, L. Wang, W. Zhang, N. Zhou, Z. Zhang, X. Zhu, *Polym. Chem.* **6**, 4669 (2015)
83. F. Zhou, Y. Li, G. Jiang, Z. Zhang, Y. Tu, X. Chen, N. Zhou, X. Zhu, *Polym. Chem.* **6**, 6885 (2015)
84. X. Wang, L. Li, X. Ye, C. Wu, *Macromolecules* **47**, 2487 (2014)
85. M.D. Hossain, D. Lu, Z. Jia, M.J. Monteiro, *ACS Macro Lett.* **3**, 1254 (2014)
86. B. Zhang, H. Zhang, Y. Li, J.N. Hoskins, S.M. Grayson, *ACS Macro Lett.* **2**, 845 (2013)
87. X. Fan, B. Huang, G. Wang, J. Huang, *Macromolecules* **45**, 3779 (2012)
88. B.A. Laurent, S.M. Grayson, *J. Am. Chem. Soc.* **133**, 13421 (2011)
89. T. Josse, O. Altintas, K.K. Oehlschlaeger, P. Dubois, P. Gerbaux, O. Coulembier, C.B. Kowollik, *Chem. Commun.* **50**, 2024 (2014)
90. W. Liu, S. Zhang, S. Liu, Z. Wu, H. Chen, *Macromol. Rapid Commun.* **40**, 1900310 (2019)
91. P. Sun, Q. Tang, Z. Wang, Y. Zhao, K. Zhang, *Polym. Chem.* **6**, 4096 (2015)
92. Q. Tang, J. Chen, Y. Zhao, K. Zhang, *Polym. Chem.* **6**, 6659 (2015)
93. J. Hu, P. Sun, X. Jiang, W. Zhu, K. Zhang, *Sci. China Chem.* **59**, 1277 (2016)
94. J.-H. Schuetz, L. Sandbrink, P. Vana, *Macromol. Chem. Phys.* **214**, 1484 (2013)
95. H. Kudo, Y. Takeshi, *J. Polym. Sci. Part Polym. Chem.* **52**, 857 (2014)
96. A. Takahashi, R. Yuzaki, Y. Ishida, A. Kameyama, *J. Polym. Sci. Part Polym. Chem.* **57**, 2442 (2019)
97. A. Takahashi, S. Tsunoda, R. Yuzaki, A. Kameyama, *Macromolecules* **53**, 5227 (2020)
98. H. Kudo, K. Naritomi, S. Onishi, H. Maekawa, E.A.Q. Mondarte, K. Suthiwanich, T. Hayashi, *Macromolecules* **53**, 4733 (2020)
99. C.D. Roland, H. Li, K.A. Abboud, K.B. Wagener, A.S. Veige, *Nat. Chem.* **8**, 791 (2016)
100. W. Niu, S.A. Gonsales, T. Kubo, K.C. Bentz, D. Pal, D.A. Savin, B.S. Sumerlin, A.S. Veige, *Chem* **5**, 237 (2019)

101. C.D. Roland, T. Zhang, S. VenkatRamani, I. Ghiviriga, A.S. Veige, *Chem. Commun.* **55**, 13697 (2019)
102. M. Ouchi, H. Kammiyada, M. Sawamoto, *Polym. Chem.* **8**, 4970 (2017)
103. H. Kammiyada, M. Ouchi, M. Sawamoto, *Macromolecules* **50**, 841 (2017)
104. H. Kammiyada, M. Ouchi, M. Sawamoto, *J. Polym. Sci. Part Polym. Chem.* **55**, 3082 (2017)
105. H.R. Kricheldorf, S.-R. Lee, *Macromolecules* **28**, 6718 (1995)
106. H.R. Kricheldorf, S. Eggerstedt, *Macromol. Chem. Phys.* **199**, 283 (1998)
107. C.W. Bielawski, D. Benitez, R.H. Grubbs, *Science* **297**, 2041 (2002)
108. A.J. Boydston, Y. Xia, J.A. Kornfield, I.A. Gorodetskaya, R.H. Grubbs, *J. Am. Chem. Soc.* **130**, 12775 (2008)
109. D.A. Culkin, W. Jeong, S. Csihony, E.D. Gomez, N.P. Balsara, J.L. Hedrick, R.M. Waymouth, *Angew. Chem.* **119**, 2681 (2007)
110. W. Jeong, J.L. Hedrick, R.M. Waymouth, *J. Am. Chem. Soc.* **129**, 8414 (2007)
111. W. Jeong, E.J. Shin, D.A. Culkin, J.L. Hedrick, R.M. Waymouth, *J. Am. Chem. Soc.* **131**, 4884 (2009)
112. L. Guo, D. Zhang, *J. Am. Chem. Soc.* **131**, 18072 (2009)
113. H.R. Kricheldorf, S.M. Weidner, F. Scheliga, *Polym. Chem.* **8**, 1589 (2017)
114. H.R. Kricheldorf, S.M. Weidner, F. Scheliga, *Macromol. Chem. Phys.* **218**, 1700274 (2017)
115. H.R. Kricheldorf, S.M. Weidner, *J. Polym. Sci. Part Polym. Chem.* **56**, 749 (2018)
116. H.R. Kricheldorf, S.M. Weidner, *Eur. Polym. J.* **105**, 158 (2018)
117. S.M. Weidner, H.R. Kricheldorf, *J. Polym. Sci. Part Polym. Chem.* **56**, 2730 (2018)
118. H.R. Kricheldorf, S.M. Weidner, F. Scheliga, *Eur. Polym. J.* **116**, 256 (2019)
119. H.R. Kricheldorf, S.M. Weidner, *J. Polym. Environ.* **27**, 2697 (2019)
120. P. Piromjitpong, P. Ratanapanee, W. Thumrongpatanaraks, P. Kongsaree, K. Phomphrai, *Dalton Trans.* **41**, 12704 (2012)
121. P. Wongmahasirikun, P. Prom-on, P. Sangtrirutnugul, P. Kongsaree, K. Phomphrai, *Dalton Trans.* **44**, 12357 (2015)
122. S. Praban, S. Yimthachote, J. Kiriratnikom, S. Chotchatchawankul, J. Tantirungrotechai, K. Phomphrai, *J. Polym. Sci. Part Polym. Chem.* **57**, 2104 (2019)
123. T. Ungpittagul, P. Wongmahasirikun, K. Phomphrai, *Dalton Trans.* **49**, 8460 (2020)
124. C.Y. Gao, Y. Li, J. Chi, P. Lecomte, R. Jérôme, C. Jérôme, L.C. Lei, H. Li, (2013)
125. S. Impemba, F.D. Monica, A. Grassi, C. Capacchione, S. Milione, *Chemsuschem* **13**, 141 (2020)
126. J. Weil, R.T. Mathers, Y.D.Y.L. Getzler, *Macromolecules* **45**, 1118 (2012)
127. S.H. Reisberg, H.J. Hurley, R.T. Mathers, J.M. Tanski, Y.D.Y.L. Getzler, *Macromolecules* **46**, 3273 (2013)
128. K. Zhang, G.N. Tew, *ACS Macro Lett.* **1**, 574 (2012)
129. K. Zhang, Y. Zha, B. Peng, Y. Chen, G.N. Tew, *J. Am. Chem. Soc.* **135**, 15994 (2013)
130. A. Blencowe, G.G. Qiao, *J. Am. Chem. Soc.* **135**, 5717 (2013)
131. S.A. Gonsales, T. Kubo, M.K. Flint, K.A. Abboud, B.S. Sumerlin, A.S. Veige, *J. Am. Chem. Soc.* **138**, 4996 (2016)
132. S.S. Nadif, T. Kubo, S.A. Gonsales, S. VenkatRamani, I. Ghiviriga, B.S. Sumerlin, A.S. Veige, *J. Am. Chem. Soc.* **138**, 6408 (2016)
133. Z. Miao, D. Pal, W. Niu, T. Kubo, B.S. Sumerlin, A.S. Veige, *Macromolecules* **53**, 7774 (2020)
134. Z. Li, C. Wu, L. Liu, M. Li, X. Yang, C. Hao, Q. Chen, Z. Hu, M. Luo, G. Lai, T.-Y. Luh, *Polym. Chem.* **8**, 1573 (2017)
135. B.J. Lidster, S. Hirata, S. Matsuda, T. Yamamoto, V. Komanduri, D. Raj Kumar, Y. Tezuka, M. Vacha, M.L. Turner, *Chem. Sci.* **9**, 2934 (2018)
136. Y. Imada, C. Okita, H. Maeda, M. Kishimoto, Y. Sugano, H. Kaneshiro, Y. Nishida, S. Kawamorita, N. Komiya, T. Naota, *Eur. J. Org. Chem.* **2014**, 5670 (2014)
137. H.A. Brown, Y.A. Chang, R.M. Waymouth, *J. Am. Chem. Soc.* **135**, 18738 (2013)
138. A.K. Acharya, Y.A. Chang, G.O. Jones, J.E. Rice, J.L. Hedrick, H.W. Horn, R.M. Waymouth, *J. Phys. Chem. B* **118**, 6553 (2014)

139. H.A. Brown, S. Xiong, G.A. Medvedev, Y.A. Chang, M.M. Abu-Omar, J.M. Caruthers, R.M. Waymouth, *Macromolecules* **47**, 2955 (2014)
140. Y.A. Chang, R.M. Waymouth, *Polym. Chem.* **6**, 5212 (2015)
141. G.O. Jones, Y.A. Chang, H.W. Horn, A.K. Acharya, J.E. Rice, J.L. Hedrick, R.M. Waymouth, *J. Phys. Chem. B* **119**, 5728 (2015)
142. T.S. Stukenbroeker, D. Solis-Ibarra, R.M. Waymouth, *Macromolecules* **47**, 8224 (2014)
143. Y.A. Chang, A.E. Rudenko, R.M. Waymouth, *ACS Macro Lett.* **5**, 1162 (2016)
144. H.A. Brown, A.G. De Crisci, J.L. Hedrick, R.M. Waymouth, *ACS Macro Lett.* **1**, 1113 (2012)
145. H. Kammiyada, A. Konishi, M. Ouchi, M. Sawamoto, *ACS Macro Lett.* **2**, 531 (2013)
146. H. Kammiyada, M. Ouchi, M. Sawamoto, *Macromol. Symp.* **350**, 105 (2015)
147. H. Kammiyada, M. Ouchi, M. Sawamoto, *Polym. Chem.* **7**, 6911 (2016)
148. H. Kubota, S. Yoshida, M. Ouchi, *Polym. Chem.* **11**, 3964 (2020)
149. I. Asenjo-Sanz, A. Veloso, J.I. Miranda, J.A. Pomposo, F. Barroso-Bujans, *Polym. Chem.* **5**, 6905 (2014)
150. I. Asenjo-Sanz, A. Veloso, J.I. Miranda, A. Alegría, J.A. Pomposo, F. Barroso-Bujans, *Macromolecules* **48**, 1664 (2015)
151. F.M. Haque, C.M. Schexnayder, J.M. Matxain, F. Barroso-Bujans, S.M. Grayson, *Macromolecules* **52**, 6369 (2019)
152. S. Wu, M. Luo, D.J. Darensbourg, D. Zeng, Y. Yao, X. Zuo, X. Hu, D. Tan, A.C.S. Sustain, *Chem. Eng.* **8**, 5693 (2020)
153. E. Piedra-Arroni, C. Ladavière, A. Amgoune, D. Bourissou, *J. Am. Chem. Soc.* **135**, 13306 (2013)
154. L. Guo, S.H. Lahasky, K. Ghale, D. Zhang, *J. Am. Chem. Soc.* **134**, 9163 (2012)
155. A. Li, L. Lu, X. Li, L. He, C. Do, J.C. Garno, D. Zhang, *Macromolecules* **49**, 1163 (2016)
156. Q. Wang, W. Zhao, J. He, Y. Zhang, E.Y.-X. Chen, *Macromolecules* **50**, 123 (2017)
157. M.L. McGraw, R.W. Clarke, E.Y.-X. Chen, *J. Am. Chem. Soc.* **143**, 3318 (2021)
158. A.V. Prasad, Z. Yinghuai, *J. Appl. Polym. Sci.* **128**, 3411 (2013)
159. A.V. Prasad, A.O. Biying, W.Y. Ling, L.P. Stubbs, Y. Zhu, *J. Polym. Sci. Part Polym. Chem.* **51**, 4167 (2013)
160. O. Coulembier, J.D. Winter, T. Josse, L. Mespouille, P. Gerbaux, P. Dubois, *Polym. Chem.* **5**, 2103 (2014)
161. Y. Zhang, R. Liu, H. Jin, W. Song, R. Augustine, I. Kim, *Commun. Chem.* **1**, 1 (2018)
162. A. Narumi, S. Hasegawa, R. Yanagisawa, M. Tomiyama, M. Yamada, W.H. Binder, M. Kikuchi, S. Kawaguchi, *React. Funct. Polym.* **104**, 1 (2016)
163. A. Narumi, T. Kobayashi, M. Yamada, W.H. Binder, K. Matsuda, M.S.A. Shaykoon, K. Enomoto, M. Kikuchi, S. Kawaguchi, *Polymers* **10**, 638 (2018)
164. A. Narumi, M. Yamada, Y. Unno, J. Kumaki, W.H. Binder, K. Enomoto, M. Kikuchi, S. Kawaguchi, *ACS Macro Lett.* **8**, 634 (2019)
165. H. Kudo, S. Makino, A. Kameyama, T. Nishikubo, *Macromolecules* **38**, 5964 (2005)
166. H. Kudo, M. Sato, R. Wakai, T. Iwamoto, T. Nishikubo, *Macromolecules* **41**, 521 (2008)
167. Z. Zhang, X. Nie, F. Wang, G. Chen, W.-Q. Huang, L. Xia, W.-J. Zhang, Z.-Y. Hao, C.-Y. Hong, L.-H. Wang, Y.-Z. You, *Nat. Commun.* **11**, 3654 (2020)
168. P.-F. Cao, A. Bunha, J. Mangadlao, M.J. Felipe, K.I. Mongcopa, R. Advincula, *Chem. Commun.* **48**, 12094 (2012)
169. P.-F. Cao, J.D. Mangadlao, A. de Leon, Z. Su, R.C. Advincula, *Macromolecules* **48**, 3825 (2015)
170. P.-F. Cao, J. Mangadlao, R. Advincula, *Angew. Chem. Int. Ed.* **54**, 5127 (2015)
171. P.-F. Cao, L.-H. Rong, J.D. Mangadlao, R.C. Advincula, *Macromolecules* **50**, 1473 (2017)

# Chapter 15

## Recent Progress on the Synthesis of Cyclic Polymers via Ring-Closure Methods



Qingquan Tang and Ke Zhang

**Abstract** Cyclic biopolymers widely exist in organisms such as cyclic DNA and cyclic peptides. The unique cyclic molecular topology endows them with intriguing properties including wonderful thermal stability and good resistance to enzymatic degradation. Inspired by this, the research on synthetic cyclic polymers has attracted intense attention in polymer science in recent years. Compared to their linear counterparts, cyclic polymers have demonstrated distinctly different physical properties such as smaller radius of gyration and hydrodynamic volume, lower melt viscosity, and higher thermostability. This provides a driving force for polymer chemists to intensely explore the efficient synthetic methods for preparing varied cyclic polymers with a high topological purity. To date, the ring-closure strategy has been demonstrated as one of the main methods for preparing pure cyclic polymers, which is developed based on the combination of click reactions and living/controlled polymerization techniques. In this strategy, living/controlled polymerization techniques are used to synthesize end-functionalized linear polymers with controlled molecular weight and narrow dispersity. The click reactions are then used to ring-close the linear precursors and produce the well-defined cyclic polymers. This chapter reviews on the recent developments of the ring-closure strategy for synthesizing cyclic polymers, especially focusing on those methods with photo-induced click chemistry and self-accelerating click chemistry as the ring-closing reactions.

---

Q. Tang

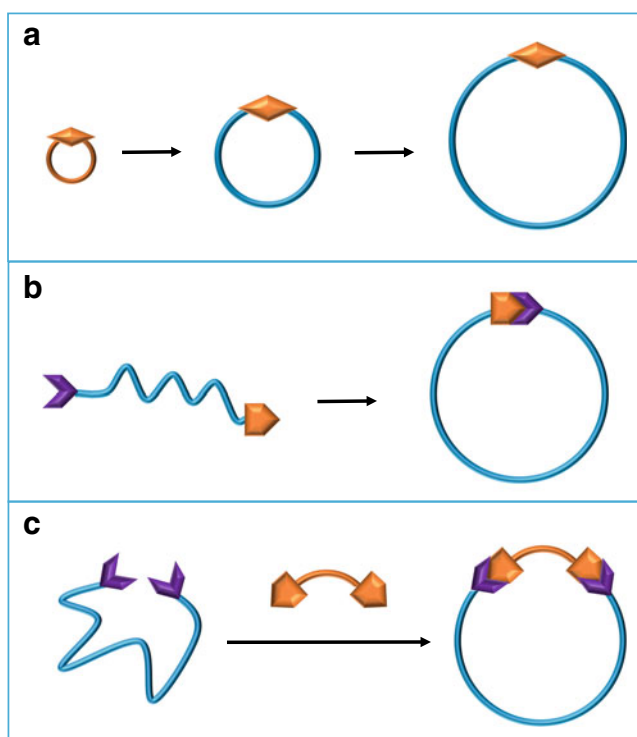
Laboratory of New Textile, College of Materials Science and Engineering, State Key, Materials and Advanced Processing Technology, Wuhan Textile University, Wuhan 430200, China

K. Zhang (✉)

Laboratory of Polymer Physics and Chemistry, Beijing National Laboratory for Molecular Sciences, Institute of Chemistry, The Chinese Academy of Sciences, Beijing 100190, China  
e-mail: [kzhang@iccas.ac.cn](mailto:kzhang@iccas.ac.cn)

## 15.1 Introduction

Cyclic polymers have drawn much attention in the past 60 years since the viral DNA of *Escherichia coli* was discovered to have a cyclic macromolecular structure in 1964 [1]. It is the unique ring macromolecular structure without chain ends that endows cyclic biopolymers with improved thermal and chemical stability [2]. For example, Kalata B1, one of the appealing cyclic peptides, shows unusual biological activity in boiling water for a few minutes [3]. Compared to their linear counterparts, the synthetic cyclic polymers also demonstrate distinctly different physical properties, such as smaller radius of gyration and hydrodynamic volume, lower melt viscosity, and higher thermostability [4–6]. This supports the functional materials from cyclic polymers with more advanced properties, including the improved fluorescence and redox behavior [7], enhanced thermal stability of the self-assembled micelles [8], and increased gene transfection efficiency and reduced cell toxicity [9]. To date, the main synthetic methods for pure cyclic polymers can be generalized into two categories: the ring-expansion (Fig. 15.1a) and the ring-closure strategies (Fig. 15.1b and c) [6, 10–15].



**Fig. 15.1** Schematic representation of the ring-expansion (a), unimolecular ring-closure (b), and bimolecular ring-closure (c) strategies

The Ring-expansion strategy produces cyclic polymers by continuously inserting the monomer units into an activated cyclic chain (Fig. 15.1a). Since the cyclic molecular structure inherited from the cyclic initiator preserves intact throughout the polymerization, the ring-expansion strategy does not require highly dilute conditions and suits for preparing high-molecular-weight cyclic polymers on large scales. A series of ring-expansion methods have been developed to date, including cyclic tin [16] and *N*-heterocyclic carbene [17]-catalyzed ring-opening polymerization (ROP) for cyclic polyesters, cyclic dithioester-based reversible addition–fragmentation chain-transfer (RAFT) polymerization for cyclic polymers [18], cyclic ruthenium alkylidene-based ring-expansion metathesis polymerization (REMP) for cyclic polynorbornenes [19], and tethered tungsten-alkylidene-catalyzed ring-expansion polymerization for conjugated cyclic poly(phenylacetylene) [20]. Although the advantages are clear when compared to ring-closure methods, disadvantages are still present in ring-expansion techniques. The main challenges include severe polymerization conditions, limited types of suitable monomers, time-consuming processes for synthesizing cyclic initiators, and the limitation to accurately control the molecular weight and dispersity of the resultant cyclic polymers [6, 11–13]. The information of ring-expansion strategy has been detailed in several recent wonderful review articles [6, 10–13, 15, 21].

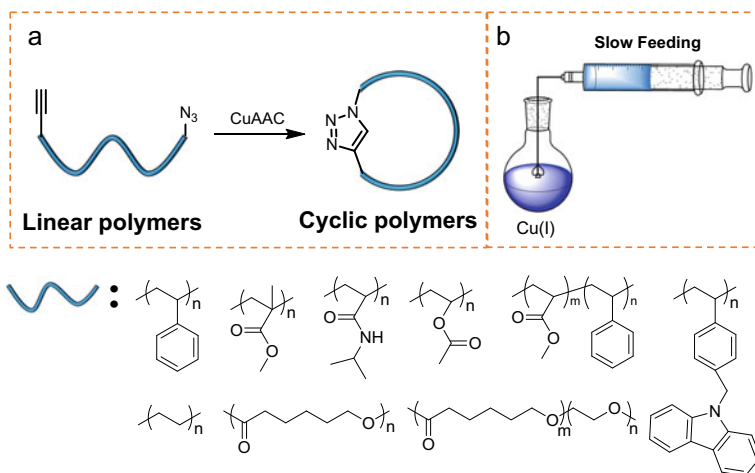
Comparatively, the ring-closure strategy produces cyclic polymers by applying highly efficient coupling reactions to ring-close end-functionalized linear telechelic polymers (Fig. 15.1b and c) [14]. Since the linear precursors are synthesized by living/controlled polymerization techniques, the ring-closure strategy can prepare cyclic polymers with widely varied molecular structure and functions, accurately controlled molecular weight, and narrow dispersity. In addition to the monocyclic polymers, the ring-closure strategy also supports a powerful tool to prepare cyclic polymer derivatives with complex architectures, such as tadpole, theta, and figure-eight shapes [22, 23]. However, disadvantages in this strategy still persist when compared to the ring-expansion strategy. Since the ring-closure of linear polymer precursor is an entropic penalty process, the ring-closure strategy is only appropriate to prepare cyclic polymers with low to medium molecular weight [14]. In addition, since a highly dilute condition is required for selecting intramolecular ring-closing reaction, the ring-closure strategy is hard to efficiently prepare cyclic polymers on large scales. The currently known ring-closure methods can be divided into two categories [11, 13, 14]: the unimolecular (Fig. 15.1b) and bimolecular (Fig. 15.1c) strategies. To date, a series of valuable review articles have been published on ring-closure strategy for cyclic polymers [6, 10–14, 24, 25]. Here, we mainly summarize the most recent progress of ring-closure methods including the unimolecular ring-closure based on photo-induced click chemistry and the bimolecular ring-closure based on self-accelerating click chemistry.

## 15.2 Unimolecular Ring-Closure Strategy

The unimolecular ring-closure strategy uses the telechelic polymers with two complementary reactive end groups as linear precursors. It can conveniently prepare cyclic polymers with a high purity by employing efficient coupling reactions to ring-close the linear precursors under highly dilute conditions. The dilute ring-closing reaction conditions are required to guarantee the selective intramolecular end group coupling but avoid the intermolecular couplings. The unimolecular ring-closure strategy becomes mature after marrying the click chemistry and the living/controlled polymerization techniques. The living/controlled polymerization techniques are used to synthesize variously well-defined linear polymers with two complementary reactive end groups. The click reactions are then used to ring-close the linear precursors and produce the well-defined cyclic polymers. According to the types of ring-closing click reactions, the unimolecular ring-closure strategy is roughly divided into the relatively traditional methods based on non-irradiated click chemistry and the novel methods based on photo-induced click chemistry in this chapter.

### 15.2.1 Unimolecular Ring-Closure Strategy Based on Non-irradiated Click Chemistry

A seminal unimolecular ring-closure method based on the combination of living/controlled polymerization and click chemistry was introduced by Grayson and co-workers in 2006 (Fig. 15.2a) [26]. They used atom transfer radical polymerization (ATRP) prepared well-defined polystyrene with alkynyl and bromine end groups. After substituting the bromine end group with sodium azide, the linear poly(styrene) precursors with alkynyl and azide end groups were successfully prepared. Subsequently, they applied the copper(I)-catalyzed azide-alkyne cycloaddition (CuAAC) click reaction to intramolecularly couple the azide and alkyne end groups of linear poly(styrene) under highly dilute conditions, successfully preparing the corresponding well-defined cyclic poly(styrene) with high purity. The cyclic molecular topology of poly(styrene) was firmly confirmed by GPC, MALDI-TOF MS, NMR, and FT-IR characterizations. Because CuAAC click reaction is tolerant to a wide range of functional groups, and because azide and alkyne groups can be easily introduced at each end of linear polymer chains, this approach has attracted intense attention in the formation of cyclic polymers. Inspired by this seminal study, CuAAC has been explored to combine with a series of living/controlled polymerization techniques such as RAFT [27], ROP [28], NMP [29], group transfer polymerization [30], and anionic polymerization [31] to successfully prepare a wide variety of cyclic homopolymers and diblock copolymers including poly(methyl methacrylate) [32], poly(*N*-isopropylacrylamide) [33], poly(4-vinylbenzyl-carbazole) [7], poly( $\epsilon$ -caprolactone) [28], poly(*N*-vinyl



**Fig. 15.2** **a** Preparation of varied cyclic polymers using CuAAC as a unimolecular ring-closing reaction. **b** Slow feeding-assisted CuAAC ring-closing reaction for the scalable formation of cyclic polymers

pyrrolidone) [34], polyethylene [35], poly(vinyl acetate) [36], poly(methyl acrylate)-*b*-poly(styrene) [37], poly(ethylene glycol)-*b*-polycaprolactone [38], poly(2-(2-methoxy-ethoxy)-ethyl methacrylate)-*b*-poly(oligo(ethylene glycol) methyl ether methacrylate) [39], and polystyrene-*b*-polyisoprene [31]. In addition, CuAAC-based unimolecular ring-closure methods have also been used to successfully prepare the cyclic polymer derivatives with complex architectures, such as multicyclic polymers [40], star cyclic polymers [41], cyclic dendronized polymers [42], and cage-shaped cyclic polymers [43]. Furthermore, the fast reaction kinetics allows CuAAC ring-closing reaction to be efficiently performed in a limited volume of solvent by slowly adding a concentrated linear polymer solution to a small amount of reaction solution containing Cu(I) catalyst (Fig. 15.2b) [44]. Compared to the one-pot ring-closing approach, the slow feeding technique significantly reduces the solvent volume of the ring-closing reaction. This allows the CuAAC-based unimolecular ring-closure methods to become ideal tools for preparing cyclic polymers in gram scales. It is the convenient preparation of cyclic polymers on large scales that facilitates to explore their applications in material science. Based on the same unimolecular ring-closure mechanism, several efficient metal-catalyzed coupling reactions, such as ring-closing metathesis (RCM) [45, 46], atom transfer radical coupling (ATRC) [47], the Glaser coupling [48], the McMurry reaction [49], and the Sonogashira coupling [50], have also been exploited to prepare cyclic polymers by combining with living/controlled polymerization techniques.

Although the usage of metal catalysts significantly speeds up the ring-closing reaction kinetics and improves the preparation efficiency of cyclic polymers, the complete removal of metal catalysts from the resultant cyclic polymers is a significant challenge. The trace amount of metal residuals may affect the application of cyclic

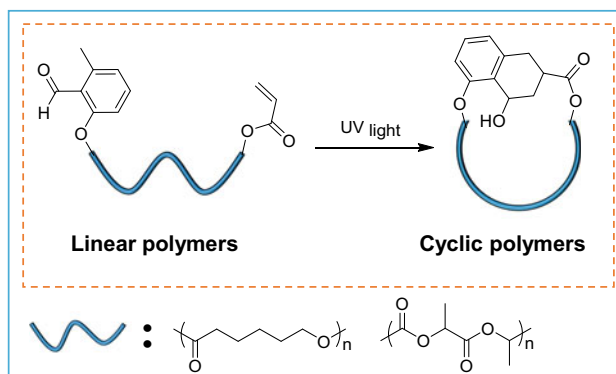


polymers in biomedical or photoelectronic research fields. To overcome this, metal-free click reactions have gained more and more interests in the ring-closure strategy for cyclic polymers. To date, three main kinds of non-irradiated metal-free click reactions have been explored in the unimolecular ring-closure methods, which includes thiol-based click reactions (thiol–thiol coupling [51–53], thiol–bromine substitution [54, 55], thiol–anthracene [56], thiol–ene [57], and thiol–Michael additions [58]), the Diels–Alder cycloaddition (maleimide–anthracene [59] and maleimide–cyclopentadiene [60]), and sulfur(VI)-fluoride exchange reaction [61]. Among them, thiol-based click reactions attracted much more attention since the thiol end-functionalized linear polymer precursors could be easily obtained by RAFT polymerization through aminolysis or reduction of RAFT chain-transfer groups at the polymer chain ends [51, 54]. In addition, RAFT polymerization synthesizes thiol end-functionalized linear polymer precursors without requiring any metal catalyst. This facilitates the combination of thiol-based click chemistry and RAFT polymerization to become a complete metal-free unimolecular ring-closure strategy for preparing cyclic polymers from the starting vinyl monomers. Although metal-free click reactions removed the usage of metal catalysts in the ring-closing reaction, most of them still required a large excess of organic chemicals to stimulate and speed up the ring-closing reaction. As a result, the cyclic polymers ring-closed by the above metal-free click reactions still suffer from the purification process to remove the chemical stimuli and the possible small byproducts.

### ***15.2.2 Unimolecular Ring-Closure Strategy Based on Photo-Induced Click Chemistry***

Due to the properties of spatiotemporal control, high efficiency, catalyst-free, and byproduct-free, photo-induced click chemistry has played an important role in polymer chemistry and materials [62–64]. Recently, the photo-induced click chemistry has also been exploited in the unimolecular ring-closure strategy for preparing cyclic polymers [65, 66]. Compared to non-irradiated click reactions, photo-induced click reactions endow the ring-closure strategy with two distinct advantages. First, the ring-closing reactions can be efficiently performed at ambient conditions under a mild light irradiation requiring no catalysts or chemical stimuli. Second, the cyclic polymers from ring-closing reaction required no further purification other than the evaporation of the solvent, due to the catalyst-free and byproduct-free properties of light-induced click reactions.

The first photo-induced unimolecular ring-closure method was developed by Barner-Kowollik and co-workers in 2014, based on the combination of living ROP technique and the UV-induced Diels–Alder reaction between photoenol and acrylate groups [66]. In this approach (Fig. 15.3), living ROP and a subsequent hydroxyl end group modification were used to prepare well-defined telechelic polyesters (polycaprolactone and polylactide) with orthoquinodimethane and acrylate end groups.

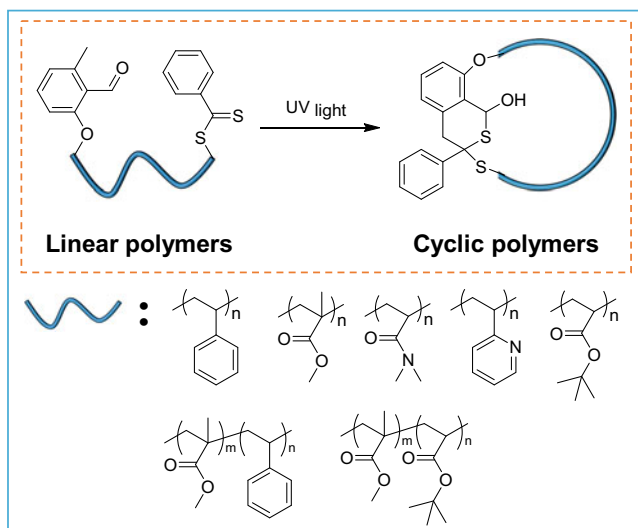


**Fig. 15.3** Preparation of cyclic polyesters using the UV-induced Diels–Alder click reaction between photoenol and acrylate groups as a unimolecular ring-closing reaction

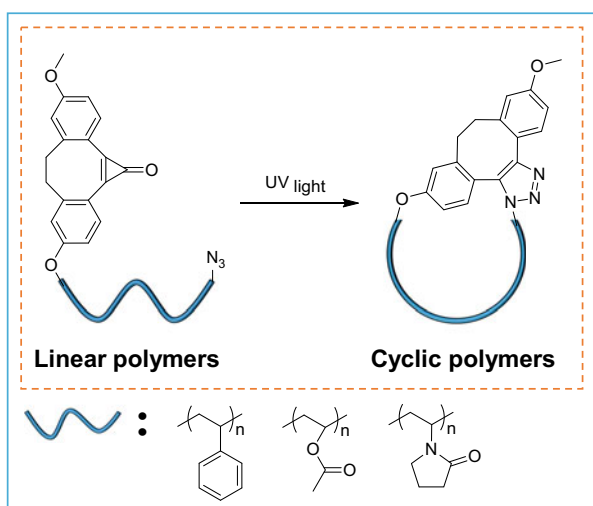
Under UV (315 nm) irradiation in dilute conditions, the orthoquinodimethane end group isomerized into a highly reactive photoenol, which efficiently reacted with the acrylate end group by a Diels–Alder cycloaddition mechanism to produce the corresponding cyclic polyesters with high purity. This ring-closing reaction can even be driven by sunlight to produce well-defined cyclic polyesters [67].

Recently, Zhang and co-workers developed a powerful ring-closure method for preparing a wide variety of cyclic polymers from vinyl monomers based on the combination of RAFT and the light-induced Diels–Alder click reaction between photoenol and dithioester groups [65]. In this approach (Fig. 15.4), a dithioester RAFT agent was designed with an orthoquinodimethane end group, by which various vinyl monomers can be polymerized by a standard RAFT process to produce a library of well-defined telechelic polymers with orthoquinodimethane and dithioester end groups. Under UV (315 nm) irradiation in dilute conditions, the in-situ formed photoenol from orthoquinodimethane isomerization efficiently reacted with the dithioester end groups to produce the corresponding cyclic polyesters with high purity. One outstanding feature of this method lies in that the linear polymer precursors can be prepared directly from RAFT polymerization, requiring no further end group modification. The universality of this method was demonstrated by successfully preparing various cyclic polymers including polystyrene, poly(methyl methacrylate), poly(*tert*-butyl acrylate), poly(*N,N*-dimethylacrylamide), poly(2-vinylpyridine), and poly(1-(4-vinylbenzyl)imidazole). In addition, this method has also been employed to successfully prepare cyclic block copolymers [65], cyclic alternating polymers [68], cyclic polymer derivatives [69, 70], and even functional cyclic polymer materials such as cyclic poly(ionic liquids) [71] and thermo-responsive cyclic polymers [72, 73].

Furthermore, Zhang and co-workers introduced UV-induced strain-promoted azide–alkyne cycloaddition (SPAAC) in the formation of cyclic polymers by combining with the ATRP technique [74]. In this approach (Fig. 15.5), well-defined



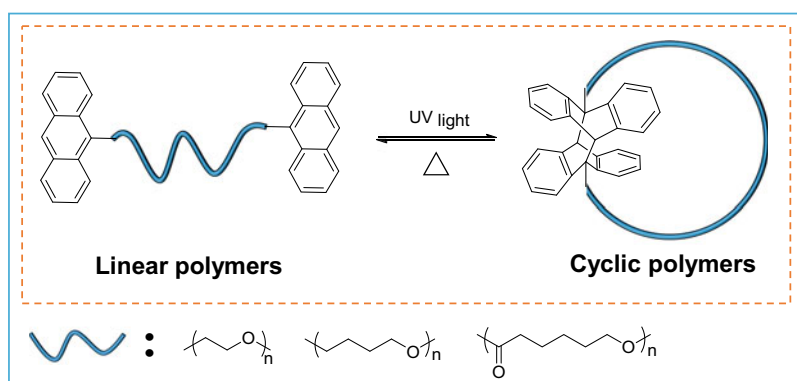
**Fig. 15.4** Preparation of varied cyclic polymers using the UV-induced Diels–Alder click reaction between photoenol and dithioester groups as a unimolecular ring-closing reaction



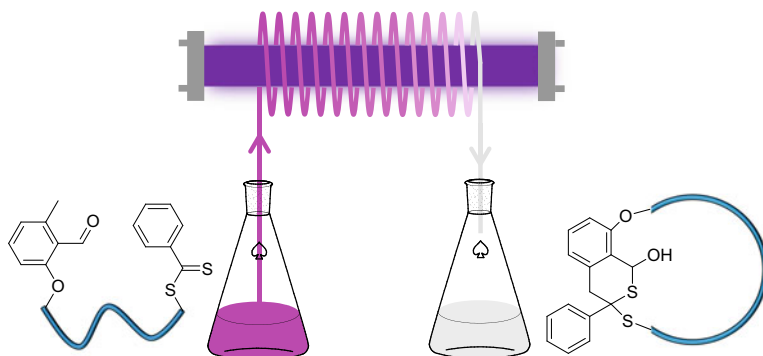
**Fig. 15.5** Preparation of varied cyclic polymers using UV-induced SPAAC as a unimolecular ring-closing reaction

telechelic polystyrene was synthesized with cyclopropanone-masked dibenzocyclooctyne and bromo end groups by ATRP of styrene from a cyclopropanone-masked dibenzocyclooctyne functionalized initiator. The linear polystyrene precursor was then obtained by using single-electron transfer-nitroxide radical coupling reaction to modify the bromo end group. Under UV irradiation (254 nm) in dilute solution, the dibenzocyclooctyne end group was quantitatively released from cyclopropanone-masked dibenzocyclooctyne, which intramolecularly reacted with the azide end group to ring-close the linear polystyrene precursor and produce the corresponding cyclic polystyrene. One distinct advantage of this method lies in that the resultant cyclic polymers can be converted back to their linear counterparts by cleaving the NO-C bond in the polymer backbone through thermolysis. Inspired by this success, Zhang and co-workers further extended the UV-induced SPAAC to prepare cyclic polymers from unconjugated vinyl monomers such as poly(vinyl acetate) and poly(*N*-vinylpyrrolidone) by combining with RAFT/macromolecular design via the interchange of xanthate (MADIX) polymerization technique [75]. Similarly, the cyclic poly(vinyl acetate) and poly(*N*-vinylpyrrolidone) could be converted back to their linear counterparts by cleaving S-C(S)O bond in the polymer backbone through aminolysis.

Photo-induced anthracene dimerization is a convenient and reversible cycloaddition reaction [76]. Yamamoto and Tezuka first introduced this chemistry in the formation of cyclic polymers with the reversible topological conversion from linear to cyclic, and back to linear again (Fig. 15.6) [77]. In this approach, the linear polymer precursors were prepared with both anthryl end groups, which were then cyclized under UV (365 nm) irradiation in a highly dilute solution to form the corresponding cyclic polymers. Upon simply heating at 150 °C, the resultant cyclic polymers could be quantitatively cleaved back to their anthryl end-functionalized linear precursors. More importantly, this approach could successfully perform the reversible topological conversion by repeating the photodimerization and thermal dissociation process.



**Fig. 15.6** Reversible topological transformation of linear and cyclic polymers based on reversible anthracene dimerization reaction



**Fig. 15.7** Scalable formation of cyclic polymers by the continuous-flow-assisted UV-induced Diels–Alder ring-closing reaction

This approach has been applied to prepare monocyclic poly(ethylene oxide) [77], poly(tetrahydrofuran) [77], polycaprolactone [78], and multicyclic polymers [79].

Since the light-induced ring-closing reactions can efficiently produce cyclic polymers at ambient conditions, they support the powerful tools to prepare cyclic polymers on large scales by combining with the continuous-flow technique [80]. Zhang and co-workers made pioneering work in this field [80]. They successfully developed a scalable formation method for cyclic polymers based on the combination of continuous-flow technique and the UV-induced Diels–Alder click reaction between photoenol and dithioester groups (Fig. 15.7). Using the telechelic polystyrene with orthoquinodimethane and dithioester end groups as exemplified linear precursors, the cyclization reaction was performed in a home-made coiled glass tube reactor under UV irradiation (310 nm, 7.5 mW/cm<sup>2</sup>) with a highly dilute polymer concentration ( $2 \times 10^{-5}$  M). Compared to the regular batch reactors, the flow reactor with a much larger surface-to-volume ratio allowed much more uniform UV irradiation on the cyclization reaction. This significantly increased the efficiency of the ring-closing reaction performed in the flow reactor, facilitating the continuous-flow technique to deal with large amounts of reaction solution in a relatively short time. By this approach, Zhang and co-workers achieved a production efficiency of 1 g/3 h for preparing cyclic polystyrene. Although a large amount of solvent (17.3 L) was used for preparing 1 g cyclic polystyrene by this approach, the solvent could be simply recycled by distillation due to the catalyst-free and byproduct-free nature of the light-induced Diels–Alder ring-closing reaction. Recently, Junkers and co-workers further improved this continuous-flow technique for the scalable formation of cyclic polymers by using a looped-flow system, which significantly reduced the required solution volumes by a factor of 43 [81]. As a result, the combination of light-induced click chemistry and continuous-flow technique provided a valuable tool for the scalable formation of cyclic polymers in practice.

### 15.3 Bimolecular Ring-Closure Strategy Based on Self-accelerating Click Chemistry

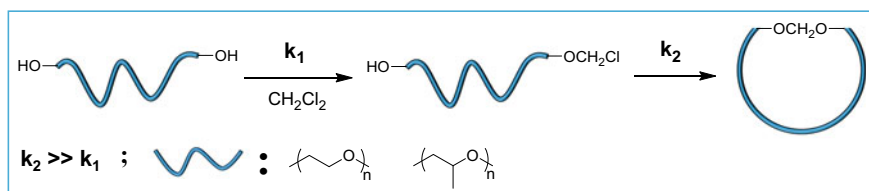
The bimolecular ring-closure strategy uses difunctional small linkers to ring-close the difunctional linear polymers to prepare the corresponding cyclic polymers (Fig. 15.1c). In this strategy, the difunctional linear polymers first reacted with the small linkers via intermolecular coupling to form the linear polymer intermediates, which were then intramolecularly ring-closed to produce the corresponding cyclic polymers. That is to say, one bimolecular cyclization process possessed two sequential reaction steps of intermolecular and then intramolecular couplings. As one of the oldest and most straightforward synthetic strategies, the traditional bimolecular ring-closure methods showed limited success for preparing pure cyclic polymers in practice. This is because the traditional methods used the same reactions to perform the sequential intermolecular and intramolecular coupling reactions. In this case, the usage of 1:1 stoichiometry between the difunctional linear polymers and small linkers was the prerequisite for preparing pure cyclic polymers. The accurate 1:1 stoichiometry, however, is hard to be achieved in practice. Even with 1:1 stoichiometry, the traditional bimolecular methods still hardly produce pure cyclic due to the issue of the kinetical paradox. The efficient intermolecular coupling prefers a high reaction concentration but the selective intramolecular cyclization requires an ultralow concentration.

To date, two specific techniques have been developed to overcome the inherent disadvantages of the traditional bimolecular ring-closure methods. The first one is the electrostatic self-assembly and covalent fixation (ESA-CF) method developed by Prof. Tezuka and co-workers [82–86]. This approach used dicarboxylate counteranions as small linkers to ring-close the telechelic polymers with cyclic ammonium salt end groups. In this approach, the electrostatic self-assembly temporarily locked the cationic end groups of telechelic polymers by anionic dicarboxylate linkers to form cyclic intermediates of the ionic complex in dilute solution. The dilute solution of the electrostatically self-assembled cyclic intermediates was then heated to induce the ring-opening reaction of the cyclic ammonium groups by the carboxylate counterions and produce the covalent cyclic polymers. The ESA-CF ingeniously employs the balance of electric charges to achieve the 1:1 stoichiometry between linear polymers and small linkers and avoid the kinetical paradox of traditional bimolecular ring-closure methods. To date, the ESA-CF method has been widely used to fabricate varied cyclic polymer topologies [87]. To date, several valuable review articles have been published by Prof. Tezuka to systematically introduce the ESA-CF bimolecular ring-closure methods for the formation of cyclic polymers and their derivatives [12, 23, 24, 87, 88].

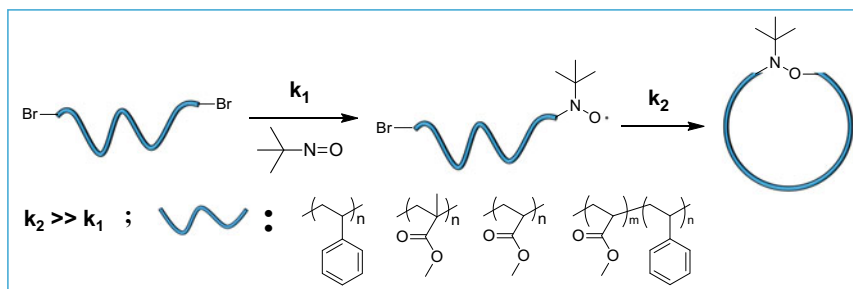
The other technique is the self-accelerating reaction-based bimolecular ring-closure strategy, which uses the self-accelerating reaction to couple the difunctional linear polymers and the small linkers [89]. In this approach, the intermolecular coupling reaction of a small linker and one end group of a polymer chain in-situ activates the second reactive moiety of the linker. The activated reactive moiety

gains a much larger rate constant to react with the other end group of the polymer chain compared to that of the original small linker. This significantly facilitates the intramolecular cyclization under dilute solution to form the cyclic polymers. In contrast to the traditional bimolecular methods using the same reaction as the intermolecular and subsequent intramolecular coupling reactions, the self-accelerating coupling reaction allows the novel bimolecular methods to produce pure cyclic polymers in the presence of an excess of small linkers. This is because the accelerated intramolecular cyclization compensates for the side effects of excess small linkers on the ring-closing process by avoiding the formation of linear polymer byproducts terminated by linkers at both ends. In this case, the presence of excess small linkers with high concentration facilitates the efficient intermolecular coupling of linear polymers and small linkers. The usage of deficient linear polymers with low concentration guarantees the selective intramolecular coupling of linear polymer intermediates to form cyclic polymers with high purity. As a result, the usage of self-accelerating ring-closing reaction ingeniously eliminates the strict stoichiometry requirement and the kinetical paradox of traditional bimolecular ring-closure methods.

The study on the self-accelerating reaction-based bimolecular ring-closure method is pioneered by Booth and co-workers, in which the Williamson reaction was used to ring-close linear polyethers with both hydroxyl end groups (Fig. 15.8) [90, 91]. In this approach, dihydroxyl end-functionalized polyethers such as HO-PEO-OH and HO-PPO-OH were dissolved in dichloromethane or its mixed solvents with a dilute concentration of  $10^{-5}$  M. In the presence of potassium hydroxide, one hydroxyl end group of linear polyether reacted with dichloromethane to form a highly reactive chloroether intermediate, which rapidly reacted with the other hydroxyl end group to form the corresponding cyclic polyether (Fig. 15.8). Because of the high reactivity of the chloroether intermediate formed from intermolecular coupling, this approach could produce cyclic polyethers by performing the following intramolecular cyclization even using dichloromethane as solvent. Although the cyclization reaction was performed in a highly dilute solution, this approach produced cyclic polyethers containing high molecular weight byproducts from the intermolecular coupling of linear polyethers. These contaminants could be removed by fractional precipitation.



**Fig. 15.8** Preparation of cyclic polyesters using the self-accelerating Williamson reaction as the bimolecular ring-closing reaction

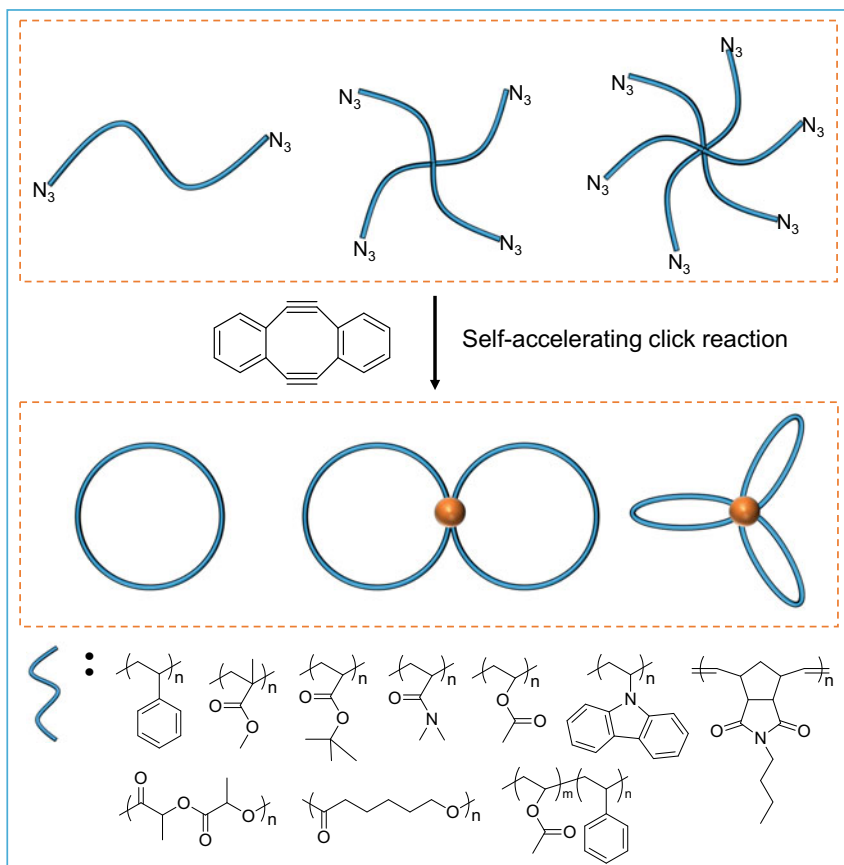


**Fig. 15.9** Preparation of varied cyclic polymers using self-accelerating RTA-ATRC as the bimolecular ring-closing reaction

Subsequently, Tillman and co-workers introduced the radical trap-assisted atom transfer radical coupling reaction (RTA-ATRC) in the bimolecular ring-closure strategy as the ring-closing reaction (Fig. 15.9) [92]. This approach used nitroso radical traps as small linkers to ring-close the dibrominated linear polymers from ATRP. In this approach, one bromine end group of the linear polymers was activated via the ATRC process under dilute solution by a nitroso radical trap, which was then efficiently reacted with the radical generated at the other end of the polymer chain to form the corresponding cyclic polymers. Due to the self-accelerating property of RTA-ATRC, this approach could produce cyclic polymers with high yield in the presence of a 250 times molar excess of nitroso radical traps over the brominated end groups. Although the RTA-ATRC-based bimolecular ring-closure method produced well-defined cyclic polystyrene, it indeed showed limited success for the formation of cyclic poly(methyl acrylate) [93] and poly(methyl methacrylate) [94]. A significant amount of byproducts with high molecular weight from the intermolecular coupling of linear polymer precursors was obtained for these two cases.

Using azide and *sym*-dibenzo-1,5-cyclooctadiene-3,7-diyne (DIBOD) as reactants, the double-strain-promoted azide–alkyne click reaction (DSPAAC) holds a significant self-accelerating property (Fig. 15.10) [95, 96]. In DSPAAC, the cycloaddition of the first alkyne with azide increased the DBA ring strain and in-situ activated the second alkyne, which reacted with azide much faster than the original DBA alkyne groups. It has been quantified that the rate constant of the second azide–alkyne cycloaddition is around 180 times larger than that of the first one. By virtue of DSPAAC as a ring-closing reaction, Zhang and co-workers have developed a powerful bimolecular ring-closure method for preparing varied cyclic polymers with high purities recently [95]. This approach used DIBOD as a small linker to ring-close linear polymers with both azide end groups. Several distinct advantages have been demonstrated in this DSPAAC-based bimolecular ring-closure method. First, the significant self-accelerating property of the DSPAAC ring-closing reaction allows this method to prepare cyclic polymers in the presence of excess DBA small linkers to the azide functionalized linear polymer precursors. Second, the click property of the DSPAAC reaction allows this method to prepare cyclic polymers at

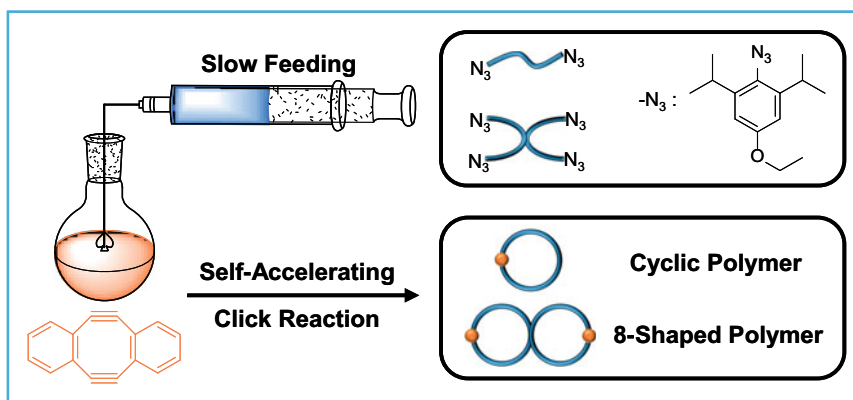




**Fig. 15.10** Preparation of varied cyclic polymers using self-accelerating DSPAAC as the bimolecular ring-closing reaction

ambient conditions requiring no metal or chemical catalysts. Thirdly, since the azide-terminated linear polymers could be easily prepared from varied living/controlled polymerization techniques including ATRP, RAFT, ROP, and ROMP, this method is a universal biomolecular ring-closure technique for preparing nearly all kinds of well-defined cyclic polymers, such as cyclic polystyrene, poly(ethylene glycol), poly(*N,N*-dimethylacrylamide), poly(*tert*-butyl acrylate), poly(lactide), poly( $\epsilon$ -caprolactone), poly( $\delta$ -valerolactone), poly(vinyl acetate), Poly(*N*-vinylcarbazole), and polynorbornene [95, 97–101]. In addition, this technique has already been used to prepare cyclic polymer derivatives like bicyclic and tricyclic polymers [95, 102].

Scalable formation of cyclic polymers is a long-term formidable challenge for bimolecular ring-closure methods. Just recently, Zhang and co-workers developed a very fast DSPAAC-based bimolecular ring-closure method for preparing cyclic polymers [103]. In this approach, DIBOD smaller linkers were used to ring-close the



**Fig. 15.11** Slow feeding-assisted DSPAAC bimolecular ring-closing reaction for the scalable formation of cyclic polymers

linear polymers with 2,6-diisopropylphenyl azide end groups connected by para-ether bonds. The kinetic investigation of this DSPAAC ring-closing reaction produced the rate constants of 0.712 and 128.16  $\text{M}^{-1} \text{s}^{-1}$  for the sterically hindered aryl azide cycloaddition with the first and the second alkyne moieties of DIBOD, respectively. Such large rate constant values supported the DSPAAC ring-closing reaction with a very fast reaction rate. Due to the significant self-accelerating property and very fast kinetics of the ring-closing reaction, the improved DSPAAC-based bimolecular method could conveniently prepare cyclic polymers on large scales by combining with the slow feeding technique (Fig. 15.11). A very low instant concentration of linear polymer precursors was maintained during the DSPAAC ring-closing reaction by slowly feeding a concentrated linear polymer solution into a small volume of DIBOD solution. This allows the fast DSPAAC-based bimolecular ring-closure method to become an ideal tool for preparing cyclic polymers in gram scales. The versatility of this slow feeding-assisted bimolecular method was demonstrated by the scalable formation of monocyclic, 8-shaped bicyclic, and flower-like tricyclic poly(lactide) with a purity above 95%. Their productivities were optimized as 1.93 g/L/12 h, 0.7 g/L/24 h, and 0.67 g/L/24 h, respectively.

## 15.4 Conclusions

This chapter presented the most recent developments of ring-closure methods for cyclic polymers, mainly focusing on the unimolecular ring-closure methods based on light-induced click reactions and the bimolecular ring-closure methods based on self-accelerating DSPAAC click reaction. Using the light-induced click reactions to ring-close linear polymers with two complementary reactive end groups, the unimolecular ring-closure methods could efficiently produce cyclic polymers at ambient conditions

under mild light irradiation. Due to the catalyst-free and byproduct-free properties of the light-induced click reactions, the pure cyclic polymers could be directly collected by simply evaporating the solvents after the ring-closing reaction. In addition, the light-induced unimolecular ring-closure methods could conveniently produce cyclic polymers on large scales by combining with the continuous-flow technique. Using self-accelerating DSPAAC click reaction as the ring-closing reaction, the bimolecular ring-closure methods could efficiently produce pure cyclic polymers by virtue of excess DIBOD small linkers to ring-close linear polymers with both azide end groups at ambient conditions. Since azide-terminated linear polymers can be easily prepared from varied living/controlled polymerization techniques, the DSPAAC-based bimolecular ring-closure method is a universal technique to prepare cyclic polymers with diverse molecular structures and functionalities. In addition, when using the sterically hindered aryl azide end group to speed up the DSPAAC ring-closing reaction, the bimolecular method could easily achieve the scalable formation of cyclic polymers by combining with the slow feeding technique. To date, the synthetic methods including ring-expansion and ring-closure strategies have become more and more mature to prepare all kinds of cyclic polymers with high purities. The success of scalable formation of pure cyclic polymers should significantly encourage the researchers to deeply explore the wide applications of cyclic polymer materials.

## References

1. D. Freifelder, R.L. Sinsheimer, A.K. Kleinschmidt, *Science* **146**, 254 (1964)
2. F.M. Haque, S.M. Grayson, *Nat. Chem.* **12**, 433 (2020)
3. O. Saether, D.J. Craik, I.D. Campbell, K. Sletten, J. Juul, D.G. Norman, *Biochemistry* **34**, 4147 (1995)
4. M. Romio, L. Trachsel, G. Morgese, S. N. Ramakrishna, N. D. Spencer, E.M. Benetti, *ACS Macro Lett.*, **9**, 1024 (2020)
5. K. Zhang, G.N. Tew, *React. Funct. Polym.* **80**, 40 (2014)
6. K. Endo, *Synthesis and Properties of Cyclic Polymers* (Advances in Polymer Science, Springer-Verlag, Berlin Heidelberg, 2008), pp. 121–183
7. X. Zhu, N. Zhou, Z. Zhang, B. Sun, Y. Yang, J. Zhu, X. Zhu, *Angew. Chem. Int. Ed.* **50**, 6615 (2011)
8. S. Honda, T. Yamamoto, Y. Tezuka, *Nat. Commun.* **4**, 1574 (2013)
9. M.A. Cortez, W.T. Godbey, Y. Fang, M.E. Payne, B.J. Cafferty, K.A. Kosakowska, S.M. Grayson, *J. Am. Chem. Soc.* **137**, 6541 (2015)
10. B.A. Laurent, S.M. Grayson, *Chem. Soc. Rev.* **38**, 2202 (2009)
11. H.R. Kricheldorf, *J. Polym. Sci. Part A: Polym. Chem.* **48**, 251 (2010)
12. T. Yamamoto, Y. Tezuka, *Polym. Chem.* **2**, 1930 (2011)
13. Z. Jia, M.J. Monteiro, *J. Polym. Sci. Part A: Polym. Chem.* **50**, 2085 (2012)
14. T. Josse, J. De Winter, P. Gerbaux, O. Coulembier, *Angew. Chem. Int. Ed.* **55**, 13944 (2016)
15. Y.A. Chang, R.M. Waymouth, *J. Polym. Sci. Part A: Polym. Chem.* **55**, 2892 (2017)
16. H.R. Kricheldorf, *J. Polym. Sci. Part A: Polym. Chem.* **42**, 4723 (2004)
17. D.A. Culkin, W. Jeong, S. Csihony, E.D. Gomez, N.R. Balsara, J.L. Hedrick, R.M. Waymouth, *Angew. Chem. Int. Ed.* **46**, 2627 (2007)
18. T. He, G.H. Zheng, C.Y. Pan, *Macromolecules* **36**, 5960 (2003)
19. K. Zhang, M.A. Lackey, Y. Wu, G.N. Tew, *J. Am. Chem. Soc.* **133**, 6906 (2011)

20. C.D. Roland, H. Li, K.A. Abboud, K.B. Wagener, A.S. Veige, *Nat. Chem.* **8**, 791 (2016)
21. H.A. Brown, R.M. Waymouth, *Acc. Chem. Res.* **46**, 2585 (2013)
22. G. Polymeropoulos, G. Zapsas, K. Ntetsikas, P. Bilalis, Y. Gnanou, N. Hadjichristidis, *Macromolecules* **50**, 1253 (2017)
23. Y. Tezuka, H. Oike, *Prog. Polym. Sci.* **27**, 1069 (2002)
24. B. Zhang, S.M. Grayson, The ring-closure approach for synthesizing cyclic polymers. *Topological polymer chemistry*, World Sci., 157–197 (2012)
25. Y. Zhu, N.S. Hosmane, *Chemistryopen* **4**, 408 (2015)
26. B.A. Laurent, S.M. Grayson, *J. Am. Chem. Soc.* **128**, 4238 (2006)
27. A.S. Goldmann, D. Quemener, P.E. Millard, T.P. Davis, M.H. Stenzel, C. Barner-Kowollik, A.H.E. Wuller, *Polymer* **49**, 2274 (2008)
28. H. Misaka, R. Kakuchi, C. Zhang, R. Sakai, T. Satoh, T. Kakuchi, *Macromolecules* **42**, 5091 (2009)
29. G. O'Bryan, N. Ningnuek, R. Braslau, *Polymer* **49**, 5241 (2008)
30. S. Kikuchi, Y. Chen, E. Ichinohe, K. Kitano, S.-I. Sato, Q. Duan, X. Shen, T. Kakuchi, *Macromolecules*, **49**, 4828 (2016)
31. A. Touris, N. Hadjichristidis, *Macromolecules* **44**, 1969 (2011)
32. X. Zhu, N. Zhou, J. Zhu, Z. Zhang, W. Zhang, Z. Cheng, Y. Tu, X. Zhu, *Macromol. Rapid Commun.* **34**, 1014 (2013)
33. X.P. Qiu, F. Tanaka, F.M. Winnik, *Macromolecules* **40**, 7069 (2007)
34. V. Mishra, R. Kumar, *Polym. Sci. Series B* **61**, 753 (2019)
35. Y. Jiang, Z. Zhang, D. Wang, N. Hadjichristidis, *Macromolecules* **51**, 3193 (2018)
36. J. Demarteau, J. De Winter, C. Detrembleur, A. Debuigne, *Polym. Chem.* **9**, 273 (2018)
37. D.M. Eugene, S.M. Grayson, *Macromolecules* **41**, 5082 (2008)
38. B. Zhang, H. Zhang, Y. Li, J.N. Hoskins, S.M. Grayson, *ACS Macro Lett.* **2**, 845 (2013)
39. Z. Ge, Y. Zhou, J. Xu, H. Liu, D. Chen, S. Liu, *J. Am. Chem. Soc.* **131**, 1628 (2009)
40. M.D. Hossain, Z. Jia, M.J. Monteiro, *Macromolecules* **47**, 4955 (2014)
41. Z. Jia, D.E. Lonsdale, J. Kulis, M.J. Monteiro, *ACS Macro Lett.* **1**, 780 (2012)
42. B.A. Laurent, S.M. Grayson, *J. Am. Chem. Soc.* **133**, 13421 (2011)
43. T. Lee, J. Oh, J. Jeong, H. Jung, J. Huh, T. Chang, H.-J. Paik, *Macromolecules*, **49**, 3672 (2016)
44. D.E. Lonsdale, C.A. Bell, M.J. Monteiro, *Macromolecules* **43**, 3331 (2010)
45. K. Adachi, S. Honda, S. Hayashi, Y. Tezuka, *Macromolecules* **41**, 7898 (2008)
46. R.P. Quirk, S.-F. Wang, M.D. Foster, C. Wesdemiotis, A.M. Yol, *Macromolecules* **44**, 7538 (2011)
47. R. Nicolay, K. Matyjaszewski, *Macromolecules* **44**, 240 (2011)
48. Y. Zhang, G. Wang, J. Huang, *Macromolecules* **43**, 10343 (2010)
49. N. Delbosq, J. De Winter, S. Moins, A. Persoons, P. Dubois, O. Coulembier, *Macromolecules* **50**, 1939 (2017)
50. T. Fukushima, H. Ishibashi, D. Suemasa, R. Nakamura, M. Yomogida, T. Isono, T. Satoh, H. Kaji, *J. Polym. Sci. Part B: Polym. Phys.* **57**, 266 (2019)
51. M.R. Whittaker, Y.K. Goh, H. Gemici, T.M. Legge, S. Perrier, M.J. Monteiro, *Macromolecules* **39**, 9028 (2006)
52. M.M. Stamenovic, P. Espeel, E. Baba, T. Yamamoto, Y. Tezuka, F.E. Du Prez, *Polym. Chem.* **4**, 184 (2013)
53. M.W. Ali, Z. Muhammad, Q. Jia, L. Li, M. Saleem, M. Siddiq, Y. Chen, *Polym. Chem.* **11**, 4164 (2020)
54. S. Long, Q. Tang, Y. Wu, L. Wang, K. Zhang, Y. Chen, *React. Funct. Polym.* **80**, 15 (2014)
55. Q. Tang, K. Zhang, *Polym. Int.* **64**, 1060 (2015)
56. B. Liu, H. Wang, L. Zhang, G. Yang, X. Liu, I. Kim, *Polym. Chem.* **4**, 2428 (2013)
57. D. Lu, Z. Jia, M.J. Monteiro, *Polym. Chem.* **4**, 2080 (2013)
58. J. Zhao, Y. Zhou, Y. Zhou, N. Zhou, X. Pan, Z. Zhang, X. Zhu, *Polym. Chem.* **7**, 1782 (2016)
59. H. Durmaz, A. Dag, G. Hizal, U. Tunca, *J. Polym. Sci., Part A: Polym. Chem.*, **48**, 5083 (2010)

60. M. Glassner, J.P. Blinco, C. Barner-Kowollik, *Macromol. Rapid. Commun.* **32**, 724 (2011)
61. W. Liu, S. Zhang, S. Liu, Z. Wu, H. Chen, *Macromol. Rapid. Commun.* **40**, 1900310 (2019)
62. M.A. Tasdelen, Y. Yagci, *Angew. Chem. Int. Ed.* **52**, 5930 (2013)
63. G. Delaittre, N.K. Guimard, C. Barner-Kowollik, *Acc. Chem. Res.* **48**, 1296 (2015)
64. E. Blasco, M. Wegener, C. Barner-Kowollik, *Adv. Mater.* **29**, 1604005 (2017)
65. Q. Tang, Y. Wu, P. Sun, Y. Chen, K. Zhang, *Macromolecules* **47**, 3775 (2014)
66. T. Josse, O. Altintas, K.K. Oehlenschlaeger, P. Dubois, P. Gerbaux, O. Coulembier, C. Barner-Kowollik, *Chem. Commun.* **50**, 2024 (2014)
67. T. Josse, J. De Winter, O. Altintas, P. Dubois, C. Barner-Kowollik, P. Gerbaux, O. Coulembier, *Macromol. Chem. Phys.* **216**, 1227 (2015)
68. W. Zhu, Z. Li, Y. Zhao, K. Zhang, *Macromol. Rapid. Commun.* **36**, 1987 (2015)
69. S. Zhang, X. Cheng, J. Wang, Z. Zhang, W. Zhang, X. Zhu, *Polym. Chem.* **9**, 5155 (2018)
70. M. Liu, L. Yin, S. Zhang, Z. Zhang, W. Zhang, X. Zhu, *Polymers* **11**, 240 (2019)
71. Q. Tang, W. Zhang, J. Yuan, Q. Zhao, *React. Funct. Polym.* **138**, 1 (2019)
72. H. Zhang, W. Wu, X. Zhao, Y. Zhao, *Macromolecules* **50**, 3411 (2017)
73. X. An, Q. Tang, W. Zhu, K. Zhang, Y. Zhao, *Macromol. Rapid. Commun.* **37**, 980 (2016)
74. P. Sun, Q. Tang, Z. Wang, Y. Zhao, K. Zhang, *Polym. Chem.* **6**, 4096 (2015)
75. Q. Tang, J. Chen, Y. Zhao, K. Zhang, *Polym. Chem.* **6**, 6659 (2015)
76. H. Meier, D. Cao, *Chem. Soc. Rev.* **42**, 143 (2013)
77. T. Yamamoto, S. Yagyu, Y. Tezuka, J. Am. Chem. Soc. **138**, 3904 (2016)
78. H. Wang, L. Zhang, B. Liu, B. Han, Z. Duan, C. Qi, D.-W. Park, I. Kim, *Macromol. Rapid. Commun.* **36**, 1646 (2015)
79. Y. Fei, C. Liu, G. Chen, C. Hong, *Polym. Chem.* **10**, 3895 (2019)
80. P. Sun, J. Liu, Z. Zhang, K. Zhang, *Polym. Chem.* **7**, 2239 (2016)
81. E. Baeten, M. Rubens, K.N.R. Wuest, C. Barner-Kowollik, T. Junkers, *React. Chem. Engin.* **2**, 826 (2017)
82. H. Oike, H. Imaizumi, T. Mouri, Y. Yoshioka, A. Uchibori, Y. Tezuka, *J. Am. Chem. Soc.* **122**, 9592 (2000)
83. Y. Tezuka, K. Fujiyama, *J. Am. Chem. Soc.* **127**, 6266 (2005)
84. N. Sugai, H. Heguri, K. Ohta, Q. Meng, T. Yamamoto, Y. Tezuka, *J. Am. Chem. Soc.* **132**, 14790 (2010)
85. T. Suzuki, T. Yamamoto, Y. Tezuka, *J. Am. Chem. Soc.* **136**, 10148 (2014)
86. K. Kyoda, T. Yamamoto, Y. Tezuka, *J. Am. Chem. Soc.* **141**, 7526 (2019)
87. Y. Tezuka, *React. Funct. Polym.*, **148**, 104489 (2020).
88. Y. Tezuka, *Acc. Chem. Res.* **50**, 2661 (2017)
89. H.R. Kricheldorf, M.G. Zolotukhin, J. Cárdenas, *Macromol. Rapid. Commun.* **33**, 1814 (2012)
90. Z.-G. Yan, Z. Yang, C. Price, C. Booth, *Makromol. Chem., Rapid Commun.*, **14**, 725 (1993)
91. G.E. Yu, P. Sinnathamby, T. Sun, F. Heatley, C. Price, C. Booth, *Macromol. Rapid. Commun.* **18**, 1085 (1997)
92. A.F. Voter, E.S. Tillman, P.M. Findeis, S.C. Radzinski, *ACS Macro Lett.* **1**, 1066 (2012)
93. S.C. Blackburn, K.D. Myers, E.S. Tillman, *Polymer* **68**, 284 (2015)
94. S.C. Blackburn, E.S. Tillman, *Macromol. Chem. Phys.* **216**, 1282 (2015)
95. P. Sun, J. Chen, J. Liu, K. Zhang, *Macromolecules* **50**, 1463 (2017)
96. J.Q. Chen, L. Xiang, X. Liu, X. Liu, K. Zhang, *Macromolecules* **50**, 5790 (2017)
97. L. Qu, P. Sun, Y. Wu, K. Zhang, Z. Liu, *Macromol. Rapid. Commun.* **38**, 1700121 (2017)
98. P. Sun, W. Zhu, J. Chen, J. Liu, Y. Wu, K. Zhang, *Polymer* **121**, 196 (2017)
99. Z. Li, L. Qu, W. Zhu, J. Liu, Q.J. Chen, P. Sun, Y. Wu, Z. Liu, K. Zhang, *Polymer* **137**, 54 (2018)
100. X. Liu, J.-Q. Chen, M. Zhang, Y. Wu, M. Yang, K. Zhang, *J. Polym. Sci. Part. A: Polym. Chem.* **57**, 1811 (2019)
101. M. Zhang, Y. Wu, Z. Liu, J. Li, L. Huang, K. Zhang, *Macromol. Rapid. Commun.* **41**, 1900598 (2020)
102. C. Liu, Y.Y. Fei, H.L. Zhang, C.Y. Pan, C.-Y. Hong, *Macromolecules*, **52**, 176 (2019)
103. L. Zhang, Y. Wu, S. Li, Y. Zhang, K. Zhang, *Macromolecules* **53**, 8621 (2020)

# Chapter 16

## Ring-Expansion Polymerization of Cycloalkenes and Linear Alkynes by Transition Metal Catalysts



Tomohiro Kubo, Rinku Yadav, and Adam S. Veige

**Abstract** This chapter communicates the synthesis of cyclic polymers via ring-expansion polymerization. Historical ring-expansion mechanisms and catalysts are discussed. The focus of the work centers on metal-catalyzed ring expansion of cyclic alkenes and alkynes. Emphasizing the benefit of ring expansion, W-based tethered alkylidenes and their use in polymerizing norbornene and acetylenes are discussed in detail. Initial stages of catalyst tuning are presented and their application in the synthesis of stereoregular cyclic polynorbornene. Some applications of the resulting cyclic polymers are presented including cyclic polypropylene, transparent cyclic polymers, and post-polymerization functionalization for AFM imaging.

**Keywords** Ring-expansion metathesis polymerization · Transition metal catalysts · Cyclic polyacetylenes · Cyclic polymer

### 16.1 Introduction

#### 16.1.1 Background

The topology of a polymer is a characteristic feature in determining its properties [1]. While the singular chemical distinction between linear and cyclic polymers is the presence or absence of chain ends, many properties of cyclic polymers such as glass transition temperature, density, and viscosity vary significantly with those of their linear analogues [2–4]. Additionally, reports indicate that cyclic polymers exhibit improved biological properties such as cytotoxicity, tumor penetrability, and

---

T. Kubo (✉)

Department of Chemical Science and Engineering, School of Materials and Chemical Technology, Tokyo Institute of Technology, Ookayama, Meguro-Ku, Tokyo 152-8550, Japan  
e-mail: [kubo@mac.titech.ac.jp](mailto:kubo@mac.titech.ac.jp)

R. Yadav · A. S. Veige

Center for Catalysis Department of Chemistry George & Josephine Butler Polymer Research Laboratory, Center for Macromolecular Science & Engineering, Department of Chemistry, University of Florida, Gainesville, FL 32611, USA

nucleic acid delivery [5–7]. Though these advantageous properties have sparked interest in cyclic polymers, their synthesis remains a challenge. Realizing an efficient and straightforward synthetic method for cyclic polymers would not only expand the boundaries of polymeric materials but also further illuminate the influence of topology on macromolecules across disciplines.

### 16.1.2 *Cyclic Polymer Synthesis*

Past research has focused on many innovative synthetic approaches for cyclic polymers that ultimately divide into two methods: ring-closing polymerization and ring-expansion polymerization (REP) [8]. The ring-closing method often involves post-polymerization modification of telechelic polymers to transform linear polymers into cyclic polymers [9]. Synthetic attempts historically began with this method because of the monomer scope; virtually any linear polymer can be a candidate for cyclization provided that appropriate chain-end modification is possible. Furthermore, the recent rapid development of precision polymerization techniques not only affords well-defined polymers but also high chain-end fidelity, which is necessary to yield highly pure cyclic polymers. However, one inherent limitation of this method is the high dilution requirement; chain-end concentration determines whether telechelic polymers undergo the desired intramolecular cyclization or intermolecular oligomerization. This limitation renders large-scale synthesis difficult and thus limits the broad use of cyclic polymers.

Alternatively, REP, which is the focus of this chapter, affords cyclic polymers through the ring expansion of a cyclic precursor to create an expandable macrocycle [10]. Initial expansion of the cyclic precursor can serve to initiate or catalyze the polymerization of monomer to yield cyclic polymers. Propagation is usually thermodynamically driven by processes such as the alleviation of ring strain in the ring opening of cyclic monomers or the conversion of less stable alkynes to more stable alkenes for linear monomers. For REP, since the starting material for polymerization is cyclic and the propagation mechanism is by monomer insertion, the products remain cyclic. Clear advantages of REP over the ring-closing method are the topological purity of polymer products and the absence of the high dilution requirement. The absence of linear contaminants allows for the precise elucidation of structure–function relationships which helps us better understand the influence of topology on various polymer properties. Compared to the ring-closing approach, however, the ring-expansion method remains underexplored, likely due to the limited available synthetic approaches. As we hope to show, synthetic methods involving catalytic cyclic precursors may offer an ideal avenue to produce highly pure cyclic polymers on a large scale. Innovating new synthetic routes expand the scope of attainable cyclic polymers and empower us to exploit the unique property profile that cyclic polymers possess.

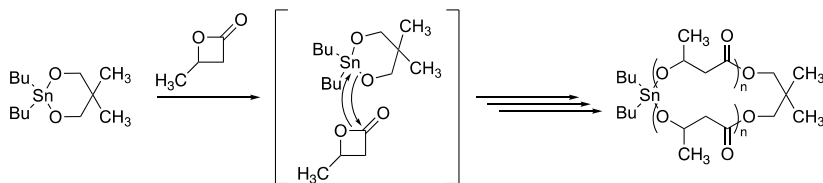
### 16.1.3 Ring-Expansion Polymerization (REP)

Kricheldorf and Lee initially pioneered REP by using cyclic lactide monomers and cyclic dibutyltin oxide as the initiator (Scheme 16.1) [11]. In this process, the lactone inserts into the tin-oxide bond which leads to a macrocyclic product. The loss in entropy with propagation is compensated by the release of ring strain which enables the synthesis of high molecular weight polymers. This method produces cyclic polymers with molecular weights up to 24 kDa and dispersities around 1.5. Kricheldorf and co-workers also developed techniques to remove the tin catalyst from the macrocycle while conserving its cyclic topology [12].

Shea and co-workers employed dimethylsulfoxonium methylide for the homologation of cyclic boranes. This process follows a migratory methylenide insertion mechanism where methylene groups insert into the boron-carbon bonds of the cyclic borane (Scheme 16.2) [13]. Propagation occurs as the electron-rich methylenide attacks the electron-deficient borane. One of the methylene groups adjacent to the boron center then migrates to the methylenide and dimethyl sulfoxide leaves, enlarging the ring by a single methylene unit. This method generates cyclic polymethylene with low molecular weight (<2 kDa) and dispersity (<1.2).

Ouchi and co-workers reported REP via living cationic polymerization using a cyclic initiator containing a hemiacetal ester with a Lewis acid catalyst to yield cyclic poly(vinyl ethers) (Scheme 16.3) [14]. The synthesis was successful for a broad scope of substrates and affords precise control over molecular weight and macrocycles with low dispersity.

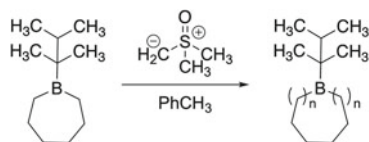
Another important catalytic ring-expansion polymerization method was developed by Waymouth and co-workers [15]. Using zwitterionic ring-opening polymerization cyclic poly(lactide) is achievable in excellent yields, low dispersity, and



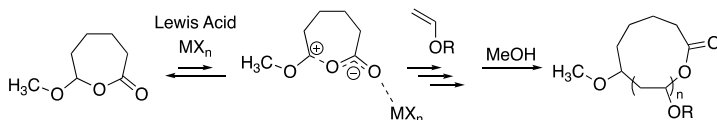
**Scheme 16.1** Ring-expansion polymerization of  $\beta$ -butyrolactone initiated by cyclic dibutyltin oxide

#### Scheme 16.2

Polyhomologation of cyclic boranes to form cyclic polymethylene



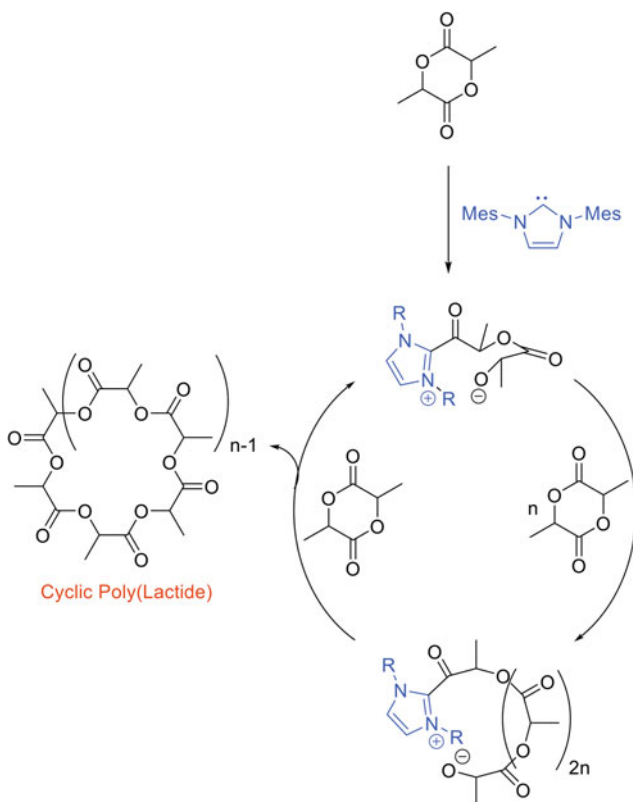




**Scheme 16.3** Ring-expansion living cationic polymerization of vinyl ether

without the need for dilute conditions (Fig. 16.1). Evidence for the columbic attraction between the chain ends comes from the production of linear polymers upon increasing the dielectric constant of the solvent.

Despite recent developments in REP, the challenge to produce large-scale cyclic polymers with high topological purity having a broad monomer scope remains. In this next section, we discuss metal-catalyzed REP that can potentially meet these



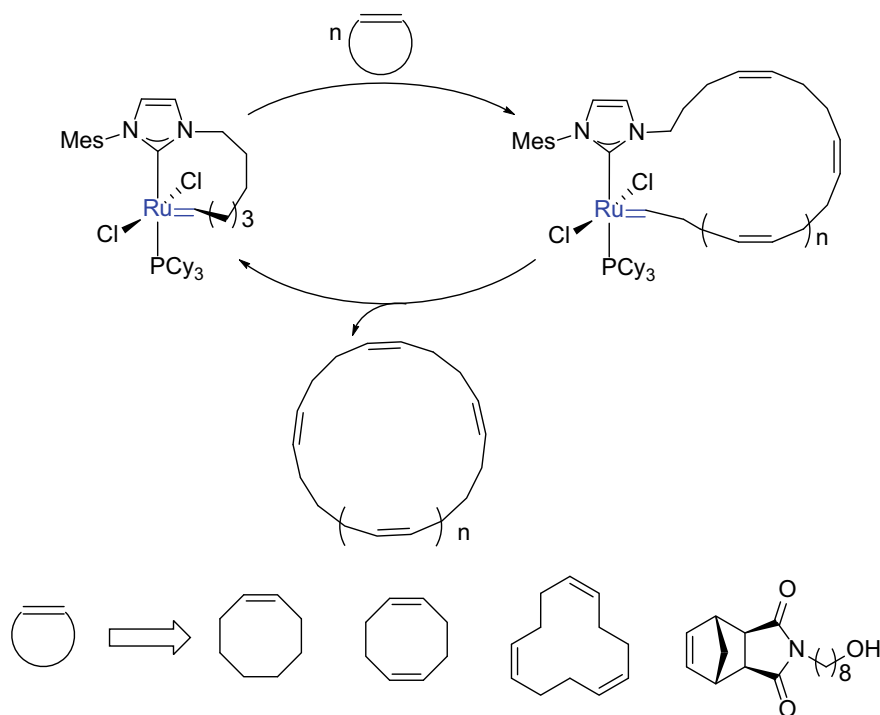
**Fig. 16.1** Synthesis of cyclic poly(lactide) via zwitterionic ring-opening polymerization

objectives with a specific focus on ruthenium- and tungsten-based metathesis-type catalysts.

## 16.2 Ring-Expansion Metathesis Polymerization (REMP)

### 16.2.1 Ruthenium Catalysts for REMP

Grubbs and co-workers initially demonstrated the utility of ring-opening metathesis polymerization to synthesize cyclic polymers using tethered ruthenium alkylidene complexes.<sup>10</sup> The tethered catalyst undergoes metathesis with cycloalkene monomers, a process that opens and inserts the cyclic monomer into the ring and initiates REP (Fig. 16.2). Propagation takes place by the repeated insertion of cyclic monomer into the growing chain through the active metal center. REMP of cyclooctene produces cyclic polymers with molecular weights up to 1,200 kDa and dispersities around 2.0. Analysis of GPC, DSC, and MALDI-TOF-MS data for the



**Fig. 16.2** Ring-opening metathesis polymerization of a cycloalkene by employing a Grubbs tethered Ru catalyst to produce cyclic polymers

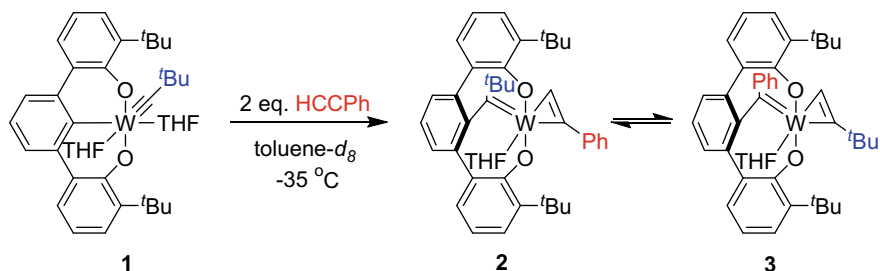
polymer products as well as characterization of any post-modified polymer products indicated a cyclic topology. This system facilitates large-scale cyclic polymer synthesis. As such, given cyclic initiators and monomers, their purity is of paramount importance for the topological purity of the polymer; a trace amount of linear impurities can result in the formation of linear polymers [16].

This Ru-based REMP approach enabled large-scale cyclic polymer synthesis as well as the synthesis of cyclic bottle brush polymers and cyclic dendrimers, among other interesting architectures [17, 18]. Polymeric networks based on cyclic polymers made with this system exhibit distinguishable gel fractions, moduli, and swelling ratios compared to gels based on linear counterparts [19].

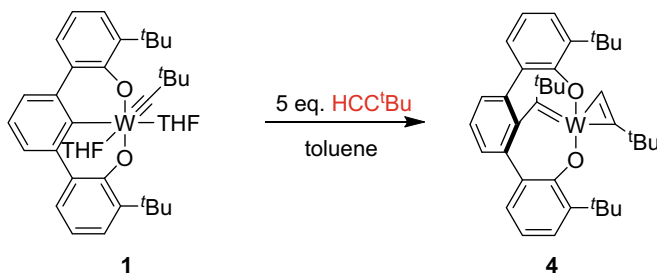
## 16.2.2 Tungsten Catalysts for Ring-Expansion Metathesis Polymerization

### 16.2.2.1 Polymerization of Linear Alkynes

In 2012, Veige and co-workers reported the activity of trianionic pincer ligand supported tungsten (VI) alkylidyne complex **1** toward alkyne polymerization [20]. With further study, the authors determined that complex **1** is not an inherently active catalyst for alkyne polymerization, but rather serves as a precatalyst that coordinates with an alkyne to generate the active catalyst in situ [21]. Complex **1** undergoes alkylidyne migratory insertion in the presence of alkynes, transforming the trianionic pincer ligand into a novel tetraanionic pincer ligand. A molybdenum catalyst with lower activity was also developed [22]. This tetraanionic pincer ligand forcibly creates a coordinatively unsaturated metal center opening a site for the alkyne monomer to bind to the metal. In the presence of phenylacetylene (PA), complex **1** converts to complexes **2** and **3**, where these products exist in equilibrium (Scheme 16.4). Both complexes **2** and **3** successfully catalyze the polymerization of alkynes though complex **2** exhibits higher activity. The authors proposed that the polymerization



**Scheme 16.4** Synthesis of complexes **2** and **3**



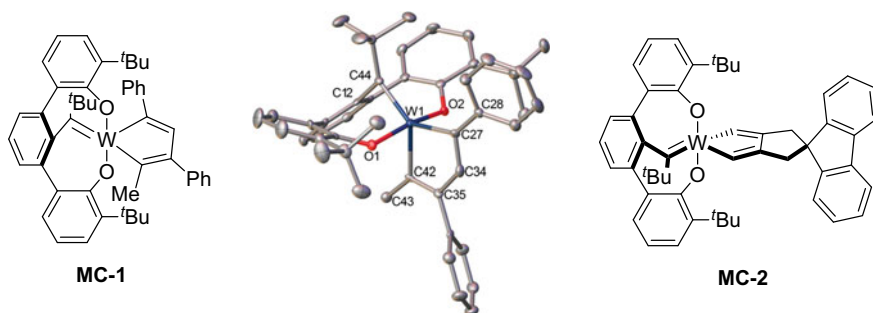
**Scheme 16.5** Synthesis of complex **4**

does not proceed through a metathesis pathway but instead follows a simple insertion pathway; the incoming alkyne inserts into the  $\eta^2$ -bound alkyne or the metallacyclopentadiene of the catalyst, resulting in a metallacyclopentadiene. Complex **2** is extremely active toward polymerization of phenylacetylene ( $5,640,000 \text{ g poly(PA)} \text{ mol}^{-1} \text{ h}^{-1}$ ) and produces polymers with molecular weights up to 119.4 kDa.

Complexes **2** and **3** have different activities toward alkyne polymerization, which necessitates their separation if one is to measure their activities independently of each other. Veige and co-workers circumvented this separation dilemma by synthesizing complex **4**, which they obtained exclusively in quantitative yield by the treatment of complex **1** with excess 3,3-dimethyl-1-butyne (Scheme 16.5). Due to the identical substitutions on the precatalyst and activating alkyne, migratory insertion results solely in complex **4**.

Complex **4** also exhibits high activity toward alkyne polymerization [23]. Complex **4** is tolerant toward a variety of functional groups on the alkyne monomer and produces cyclic polymers with molecular weights up to 350 kDa. The initial monomer concentration was approximately 1 M. Most importantly, complex **4** represents the first ever reported catalyst for the REP of alkynes. Suggested based on the synthesis and isolation of metallacyclopentadiene intermediates that are also active catalysts, the proposed mechanism involves sequential insertion of alkynes into a growing metallacycle. Propagation continues with the step-wise insertion of alkyne monomer into the metallacycle, effectively expanding the ring. Reductive elimination of the growing chain yields cyclic polyenes [23]. Figure 16.3 depicts two metallacyclopentadienes (**MC-1** and **MC-2**) characterized by solution phase methods and X-ray diffraction that inspired the proposed ring-expansion mechanism [24]. The mechanism did not originally involve the alkyldiene present in the ligand backbone. The reason at the time for exclusion was that no reaction occurs upon exposing complex **4** to preformed cyclic polyphenylacetylene, i.e., no backbiting into the ring. Future experiments need to be done that generate the active catalyst in situ and then trap the propagating species. The mechanism continues to unravel and a ring-expansion metathesis (REMP) mechanism involving a tethered alkyldiene intermediate cannot be ruled out at this time.

Veige and co-workers further demonstrated the utility of tungsten alkyldiene catalysts by extending REP to commercially relevant monomers. Linear polypropylene

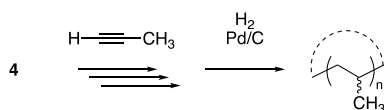


**Fig. 16.3** Metallacyclopentadiene intermediates in the ring expansion polymerization of alkynes

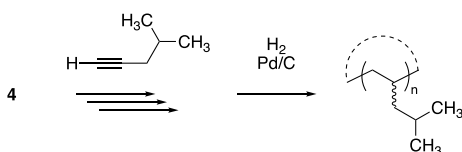
is arguably one of the most important commercial polymers, yet its cyclic version was unknown. To this end, the authors began with the REP of propyne followed by exhaustive hydrogenation to produce cyclic polypropylene (Scheme 16.6) [25]. The polymerization of propyne affords cyclic polypropyne, which possesses conjugated double bonds along the backbone. Complete hydrogenation of cyclic polypropyne with palladium on carbon (Pd/C) yields atactic cyclic polypropylene. GPC analysis indicated a cyclic topology for the product given the relative smaller size compared to a linear analogue. Interestingly, the glass transition temperature of the cyclic polymer is drastically higher than the linear analogue, which is explained in part by the smaller free volume of cyclic polymers. Rheological studies also showed distinguishable diffusion and relaxation processes for cyclic and linear polypropylene.

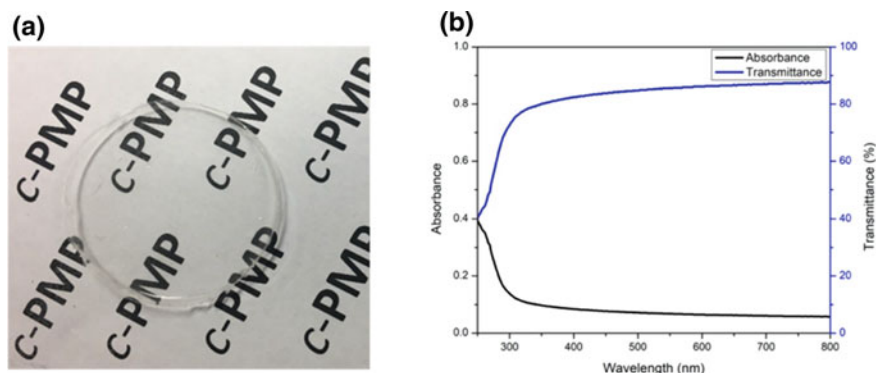
These authors also successfully polymerized 4-methyl-1-pentyne by REP and exhaustively hydrogenated the cyclic product to yield poly(4-methyl-1-pentene), an important commercially relevant transparent thermoplastic (Scheme 16.7) [26]. Rheological and thermal analysis indicated a cyclic topology, and the transparency was comparable to traditional linear polyolefins (Fig. 16.4). Finally, to show the versatility of this catalytic ring-expansion approach to synthesize a variety of large-scale commercially relevant polymers, Veige and co-workers used REP and hydrogenation to afford poly(1-pentyne) on a >10 g scale.

**Scheme 16.6** Synthesis of cyclic polypropylene

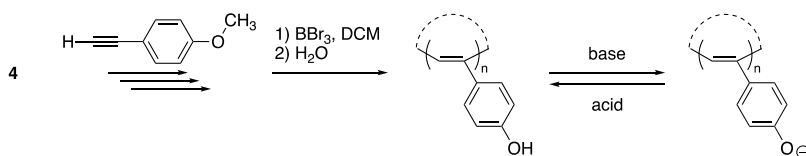


**Scheme 16.7** Synthesis of cyclic poly(4-methyl-1-pentene)





**Fig. 16.4** **a** Solvent-cast thin film of poly(4-methyl-1-pentene). **b** UV–Vis absorbance and transmittance of a poly(4-methyl-1-pentene) thin film. Adapted with permission from Ref. [23]. Copyright 2020 American Chemical Society

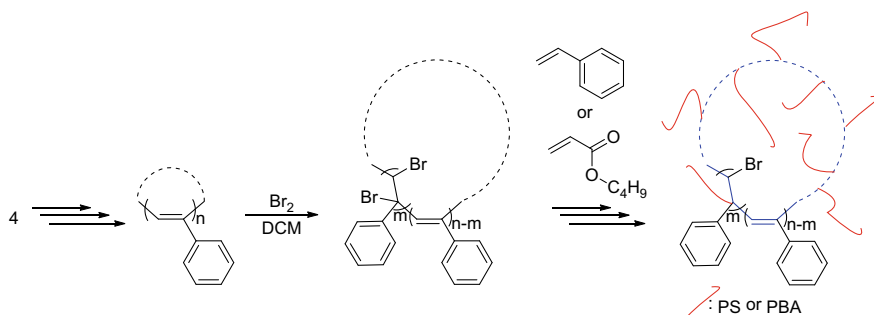
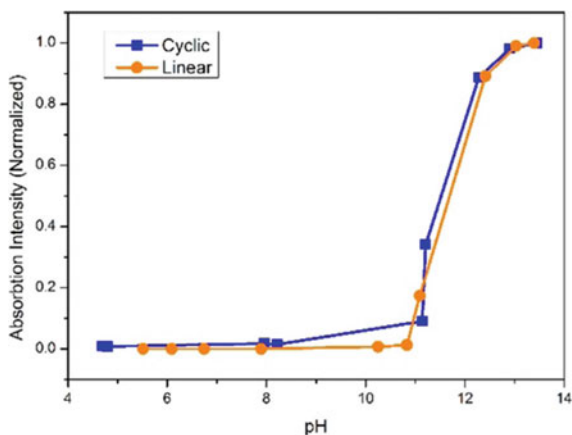


**Scheme 16.8** Synthesis of poly(4-ethynylphenol) and its pH-dependent structure

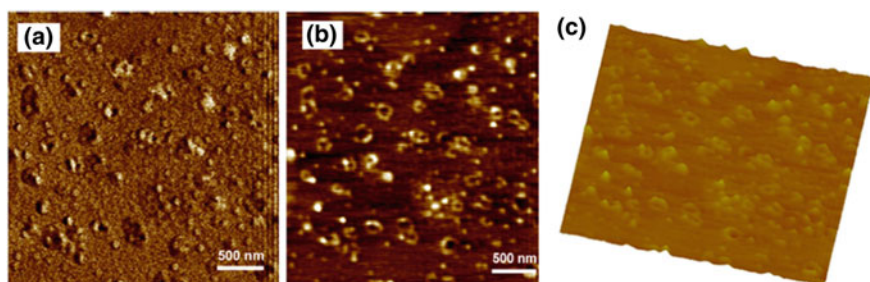
Because cyclic polymers are useful in some biomedical applications, it is important to determine the character of water-soluble cyclic polymers. To better understand the aqueous solution properties of cyclic polymers, Veige and co-worker synthesized poly(4-ethynylphenol), which contains a pendant pH-responsive phenol group (Scheme 16.8) [27]. In comparing the UV absorption of the cyclic product to linear analogues with similar molecular weights, the authors found that topology does not play a key role in pH responsiveness (Fig. 16.5).

Although comparative GPC analysis as well as thermal and rheological data clearly support the cyclic topology of the polymers produced using catalyst **4**, imaging from AFM can provide confirmation of cyclic architecture provided adequate resolution. Depending on graft lengths, AFM of cyclic bottlebrush polymers synthesized by “grafting from” a cyclic polymer provides unquestionable evidence for cyclic topology. Sumerlin and co-workers employed REP using catalyst **4** to make poly(PA) and subsequently brominated the double bonds in the backbone, creating atom transfer radical polymerization (ATRP) initiating sites throughout the ring. Grafting from ATRP with styrene or butylacrylate yields cyclic bottlebrush polymers (Scheme 16.9) [28]. AFM images clearly show the cyclic topology of the resulting brush polymers (Fig. 16.6), thus proving the formation of cyclic polymers by REP.

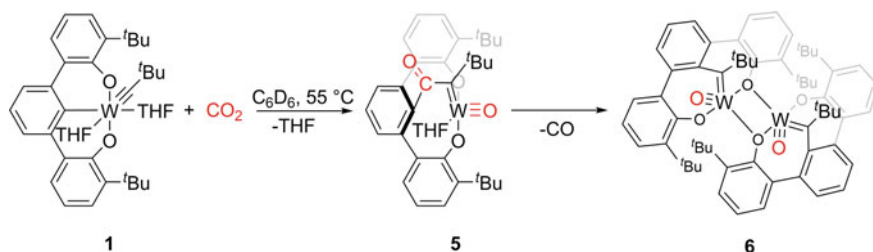
**Fig. 16.5** The pH-dependent UV absorption intensity at 294 nm of cyclic and linear poly(4-ethynylphenol). Reprinted with permission from Ref. [24]. Copyright 2019 American Chemical Society



**Scheme 16.9** Cyclic bottlebrush polymer synthesis via ring-expansion polymerization and atom transfer radical polymerization



**Fig. 16.6** AFM phase (a), height (b), and three-dimensional (c) images of cyclic bottlebrush polymers (styrene/macroiinitiator = 200/1). Adapted with Permission from Ref. [25]. Copyright 2020 American Chemical Society

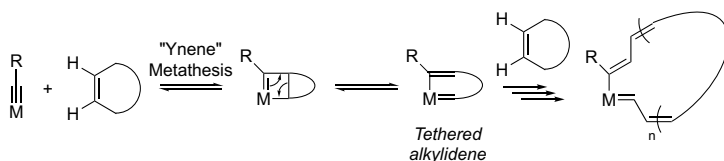


**Scheme 16.10** Synthesis of complexes **5** and **6**

### 16.2.2.2 Polymerization of Cycloalkenes

Veige and co-workers reported continued advances in REMP catalysis with the use of a novel tethered tungsten oxo alkylidene complex **5** for the REMP of norbornene [29]. The reaction of complex **1** with  $\text{CO}_2$  produces complexes **5** and **6** (Scheme 16.10) and extended heating of the product mixture results in complete conversion of **5** to **6**. Complexes **5** and **6** can be separated and complex **5** is more active toward the REMP of norbornene than complex **6** and treatment of a mixture of **5** and **6** with norbornene selects for catalysis by complex **5**. When treating each complex with excess norbornene, complex **5** yields *cis*-syndiotactic cyclic polynorbornene in good yields and complex **6** yields polynorbornene in relatively lower yields with no apparent stereoselectivity or regular tacticity. GPC data showed reduced intrinsic viscosities, reduced radii of hydration, and longer retention times for polynorbornene products indicating cyclic topology, while NMR analysis of the polynorbornene revealed its tacticity. The optimal REMP system using complex **5** produces cyclic polymers with molecular weights up to 578 kDa.

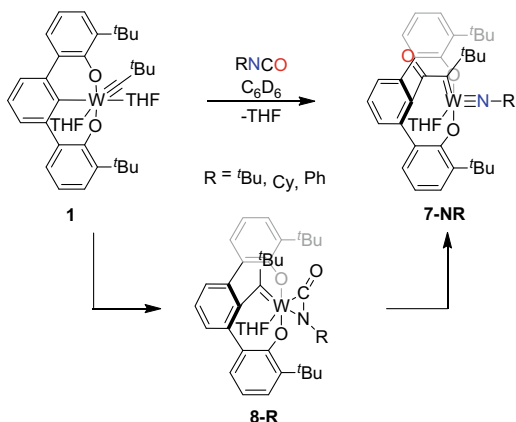
The Veige group later demonstrated that complex **1** can also catalyze the REMP of norbornene with high stereoselectivity and tacticity [30]. REMP of norbornene catalyzed by complex **1** follows an “Ynene” metathesis initiation, i.e., metathesis between an alkylidyne and an olefin (Scheme 16.11). Contrary to “Enyne” metathesis, defined by the metathesis of an alkylidene and an alkyne, the metathesis reactions between alkylidynes and olefins are rare [31]. The authors proposed that “Ynene” metathesis leads to a tethered alkylidene which acts as a catalyst for the stereoselective REMP of norbornene. Cyclic polynorbornene produced by **1** has a >99% *cis* conformation and is >95% syndiotactic.



**Scheme 16.11** “Ynene” metathesis to generate tethered alkylidene



**Scheme 16.12** Synthesis of complexes **8-R** and **7-NR**, where R = <sup>t</sup>Bu, Cy, and Ph

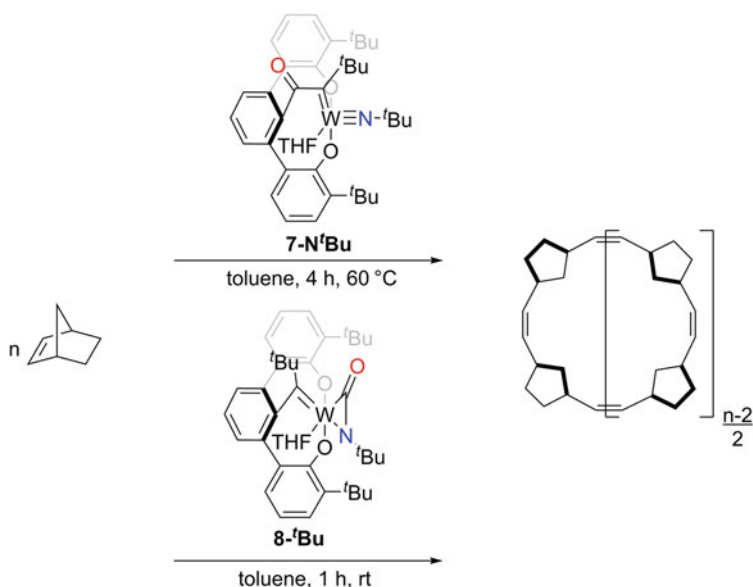


Carbon dioxide contains two symmetric C = O bonds, whereas isocyanates (R-N = C = O) are unsymmetrical. Both unsaturation sites in isocyanates are potentially susceptible to activation by alkylidyne **1**. C = O activation would lead to a W-oxo complex and C = N activation would lead to a W-imido complex. Treating complex **1** with isocyanates provides exclusively the W-imido complexes **7-NR** (Scheme 16.12) [32]. Distinct from the reaction with CO<sub>2</sub> complexes **7-NR** allow for modification. In fact, employing the larger <sup>t</sup>BuC = N = O lead to the isolation of the η<sup>2</sup>-(C,N) ligated intermediate (O<sub>2</sub>C<sup>t</sup>BuC = )W(η<sup>2</sup>-(C,N)-RN = C = O)(THF) (**8-<sup>t</sup>Bu**). Complex **8-<sup>t</sup>Bu** is an intermediate on the pathway to form **7-<sup>t</sup>Bu** (Scheme 16.12). The size of the R-group in the isocyanate indicates whether the η<sup>2</sup>-(C,N) complex is isolable, where smaller isocyanates are too fleeting to capture. Finally, adding to the short list of catalysts capable of REMP, complexes **6-NR** are active catalysts for the stereoselective synthesis of cyclic polynorbornene.

Complex **7-N<sup>t</sup>Bu** is an active catalyst for the stereoselective REMP of norbornene to give cyclic polynorbornene (Scheme 16.13; Table 16.1). <sup>1</sup>H and <sup>13</sup>C NMR spectra are consistent with *cis*-syndiotactic polynorbornene (>95% *cis*, >97% syndiotactic). The imido ligand on **7-<sup>t</sup>Bu**, not surprisingly, must slow the polymerization rate since **8-<sup>t</sup>Bu** does not require heating and the reactions are complete within 1 h (Table 16.2).

## 16.3 Conclusion

Historically, synthesizing pure cyclic polymers on a large scale with a broad monomer scope is challenging. The recent advances in ring-expansion polymerization using novel tethered transition metal catalysts offer unparalleled advantages due to the modularity and efficiency of these systems. Commercially relevant cyclic polymers are now attainable on scales that may enable large-scale applications. Metal catalysts containing a tethered structure afford highly pure cyclic polymers from cycloalkenes



**Scheme 16.13** Polymerization of norbornene by catalyst 7-N<sup>t</sup>Bu and 8-tBu to generate stereoregular cyclic polynorbornene

**Table 16.1** Polymerization of norbornene<sup>a</sup> with catalyst 7-N<sup>t</sup>Bu

[mon]/[cat] <sub>0</sub>	[mon] <sub>0</sub> <sup>b</sup>	Yield (%)	% <i>cis</i> <sup>c</sup>	<i>M<sub>n</sub></i> <sup>d</sup> (kDa)	<i>M<sub>w</sub></i> / <i>M<sub>n</sub></i> <sup>d</sup>
50:1	0.25	75	95	1,940	1.53
100:1	0.25	67	95	633	3.23
200:1	0.25	42	94	677	3.19
400:1	0.25	27	95	727	2.45

<sup>a</sup> The appropriate amount of a catalyst solution in toluene (10 mg/mL) is added to norbornene (50 mg) dissolved in toluene and stirred for 4 h at 60 °C

<sup>b</sup> mol L<sup>-1</sup>

<sup>c</sup> Determined by <sup>1</sup>H NMR spectroscopy

<sup>d</sup> Determined by size-exclusion chromatography (SEC) using dichlorobenzene as the mobile phase at 140 °C with a conventional calibration based on narrow polystyrene standards

and linear alkynes. Innovation in the post-polymerization modification of cyclic polymers is expanding the scope of attainable polymeric materials while providing a creative way to determine the topology of the initial polymer. Exploring REP and REMP using tethered transition metal catalysts is paving a path toward a deeper understanding and potentially broader application of cyclic polymers. The field of cyclic polymer chemistry is expanding by adopting catalytic methods that allow for catalyst tuning. A clear example of successful tuning comes from the stereoselective synthesis of cyclic polynorbornene. Understanding the mechanism for polymerization using these tethered alkylidene complexes continues to unfold. The origin of

**Table 16.2** Polymerization of norbornene<sup>a</sup> with catalyst 8-N<sup>t</sup>Bu

[mon]/[cat] <sub>0</sub>	[mon] <sub>0</sub> <sup>b</sup>	Yield (%)	% <i>cis</i> <sup>c</sup>	<i>M</i> <sub>n</sub> <sup>d</sup> (kDa)	<i>M</i> <sub>w</sub> / <i>M</i> <sub>n</sub> <sup>d</sup>
50:1	0.25	95	99	436	2.02
100:1	0.25	93	99	546	3.61
200:1	0.25	80	99	458	2.09
400:1	0.25	64	99	1,499	2.11

<sup>a</sup> The appropriate amount of a catalyst solution in toluene (10 mg/mL) is added to norbornene (50 mg) dissolved in toluene and stirred for 1 h at ambient temperature

<sup>b</sup> mol L<sup>-1</sup>

<sup>c</sup> Determined by <sup>1</sup>H NMR spectroscopy

<sup>d</sup> Determined by size-exclusion chromatography (SEC) using dichlorobenzene as the mobile phase at 140 °C with a conventional calibration based on narrow polystyrene standards

the stereoselectivity in REMP of norbornene with catalysts **1** remains unknown and more vetting of the proposed ring expansion of alkynes with catalyst **4** is needed.

Now with many methods for producing cyclic polymers available, the next phase of cyclic polymer chemistry is ready for exploitation. The cyclic polymers described in this work are amenable to further functionalization. Perhaps the next step in cyclic polymer synthesis is not to produce new polymers from new monomers, but to functionalize the polymers already available. Post-polymerization modification can significantly expand the current synthetic space. Imaging of bottlebrush cyclic polymers derived from post-polymerization functionalization was the goal in Fig. 16.6, but the area is ripe for other applications. The polymers produced from alkynes offer easy entry to functionalization through the double bonds. Only a decade ago the scope of cyclic polymers was limited to a few archetypes. With the new methods described in this chapter, it is reasonable to expect an exponential growth and we will be able to answer using large-scale samples, lingering fundamental questions regarding cyclic polymer properties in the solid, melt, dilute, and liquid phases.

**Acknowledgements** Ongoing catalyst development and study is supported by the National Science Foundation under grant CHE-1265993 and CHE-1856674. Application of cyclic polymers, their synthesis, and characterization are supported by CHE-1808234.

## References

1. Y. Tezuka, H. Oike, Prog. Polym. Sci. **27**, 1069 (2002)
2. J.M. García Bernal, M.M. Tirado, J.J. Freire, J. de la Torre García, Macromolecules **24**, 593 (1991)
3. D.J. Orrah, J.A. Semlyen, S.B. Ross-Murphy, Polymer (Guildf) **29**, 1455 (1988)
4. S.J. Clarson, K. Dodgson, J.A. Semlyen, Polymer (Guildf) **26**, 930 (1985)
5. N. Nasongkia, B. Chen, N. Macaraeg, M.E. Fox, J.M.J. Fréchet, F. Szoka, J. Am. Chem. Soc. **131**, 3842 (2009)
6. H. Wei, C.E. Wang, N. Tan, A.J. Boydston, S.H. Pun, ACS Macro Lett. **4**, 938 (2015)

7. B. Chen, K. Jerger, J.M.J. Fréchet, F.C. Szoka, J. Control. Release **140**, 203 (2009)
8. B.A. Laurent, S.M. Grayson, Chem. Soc. Rev. **38**, 2202 (2009)
9. B.A. Laurent, S.M. Grayson, J. Am. Chem. Soc. **128**, 4238 (2006)
10. C.W. Bielawski, D. Benitez, R.H. Grubbs, Science **297**, 2041 (2002)
11. H.R. Kricheldorf, S.R.P. Lee, Macromolecules **28**, 6718 (1995)
12. H.R. Kricheldorf, M. Al-Masri, G. Schwarz, Macromolecules **35**, 8936 (2002)
13. K.J. Shea, S.Y. Lee, B.B. Busch, J. Org. Chem. **63**, 5746 (1998)
14. M. Ouchi, H. Kammiyada, M. Sawamoto, Polym. Chem. **8**, 4970 (2017)
15. D.A. Culkun, W. Jeong, S. Csihony, E.D. Gomez, N.P. Balsara, J.L. Hedrick, R.M. Waymouth, Angew. Chem. Int. Ed. **46**, 2627 (2007)
16. C.W. Bielawski, D. Benitez, R.H. Grubbs, J. Am. Chem. Soc. **125**, 8424 (2003)
17. Y. Xia, A.J. Boydston, R.H. Grubbs, Angew. Chem. Int. Ed. **50**, 5882 (2011)
18. A.J. Boydston, T.W. Holcombe, D.A. Unruh, J.M.J. Fréchet, R.H. Grubbs, J. Am. Chem. Soc. **131**, 5388 (2009)
19. K. Zhang, M.A. Lackey, J. Cui, G.N. Tew, J. Am. Chem. Soc. **133**, 4140 (2011)
20. S. Sarkar, K.P. McGowan, S. Kuppaswamy, I. Ghiviriga, K.A. Abboud, A.S. Veige, J. Am. Chem. Soc. **134**, 4509 (2012)
21. K.P. McGowan, M.E. O'Reilly, I. Ghiviriga, K.A. Abboud, A.S. Veige, Chem. Sci. **4**, 1145 (2013)
22. C.D. Roland, S. VenkatRamani, V.K. Jakhar, I. Ghiviriga, K.A. Abboud, A.S. Veige, Organometallics **37**, 4500 (2018)
23. C.D. Roland, H. Li, K.A. Abboud, K.B. Wagener, A.S. Veige, Nat. Chem. **8**, 791 (2016)
24. C.D. Roland, T. Zhang, S. VenkatRamani, I. Ghiviriga, A.S. Veige, Chem. Commun. **55**, 13697 (2019)
25. W. Niu, S.A. Gonsales, T. Kubo, K.C. Bentz, D. Pal, D.A. Savin, B.S. Sumerlin, A.S. Veige, Chem **5**, 237 (2019)
26. Z. Miao, D. Pal, W. Niu, T. Kubo, B.S. Sumerlin, A.S. Veige, Macromolecules **53**, 7774 (2020)
27. Z. Miao, T. Kubo, D. Pal, B.S. Sumerlin, S.A. Veige, Macromolecules **52**, 6260 (2019)
28. D. Pal, Z. Miao, J.B. Garrison, A.S. Veige, B.S. Sumerlin, Macromolecules **53**, 9717 (2020)
29. S.A. Gonsales, T. Kubo, M.K. Flint, K.A. Abboud, B.S. Sumerlin, A.S. Veige, J. Am. Chem. Soc. **138**, 4996 (2016)
30. S.S. Nadif, T. Kubo, S.A. Gonsales, S. VenkatRamani, I. Ghiviriga, B.S. Sumerlin, A.S. Veige, J. Am. Chem. Soc. **138**, 6408 (2016)
31. F.R. Kreibl (ed.), *Transition Metal Carbyne Complexes* (Springer, Dordrecht, The Netherlands, 1993)
32. V. Jakhar, D. Pal, I. Ghiviriga, K.A. Abboud, D.W. Lester, B.S. Sumerlin, A.S. Veige, J. Am. Chem. Soc. **143**, 1235 (2021)

# Chapter 17

## Synthesis of Cyclic Vinyl Polymers via *N*-Heterocyclic Carbene (NHC)-Initiated Anionic Polymerization and Subsequent Ring-Closure Without Highly Dilute Conditions



Yuki Muramatsu and Akinori Takasu

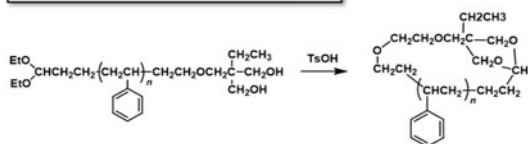
In this chapter, we introduce recent progress on cyclic polymer synthesis using chain polymerization techniques including controlled radical polymerizations of vinyl monomers combined with click chemistries as well as metathesis polymerization of cyclic olefins or several alkynes. In order to eliminate highly diluted conditions ( $[M]_0 < 1.0$  mM) for the ring-closure, supra chemistries including electrostatic self-assembly and rotaxane are practical. We introduce our original procedure, *N*-heterocyclic carbene-initiated anionic polymerization of vinyl monomers and subsequent ring-closing, in which we do not have to use highly diluted condition ( $[M]_0 = 1.0$ – $2.0$  M).

### 17.1 Research Background in Synthesis of Cyclic Polymers via Chain Polymerization

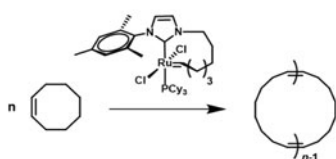
Advanced chemical procedures allowing precise control of the structure also enable us to discuss topological effects on the properties. Cyclic polymers possess unique characteristics due to the absence of polymer termini. They show different bulk and solution properties from their corresponding linear counter parts, i.e., smaller hydrodynamic volume and radius of gyration ( $R_g$ ), [1] lower intrinsic viscosity, [2] higher critical solution temperature, [2] increased rate of crystallization, [3] and higher refractive index [4]. In order to make progress in this research field, innovative synthetic procedures, particularly in chain polymerization, are essential, although cyclic polymers are well-known as a byproduct in step polymerization. A facile

---

Y. Muramatsu · A. Takasu (✉)  
Gokiso-Cho, Nagoya 466-855, Japan  
e-mail: [takasu.akinori@nitech.ac.jp](mailto:takasu.akinori@nitech.ac.jp)

**Ring-closure**A. Deffieux, et al. *Macromolecules*, 2001.

- Applicable to many monomers
- Requires highly dilute conditions
- Tedious multistep procedure

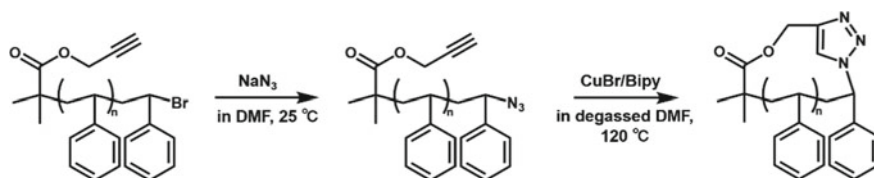
**Ring-expansion polymerization**R. H. Grubbs et al. *Science*, 2002.

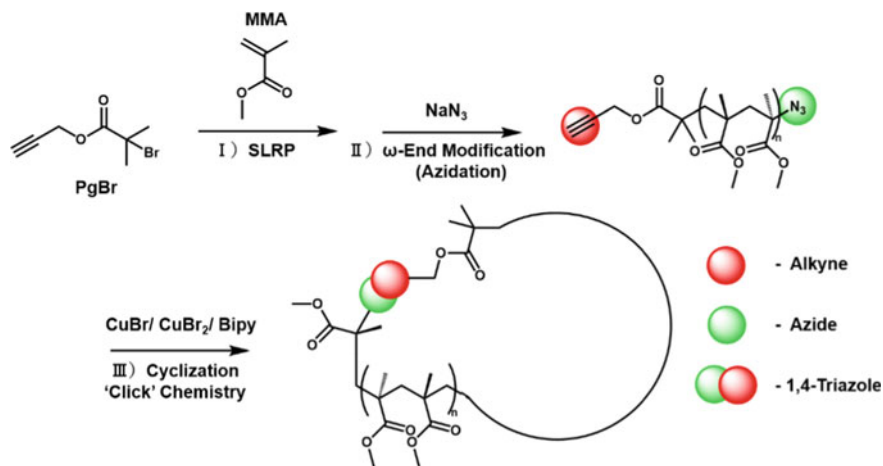
- Does not require high dilutions
- Limited to cyclic monomers and initiators

**Fig. 17.1** Two independent pathways for synthesis of cyclic polymers

synthetic pathway has made it possible to synthesize a series of cyclic polymers—a “cyclic polymer library”. The synthetic strategy for cyclic polymers via chain polymerization principally has two typical types, one being ring-closure of functional linear polymers and the other ring-expansion polymerization using cyclic monomers, initiator, or catalyst (Fig. 17.1).

For ring-closure of polymer precursors, functionalization of polymer termini [5, 6] is essential, but it is a tedious multistep procedure and needs excess amounts of reagent in order to attain high functionalization. Alternatively, controlled polymerization of vinyl monomers, including atom transfer radical polymerization (ATRP) and reversible addition-fragmentation chain transfer (RAFT) polymerization is useful for the parent linear precursors and molecular weight control is easy to achieve. However, fidelity of terminal functionality and high dilution in order to avoid intermolecular functionalization are requisites. Depending on the terminal functionality, [7, 8] recent progress in click chemistry has played an important role in intramolecular cyclization. In 2006, Laurent and Grayson [9] showed the first example of intramolecular ring-closing of a linear precursor having  $\alpha$ -alkynyl and  $\omega$ -azido termini combined with ATRP (Fig. 17.2). Later, cyclic poly(*N*-isopropylacrylamide) [10] and poly(acrylic acid) [11] were synthesized using this synthetic strategy.

**Fig. 17.2** First report of the synthesis of a cyclic vinyl polymer via ATRP and intramolecular click reaction of an  $\alpha$ -alkynyl- $\omega$ -azido linear precursor



**Fig. 17.3** Synthesis of cyclic syndiotactic poly(methyl methacrylate) via ATRP and “click” cyclization. From Ref. [12] Copyright © 2014 by John Wiley Sons, Inc. Reprinted by permission of John Wiley & Sons, Inc.

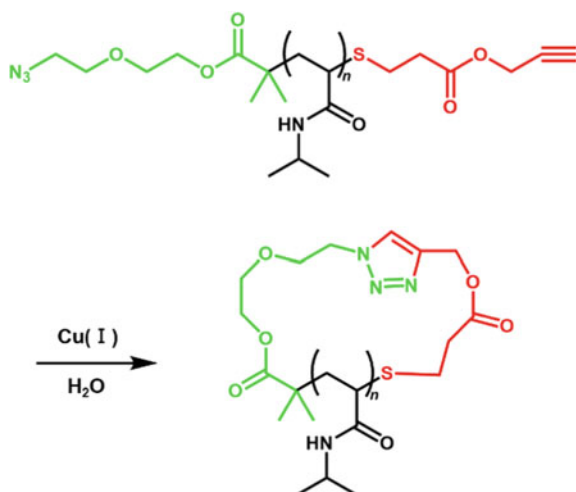
Now this powerful tool enabled us to synthesize even a stereoregular polymer, i.e., syndiotactic cyclic poly(methyl methacrylate) (Fig. 17.3), which inspired the field of self-assembly, also known as supramolecular science. Kamigaito et al. prepared syndiotactic cyclic poly(methyl methacrylate) stereo-complexed with linear isotactic poly(methyl methacrylate) to give a necklace-type “polypseudorotaxane”, which showed remarkable different thermal properties from the stereo-complex consisting of linear stereoregular poly(methyl methacrylate)s [12].

The combination of this approach with RAFT polymerization is also a versatile tool. In 2007, Winnik<sup>2</sup> reported a typical example of cyclic poly(*N*-isopropylacrylamide) made via RAFT polymerization and subsequent ring-closing of the telechelic polymer (Fig. 17.4), although this seems to suffer from a complicated pathway and severe reaction conditions. Stamenovic et al. [13] reported a thiolactone-containing RAFT agent, which initiated styrene monomer to give poly(styrene) containing  $\alpha$ -thiolactone and  $\omega$ -dithiobenzoate groups, followed by aminolysis to afford the corresponding  $\alpha$ ,  $\omega$ -dithiol linear precursor. The cyclization was induced under highly dilute conditions. Similar combinations were applied to synthesize cyclic poly(*tert*-butyl acrylate), poly(*N*-isopropylacrylamide), and poly(*N,N'*-dimethylacrylamide).

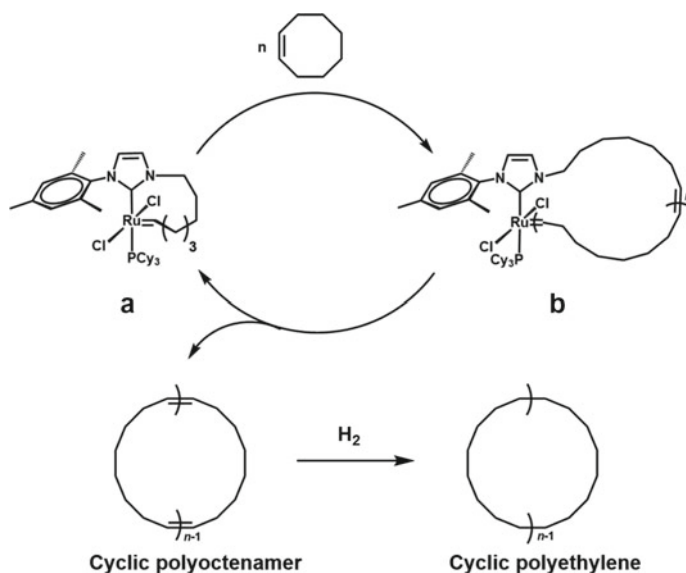
Although the combination of controlled polymerization with click chemistry shed light on the synthesis of cyclic polymers, extremely low concentrations were still essential to avoid intermolecular coupling in this cyclization procedure [14, 15].

One solution for removing the highly dilute condition in the chain polymerization mechanism is the ring-expansion metathesis polymerization (REMP) of cycloalkenes developed by Grubbs and co-workers [16, 17]. Using a cyclic ruthenium

**Fig. 17.4** Synthesis of cyclic poly(*N*-*iso*-propylacrylamide) via RAFT polymerization and “click” ring-closure



initiator/catalyst, generally known as a “Grubbs catalyst”, ring-expansion polymerization was carried out on strained cyclic olefins and after monomer depletion a backbiting termination occurs to remove the ruthenium catalyst giving the expected cyclic polyolefins (Fig. 17.5).

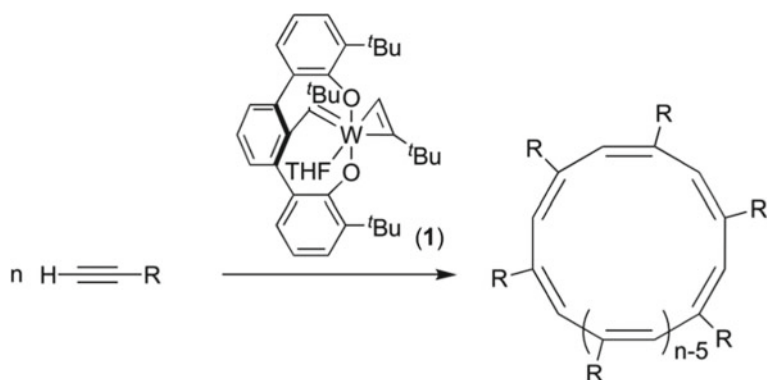


**Fig. 17.5** Synthesis of cyclic polymers using REMP. Addition of *cis*-cyclooctene (monomer) to cyclic complex **a** resulted in the transient formation of macrocyclic complex **b**. Subsequent intramolecular chain transfer provided cyclic polyoctenamer and regenerated **a**. Hydrogenation of the cyclic polyoctenamer afforded cyclic polyethylene

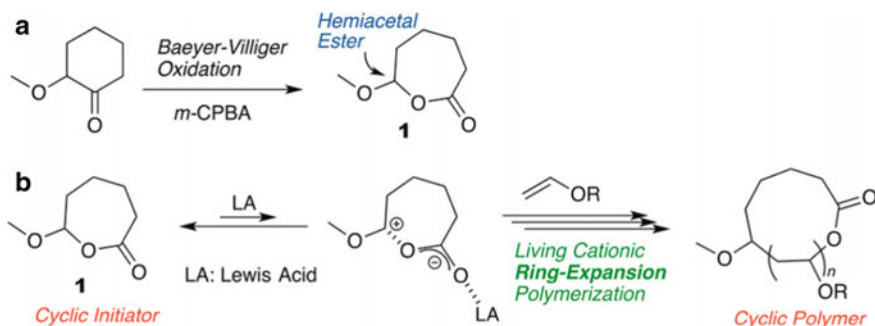


Recently, Veige et al. demonstrated REMP of propynes with a tungsten complex catalyst, followed by subsequent hydrogenation to generate cyclic polypropylene [18]. This work allows for the study of the cyclic analogue of a widely used commodity polymer. For example, recently, Miao et al. [19] discovered chain polymerization of an alkyne, 4-methyl-1-pentyne, with a tungsten alkylidyne catalyst and subsequent hydrogenation (>99%) provided cyclic poly(4-methyl-1-pentene) (Fig. 17.6). Evidence of a cyclic topology comes from rheology/viscosity studies, light scattering measurements, and size-exclusion chromatography.

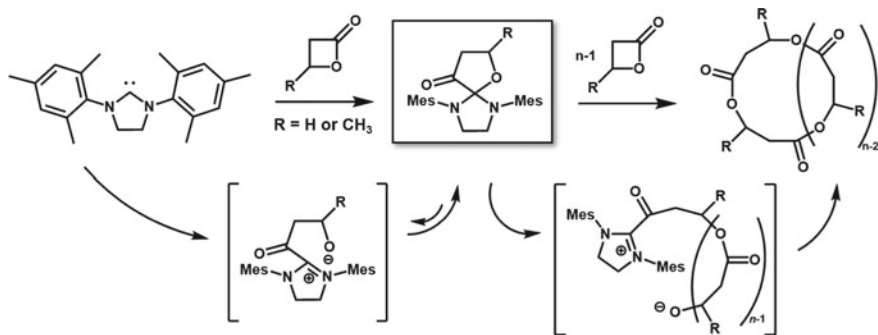
According to REMP of vinyl monomers, Ouchi et al. reported a synthesis of cyclic poly(vinyl ether)s. In their trials, a cyclic acetal was used as the cationic initiator and the quantitative monomer consumption was demonstrated but highly dilution was necessary to avoid fusion between cyclic propagating chains [20, 21] (Fig. 17.7). They also extended this synthetic procedure to ring-expansion cationic polymerization of acyclic divinyl monomers to give a cyclic “cyclopolymer” [22].



**Fig. 17.6** Schematic representation of catalytic synthesis of cyclic polyenes from alkynes. Reprinted from Ref. [19]. Copyright (2020) American chemical Society



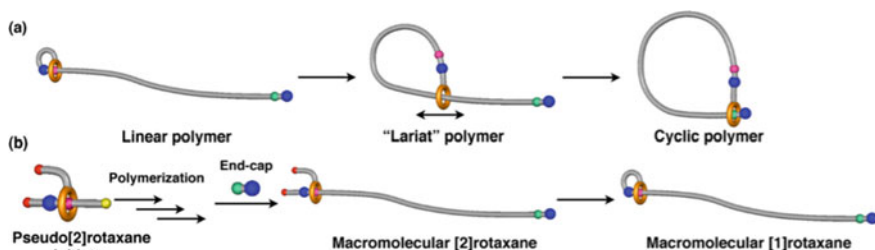
**Fig. 17.7** Schematic representation of (a) synthesis of cyclic initiator (**1**) and (b) ring-expansion living cationic polymerization of vinyl ethers with **1** (*m*-CPBA: *m*-chloroperoxybenzoic acid). Reprinted from Ref. [20]. Copyright (2013) American chemical Society



**Fig. 17.8** Organic spirocyclic initiators for the ring-expansion polymerization of  $\beta$ -lactones [23]

Pioneering work using ring-expansion of heterocyclic monomers by zwitterionic propagation (RE) is an alternative ring-expansion technique using metal-free organocatalytic *N*-heterocyclic carbene (NHC) catalysts, termed zwitterionic ring-expansion polymerization (RE), to generate cyclic polyesters from lactone (cyclic) monomers (Fig. 17.8) [23–25]. This work has also been extended using similar catalysts to prepare cyclic polypeptides [26] and polypeptoids [27].

In order to eliminate highly dilute conditions, electrostatic self-assembly and covalent fixation (ESA-CF), [28] a method where polymers with ionic end groups self-assemble with counter ionic linkers to impart various polymer topologies, was investigated by Suzuki et al. [29] By employing rotaxanes to promote cyclization, Ogawa et al. [30] and Aoki et al. [31] eliminated the need for dilute conditions and permitted multigram-scale synthesis. In their work, cyclic PCL was prepared by ring-opening polymerization of  $\epsilon$ -caprolactone ( $\epsilon$ -CL) initiated by a pseudo[2]rotaxane initiator in the presence of diphenylphosphate (DPP) as a catalyst, followed by capping of the propagation end by using a bulky isocyanate to afford macromolecular[2]rotaxane. The following intramolecular cyclization to macromolecular [1]rotaxane at the polymer terminus proceeded with good yield (Fig. 17.9b). The attractive interaction of the terminal ammonium/crown ether moiety was removed via *N*-acetylation.



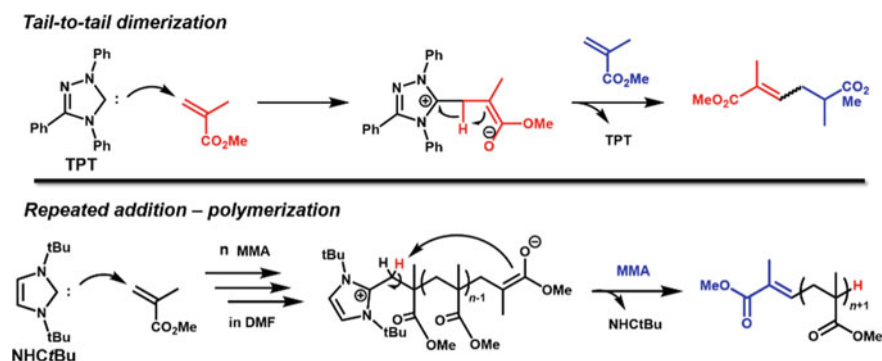
**Fig. 17.9** **a** Structural transformation to cyclic polymer and **b** synthetic strategy using the rotaxane-from method of macromolecular [1]rotaxane. Reprinted from Ref. [30]. Copyright (2015) American chemical Society

This enabled movement of the crown ether wheel along the axle PCL chain to the urethane region of the other terminus in the solution state (Fig. 17.9a).

Among the synthetic techniques for generating cyclic polymers, there is still no single technique that surpasses the rest, but rather each technique exhibits a unique set of advantages and disadvantages. The REMP technique, categorized in chain polymerization, is a powerful tool for affording polymers of high purity and high molecular weight, though it is still very difficult to attain controlled molecular weights and polydispersities, because we cannot control when the ring-expansion is terminated in each macrocycle. Therefore, molecular weight control using chain polymerization technique, including living polymerization, without highly diluted conditions is still a challenging subject.

## 17.2 NHC-Initiated Anionic Polymerization of Alkyl Sorbate in the Presence of Bulky Lewis Acid and Subsequent Ring-Closure Without Highly Dilution

Since Arduengo succeeded in isolation of a carbene, *N*-heterocyclic carbene (NHC), [32] a series of reactive carbenes have turned out to be versatile nucleophiles. According to trials of the polymer synthesis, Matsuoka et al. first tried for NHC-initiated anionic polymerization of methyl methacrylate (MMA) [33]. They used an NHC, 1,3,4-triphenyl-4,5-dihydro-1H-1,2,4-triazol-5-ylidene (TPT), as the anionic initiator. However, using a weaker nucleophile but a better leaving group than those found in a typical initiator, such as alkylolithium, MMA undergoes 1,2-proton transfer to generate the enamine; this is followed by nucleophilic attack on a second MMA monomer, to afford a tail-to-tail dimer of MMA via umpolung (Fig. 17.10, upper)

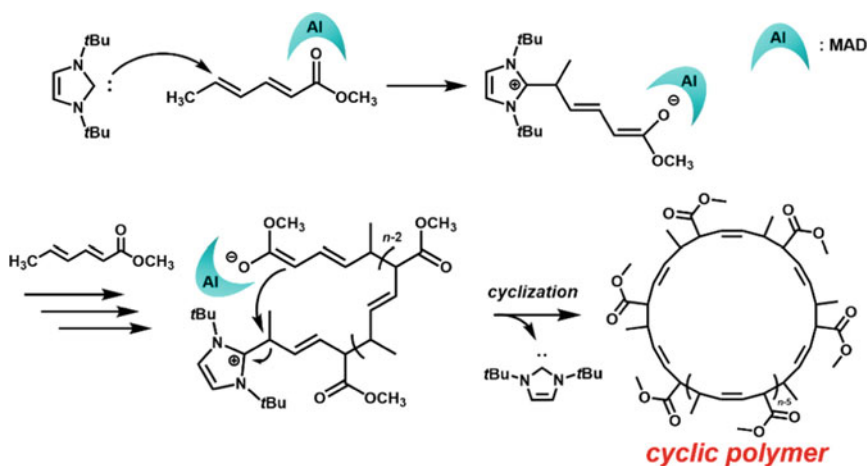


**Fig. 17.10** TPT catalyzed tail–tail dimerization (above) and NHC*t*Bu-initiated anionic polymerization of MMA

[33, 34]. Similar umpolung of a 1:1 adduct of TPT and MMA was reported by Glorius et al. and a similar tendency is well-recognized [35].

In 2013, Chen et al. [36] found that another NHC, 1,3-di-*tert*-butylimidazolin-2-ylidene (NHC*t*Bu) initiated anionic polymerization of MMA, but after monomer consumption, umpolung occurs to give linear poly(MMA) via an enamine intermediate (Fig. 17.10, lower).

We considered that addition of a Lewis acid lowers the basicity of the propagating anion by sharing the negative charge of the enolate oxygen and thus raises the barrier of the intra- or inter-molecular proton transfers. In 2017, we reported a first trial of NHC*t*Bu-initiated anionic polymerization of methyl sorbate (MS) in the presence of a bulky aluminum Lewis acid, aluminum di(2,6-di-*tert*-butyl-4-methylphenoxy) (MAD) [37]. MAD is well-known as a versatile Lewis acid [38] and is commercially available. Sorbates, a bio-refinery monomer containing two carbon–carbon double bonds conjugated to an ester, were thus added to the scope of cyclic polymers and are interesting because of the unique tritactic polymer structure (two chiral centers and *cis*-/*trans*-geometry per repeat unit). We had a previous experience of anionic polymerization of sorbates in the presence of MAD in a collaborative project with Prof. Hirabayashi [39–41], in which threeo-disyndiotactic poly(MS) was synthesized via a 1,4-*trans* addition mode [41]. This research background prompted us to try NHC*t*Bu-initiated anionic polymerization of sorbates with the expectation of simultaneous control of the primary structure, such as the 1,4-addition regioselectivity and stereoregularity (threeo-disyndiotactic), as well as the topological control induced by S<sub>N</sub>2-type macrocyclization to form cyclic poly(MS) (Fig. 17.11) [37]. In fact, quantitative monomer consumption in the anionic polymerization of MS ([M]<sub>0</sub>: 1.0–2.0 M) was observed in the presence of MAD to afford the cyclic poly(MS) with a 1,4-*trans* structure, 86% of threeo diastereoselectivity, and an *M*<sub>n</sub> of 23.0 ×



**Fig. 17.11** NHC*t*Bu-initiated anionic polymerization of MS and subsequent ring-closing without highly dilute condition

$10^3$  with a narrow molecular weight distribution ( $M_w/M_n = 1.17$ ) without the need for highly dilute conditions [37]. The narrow molecular weight distribution was attained because MAD accelerated propagation compared with ring-closure, i.e., after monomer consumption, ring-closing occurred via nucleophilic attack of a  $\omega$ -terminal enolate toward the  $\alpha$ -terminal carbon-covalently bonded to NHC*t*Bu, which acted an excellent leaving group. It seems that NHC*t*Bu acted not only as initiator in the initiation process but also as counter cation, an imidazolium, during the propagation. The neighboring ion pair compensates the entropic penalty of coupling of two polymer termini. This finding is a remarkable revolution in the frontier synthesis of cyclic polymers via a ring-closure procedure.

### 17.3 Expansion of Range of Acceptable Vinyl Monomers

First, we tried a simple application using one of the most common vinyl monomers, methyl methacrylate (MMA). NHC*t*Bu-initiated anionic polymerization of MMA underwent in the presence of MAD ( $[MAD]_0/[NHCtBu]_0 = 3/1$ ) and, after quantitative monomer depletion, a methylene proton neighboring the  $\alpha$ -terminal NHC*t*Bu residue was abstracted by the propagating anion to afford linear poly(MMA) (Fig. 17.12a). When we used methyl crotonate (MC),  $\alpha$ ,  $\beta$ -disubstituted vinyl monomer, as the monomer, NHC*t*Bu attacked first one monomer and subsequently a second monomer was inserted into the produced anion. However, the propagating anion abstracted the  $\alpha$ -carbonyl (acidic) proton to give a head-to-tail dimer, accompanied with the release of NHC*t*Bu (Fig. 17.12b). From these results, we concluded that the MS unit in the  $\alpha$ -terminal unit, the methine and vinyl protons are difficult to abstract, which induced anionic polymerization until monomer consumption (Fig. 17.12c).

In order to expand the range of acceptable monomers, a more general methodology for synthesizing cyclic polymers from any methacrylate was demonstrated by initiating polymerization on only 1 equiv of MS and subsequently adding to the reaction many more equivalents of MMA which proceeded to polymerize until monomer consumption, at which point the PMMA-enolate performs a  $S_N2$  type of ring-closure to afford a well-defined cyclic PMMA (Fig. 17.13) [42].

This study triggered us to extensively investigate a range of acceptable vinyl monomers. In our attempts [42–44] using an adduct of NHC*t*Bu and MS as the initiation species, umpolung (dipole inversion) [33–35] of Michael acceptors via  $\alpha$ -terminal proton abstraction by the propagating anion was suppressed, while the MAD-assisted polymerization accelerated the propagation of the methacrylates before quantitative monomer depletion, which enabled us to synthesize cyclic poly(allyl methacrylate) [poly(AMA)] [43] and poly(*N*-substituted maleimide)s [44] (Fig. 17.14).

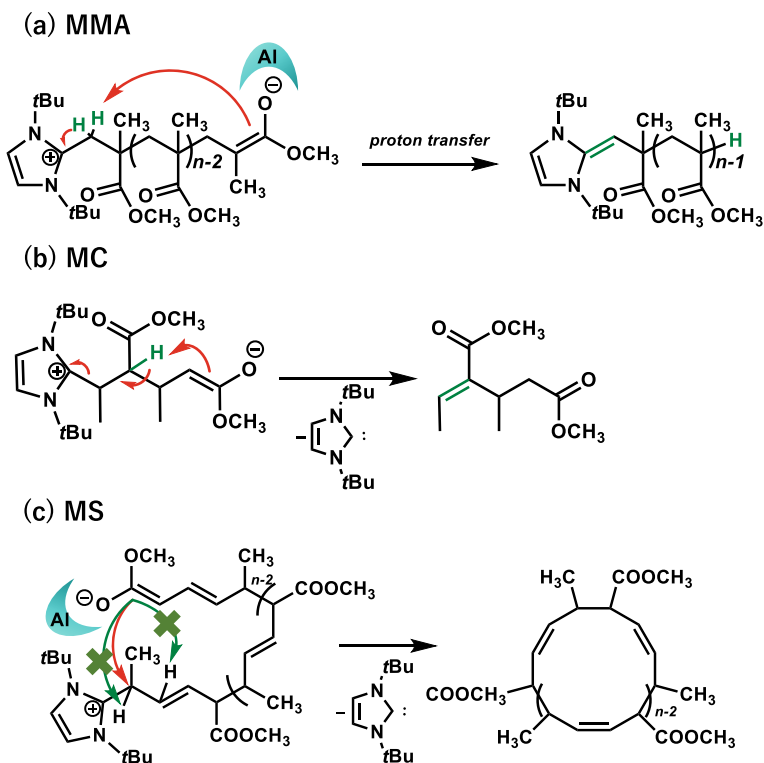


Fig. 17.12 Expansion of acceptable vinyl monomers

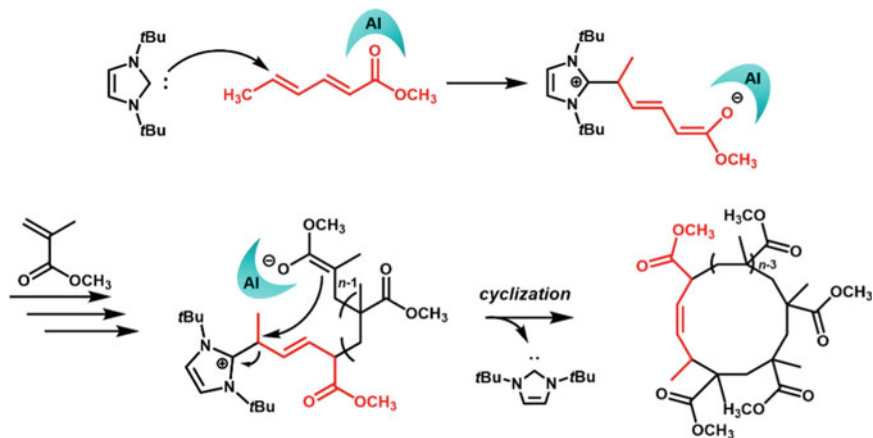
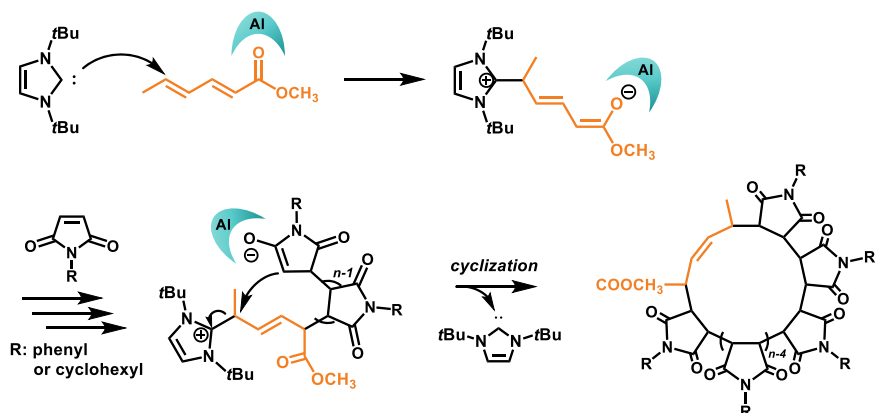


Fig. 17.13 Anionic polymerization initiated by 1:1 adduct of MS and NHCtBu and subsequent ring-closure affording cyclic poly (MMA)

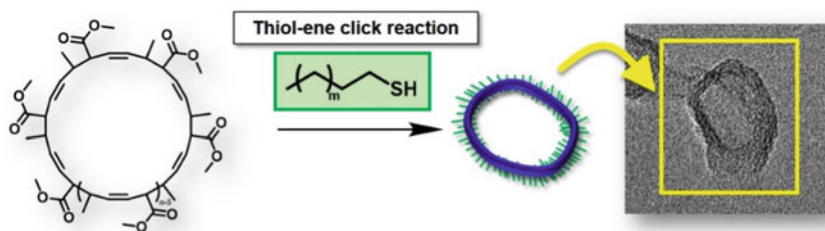


**Fig. 17.14** Anionic polymerization initiated by 1:1 adduct of MS and NHC*t*Bu and subsequent ring-closure affording cyclic poly(*N*-substituted maleimide)s [44]

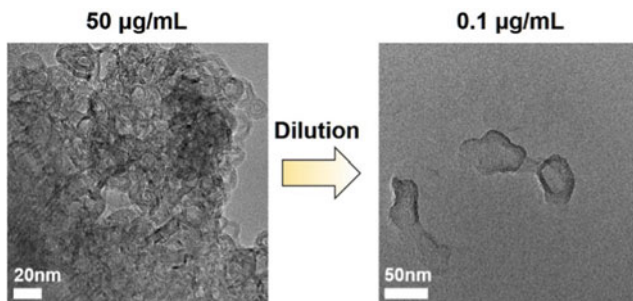
## 17.4 Direct Observation of Cyclic Structures

In the ring-closure procedure, reducing contamination by linear counterparts is critical because such contamination often influences the physical properties. In order to prove the reliability of this new synthetic concept, we decided that microscopic observation using transmission electron microscope (TEM) would be one of the powerful tools at our disposal. As described in our first report on cyclic poly(MS), longer alkylthiols were inserted onto the internal double bonds of the poly(MS) main chain via a thiol-ene click reaction (Fig. 17.15) [45].

After the click reaction between the thiol group of 1-octadecanethiol and the internal double bonds of poly(MS), the intensity of the <sup>1</sup>H peak assigned to the internal double bond of MS units decreased and a new peak was observed. The new peak originated from the methylene group (CH<sub>2</sub>) adjacent to the thiol group. The change of NMR signals was accompanied with a shift of the SEC trace to a high



**Fig. 17.15** Direct TEM observation of cyclic poly(MS) prepared via NHC*t*Bu initiated anionic polymerization



**Fig. 17.16** TEM observation of cyclic-poly(MS)-35-C<sub>18</sub> prepared by the toluene solution with 50 g/mL and 0.1 g/mL

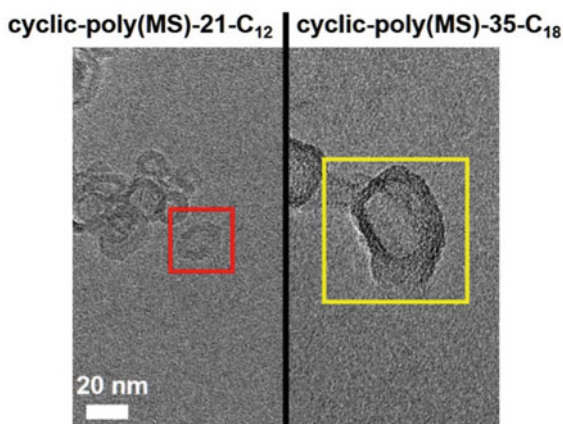
elution region compared with the parent cyclic poly(MS). The thiol-ene reaction using another alkanethiol, i.e., 1-dodecanethiol, was also carried out using a similar experimental procedure. Herein, the sample is coded as cyclic-poly(MS)-35-C<sub>18</sub>, where “35” and “C<sub>18</sub>” represents the molecular weight of the component cyclic-poly(MS) with a unit of kg/mol and the number of carbons of 1-octadecanethiol used in the thiol-ene reaction. Similarly, the sample using 1-dodecanethiol is coded as cyclic-poly(MS)-21-C<sub>12</sub>.

The synthesized graft-like cyclic polymers were dissolved in toluene and poured onto water to form a molecular layer, followed by deposition on a TEM grid. As shown in Fig. 17.16, the TEM image of cyclic poly(MS)s containing side chains displayed a cyclic structure, and the presence of a linear counterpart could not be observed. When a high concentration solution (50 g/mL) of cyclic-poly(MS)-35-C<sub>18</sub> was used for the TEM sample preparation, the cyclic structures appeared to aggregate (Fig. 17.16, left). The concentration was thus lowered to 0.1 g/mL, resulting in observation of the isolated cyclic structure (Fig. 17.16, right). To identify the cyclic object in the TEM photographs, an elemental mapping of the scanning TEM images (=STEM image) was carried out, which can provide information on the distribution of carbon and oxygen. It was revealed that the cyclic object was composed of carbon and oxygen and thus the TEM photograph was concluded to reflect the cyclic structure of poly(MS)s with pendent long alkyl side chains.

We finally compared the theoretical and experimental chain diameter and width as follows; the visualized diameter of cyclic-poly(MS)-35-C<sub>18</sub> was 34.9 nm (averaged value of 10 cyclic objects in Fig. 17.17), which was in agreement with the calculated diameter of 39.0 nm ( $L_d$ ) obtained by the absolute value of  $M_n$ . For the estimation of 39.0 nm, we first calculated the diameter ( $L_{6mer} = 0.836$  nm) of a 6 mer cyclic poly(MS) based on a semi-empirical molecular orbital method (MM2). Note that the MM2 method does not provide the value of a fully stretched chain length, but the value of the chain length under the condition of energetic optimization. The value of  $L_{6mer}$  was then multiplied by  $n/6$ , where  $n$  represents the degree of polymerization ( $n = 280$ ), providing  $L_d = 39$  nm. The chain width was calculated based on the

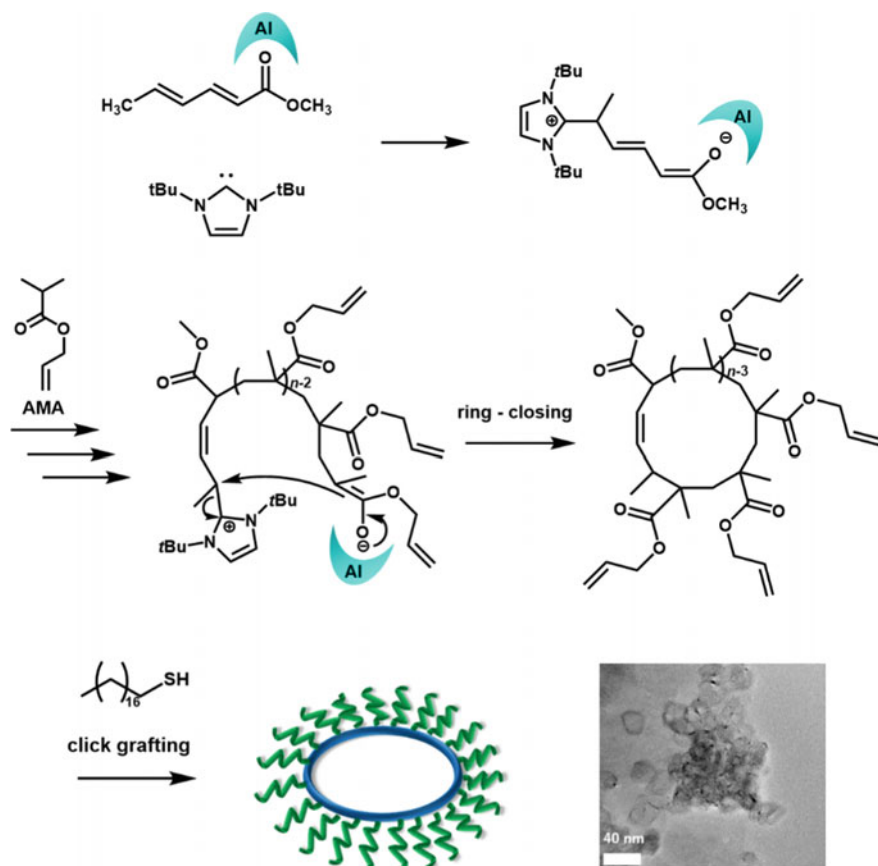


**Fig. 17.17** TEM image of isolated cyclic-poly(MS)-21-C<sub>12</sub> (left), and cyclic-poly(MS)-35-C<sub>18</sub> (right)



zig-zag conformation of the longer alkyl side chain and found to be 5.5 nm for 1-octadecanethiol. The observed width of 5.0 nm agreed well with the calculated value. Furthermore, for cyclic-poly(MS)-21-C<sub>12</sub>, a shorter width of 2.8 nm was observed, as shown in Fig. 17.17, which also corresponded to the estimated value of 3.5 nm. The observed  $L_d$  (18.0 nm, averaged value of 10 cyclic objects from Fig. 17.11) was comparable with the calculated value of 23.4 nm, while the diameter was smaller than that of cyclic-poly(MS)-35-C<sub>18</sub> (= 34.9 nm) due to the smaller  $M_n$  of the parent poly(MS). These obtained results demonstrated that the synthesized cyclic poly(MS) was truly generated upon chain polymerization of MS using the NHC*t*Bu as anionic initiator.

To allow another TEM observation, a long alkyl chain was also introduced into the pendent allyl groups in poly(AMA) initiated from a 1:1 adduct of NHC*t*Bu and MS. In concrete terms, a 1:1 adduct of MS and NHC*t*Bu initiates anionic polymerization of another methacrylate, allyl methacrylate (AMA) in toluene. After the monomer is consumed quantitatively using MAD as an additive, successive ring-closure occurs without highly dilute conditions to give a cyclic poly(AMA) containing an  $\alpha$ -terminal MS unit, and an  $M_n$  of  $8.8 \times 10^3 - 58.5 \times 10^3$  with a narrow molecular dispersity index ( $M_w/M_n = 1.14-1.37$ ). The cyclic structure was actually observed after the long alkyl side chains were grafted to the pendent allyl groups (Fig. 17.18). After the thiol-ene click reaction of 1-octadecanethiol and pendent allyl groups, NMR peaks assigned to allyl groups in the AMA unit disappeared and a new signal ascribed to a saturated allyl group appeared. The SEC trace shifted to a higher molecular weight region. The peak maximum ( $M_n$ ) of  $58.5 \times 10^3$  ( $M_w/M_n = 1.22$ ) shifted to a value of  $150.0 \times 10^3$  ( $M_w/M_n = 1.35$ ) after the click reaction. As shown in Fig. 17.18, the TEM image shows a cyclic structure and we could not detect the presence of a linear counterpart. The observed diameter of the cyclic structure was 25 nm, which was reasonably close to the estimated diameter of 40 nm using the  $M_n$  (SEC) and a semi-empirical molecular orbital method (AM1) calculations [43]. These results



**Fig. 17.18** Preparation of cyclic poly(AMA) via ionic polymerization initiated by a 1:1 adduct of NHC*t*Bu and MS and subsequent ring-closure without highly dilute solutions

proved that a cyclic poly(AMA) was indeed prepared by the chain polymerization of AMA using a 1:1 adduct of MS and NHC as the anionic initiator.

The ring-expansion (REMP) technique is a powerful tool for affording polymers of high purity and high molecular weight, though it is still very difficult to attain controlled molecular weights and polydispersities, because we cannot control when the ring-expansion is terminated in each macrocycle. This technique has been optimized for a handful of specific monomers, but lacks the backbone variation observed with other techniques [46]. In contrast, the ring-closure techniques that avoid high dilutions have a wide range of adaptable monomers. When employing highly enhanced propagation compared with termination, i.e., ring-closure, molecular weight control was also realized, as described in this chapter. The results of this chapter will help to shed light on the reliability of this newly developed synthetic procedure for a library of cyclic vinyl polymers at normal solution concentrations.

## References

1. D.E. Lonsdale, C.A. Bell, M.J. Monteiro, *Macromolecules* **43**, 3331–3339 (2010)
2. X.P. Qiu, F. Tanaka, F.M. Winnik, *Macromolecules* **40**, 7069–7071 (2007)
3. E.J. Shin, W. Jeong, H.A. Brown, B.J. Koo, J.L. Hedrick, R.M. Waymouth, *Macromolecules* **44**, 2773–2779 (2011)
4. D.J. Bannister, J.A. Semlyen, *Polymer* **22**, 377–381 (1981)
5. D. Geiser, H. Hocker, *Macromolecules* **13**, 653–656 (1980)
6. G. Hild, A. Kohler, P. Rempp, *Eur. Polym. J.* **16**, 525–527 (1980)
7. M. Schappacher, A. Deffieux, *Makromol. Chem. Rapid Commun.* **12**, 447–453 (1991)
8. M. Schappacher, A. Deffieux, *Macromolecules* **34**, 5827–5832 (2001)
9. B.A. Laurent, S.M. Grayson, *J. Am. Chem. Soc.* **128**, 4238–4239 (2006)
10. J. Xu, J. Ye, S.Y. Liu, *Macromolecules* **40**, 9103–9110 (2007)
11. F.G. Chen, G.M. Liu, G.Z. Zhang, *J. Polym. Sci. Part A Polym. Chem.* **50**, 831–835 (2012)
12. J.M. Ren, K. Satoh, T.K. Goh, A. Blencowe, K. Nagai, K. Ishitake, A.J. Christofferson, G. Yiapanis, I. Yarovsky, M. Kamigaito, G.G. Qiao, *Angew. Chem., Int. Ed.*, **53**, 459–464 (2014)
13. M.M. Stamenovic, P. Espeel, E. Baba, T. Yamamoto, Y. Tezuka, F.E. Du Prez, *Polym. Chem.* **4**, 184–193 (2013)
14. M.L. McGraw, E.Y.-X. Chen, *Macromolecules* **2020**(53), 6102–6122 (2020)
15. F.M. Haque, S.M. Grayson, *Nat. Chem.* **12**, 433–444 (2020)
16. C.W. Bielawski, D. Benitez, R.H. Grubbs, *Science* **297**, 2041–2044 (2002)
17. A.J. Boydston, Y. Xia, J.A. Kornfield, I.A. Gorodetskaya, R.H. Grubbs, *J. Am. Chem. Soc.* **130**, 12775–12782 (2008)
18. C.D. Roland, H. Li, K.A. Abboud, K.B. Wagener, A.S. Veige, *Nat. Chem.* **8**, 792–796 (2016)
19. Z. Miao, D. Pal, W. Niu, T. Kubo, B.S. Sumerlin, A.S. Veige, *Macromolecules* **53**, 7774–7782 (2020)
20. H. Kammiyada, A. Konishi, M. Ouchi, M. Sawamoto, *ACS Macro Lett.* **2**, 531–534 (2013)
21. H. Kammiyada, A. Konishi, M. Ouchi, M. Sawamoto, *Macromolecules* **50**, 841–848 (2017)
22. H. Kubota, S. Yoshida, M. Ouchi, *Polym. Chem.* **11**, 3964–3971 (2020)
23. W. Jeong, J.L. Hedrick, R.M. Waymouth, *J. Am. Chem. Soc.* **129**, 8414–8415 (2007)
24. N.E. Kamber, W. Jeong, S. Gonzalez, J.M. Hedrick, R.M. Waymouth, *Macromolecules* **42**, 1634–1639 (2009)
25. D.A. Culkin, W. Jeong, S. Csihony, E.D. Gomez, N.P. Balsara, J.M. Hedrick, R.M. Waymouth, *Angew. Chem. Int. Ed.* **46**, 2627–2630 (2007)
26. Y. Zhang, R. Liu, H. Jin, W. Song, *Commun. Chem.* **1**, 40 (2018)
27. L. Guo, D. Zhang, *J. Am. Chem. Soc.* **131**, 18072–18074 (2009)
28. H. Oike, H. Imaizumi, T. Mouri, Y. Yoshioka, A. Uchibori, Y. Tezuka, *J. Am. Chem. Soc.* **122**, 9592–9599 (2000)
29. T. Suzuki, T. Yamamoto, Y. Tezuka, *J. Am. Chem. Soc.* **136**, 10148–10155 (2014)
30. T. Ogawa, K. Nakazono, D. Aoki, S. Uchida, T. Takata, *ACS Macro Lett.* **4**, 343–347 (2015)
31. D. Aoki, G. Aibara, S. Uchida, T. Takata, *J. Am. Chem. Soc.* **139**, 6791–6794 (2017)
32. A.J. Arduengo, R.L. Harlow, M. Kline, *J. Am. Chem. Soc.* **113**, 361–363 (1991)
33. S.-I. Matsuoka, Y. Ota, A. Washio, A. Katada, K. Ichioka, K. Takagi, M. Suzuki, *Org. Lett.* **13**, 3722–3725 (2011)
34. T. Kato, Y. Ota, S.-I. Matsuoka, K. Takagi, M. Suzuki, *J. Org. Chem.* **78**, 8739–8747 (2013)
35. A.T. Biju, M. Padmanaban, N.E. Wurz, F. Glorius, *Angew. Chem., Int. Ed.*, **50**, 8412–8415 (2011)
36. Y.T. Zhang, M. Schmitt, L. Falivene, L. Caporaso, L. Cavallo, E.Y.X. Chen, *J. Am. Chem. Soc.* **135**, 17925–17941 (2013)
37. Y. Hosoi, A. Takasu, S. Matsuoka, M. Hayashi, *J. Am. Chem. Soc.* **139**, 15005–15012 (2017)
38. K. Maruoka, T. Itoh, M. Sakurai, K. Nonoshita, H. Yamamoto, *J. Am. Chem. Soc.* **110**, 3588–3597 (1988)
39. T. Hirabayashi, H. Yamamoto, T. Kojima, A. Takasu, Y. Inai, *Macromolecules* **33**, 4304–4306 (2000)

40. A. Takasu, M. Ishii, Y. Inai, T. Hirabayashi, *Macromolecules* **34**, 6548–6550 (2001)
41. A. Takasu, M. Ishii, Y. Inai, T. Hirabayashi, K. Inomata, *Macromolecules* **36**, 7055–7064 (2003)
42. Y. Oga, Y. Hosoi, A. Takasu, *Polymer*, **186**, 122019 (2020)
43. K. Naruse, A. Takasu, M. Higuchi, *Macromol. Chem. Phys.* **221**, 2000042 (2020)
44. Y. Muramatsu, Y. Oga, A. Takasu, M. Higuchi, *Polym. J.* **52**, 1253–1261 (2020)
45. Y. Muramatsu, A. Takasu, M. Higuchi, M. Hayashi. *J. Polym. Sci.* **52**, 2936–2942 (2020)
46. Y. Tezuka (ed.), *Topological Polymer Chemistry: Progress of Cyclic Polymers in Syntheses, Properties and Functions* (World Scientific, Singapore, 2013)

# Chapter 18

## Controlled Ring-Expansion Polymerization Based on Acyl-Transfer Polymerization of Thiiranes with Aromatic Heterocycles as Initiators



Atsushi Kameyama and Akira Takahashi

**Abstract** This chapter describes the ring-expansion polymerization (REP) of thiiranes using aromatic benzothiazolone derivatives as initiators, including key fundamental addition reactions between thiiranes and active ester species in the presence of quaternary onium halides. This regiospecific addition reaction proceeds via selective intramolecular rearrangement, which results in the insertion of the thiirane-derived thioethylenes into the active ester structures. Such reaction mode enables the design of the controlled polymerization of thiiranes using the active esters as initiators. Since the acyl-group in the initiators repeatedly transfers at the propagating terminus, the polymerization is named “acyl-transfer polymerization”. When cyclic aromatic heterocycles with *S*-thiocarbamate moieties are used as initiators, the acyl-transfer polymerization proceeds in a ring-expanding fashion to produce cyclic polysulfides. The unique polymerization behavior was observed based on the rigid 5-membered structures of the initiators, while the living-like nature of the REP was confirmed by careful investigation. Successful synthesis of cyclic block copolymers and the characteristic glass transition properties of the obtained cyclic polysulfides are also described.

**Keywords** Cyclic polymer · Thiirane · Acyl-transfer polymerization

### 18.1 Introduction

Cyclic polymers have characteristic properties such as smaller hydrodynamic volume and higher glass transition temperature due to their specific topology with no chain terminus. In synthesizing cyclic polymers, controlled ring-expansion polymerization (REP) is a useful method, in which the continuous insertion of monomers into the active group of cyclic initiators proceeds in a chain-growth mode. In the last 20 years, REP has made remarkable progress in the synthesis of cyclic polyesters, cyclic polyolefins, cyclic polystyrene, and cyclic polysulfide, among others. Controlled

---

A. Kameyama (✉) · A. Takahashi  
Department of Chemistry, Faculty of Engineering, Kanagawa University, Yokohama, Japan  
e-mail: [kameya01@kanagawa-u.ac.jp](mailto:kameya01@kanagawa-u.ac.jp)

REP employs a strategy similar to the synthesis of well-defined linear polymers by controlled polymerization. The strategy involves a reversible activation of dormant groups into active species at the propagating terminus.

The key step in establishing controlled REP is a molecular design and synthesis of cyclic compounds as initiators for specific monomers, such as vinyl monomers, cyclic monomers, and more. Considering the dormant groups of cyclic initiators and the correlation between reactivity and ring sizes, several cyclic initiators have been synthesized. Radical REP of methacrylates was performed with a cyclic benzodithioate compound [1] as a cyclic initiator using  $^{60}\text{Co}$   $\gamma$ -ray at low temperatures to provide well-defined cyclic poly(methacrylate)s. Cyclic alkoxyamine compounds with moderate ring-size [2, 3] were synthesized as cyclic initiators to demonstrate nitroxide-mediated radical polymerization proceeding in ring-expansion mode to produce cyclic polystyrene. A 7-membered cyclic hemiacetal was synthesized to achieve ring-expansion cationic polymerization of vinyl ethers with a suitable Lewis acid to provide controlled poly(vinyl ethers) and block copoly(vinyl ethers) [4, 5]. On the other hand, the first example of REP of cyclic monomers is the REP of  $\epsilon$ -caprolactone with cyclic tin alkoxide reported [6] in 1998. Based on the ring opening metathesis polymerization of cyclooctene, REP was successful using cyclic ruthenium carbene complex to provide a controlled cyclic polymer. REP based on acyl-transfer polymerization of thiiranes with *S*-dithioesters [7] cyclic initiator and tetrabutyl ammonium chloride (TBAC) providing cyclic polysulfides was reported by Nishikubo et al. Cyclic polymers with higher molecular weights were produced as side products from the ring-crossover reaction of the initial cyclic polysulfides. The same group then improved the REP of thiiranes using a 5-membered cyclic *N*-keto-thiourethane [8]. Furthermore, recent reports of REP of thiiranes involved a newly designed 5-membered cyclic *N*-keto-thiourethane compound and TBAC catalyst [9]. These reports suggest that a well-structured 5-membered cyclic compound, which is relatively stable due to its small plane structures in basic organic chemistry, works well as a cyclic initiator for REP of thiiranes.

From these backgrounds, we developed the REP of thiiranes using simple aromatic cyclic thiourethanes as initiators and TBAC as catalyst. In this chapter, the unique polymerization behavior, living character of REP, and successful synthesis of block copolysulfides are described. Furthermore, we demonstrate that cyclic polysulfide has a higher glass transition temperature ( $T_g$ ) than its linear counterpart.

## 18.2 Ring-Opening Reaction of Thiiranes with Active Ester Groups Catalyzed by Quaternary Onium Halides

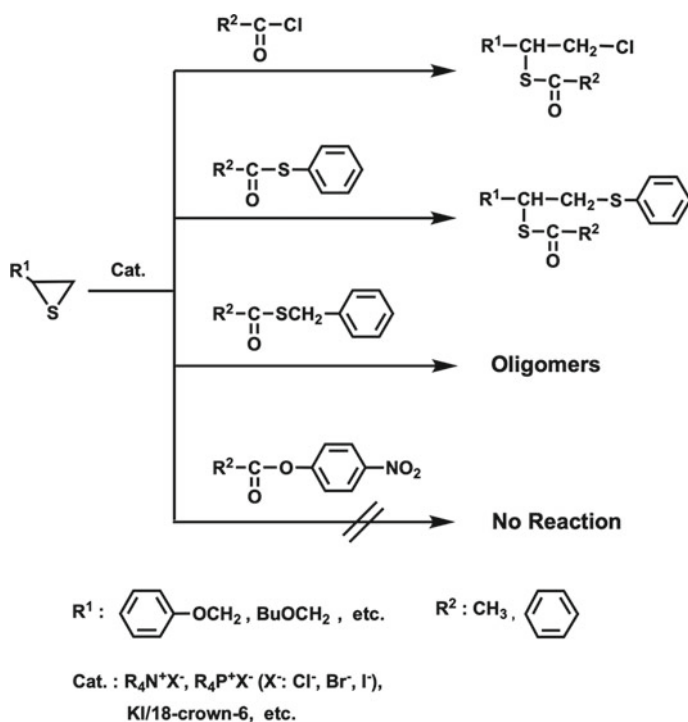
In a series of studies of a new ring-opening reaction of cyclic ethers [10] and cyclic sulfides, regioselective ring-opening reaction of thiiranes with carboxylic acid derivatives catalyzed by quaternary onium halides was developed [11]. It was proven that

the reaction behavior strongly depends on the structure of the carboxylic acid derivatives as shown in Scheme 1. The reaction of thiiranes with acyl chlorides or *S*-phenyl esters using quaternary ammonium halides, such as TBAC, proceeds efficiently to selectively produce  $\beta$ -addition products. It implies that the  $\beta$ -cleavage of the covalent bond between sulfur and non-substituted carbon (*S*-CH<sub>2</sub>) selectively occurs in the reaction. On the other hand, the reaction with *S*-benzyl ester produced oligomers with terminal *S*-thioester groups, instead of the  $\beta$ -addition product. In cases involving *O*-aryl esters, the reaction did not proceed under the same conditions as the reactions with the above reagents.

The general order of reactivity of carboxylic acid derivatives is explained by considering the leaving ability that is based on the basicity of the leaving groups. In this case,  $\text{Cl}^- > \text{PhS}^- > \text{PhCH}_2\text{S}^-$  (alkyl-S<sup>-</sup>)  $> \text{PhO}^-$ . In addition, rate Eq. (18.1) derived from a kinetic study suggests that thiiranes and catalysts were related to the rate-determining step.

$$v = k[\text{thiirane}][\text{catalyst}] \quad (18.1)$$

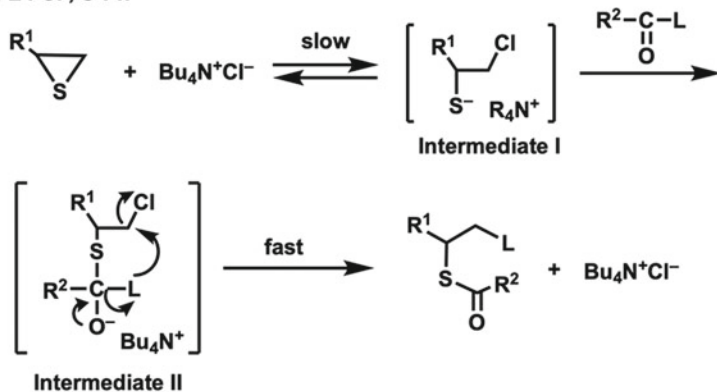
*k*: rate constant.



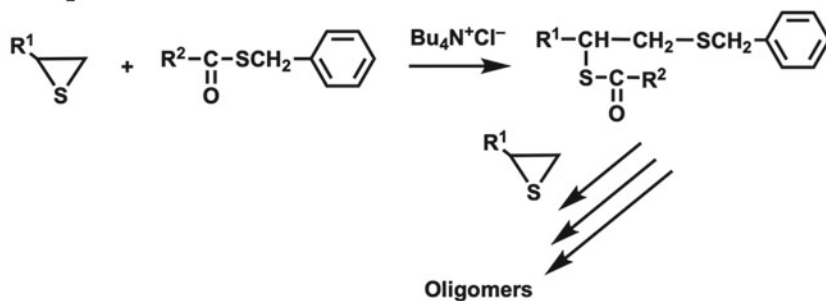
**Scheme 1** Regioselective addition reaction of thiiranes with carboxylic acid compounds

**Leaving ability :  $\text{Cl}^- > \text{PhS}^- > \text{PhCH}_2\text{S}^- > \text{PhO}^-$**

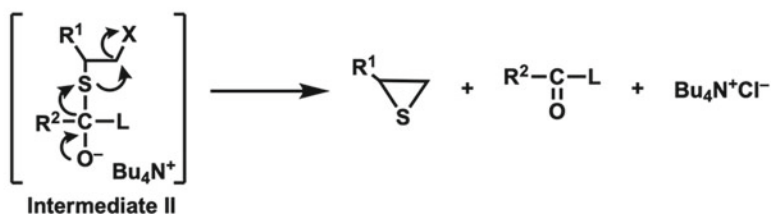
1) L : Cl, S-Ph



2) L : SCH<sub>2</sub>Ph



3) L : OPh (p-NO<sub>2</sub>)



**Scheme 2** Speculated reaction mechanism of addition reaction of thiranes with carboxylic acid compounds catalyzed by TBAC (Bu<sub>4</sub>N<sup>+</sup>Cl<sup>-</sup>)



From these results, the reaction mechanism can be understood by Scheme 2 [12]. At first,  $\text{Cl}^-$  of TBAC attacks the  $\beta$ -carbon of the thiirane to form an alkyl thiolate ( $\text{RS}^-$ ) Intermediate I. Then, Intermediate I reacts with carboxylic acid derivatives to form Intermediate II. When the leaving ability of the leaving group (L) is greater than that of the alkyl thiolate, L is released to replace  $\text{Cl}^-$ . The high regioselectivity of the reactions is attributable to a steric hindrance between the substituent group of thiirane and the quaternary onium halides used.

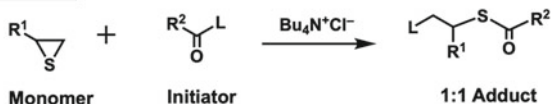
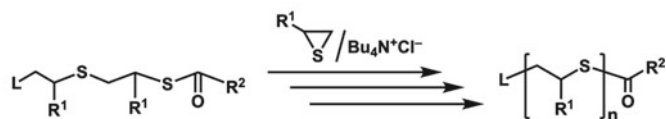
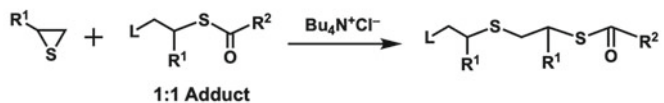
Initially, the reaction of thiiranes with *S*-benzyl esters produces an *S*-alkyl thioester. The reactivity of the alkyl thioester group toward thiiranes is the same as that of the starting *S*-benzyl esters. Thus, the reaction of *S*-alkyl thioester with thiiranes occurred in a chain reaction mode to produce oligomers with terminal *S*-thioester groups. In reactions with *O*-aryl esters, Intermediate II would form. However, it reverts to the starting materials at equilibrium due to the lower leaving ability of  $\text{PhO}^-$  than alkyl thiolate ( $\text{RS}^-$ ).

It is demonstrated that the novel ring-opening reaction of thiiranes with certain carboxylic acid derivatives catalyzed by quaternary onium halides proceed regioselectively to provide the corresponding  $\beta$ -addition product. It is also noteworthy that the regioselective reactions of thiiranes have high potential in synthesizing sulfur-containing compounds and polymers with well-defined structures.

### 18.3 Acyl-Transfer Polymerization of Thiiranes

Based on the results of the regioselective reaction of thiiranes with the carboxylic acid derivatives, A. Kameyama et al. developed the acyl-transfer polymerization of thiiranes with acyl chlorides or carboxylic ester initiators catalyzed by quaternary onium halides [13–15]. The polymerization mechanism is understood based on the ring-opening reaction mechanism of thiiranes. Here, the polymerization proceeds in the activated monomer mechanism. The polymerization mechanism is also supported by the result of a reference experiment [16]; the reaction of phenoxypropylene sulfide (PPS) with 5 mol% of TBAC under the same condition as in the aforementioned ring-opening reaction of thiiranes resulted in a linear polysulfide of PPS. Here, the chloride of TBAC attacked the carbon to produce thiolate (anion), which in turn attacked another PPS in a chain-growth mode. It is noteworthy that the polymerization mechanism is different from living polymerization systems such as in living radical polymerizations, living anionic polymerizations, or cationic polymerizations that proceed in a propagating terminus activation mechanism.

In the initiation process, thiiranes react readily with highly active carboxylic acid derivatives, such as acyl chlorides or *S*-phenyl thioesters, to produce the addition products (1:1 adducts), *S*-alkyl thioesters. The *S*-alkyl thioesters react with the thiiranes to produce the corresponding addition products. Then, similar addition reactions of the terminal *S*-alkyl thioester groups proceed in a chain-growth manner (Scheme 3). A remarkably interesting feature of the polymerization is that the acyl

**Initiation****Propagation**

$\text{R}^1$  :  $-\text{CH}_2-\text{O}-\text{Ph}$ ,  $-\text{CH}_2-\text{O}-\text{Bu}$ , etc.

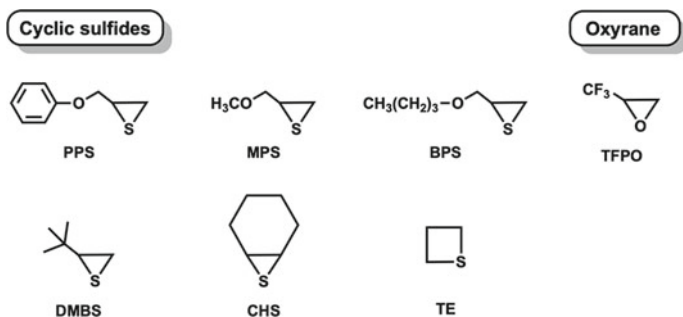
$\text{R}^2$  :  $-\text{CH}_3$ ,  $-\text{Ph}$ , etc.

$\text{L}$  :  $-\text{Cl}$ ,  $-\text{S}-\text{Ph}$ , etc.

**Scheme 3** Acyl-transfer polymerization of thiiranes with carboxylic acid compound initiators catalyzed by TBAC ( $\text{Bu}_4\text{N}^+\text{Cl}^-$ )

groups of the used initiators transfer at the propagating terminus. Therefore, the process is called as ‘‘acyl-transfer polymerization’’.

Several mono-substituted 3-membered cyclic sulfides (thiiranes) such as butoxy propylene sulfide (BPS), 3-dimethyl-1-butene sulfide (DMBS), di-substituted 3-membered cyclic sulfide, cyclohexene sulfide (CHS), and 4-membered cyclic sulfide (thietane) are applicable for the acyl-transfer polymerization. Apart from 3-membered or 4-membered cyclic sulfides, trifluoromethyl ethylene oxide, which is an oxirane with a strong electron withdrawing group, is also useful for the acyl-transfer polymerization (Scheme 4).



**Scheme 4** Monomers for the acyl-transfer polymerization

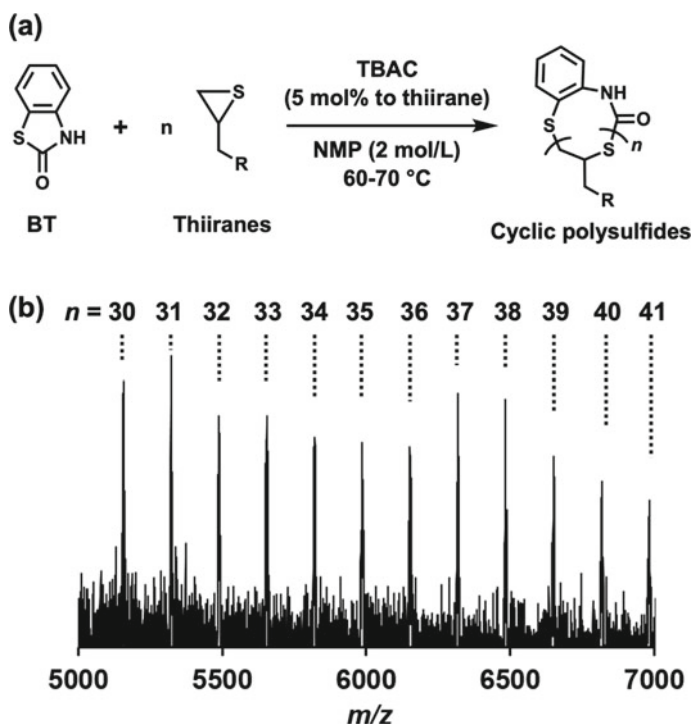
Furthermore, a variety of block copolymers of these cyclic monomers are successfully synthesized based on the post-polymerization method using isolated polysulfides with terminus *S*-acyl groups as macroinitiators [14].

#### 18.4 Ring-Expansion Acyl-Transfer Polymerization of Thiiranes with Cyclic Initiators

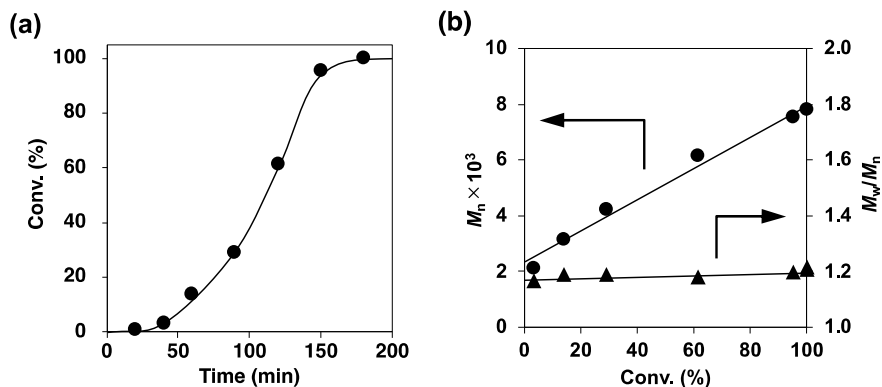
As described above, the acyl-transfer polymerization of thiiranes proceeds via monomer insertion into the active ester moiety by successive addition and rearrangement reactions. These reactions do not involve the dissociation reactions at the chain terminus, which indicates that acyl-transfer polymerization using cyclic initiator can maintain the cyclic topology of the formed macrocycles throughout the polymerization. In addition, the intermediate thiolate anions are relatively tolerant to oxygen and water compared to the other active species used in common living polymerizations, further assuring the cyclic topology of the products. These characteristics of acyl-transfer polymerization of thiiranes are highly favorable for REP within the context of the selective and facile preparation of cyclic polymers. Kudo and Nishikubo first investigated the REP of thiiranes with several cyclic thioester derivatives as initiators. They found that the REP successfully proceeded to afford cyclic polysulfides, and that the suppression of the ring-crossover reactions of the products was important to ensure the well-defined cyclic structure of the products [7, 8, 17, 18]. These polymerization systems were also investigated in detail by Vana and co-workers using a Gaussian fitting method, which revealed detailed time-course polymerization and crossover behaviors [19, 20]. The more suppressed crossover reaction with *N*-ketothiocarbamate than with *S*-thioester suggests that the crossover properties would depend on the reactivity of the initiating structures. Specifically, it would depend on the electrophilicity of the carbonyl carbon in the active *S*-thioester moiety. Based on this consideration, our group has focused on cyclic *N*-aromatic thiocarbamate structures. The reactivity of these structures is suppressed by resonance stabilization of aromatic heterocycles. On the other hand, a preceding study of controlled acyl-transfer polymerization using *N*-(4-tolyl)-*S*-phenyl thiocarbamate initiator guaranteed the initiating ability of the *N*-aromatic thiocarbamates [8, 21]. The following sections describe the controlled REP of thiiranes and the preparation of cyclic block copolymers using two benzothiazolone derivatives as initiators. These initiators are associated with the unique thermal properties of the obtained cyclic polysulfides [16, 22].

### 18.4.1 Ring-Expansion Polymerization of Thiiranes with Cyclic Aromatic Thiourethane Initiator: The Polymerization Properties

3*H*-Benzothiazol-2-one (BT) is the simplest cyclic analog of *N,S*-diaryl thiocarbamate, and was investigated as a cyclic initiator for the REP of thiiranes. The REP of PPS in the presence of BT initiator and TBAC catalyst in *N*-methylpyrrolidone (NMP, 2 mol/L) at 60 °C (Fig. 1a, R = PhOCH<sub>2</sub>) produced a poly(PPS) with number average molecular weight ( $M_n$ ) of 6150 and a relatively narrow dispersity ( $M_w/M_n$ ) of 1.18. MALDI-TOF MS measurement revealed a well-defined cyclic structure of the obtained polysulfides with one BT moiety per macrocycle (Fig. 1b). These results show that BT-initiated REP selectively proceeded in a controlled fashion. The REP of the other thiirane monomers such as BPS and propylene sulfide (PS) using BT initiator also proceeded at 70 °C in the same manner and yielded cyclic polysulfides with well-defined cyclic structures and narrow dispersity (*ca.* 1.15). This result demonstrates the versatility of BT-initiated REP.

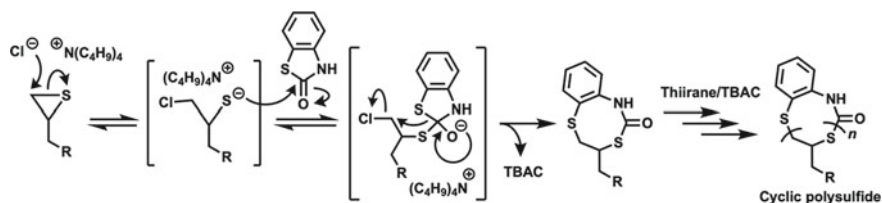


**Fig. 18.1** **a** REP of PPS using BT as the cyclic initiator and TBAC as the catalyst. **b** MALDI-TOF MS spectrum of BT-initiated cyclic poly(PPS). From [16] Copyright © 2021 by John Wiley Sons, Inc. Adapted by permission of John Wiley & Sons, Inc



**Fig. 18.2** **a** Time–conversion and **b** conversion– $M_n$  and  $M_w/M_n$  plots for the REP of PPS using BT initiator. From [16] Copyright © 2021 by John Wiley Sons, Inc. Adapted by permission of John Wiley & Sons, Inc

The BT-initiated REP of thiiranes showed a unique time-conversion behavior with a sigmoidal form, where the conversion rate was initially low, but subsequently increased with the reaction time (Fig. 2a). This behavior can be explained by the acyl-transfer polymerization mechanism (Scheme 5), where the rigid, 5-membered ring of BT may slow down the initial thiolate addition and rearrangement reactions. On the other hand, the once-expanded carbamate ring by the monomer insertion should have better reactivity and lead to a faster reaction rate than BT due to the lack of steric stability. Indeed,  $M_n$  of the product was higher than the theoretical value (3476) calculated from the PPS/BT feed ratio. This difference suggests that the required amount of BT initiator is lower than what was fed, because the thiirane monomer preferentially reacts with the ring-expanded products than with BT. Despite such unusual characteristics, a proportional increase in  $M_n$  with conversion and a nearly constant dispersity up to  $\sim 1.2$  during the polymerization were observed (Fig. 2b). This observation demonstrates the living-like nature of the BT-initiated REP of thiiranes. In fact, a control experiment using PPS monomer and TBAC catalyst in the absence of BT resulted in the formation of the linear poly(PPS) with  $M_n$  and  $M_w/M_n$  of 160,000



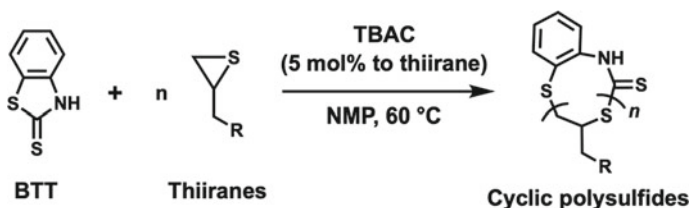
**Scheme 5** Speculated mechanism of the REP of PPS in the presence of BT as the cyclic initiator and TBAC as the catalyst. From [16] Copyright © 2021 by John Wiley Sons, Inc. Adapted by permission of John Wiley & Sons, Inc.

and 2.36, respectively, indicating that the intrinsic ring-opening polymerization of PPS proceeded. This result clearly shows the efficiency of the BT initiator and the herein proposed REP mechanism that initiates from the nucleophilic attack of the chloride anion of TBAC to PPS.

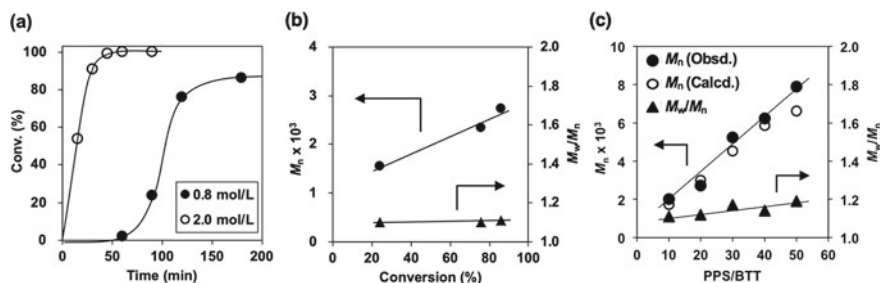
### 18.4.2 Ring-Expansion Polymerization of Thiiranes with Cyclic Aromatic Dithiocarbamate Initiator: Comparison of Acyl-Transfer and Thioacyl-Transfer Polymerization

Candidates for cyclic initiators for the REP of thiiranes include various ester derivatives that allow the acyl-transfer mechanism, examples of which are mostly limited to cyclic *S*-thioesters [7, 17–19] and *S*-thiourethanes [8, 16, 20]. In this context, we investigated 3*H*-benzothiazol-2-thione (BTT), which is a thiocarbonyl analog of BT, as the cyclic dithiocarbamate initiator. This section describes the characteristics of the BTT-initiated REP, and the difference between the REP properties using BTT and BT as initiators.

The REP of PPS using BTT (5 mol%) and TBAC (5 mol%) in NMP (0.8 mol/L) at 60 °C (Scheme 6) showed a sigmoidal time–conversion plot (Fig. 3a) similar to the one using BT. This result indicates that BTT-initiated REP proceeds through the same polymerization mechanism in a thioacyl-transfer fashion. A proportional increase in  $M_n$  versus conversion and a constant dispersity throughout the polymerization were observed (Fig. 3b), showing that the BTT-initiated REP proceeded in a controlled manner. REP at 3 h gave a cyclic poly(PPS) with  $M_n$  of 2760 and  $M_w/M_n$  as narrow as 1.10. The cyclic topology of the product with one BTT moiety per macrocycle was clearly confirmed by MALDI-TOF MS. Importantly, the  $M_n$  of the obtained cyclic polysulfides with different PPS/BTT feed agreed with the calculated values (Fig. 3c), demonstrating the living-like nature of the BTT-initiated REP. The generality of the REP was also examined using BPS and PS monomer instead of PPS, resulting in cyclic polysulfides with narrow dispersity (1.12 and 1.15, respectively) in each REP.



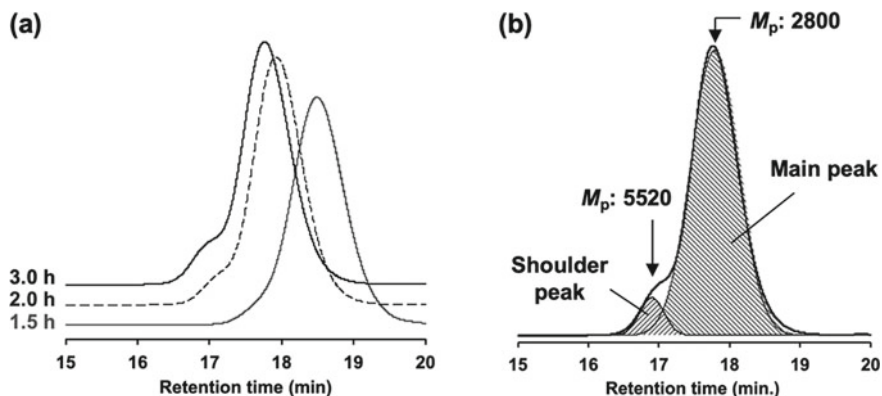
**Scheme 6** Ring-expansion polymerization using BTT as the initiator. Adapted with permission from [22]. Copyright 2021 American Chemical Society



**Fig. 18.3** **a** Time–conversion plot and **b**  $M_n$  and  $M_w/M_n$  plots as a function of conversion and **c** PPS/BTT feed for the BTT-initiated REP of PPS. Adapted with permission from [22]. Copyright 2021 American Chemical Society

When carried out at the 2.0 mol/L condition, which is the same as the REP using BT initiator, the BTT-initiated REP of PPS showed no lead time and resulted in a quantitative monomer conversion in only 45 min (Fig. 3a). The conversion was much more rapid than that of the BT-initiated one that required 150 min to reach a comparable conversion (Fig. 2a). At those reaction times, the  $M_n$  of the BTT-initiated poly(PPS) was 3650, which is closer to the theoretical value of 3492. In contrast,  $M_n$  of the BT-initiated poly(PPS) was higher at 7570 than the theoretical value of 3480. In addition, the  $M_w/M_n = 1.11$  of the BTT-initiated cyclic poly(PPS) is narrower than the BT-initiated ones ( $\sim 1.20$ ). These results indicate that the initiator efficiency of BTT is higher than BT, which implies that the dithiocarbamate moieties are more reactive than the *S*-thiocarbamate ones. This consideration was supported by the  $^{13}\text{C}$ -NMR spectra of BTT and BT. The chemical shift of the thiocarbonyl carbon of BTT (191 ppm) was much lower compared to that of the carbonyl carbon of BT (174 ppm). These values indicate that BTT is more susceptible to the nucleophilic attack from the thiolate anion than BT.

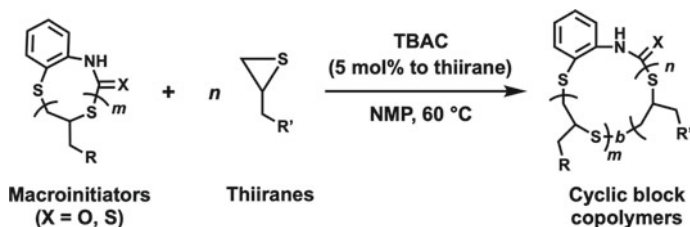
Herein, the GPC measurement of the BTT-initiated polysulfides showed a sharp main peak accompanied by a shoulder that corresponds to a higher molecular-weight fraction. The shoulder appeared as the polymerization proceeded (Fig. 4a). Gaussian fitting analysis of the GPC curves revealed a two-fold peak molecular weight ( $M_p$ ) of the shoulder compared to the  $M_p$  of the main peak (Fig. 4b). This minor fraction can be attributed to the fused ring of two BTT-initiated polysulfides by the ring-crossover reaction [17, 18], as supported by the detailed MALDI-TOF MS measurement. Such fused ring formation was fewer in the BTT-initiated REP at 0.8 mol/L than 2.0 mol/L because the crossover reactions should be entropically unfavorable under diluted conditions [23]. On the other hand, the  $M_w/M_n$  of the BTT-initiated cyclic polysulfides were less than 1.20 despite their bimodal form in the GPC curve. Furthermore, the dispersity of the main peak calculated from the fitted curve was as narrow as less than 1.10. These data demonstrate the superior initiator efficiency of the BTT for the controlled REP of thiiranes.



**Fig. 18.4** **a** Time-course GPC traces of the BTT-initiated cyclic poly(PPS) at different polymerization times. **b** Gaussian fitting profiles of the BTT-initiated cyclic poly(PPS) after the REP for 3 h. Adapted with permission from [22]. Copyright 2021 American Chemical Society

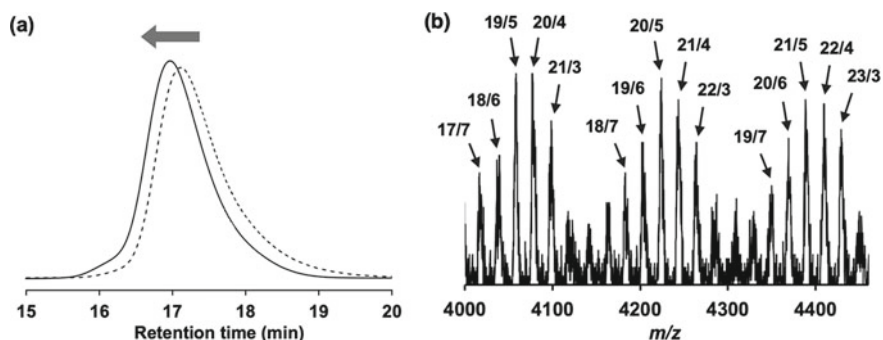
### 18.4.3 Post-polymerization and Block Copolymerization Based on Cyclic Aromatic (Di)thiocarbamates-Initiated Polysulfides as Macro-initiators

The living properties of the BT- and BTT-initiated REP were further explored by the post-polymerization and block copolymerization experiments using the obtained cyclic polysulfides as macroinitiators (Scheme 7). The REP using the BT-initiated cyclic poly(PPS) macroinitiator and PPS monomer reached a quantitative monomer conversion within 30 min, which is faster than the REP using the BT initiator. The faster polymerization rate is because of the absence of the steric stability in the macroinitiator, which leads to a higher reactivity of the *S*-thiocarbamate moiety than the one in BT. The increase in  $M_n$  (from 3570 to 5630) and narrowing of the dispersity (from 1.20 to 1.13) were observed by GPC measurement, indicating the occurrence



**Scheme 7** Post-polymerization and block copolymerization using BT- and BTT-initiated poly(PPS) as the macroinitiators. Adapted with permission from [22]. Copyright 2021 American Chemical Society

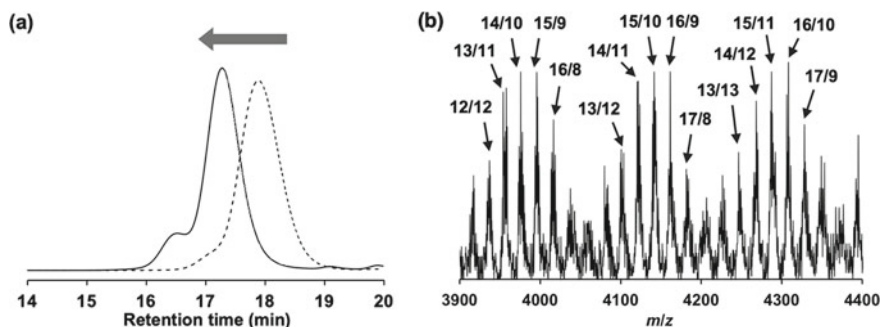




**Fig. 18.5** **a** GPC curve transition with block copolymerization using the BT-initiated cyclic poly(PPS) macroinitiator and BPS monomer. **b** MALDI-TOF MS spectrum of the BT-initiated cyclic poly(PPS-*b*-BPS). The values of each peak are the degree of polymerization (PPS/BPS). From [16] Copyright © 2021 by John Wiley Sons, Inc. Adapted by permission of John Wiley & Sons, Inc

of post-polymerization. Importantly, the clear cyclic structure was confirmed by MALDI-TOF MS spectrometry, implying that a well-defined cyclic structure was maintained through post-polymerization. Such living properties of the BT-initiated cyclic polysulfides also enabled the precise synthesis of cyclic block copolymers. The polymerization using the poly(PPS) macroinitiator and BPS monomer proceeded to produce cyclic poly(PPS-*b*-BPS) with larger  $M_n$  of 5170 and narrower dispersity of 1.13 (Fig. 5a). The well-defined cyclic structure of the obtained block copolymer was confirmed by MALDI-TOF MS spectrometry, which showed the peaks corresponding to the targeted block copolymer with one BT per macrocycle and different PPS/BPS compositions (Fig. 5b).

When post-polymerization was carried out with the BTT-initiated cyclic poly(PPS) macroinitiator ( $M_n$ : 2420,  $M_w/M_n$ : 1.11) and PPS monomer (Scheme 7, X = S), the ring-expanded cyclic poly(PPS) was obtained and the dispersity increased ( $M_n$ : 6030,  $M_w/M_n$ : 1.17). The increase in the dispersity is due to the increase in the fused ring fraction from 2.5 to 15%, as revealed by the Gaussian fitting analysis. This result indicates a higher reactivity of the dithiocarbamate moiety not only for REP but also for the ring-crossover reactions. On the other hand, MALDI-TOF MS clearly confirmed the cyclic structure of the product, showing that the topology was not disturbed during the post-polymerization. The block copolymerization using the same macroinitiator and BPS monomer also proceeded in a similar fashion, and yielded cyclic poly(PPS-*b*-BPS) ( $M_n$ : 4290,  $M_w/M_n$ : 1.11, Fig. 6a) with a cyclic topology, as confirmed by MALDI-TOF MS measurement (Fig. 6b).

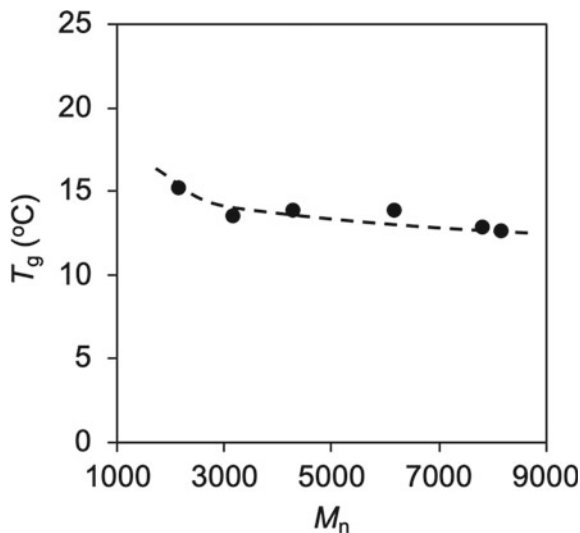


**Fig. 18.6** **a** GPC curve transition with block copolymerization using the BTT-initiated cyclic poly(PPS) macroinitiator and BPS monomer. **b** MALDI-TOF MS spectrum of the BTT-initiated cyclic poly(PPS-*b*-BPS). The values of each peak are the degree of polymerization (PPS/BPS). Adapted with permission from [22]. Copyright 2021 American Chemical Society

#### 18.4.4 Glass Transition Properties of BT-Initiated Cyclic Polysulfides with Well-Defined Cyclic Topology

The well-defined cyclic structure of the BT-initiated polysulfides enabled the investigation of  $T_g$  of cyclic polysulfides with different ring sizes. The cyclic poly(PPS) with  $M_n$  from 2120 to 8150 were prepared by the BT-initiated REP under various PPS/BT ratios and subjected to differential scanning calorimetry (DSC). The DSC measurement revealed that the  $T_g$  (midpoint) of the BT-initiated cyclic poly(PPS) ranges from 15.2 to 12.6 °C. These values were higher than those of the poly(PPS) with a well-defined linear topology (9 °C) that was previously reported [24]. A well-known characteristic of cyclic polymers is that they possess no chain terminus and thus lower segmental mobility of polymeric chains compared to those in their linear counterparts [25]. In addition, the  $T_g$  of the BT-initiated cyclic poly(PPS) unexpectedly decreased as  $M_n$  increased (Fig. 18.7). This result is opposite to the general  $M_n$ - $T_g$  relationship observed with linear polymers, which shows higher  $T_g$  with larger  $M_n$  polymers due to the decreasing chain mobility. Meanwhile, a unique  $T_g$  property was reported with cyclic polydimethylsiloxanes and was explained as the result of a larger configurational entropy of the smaller rings. The segmental rotation of these rings is relatively restricted compared to those from the linear counterparts [26, 27]. The  $T_g$  properties of the BT-initiated cyclic polysulfides we observed can be explained by the above-mentioned mechanism and can further support the well-defined cyclic topology of the BT-initiated cyclic polysulfides.

**Fig. 18.7**  $M_n$ - $T_g$  (midpoint) plot of the BT-initiated cyclic poly(PPS). From [16] Copyright © 2021 by John Wiley Sons, Inc. Adapted by permission of John Wiley & Sons, Inc



## References

1. T. He, G.H. Zheng, C.Y. Pan, *Macromolecules* **36**, 5960–5966 (2003)
2. J. Ruehl, N. Ningnuek, T. Thongpaisanwong, R. Braslau, *J. Polym. Sci. Part A Polym. Chem.*, **46**, 8049–8069 (2008)
3. A. Narumi, S. Zeidler, H. Barqawi, C. Enders, W. H. Binder, *J. Polym. Sci. Part A Polym. Chem.*, **48**, 3402–3416 (2010)
4. H. Kammiyada, A. Konishi, M. Ouchi, M. Sawamoto, *ACS Macro Lett.* **2**, 531–534 (2013)
5. M. Ouchi, H. Kammiyada, M. Sawamoto, *Polym. Chem.* **8**, 4970–4977 (2017)
6. H.R. Kricheldorf, S.R. Lee, N. Schittenhelm, *Macromol. Chem. Phys.* **199**, 273–282 (1998)
7. H. Kudo, S. Makino, A. Kameyama, T. Nishikubo, *Macromolecules* **38**, 5964–5969 (2005)
8. H. Kudo, M. Sato, R. Wakai, T. Iwamoto, T. Nishikubo, *Macromolecules* **41**, 521–523 (2008)
9. H. Kudo, K. Naritomi, S. Onishi, H. Maekawa, E.A.Q. Mondarte, K. Suthiwanich, T. Hayashi, *Macromolecules* **53**, 4733–4740 (2020)
10. T. Nishikubo, A. Kameyama, *Prog. Polym. Sci.* **18**, 963–995 (1993)
11. A. Kameyama, M. Kiyota, T. Nishikubo, *Tetrahedron Lett.* **35**, 4571–4572 (1994)
12. A. Kameyama, T. Nishikubo, *Polym. J.* **41**, 1–15 (2009)
13. A. Kameyama, K. Shimotsuma, T. Nishikubo, *Macromol. Rapid Commun.* **15**, 335–342 (1994)
14. A. Kameyama, K. Shimotsuma, T. Nishikubo, *Polym. J.* **28**, 68–75 (1996)
15. S. Kawakami, A. Kameyama, M. Miyata, T. Nishikubo, *Polym. J.* **29**, 550–552 (1997)
16. A. Takahashi, R. Yuzaki, Y. Ishida, A. Kameyama, *J. Polym. Sci. Part A Polym. Chem.*, **57**, 2442–2449 (2019).
17. H. Kudo, S. Makino, T. Nishikubo, *J. Polym. Sci. Part A Polym. Chem.* **45**, 680–687 (2007).
18. H. Kudo, Y. Takeshi, *J. Polym. Sci. Part A Polym. Chem.* **52**, 857–866 (2014).
19. J.-H. Schuetz, P. Vana, *Macromol. Chem. Phys.* **212**, 1263–1275 (2011)
20. J.-H. Schuetz, L. Sandbrink, P. Vana, *Macromol. Chem. Phys.* **214**, 1484–1495 (2013)
21. H. Kudo, K. Sato, T. Nishikubo, *Macromolecules* **43**, 9655–9659 (2010)
22. A. Takahashi, S. Tsunoda, R. Yuzaki, A. Kameyama, *Macromolecules* **53**, 5227–5236 (2020)
23. H. Kammiyada, M. Ouchi, M. Sawamoto, *Polym. Chem.* **7**, 6911–6917 (2016)
24. Z. Zhang, T.-Y. Zeng, L. Xia, C.-Y. Hong, D.-C. Wu, Y.-Z. You, *Nat. Commun.* **9**, 2577 (2018)

25. T. Yamamoto, Y. Tezuka, *Soft Matter* **11**, 7458–7468 (2015)
26. E.A.D. Marzio, C.M. Guttman, *Macromolecules* **20**, 1403 (1987)
27. V. Arrighi, S. Gagliardi, F. Ganazzoli, J.S. Higgins, G. Raffaini, J. Tanchawanich, J. Taylor, M.T.F. Telling, *Macromolecules* **51**, 7209–7223 (2018)

# Chapter 19

## A Conjunctive RC and RE Polymer Cyclization with Zwitterionic Telechelic Precursors



Yasuyuki Tezuka

**Abstract** An efficient polymer cyclization process has been developed with a series of zwitterionic telechelic precursors having a pair of a cyclic ammonium and a carboxylate end groups. As showcase examples, zwitterionic telechelic poly(THF)s were prepared by taking advantage of a living cationic polymerization technique, and were subjected to the polymer cyclization under dilution to afford cyclized poly(THF)s in high yields. Likewise, a series of cyclic polystyrenes have been prepared conveniently by adopting the relevant zwitterionic telechelic polystyrenes prepared through a living anionic polymerization technique.

### 19.1 Introduction

A class of topological polymers comprising a monocyclic (simple ring) unit, i.e., ring polymers, optionally possessing designated functional groups along the circular chain segment (*kyklo*-telechelics), as well as tadpole type polymers having both cyclic and branched segments, have attracted growing interests both from the precision designing of macromolecular architectures and applied polymer materials engineering [1]. Notably, in particular, a variety of *monocyclic* or simple ring polymers have now become accessible through newly developed synthetic protocols, either a ring-closure (RC) of linear polymer precursors [2, 3], or an alternative ring-expansion polymerization (RE) [4–6]. They have been applied broadly to uncover unprecedented cyclic topology effects attributed to the elimination of the chain termini from their relevant linear and branched counterparts [7, 8]. In order to achieve further evolution in this research endeavor and to realize eventually any practical applications of cyclic polymers, an urgent and crucial quest should be a versatile and scalable means for those with any prescribed chemical compositions.

Since a variety of either *hetero*- or *homo*-difunctional telechelic polymer precursors is obtainable conveniently through the end-capping of living/controlled polymerizations, *unimolecular* RC processes have now routinely employed by making use

---

Y. Tezuka (✉)  
Tokyo Institute of Technology, Tokyo, Japan  
e-mail: [ytezukak33@gmail.com](mailto:ytezukak33@gmail.com)

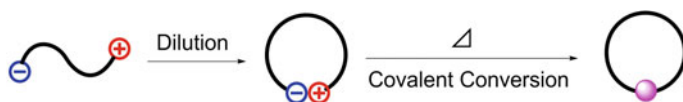
of highly efficient linking protocols, including in particular an alkyne-azide addition (*click*) [9], or an olefin-metathesis condensation (*clip*) process [10]. Under dilution, the intramolecular polymer cyclization tends to proceed preferentially over the intermolecular chain extension, while the reducing chain-end concentration inevitably induces the significant kinetic suppression, limiting, in particular, their practical use toward the scalable preparation of high molecular weight products.

Alternative ring-expansion polymerization (RE) processes have been developed, typically with the transition metal complex catalysts having deliberately designed cyclic ligands, as in the ring-expansion metathesis polymerization (REMP) of cycloalkenes [4] as well as in the relevant ring-expansion polymerization of alkynes [6]. Remarkably, the repetitive monomer insertion into a cyclic initiator moiety takes place under the even low concentration of the propagation species, and the following elimination of the active propagating group either during and/or after the propagation step can produce ring polymer products free of unstable propagating/catalyst moieties.

A zwitterionic ring-opening polymerization has also been applied to extend the scope of the RE process [5]. By introducing a class of new initiators, including *N*-heterocyclic carbenes or strong organic base reagents like DBU, the ring-opening RE polymerization of such heterocyclic monomers as lactones, lactides, lactams, as well as several Si- or P-containing cyclic compounds, was found to proceed with the zwitterionic propagating species [5]. The subsequent covalent recombination of a pair of cationic and anionic species either after the complete monomer consumption or during the course of the propagation could afford cyclic polymer products [11].

A *conjunctive* RC and RE polymer cyclization processes has now been introduced as an innovative strategy, in order to address key issues encountered in the current RC and RE techniques, in particular the kinetic suppression by dilution in the former and the limited choice of monomer types in the latter [12]. Thus, a series of telechelic precursors having a pair of zwitterionic, i.e., a cyclic ammonium cation and a carboxylate anion, end groups has deliberately been introduced for a unimolecular RC polymer cyclization. They are regarded as a relevant RE intermediate polymer analog with the propagating zwitterionic species, in which the complementary cation/anion groups in the propagating active site species inherently balance the charges. Accordingly, these zwitterionic telechelic precursors are applied to a versatile and effective polymer cyclization by the conjunction of RC and RE processes (Fig. 19.1).

Notably, moreover, the ESA-CF polymer cyclization process involves exclusively organic reagents, and obtained cyclic polymer products are free from any trace contamination by heavy metals, and thus are suitable for some of the electronics



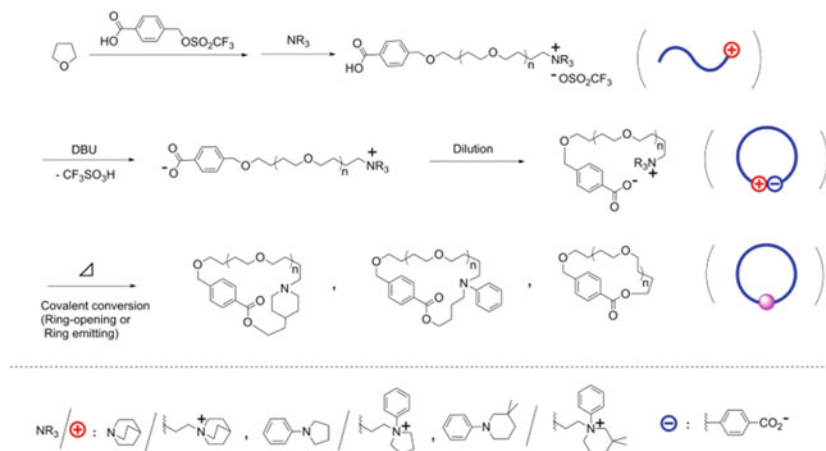
**Fig. 19.1** Unimolecular ESA-CF polymer cyclization upon conjunctive RC and RE processes

and biomedical applications, in contrast to those prepared by the relevant alkyne-azide click RC process in the presence of Cu complex catalysts, or either by the metathesis RC or RE processes requiring typically Ru complex catalysts [4, 6, 9]

## 19.2 Telechelic Poly(THF)s Having a Pair of a Cyclic Ammonium and a Carboxylate Groups for Unimolecular ESA-CF Polymer Cyclization

A series of telechelic poly(THF)s having three types of the zwitterionic pair by cyclic ammonium and benzoate groups were prepared. Thus, the living cationic polymerization of THF was carried out using a new functional initiator, i.e., a benzyl triflate ester derivative having a benzoic acid unit, which is obtainable *in situ* by the reaction of triflic anhydride with 4-hydroxymethyl benzoic acid [12]. (Scheme 1) It is notable that the employed initiator possessing a free benzoic acid group was found to be effective for the living cationic polymerization process of THF, involving an oxonium/triflate ester as a propagation species.

The end-group conversion of the living propagating oxonium site of poly(THF) with either quinuclidine, with *N*-phenylpyrrolidine, or with 3,3-dimethyl-*N*-phenylpiperidine was subsequently performed to produce the corresponding poly(THF)s having a zwitterionic pair of a cyclic quaternary ammonium accompanying a triflate counteranion and a benzoic acid groups. The subsequent deprotonation of the benzoic acid unit was performed by the treatment typically with such a



**Scheme 1** Unimolecular polymer cyclization with telechelic poly(THF)s having a zwitterionic pair of a cyclic ammonium and a carboxylate groups. Adapted with permission from [12]. Copyright 2019 American Chemical Society (ACS AuthorChoice)

strong base reagent like DBU, to form the zwitterionic telechelic poly(THF)s having a pair of a quaternized ammonium and benzoate groups. (Scheme 1)

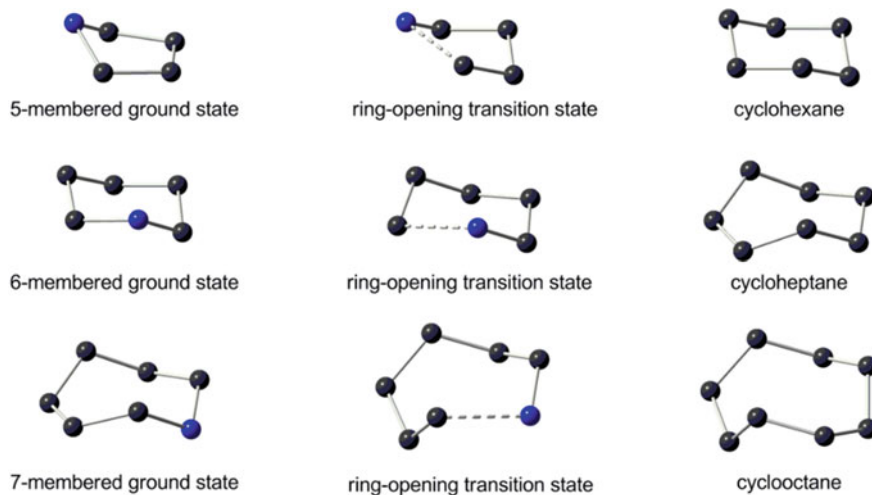
The zwitterionic pair of either quinuclidinium or *N*-phenylpyrrolidinium cation and benzoate anion undergoes the covalent transformation via the *ring-opening* reaction of the cyclic ammonium unit by the benzoate counteranion. Accordingly, the cyclic polymer product having an aminoester linking unit is formed from these pairs. In contrast, the distinctive chemical mode of the *ring-emitting* (elimination of cyclic amine unit) reaction takes place with 3,3-dimethyl-*N*-phenylpiperidinium cation and benzoate anion [1, 13, 14]. Thus, notably, the covalently converted product having a simple ester, and thus hydrolytically and/or thermally robust linkage unit is obtainable from the latter telechelic precursor [13, 14].

In this connection, it is noteworthy that the  $S_N2$  esterification reactions involving 5-, 6- and 7-membered cyclic ammonium salts proceeds under a counterintuitive regioselectivity [13, 14]. Thus, the quantitative ring-opening reaction occurs with the 5-membered cyclic (pyrrolidinium) and 6-membered bicyclic ammonium (quinuclidinium) salts by carboxylate anions, and the regioselectivity has been intuitively ascribed to their ground-state ring strains. To our surprise, however, the predominant ring-emitting reaction (80–90%) was observed for the  $S_N2$  reaction of the apparently strain-free 6-membered ring, *N*-phenylpiperidinium salt end groups by carboxylate anions, occurring at the *exo*-position, i.e., the *N*-adjacent methylene unit of the polymer chain [13, 14]. In a consistent manner, the 7-membered counterpart was found to cause also the predominant  $S_N2$  ring-emitting reaction, despite their ground-state ring strains are comparable with the 5-membered counterpart (both 25.9 kJ/mol, as for cyclopentane and cycloheptane) [14].

The DFT analysis has subsequently been conducted and the results are summarized in Fig. 19.2 [14]. It is recognized that the skeletal 5-membered ring, azacyclopentane conformation at the ground state apparently transforms into a hypothetically strain-free 6-membered, azacyclohexane ring structure at the  $S_N2$  ring-opening transition state. More interestingly, the strain-free 6-membered ring, azacyclohexane structure at the ground state tends to transform into the sterically frustrated 7-membered ring, hypothetical azacycloheptane conformation at the ring-opening transition state [14]. And in a consistent manner, the 7-membered azacycloheptane ring conformation rearranges into a hypothetical 8-membered ring, thus incrementally strained, azacyclooctane structure at the ring-opening transition state. These DFT results clearly indicate that the steric frustration at the transition state rather than the ring strain energy at the ground state is dictating the regioselectivity in these  $S_N2$  reactions involving the cyclic ammonium salts [13, 14].

Notably, moreover, the further DFT study with *N*-phenyl-3,3-dimethylpiperidinium salts has indicated that the 1,3-diaxial interaction on the 6-membered ring, azacyclohexane unit could affect pronouncedly on the  $S_N2$  transition state energy profile, to achieve the quantitative ring-emitting reaction, which was subsequently confirmed experimentally [13].





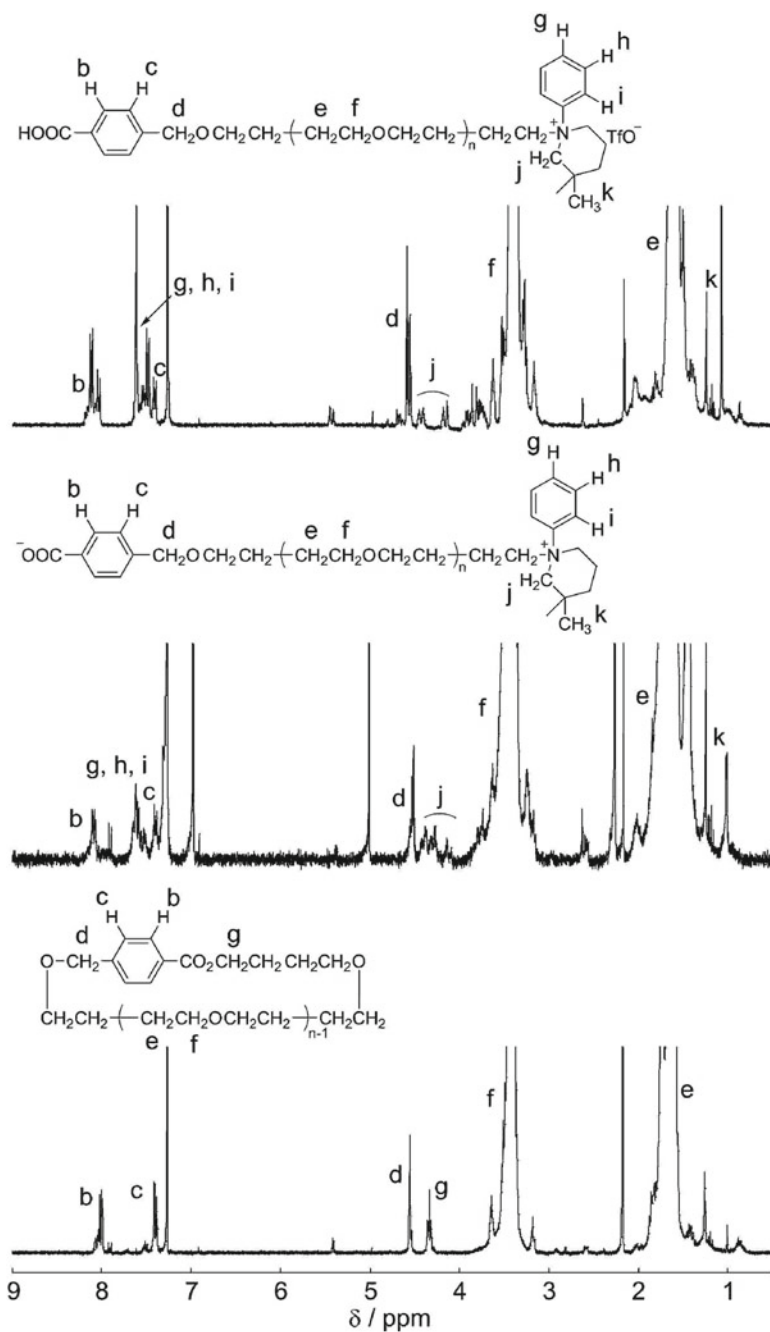
**Fig. 19.2** DFT-optimized skeletal conformations for 5-, 6- and 7-membered ring, azacycloalkanes at their ground states (left), at their ring-opening transition states (center), and their relevant cycloalkane conformations (right). Reprinted with permission from [16]. Copyright 2017 American Chemical Society

### 19.3 Unimolecular Polymer Cyclization with Telechelic Poly(THF)s Having a Pair of a Cyclic Ammonium and a Carboxylate Groups

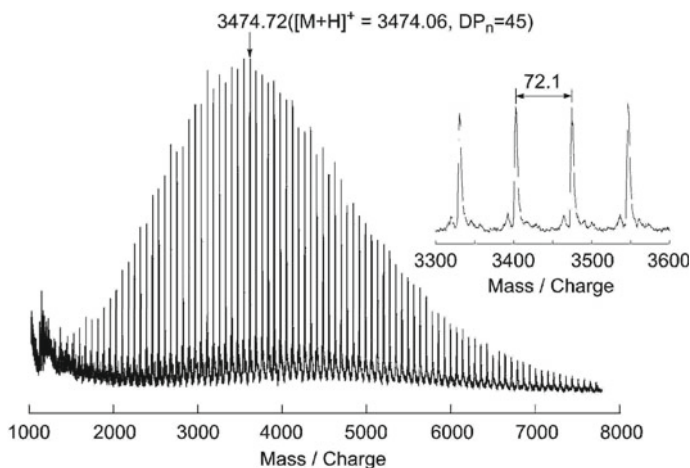
As a showcase example of the polymer cyclization with a zwitterionic telechelic precursors, the poly(THF) precursor having specifically a 3,3-dimethyl-*N*-phenylpiperidinium end group is outlined. Since the ESA-CF polymer cyclization of this telechelic precursor proceeds through the covalent conversion with the selective *ring-emitting* (elimination of cyclic amine unit) reaction, the practically attractive cyclic polymer product having a simple and robust ester linkage unit is produced [13]. On the other hand, alternative polymer products having aminoester linking units are formed through the *ring-opening* covalent conversion of such cyclic ammonium cations of either quinuclidinium or *N*-phenylpyrrolidinium groups.

Thus, the zwitterionic telechelic poly(THF) was obtained by the base treatment of the relevant poly(THF) precursor having a pair of the cyclic ammonium and a free benzoic acid end groups to cause the deprotonation of the acid unit. The zwitterionic telechelic poly(THF) was characterized by the  $^1\text{H NMR}$  inspection (Fig. 19.3), where the  $N^+$ -adjacent methylene proton signals were observed to shift from 3.74–4.47 ppm to 4.07–4.38 ppm, while the *N*-phenyl proton signals at 7.53–7.63 ppm and the methyl proton signal on the piperidinium unit at 1.08 ppm were unaffected.

The subsequent unimolecular polymer cyclization of the zwitterionic poly(THF) was performed under optimized dilution (0.2 g/L) in THF under reflux condition, and the product was finally recovered after silica gel column treatment. The obtained



**Fig. 19.3**  $^1\text{H}$  NMR spectra of the zwitterionic poly(THF) precursor of (top) before and (middle) after the deprotonation treatment, and of (bottom) the polymer cyclization product. Reprinted with permission from [12]. Copyright 2019 American Chemical Society (ACS AuthorChoice)

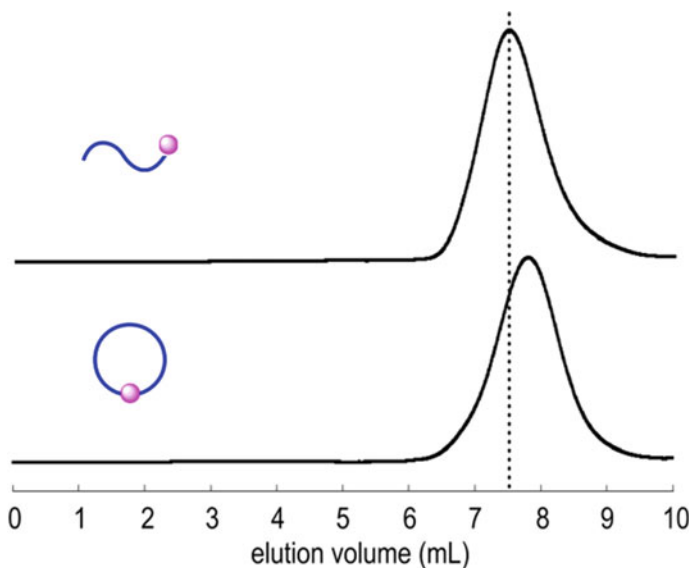


**Fig. 19.4** A MALDI-TOF mass spectrum of the polymer cyclization product obtained from the zwitterionic telechelic poly(THF) precursor. Reprinted with permission from [12]. Copyright 2019 American Chemical Society (ACS AuthorChoice)

cyclic poly(THF) product having a benzoate ester linkage was characterized by means of  $^1\text{H}$  NMR (Fig. 19.3), MALDI TOF mass (Fig. 19.4), and SEC (Fig. 19.5) techniques. Thus, the  $^1\text{H}$  NMR showed that the ester methylene signals appeared at 4.34 ppm along with the total elimination of the *N*-phenyl signals due to the cyclic ammonium group visible in the precursor (Fig. 19.3), to be consistent with the simple benzoate ester unit by the selective and quantitative covalent conversion with 3,3-dimethyl-*N*-phenylpiperidinium unit.

The MALDI TOF analysis of the cyclized poly(THF) (Fig. 19.4) showed, moreover, the peak at  $m/z = 3474.72$ , which was assumed to be the adduct with  $\text{Na}^+$ , corresponds to the product possessing the simple benzoate ester as the linking unit with a  $\text{DP}_n$  of 45;  $(\text{C}_4\text{H}_8\text{O}) \times 45 + \text{C}_{12}\text{H}_{14}\text{O}_3$  plus  $\text{Na}^+$  equals 3474.06.

The SEC trace of the cyclized product was compared with that of the linear precursor analogs, obtained by the treatment with an excess amount of benzoate anion to cause the covalent conversion of the cyclic ammonium into the benzoate ester species (Fig. 19.5). The SEC traces remained unimodal with the PDI of around 1.1, to show the selective covalent conversion and the absence of any polymer degradation during the covalent conversion process. The significant reduction of the apparent peak molecular weight, corresponding to their respective 3D sizes, observed evidently along with the polymer cyclization, further substantiated the transformation of the linear telechelic precursor into the cyclic product retaining their chain lengths.



**Fig. 19.5** SEC traces of (top) the zwitterionic poly(THF) precursor after the covalent conversion of the ionic group, and (bottom) the ESA-CF polymer cyclization product therefrom. Reprinted with permission from [12]. Copyright 2019 American Chemical Society (ACS AuthorChoice)

## 19.4 Perspectives of Unimolecular Polymer Cyclization with Zwitterionic Telechelic Precursors

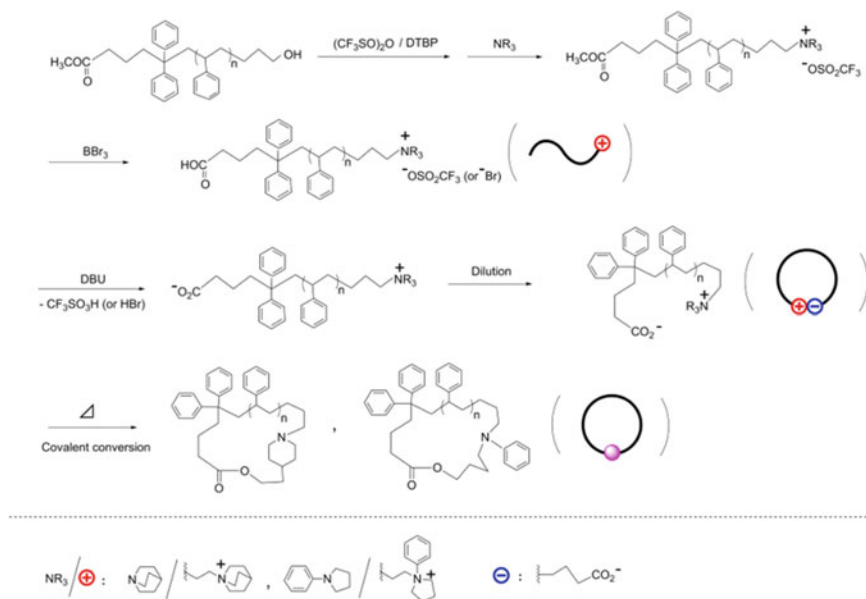
The present unimolecular polymer cyclization using zwitterionic telechelic precursors is apparently an extension of an *pseudo-bimolecular* ESA-CF polymer cyclization process [15, 16], in which a variety of linear and branched telechelic precursors having appropriately reactive cyclic ammonium, typically 5-membered *N*-phenylpyrrolidinium, groups carrying relevantly nucleophilic carboxylate counteranions, have been widely employed as key prepolymers. The attractive interaction between cationic and anionic species among the polymer components, with the inherent balance between opposite charges, tends to mitigate the kinetic suppression under dilution (apparent low overall concentration). The subsequent quantitative conversion of the ionic pair species effectively produces the corresponding polymer products having the robust covalent bond by the selective nucleophilic ring-opening or ring-emitting reaction at the prescribed elevated temperature.

While the *pseudo-bimolecular* ESA-CF protocol has been applied extensively to prepare diverse cyclic and multicyclic polymers [15, 16], the anion-replacing process to introduce the designated carboxylate has often been laborious or inefficient in practice. The repetitive reprecipitation treatment is usually required, in turn to bring a loss of a part of the sample material having, in particular, high molecular weights during the recovery. In contrast, the relevant *unimolecular* process could

inherently proceed with the equimolar combination of counterion pairs by introducing them as the end group. Indeed, in the *pseudo-bimolecular* ESA-CF procedure reported before [13], a bifunctional poly(THF) precursor having 3,3-dimethyl-*N*-phenylpiperidinium groups at both chain ends was subjected to the repeated reprecipitation/recovery treatment in order to accommodate the high portion of the biphenyl dicarboxylate counteranion. In contrast, this ion-exchange step is eliminated in the corresponding *unimolecular* process to improve the final yield of the cyclic polymer product.

In order to further demonstrate the promising feature of the *unimolecular* polymer cyclization process, a series of cyclic polystyrenes having the MW of up to 10 kDa with the narrow size distributions were produced in good isolated yields. A series of zwitterionic telechelic polystyrenes having a zwitterionic pair of cyclic ammonium and carboxylate groups were obtained accordingly by taking advantage of a living anionic polymerization technique (Scheme 2) [12].

To conclude, the ESA-CF polymer cyclization process with zwitterionic telechelic precursors has been proven as a prominent protocol to produce diverse cyclic polymers, where either cationic or anionic living polymerization technique are applied to prepare the relevant telechelic precursors with a versatile choice of polymer segment structures [12]. By the conjunction of the RC and the RE processes, moreover, the kinetic suppression inherently encountered in the conventional RC processes under



**Scheme 2** Unimolecular polymer cyclization with zwitterionic telechelic polystyrenes having a pair of a cyclic ammonium and a carboxylate groups. Adapted with permission from [12]. Copyright 2019 American Chemical Society (ACS AuthorChoice)

dilution could be mitigated through the association of the ionic chain ends as in the RE propagation species, to enhance the local concentration of the ionic pair units eventually converted into the covalent linkage.

## References

1. Y. Tezuka (ed.), *Topological Polymer Chemistry: Progress of cyclic polymers in syntheses, properties and functions* (World Scientific, Singapore, 2013)
2. S.M. Grayson, Y.D. Getzler, D. Zhang, D., Eds. *Cyclic polymers: New developments*, (Special issue in *Reactive and Functional Polymers*, vol. 80, 2014)
3. Z. Jia, M.J. Monteiro, *Adv. Polym. Sci.* **262**, 295 (2013)
4. J.P. Edwards, W.J. Wolf, R.H. Grubbs, *J. Polym. Sci., Part-A, Polym. Chem.* **57**, 228 (2019)
5. Y.A. Chang, R.M. Waymouth, *J. Polym. Sci., Part-A, Polym. Chem.* **55**, 2892 (2017)
6. C.D. Roland, H. Li, K.D. Abboud, K.B. Wagener, A.S. Veige, *Nature Chem.* **8**, 791 (2016)
7. T. Yamamoto, Y. Tezuka, *Soft Matter* **11**, 7458 (2015)
8. F.M. Haque, S.M. Grayson, *Nature Chem.* **12**, 433 (2020)
9. B.A. Laurent, S.M. Grayson, *J. Am. Chem. Soc.* **128**, 4238 (2006)
10. Y. Tezuka, R. Komiya, *Macromolecules* **35**, 8667 (2002)
11. H.M. Brown, S. Xiong, G.A. Medvedev, Y.A. Chang, M.M. Abu-Omar, J.M. Caruthers, R.M. Waymouth, *Macromolecules* **47**, 2955 (2014)
12. T. Konomoto, K. Nakamura, T. Yamamoto, Y. Tezuka, *Macromolecules* **52**, 9208 (2019)
13. A. Kimura, S. Takahashi, S. Kawauchi, T. Yamamoto, Y. Tezuka, *J. Org. Chem.* **78**, 3086 (2013)
14. A. Kimura, S. Kawauchi, T. Yamamoto, Y. Tezuka, *Org. Biomol. Chem.* **12**, 6717 (2014)
15. H. Oike, H. Imaizumi, T. Mouri, Y. Yoshioka, A. Uchibori, Y. Tezuka, *J. Am. Chem. Soc.* **122**, 9592 (2000)
16. Y. Tezuka, *Acc. Chem. Res.* **50**, 2661 (2017)

# Chapter 20

## Cyclic Polymers Synthesized by Spontaneous Selective Cyclization Approaches



Daisuke Aoki, Hideyuki Otsuka, and Toshikazu Takata

**Abstract** The status quo of synthetic routes to cyclic polymers via spontaneously occurring cyclization processes using dynamic covalent chemistry and rotaxane chemistry is introduced. Systems based on dynamic covalent chemistry utilize bis(2,2,6,6-tetramethylpiperidin-1-yl)disulfide (BiTEMPS) units that behave as stable covalently bound structures at room temperature, while they exchange disulfide bonds above 80 °C, providing cyclic polymers. Systems with rotaxane-based structures proceed via the spontaneous and selective cyclization of two self-complementary *sec*-ammonium-containing crown ether monomers and a macromolecular rotaxane switch, where the relative position of each component can be controlled, which results in the synthesis of cyclic polymers.

### 20.1 General Approaches for Synthesizing Cyclic Polymers

Cyclic polymers, i.e., polymers with cyclic topologies, have been synthesized due to their unique properties in both solution and bulk, which arise from a lack of polymer chain ends [1–16]. Accordingly, cyclic polymers have attracted substantial attention from a wide range of scientists. However, because of their unique topology, cyclic

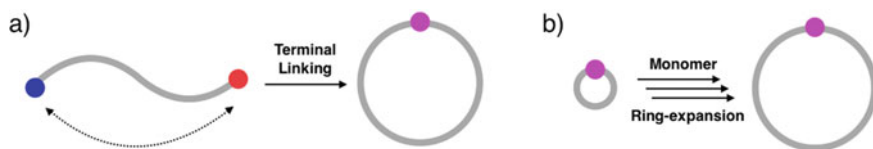
---

D. Aoki (✉) · H. Otsuka  
Department of Chemical Science and Engineering, Tokyo Institute of Technology, Tokyo  
152-8550, Japan  
e-mail: [aoki.d.aa@m.titech.ac.jp](mailto:aoki.d.aa@m.titech.ac.jp)

D. Aoki  
JST PRESTO, Meguro, Tokyo 152-8550, Japan

T. Takata  
Department of Chemical Science and Engineering, Tokyo Institute of Technology, Yokohama  
226-8503, Japan

Graduate School of Advanced Science and Engineering, Hiroshima University, Hiroshima  
739-8527, Japan



**Fig. 20.1** General methods for synthesizing cyclic polymers: **a** intramolecular cyclization of linear polymers with terminal homo- or heterobifunctional groups and **b** ring-expansion polymerization (REP)

polymers are difficult to synthesize. Accordingly, the development of appropriate methods for synthesizing cyclic polymers remains a challenge.

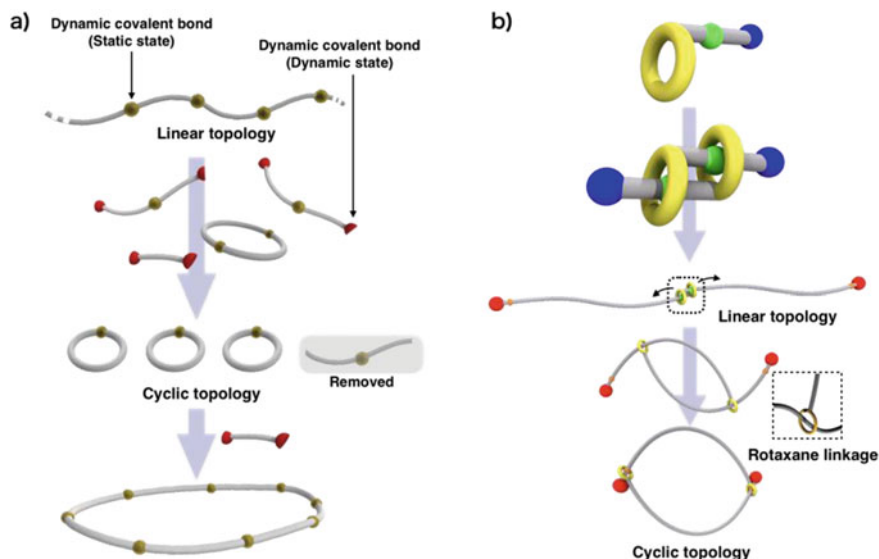
Cyclic polymers are generally synthesized via two primary approaches (Fig. 20.1): (a) intramolecular cyclization of linear polymers with terminal homo- or heterobifunctional groups [1, 12, 16–19] and (b) ring-expansion polymerization (REP) [3, 4, 6, 8, 9, 11, 14, 15, 20–23].

Figure 20.1a illustrates the cyclization of linear polymers with reactive groups at the polymer termini, which is a common method for synthesizing cyclic polymers that have the same composition and polydispersity as their precursors. However, this approach requires high-dilution conditions to prevent intermolecular reactions and elaborate purification processes to remove undesired products. In contrast, REP approaches, which are based on the insertion of monomer units into an activated cyclic initiator or monomer, can efficiently synthesize cyclic polymers with high molar mass at a relatively high yield. However, most REP processes require specific substances, such as cyclic initiators and monomers that are difficult to synthesize, as well as reaction conditions that require special catalysts and degassing. Because these methods both have advantages and disadvantages, as have been well summarized by several other experts in this field [14, 24–26], a universal strategy for synthesizing cyclic polymers is still in high demand. As cyclization reactions are inevitable in the synthesis of cyclic polymers, the issues of when and how these cyclization reactions are performed in the synthesis sequence should be a key point to success. A system capable of spontaneous, selective cyclization would be ideal. In this chapter, we describe recent progress on unique approaches for synthesizing cyclic polymers via spontaneous selective cyclization approaches.

## 20.2 Unique Approaches for Synthesizing Cyclic Polymers via Spontaneous Selective Cyclization Approaches

We have developed two approaches for synthesizing cyclic polymers via spontaneous selective cyclization. The first approach uses a topological change under a concomitant cleavage of covalent bonds, i.e., a cyclization process induced by cleaving and forming covalent bonds. This approach is enabled by dynamic covalent chemistry (DCC) (Fig. 20.2a) [27–29].





**Fig. 20.2** Spontaneous selective cyclization approaches for synthesizing cyclic polymers via **a** DCC or **b** rotaxane chemistry

The second approach utilizes a topological change without the cleavage or formation of covalent bonds in the main polymer chain. This approach is enabled by a mechanically linked structure. In this context, the rotaxane linkage is the most promising tool, as the components in the rotaxane structure exhibit a high degree of mobility (Fig. 20.2b) [30–37].

### 20.3 Synthesis of Cyclic Polymers via DCC: Using Ring/Chain Equilibria

DCC is conceptually related to reversible chemical reactions under equilibrium control. DCC is dependent on the reversible formation and cleavage of relatively strong covalent bonds in molecules. Therefore, this approach combines the error-correction ability of supramolecular interaction and the strength of covalent bonding [27, 28]. Given that the reaction occurs under thermodynamic control, the obtained product variety depends only on the relative stability of the final products. DCC has been applied to obtain cyclic polymers via exchange reactions in dilute conditions based on the ring/chain equilibria in solution (Fig. 20.3).

To obtain a cyclic structure via the ring/chain equilibria of polymers possessing dynamic covalent bonds in their repeat units, shuffling reactions via DCC must occur under dilute concentrations [38, 39]. The cyclodepolymerization reaction is well

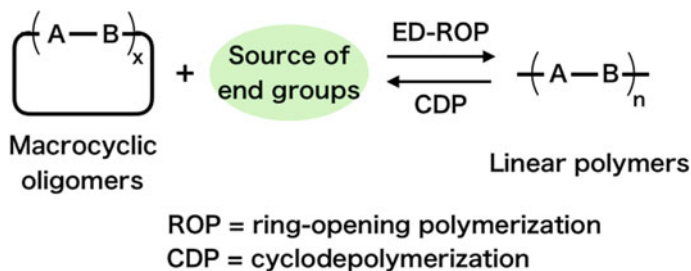


Fig. 20.3 Ring/chain equilibria

known and has been widely applied to prepare macrocycles (MCs) by the decomposition of corresponding linear polymers. We note that the ring/chain equilibria in DCC are spontaneous but not selective toward specific cyclic compounds and polymers. If selectivity could be attained in a DCC system, this approach would be an attractive method for synthesizing cyclic polymers. Otsuka et al. reported that the bis(2,2,6,6-tetramethylpiperidin-1-yl)disulfide (BiTEMPS) structure is a stable covalently bound moiety at room temperature, which also exchanges disulfide bonds at temperatures exceeding 80 °C [40]. Accordingly, BiTEMPS units can be applied to ring/chain equilibria: solutions of polyurethanes containing BiTEMPS units in the polymer repeat units undergo cyclodepolymerization from linear polymers to oligomers in highly diluted conditions, a process that is reversed upon heating under high-concentration conditions (Fig. 20.4).

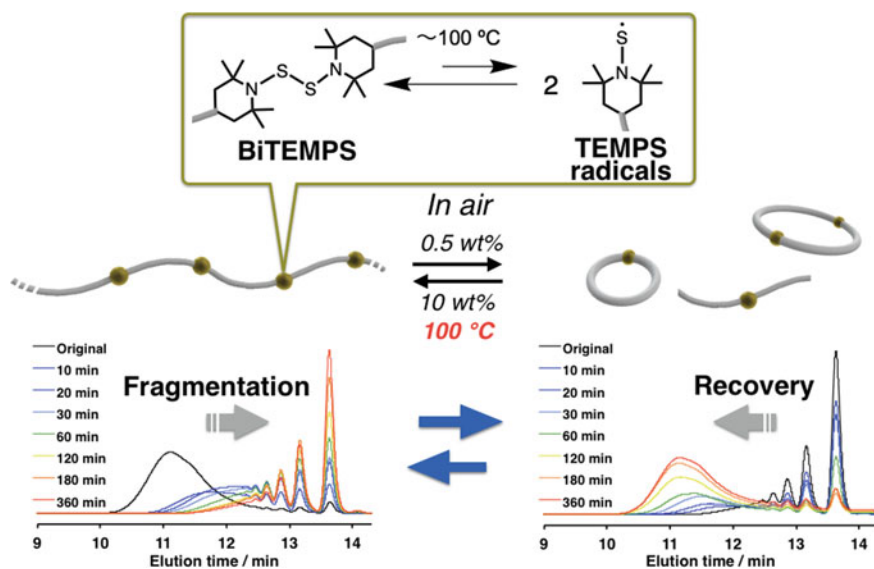
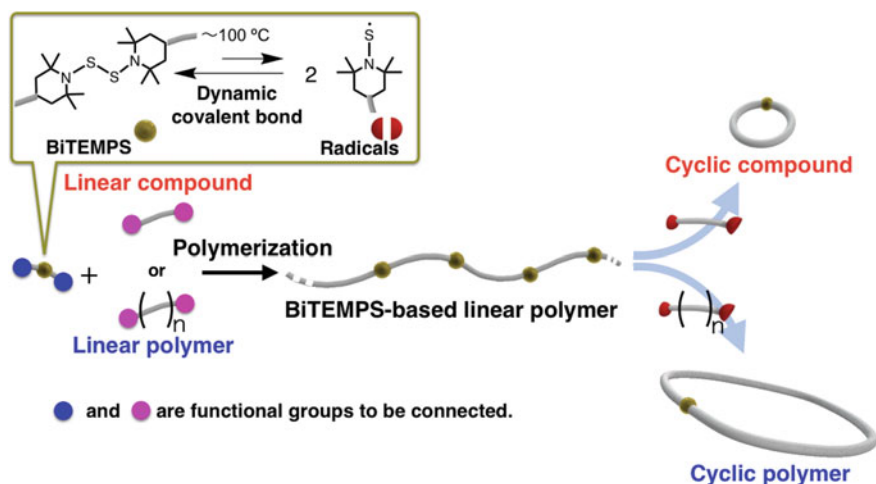


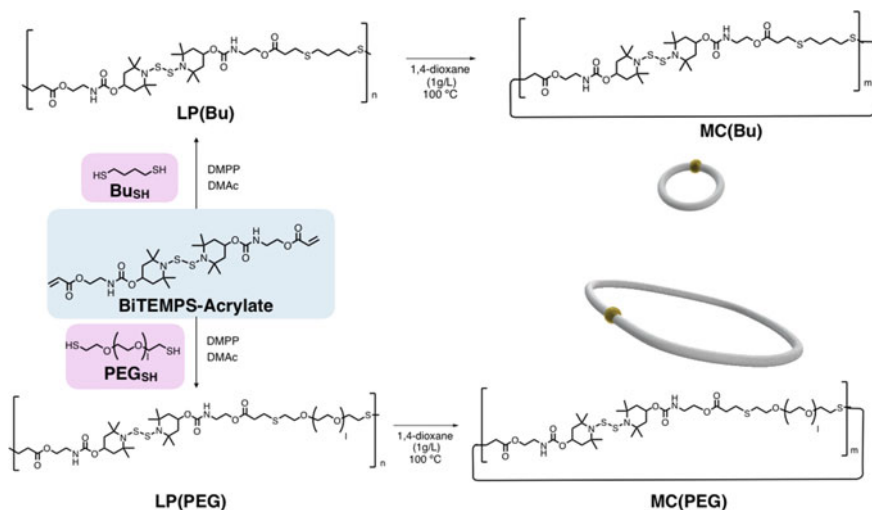
Fig. 20.4 Ring/chain equilibrium derived from BiTEMPS units



**Fig. 20.5** Schematic of the strategy for obtaining cyclic compounds and polymers via the ring/chain equilibria induced by BiTEMPS units

This finding inspired us to develop a universal strategy for achieving the cyclic topology, as BiTEMPS units have unique features that are not exhibited by other dynamic covalent bonds. BiTEMPS units exhibit the following dynamic features: (i) The linear precursors can be cyclized if they can react with BiTEMPS derivatives, i.e., by linking the target molecule and the BiTEMPS unit with covalent bonds. (ii) The radicals generated from BiTEMPS have a high tolerance toward various functional groups because of their poor reactivity with a wide range of chemical species, including oxygen. Moreover, BiTEMPS shows high reactivity in exchange reactions, rendering it applicable to a variety of skeletons. (iii) Simple heating can induce cyclization reactions; thus, there is no need to supply additional catalysts or additives. The primary concept of obtaining cyclic compounds and polymers via the dynamic nature of BiTEMPS is shown in Fig. 20.5. The target molecules (including the polymer chain) toward the cyclic topology react with a BiTEMPS derivative to give the corresponding BiTEMPS-based linear polymer, which is subsequently cyclized.

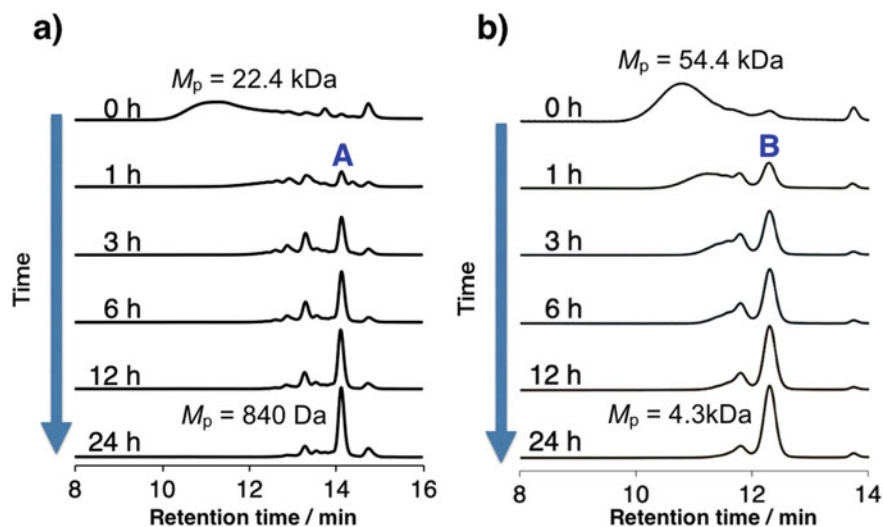
Based on the strategy shown in Fig. 20.5, we applied a BiTEMPS derivative with diacrylate groups (**BiTEMPS-Acrylate**) as the BiTEMPS source, combined with two types of thiols as the target skeleton for the cyclic structure: (1) 1,4-butanedithiol (**Bu<sub>SH</sub>**) and (2) polyethylene glycol (PEG) with thiol groups at the end of the polymer chain (**PEG<sub>SH</sub>**). This combination was achieved via thiol-ene reactions in the presence of dimethylphenylphosphine (DMPP) as a catalyst (Fig. 20.6). For the present method, polymers with high molar mass are not suitable due to difficulties associated with controlling the stoichiometry in the reaction feed (AA monomer vs. BB monomer). Therefore, we used a moderate-weight polymer (PEG:  $M_n = 3400$ ), as



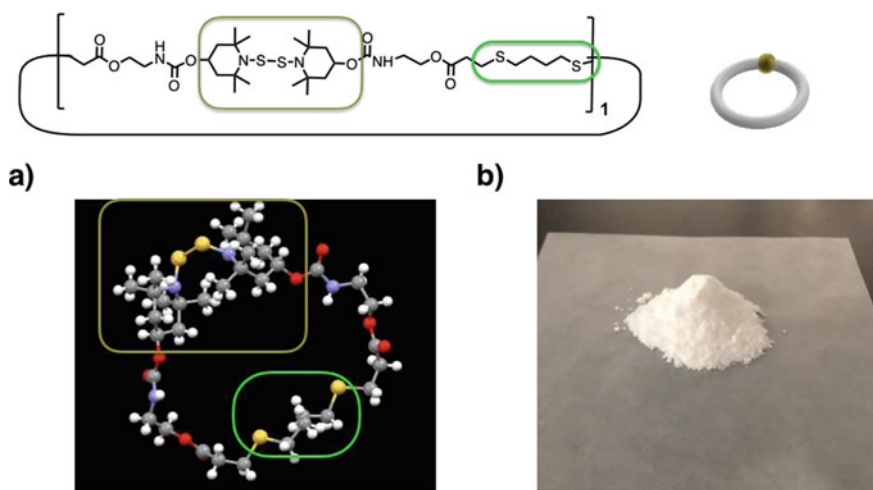
**Fig. 20.6** Synthesis of cyclic compounds and polymers via ring/chain equilibria derived from BiTEMPS units

a target skeleton. Reprecipitation of the obtained polymers, **LP(Bu)** and **LP(PEG)**, was conducted to quantitatively afford linear polymers.

Subsequently, cyclodepolymerization, i.e., a change in topology from linear precursors to cyclic polymers, was performed. **LP(Bu)** and **LP(PEG)** were both cyclized in 1,4-dioxane (1.0 g/L) at 100 °C and monitored by gel permeation chromatography (GPC). As shown in Fig. 20.7, the peaks of **LP(Bu)** (peak top molecular weight:  $M_p = 22.4$  kDa) and **LP(PEG)** ( $M_p = 54.4$  kDa) disappeared, with a new peak appearing after the cyclization reaction, occurring at  $M_p = 840$  Da (marked as A in Fig. 20.7a) for **LP(Bu)** and  $M_p = 4.3$  kDa (marked as B in Fig. 20.7b) for **LP(PEG)**. Each peak (marked as A and B in Fig. 20.7) grew in intensity with increasing heating time. After heating for 24 h, the solvent was evaporated by a freeze-drying technique. Although purification was not performed for the products [**MC(PEG)**] obtained from **LP(PEG)**, the residue from **LP(Bu)** was purified by flash column chromatography and/or recrystallization to give white crystals of **MC(Bu)**. With these purification techniques, the isolated yield of **MC(Bu)** [ $m = 1$ ] was ~60%. A single crystal of **MC(Bu)** [ $m = 1$ ] was characterized by X-ray diffraction analysis, demonstrating a cyclic structure (Fig. 20.8a). Moreover, a MALDI-TOF MS spectrum of **MC(PEG)** revealed only one series of peaks corresponding to cyclic polymers with one BiTEMPS unit, thus confirming the synthesis of cyclic polymers (Fig. 20.9a). GPC profiles of **MC(PEG)** were compared with the corresponding linear model polymer (**linear-PEG**) for PEG at the same molecular weight (Fig. 20.9b), which demonstrated a decreased hydrodynamic radius due to the cyclic structure. The crystallization behavior of these polymers differed, indicating a cyclic topology effect (Fig. 20.9c).

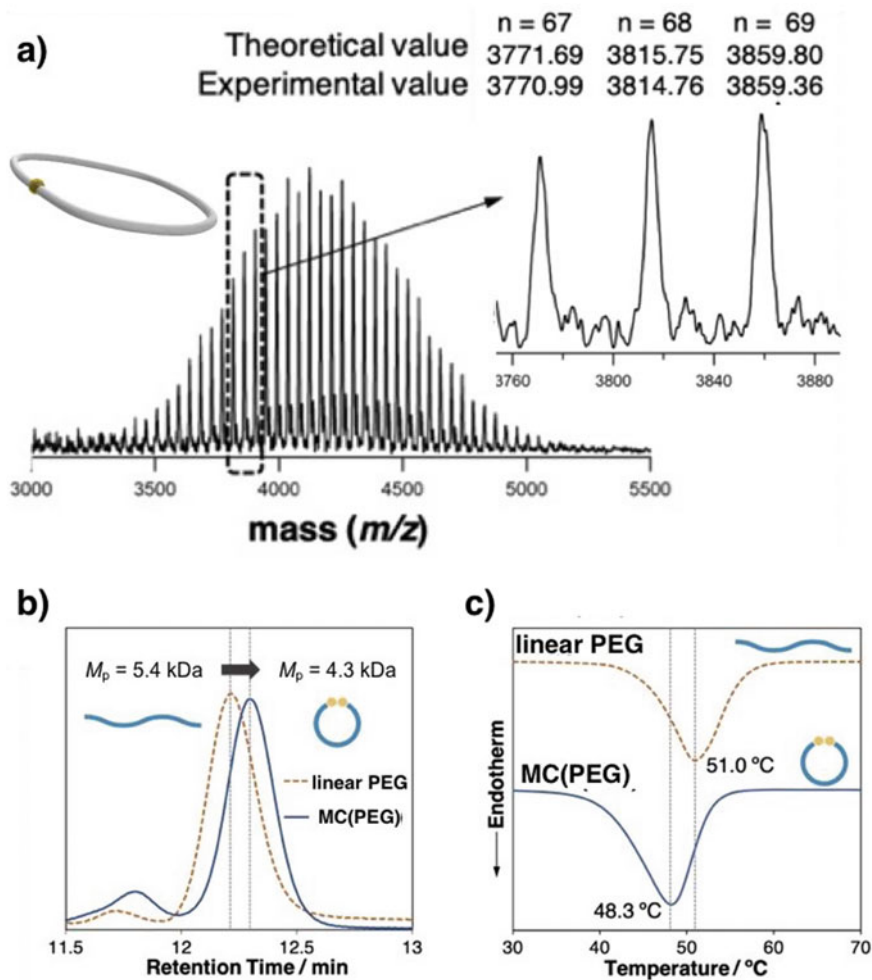


**Fig. 20.7** GPC profiles of the cyclization of **a** LP(Bu) and **b** LP(PEG) in 1,4-dioxane (1 g/L) at 100 °C



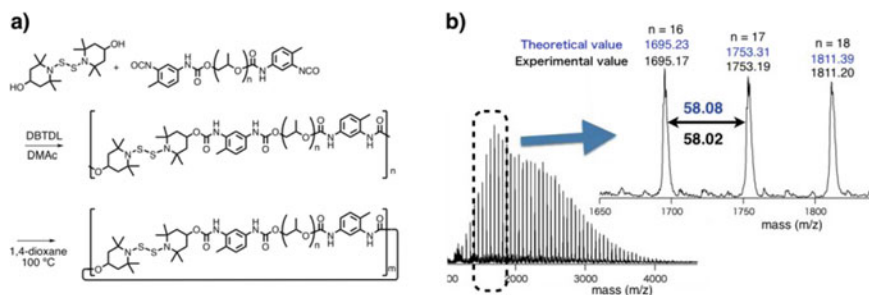
**Fig. 20.8** **a** Molecular structure of MC(Bu) in single crystals and **b** isolated MC(Bu) on the gram scale

The DCC-based cyclodepolymerization approach has been applied to produce MCs from linear polymers since the early 2000s, resulting in the syntheses of “cyclic oligomers” [41]. Conversely, we achieved spontaneous selective cyclization reactions via the exchange reaction of BiTEMPS, which resulted in the selective synthesis and isolation of a specific macrocycle ( $m = 1$ ) when a small molecule was applied, while



**Fig. 20.9** **a** MALDI-TOF MS profile of MC(PEG), **b** GPC profiles of linear PEG and MC(PEG), and **c** differential scanning calorimetry (DSC) curves of linear PEG and MC(PEG)

resulting in a transformation to a cyclic polymer ( $m = 1$ ) as the main product when a macromolecule was applied. We screened the reaction conditions, revealing that the cyclization process can be induced by a concentration of 18 mmol (10 g/L) in **MC(Bu)**; thus, purified cyclic compounds ( $m = 1$ ) are easily accessible on a gram scale with a relatively small amount of solvent. In fact, we have successively isolated cyclic **MC(Bu)** ( $m = 1$ ) on a gram scale using less than 200 mL of solvent (Fig. 20.8b). For **MC(PEG)**, a concentration of 2 g/L (mM scale) gives cyclic products. Notably, the present concentration is much higher than that generally used in the synthesis of



**Fig. 20.10** **a** Synthesis of cyclic poly(propylene glycol) via BiTEMPS-based cyclodepolymerization and **b** MALDI-TOF MS profile of cyclic poly(propylene glycol) with one BiTEMPS unit ( $m = 1$ )

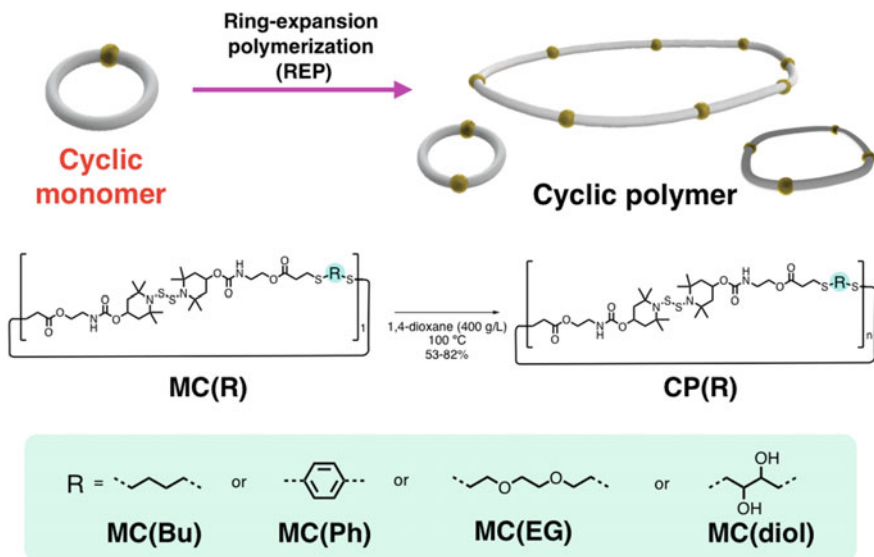
cyclic polymers under dilute conditions. Furthermore, the reactions in Fig. 20.6 can be conducted in air, enabling a simple operation.

We, thus, concluded that the occurrence of this cyclization reaction under relatively high concentrations can be attributed to the error-checking ability enabled by the dynamic nature of BiTEMPS and a high susceptibility toward bond exchange. The present method can be applied to the gram-scale synthesis of cyclic polymers with moderate molar mass. For example, we cyclized commercially available poly(propylene glycol) with functional groups at the polymer termini ( $M_n = 2.3$  kDa) on the gram scale via the present method as a demonstration (Fig. 20.10) [42].

## 20.4 Synthesis of Cyclic Polymers via DCC: Using REP

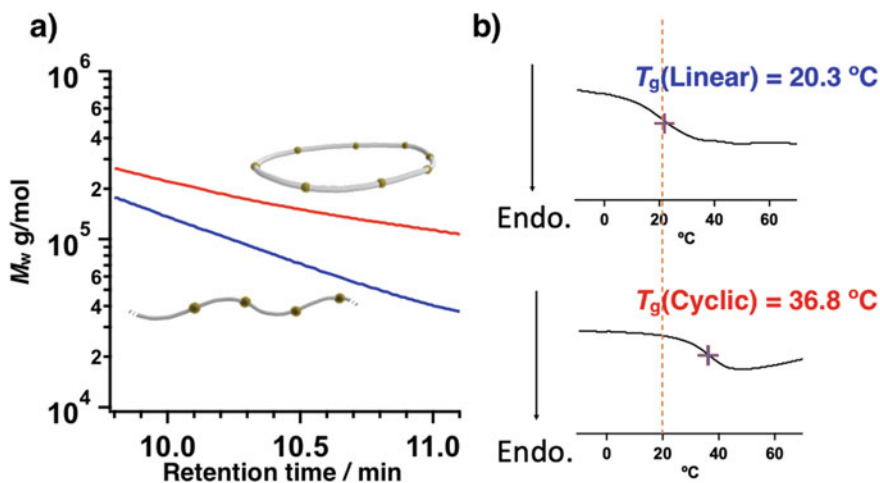
In the previous section, we discussed a synthetic method that produces cyclic compounds and polymers via ring/chain equilibria. In this section, we introduce a simple approach for synthesizing cyclic polymers by applying REP to the MCs obtained in the previous section. This process utilizes another equilibrium without terminal structures in the polymer chain. By combining the BiTEMPS-based ring/chain equilibria and purification techniques, a series of specific MCs ( $m = 1$ ) can be synthesized as shown in Fig. 20.11 [42]. These MCs can then be expanded to give cyclic polymers. As shown in Fig. 20.11, with these entropically driven REP reactions, in which terminal structures are not present, spontaneous selective cyclization can be attained in the synthesis of cyclic polymers by simply heating MCs.

Various MCs, i.e., **MC(Bu)**, **MC(Ph)**, **MC(EG)**, and **MC(diols)**, were prepared by cyclodepolymerization based on BiTEMPS units and were then isolated by purification techniques. Subsequently, heat-induced REP was performed for the resulting MCs. At high concentrations, the conversion of MCs was high (>95% in 400 g/L after 3 h), although 100% conversion was not achieved because of the thermodynamic system. To determine their topology, SEC equipped with multi-angle light scattering (SEC-MALS) was applied to compare the hydrodynamic volume and



**Fig. 20.11** Synthesis method for producing cyclic polymers via the REP of MCs

absolute molecular weights of **CP(Bu)** and **LP(Bu)**. The SEC-MALS results for **CP(Bu)** and **LP(Bu)** show clear differences with respect to their topology: a lower hydrodynamic volume was confirmed for **CP(Bu)** versus **LP(Bu)**, suggesting that **CP(Bu)** is cyclic (Fig. 20.12a).



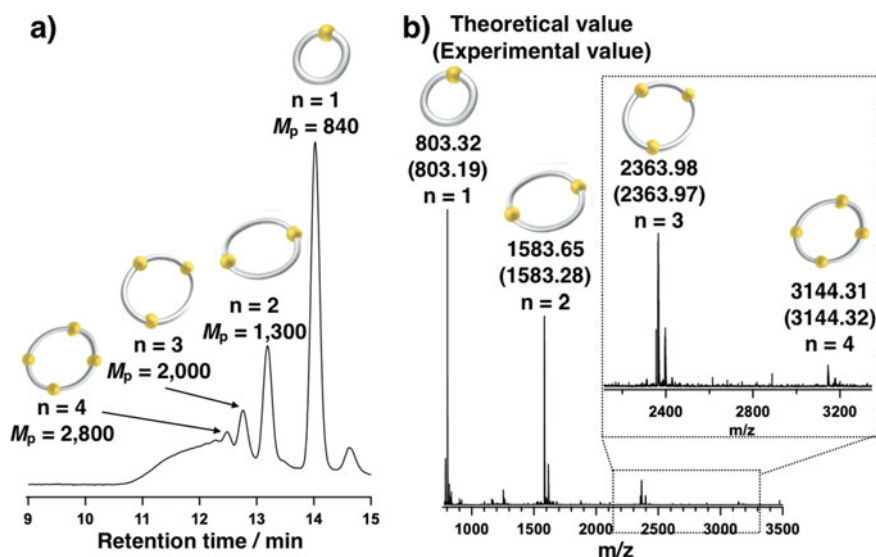
**Fig. 20.12** **a** Logarithmic plot of the absolute molecular weight versus retention time for **CP(Bu)** (red) and **LP(Bu)** (blue). **b** DSC curves for **LP(Bu)** (top) and **CP(Bu)** (bottom) samples with the same molecular weight, as estimated by SEC



Using differential scanning calorimetry (DSC), the thermophysical properties of the polymers were also characterized, revealing a significant change in the glass-transition temperature ( $T_g$ ) for **CP(Bu)** ( $T_{g(\text{cyclic})} = 37\text{ }^\circ\text{C}$ ;  $M_{n\text{SEC}} = 55.0\text{ kDa}$ ) and **LP(Bu)** ( $T_{g(\text{linear})} = 20\text{ }^\circ\text{C}$ ;  $M_{n\text{SEC}} = 56.0\text{ kDa}$ ). This result provides further evidence that the obtained polymer is cyclic, as the  $T_g$  for a cyclic polymer is generally higher than that of a linear polymer (Fig. 20.12b) [43]. Cyclic oligomers [**Oligo CM(Bu)**] were also synthesized when the reaction was conducted under relatively dilute conditions (20 g/L), as confirmed by electrospray ionization time-of-flight MS (ESI-TOF MS). The peaks in the SEC elution curves and ESI-TOF MS results are consistent with the theoretical value calculated for cyclic oligomers ( $n = 2\text{--}4$ ), demonstrating that cyclic polymers were formed (Fig. 20.13).

The present method, i.e., the ring-expansion strategy based on MCs, can also be applied to produce cyclic copolymers by combining different monomers (Fig. 20.14).

MCs with BiTEMPS units can be synthesized on the gram scale with a relatively small amount of solvent; thus, one can synthesize cyclic polymers on a large scale via the present simple route. This facile and selective synthetic method enables the introduction of functional groups into cyclic polymers, e.g., using **MC(EG)** and **MC(diol)** as monomers. The procedural simplicity of this approach is expected to encourage further characterization of cyclic polymers and novel applications [44].



**Fig. 20.13** **a** SEC curves for a mixture of *Oligo CM(Bu)* (PS standards; eluent: THF; flow rate: 0.6 mL/min; UV detector). **b** ESI-TOF MS spectrum for a mixture of *Oligo CM(Bu)* ( $M_n < 3.5\text{ kDa}$ ); all peaks were detected as  $[M + Na]^+$ ). **c** Enlarged view of the ESI-TOF MS spectrum shown in (b). Reprinted with permission from Ref. [44]. Copyright (2020) American Chemical Society

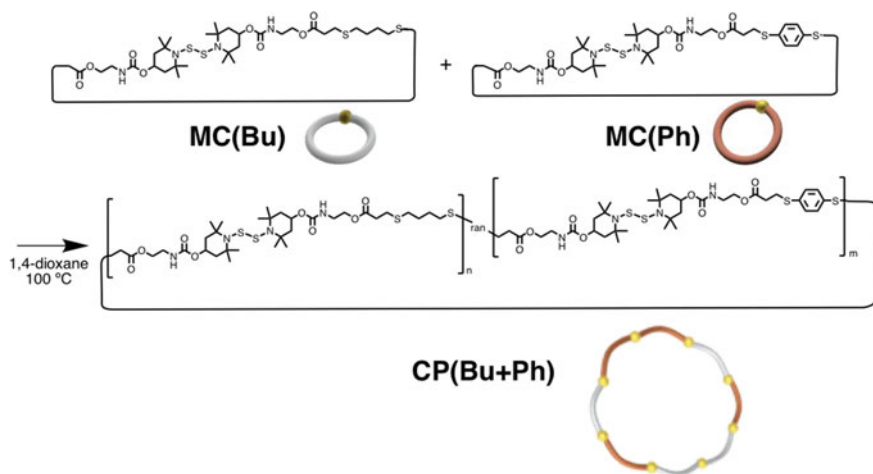


Fig. 20.14 Copolymerization of MC(Bu) and MC(Ph)

## 20.5 Synthesis of Cyclic Polymers via Rotaxane Chemistry

In this section, we combine a spontaneously occurring self-assembly process in the synthesis of a rotaxane structure and a topological change without the cleavage or formation of covalent bonds in the main polymer chain via the rotaxane structure. This combination is introduced as a novel approach for producing cyclic polymers. A rotaxane is a mechanically interlocking pair of molecules consisting of an axle component and a wheel component. In the rotaxane structure, the relative positions of the components can be changed by altering their interactions. Thus far, several rotaxane molecular switches have been reported (Fig. 20.15a), [45–47] and even long-range switches have been achieved (Fig. 20.15b) [48]. To synthesize a

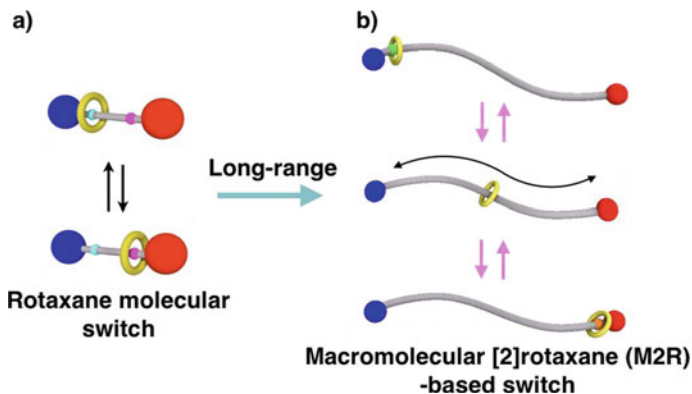
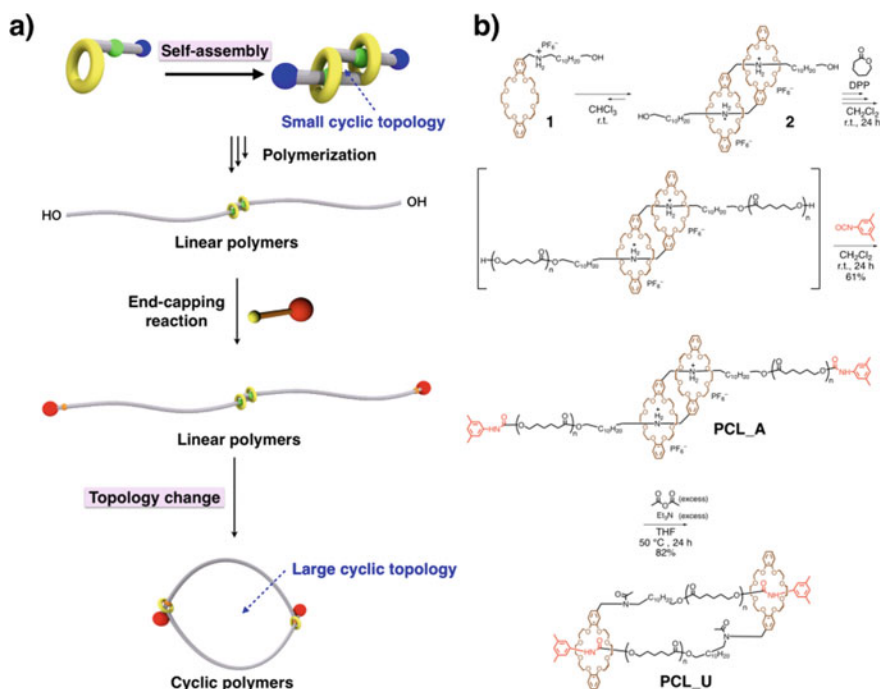


Fig. 20.15 Rotaxane-based molecular switches

rotaxane structure, the interaction between components, such as the *sec*-ammonium salt/dibenzo-24-crown-8-ether (DB24C8) interaction, provides the driving force to thread the cavity of the wheel component. The threaded structure is then maintained by end-capping with bulky stoppers.

We focused on the “space” formed by self-complementary molecules that contain two mutually recognizing moieties in the process of forming the threading structure (Fig. 20.16a). Such monomers can spontaneously and selectively self-assemble into [c2] daisy chain units. As the space between [c2] daisy chain units is cyclic, we regarded this self-assembly as a cyclization step in the preparation of cyclic polymers. The thus-obtained small space that appears as a cyclic structure, consisting of [c2] daisy chain dimers, can be enlarged into larger circles by introducing polymer chains as axle components. This step is followed by a change in topology, induced by a change in the interaction.

Using this method, we synthesized crown ethers containing a *sec*-ammonium part and a terminal hydroxy group (**1**) (Fig. 20.16b). In a solvent with moderate polarity, such as chloroform or dichloromethane, **1** dimerizes spontaneously into [c2]-daisy-chain-type intermediate **2** via a self-assembly process. The self-assembled structure (**2**) was confirmed using  $^1\text{H}$  NMR spectroscopy in  $\text{CDCl}_3$ , as well as using



**Fig. 20.16** Synthesis of cyclic polymers via rotaxane chemistry: **a** synthesis strategy and **b** reaction scheme

MALDI-TOF MS and ESI-TOF MS spectra, demonstrating that the self-assembly-induced cyclization occurs spontaneously and selectively under both dilute and high-concentration conditions.

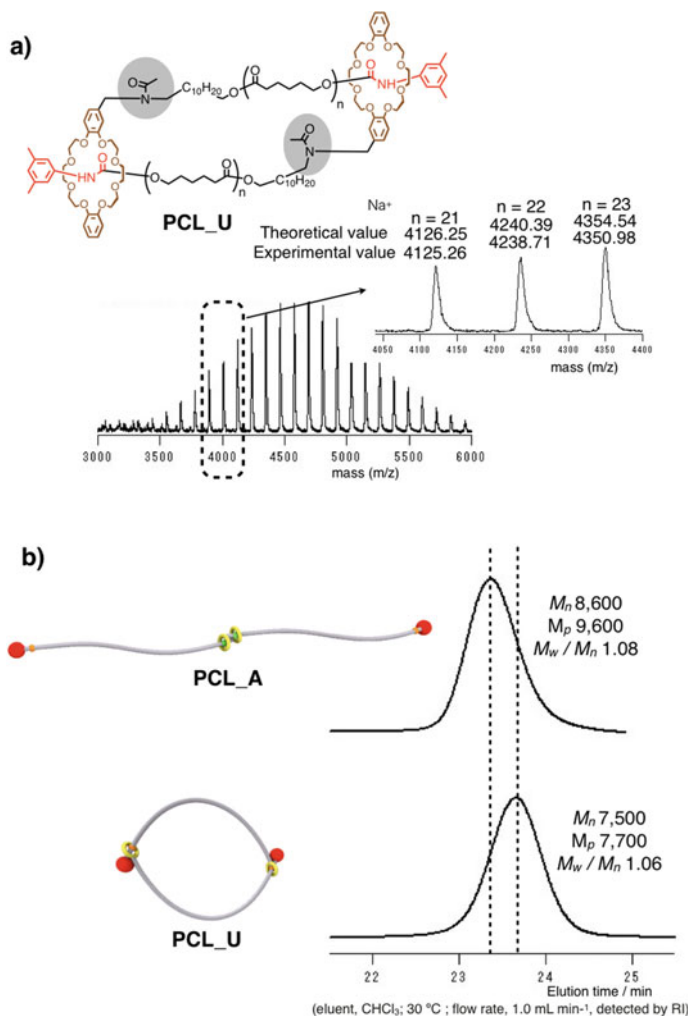
The polymer chains were introduced to **2** by diphenyl phosphate (DPP)-catalyzed living ring-opening polymerization of  $\epsilon$ -caprolactone (CL), which was initiated by hydroxy groups on **2** [49]. After polymerization, 3,5-dimethylphenyl isocyanate was added to cap the propagating end with a bulky stopper and to introduce a urethane moiety at the  $\omega$ -end on the axle, which works as a second recognition site. This one-pot reaction afforded poly( $\epsilon$ -caprolactone) (PCL)-based polymer **PCL\_A** with an overall isolated yield of 61% relative to **2** (the suffix “A” in the polymer name indicates that the crown ether is fixed on the *sec*-ammonium moiety). Subsequently, linear **PCL\_A**, which is maintained by the stable [c2] daisy chain structure, was converted to a cyclic structure when the strong *sec*-ammonium moiety/crown ether interaction was disrupted at the center of the polymer chain via *N*-acetylation. This rotaxane protocol produced cyclic polymer **PCL\_U** with an isolated yield of 82% (the suffix “U” indicates that the crown ether is fixed on the urethane moiety).

The cyclic topology of **PCL\_U** was confirmed by  $^1\text{H}$  NMR spectroscopy, MALDI-TOF MS, and the change in hydrodynamic volume characterized by GPC and DOSY NMR spectroscopy (Fig. 20.17).

The present method requires neither high dilution, which is often used in conventional approaches to promote intramolecular cyclization in favor of intermolecular polymerization of multiple linear chains, nor special purification steps such as preparative GPC, which is commonly used in research laboratories but ill-suited to mass production. Therefore, this method enables gram-scale synthesis of cyclic polymers [50].

## 20.6 Foresight

In this chapter, novel approaches for synthesizing cyclic polymers via spontaneous selective cyclization have been introduced. The synthesis routes reported herein can provide facile, large-scale access to a wide variety of cyclic polymers that may exhibit specific functionality. These methods are expected to encourage further characterization of cyclic polymers and advance their industrial applications. Thus, the methods introduced here show great potential to remarkably expand the field of cyclic polymers.



**Fig. 20.17** a MALDI-TOF MS spectrum of **PCL\_U**. b GPC profiles for **PCL\_A** and **PCL\_U**

## References

1. B.A. Laurent, S.M. Grayson, *Chem. Soc. Rev.* **38**, 2202 (2009)
2. B.T. Dong, Y.Q. Dong, F.S. Du, Z.C. Li, *Macromolecules* **43**, 8790 (2010)
3. J.A. Castro-Osma, C. Alonso-Moreno, J.C. Garcia-Martinez, J. Fernandez-Baeza, L.F. Sanchez-Barba, A. Lara-Sanchez, A. Otero, *Macromolecules* **46**, 6388 (2013)
4. C.W. Bielawski, D. Benitez, R.H. Grubbs, *J. Am. Chem. Soc.* **125**, 8424 (2003)
5. H.R. Kricheldorf, *J. Polym. Sci. Part A Polym. Chem.* **48**, 251 (2010)
6. D.A. Culkin, W.H. Jeong, S. Csihony, E.D. Gomez, N.R. Balsara, J.L. Hedrick, R.M. Waymouth, *Angew. Chem. Int. Ed.* **46**, 2627 (2007)

7. C.E. Willans, M.A. Sinenkov, G.K. Fukin, K. Sheridan, J.M. Lynam, A.A. Trifonov, F.M. Kerton, *Dalton Trans*, 3592 (2008)
8. H. Kammiyada, A. Konishi, M. Ouchi, M. Sawamoto, *ACS Macro Lett.* **2**, 531 (2013)
9. C.D. Roland, H. Li, K.A. Abboud, K.B. Wagener, A.S. Veige, *Nat. Chem.* **8**, 791 (2016)
10. Z. Li, L. Qu, W. Zhu, J.A. Liu, J.Q. Chen, P. Sun, Y. Wu, Z.P. Liu, K. Zhang, *Polymer* **137**, 54 (2018)
11. K. Zhang, M.A. Lackey, Y. Wu, G.N. Tew, *J. Am. Chem. Soc.* **133**, 6906 (2011)
12. S. Honda, T. Yamamoto, Y. Tezuka, *Nat. Commun.* **4**, 1574 (2013)
13. H. Oike, T. Mouri, Y. Tezuka, *Macromolecules* **34**, 6229 (2001)
14. Y.A. Chang, R.M. Waymouth, *J. Polym. Sci. Part A Polym. Chem.* **55**, 2892 (2017)
15. G. Yamaguchi, Y. Higaki, H. Otsuka, A. Takahara, *Macromolecules* **38**, 6316 (2005)
16. M. Schulz, S. Tanner, H. Barqawi, W.H. Binder, *J. Polym. Sci. Part A Polym. Chem.* **48**, 671 (2010)
17. B. Laurent, S.M. Grayson, *J. Am. Chem. Soc.* **128**, 4238 (2006)
18. Y. Tezuka, H. Oike, *J. Am. Chem. Soc.* **123**, 11570 (2001)
19. T. Yamamoto, M. Hosokawa, M. Nakamura, S. Sato, T. Isono, K. Tajima, T. Satoh, M. Sato, Y. Tezuka, A. Saeki, Y. Kikkawa, *Macromolecules* **51**, 9284 (2018)
20. A. Takahashi, R. Yuzaki, Y. Ishida, A. Kameyama, *J. Polym. Sci. Part A: Polym. Chem.* (2019)
21. A. Narumi, M. Yamada, Y. Unno, J. Kumaki, W.H. Binder, K. Enomoto, M. Kikuchi, S. Kawaguchi, *ACS Macro Lett.* **8**, 634 (2019)
22. K. Zhang, M.A. Lackey, J. Cui, G.N. Tew, *J. Am. Chem. Soc.* **133**, 4140 (2011)
23. A.J. Boydston, Y. Xia, J.A. Kornfield, I.A. Gorodetskaya, R.H. Grubbs, *J. Am. Chem. Soc.* **130**, 12775 (2008)
24. F.M. Haque, S.M. Grayson, *Nat. Chem.* **12**, 433 (2020)
25. S.S. Zhang, Y. Tezuka, Z.B.A. Zhang, N. Li, W. Zhang, X.L. Zhu, *Polym. Chem.* **9**, 677 (2018)
26. T. Yamamoto, Y. Tezuka, *Polym. Chem.* **2**, 1930 (2011)
27. Y.H. Jin, C. Yu, R.J. Denman, W. Zhang, *Chem. Soc. Rev.* **42**, 6634 (2013)
28. S.J. Rowan, S.J. Cantrill, G.R.L. Cousins, J.K.M. Sanders, J.F. Stoddart, *Angew. Chem. Int. Ed.* **41**, 898 (2002)
29. H. Otsuka, *Polym. J.* **45**, 879 (2013)
30. M. Xue, Y. Yang, X.D. Chi, X.Z. Yan, F.H. Huang, *Chem. Rev.* **115**, 7398 (2015)
31. A. Harada, A. Hashidzume, H. Yamaguchi, Y. Takashima, *Chem. Rev.* **109**, 5974 (2009)
32. F. Raymo, J.F. Stoddart, *Chem. Rev.* **99**, 1643 (1999)
33. S. Erbas-Cakmak, D.A. Leigh, C.T. McTernan, A.L. Nussbaumer, *Chem. Rev.* **115**, 10081 (2015)
34. M. Arunachalam, H.W. Gibson, *Prog. Polym. Sci.* **39**, 1043 (2014)
35. R.S. Forgan, J.P. Sauvage, J.F. Stoddart, *Chem. Rev.* **111**, 5434 (2011)
36. T. Takata, *Polym. J.* **38**, 1 (2006)
37. C.O. Dietrich-Buchecker, J.P. Sauvage, *Chem. Rev.* **87**, 795 (1987)
38. A.M. Ildarova, S.M. Guerra, *Polym. Chem.* (2020)
39. S. Honda, M. Oka, H. Takagi, T. Toyota, *Angew. Chem. Int. Ed.* **58**, 144 (2019)
40. A. Takahashi, R. Goseki, H. Otsuka, *Angew. Chem. Int. Ed.* **56**, 2016 (2017)
41. P. Hodge, *Chem. Rev.* **114**, 2278 (2014)
42. N. Tsurumi, R. Takashima, D. Aoki, S. Kuwata, H. Otsuka, *Angew. Chem. Int. Ed.* **59**, 4269 (2020)
43. L.F. Gao, J. Oh, Y.F. Tu, T. Chang, C.Y. Li, *Polymer* **170**, 198 (2019)
44. R. Takashima, D. Aoki, H. Otsuka, *Macromolecules* **53**, 4670 (2020)
45. J.P. Sauvage, C.O. Dietrich-Buchecker, *Molecular Catenanes (Rotaxanes and Knots)*; Wiley, New York, 1999)
46. J.D. Badjic, V. Balzani, A. Credi, S. Silvi, J.F. Stoddart, *Science* **303**, 1845 (2004)
47. C. Bruns, J.F. Stoddart, *The Nature of the Mechanical Bond: From Molecules to Machines* (Wiley, Hoboken, NJ, 2016)
48. T. Takata, *ACS Central Sci.* **6**, 129 (2020)
49. K. Makiguchi, T. Satoh, T. Kakuchi, *Macromolecules* **44**, 1999 (2011)
50. D. Aoki, G. Aibara, S. Uchida, T. Takata, *J. Am. Chem. Soc.* **139**, 6791 (2017)

# Chapter 21

## Unstoichiometric Polycondensation for the Synthesis of Aromatic Cyclic Polymers



Tsutomu Yokozawa, Hajime Sugita, and Yoshihiro Ohta

**Abstract** This chapter describes the synthesis of cyclic polymers by means of conventional polycondensation and by unstoichiometric Suzuki–Miyaura polycondensation. The most of polymers obtained by conventional polycondensation have been found to include cyclic polymers since matrix-assisted laser desorption ionization time-of-flight (MALDI-TOF) mass spectrometry was developed. Only cyclic polymers are obtained under optimized conditions in which side reactions do not take place. For example, cyclic polymers of polycarbonate, poly(ether sulfone), polyester, poly(ether ketone), polyimide, and polyurethane have been reported. However, if condensation polymers do not have bent structures or flexible backbones, then cyclic polymers have not been obtained; for example, aromatic polyamides and  $\pi$ -conjugated polymers. Suzuki–Miyaura polycondensation of dibromoarylene and arylenediboronic acid (ester) with *t*-Bu<sub>3</sub>PPd, which has a propensity for intramolecular catalyst transfer on  $\pi$ -electron face of aromatics, affords high-molecular-weight  $\pi$ -conjugated polymers with a boronate at both ends, even though excess dibromoarylene is used, whereas similar polycondensation of monomers, at least one of which has a kinked structure, yields selectively cyclic aromatic polymers when excess dibromoarylene is used. In this unstoichiometric Suzuki–Miyaura polycondensation, cyclic poly(*m*-phenylene-*alt-p*-phenylene)s, cyclic poly(*m*-phenylene-*alt*-linearly extended conjugated arylene), cyclic poly(extensively conjugated, kinked arylene-*alt-p*-phenylene)s, cyclic poly(*m*-phenylene-*alt*-heteroarylene)s, and cyclic poly(heteroarylene-*alt-p*-phenylene)s are obtained.

**Keywords** Polycondensation · Suzuki polycondensation · Unstoichiometric polycondensation · Cyclic aromatic polymer · Catalyst transfer · Pd catalyst

---

T. Yokozawa (✉) · H. Sugita · Y. Ohta  
Department of Materials and Life Chemistry, Kanagawa University, Rokkakubashi,  
Kanagawa-ku, Yokohama 221-8686, Japan  
e-mail: [yokozi01@kanagawa-u.ac.jp](mailto:yokozi01@kanagawa-u.ac.jp)

## 21.1 Introduction

Recent advances in the synthesis of cyclic polymers are generally classified as ring-closure of polymer precursors and ring-expansion polymerization. However, Kricheldorf found in many polycondensations that the percentage and molecular weight of the cyclic polymers increase when the reaction conditions favor high molecular weights. In the absence of side reactions, all polycondensation products will be cyclic polymers when conversion approaches 100% [1]. The formation of cyclic polymer in polycondensation of AA monomer and BB monomer is accounted for by the intramolecular reaction of the A end with the B end in polymer under pseudo high-dilution conditions of both ends in high conversion of the monomers. Accordingly, cyclic polycondensation might be classified as ring-closure of polymer precursors, although cyclization spontaneously takes place, in contrast to the case of introduction of reacting groups at both ends of polymer, obtained by living polymerization, for the synthesis of cyclic polymer. For quantitative formation of cyclic polymer in polycondensation, exactly equal amount of AA and BB monomers should be used, leading to the same amount of the A and B ends in the polymer. However, we found polycondensation that affords cyclic polymer selectively when excess one of the two monomers, rather than equimolar two monomers, are used [2]. In this chapter, we describe the synthesis of cyclic polymers by means of conventional polycondensation and this unstoichiometric polycondensation.

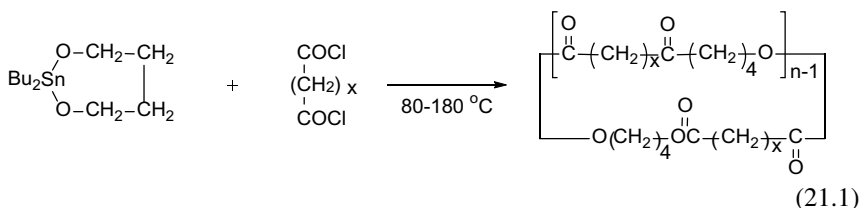
## 21.2 Cyclic Polymer from Conventional Polycondensation

Polycondensation was not thought to afford cyclic polymer, as indicated by the fact that Carothers and Flory did not take into account cyclization reactions in their theory of step-growth polymerization [3–5]. However, the development of MALDI-TOF mass spectrometry has made it possible to analyze cyclic polymer.

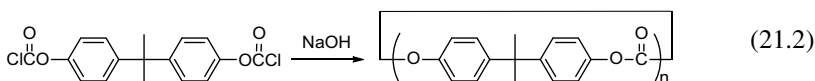
Kricheldorf first investigated the polycondensation of tin-containing cyclic oligoester or oligo(ether-ester) with dicarboxylic acid dichloride [6, 7]. The molecular weight of the obtained polymer was limited, and he speculated that this result might be due to the formation of cyclic polymer [7]. He then conducted the polycondensation of 2,2-dibutyl-2-stanna-1,3-dioxepane with dicarboxylic dichloride and found that the main products were cyclic polyester by means of MALDI-TOF mass spectrometry (Eq. 21.1) [8]. The polycondensation of acyclic 1,4-bis(tributylstannoxy)butane and dicarboxylic acid dichlorides also afforded cyclic polyesters. Accordingly, the cyclic tin monomer was not responsible for the formation of cyclic polyester. Furthermore, he has demonstrated that cyclization takes place at any concentration and at any stage of polymerization in numerous, conventional polycondensations. This is the reason for the limitation of the molecular weight of the polymer in polycondensation [1]. Furthermore, Kricheldorf made the following



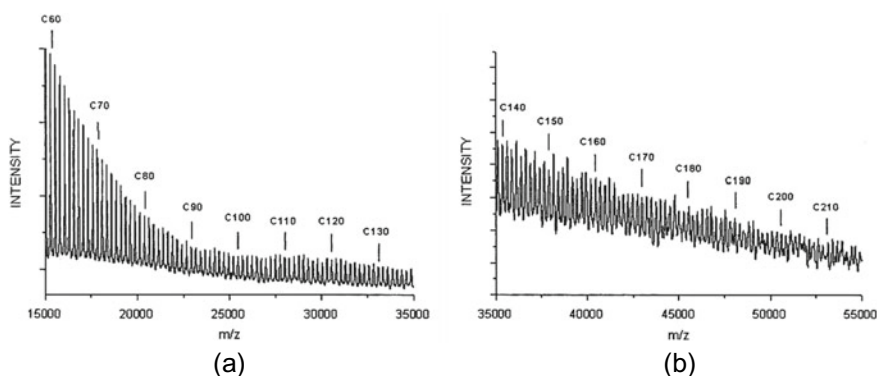
statement: “all step-growth polymerizations possess the fundamental tendency to yield cycles as stable endproducts with linear chain being the reactive intermediates or endproducts of side reaction” [9].



Several examples of polycondensations affording cyclic polymers are described below. Interfacial hydrolytic polycondensation of bisphenol-A bis(chloroformate) afforded polycarbonate with  $M_n$  of 65,000 (Eq. 21.2). The MALDI-TOF mass spectrum of this polymer showed a series of peaks due to cyclic polymer up to 18,000 Da and no peaks for linear polymer (Fig. 21.1a). Furthermore, the spectrum of polymer fractionated in the higher-molecular-weight region showed cyclic polymer peaks up to 55,000 Da corresponding to the  $DP$  around 210 (Fig. 21.1b) [10]. This result indicates that cyclization competes with propagation at any chain length.

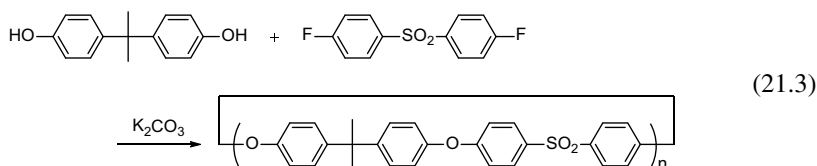


Commercial poly(ether sulfone)s are generally produced by the polycondensation of a bisphenol with 4,4'-dichlorodiphenyl sulfone in the presence of  $\text{K}_2\text{CO}_3$  in DMSO, and the MALDI-TOF mass spectrum showed a moderate content of cyclic polymer and linear polymer with OH and Cl end groups. Since the linear

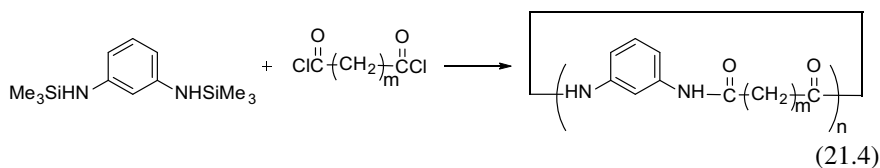


**Fig. 21.1** MALDI-TOF mass spectrum of a fraction of a polycarbonate prepared by triethylamine-catalyzed hydrolytic polycondensation of bisphenol-A bis(chloroformate). (Ref. [10]). From ref. 1 Copyright © 2000 by John Wiley Sons, Inc. Reprinted by permission of John Wiley & Sons, Inc.

polymer was thought to be obtained before the reaction was completed, more reactive 4,4'-difluorodiphenyl sulfone was used instead of the dichloro-counterpart. In the MALDI-TOF mass spectrum of the products, only one series of peaks due to cyclic polymer were observed without detection of peaks of linear polymers (Eq. 21.3) [11].



If condensation polymers do not have bent structures or flexible backbones, cyclic polymers have not been obtained. For example, rigid-rod poly(*p*-phenylene terephthalamide) analogs having alkyl side chains did not contain cyclic polymers. However, the polycondensation of silylated *m*-phenylenediamine and aliphatic dicarboxylic acid chloride afforded cyclic polyamides predominately (Eq. 21.4) [12].



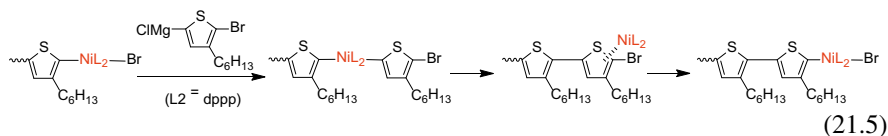
Furthermore, cyclic polymers of polyesters, poly(ether ketone)s, polyimides, and polyurethanes are obtained in the corresponding polycondensations [9]. Cyclization of oligomer and polymer was also investigated in polycondensation of AB<sub>2</sub> monomers [13–20] and “A<sub>2</sub> + B<sub>3</sub>” [21–27] and “A<sub>2</sub> + B<sub>4</sub>” polycondensations [28–31].

## 21.3 Cyclic Polymer from Unstoichiometric Polycondensation

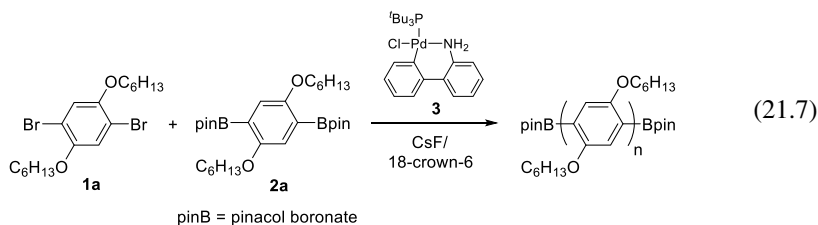
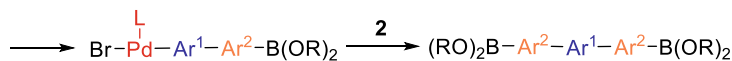
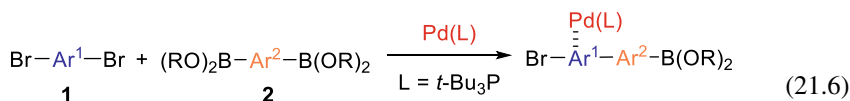
### 21.3.1 Background and Discovery

Metal-catalyzed coupling polymerization had regarded as a polycondensation that proceeds in a step-growth polymerization. However, we [32–34] and McCullough [35, 36] independently discovered that Ni-catalyzed Kumada-Tamao coupling polymerization of bromothiophene Grignard monomer proceeded in a chain-growth polymerization manner, affording well-defined poly(3-hexylthiophene) (P3HT). The

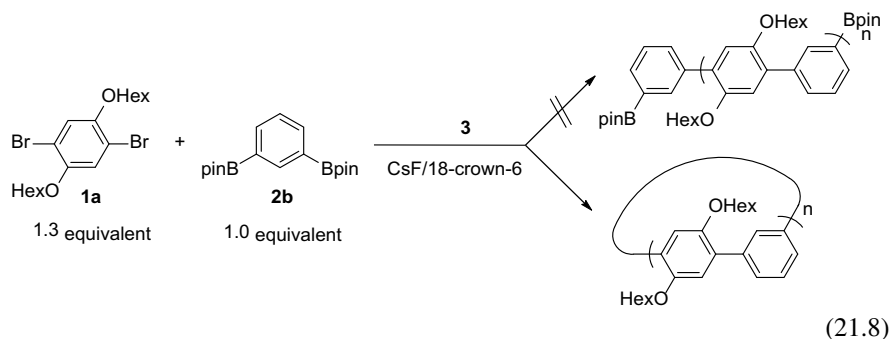
polymerization involved intramolecular transfer of the Ni catalyst on the polymer backbone; the Grignard monomer reacts with the polymer-Ni-Br end, and regenerated Ni(0) catalyst is transferred on the thiophene ring, newly connected to the polymer end, and inserts the C–Br bond of the thiophene, to generate the same polymer-Ni-Br end (Eq. 21.5). We [37] also found that similar catalyst transfer chain-growth condensation polymerization took place in Suzuki–Miyaura polycondensation by using *t*-Bu<sub>3</sub>PPd catalyst, which has a propensity for intramolecular catalyst transfer on the  $\pi$ -electron face [38–42].



When this Pd catalyst was used for Suzuki–Miyaura polycondensation of dibromoarylene **1** and arylenediboronic acid ester **2** (A<sub>2</sub> + B<sub>2</sub> polycondensation), successive substitution of **1** with **2** took place through the intramolecular transfer of the Pd catalyst on **1** (Eq. 21.6). Accordingly, the polycondensation proceeded while maintaining boronic acid ester ends, although excess **1** was used, affording high-molecular-weight polymer with boronic acid ester ends (unstoichiometric polycondensation) [43–47]. For example, the polycondensation of equimolar dibromophenylene **1a** and phenylenediboronic acid ester **2a** in the presence of *t*-Bu<sub>3</sub>PPd precatalyst **3** and CsF/crown-6 as a base afforded polyphenylene with *M<sub>n</sub>* of 15,600, whereas the polycondensation of 1.3 equivalents of **1a** with 1.0 equivalent of **2a** resulted in the increase of *M<sub>n</sub>* up to 19,600 (Eq. 21.7). The MALDI-TOF mass spectrum of the polymer obtained by the latter feed ratio showed essentially one series of peaks due to polyphenylene with a pinacol boronate (Bpin) moiety at both ends [44].

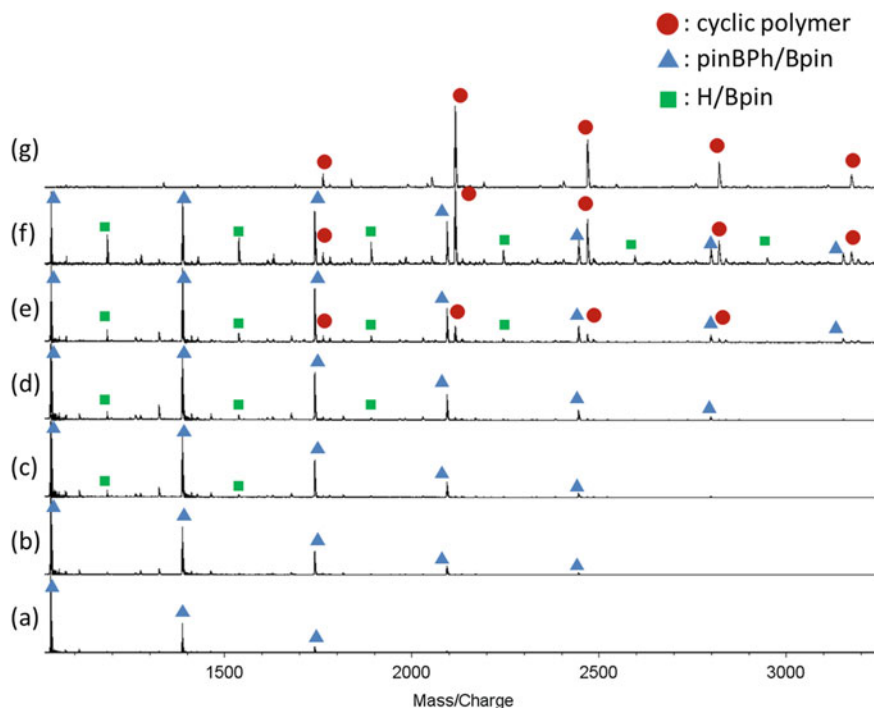


In order to extend the range of unstoichiometric Suzuki–Miyaura polycondensation, we carried out similar polycondensation using *m*-phenylenediboric acid ester **2b** instead of **2a**. However, the product was not linear polymer with Bpin at both ends but cyclic polyphenylene (Eq. 21.8) [2]. This cyclic polycondensation under unstoichiometric condition is unprecedented, because normal unstoichiometric polycondensation affords low-molecular-weight polymer with excess monomer ends, whereas the above abnormal unstoichiometric polycondensation affords high-molecular-weight polymer with insufficient monomer ends [48]. Accordingly, cyclic polymer should not be obtained by the reaction of the same end groups in either normal or abnormal unstoichiometric polycondensation. We then started to investigate unstoichiometric cyclic polycondensation.



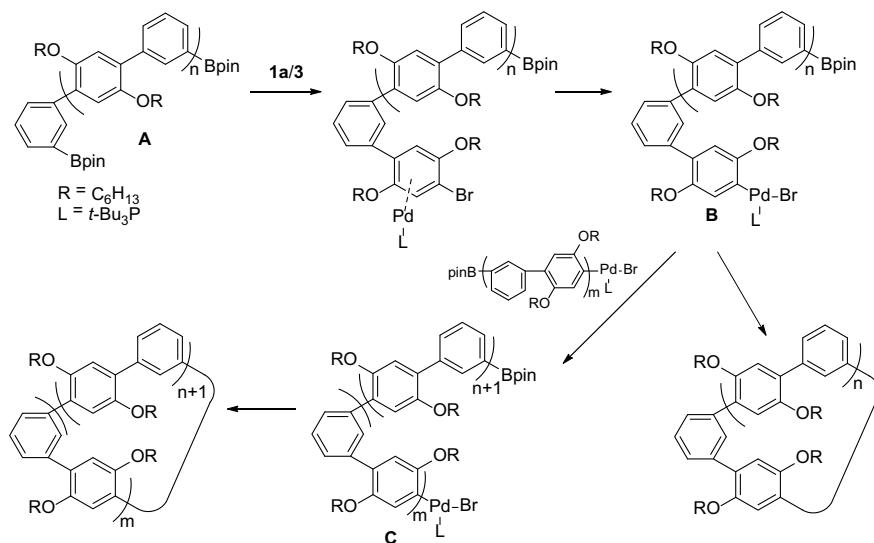
### 21.3.2 Cyclic Polyphenylenes

We first studied the mechanism of cyclic polymerization under unstoichiometric condition [2]. The conversion of **2b** and the change of the products with polymerization time was monitored (Fig. 21.2). The MALDI-TOF mass spectra indicated that linear polyphenylene with pinBPh/Bpin ends was predominantly formed until the conversion reached 89% (1 h) (Fig. 21.2a–d). This behavior is the same as in the case of unstoichiometric polycondensation of 1.3 equivalents of **1a** and 1.0 equivalent of **2a** with **3**. Cyclic polymer and polymer with H/Bpin ends were observed at 97% conversion (5 h) (Fig. 21.2e), and both peaks then increased until 100% conversion (5 h) (Fig. 21.2f). After 24 h, the products converted to cyclic polymer (Fig. 21.2e). Since the H/Bpin-ended polymer was converted to cyclic polymer, the hydrogen end was presumably formed by hydrolysis of a polymer-Pd-Br end during quenching with hydrochloric acid. In addition, cyclic polymer was obtained even at high monomer concentration, and the molecular weight of the cyclic polymer increased up to  $M_n = 8540$  with increasing concentration.



**Fig. 21.2** Changes of products with polymerization time and conversion of **2b** in the polymerization of 1.3 equivalents of **1a** and 1.0 equivalent of **2b** with 5.0 mol % of **3**, CsF (4 equivalents), and 18-crown-6 (8 equivalents) in THF ( $[\mathbf{2b}]_0 = 16.6 \times 10^{-3}$  M) and water (THF/water = 3.0/0.1, v/v) at rt: time, conversion of **2b**, and  $M_n$  are (a) 15 min, 72%, 1640; (b) 30 min, 83%, 1720; (c) 45 min, 86%, 1810; (d) 1 h, 89%, 1940; (e) 3 h, 97%, 2770; (f) 5 h, 100%, 3790; (g) 24 h, 100%, 4920

On the basis of these results, we proposed the following mechanism (Fig. 21.3). Suzuki–Miyaura polycondensation of **1a** and **2b** proceeded through intramolecular catalyst transfer on **1a** to afford polyphenylene **A** with pinBPh/Bpin ends until **2b** was almost completely consumed. Excess **1b** reacted with the pinB end, followed by intramolecular oxidative addition to generate polymer **B**. If polymer **B** has a favorable conformation for cyclization, the two chain ends would react to yield cyclic polymer. Cyclic polymer could be also formed by intramolecular reaction of the two chain ends of polymer **C** formed by intermolecular coupling reaction between polymer **B**s. Excess **1a** should promote the generation of cyclization precursor **B** and **C** because this polymerization proceeds through the formation of polymer **A** with pinBPh/Bpin ends until **2b** was almost completely consumed. Furthermore, the kinked structure of *meta*-monomer is crucial for cyclization polymerization, because the combination of *para*-monomers affords linear polymer with Bpin at both ends.



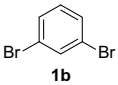
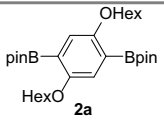
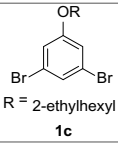
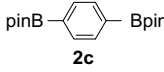
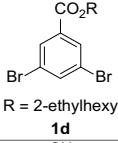
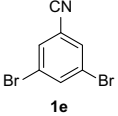
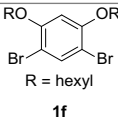
**Fig. 21.3** Proposed mechanisms for cyclic polymerization of excess **1a** and 1.0 equivalent of **2b** with **3**

Cyclic polycondensation of other phenylene monomers was examined under unstoichiometric condition (Table 21.1) [2]. The reverse combination of monomers, i.e., 1.3 equivalents of *m*-dibromophenylene **1b** and 1.0 equivalent of pinacol *p*-phenylenediboronate **2a**, afforded cyclic polymer with similar molecular weight (Entry 1). Electron-donating and electron-withdrawing substituents on *m*-dibromophenylenes **1c–1e** did not affect the reaction, affording cyclic polyphenylene with similar molecular weights (Entries 2–4). Furthermore, the combination of *m*-dibromophenylene **1f** and *m*-phenylenediboronate **2b** also afforded cyclic polyphenylene. When *o*-phenylene monomers were used in any combination of monomers, linear polymer was mainly obtained.

### 21.3.3 Extensively Conjugated Cyclic Polyarylenes

Since *t*-Bu<sub>3</sub>PPd catalyst undergoes intramolecular transfer not only on benzene rings [41, 49], but also on a variety of aromatics [37, 41, 42, 50–56] and multiple bonds [45, 57, 58], we extended unstoichiometric Suzuki–Miyaura cyclic polycondensation to

**Table 21.1** Cyclic polymerization of 1.3 equivalents of dibromophenylene **1** and 1.0 equivalent of **2** with **3** and CsF/18-crown-6<sup>a</sup>

Entry	<b>1</b> <sup>b</sup>	<b>2</b>	Yield (%) <sup>c</sup>	$M_n (M_w/M_n)$ <sup>d</sup>
1	 <b>1b</b>	 <b>2a</b>	83	5610 (1.86)
2	 <b>1c</b> R = 2-ethylhexyl	 <b>2c</b>	93	5030 (1.72)
3	 <b>1d</b> R = 2-ethylhexyl	<b>2c</b>	90	5320 (1.65)
4	 <b>1e</b>	<b>2a</b>	88	5600 (1.64)
5	 <b>1f</b> R = hexyl	<b>2b</b>	94	2580 (1.42)

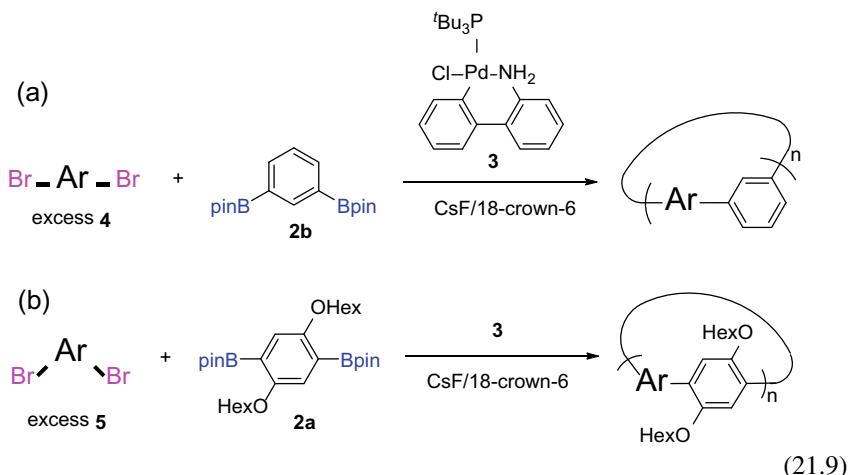
<sup>a</sup> Polymerization of 1.3 equivalents of **1** and 1.0 equivalent of **2** was carried out with 5.0 mol% of **3**, CsF (4 equivalents), and 18-crown-6 (8 equivalents) in THF ( $[2]_0 = 16.1 \times 10^{-3}$  M) and water (THF/water = 3/0.1, v/v) at rt for 24 h, followed by quenching with 1 M hydrochloric acid

<sup>b</sup> 1.3 equivalents

<sup>c</sup> Isolated yield after preparative HPLC

<sup>d</sup> Estimated by GPC based on polystyrene standards (eluent: THF)

yield a variety of cyclic aromatic polymers. Thus, we investigated polymerization of linearly extended, conjugated dibromo monomer **4** with *meta*-phenylenediboronic acid ester **2b** (Eq. 21.9a) and of the extensively conjugated, kinked dibromo monomer **5** with *para*-phenylenediboronic acid ester **2a** (Eq. 21.9b) [59].

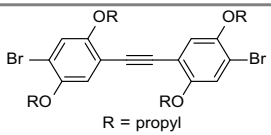
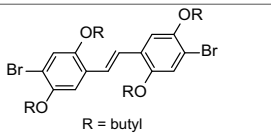
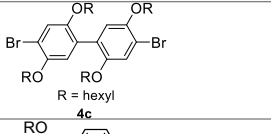
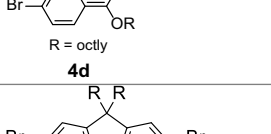
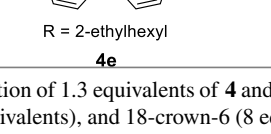


The results of the former polycondensation of 1.3 equivalents of **4** with **2b** was shown in Table 21.2. When dibromotolane (**4a**) containing a carbon–carbon triple bond was used, a high-molecular-weight cyclic polymer was obtained ( $M_n = 12,400$ ) (Entry 1). In the case of polycondensation of dibromostilbene **4b** and **2b**, the molecular weight of the obtained cyclic polymer was also high ( $M_n = 10,200$ ) (Entry 2). Furthermore, the polycondensation of dibromobiphenyl **4c** and **2b** afforded cyclic polymer with  $M_n$  of 8650 (Entry 3). Thus, it turned out that linearly extended dibromoarylenes containing a carbon–carbon triple bond, double bond, or single bond reacted with **2b** under unstoichiometric conditions, affording cyclic polymers with  $M_n$  more than 8600, which is higher than that in the case of cyclic polymerization of *para*- and *meta*-phenylene monomers ( $M_n \approx 5000$ ) [2]. The formation of higher-molecular-weight polymer by using stiff, long dibromo monomers **4a–4c** might be accounted for by less chance to take a favorable conformation for cyclization of the intermediary linear polymer. Regarding condensed aromatic dibromides, naphthalene **4d** and fluorene **4e** also lead to cyclic polymers (Entries 4 and 5).

Furthermore, the polycondensation of 1.3 equivalents of extensively conjugated, kinked dibromo monomer **5** with **2a** was conducted (Table 21.3). The polycondensation of 3,5-dibromotolane **5a** with **2a** afforded cyclic polymer with  $M_n$  of 8720 (Entry 1). In the polycondensation of 3,5-dibromostilbene **5b**, however, linear polymer with Br/**5b**-Br became the major product (Entry 2). This linear polymer was formed by end-capping with excess **5b**, indicating that subsequent substitution of **5b** with **2a** did not take place due to the occurrence of intermolecular transfer of the Pd catalyst after the first substitution. This result is consistent with the fact that Suzuki–Miyaura coupling reaction of 4,4'-dibromostilbene with phenylboronic acid in the presence of **3** did not selectively afford diphenyl-substituted stilbene through intramolecular transfer of the Pd catalyst; unsubstituted stilbene favored intermolecular transfer because of trapping the Pd catalyst with the carbon–carbon double bond of another stilbene during intramolecular transfer of the Pd catalyst on dibromostilbene [58]. Furthermore, this result strongly supports the idea that



**Table 21.2** Cyclic polymerization of 1.3 equivalents of linearly extended, conjugated dibromo monomer **4** and 1.0 equivalent of **2b** with **3** and CsF/18-crown-6<sup>a</sup>

Entry	<b>4</b> <sup>b</sup>	Yield (%) <sup>c</sup>	$M_n (M_w/M_n)$ <sup>d</sup>
1	 <p style="text-align: center;"><b>4a</b></p>	94	12,400 (2.41)
2 <sup>e</sup>	 <p style="text-align: center;"><b>4b</b></p>	82	10,200 (2.39)
3 <sup>f</sup>	 <p style="text-align: center;"><b>4c</b></p>	74	8650 (1.64)
4	 <p style="text-align: center;"><b>4d</b></p>	98	6440 (1.90)
5	 <p style="text-align: center;"><b>4e</b></p>	88	5890 (2.21)

<sup>a</sup> Polymerization of 1.3 equivalents of **4** and 1.0 equivalent of **2b** was carried out with 5.0 mol % of **3**, CsF (4 equivalents), and 18-crown-6 (8 equivalents) in THF ( $[2b]_0 = 16.6 \times 10^{-3}$  M) and water (THF/water = 3/0.1, v/v) at rt for 24 h, followed by quenching with 1 M hydrochloric acid

<sup>b</sup> 1.3 equivalents

<sup>c</sup> Isolated yield after preparative HPLC

<sup>d</sup> Estimated by GPC based on polystyrene standards (eluent: THF).

<sup>e</sup>  $[2b]_0 = 8.3$  mM; polymerization was carried out for 48 h

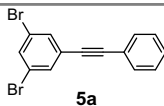
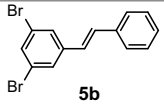
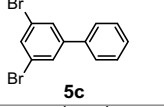
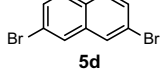
<sup>f</sup> Polymerization was carried out for 51 h

intramolecular catalyst transfer is essential for unstoichiometric Suzuki–Miyaura cyclic polycondensation.

In the polycondensation using 3,5-dibromobiphenyl **5c** and 2,7-dibromonaphthalene **5d**, cyclic polymers were obtained (Entries 3 and 4). Consequently, it turned out that dibromo monomers containing a moiety that disturbs intramolecular catalyst transfer should not be used for unstoichiometric Suzuki–Miyaura cyclic polycondensation.

During the course of the investigation of Pd-catalyst transfer on functional groups between benzene rings [47], we found that the polycondensation of 1.3 equivalents of dibromo monomer **6** (X = CH<sub>2</sub>, N-Bu, and O) and 1.0 equivalent of *p*-phenylenediboronic acid **2e** in the presence of **3** afforded cyclic polymers, the  $M_n$  of

**Table 21.3** Cyclic polymerization of 1.3 equivalents of extensively conjugated, kinked dibromo monomer **5** and 1.0 equivalent of **2a** with **3** and CsF/18-crown-6<sup>a</sup>

Entry	<b>5</b> <sup>b</sup>	Yield (%) <sup>c</sup>	$M_n$ ( $M_w/M_n$ ) <sup>d</sup>
1		98	8720 (2.56)
2		86 <sup>e</sup>	3770 (1.41)
3		80	6580 (1.81)
4		86	8310 (2.37)

<sup>a</sup> Polymerization of 1.3 equivalents of **5** and 1.0 equivalent of **2a** was carried out with 5.0 mol % of **3**, CsF (4 equivalents), and 18-crown-6 (8 equivalents) in THF ( $[\mathbf{2a}]_0 = 16.6 \times 10^{-3}$  M) and water (THF/water = 3/0.1, v/v) at rt for 24 h, followed by quenching with 1 M hydrochloric acid

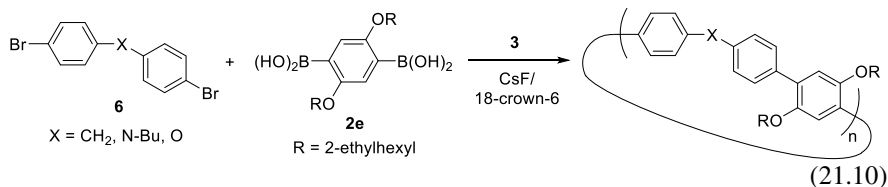
<sup>b</sup> 1.3 equivalents

<sup>c</sup> Isolated yield after preparative HPLC

<sup>d</sup> Estimated by GPC based on polystyrene standards (eluent: THF)

<sup>e</sup> Linear polymer with Br/**5b**-Br was mainly obtained

which were high (X = CH<sub>2</sub>: 10,400; N-Bu: 15,500; O: 20,500) (Eq. 21.10). Formation of cyclic polymer, even though *p*-phenylene monomer was used, implied that **6** acts as monomers with kinked structures due to the presence of the sp<sup>3</sup> X groups. The long structure of **6** is presumably responsible for obtaining high-molecular-weight cyclic polymers, as in the case of the polymerization of **4a** or **4b**, containing carbon-carbon triple and double bonds, with **2b**.

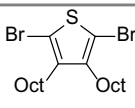
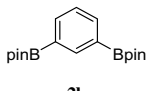
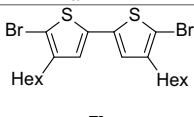
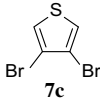
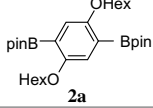
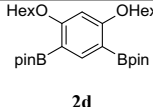
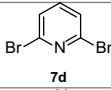
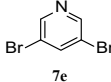


### 21.3.4 Cyclic Polyheteroarylenes

Unstoichiometric cyclic polycondensation using thiophene and pyridine dibromides was investigated (Table 21.4) [60] because intramolecular catalyst transfer on thiophene in Kumada-Tamao [36] and Suzuki–Miyaura [52, 61] reactions and on pyridine in Kumada-Tamao reaction [62, 63] were observed.

We first examined polycondensation of 1.3 equivalents of 2,5-dibromothiophene **7a** and 1.0 equivalent of pinacol *m*-phenyleneboronate **2b** in the presence of **3**. The most of products were cyclic polymers; however, a small amount of linear polymers with a hydrogen end were also obtained. Side reactions such as deboronation and

**Table 21.4** Cyclic polymerization of 1.3 equivalents of dibromoheteroarylene **7** and 1.0 equivalent of **2** with **3** and CsF/18-crown-6<sup>a</sup>

Entry	<b>7</b> <sup>b</sup>	<b>2</b>	Yield (%) <sup>c</sup>	$M_n (M_w/M_n)^d$
1	 <b>7a</b>	 <b>2b</b>	82	4210 (1.64)
2	 <b>7b</b>	<b>2b</b>	88	2950 (1.39)
3	 <b>7c</b>	 <b>2a</b>	86 <sup>e</sup>	1350 (1.18)
4	<b>7c</b>	 <b>2d</b>	98 <sup>e</sup>	1730 (1.31)
5	 <b>7d</b>	<b>2a</b>	– <sup>f</sup>	4910 (1.55) <sup>g</sup>
6	 <b>7e</b>	<b>2a</b>	72	3480 (1.37)

<sup>a</sup> Polymerization of 1.3 equivalents of **7** and 1.0 equivalent of **2** was carried out with 5.0 mol % of **3**, CsF (4 equivalents), and 18-crown-6 (8 equivalents) in THF ( $[2]_0 = 16.1 \times 10^{-3}$  M) and water (THF/water = 3/0.1, v/v) at rt for 24 h, followed by quenching with 1 M hydrochloric acid

<sup>b</sup> 1.3 equivalents

<sup>c</sup> Yield after isolation by means of HPLC (entries 1–4) or precipitation into hexane (entry 6)

<sup>d</sup> Estimated by GPC based on polystyrene standards (eluent: THF)

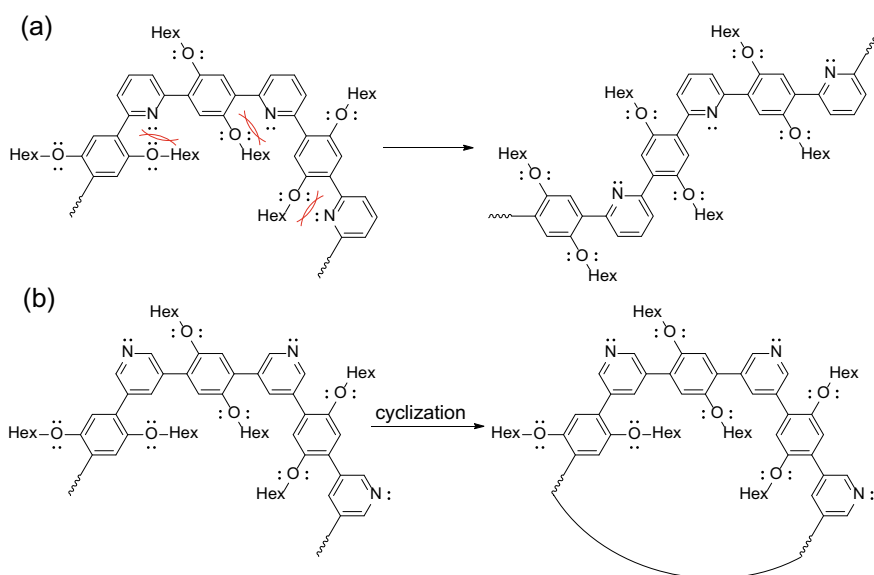
<sup>e</sup> Linear polymer with Br/**7c**-Br was mainly obtained

<sup>f</sup> Polymer was precipitated during polymerization

<sup>g</sup> Polymer soluble in the reaction mixture, and linear polymers with several end groups were obtained

dehalogenation might take place in the final stage of polymerization from the results obtained by tracing the products by means of MALDI-TOF mass spectrometry (Entry 1). When bithiophene **7b** was used instead of **7a**, only cyclic polymer was formed (Entry 2). On the other hand, the polycondensation using 3,4-dibromothiophene **7c** afforded low-molecular-weight, linear polymer with the **7c** unit at both ends even when *p*- or *m*-phenylenediboronate was reacted with **7c** (Entries 3 and 4). These results indicated that the polymers were end-capped by excess **7c**; abnormal unstoichiometric polycondensation via intramolecular transfer of the Pd catalyst on **7c** did not occur. The model reaction of **7c** with phenylboronic acid resulted in the selective formation of mono-substituted thiophene. Consequently, it turned out that the Pd catalyst is transferred from the 2 to 5 position of thiophene, but not from the 3 to 4 position. The reason for this difference is not clear at present.

We next investigated the polymerization of dibromopyridine with *p*-phenylenediboronic acid ester **2a**. In the polymerization of 2,6-dibromopyridine **7d** with **2a**, the polymer was precipitated during the reaction. The polymer soluble in the reaction mixture was turned out to be linear polymers with several kinds of polymer ends (Entry 5). In contrast, the polymerization of 3,5-dibromopyridine **7e** with **2a** proceeded homogeneously, to afford cyclic polymer (Entry 6). The different polymerization behavior may be accounted for by the presence of the lone pairs of pyridine and the alkoxy side chain in **2a** (Fig. 21.4). Thus, a zigzag conformation, leading to linear polymer, would be favored in the polymerization of **7d** with **2a** because of the electronic repulsion between the lone pairs of pyridine and the alkoxy group in **2a**, whereas a conformation leading to cyclization could be adopted without such



**Fig. 21.4** Proposed mechanism accounting for the different polymerization behaviors of **a 7d** with **2a** and **b 7e** with **2a**

electronic repulsion in the polymerization of **7e** with **2a**. These results demonstrate that the position of bromine in dibromoheteroarylenes strongly influences whether cyclic polymer or linear polymer is formed in unstoichiometric Suzuki–Miyaura polycondensation with **3** in the presence of excess dibromo monomer.

## 21.4 Conclusion

Polycondensation is a fundamental approach to cyclic polymers, although the molecular weight and dispersity are difficult to control. In conventional polycondensation, the whole products are cyclic polymer unless side reactions take place and the polymer backbone is rigid. For example, the MALDI-TOF mass spectra of polycarbonate, poly(ether sulfone), polyester, poly(ether ketone), polyimide, and polyurethane, obtained under optimized conditions, displayed peaks due to cyclic polymer, and no linear polymer species was detectable.

We investigated Suzuki–Miyaura polycondensation of dibromoarylenes and arylenediboronic acid (ester) with *t*-Bu<sub>3</sub>PPd catalyst under excess use of the former monomer and found that cyclic aromatic polymers were selectively obtained when one of the two monomers has a kinked structure. The mechanism of unstoichiometric cyclic polycondensation of *p*-dibromophenylene and pinacol *m*-phenylenediboronate was investigated. Linear polymer with a boronate moiety at both ends was first formed through intramolecular Pd-catalyst transfer on the dibromo monomer until almost all of the diboronate monomer was consumed. Excess dibromo monomer, activated with the Pd catalyst, was then reacted with the polymer with boronate at both ends, affording cyclic polymer. This approach yielded a variety of cyclic aromatic polymers containing tolane, stilbene, fluorene, naphthalene, thiophene, pyridine, and so on. We are currently investigating the optical properties of these cyclic aromatic polymers, as well as new polymer synthesis by utilizing the merit of unstoichiometric condition in this Suzuki–Miyaura polycondensation.

**Acknowledgements** This study was supported by a Grant in Aid (No. 15H03819) for Scientific Research from the Japan Society for the Promotion of Science (JSPS) and by the MEXT-Supported Program for the Strategic Research Foundation at Private Universities (No. S1311032), 2013–2018.

## References

1. H.R. Kricheldorf, G. Schwarz, *Macromol. Rapid Commun.* **24**, 359 (2003)
2. H. Sugita, M. Nojima, Y. Ohta, T. Yokozawa, *Chem. Commun.* **53**, 396 (2017)
3. P.J. Flory, *J. Am. Chem. Soc.* **58**, 1877 (1936)
4. W.H. Carothers, *Trans. Faraday Soc.* **32**, 39 (1936)
5. P.J. Flory, *Chem. Rev.* **39**, 137 (1946)
6. H.R. Kricheldorf, S. Eggerstedt, *J. Polym. Sci., Part A Polym. Chem.* **36**, 1373 (1998)
7. H.R. Kricheldorf, D. Langanke, *Macromol. Chem. Phys.* **200**, 1183 (1999)
8. H.R. Kricheldorf, D. Langanke, J. Spickermann, M. Schmidt, *Macromolecules* **32**, 3559 (1999)

9. H.R. Kricheldorf, *Macromolecules* **36**, 2302 (2003)
10. H.R. Kricheldorf, S. Bohme, G. Schwarz, C.L. Schultz, *Macromol. Rapid Commun.* **23**, 803 (2002)
11. H.R. Kricheldorf, S. Boehme, G. Schwarz, R.-P. Krueger, G. Schulz, *Macromolecules* **34**, 8886 (2001)
12. H.R. Kricheldorf, S. Böhme, G. Schwarz, *Macromolecules* **34**, 8879 (2001)
13. V. Percec, P. Chu, M. Kawasumi, *Macromolecules* **27**, 4441 (1994)
14. F. Chu, C.J. Hawker, P.J. Pomery, D.J.T. Hill, *J. Polym. Sci., Part A Polym. Chem.* **35**, 1627 (1997)
15. J.K. Gooden, M.L. Gross, A. Mueller, A.D. Stefanescu, K.L. Wooley, *J. Am. Chem. Soc.* **120**, 10180 (1998)
16. K. Dusek, J. Somvarsky, M. Smrckova, W.J. Simonsick Jr., L. Wilczek, *Polym. Bull. (Berlin)* **42**, 489 (1999)
17. D. Parker, W.J. Feast, *Macromolecules* **34**, 2048 (2001)
18. C. A. Martinez, and A. S. Hay, *J. Polym. Sci., Part A: Polym. Chem.*, **35**, 2015 (1997).
19. A. Burgath, A. Sunder, H. Frey, *Macromol. Chem. Phys.* **201**, 782 (2000)
20. H.R. Kricheldorf, L. Vakhtangishvili, G. Schwarz, R.-P. Krueger, *Macromolecules* **36**, 5551 (2003)
21. H.R. Kricheldorf, D. Fritsch, L. Vakhtangishvili, G. Schwarz, *Macromolecules* **36**, 4337 (2003)
22. H.R. Kricheldorf, R. Hobzova, G. Schwarz, L. Vakhtangishvili, *Macromolecules* **38**, 1736 (2005)
23. H.R. Kricheldorf, L. Vakhtangishvili, G. Schwarz, M. Prosenec, *J. Polym. Sci., Part A Polym. Chem.* **43**, 6233 (2005)
24. H.R. Kricheldorf, L. Vakhtangishvili, G. Schwarz, *J. Polym. Sci. Part A Polym. Chem.* **42**, 5725 (2004)
25. H.R. Kricheldorf, R. Hobzova, L. Vakhtangishvili, G. Schwarz, *Macromolecules* **38**, 4630 (2005)
26. H.R. Kricheldorf, R. Hobzova, L. Vakhtangishvili, G. Schwarz, *Macromol. Chem. Phys.* **206**, 2133 (2005)
27. H.R. Kricheldorf, N. Lomadze, C. Polefka, G. Schwarz, *Macromolecules* **39**, 2107 (2006)
28. H.R. Kricheldorf, J. Schellenberg, G. Schwarz, *Macromol. Chem. Phys.* **207**, 1556 (2006)
29. H.R. Kricheldorf, J. Schellenberg, G. Schwarz, *Macromolecules* **39**, 6445 (2006)
30. H.R. Kricheldorf, J. Schellenberg, G. Schwarz, *J. Polym. Sci. Part A Polym. Chem.*, **44**, 5546 (2006)
31. H.R. Kricheldorf, K. Bornhorst, G. Schwarz, *Macromolecules* **40**, 199 (2007)
32. A. Yokoyama, R. Miyakoshi, T. Yokozawa, *Macromolecules* **37**, 1169 (2004)
33. R. Miyakoshi, A. Yokoyama, T. Yokozawa, *Macromol. Rapid Commun.* **25**, 1663 (2004)
34. R. Miyakoshi, A. Yokoyama, T. Yokozawa, *J. Am. Chem. Soc.* **127**, 17542 (2005)
35. M.C. Iovu, E.E. Sheina, R.R. Gil, R.D. McCullough, *Macromolecules* **38**, 8649 (2005)
36. E.E. Sheina, J.S. Liu, M.C. Iovu, D.W. Laird, R.D. McCullough, *Macromolecules* **37**, 3526 (2004)
37. A. Yokoyama, H. Suzuki, Y. Kubota, K. Ohuchi, H. Higashimura, T. Yokozawa, *J. Am. Chem. Soc.* **129**, 7236 (2007)
38. H. Suzuki, Kanagawa University (2005)
39. T. Yokozawa, H. Higashimura, Japan Patent Kokai 2005-0388532005
40. T. Yokozawa, K. Okuchi, Y. Kubota, H. Higashimura, Japan Patent Kohkai 2006-0390652006
41. C.-G. Dong, Q.-S. Hu, *J. Am. Chem. Soc.* **127**, 10006 (2005)
42. S.K. Weber, F. Galbrecht, U. Scherf, *Org. Lett.* **8**, 4039 (2006)
43. M. Nojima, K. Kosaka, M. Kato, Y. Ohta, T. Yokozawa, *Macromol. Rapid Commun.* **37**, 79 (2016)
44. M. Nojima, Y. Ohta, T. Yokozawa, *Chem. Lett.* **46**, 35 (2017)
45. T. Kamigawara, H. Sugita, K. Mikami, Y. Ohta, T. Yokozawa, *Catalysts* **7**, 195 (2017)
46. K. Kosaka, K. Nanjyo, Y. Ohta, T. Yokozawa, *Chem. Lett.* **47**, 1040 (2018)
47. T. Yokozawa, N. Harada, H. Sugita, Y. Ohta, *Chem. Eur. J.* **25**, 10059 (2019)

48. H.R. Kricheldorf, M.G. Zolotukhin, J. Cárdenas, *Macromol. Rapid Commun.* **33**, 1814 (2012)
49. T. Yokozawa, H. Kohno, Y. Ohta, A. Yokoyama, *Macromolecules* **43**, 7095 (2010)
50. T. Yokozawa, R. Suzuki, M. Nojima, Y. Ohta, *Macromol. Rapid Commun.* **32**, 801 (2011)
51. M. Verswyvel, C. Hoebbers, J. De Winter, P. Gerbaux, G. Koeckelberghs, *J. Polym. Sci. Part A Polym. Chem.* **51**, 5067 (2013)
52. K. Kosaka, Y. Ohta, T. Yokozawa, *Macromol. Rapid Commun.* **36**, 373 (2015)
53. E. Elmalem, A. Kiriya, W.T.S. Huck, *Macromolecules* **44**, 9057 (2011)
54. P. Willot, G. Koeckelberghs, *Macromolecules* **47**, 8548 (2014)
55. R. Tkachov, Y. Karpov, V. Senkovskyy, I. Raguzin, J. Zessin, A. Lederer, M. Stamm, B. Voit, T. Beryozkina, V. Bakulev, W. Zhao, A. Facchetti, A. Kiriya, *Macromolecules* **47**, 3845 (2014)
56. W. Liu, R. Tkachov, H. Komber, V. Senkovskyy, M. Schubert, Z. Wei, A. Facchetti, D. Neher, A. Kiriya, *Polym. Chem.* **5**, 3404 (2014)
57. S. Kang, R.J. Ono, C.W. Bielawski, *J. Am. Chem. Soc.* **135**, 4984 (2013)
58. M. Nojima, Y. Ohta, T. Yokozawa, *J. Am. Chem. Soc.* **137**, 5682 (2015)
59. H. Sugita, M. Nojima, Y. Ohta, T. Yokozawa, *Polym. Chem.* **10**, 1182 (2019)
60. H. Sugita, Y. Ohta, T. Yokozawa, *J. Polym. Sci.* **58**, 1236 (2020)
61. K. Kosaka, T. Uchida, K. Mikami, Y. Ohta, T. Yokozawa, *Macromolecules* **51**, 364 (2018)
62. Y. Nanashima, A. Yokoyama, T. Yokozawa, *Macromolecules* **45**, 2609 (2012)
63. Y. Nanashima, R. Shibata, R. Miyakoshi, A. Yokoyama, T. Yokozawa, *J. Polym. Sci. Part A Polym. Chem.*, **50**, 3628 (2012)

**Part IV**  
**Cyclic Polymer Innovations: Topology**  
**Effects**



# Chapter 22

## Entanglement in Solution of Non-concatenated Rings



### Dynamical Entanglement Analysis

Takahiro Sakaue and Davide Michieletto

**Abstract** Most conventional analysis of entanglements in polymer systems is focused on measuring the chains' self-correlations. This is mainly motivated by the popular mean field picture in which a single chain moves in a sea of static topological obstacles representing the surrounding chains. Recently, we have proposed an alternative approach to understand the behaviours of polymeric systems, which is based on the analysis of cooperative motions between entangled chains. This method, which we call *dynamical entanglement analysis* (DEA), captures the spatio-temporal structures of correlated dynamics as a footprint of dynamic entanglement structures. Here, we summarize the principle and some of the results obtained in our recent studies and demonstrate that the entanglement structures are different between linear polymers and non-concatenated ring polymers in their concentrated solutions.

**Keywords** Entanglement · Topology · Ring polymers

### 22.1 Introduction

A cyclic polymer, also called ring polymer, can be made from a linear polymer by joining its ends. This seemingly simple closure operation carries an important consequence as it introduces a topological invariant into the system. One can think of various types of knots tied within a ring, and also various types of links made from several rings. Importantly, such a topological state is fixed at the stage of the

---

T. Sakaue (✉)

Department of Physical Sciences, Aoyama Gakuin University, 5-10-1 Fuchinobe, Chuo-ku, Sagamihara, Kanagawa 252-5258, Japan  
e-mail: [sakaue@phys.aoyama.ac.jp](mailto:sakaue@phys.aoyama.ac.jp)

D. Michieletto

School of Physics and Astronomy, University of Edinburgh, Peter Guthrie Tait Road, EH9 3FD Edinburgh, UK  
e-mail: [davide.michieletto@ed.ac.uk](mailto:davide.michieletto@ed.ac.uk)

preparation and acts as a frozen variable thereafter. The fundamental question is how such topological constraint affects the physical and statistical properties of ring polymers in solution [1–8].

In this chapter, we shall mainly consider the dynamics of dense non-concatenated, unknotted rings. Thus, our target is a very dense solution of ring polymers (each composed of  $N$  monomers of size  $a$ ), in which any ring is knot-free, and also free from any linking with any other ring. Of course, rings constantly change their positions and shape kicked by thermal noise, but all these fluctuations have to preserve the original topology. For instance, one can imagine creating such a system with DNA molecules: a tube with 1 ml of solution made of 50'000 base-pair-long DNA at 1 mg/ml contains  $10^{13}$  molecules, an impressive number of topological constraints to be satisfied!

This chapter is structured as follows: in Sect. 22.2, we give a brief review on the conformation of non-concatenated rings in melt, and see how it differs from the linear polymer counterpart. In Sect. 22.3, we recall the concept of entanglement familiar in linear polymer solution and raise a question about entanglements in solutions of non-concatenated rings. We then propose a method, i.e., the *dynamical entanglement analysis* [9], to probe the spatio-temporal evolution of entanglements, and apply it to solutions of non-concatenated ring and linear chains.

## 22.2 Brief Reminder on Ring Conformation

### 22.2.1 Size Scaling

In textbooks, we learn that excluded volume interactions swell polymers in dilute solution [10, 11]. On the other hand, this excluded volume effect is screened in melt and concentrated solutions of polymers [12]. It is well known that the conformation of individual chains in melt of linear polymers follows very closely the ideal chain statistics such that the average chain size, e.g. the radius of gyration, is given by  $R \simeq aN^{1/2}$  [10, 11]. This simple result, however, breaks down for rings because of the topological invariance discussed above.

To get a better feeling for this, suppose rings in dense solutions obey the  $R \sim N^{1/2}$  scaling. Then the volume occupied by one reference ring is  $R^3 \sim N^{3/2}$ , and there would be, on average,  $R^3/N \sim N^{1/2}$  other overlapping rings invading that volume. The same applies to all the rings, and it is not difficult to imagine that the unlinking (non-concatenation) topological invariant will become harder and harder to satisfy at larger values of  $N$ . For rings, a way out of this problem is to shrink, i.e.,  $R \sim N^\nu$  with  $\nu < 1/2$ . Simulations have found that  $\nu = 1/2$  for short rings, but at large enough  $N$  the most recent results strongly suggest an exponent  $\nu = 1/3$  [13–17]; a similar exponent was also observed in experiments using neutron scattering [18–20].

### 22.2.2 Topological Volume

Intuitively, the unlinking topological invariance generates an effective entropic repulsion between rings, which may also be interpreted as an effective excluded volume. We have recently exploited such a notion of *topological volume* to describe the above mentioned size scaling behavior [5, 21], i.e., from ideal chain statistics ( $\nu = 1/2$ ) for short rings ( $N < N_e$ ; see the discussion in Sect. 22.3) to the compact statistics ( $\nu = 1/3$ ) for asymptotically long rings with a broad crossover ( $\nu \simeq 0.4$ ) in between. With its appealing physical picture, the idea of topological volume has turned out to be useful in various problems in ring polymers; so far it has been applied to describe the slow dynamics in ring polymer melts [22], and the problem of phase behavior of blends including ring polymers [23]; see also the corresponding experiment [24].

## 22.3 Entanglement

Long linear polymers in concentrated solutions are said to be “entangled”. Entanglements originate from the uncrossability of bonds and make the dynamics of polymers slower, yielding an often spectacular viscoelastic behavior [10, 11], which makes solutions of polymers resist stress at short timescales and yet flow at long timescales. Importantly, there is a characteristic chain length, called “entanglement length”  $N_e$ , such that the entanglement effect shows up for  $N > N_e$ . The dynamics of shorter unentangled chains in the melt can be described by the Rouse model [10, 11]. For rings too there exists a  $N_e$ , which marks the transition from unentangled to entangled regime. Note that the term entanglement here is strictly referring to phenomena arising due to the uncrossability of polymer bonds and is not meant to include the topological invariance of the system (recall our target is the non-concatenated rings!). Rather, similarly to linear polymers, rings in the entangled regime are also under the influence of generic topological constraint due to bond uncrossability; however, the way rings entangle should be very different than the way linear chains entangle, indeed because of the additional topological invariance in place in systems of rings. As discussed in Sect. 22.2, unlike the linear case, topological constraints in systems of rings have a pronounced effect on their conformation (scaling with a metric exponent  $\nu = 1/3$ ). In turn, we expect a stark difference in the number of overlapping chains and markedly different entanglement structures, both of which should be reflected in their dynamics.

## 22.4 Dynamical Entanglement Analysis

A standard theory for the dynamics of entangled linear polymer solution is the reptation theory [10, 11]. Here, a reference chain is pictured as moving in an array of fixed obstacles representing the topological constraints from surrounding chains. The

entanglement effect is enforced by the rule that the reference chain cannot cross the obstacles. This picture is equivalent to a (non-self-consistent) mean field approach, where the effect of neighboring chains on the test chain is exchanged by an average and static set of constraints. Largely due to such modeling philosophy which has been very successful in the past [12], the dynamics of entangled polymers are conventionally analyzed in terms of single-chain quantities, such as the mean square self-displacement of the center of mass of chains or of some tagged monomers along the chains.

What happens if we remove the (rather strong) assumption of fixed obstacles? Imagine that a reference chain makes a displacement in a certain direction; then, other chains entangled with the reference chain can also move in the same direction thanks to the transient vacancy left by the reference chain; in turn, this may also entail that the reference chain cannot reverse its displacement, as there is a new obstacle in its way. Following this intuition, i.e., that entangled chains may display coordinated motion due to “entrainment”, we have recently proposed a method, which we call *dynamical entanglement analysis* (DEA), to probe and quantify the nature of polymer entanglement by measuring the cooperative motion of entangled polymers [9]. Below, we first illustrate the idea and its formulation and then apply it to data obtained from molecular dynamics simulations.

### 22.4.1 Displacement Correlation

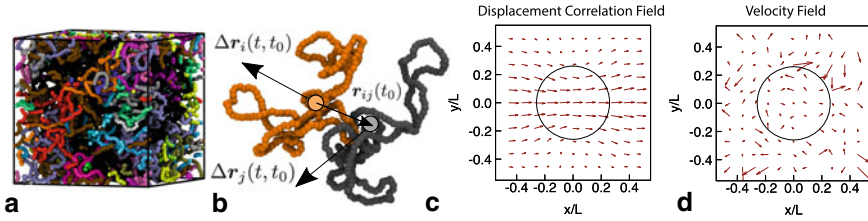
Let  $\mathbf{r}_i(t)$  be the position of the center of mass of the  $i$ th polymer at time  $t$ , and  $\Delta\mathbf{r}_i(t, t_0) = \mathbf{r}_i(t_0 + t) - \mathbf{r}_i(t_0)$  be its displacement during the time interval  $t$ . In the dynamical entanglement analysis, we compute the correlation between displacements of different polymers (see Fig. 22.1a, b for a sketch)

$$H_{\alpha\beta}(t, \mathbf{r}) \equiv \langle \Delta r_{i,\alpha}(t, t_0) \Delta r_{j,\beta}(t, t_0) \rangle_{\mathbf{r}} \quad (22.1)$$

where the Greek indexes stand for Cartesian components. Noting that the “initial” time does not enter the statistical quantities in stationary state, the average  $\langle \dots \rangle_{\mathbf{r}}$  is intended over times  $t_0$ , and pairs of polymers  $(i, j)$  which satisfy  $\mathbf{r}_j(t_0) - \mathbf{r}_i(t_0) = \mathbf{r}(t_0)$ .

### 22.4.2 Vector Field Representation

Equation (22.1), which we call the displacement correlation tensor, carries the detailed information on cooperative motion in the system of entangled polymers on the time scale  $t$ . Now, let us imagine to apply an external force to the polymer  $i$  at the origin  $\mathbf{r}_i = \mathbf{0}$  and measure the resultant induced displacement of other polymers at different distances from it. Such a displacement vector field is visualized



**Fig. 22.1** **a** Snapshot of the simulated system. **b** Sketch of the DEA calculation for a pair of rings. **c** 2D slice of the vector field  $\mathbf{v}(t, \mathbf{r}) = H(t, \mathbf{r}) \cdot \mathbf{e}_x$  for ring polymers  $N = 512$  beads long at the lag-time  $t = 10^4 \tau_0$ , where  $\mathbf{e}_x = (1, 0, 0)$  is a unit vector in the direction of applied force, and  $\tau_0$  is the monomeric time scale. The spatial coordinate is normalized by the box length  $L$ , which is about four times larger than the average radius of gyration of rings; see the circle in figures, which is drawn using the average radius of gyration as radius. Note that the vectors are scaled up ( $\times 2.5$ ) for visualization purposes. **d** Velocity field  $\mathbf{b}(t, \mathbf{r}) = \langle \sum_i [\Delta \mathbf{r}_i(t, t_0)] / t \delta(\mathbf{r}_i(t_0) - \mathbf{r}) \rangle$  at fixed lagtime  $t = 10^4 \tau_0$  and averaged over 200 consecutive values of  $t_0$  over  $0.2 \times 10^4 \tau_0$  in order to fill up the space with instantaneous velocity vectors. Vectors are scaled up by 80 times to better visualize their random direction (they would be too small otherwise). Adapted with permission from Ref. [9]. Copyright (2021) American Chemical Society

in Fig. 22.1c, where we set the direction of the applied fictitious force oriented to positive  $x$  axis. We emphasize that Fig. 22.1c is *not* the velocity field of rings; in fact, we can measure the instantaneous velocity of rings via their displacement over a lagtime  $t$  as

$$b_\alpha(t, \mathbf{r}) \equiv \langle \Delta r_{i,\alpha}(t, t_0) / t \rangle_{\mathbf{r}}. \quad (22.2)$$

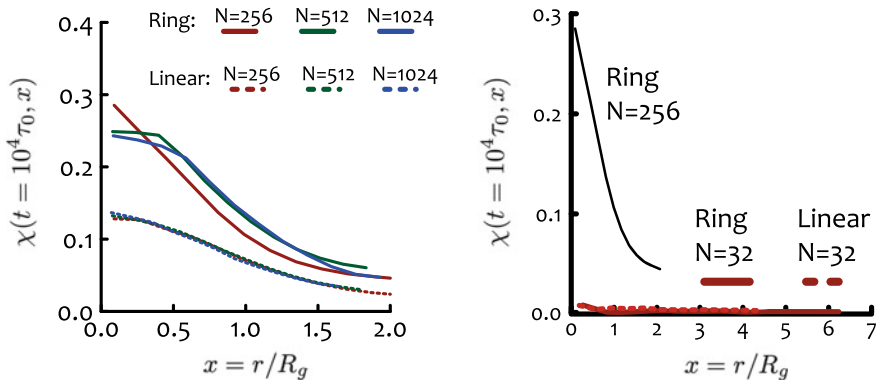
This quantity looks more chaotic due to the thermal noise and we do not expect any structure in time or space (Fig. 22.1d). Nonetheless, the correlation of mutual displacements strongly suggests that there are cooperative dynamics in entangled chains, which persists over long length and time scales.

### 22.4.3 Spatial-Temporal Entanglement Structure

For more quantitative analysis, we can construct a scalar quantity

$$\chi(t, r) = \frac{\text{Tr}[H(t, \mathbf{r})]}{g_3(t)} \quad (22.3)$$

where  $\text{Tr}[H(t, \mathbf{r})]$  depends only on the separation  $r = |\mathbf{r}|$  for a homogeneous and isotropic system, and the normalizing factor  $g_3(t)$  is the mean squared displacement of the polymers' center of mass. Thus,  $\chi(t, r)$  measures the degree of the dynamic cooperativity between polymers on time scale  $t$  and the spatial scale  $r$ .

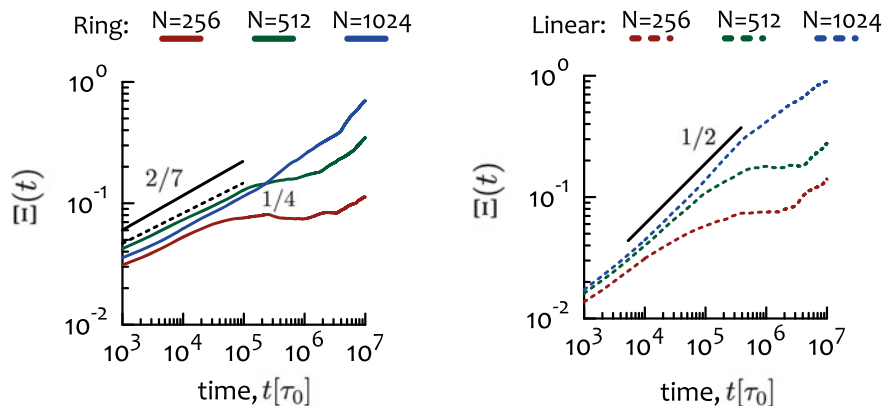


**Fig. 22.2** Spatial profile of cooperative motion  $\chi(t, r)$  at the time scale  $t = 10^4 \tau_0$ , where the spatial scale is normalized by the radius of gyration  $R_g$ . (Left) The profile of ring (solid) or linear (dashed) exhibits chain length independent master curve (chain length examined are  $N = 256, 512$  and  $1024$  as indicated). However, distinct profiles between ring and linear systems indicate qualitatively different entanglement structures in these systems. (Right) Comparison with unentangled systems. Here, we show the spatial profile of  $\chi(t, r)$  at  $t = 10^4 \tau_0$  for ring and linear systems with the chain length  $N = 32$ , which is shorter than the entanglement length  $N_e (\simeq 40)$  in our model. As a reference, we also plot  $\chi(t, r)$  at  $t = 10^4 \tau_0$  for the ring system with  $N = 256$ , which is also shown (Left). Adapted with permission from Ref. [9]. Copyright (2021) American Chemical Society

In Fig. 22.2, we plot the spatial dependence of  $\chi(t, r)$  at the time scale  $t = 10^4 \tau_0$  for ring and linear systems with various chain lengths. Interestingly, on this time scale, the spatial profile of the dynamic cooperativity does not depend on chain length  $N$  once scaled by the gyration radius  $R_g$  but exhibits a marked difference between ring and linear polymer systems. For rings, the steeper spatial gradient suggests that mutually overlapping (and hence, likely interpenetrating or threading [16, 25, 26]) rings are more correlated than distant ones. Instead, the weaker spatial dependence seen for linear chains reflects a more uniformly distributed entanglement structure over the whole contour of the chain, in qualitative agreement with the picture of the tube and reptation model. In this way, we can access the difference in the structure of entanglements between ring and linear chains from our dynamical entanglement analysis. We also stress that, for unentangled chains ( $N < N_e$ ),  $\chi(t, r)$  remains close to zero, there is no correlation at any spatial or temporal scales for unentangled chains, which supports our intuition that the observed cooperative motion is a footprint of polymer entanglements.

#### 22.4.4 Mean Field Picture

By taking the spatial average of  $\chi(t, r)$ , we can discuss how the average entanglement structure evolves over the time scale. This leads to a mean field picture in which the surrounding entanglements are replaced by a uniform field of constraints, and



**Fig. 22.3** Plot of  $\overline{\chi}(t)$ , defined as the spatial average of  $\chi(t, r)$ , as a function of the lag time for ring (Left) and linear (Right) systems. Adapted with permission from Ref. [9]. Copyright (2021) American Chemical Society

which can thus be compared with the prediction of, e.g., reptation theory. As shown in Fig. 22.3, the spatial average of  $\chi(t, r)$ , which we call  $\overline{\chi}(t)$ , exhibits a power-law behavior in the short-medium time scale. Now, recalling the physical picture behind the dynamical entanglement analysis that the cooperative motion is due to the entrainment/entanglement of two polymers, one can argue that  $\overline{\chi}(t)$  is proportional to the friction coefficient  $\Gamma(t)$  experienced by each chain at the time scale  $t$  [9]. The reptation theory predicts  $\Gamma(t) \sim t^{1/2}$  up to Rouse time  $t_R \simeq \tau_0 N^2$ . Thus, the observed  $\overline{\chi}(t) \sim t^{1/2}$  for linear systems supports our reasoning. On the other hand, we observe a very different scaling  $\overline{\chi}(t) \sim t^{2/7}$  for rings, which again indicates (i) qualitatively different entanglement structures and (ii) that their evolution is different from that of entanglements in linear polymers. A detailed analysis suggests that the *tube dilation* mechanism is at work for rings, where the number of entangled rings decreases with time scale [9]. However, we have found that there are yet remnants of entangled rings even at the conformational relaxation time scale, which may be the origin of slow dynamics expected and observed in dense solution of non-concatenated rings [4, 16, 18, 22, 27].

## 22.5 Outlooks

“What is an entanglement?” is a simple yet deep question in polymer science with a long history of research, still attracting many researchers today. The consequences brought about by entanglements are particularly challenging to understand especially in systems of non-concatenated ring polymers (Sect. 22.3); as we discussed in this

section, their nature appears to be different than the entanglement populating systems of linear chains. In this respect, systems of ring polymers provide a unique standpoint to address this fundamental question.

We have demonstrated that the recently proposed method dubbed “dynamical entanglement analysis” (DEA) is able to capture the spatio-temporal entanglement structure from the cooperative motion of polymers.

While we have focused here on the motion of polymers’ center of mass, it may be interesting to analyze the cooperative dynamics in various spatial resolutions, say at the segment scale or, perhaps more interestingly, over an entanglement length scale.

Compared with the intermediate time scale, we have not obtained a clear picture in the long time-scale dynamics (see the last part in Sect. 22.4). It is an interesting challenge to unveil the molecular origin of the slow dynamics in ring polymer systems [16, 22, 27]. The dynamical entanglement analysis will be useful here, although longer simulations are needed in order to gather enough statistics at long time scales.

The DEA method can be applied not only to linear and ring polymers but also to other polymeric systems. Thus, it may be used in the future to characterize entanglements in other types of polymers. Interesting examples include topologically designed polymers [28, 29], such as tadpoles [30, 31] and dumbbells [32], in which linear and ring polymers are covalently bonded within a single chain.

**Acknowledgements** T.S is supported by JSPS KAKENHI (Number JP18H05529) from MEXT, Japan. D.M. is a Royal Society University Research Fellow and is supported by the ERC (TAP, 947918).

## References

1. M. Rubinstein, *Phys. Rev. Lett.* **57**(24), 3023 (1986)
2. M. Cates, J. Deutsch, *J. Phys.* **47**(12), 2121 (1986)
3. T. McLeish, *Science* **297**(5589), 2005 (2002)
4. M. Kapnistos, M. Lang, D. Vlassopoulos, W. Pyckhout-Hintzen, D. Richter, D. Cho, T. Chang, M. Rubinstein, *Nat. Mater.* **7**(12), 997 (2008)
5. T. Sakaue, *Phys. Rev. Lett.* **106**(16), 167802 (2011)
6. J.D. Halverson, J. Smrek, K. Kremer, A.Y. Grosberg, *Reports Prog. Phys.* **77**(2) (2014)
7. A. Narros, C.N. Likos, A.J. Moreno, B. Capone, *Soft Matter* **10**(48), 9601 (2014)
8. T. Ge, S. Panyukov, M. Rubinstein, *Macromolecules* **49**(2), 708 (2016)
9. D. Michieletto, T. Sakaue, *ACS Macro Lett.* **10**(1), 129 (2021)
10. P.G.D. Gennes, *Scaling concepts in polymer physics* (Cornell University Press, 1979)
11. M. Rubinstein, H.R. Colby, *Polymer Physics* (Oxford University Press, Oxford, 2003)
12. M. Doi, S.F. Edwards, *The Theory of Polymer Dynamics*, vol. 73 (Oxford University Press, Oxford, 1988)
13. J. Suzuki, A. Takano, T. Deguchi, Y. Matsushita, *J. Chem. Phys.* **131**(14), 144902 (2009)
14. T. Vettorel, A.Y. Grosberg, K. Kremer, *Phys. Biol.* **6**(2), 025013 (2009)
15. J.D. Halverson, W.B. Lee, G.S. Grest, A.Y. Grosberg, K. Kremer, *J. Chem. Phys.* **134**(20), 204904 (2011)
16. D. Michieletto, M.S. Turner, *Proc. Natl. Acad. Sci.* **113**(19), 5195 (2016)
17. A. Rosa, R. Everaers, *Phys. Rev. Lett.* **112**(11), 118302 (2014)



18. S. Gooßen, A. Brás, M. Krutyeva, M. Sharp, P. Falus, A. Feoktystov, U. Gasser, W. Pyckhout-Hintzen, A. Wischnewski, D. Richter, *Phys. Rev. Lett.* **113**(16), 168302 (2014)
19. A. Brás, S. Gooßen, M. Krutyeva, A. Radulescu, B. Farago, J. Allgaier, W. Pyckhout-Hintzen, A. Wischnewski, D. Richter, *Soft Matter* **10**, 3649 (2014)
20. M. Kruteva, J. Allgaier, M. Monkenbusch, L. Porcar, D. Richter, *ACS Macro Lett.* **9**(4), 507 (2020)
21. T. Sakaue, *Phys. Rev. E* **85**(2), 021806 (2012)
22. T. Sakaue, *Soft Matter* **14**(7507), 7507 (2018)
23. T. Sakaue, C.H. Nakajima, *Phys. Rev. E* **93**(04), 2502 (2016)
24. Y. Kobayashi, Y. Doi, S.S. Abdul Rahman, E. Kim, T.H. Kim, A. Takano, Y. Matsushita, *Macromolecules* **51**(5), 1885 (2018)
25. J. Smrek, A.Y. Grosberg, *ACS Macro Lett.* **5**(6), 750 (2016)
26. F. Landuzzi, T. Nakamura, D. Michieletto, T. Sakaue, *Phys. Rev. Res.* **2**, 033529 (2020)
27. D.G. Tsalikis, V.G. Mavrantzas, D. Vlassopoulos, *ACS Macro Lett.* **5**(6), 755 (2016)
28. E. Uehara, T. Deguchi, *J. Chem. Phys.* **145**(16) (2016)
29. T. Deguchi, E. Uehara, *Polymers* **9**(7), 13 (2017)
30. Y. Doi, A. Takano, Y. Takahashi, Y. Matsushita, *Macromolecules* **48**(23), 8667 (2015)
31. A. Rosa, J. Smrek, M.S. Turner, D. Michieletto, *ACS Macro Lett.* **9**(5), 743 (2020)
32. Y. Doi, A. Takano, Y. Takahashi, Y. Matsushita, *Macromolecules* **54**(3), 1366 (2021)

# Chapter 23

## Dilute Solution Properties of Ring Polymers



Daichi Ida

**Abstract** Molecular characterization of ring polymers on the basis of their dilute solution properties is still required even with recent development of various experimental techniques. In this chapter, the theories and procedures for analyzing experimental data of dilute solution properties of ring polymers are summarized. First, the conventional theory on the basis of the *Gaussian ring model* is briefly mentioned along with the introduction of typical dilute solution properties of polymers. Then, the theory on the basis of the *wormlike ring model* taking into account effects of *chain stiffness*, which are outside of the scope of the Gaussian ring theory, is presented. Finally, some examples of analyses of experimental data on the basis of the latter model are shown.

### 23.1 Gaussian Ring

Studies of dilute solution properties of ring polymers have been made mainly for *flexible* ring polymers, such as atactic polystyrene (a-PS), poly(dimethylsiloxane) (PDMS), and so on [1, 2]. In particular, experimental data for flexible rings without (ordinary) excluded-volume effects in the  $\Theta$  state or bulk have been analyzed on the basis of the ideal Gaussian ring or its analogue, and then, a comparison has been made between the results for the rings and those for the corresponding linear polymers.

The ideal Gaussian ring model is composed of infinitely thin  $n$  Hookean springs of equilibrium length 0 and root-mean-square length  $l$ , two adjacent springs being jointed freely. For convenience, the *intramolecular topological constraints*, which work to preserve the type of knot for a given ring polymer, are ignored. The ideal Gaussian ring may then be regarded as a “phantom” ring, for which the springs (bonds) are allowed to cross each other. On the basis of the ideal Gaussian ring model, analytical expressions have been obtained for typical dilute solution properties.

---

D. Ida (✉)

Department of Polymer Chemistry, Kyoto University, Katsuta, Kyoto 615-8510, Japan  
e-mail: [ida@molsci.polym.kyoto-u.ac.jp](mailto:ida@molsci.polym.kyoto-u.ac.jp)

The *mean-square radius of gyration*  $\langle S^2 \rangle$ ,<sup>1</sup> which may be determined from static light scattering (SLS) and small-angle X-ray or neutron scattering (SAXS or SANS), may be given by [1, 3, 4]

$$\langle S^2 \rangle = nl^2/12 \quad (\text{Gaussian ring}). \quad (23.1)$$

The *scattering function*  $P(k)$ <sup>2</sup> as a function of the magnitude  $k$  of the scattering vector, which reflects the distribution of the repeating units of a polymer molecule around its center of mass and is determined from scattering experiments as in the case of  $\langle S^2 \rangle$ , is given by [5]

$$P(k) = \left( \frac{2}{\langle S^2 \rangle k^2} \right)^{1/2} e^{-\langle S^2 \rangle k^2 / 2} \int_0^{(\langle S^2 \rangle k^2 / 2)^{1/2}} e^{x^2} dx \quad (\text{Gaussian ring}), \quad (23.2)$$

where  $\langle S^2 \rangle$  is given by Eq. (23.1).

The *translational diffusion coefficient*  $D$  of a polymer molecule, which may be determined from dynamic light scattering measurements, is related to the *effective hydrodynamic radius*  $R_H$  of a polymer molecule by the Stokes–Einstein relation  $D = k_B T / 6\pi\eta_0 R_H$  with  $k_B$  the Boltzmann constant,  $T$  the absolute temperature, and  $\eta_0$  the solvent viscosity. The quantity  $R_H$  for the Gaussian ring is given by [1, 6, 7]

$$R_H = (6\pi)^{-1/2} (nl^2)^{1/2} \quad (\text{Gaussian ring}). \quad (23.3)$$

The *intrinsic viscosity*  $[\eta]$  determined from viscometry is proportional to the *effective hydrodynamic volume*  $V_H$  in steady shear flow.<sup>3</sup> The quantity  $[\eta]$  for the Gaussian ring is given by [1, 6, 7]

$$[\eta] = 5N_A V_H / 2M = \Phi_r (nl^2)^{3/2} / M \quad (\text{Gaussian ring}), \quad (23.4)$$

where  $N_A$  is the Avogadro constant,  $M$  is the molecular weight, and  $\Phi_r = 1.854 \times 10^{23} \text{ mol}^{-1}$ . We note that Eqs. (23.3) and (23.4) are obtained on the basis of the Kirkwood–Risemann approximation [1, 8].

The quantities  $\langle S^2 \rangle$ ,  $R_H$ , and  $V_H$  (or  $M[\eta]$ ) are measures of the *average chain dimension* of a polymer molecule in solutions at infinite dilution. For the ideal Gaussian ring, of course, the length scale characterizing the average chain dimension should be proportional to  $n^{1/2}$  as in the case of the ideal linear Gaussian chain. Indeed, Eqs. (23.1), (23.3), and (23.4) represent the relations  $\langle S^2 \rangle \propto n$ ,  $R_H \propto n^{1/2}$ , and  $M[\eta] \propto V_H \propto n^{3/2}$ , respectively. Such results for the Gaussian ring are often com-

<sup>1</sup> The root-mean-square radius of gyration  $\langle S^2 \rangle^{1/2}$  is often denoted by  $R_g$  elsewhere.

<sup>2</sup> There holds the relation

$$P(k) = 1 - \langle S^2 \rangle k^2 / 3 + \mathcal{O}(k^4).$$

<sup>3</sup> Note that  $V_H \neq 4\pi R_H^3 / 3$ .

pared with those for the corresponding linear Gaussian chain having the same  $n$  and  $l$  by the use of the so-called  $g$ -factors defined as  $g_S = \langle S^2 \rangle(\text{ring}) / \langle S^2 \rangle(\text{linear})$ ,  $g_H = R_H(\text{ring}) / R_H(\text{linear})$ , and  $g_\eta = [\eta](\text{ring}) / [\eta](\text{linear})$ . The factors  $g_S$ ,  $g_H$ , and  $g_\eta$  become constants  $1/2$ ,  $8/3\pi$ , and  $0.646$ , respectively, independent of  $n$ , since  $\langle S^2 \rangle = nl^2/6$ ,  $R_H = (3/8)(\pi/6)^{1/2}(nl^2)^{1/2}$ , and  $[\eta] = (2.870 \times 10^{23} \text{ mol}^{-1} / M)(nl^2)^{3/2}$  for the linear Gaussian chain [1, 9].

The *second virial coefficient*  $A_2$ , which may be determined from SLS measurements or osmometry, reflects the intermolecular interaction between a pair of polymers in solutions. Usually, the interactions between repeating units of polymers become repulsive, i.e., the (ordinary) excluded-volume effects work, if  $A_2 > 0$  and become attractive if  $A_2 < 0$ . When  $A_2$  vanishes (in the limit of  $M \rightarrow \infty$ , strictly speaking [9]), the contributions of the repulsive and attractive forces to the interactions between repeating units cancel apparently each other, and then, the polymers in solutions behave as ideal polymers without excluded volume. Such state is called the  $\Theta$  state [1, 9]. For an unlinked pair of ring polymers, in addition to the ordinary excluded-volume effects, the repulsive force results from the so-called *topological interaction* which works to conserve a given link type of a pair of ring polymers. Consequently,  $A_2$  of ring polymers becomes positive even in the  $\Theta$  or ideal state without excluded-volume effects, as explicitly shown by Frank-Kamenetskii et al. [10, 11]. If  $A_2 > 0$ ,  $A_2$  may be related to the *effective intermolecular excluded volume*  $V_E$ , which is another measure of the average chain dimension. For the Gaussian ring, the second virial coefficient  $A_{2,\Theta}$  at the  $\Theta$  or ideal state may be given by [12–15]

$$A_{2,\Theta} = 4N_A V_E / M^2 \propto \langle S^2 \rangle^{3/2} / M^2 \propto n^{-1/2} \quad (\text{Gaussian ring}). \quad (23.5)$$

It is important to note here that all the results for the Gaussian ring described above are the asymptotic forms valid only in the limit of  $n \rightarrow \infty$  (or  $M \rightarrow \infty$ ), and also, that  $n$  and  $l$  are never determined separately from analyses of experimental data on the basis of the Gaussian ring theory.

## 23.2 Wormlike Ring

For real polymers, their backbone is, of course, subject to the constraints on bond lengths, bond angles, and internal rotation angles corresponding to the chemical structures of repeating units, and then, are not so flexible as expected from the picture of the Gaussian chain model. In other words, all real polymers have the characteristic chain stiffness even in the cases of a-PS, PDMS, and other polymers known as flexible polymers and exist in the range of the crossover from the rigid-rod limit to the random-coil (Gaussian) one. It is well known that linear polymers in the range of crossover may be well described by the Kratky–Porod wormlike chain model [9, 16].

The (linear) wormlike chain model (without excluded volume) may be defined as a continuous limit of the freely rotating chain or as a statistical elastic wire with bending energy in a thermal bath [9]. The wormlike chain takes into account the effects of chain stiffness by the *persistence length*  $q$  in the case of the former definition or the *stiffness parameter*  $\lambda^{-1}$  proportional to the bending force constant in the latter. Both the parameters  $q$  and  $\lambda^{-1}$  have the dimension of length and the equality  $\lambda^{-1} = 2q$  holds in the case of the wormlike chain.<sup>4</sup> For the wormlike chain of contour length  $L$  and stiffness parameter  $\lambda^{-1}$ , the dimensional and conformational properties reduced by  $\lambda^{-1}$  may be expressed as functions of the reduced contour length  $\lambda L$ . The wormlike chain becomes stiffer and more flexible with decreasing and increasing  $\lambda L$ , respectively, the limits of  $\lambda L \rightarrow 0$  and  $\lambda L \rightarrow \infty$  corresponding to the rigid-rod and random-coil (Gaussian) limits, respectively. The wormlike chain model may then describe the dilute solution behavior of all flexible, *semiflexible*, and stiff polymers with various length (molecular weight) and stiffness.<sup>5</sup>

The wormlike chain model may be extended, in principle, to any non-linear polymers. The wormlike ring model is constructed from the linear wormlike chain with connecting its both ends such that the unit tangent vectors at both the ends coincide with each other. For the wormlike ring, the limits of  $\lambda L \rightarrow 0$  and  $\lambda L \rightarrow \infty$  correspond to the rigid and random-coiling (Gaussian) rings, respectively. As in the case of the linear wormlike chain model, the wormlike ring may be considered to describe well the dilute solution behavior of all ring polymers in the range of the crossover from the rigid ring to the random-coiling one. Note that for the results explained in this section effects of the intramolecular topological constraints are also ignored as in the case of the Gaussian ring described in the previous section.

The mean-square radius of gyration  $\langle S^2 \rangle$  for the wormlike ring model (without thickness) is given by [9, 17, 18]

$$\begin{aligned} \lambda^2 \langle S^2 \rangle &= \frac{(\lambda L)^2}{4\pi^2} [1 - 0.1140\lambda L - 0.0055258(\lambda L)^2 \\ &\quad + 0.0022471(\lambda L)^3 - 0.00013155(\lambda L)^4] \quad \text{for } \lambda L < 6 \\ &= \frac{\lambda L}{12} \left[ 1 - \frac{7}{6\lambda L} - 0.025e^{-0.01(\lambda L)^2} \right] \quad \text{for } \lambda L \geq 6 \end{aligned}$$

(wormlike ring). (23.6)

It is seen that  $\lambda^2 \langle S^2 \rangle$  in the left-hand side of Eq. (23.6), which represents  $\langle S^2 \rangle$  reduced by  $\lambda^{-1}$  (having the dimension of length), becomes a function only of  $\lambda L$ . It is also seen from Eq. (23.6) that  $\lim_{\lambda L \rightarrow 0} \lambda^2 \langle S^2 \rangle = (\lambda L)^2/4\pi^2$  and  $\lim_{\lambda L \rightarrow \infty} \lambda^2 \langle S^2 \rangle = \lambda L/12$

<sup>4</sup> Note that in general  $\lambda^{-1} \geq 2q$  [9].

<sup>5</sup> For flexible polymers, strictly speaking, we should use a more general model, the *helical wormlike chain model* [9], which includes the wormlike chain model as a special case, to analysis of experimental data.

recover the asymptotic forms in the rigid and random-coiling limits, respectively. Note that the latter asymptotic relation is reduced to Eq. (23.1) with  $\lambda^{-1} = l$  and  $L = nl$ .

The scattering function  $P(k)$  of the wormlike ring (without thickness), for which analytical expression may be obtained only in the range of  $\lambda L \gg 1$ , is given by [9, 19]

$$P(k) = 2L^{-2} \int_0^L (L-t) e^{-t(L-t)k^2/6L} \left[ 1 + \frac{k^2}{12} - \frac{11t(L-t)k^2}{36L^2} - \frac{11t^4(L-t)k^4}{1080L^4} - \frac{11t(L-t)^4k^4}{1080L^4} + \dots \right] dt \quad \text{for } \lambda L \gtrsim 10$$

(wormlike ring). (23.7)

This expression takes into account the deviation of order  $\mathcal{O}[(\lambda L)^{-1}]$  due to the effects of chain stiffness from the asymptotic form Eq. (23.2) for the random-coiling ring, and then, recovers Eq. (23.2) in the limit of  $\lambda L \rightarrow \infty$ . For the rigid ring (or in the limit of  $\lambda L \rightarrow 0$ ),  $P(k)$  is given by [20, 21]

$$P(k) = \int_0^{\pi/2} [J_0(\langle S^2 \rangle^{1/2} k \sin \phi)]^2 \sin \phi d\phi \quad \text{(rigid ring)}, \quad (23.8)$$

where  $J_0(x)$  is the zeroth-order Bessel function of the first kind with  $\langle S^2 \rangle = L^2/4\pi^2$ . In the range of  $\lambda L$  where Eqs. (23.7) and (23.8) are not valid, experimental data may be analyzed by the Monte Carlo (MC) data obtained on the basis of the discrete version of the wormlike ring model [22, 23] as described later.

For calculation of  $R_H$  and  $[\eta]$  of the wormlike ring, effects of the hydrodynamic thickness of the ring contour should be taken into account. Note that for the Gaussian ring (in the limit of  $\lambda L \rightarrow \infty$ ) the “finite” hydrodynamic thickness may be regarded as infinitesimal compared to the contour length and then ignored in Eqs. (23.3) and (23.4). Here, the wormlike ring is extended to the wormlike cylinder ring model having a uniform circular cross section of diameter  $d$  whose center is on the wormlike ring contour [9, 17]. On the basis of the Oseen–Burgers procedure [9] in the Kirkwood–Risemann approximation [1], the effective hydrodynamic radius  $R_H$  of the wormlike cylinder ring is calculated as follows [9, 17]:

$$\lambda R_H = (6\pi)^{-1/2} (\lambda L)^{1/2} F_H(\lambda L, \lambda d) \quad \text{(wormlike ring)}, \quad (23.9)$$

where

$$\begin{aligned}
[F_H(L, d)]^{-1} = & \frac{2}{\pi} \left[ \left( 1 - \frac{11}{120L} \right) \arcsin \left( 1 - \frac{2\sigma}{L} \right) - \frac{(L - 2\sigma)(1 + 5d^2)}{20L\sigma^{1/2}(L - \sigma)^{1/2}} \right] \\
& + \ln \left[ \frac{2\sigma + (4\sigma^2 + d^2)^{1/2}}{d} \right] + f_1 \left[ \left( \sigma^2 + \frac{1}{4}d^2 \right)^{1/2} - \frac{1}{2}d \right] \\
& + \frac{1}{2}f_2 \left\{ \sigma \left( \sigma^2 + \frac{1}{4}d^2 \right)^{1/2} - \frac{1}{4}d^2 \ln \left[ \frac{2\sigma + (4\sigma^2 + d^2)^{1/2}}{d} \right] \right\} \\
& + \frac{1}{3}f_3 \left( \sigma^2 - \frac{1}{2}d^2 \right) \left( \sigma^2 + \frac{1}{4}d^2 \right)^{1/2} \quad \text{for } L \geq 3.480.
\end{aligned} \tag{23.10}$$

In Eq. (23.10),  $\sigma = \sigma(L)$  and  $f_i = f_i(L, d)$  are given by

$$\begin{aligned}
\sigma &= 2.18559 - 0.467985/L + 0.491581/L^2 - 15.0334/L^3, \\
f_1 &= 0.333333 - 0.0450040d^2 - 0.0220160d^4 \\
&\quad - (0.275430d^2 + 0.0822244d^4)/L + (1.19325d^2 + 0.457470d^4)/L^2 \\
&\quad - (5.59657d^2 - 2.97966d^4)/L^3, \\
f_2 &= 0.119083 + 0.00518804d^2 + 0.0158136d^4 \\
&\quad + (0.530304 + 0.140740d^2 + 0.0754396d^4)/L \\
&\quad + (0.999369 - 2.39261d^2 - 0.620245d^4)/L^2 \\
&\quad - (4.99560 - 9.30255d^2 - 3.39914d^4)/L^3, \\
f_3 &= -0.0265957 + 0.000915166d^2 - 0.00297808d^4 \\
&\quad - (0.0149946 + 0.0533328d^2 + 0.0187217d^4)/L \\
&\quad - (0.688179 - 1.03760d^2 - 0.193592d^4)/L^2 \\
&\quad + (4.85298 - 4.61578d^2 - 0.982380d^4)/L^3,
\end{aligned} \tag{23.11}$$

respectively. The wormlike cylinder ring becomes the rigid torus of thickness  $d$  in the limit of  $\lambda L \rightarrow 0$  with finite  $d$ . For the rigid torus,  $R_H$  is given by [9, 17]

$$R_H = L/2 \left( \frac{4p^2}{4p^2 + \pi^2} \right)^{1/2} K \left[ \left( \frac{4p^2}{4p^2 + \pi^2} \right)^{1/2} \right] \quad (\text{rigid torus}), \tag{23.12}$$

where  $p = L/d$  and  $K(x)$  is the complete elliptic integral of the first kind given by

$$K(x) = \int_0^{\pi/2} (1 - x^2 \sin^2 \theta)^{-1/2} d\theta. \tag{23.13}$$

Further,  $R_H$  for the rigid ring without thickness may be obtained as the asymptotic form of Eq. (23.12) in the limit of  $p \rightarrow \infty$  ( $d \rightarrow 0$ ) as follows [9, 17]:

$$R_H = L/2 \ln(L/d) \quad (\text{rigid ring}). \tag{23.14}$$

By the use of the same model and procedure as in the case of  $R_H$ , the intrinsic viscosity  $[\eta]$  of the wormlike cylinder ring is given by [9, 17]

$$\frac{\lambda^{3/2} M [\eta]}{L^{3/2}} = \Phi_r F_\eta(\lambda L, \lambda d) \quad (\text{wormlike ring}), \quad (23.15)$$

where

$$[F_\eta(L, d)]^{-1} = 1 + \sum_{i=1}^4 C_i L^{-i/2} \quad \text{for } L \geq 3.480. \quad (23.16)$$

In Eq. (23.16), the coefficients  $C_i = C_i(d)$  are given by

$$\begin{aligned} C_1 &= 0.809231 - 40.8202d - 483.899d^2 - (2.53944 + 339.266d^2) \ln d, \\ C_2 &= -13.7690 + 380.429d + 5197.48d^2 + (0.818816 + 3517.90d^2) \ln d, \\ C_3 &= 35.0883 - 1079.70d - 14530.3d^2 - (1.44344 + 9855.73d^2) \ln d, \\ C_4 &= -28.6643 + 927.876d + 12010.0d^2 + (0.571812 + 8221.82d^2) \ln d \end{aligned}$$

for  $0.001 \leq d \leq 0.1$

(23.17)

and

$$\begin{aligned} C_1 &= -2.17381 - 11.3578d + 249.523d^2 - 729.371d^3 \\ &\quad + 489.172d^4 - (3.58885 - 74.3257d^2 + 335.732d^4) \ln d, \\ C_2 &= 112.769 - 851.870d - 21390.1d^2 + 56909.8d^3 \\ &\quad - 34787.5d^4 + (41.8243 - 9944.26d^2 + 22067.0d^4) \ln d, \\ C_3 &= -1680.23 + 24753.1d + 498848d^2 - 1314310d^3 \\ &\quad + 792477d^4 - (526.628 - 244353d^2 + 497280d^4) \ln d, \\ C_4 &= 7043.32 - 142907d - 2883470d^2 + 7668650d^3 \\ &\quad - 4648720d^4 + (2177.01 - 1407520d^2 + 2937180d^4) \ln d \end{aligned}$$

for  $0.1 < d < 1$ . (23.18)

From Eq. (23.15),  $[\eta]$  of the rigid ring is obtained as the asymptotic form in the rigid ring limit ( $\lambda L \rightarrow 0$  and  $p \rightarrow \infty$ ) as follows [9, 17]:

$$[\eta] = \frac{N_A L^3}{8\pi M} \left[ \ln p + \ln \left( \frac{8}{\pi} \right) - 2 \right]^{-1} \quad (\text{rigid ring}). \quad (23.19)$$

We note that in the range of  $0 < \lambda L < 3.480 R_H$  and  $[\eta]$  [24] should be calculated by MC simulations because of the difficulty of analytical calculations.



On the basis of MC simulations by the use of the discrete version of the wormlike ring without ordinary excluded volume, the interpolation formula for the second virial coefficient  $A_{2,\theta}$  is constructed as follows [9, 25]:

$$A_{2,\theta} = \frac{4N_A}{M^2} V_E(\lambda L) \quad (\text{wormlike ring}), \tag{23.20}$$

where

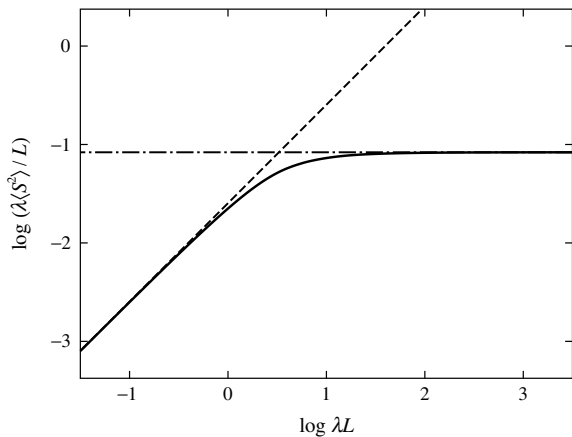
$$V_E(L) = \frac{L^3}{24\pi^2} \left[ e^{-0.6014L} + \frac{0.5700L}{1 + 0.9630L^{1/2} - 0.7345L + 0.4887L^{3/2} + 0.07915L^2} \right]^{3/2} \tag{23.21}$$

for  $L \lesssim 10^3$ .

It is seen that, as in the case of  $\lambda^2 \langle S^2 \rangle$ ,  $\lambda V_E/L^2$  (proportional to  $A_{2,\theta}$ ) becomes a function only of  $\lambda L$ . The asymptotic relations  $V_E = L^3/24\pi^2$  [14] and  $\lambda V_E/L^2 = 0.082(\lambda L)^{-1/2}$  [25] hold in the limits of  $\lambda L \rightarrow 0$  and  $\lambda L \rightarrow \infty$ , respectively, the latter relation recovering Eq. (23.5). It is pertinent to noting that although the original MC values of  $A_{2,\theta}$  have been evaluated by the procedure on the basis of the Gauss linking number instead of more accurate procedure on the basis of the Alexander polynomials, the difference in the values of  $A_{2,\theta}$  evaluated by the two procedures has been shown to negligibly small in the range of  $\lambda L \lesssim 10^3$  [25].

Here, taking  $\langle S^2 \rangle$  as an example, an overview of the crossover behavior from the rigid ring to the random-coiling one of the wormlike ring is provided. Figure 23.1 shows double-logarithmic plots of  $\lambda \langle S^2 \rangle / L$  against  $\lambda L$ , corresponding to the double-logarithmic plots of  $\langle S^2 \rangle / M$  against  $M$  in experiments, for the wormlike ring. The solid curve represents the theoretical values of the wormlike ring calculated from

**Fig. 23.1** Double-logarithmic plots of  $\lambda \langle S^2 \rangle / L$  against  $\lambda L$  for the wormlike ring model. The *solid curve* represents the theoretical values of the wormlike ring model calculated from Eq. (23.6). The *dashed and chain line segments* represent the theoretical values for the rigid ring and random-coiling ring, respectively

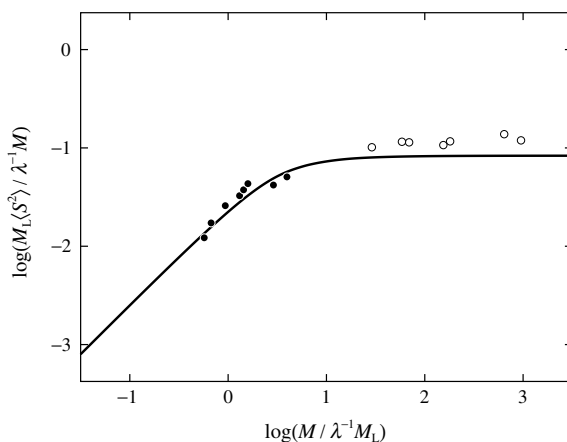


Eq. (23.6). The theoretical values of the wormlike ring first increase monotonically along those of the rigid ring ( $\langle S^2 \rangle = L^2/4\pi^2$ ) represented by the dashed line segment of slope unity in the range of  $\lambda L \lesssim 1$ , and then, approach the random-coil limiting value  $1/12$  ( $\lambda^2 \langle S^2 \rangle = \lambda L/12$ ) represented by the chain horizontal line segment in the range of  $\lambda L \gtrsim 10^2$ , with increasing  $\lambda L$  (the ring becoming longer and/or more flexible). Other properties also exhibit such crossover behavior from the rigid ring to the random-coiling one as a function of  $\lambda L$ , except for the dependence of  $\lambda d$ .

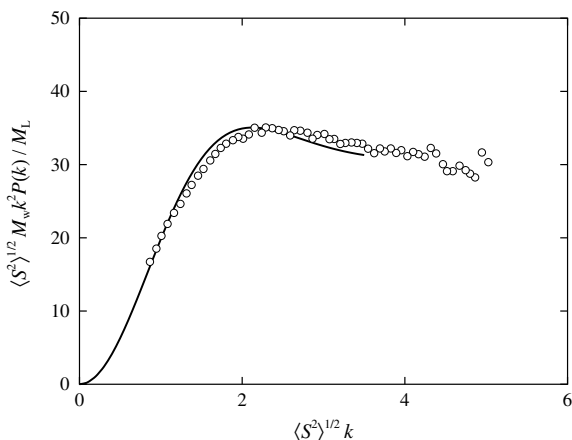
### 23.3 Analyses of Experimental Data

In this section, some examples of analyses of experimental data on the basis of the wormlike ring model are shown.

Figure 23.2 shows double-logarithmic plots of  $M_L \langle S^2 \rangle / \lambda^{-1} M$  ( $= \lambda \langle S^2 \rangle / L$ ) against  $M / \lambda^{-1} M_L$  ( $= \lambda L$ ), where  $M_L = M/L$  is the molecular weight per unit contour length of the wormlike ring, i.e., the so-called *shift factor* [9]. The open and closed circles represent the data for ring a-PS in cyclohexane- $d_{12}$  at 44 °C ( $\Theta$ ) by Takano et al. [26] and those for cyclic amylose tris(*n*-butylcarbamate) (cATBC) in 2-propanol at 35 °C ( $\Theta$ ) by Terao et al. [27], respectively. Note that the data for cATBC have been obtained from SAXS measurements and then proper corrections for chain thickness (the spatial distribution of electrons around the chain contour) [9] have been made by subtraction of the value of the mean-square radius of gyration of cross section of the contour  $d^2/4$  with  $d = 13$  Å from the (raw) values of  $\langle S^2 \rangle$  [27]. The solid curve represents the theoretical values of the wormlike ring (with-



**Fig. 23.2** Double-logarithmic plots of  $M_L \langle S^2 \rangle / \lambda^{-1} M$  against  $M / \lambda^{-1} M_L$  for ring a-PS in cyclohexane- $d_{12}$  at 44 °C ( $\Theta$ ) (open circles) [26] and cATBC in 2-propanol at 35 °C ( $\Theta$ ) (closed circles), with corrections of chain thickness for cATBC [27]. The solid curve represents the theoretical values of the wormlike ring model calculated from Eq. (23.6)



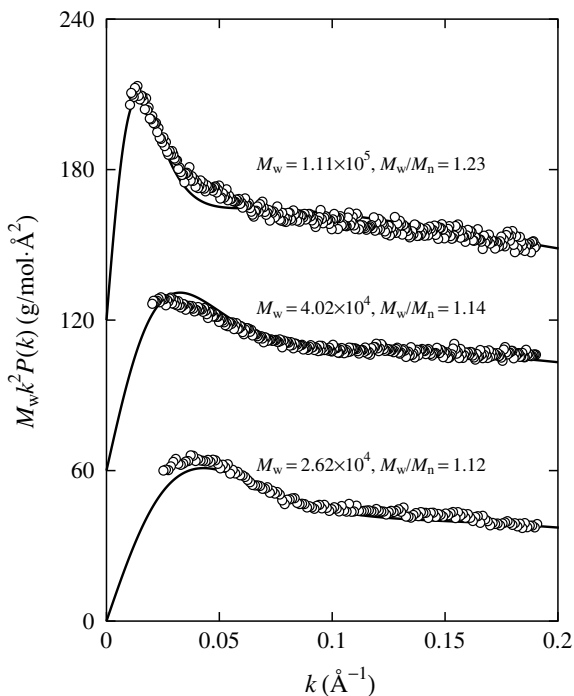
**Fig. 23.3** Reduced Kratky plots for the ring a-PS sample with  $M_w = 4.50 \times 10^4$  and  $\langle S^2 \rangle^{1/2} = 44.0 \text{ \AA}$  in cyclohexane- $d_{12}$  at  $33 \text{ }^\circ\text{C}$  (near  $\Theta$ ) (open circles) [37]. The solid curve represents the theoretical values of the wormlike ring model (without chain thickness) calculated from Eq. (23.7) with  $\lambda L = 61.0$  and with the values of  $\langle S^2 \rangle$  calculated from Eq. (23.6) with considering the deviation up to  $\mathcal{O}[(\lambda L)^{-1}]$  from the random-coil limit

out thickness) calculated from Eq. (23.6). The values of  $\lambda^{-1}$  and  $M_L$  for cATBC have been determined to be  $200 \text{ \AA}$  and  $140 \text{ \AA}^{-1}$ , respectively, from a best fit of the theoretical values to the data [27]. As for ring a-PS, the values  $\lambda^{-1} = 16.8 \text{ \AA}$  and  $M_L = 35.8 \text{ \AA}^{-1}$  determined from the analysis of the experimental data for linear a-PS in cyclohexane at  $34.5 \text{ }^\circ\text{C}$  ( $\Theta$ ) on the basis of the linear wormlike chain are used [28]. Although for ring a-PS the data are slightly larger than the theoretical values because of the difference in the solvent conditions between the ring and linear a-PS, it is seen that the wormlike ring model may describe quantitatively the behavior of all the data by the use of the “molecular parameters”  $\lambda^{-1}$  and  $M_L$ .

Figure 23.3 shows reduced Kratky plots for the ring a-PS sample with the weight-average molecular weight  $M_w = 4.50 \times 10^4$  and  $\langle S^2 \rangle^{1/2} = 44.0 \text{ \AA}$  in cyclohexane- $d_{12}$  at  $33 \text{ }^\circ\text{C}$  (near  $\Theta$ ) [37]. The solid curve represents the best-fit theoretical values of the wormlike ring calculated from Eq. (23.7) with  $\lambda L = 61.0$ ,  $M_L = 35.8 \text{ \AA}^{-1}$ , and the values of  $\langle S^2 \rangle$  calculated from Eq. (23.6) with considering the deviation up to  $\mathcal{O}[(\lambda L)^{-1}]$  from the random-coil limit. Although the value of  $\lambda^{-1}$  calculated from the above-mentioned values of  $M_w$ ,  $\lambda L$ , and  $M_L$  is  $20.6 \text{ \AA}$  and somewhat larger than the value  $16.8 \text{ \AA}$  used in Fig. 23.2, the theoretical values of the wormlike ring may well describe the behavior of the experimental data in the range of  $\langle S^2 \rangle^{1/2} k \lesssim 3$ . It is noted that in the range of  $\langle S^2 \rangle^{1/2} k \lesssim 3$  the effects of chain thickness are negligibly small if the thickness is not very large [19].

Figure 23.4 shows Kratky plots for the cATBC samples, with the indicated values of  $M_w$  and the ratio of  $M_w$  to the number-average molecular weight  $M_n$ , in tetrahydrofuran (THF) at  $25 \text{ }^\circ\text{C}$  by SAXS measurements [22]. The plots for the samples  $M_w = 4.02 \times 10^4$  and  $1.11 \times 10^5$  are shifted upward by 60 and  $120 \text{ g/mol} \cdot \text{\AA}^2$ ,

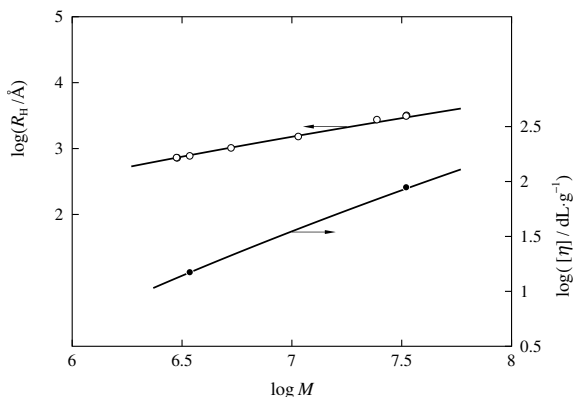
**Fig. 23.4** Kratky plots for the cATBC samples, with the indicated values of  $M_w$  and  $M_w/M_n$ , in THF at 25 °C (open circles) [22]. The plots for the samples  $M_w = 4.02 \times 10^4$  and  $1.11 \times 10^5$  are shifted upward by 60 and 120 g/mol·Å<sup>2</sup>, respectively. The solid curves represent the corresponding best-fit MC values of the discrete version of the wormlike ring, with the corrections both for chain thickness and polydispersity [22] (see text)



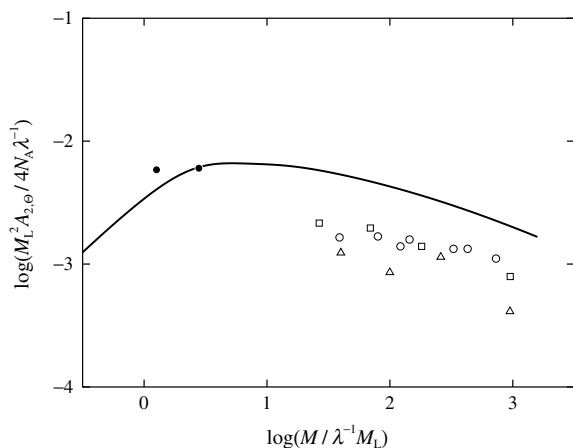
respectively. The chain thickness (the spatial distribution of electrons around the chain contour) [9] may affect largely  $P(k)$  in the range of large  $k$ , and also, effects of polydispersity of the samples are significant since  $P(k)$  is a z-averaged quantity. In Fig. 23.4, the solid curves represent the corresponding best-fit MC values of the discrete version of the wormlike ring with the corrections for the chain thickness and polydispersity with the following assumption: The scatterers are uniformly distributed in the spheres of diameter  $d_b$  touched with each other, whose centers are located on the wormlike ring contour, with the log-normal distribution of  $M$  with  $M_w/M_n = 1.2$  for all the cATBC samples [22]. Agreement of the MC values with the experimental data is almost complete and leads  $\lambda^{-1} = 250 \text{ \AA}$ ,  $M_L = 123 \text{ \AA}^{-1}$ , and  $d_b = 12 \text{ \AA}$ .

Figure 23.5 shows double-logarithmic plots of  $R_H$  [29–36] and  $[\eta]$  [34, 35] against  $M$  for (nicked) circular DNA in buffers at room temperature. The solid curves represent the respective best-fit theoretical values of the wormlike ring calculated from Eq. (23.9) for  $R_H$  and Eq. (23.15) for  $[\eta]$ . The value of  $d$  as a fitting parameter is determined to be 25 Å and 15 Å from the analyses of  $R_H$  and  $[\eta]$ , respectively, using with  $\lambda^{-1} = 1200 \text{ \AA}$  and  $M_L = 195 \text{ \AA}^{-1}$  determined for linear DNA in 0.2 M aqueous NaCl solution at 25 °C [9]. For both the cases of  $R_H$  and  $[\eta]$ , the theoretical values reproduce quantitatively the behavior of the experimental data.

Figure 23.6 shows double-logarithmic plots of  $M_L^2 A_{2,\theta} / 4N_A \lambda^{-1}$  ( $= \lambda V_E / L$ ) against  $M / \lambda^{-1} M_L$  ( $= \lambda L$ ). The open circles, triangles, and squares represent the



**Fig. 23.5** Double-logarithmic plots of  $R_H$  (*open circles*) [29–36] and  $[\eta]$  (*closed circles*) [34, 35] against  $M$  for (nicked) circular DNA in buffers at room temperature. The *solid curves* represent the respective theoretical values of the wormlike ring model calculated from Eq. (23.9) for  $R_H$  and Eq. (23.15) for  $[\eta]$  with the values of  $\lambda^{-1}$  and  $M_L$  determined for linear DNA in 0.2 M aqueous NaCl solutions at 25 °C [9] (see text)



**Fig. 23.6** Double-logarithmic plots of  $M_L^2 A_{2,\theta} / 4N_A \lambda^{-1}$  against  $M / \lambda^{-1} M_L$  for ring a-PS in cyclohexane at  $\Theta$  by Roovers and Toporowski (*open circles*) [38], by Huang et al. (*triangles*) [39], and by Takano et al. (*squares*) [26], and for cATBC in 2-propanol at 35 °C ( $\Theta$ ) (*closed circles*) [27]. The *solid curve* represents the theoretical values of the wormlike ring model calculated from Eq. (23.20)

**Table 23.1** Values of the parameters  $\lambda^{-1}$ ,  $M_L$ , and  $d$  (or  $d_b$ ) for the polymers illustrated as examples

Polymer	Solvent condition	$\lambda^{-1}$ (Å)	$M_L$ (Å <sup>-1</sup> )	$d$ ( $d_b$ ) (Å)	Observed quantity
Ring a-PS	Cyclohexane at 34.5 °C ( $\Theta$ )	16.8 <sup>a</sup>	35.8 <sup>a</sup>		$\langle S^2 \rangle$
	Cyclohexane- <i>d</i> <sub>12</sub> at 33 °C (near $\Theta$ )	20.6	35.8 <sup>a</sup>		$P(k)$
cATBC	2-propanol at 35 °C ( $\Theta$ )	200	140	13	$\langle S^2 \rangle$
	THF at 25 °C	250	123	(12)	$P(k)$
Circular DNA	Buffers at room temperature	1200 <sup>b</sup>	195 <sup>b</sup>	25	$R_H$
		1200 <sup>b</sup>	195 <sup>b</sup>	15	$[\eta]$

<sup>a</sup>Determined for linear a-PS in cyclohexane at 34.5 ( $\Theta$ )

<sup>b</sup>Determined for linear DNA in 0.2 M aqueous NaCl solution at 25 °C

experimental data for ring a-PS in cyclohexane at  $\Theta$  determined by Roovers and Toporowski (at 34.5 °C) [38], by Huang et al. (at 35 °C) [39], and by Takano et al. (at 34.5 °C) [40], respectively. The closed circles represent the experimental data for cATBC in 2-propanol at 35 °C ( $\Theta$ ) [27]. For both ring a-PS and cATBC, the same values of  $\lambda^{-1}$  and  $M_L$  are used as in the case of Fig. 23.2. It is seen that the wormlike ring may describe semi-quantitatively the behavior of all the experimental data, although the data for ring a-PS are definitely smaller than the theoretical values. It is noted that the cause of the discrepancy between the theory and experiments for ring a-PS is still unresolved [25, 41].

In Table 23.1, the values of the model parameters  $\lambda^{-1}$ ,  $M_L$ , and  $d$  (or  $d_b$ ) for the polymers illustrated as examples in Figs. 23.2–23.6 are summarized. For cATBC, the values of  $\lambda^{-1}$  and  $M_L$  are much larger than those for ring a-PS as a typical example of flexible rings having the backbone composed from C–C single bonds, and, the values of  $d$  (or  $d_b$ ) are comparable to those for DNA. This is due to the fact that the backbone of cATBC, having large side chains (*n*-butyl group), retains a helix in dilute solutions. Circular DNA, whose backbone has the double helix structure, has the largest values of  $\lambda^{-1}$ ,  $M_L$ , and  $d$ . Such molecular characterization of ring polymers may never, of course, be achieved by the Gaussian ring theory.

## References

1. H. Yamakawa, *Modern Theory of Polymer Solutions* (Haper & Row, New York, 1971), its electric edition is available on-line at the <http://hdl.handle.net/2433/50527>
2. J.A. Semlyen (ed.), *Cyclic Polymers* (Elsevier, London, 1986)
3. H.A. Kramers, *J. Chem. Phys.* **14**, 415 (1946)
4. B.H. Zimm, W.H. Stockmayer, *J. Chem. Phys.* **17**, 1301 (1949)
5. E.F. Casassa, *J. Polym. Sci. Part A* **3**, 605 (1965)

6. V.A. Bloomfield, B.H. Zimm, *J. Chem. Phys.* **44**, 315 (1966)
7. M. Fukatsu, M. Kurata, *J. Chem. Phys.* **44**, 4539 (1966)
8. J.G. Kirkwood, J. Riseman, *J. Chem. Phys.* **16**, 565 (1948)
9. H. Yamakawa, T. Yoshizaki, *Helical Wormlike Chains in Polymer Solutions*, 2nd edn. (Springer, Berlin, 2016)
10. A.V. Vologodskii, A.V. Lukashin, M.D. Frank-Kamenetskii, *Zh. Eksp. Teor. Fiz.*, **67**, 1875 (1974) [*Soviet Phys. JETP*, **40**, 932 (1975)]
11. M.D. Frank-Kamenetskii, A.V. Lukashin, A.V. Vologodskii, *Nature* **258**, 398 (1975)
12. K. Iwata, T. Kimura, *J. Chem. Phys.* **74**, 2039 (1981)
13. K. Iwata, *Macromolecules* **18**, 115 (1985)
14. J. des Cloizeaux, *J. Phys. Lett.* **42**, L-433 (1981)
15. F. Tanaka, *J. Chem. Phys.* **87**, 4201 (1987)
16. O. Kratky, G. Porod, *Recl. Trav. Chim. Pay-Bas.* **68**, 1106 (1949)
17. M. Fujii, H. Yamakawa, *Macromolecules* **8**, 792 (1975)
18. J. Shimada, H. Yamakawa, *Biopolymers* **27**, 657 (1988)
19. R. Tsubouchi, D. Ida, T. Yoshizaki, H. Yamakawa, *Macromolecules* **47**, 1449 (2014)
20. G. Oster, D.P. Riley, *Acta. Cryst.* **5**, 272 (1952)
21. K. Huber, W.H. Stockmayer, *Polymer* **28**, 1987 (1987)
22. A. Ryoki, D. Ida, K. Terao, *Polym. J.* **49**, 633 (2017)
23. A. Ryoki, H. Yokobatake, H. Hasegawa, A. Takenaka, D. Ida, S. Kitamura, K. Terao, *Macromolecules* **50**, 4000 (2017)
24. Y. Ono, D. Ida, *Polym. J.* **47**, 487 (2015)
25. D. Ida, D. Nakatomi, T. Yoshizaki, *Polym. J.* **42**, 735 (2010)
26. A. Takano, Y. Ohta, K. Masuoka, K. Matsubara, T. Nakano, A. Hieno, M. Itakura, K. Takahashi, S. Kinugasa, D. Kawaguchi, Y. Takahashi, Y. Matsushita, *Macromolecules* **45**, 369 (2012)
27. K. Terao, K. Shigeuchi, K. Oyamada, S. Kitamura, T. Sato, *Macromolecules* **46**, 5355 (2013)
28. H. Yamakawa, T. Yoshizaki, *J. Chem. Phys.* **119**, 1257 (2003)
29. L.V. Crawford, P.H. Bleck, *Virology* **24**, 388 (1964)
30. J. Vinograd, J. Lebowitz, R. Radloff, R. Watson, P. Laipis, *Proc. Natl. Acad. Sci. U.S.A.* **53**, 1104 (1965)
31. L.V. Crawford, *J. Mol. Biol.* **13**, 362 (1965)
32. C. Bode, A.D. Kaiser, *J. Mol. Biol.* **14**, 399 (1965)
33. I.B. David, D.R. Wolstenholme, *J. Mol. Biol.* **28**, 233 (1967)
34. A. Opschoor, P.H. Pouwels, C.M. Knijnenburg, J.B.T. Aten, *J. Mol. Biol.* **37**, 13 (1968)
35. J.R. Dawson, J.A. Harpst, *Biopolymers* **10**, 2499 (1971)
36. D.A. Ostrander, H.B. Gray Jr., *Biopolymers* **12**, 1387 (1973)
37. G. Hadziioannou, P.M. Cotts, G. ten Brinke, C.C. Han, P. Lutz, C. Strazielle, P. Rempp, A.J. Kovacs, *Macromolecules* **20**, 493 (1987)
38. J. Roovers, P.M. Toporowski, *Macromolecules* **16**, 843 (1983)
39. J. Huang, J. Shen, C. Li, D. Liu, *Makromol. Chem.* **192**, 1249 (1991)
40. A. Takano, Y. Kushida, Y. Ohta, K. Masuoka, Y. Matsushita, *Polymer* **50**, 1300 (2009)
41. D. Ida, T. Yoshizaki, *Polym. J.* **48**, 883 (2016)

# Chapter 24

## Cyclic Polymers for Innovative Functional Materials



Takuya Yamamoto

Due to the absence of ends, cyclic topological polymers are conformationally limited and exhibit different physical and chemical properties than linear polymers, even though they have the same composition and molecular weight. To achieve functionality based on polymer topology, we developed the synthesis of cyclic polymers and built nanostructures by self-assembly. In addition, the first defect-free cyclic poly(3-hexylthiophene) (P3HT) synthesis was achieved by GRIM polymerization, using a proper initiators, cyclization by an end-to-end coupling reaction mediated by Pd catalyst, and two separations by functionalized resins, selectively trapping impurities by differentiable end groups. These topologies were visualized by STM. In particular, fluorescence spectroscopy reveals an intrinsically forbidden transition of 0–0. Finally, cyclized poly(ethylene glycol) (*c*-PEG) exhibited a topology-based dispersion of gold nanoparticles (AuNPs) via simple mixing of *c*-PEG. The modified AuNPs showed dispersibility after freezing, lyophilization, or at high temperature. Surprisingly, *c*-PEG showed even better dispersibility than the thiolated PEG (HS-PEG-OMe).

### 24.1 Introduction

Topology is one of the most important factors that affect the properties and functions of materials. There are many examples where properties depend on topology, ranging from the atomic level to huge scales such as celestial bodies and the universe. In the case of polymers, topology has been mostly limited to linear and branched

---

T. Yamamoto (✉)

Faculty of Engineering, Division of Applied Chemistry, Hokkaido University, Sapporo 060-8628, Hokkaido, Japan

e-mail: [yamamoto.t@eng.hokudai.ac.jp](mailto:yamamoto.t@eng.hokudai.ac.jp)



chains. In recent years, however, advances in living polymerization and the introduction of specific functional groups at the ends of molecular chains have enabled the selective synthesis of precisely controlled cyclic polymers [1, 2]. In particular, the combination of monocyclic structures, polymers containing various ring structures, and the establishment of methods to remove impurities have enabled highly efficient and high-purity syntheses, as well as the measurement and application of physical and chemical properties. Such advances in the synthesis and purification of cyclic polymers are expected to contribute to the development of state-of-the-art polymer chemistry, polymer physics, and polymer materials that depend on polymer topology.

Since cyclic polymers exhibit specific properties (topological effects) derived from their “topology,” various attempts have been made both theoretically and experimentally. For example, in contrast to linear polymers of the same molecular weight and chemical composition, cyclic polymers are known to exhibit lower viscosity, smaller hydrodynamic volume, and higher glass transition temperature ( $T_g$ ) [1]. Furthermore, it has been recently reported that the topological effects of cyclic polymers affect their high lubricity [3, 4] and miscibility among polymers [5]. In biological applications, cyclic comb-shaped polymers have been reported to exhibit strong cytotoxicity [6]. The effects of polymer topology are advancing day by day, as exemplified by these series of studies. In addition, computer simulations of cyclic polymers have been actively carried out [7]. Furthermore, high-performance liquid chromatography has enabled the separation of polymers depending on their topology, such as rings, linear chains, and branches, which has been difficult in the past.

Here, we will discuss two main factors that contribute to the topological effects exhibited by cyclic polymers. The first is the effect of the presence or absence of a terminal, represented by the change in  $T_g$  mentioned above. The other factor is the effect dependent on the cyclic structure itself, i.e., the reduction of the radius of gyration. In other words, the effect of the topology of cyclic polymers is brought about by these two different factors. The former factor, which depends on molecular weight, is the nature of the polymer chain ends, while the latter, which is not affected by molecular weight, is an intrinsic feature of the ring structure. These two factors, in conjunction with various intra- and intermolecular interactions, are expressed as polymeric properties.

In order to explore the topological effects, it is necessary to synthesize cyclic polymers, and there are two typical synthesis methods: end-to-end linkage of linear polymers and ring-expansion polymerization. Typical end-to-end linkage methods include click chemistry, metathesis, and disulfide bond formation, while ring-expansion polymerization methods using tin catalysts and derivatives of Grubbs catalysts are well known. In designing functional polymers, a variety of polymer main chains are required, and for this purpose, end-linking methods that can be used in conjunction with living polymerization are frequently used. As a specific example, a cyclic block copolymer with amphiphilic properties can be synthesized by extending hydrophobic chains from hydrophilic chains by living polymerization and linking the allyl groups introduced at both ends by metathesis. Furthermore, micelles were constructed by self-assembling the polymer [8–10], and unlike the micelles of linear BAB triblock copolymers, the hydrophobic portions of the micelles

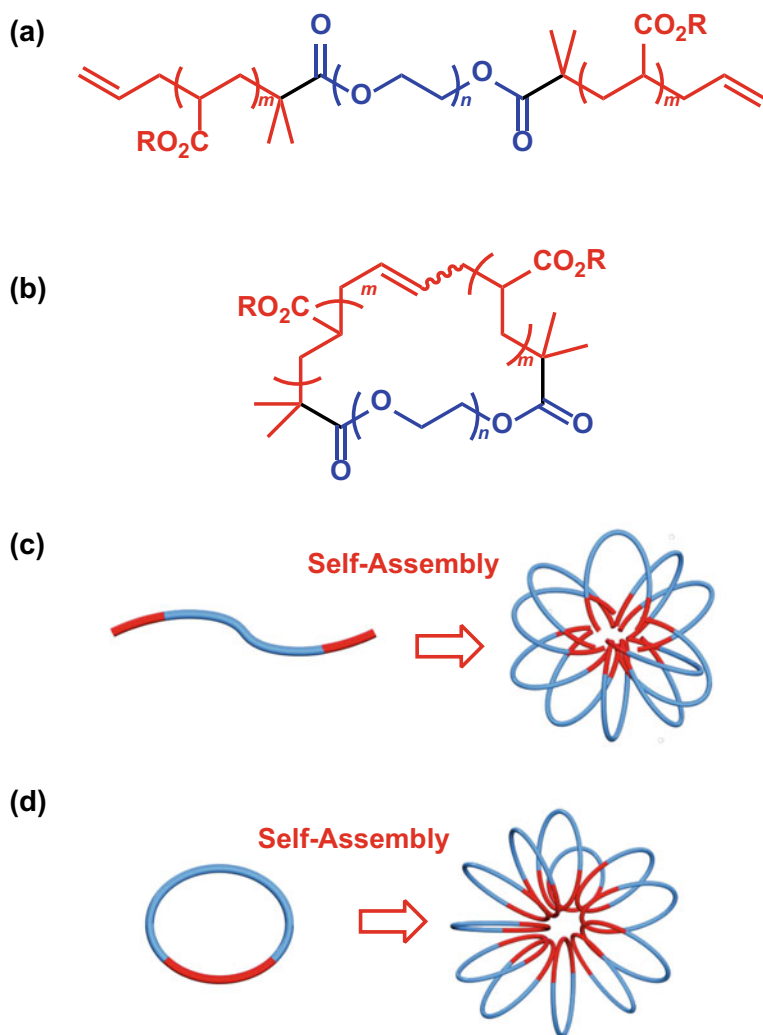
prevented dynamic cross-linking between the micelles, resulting in the discovery of surprisingly high thermal stability. Furthermore, cyclic amphiphilic block copolymers of poly(ethylene oxide) (PEO) and polystyrene (PS) synthesized by a similar method have been reported for the preparation of vesicles [11, 12]. In addition, reversible and repeatable topological transformations of linear chains and rings using hydrophobic interactions at the PEO ends [13] and the synthesis of all  $\pi$ -conjugated cyclic polymers have been achieved [14].

## 24.2 Amphiphilicity and Self-assembly

One of the most powerful methods for constructing practical nanostructures with molecular-level accuracy is self-assembly. Micelles and vesicles formed from amphiphilic block copolymers by this method have very different physical properties from structures made from linear copolymers. When self-assembly is induced in the aforementioned cyclic amphiphilic block copolymers, they mimic the cyclic lipid molecules that are the building blocks of the cell membranes of thermophilic archaea that live under high temperature conditions such as hot springs and underwater volcanoes. By following the example of this curious molecule found in ecosystems, we were able to obtain high thermal stability in the self-assembled structure. We have synthesized amphiphilic block copolymers of linear poly(*n*-butyl acrylate)–poly(ethylene oxide)–poly(*n*-butyl acrylate) (PBA–PEO–PBA) and cyclic PBA–PEO (Fig. 24.1) [8]. The self-assembly of these macromolecules has produced micelles with high thermal stability. Measurement of the cloud point ( $T_c$ ) of the micelles prepared by self-assembly of these polymers revealed that the cyclic polymer micelles were stable up to high temperatures of 71–74 °C, whereas the linear polymer micelles were suspended at 24–27 °C. This means that the temperature resistance of the micelles was dramatically enhanced by the change in polymer topology from linear to cyclic. Furthermore, the  $T_c$  of the micelles was controlled by combining cyclic and linear block copolymers in a variety of the proportions.

Next, we synthesized amphiphilic linear and cyclic block copolymers using poly(methyl acrylate) (PMA) as the hydrophobic part, and compared the heat and salt resistance of the micelles [9]. As a result, the micelles made from cyclic PMA–PEO were stable up to 270 mg/mL NaCl concentration, while the linear PMA–PEO–PMA micelles were precipitated by salt precipitation at 10 mg/mL. In other words, the cyclic polymer micelles were not only stable at high temperature, but also showed high stability against salt concentration. Furthermore, the control of the  $T_c$  of the micelles was achieved over a wide range of temperatures and salt concentrations and could also be adjusted by changing the ratio of the cyclic and linear polymers in the mixture. When this topology effect was applied to the catalytic reaction of halogen exchange, the conversion with the cyclic polymer was improved by about 50% over that of the corresponding linear polymer.

Furthermore, small-angle X-ray scattering using a synchrotron revealed the high density of cyclic polymer micelles [15]. In particular, the density of the PBA core of



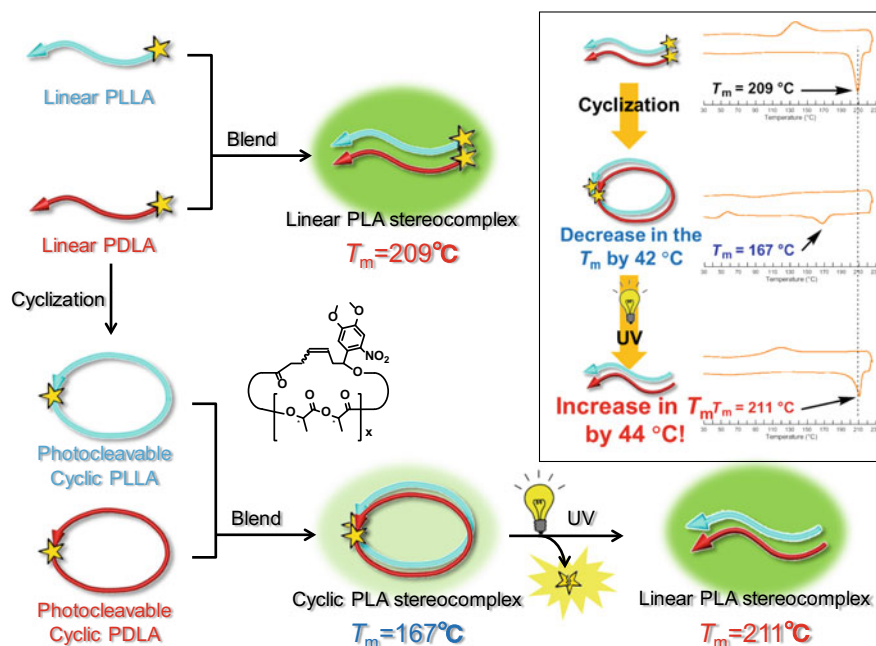
**Fig. 24.1** Chemical structures of **a** linear and **b** cyclic block copolymers. Schematics of micelle formation by self-assembly of **c** linear and **d** cyclic block copolymers

cyclic polymer micelles was found to be higher than that of linear polymer micelles. This is attributed to the fact that the density of the core is comparable to or higher than that of bulk PBA because the free volume is limited by the absence of ends in cyclic polymers. In other words, this density difference is thought to have an effect on heat and salt resistance.

Referring to the phase transition mechanism of micelles from the dispersed state to the suspended state, it is thought that in linear polymer micelles, one of the polymer chain ends desorbs from the center of the micelle and dynamic cross-linking occurs

between the micelles with dehydration summation. Therefore, the linear polymeric micelles are considered to aggregate and suspend at low temperatures, in contrast to the cyclic polymeric micelles where cross-linking reactions do not occur intrinsically. To verify this, spin–lattice ( $T_1$ ) and spin–spin ( $T_2$ ) relaxation times were measured by NMR relaxation time measurements [10]. As a result, the  $T_2$  of the PEO portion of the linear and cyclic block copolymers decreased even at higher temperatures than  $T_c$ . On the other hand, the  $T_2$  of the PEO portion of the linear and cyclic block copolymers decreased even at higher temperatures than  $T_c$ , which means that relatively large molecular motions, such as micelle cross-linking and interpenetration, were suppressed. In the meantime, the  $T_1$  of the PEO portion of the linear polymer continued to increase. This indicates that dehydration and aggregation proceeded even beyond  $T_c$ . However, for the cyclic block copolymer,  $T_1$  did not exceed a certain value even above  $T_c$ . In other words, the rotational movement of the PEO skeleton due to dehydration and summation is considered to be suppressed.

Cyclic poly(L-lactide) (PLLA) and poly(D-lactide) (PDLA) incorporating an *o*-nitrobenzyl group as a photocleavable unit were synthesized [16]. The  $T_m$  of the photocleavable cyclic PLLA/cyclic PDLA blend decreased by more than 40 °C from that of the linear PLLA/linear PDLA counterpart despite their essentially identical molecular weights and chemical structure (Fig. 24.2). Moreover, through the



**Fig. 24.2** Stereocomplexation of photocleavable linear and cyclic poly(lactides). The stereocomplex of linear poly(lactides) had a melting point at 209 °C, while that of the cyclized poly(lactides) was 167 °C. After the linearization of the cyclized PLAs, melting point increased to 211 °C

cyclic-to-linear topological transformation by UV, the photocleaved linear polylactide showed almost an identical  $T_m$  as the linear precursors before cyclization. The change in  $T_m$  by the cyclic topology was also observed between cyclic PLLA/cyclic PDLA and linear PLLA/linear PDLA blends.

In addition, the block copolymers of cyclic poly(L-lactide)-poly(ethylene oxide) (PLLA-PEO) and the corresponding cyclic poly(D-lactide)-poly(ethylene oxide) (PDLA-PEO) micelles, respectively, were mixed and heated, but no phase transition occurred [17]. However, heating the mixture of linear PLLA-PEO-PLLA and linear PDLA-PEO-PDLA micelles resulted in progressive gelation. This suggests that the polymer topology affected the progression of network formation. Furthermore, cyclic PLLA-PEO and cyclic PDLA-PEO with *o*-nitrobenzyl groups as photocleavable moieties were synthesized, and gelation was achieved by converting them into linear chains by photoirradiation.

By using linear polystyrene-poly(ethylene oxide)-polystyrene (PS-PEO-PS) and cyclic PS-PEO by self-assembly, a spherically closed structure of bilayers called vesicles was formed. These structures were confirmed by TEM, DLS, and SLS. It is noteworthy that the linear polymer vesicles showed higher structural stability than the cyclic polymer vesicles. This means that, contrary to intuition, the stability of vesicles was opposite to that of micelles. In addition, as in the case of micelles, the  $T_c$  of the vesicles could be controlled by the mixing ratio of linear and cyclic polymers.

Liquid crystalline polymers have been extensively studied because they respond to electric and magnetic fields depending on their rigid nature and anisotropic dielectric constant. Applying their properties, linear and cyclic block copolymers with a liquid crystalline segment as the hydrophobic part and poly(acrylic acid) as the hydrophilic parts have been newly synthesized and the topological effects of self-assembly and application of external electric fields have been investigated [11].

In addition, investigations of the behavior of cyclic and linear amphiphilic block copolymers at interfaces have been reported. That is, copolymers with linear diblock PBA-PEO and triblock PBA-PEO-PBA and cyclic PBA-PEO structures were used to construct Langmuir-Blodgett (LB) membranes [18]. The LB membranes of PBA-PEO-PBA were formed of a fibrous structure by crystallization. On the other hand, no clear domain formation was observed in cyclic PBA-PEO. For the detailed structural investigation of these LB films, temperature-dependent X-ray diffraction measurements were performed, and all these block copolymers showed diffraction at low temperatures, confirming a clear self-assembled structure. However, the LB films formed from linear PBA-PEO and PBA-PEO-PBA gradually lost their layered structure upon heating, whereas the LB films constructed from cyclic PBA-PEO were relatively stable up to high temperature and showed a remarkable tendency to show a higher structural order when moderately heated.

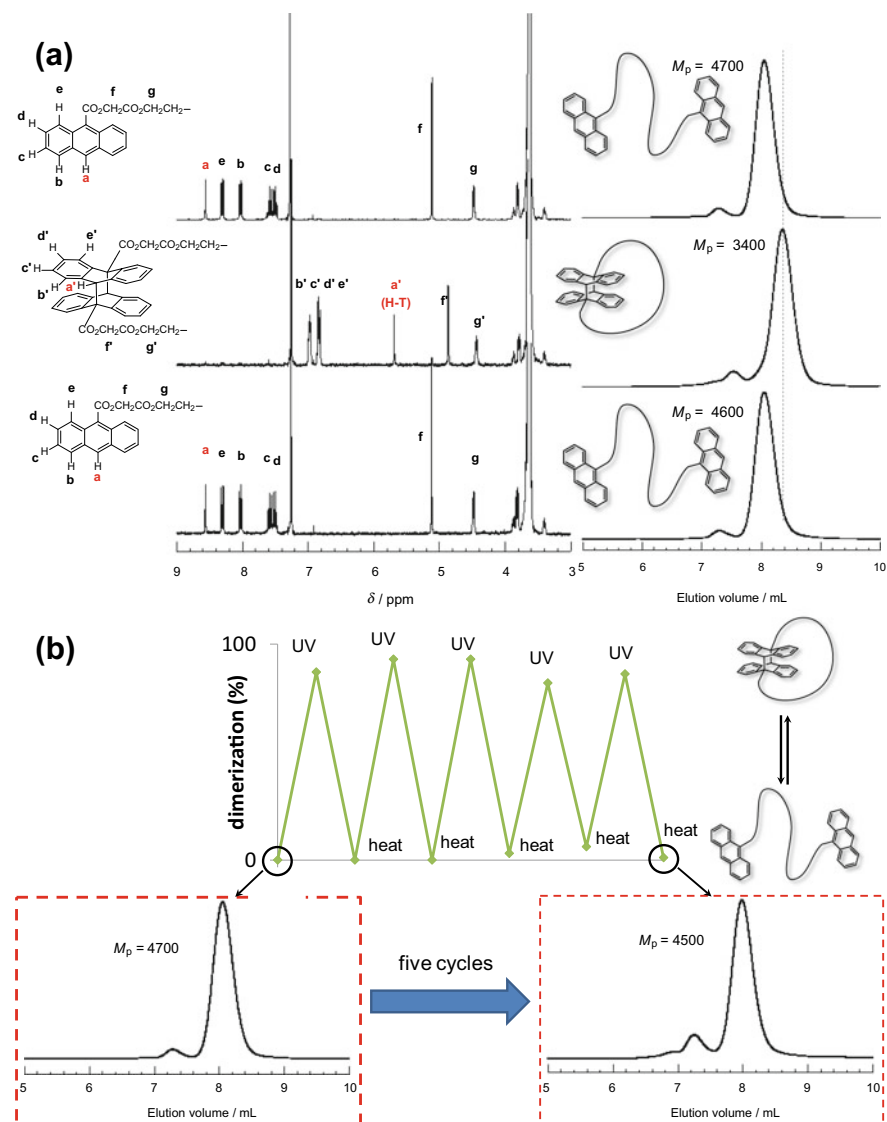
### 24.3 Reversible Topological Transformations

Reversible and repeatable polymer topological transformations have been reported for hydrophobic and hydrophilic polymer chains of various molecular weights (Fig. 24.3) [13]. They are based on reversible dimerization of anthracene and coumarin at the end of polymer chains using photo- and thermal reactions. First, we synthesized and investigated PEOs with anthracene ends connected by electron-donating or electron-withdrawing groups. The polymers connected with electron-donating groups decomposed upon photoirradiation, but those connected with electron-withdrawing groups were stable, and the cyclization reaction proceeded in water and organic solvents. The shorter the polymer chain, the faster the cyclization reaction proceeded. When the cyclized polymer was heated to 150 °C, it quantitatively switched to a linear structure, confirming that this conversion was reversible. This reversible control of polymer topology was equally effective for the hydrophobic poly(tetrahydrofuran).

On the other hand, the coumarin-terminated PEO changed to a cyclic form by irradiation of 365 nm light in water, but the reaction did not proceed completely and formed an equilibrium state with the linear chain even though 254 nm light irradiation was applied for the reverse conversion.

### 24.4 All $\pi$ -Conjugated Cyclic Polymers

All  $\pi$ -conjugated macrocyclic molecules with a well-defined chemical structure are among the most interesting materials theoretically and experimentally because of their potential to form “infinite conjugated systems” that exhibit unprecedented optical and electronic properties. As such particles are expected to exhibit excellent properties, they are very interesting for applications in organic electronic devices. In particular, cyclic conjugated polymers have been actively studied and unique properties such as non-linear optical and light-collecting properties have been reported [19]. Through cyclization, maximum absorption is shifted to shorter wavelengths compared to the corresponding linear polymers. However, although these polymers are  $\pi$ -conjugated in whole, in fact, the molecule tends to disintegrate due to the main chain distortion and ring deformation. One of the most important phenomena confirming completely  $\pi$ -conjugated at any given time is the prohibition of the 0–0 spectral transition based on the selection rules established for polycyclic aromatic hydrocarbons [20]. For example, for cyclic poly(*p*-phenylene), 0–0 transition is prohibited for octamers. Larger cyclic poly(*p*-phenylene) compounds have been synthesized, but often the 0–0 transition was allowed due to distortion of the main chain and ring structure. In the case of poly(*p*-phenylene) and its derivatives, a macrocyclic compound with a total of twelve thiophene units showed an inhibition of the 0–0 transition. This molecule is believed to form a metastable ring structure because the formation of the most stable trans structure is sterically difficult.



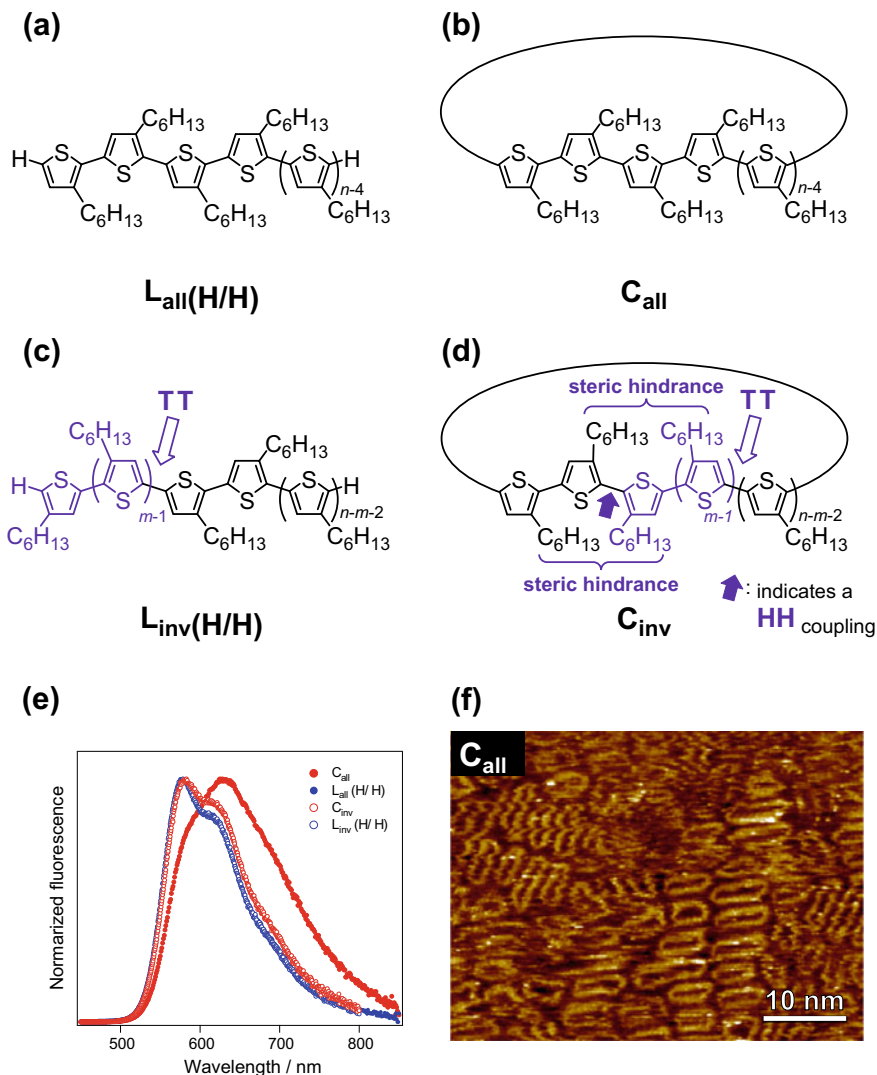
**Fig. 24.3** **a** Reversible linear–cyclic conversion of polymers terminated with anthracene using photo- and thermal reactions determined by NMR and SEC. Before cyclization (top), after cyclization (middle), and after linearization (bottom). **b** Repeated reversible linear–cyclic conversion

However, the ring structure is expected to be similar to the planar structure of less than fourteen thiophene units, but it is considered highly deformed for larger sizes. In cyclic poly(thienylene ethynylene), the 0–0 transition inhibition is up to six thiophene units. In addition, the inclusion of heterogeneous functional groups, such as vinylene rather than acetylene groups, makes it very difficult to delocalize an exciton. Therefore, the new molecular design is necessary to construct fully conjugated macrocyclic compounds that achieve an “infinite conjugation” for complete excitation delocalization. We established the synthesis and purification of an ideally conjugated cyclic polymer type all  $\pi$ -conjugated, poly(3-hexylthiophene) (P3HT), which is an all-head-to-tail regioregularity without structural defects.

P3HT is a typical organosemiconductor having good optoelectronic properties and solubility among those so far examined. Cyclic P3HT has been described by aldol reaction [21], Glaser [22], and McMurry couplings [23]. However, these ring-shaped P3HTs contained discontinuities or heterogeneities in the  $\pi$ -conjugation system at the point where the cyclization reaction took place. Therefore, the cyclic polymer skeleton should be conjugated in full to show the properties, and it is crucial to address this issue. In addition, the physical properties of P3HT are strongly influenced by the regularity of the substitutes. In other words, P3HT has three bonding modes: head-to-tail (HT), head-to-head (HH), and tail-to-tail (TT). Among them, HT bonding can be used to relieve the steric repulsion between hexyl groups so that the thiophene ring can form in the same plane in the excited state. Thus, the high proportion of HT bonds, i.e., high regioregularity, indicates excellent electrical conductivity. The Grignard metathesis polymerization (GRIM) is widely used because it allows P3HT synthesis with high regioregularity and controlled molecular weight and molecular weight distribution. However, the initial reaction produces a TT-coupled 3-hexylthiophene dimer, which are located in the main chain. For linear P3HT, TT bonding is less of a problem. But, TT bonding is inevitably accompanied by the formation of a HH bond, which disturbs the  $\pi$ -conjugation due to a steric repulsion between the 3-hexyl groups in cyclic P3HT. It is known that HH bonds severely interfere with the coplanarization for  $\pi$ -conjugation due to a steric repulsion between the 3-hexyl groups. In other words, full control of the correct position is essential for cyclic P3HT, and therefore the elimination of counter-directional 3-hexyl thiophene resulting from the initiation reaction is crucial.

We conducted the following experiments to synthesize cyclic P3HT with a fully regioregular and  $\pi$ -conjugated structure (Fig. 24.4,  $C_{all}$ ) [14]. First, linear P3HT ( $L_{all}(H/H)$ ) of all-head-to-tail type were synthesized by GRIM polymerization using appropriate initiators (Fig. 24.5). The separation of the byproducts produced during polymerization was performed using the Suzuki–Miyaura cross coupling with boronic acid-loaded resin. The ring-formation reaction by a Pd catalysis between the  $SnMe_3$  end groups, which was used for the first time for P3HT coupling. In this process, as a result of the capture reaction with an aminomethyl resin, intermolecular coupling products as well as the unreacted linear precursor were removed





**Fig. 24.4** a–d show the structures of  $L_{\text{all}}(\text{H}/\text{H})$ ,  $C_{\text{all}}$ ,  $L_{\text{inv}}(\text{H}/\text{H})$ , and  $C_{\text{inv}}$ , respectively. The purple segments indicate inverted units;  $C_{\text{inv}}$  has a highly sterically hindered HH bond. **e** Fluorescence spectra (normalized) of  $L_{\text{all}}(\text{H}/\text{H})$ ,  $C_{\text{all}}$ ,  $L_{\text{inv}}(\text{H}/\text{H})$ , and  $C_{\text{inv}}$  shown in solid blue, solid red, dotted blue, and dotted red, respectively. **f** STM image of  $C_{\text{all}}$

in order to obtain pure  $C_{\text{all}}$ . Similarly, cyclic P3HT with a partially inverted 3-hexylthiophene segment ( $C_{\text{inv}}$ ) and linear P3HT formed by the regular polymerization technique ( $L_{\text{inv}}(\text{H}/\text{H})$ ) were prepared. SEC–MALS–Visco, absorption and fluorescence spectroscopy, FP–TRMC, and STM measurements were used to investigate

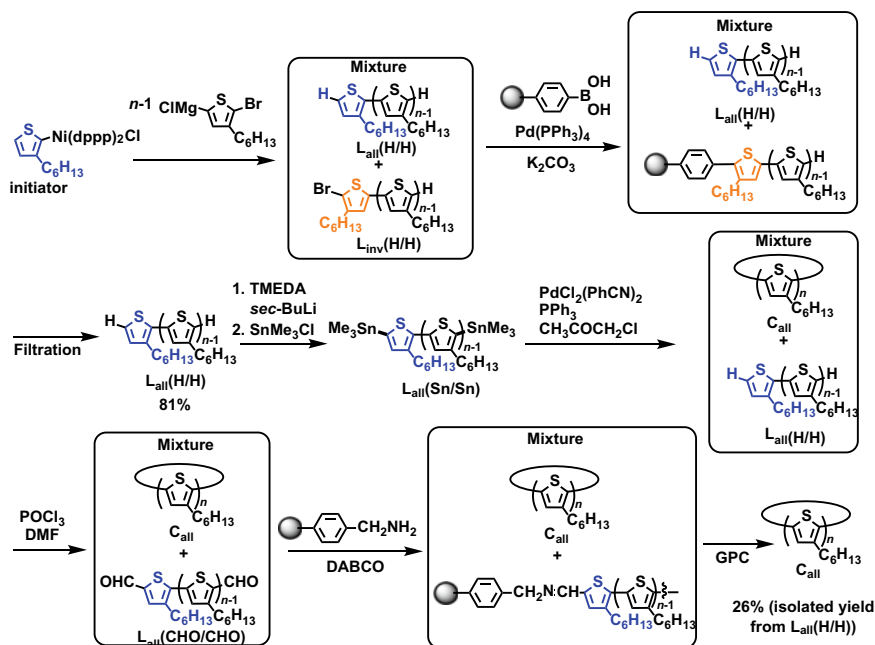


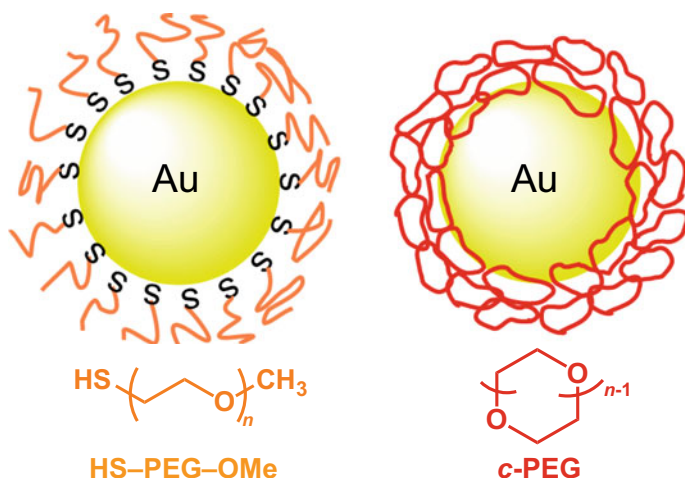
Fig. 24.5 Synthetic scheme of  $L_{all}(H/H)$  and  $C_{all}$

the effect of the topology and regioregularity, showing that  $C_{all}$  has an excitation with delocalization.

## 24.5 Stabilization of Gold Nanoparticles

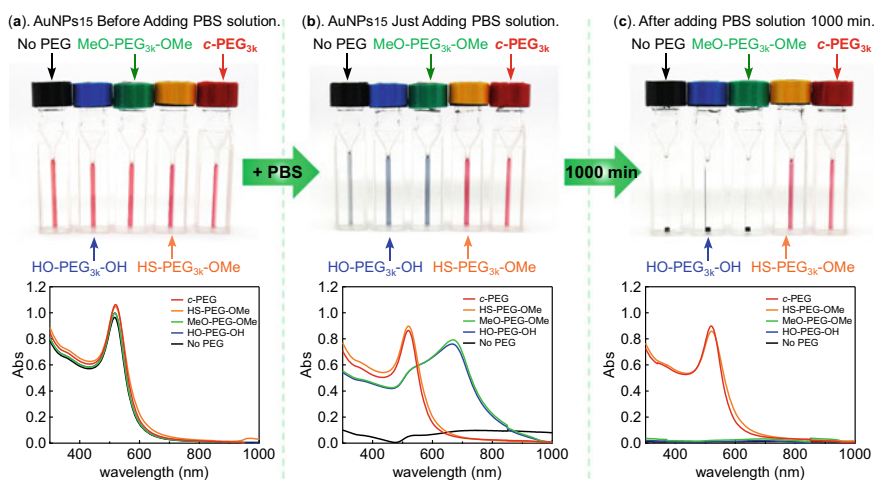
Many nanoparticle-based drugs, including metal nanoparticles, are currently actively studied, and their surface is often covered with biocompatible polyethylene glycol (PEG) [24–28]. This modification by PEG is called PEGylation and is essential for biological applications because it provides dispersion stability under physiological conditions [29]. PEGylation also protects them from detection by the immune system in vivo. However, since PEGylation of nanoparticle-based drugs is based on chemisorption represented by thiols (Fig. 24.6), the synthesis of the corresponding PEGylating agent is necessary, the procedure is complicated, and sufficient dispersion stability is often not achieved. In other words, simple and stable PEGylation of nanoparticles is a technology that is strongly required not only in biological applications but also in a wide range of areas where nanoparticles are used.

To an aqueous dispersion of gold nanoparticles with a diameter of about 15 nm, linear HO–PEG–OH with a hydroxyl group at both ends, linear MeO–PEG–OMe,

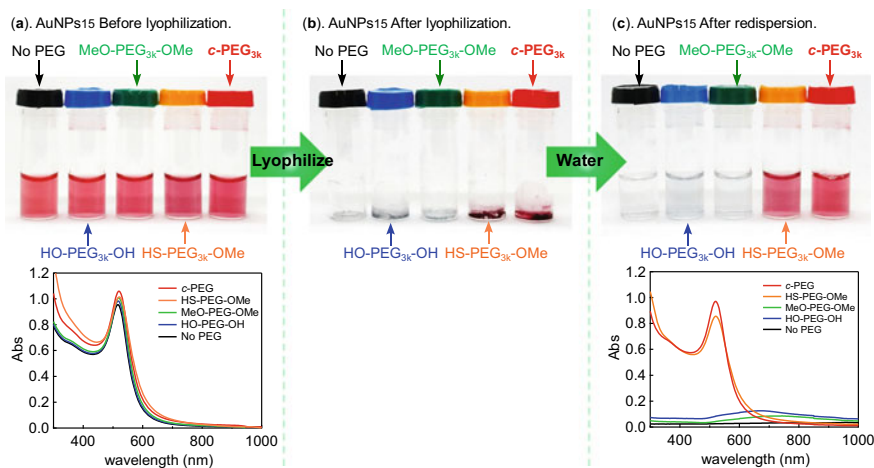


**Fig. 24.6** Schematic illustration of AuNPs treated with HS-PEG-OMe (left) and *c*-PEG (right)

linear HS-PEG-OMe, which is widely used as a PEGylating agent for nanoparticles by the chemical reaction between thiol and metal nanoparticles, or cyclic PEG (*c*-PEG) was added [30]. Physiological condition (Fig. 24.7), redispersion after freeze-drying (Fig. 24.8), and a heating condition were evaluated. Furthermore, we conducted animal experiments using mice to evaluate biocompatibility, retention



**Fig. 24.7** UV-Vis spectra and photographs of AuNPs<sub>15</sub>/No PEG (black), AuNPs<sub>15</sub>/HO-PEG<sub>3k</sub>-OH (blue), AuNPs<sub>15</sub>/MeO-PEG<sub>3k</sub>-OMe (green), AuNPs<sub>15</sub>/HS-PEG<sub>3k</sub>-OMe (orange), and AuNPs<sub>15</sub>/*c*-PEG<sub>3k</sub> (red). **a** Before the addition of PSB, **b** immediately after the addition of PBS, and **c** 1000 min after the addition of PBS. The resulting dispersions were pH 7.4 and 150 mM of NaCl



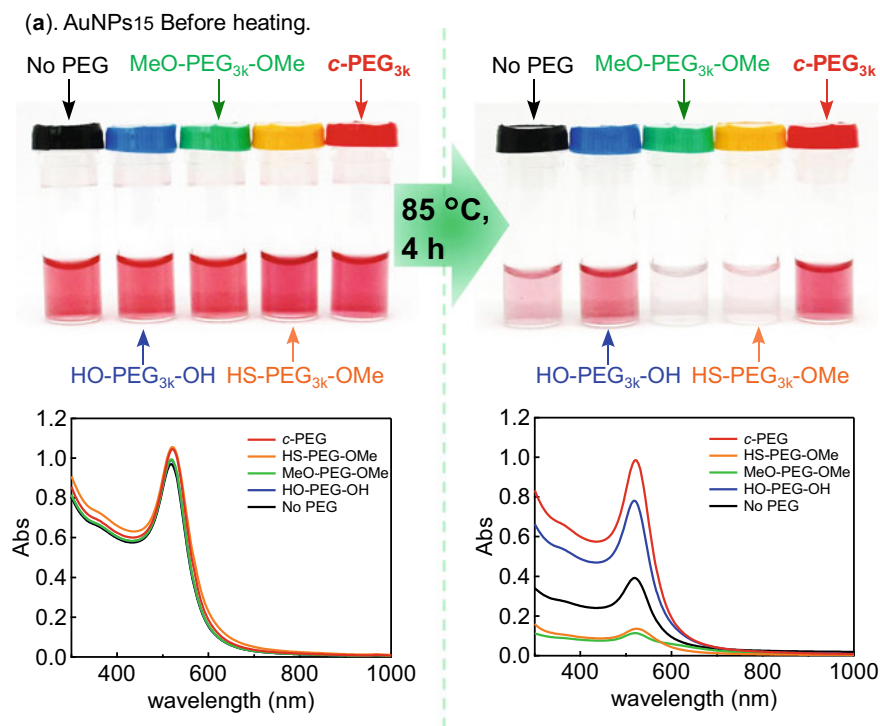
**Fig. 24.8** UV-Vis spectra and photographs of AuNPs<sub>15</sub>/No PEG (black), AuNPs<sub>15</sub>/HO-PEG<sub>3k</sub>-OH (blue), AuNPs<sub>15</sub>/MeO-PEG<sub>3k</sub>-OMe (green), AuNPs<sub>15</sub>/HS-PEG<sub>3k</sub>-OMe (orange), and AuNPs<sub>15</sub>/c-PEG<sub>3k</sub> (red). **a** Before lyophilization, **b** after lyophilization, and **c** after redispersion in water

in blood, and accumulation in tumors. The gold nanoparticles with HO-PEG-OH and MeO-PEG-OMe precipitated irreversibly, almost the same as unmodified gold nanoparticles. In contrast, the gold nanoparticles with *c*-PEG retained their dispersion stability even under these harsh conditions. Interestingly, even when HS-PEG-OMe was used, the gold nanoparticles could not withstand the above-mentioned heating conditions and could hardly be redispersed (Fig. 24.9). In other words, cyclic PEG was shown to be a better dispersion stabilizer than conventional HS-PEG-OMe. Furthermore, in animal experiments, the biocompatibility, retention in blood, and tumor accumulation of the *c*-PEG-modified gold nanoparticles were confirmed.

The modification and stabilization of nanoparticles by cyclic PEGs developed in this study is simple and applicable to a wide range of metal species and is expected to lead to the development of innovative products in the field of biotechnology applications. For example, gold nanorods, silver nanoparticles, and ultrafine iron oxide nanoparticles modified by cyclic PEGs are expected to be applied as bioimaging devices and as new tools for photothermal therapy of tumors.

## 24.6 Conclusions

Recently, significant advances have been reported in their synthesis and purification, which will allow us to exploit the excellent properties of cyclic polymers in molecularly dispersed and self-assembled states. In addition, topological effects are beginning to be recognized as a way to control polymer properties without changing the



**Fig. 24.9** UV-Vis spectra and photographs of AuNPs<sub>15</sub>/No PEG (black), AuNPs<sub>15</sub>/HO-PEG<sub>3k</sub>-OH (blue), AuNPs<sub>15</sub>/MeO-PEG<sub>3k</sub>-OMe (green), AuNPs<sub>15</sub>/HS-PEG<sub>3k</sub>-OMe (orange), and AuNPs<sub>15</sub>/c-PEG<sub>3k</sub> (red). **a** Before heating and **b** after heating at 85 °C for 4 h

molecular weight or chemical structure. In other words, it is expected that the application of topology effects to material design can be used to improve the functionality of current polymer materials. Similarly, topology effects in polycyclic polymers have recently been discovered, which may lead to the creation of new materials [31, 32].

## References

1. J.A. Semlyen (ed.), *Cyclic Polymers* (Kluwer, Dordrecht, 2000)
2. Y. Tezuka, *Acc. Chem. Res.* **50**, 2661–2672 (2017)
3. M. Divandari, L. Trachsel, W. Yan, J.-G. Rosenboom, N.D. Spencer, M. Zenobi-Wong, G. Morgese, S.N. Ramakrishna, E.M. Benetti, A.C.S. *Macro. Lett.* **7**, 1455–1460 (2018)
4. G. Morgese, E. Cavalli, J.-G. Rosenboom, M. Zenobi-Wong, and E. M. Benetti, *Angew. Chem. Int. Ed.* **57**, 1621–1626 (2018)
5. Y. Kobayashi, Y. Doi, S.S.A. Rahman, E. Kim, T.-H. Kim, A. Takano, Y. Matsushita, *Macromolecules* **51**, 1885–1893 (2018)
6. Z. Liu, Y. Huang, X. Zhang, X. Tu, M. Wang, L. Ma, B. Wang, J. He, P. Ni, H. Wei, *Macromolecules* **51**, 7672–7679 (2018)

7. D.G. Tsalikis, P.V. Alatas, L.D. Peristeras, V.G. Mavrantzas, A.C.S. Macro, Lett. **7**, 916–920 (2018)
8. S. Honda, T. Yamamoto, Y. Tezuka, J. Am. Chem. Soc. **132**, 10251–10253 (2010)
9. S. Honda, T. Yamamoto, Y. Tezuka, Nat. Commun. **4**, 1574 (2013)
10. H. Wada, Y. Kitazawa, S. Kuroki, Y. Tezuka, T. Yamamoto, Langmuir **31**, 8739–8744 (2015)
11. S. Honda, M. Koga, M. Tokita, T. Yamamoto, Y. Tezuka, Polym. Chem. **6**, 4167–4176 (2015)
12. E. Baba, T. Yatsunami, Y. Tezuka, T. Yamamoto, Langmuir **32**, 10344–10349 (2016)
13. T. Yamamoto, S. Yagyū, Y. Tezuka, J. Am. Chem. Soc. **138**, 3904–3911 (2016)
14. T. Yamamoto, M. Hosokawa, M. Nakamura, S. Sato, T. Isono, K. Tajima, T. Satoh, M. Sato, Y. Tezuka, A. Saeki, Y. Kikkawa, Macromolecules **51**, 9284–9293 (2018)
15. B. J. Ree, T. Satoh, T. Yamamoto, Polymers, **11** (2019)
16. N. Sugai, S. Asai, Y. Tezuka, T. Yamamoto, Polym. Chem. **6**, 3591–3600 (2015)
17. T. Yamamoto, K. Inoue, Y. Tezuka, Polym. J. **48**, 391–398 (2016)
18. Q. Meng, S. Honda, Y. Tezuka, T. Yamamoto, A. Fujimori, J. Polym. Sci. Part B: Polym. Phys. **54**, 486–498 (2016)
19. M. Iyoda, H. Shimizu, Chem. Soc. Rev. **44**, 6411–6424 (2015)
20. K. H. Park, P. Kim, W. Kim, H. Shimizu, M. Han, E. Sim, M. Iyoda, D. Kim, Angew. Chem. Int. Ed., **54**, 12711–12715 (2015)
21. O. Coulembier, G. Deshayes, M. Surin, J. De Winter, F. Boon, C. Delcourt, P. Leclère, R. Lazzaroni, P. Gerbaux, P. Dubois, Polym. Chem. **4**, 237–241 (2013)
22. G.R. McKeown, Y. Fang, N.K. Obhi, J.G. Manion, D.F. Peregichka, D.S. Seferos, A.C.S. Macro, Lett. **5**, 1075–1079 (2016)
23. N. Delbosc, J. De Winter, S. Moins, A. Persoons, P. Dubois, O. Coulembier, Macromolecules **50**, 1939–1949 (2017)
24. M. Elsbahy, K.L. Wooley, Chem. Soc. Rev. **41**, 2545–2561 (2012)
25. D. Sutton, N. Nasongkla, E. Blanco, J.M. Gao, Pharm. Res. **24**, 1029–1046 (2007)
26. S.S. Agasti, S. Rana, M.H. Park, C.K. Kim, C.C. You, V.M. Rotello, Adv. Drug Delivery Rev. **62**, 316–328 (2010)
27. K. Knop, R. Hoogenboom, D. Fischer, U. S. Schubert, Angew. Chem. Int. Ed. **49**, 6288–6308 (2010)
28. H. Otsuka, Y. Nagasaki, K. Kataoka, Adv. Drug Delivery Rev. **55**, 403–419 (2003)
29. G. Zhang, Z. Yang, W. Lu, R. Zhang, Q. Huang, M. Tian, L. Li, D. Liang, C. Li, Biomaterials **30**, 1928–1936 (2009)
30. Y. Wang, J.E.Q. Quinsaat, T. Ono, M. Maeki, M. Tokeshi, T. Isono, K. Tajima, T. Satoh, S. Sato, Y. Miura, T. Yamamoto, Nat. Commun. **11**, 6089 (2020)
31. A.K. Mohanty, J. Ye, J. Ahn, T. Yun, T. Lee, K.-S. Kim, H.B. Jeon, T. Chang, H.-J. Paik, Macromolecules **51**, 5313–5322 (2018)
32. A. Pipertzis, M.D. Hossain, M.J. Monteiro, G. Floudas, Macromolecules **51**, 1488–1497 (2018)

# Chapter 25

## Surface Functionalization with Cyclic Polymers



Edmondo M. Benetti

The application of cyclic polymers in surface functionalization enables an extremely broad modulation of technologically relevant, interfacial physicochemical properties, surpassing the attractive characteristics provided by linear polymer “brushes”. This is valid on model inorganic surfaces, where cyclic polymer brushes provide enhanced steric stabilization and superlubricious behavior. Alternatively, when cyclic brushes form shells on inorganic nanoparticles (NPs), their highly compact and ultra-dense character make them impenetrable and long-lasting shields, which extend the stability of NP dispersions and hinder any interaction with serum proteins.

The unique characteristics of cyclic polymer brushes can be further exploited to formulate biocompatible surface modifiers for human cartilage, which are capable of binding to the tissue, and generating a bioinert and highly lubricious polymer layer that halt the progression of degenerative syndromes affecting articular joints.

Polymer topology effects are amplified by adding an additional boundary such as a grafting surface. Their precise tuning translates into synthetic interfaces with unprecedented properties and extremely high applicability.

### 25.1 Introduction

In solution, bulk and melts topology effects by ring macromolecules are determined by their intrinsic architecture, *i.e.*, the steric pressure induced by cyclization, and the lack of chain ends. For instance, in solution cyclic polymers typically feature a smaller hydrodynamic volume compared to their linear counterparts with similar molar mass [1–4]. In addition, cyclic polymers present a lower intrinsic viscosity within melts,

---

E. M. Benetti (✉)

Laboratory for Surface Science and Technology, Department of Materials, ETH Zürich, Vladimir-Prelog-Weg 5, 8093 Zürich, Switzerland

e-mail: [edmondo.benetti@unipd.it](mailto:edmondo.benetti@unipd.it)

while in bulk they are characterized by higher glass-transition temperature ( $T_g$ ) and greater density [5–7]. These unique properties also affect the characteristics of assemblies when cyclic polymers are immobilized or “grafted” onto surfaces through physical or chemical interactions.

Polymer topology effects translate into a significant broadening of tuning capability for several, technologically relevant interfacial properties. In particular, when cyclic macromolecules are assembled to form polymer “brush” layers on macroscopic surfaces and nanoparticles (NPs) the steric constraints within their structure substantially alter hydration, steric stabilization, and exposure of functional groups, consequently influencing the interaction of the functionalized supports with the surrounding environment [8, 9]. The density, nanomechanical and nanotribological properties of polymer brushes were demonstrated to be topology-dependent, thus enabling the design of polymeric films with physicochemical properties that could not be otherwise attained by simply applying linear adsorbates.

Topological polymer chemistry applied to materials science is thus paving the way for the development of new molecular strategies to functionalize biomaterials and modulate their interaction with biological media, as well as to design nanomedicine and bioimaging tools with radically new properties.

In this chapter the recent applications of cyclic polymer adsorbates are summarized, especially highlighting how their structural characteristics translate into unprecedented surface properties.

## 25.2 Cyclic Polymers on Macroscopic Surfaces

The unique properties of surface assemblies of cyclic polymers were initially revealed while studying polymer brush coatings based on poly(2-alkyl-2-oxazoline)s (PAOXAs), which were applied on various inorganic and organic supports [8–11].

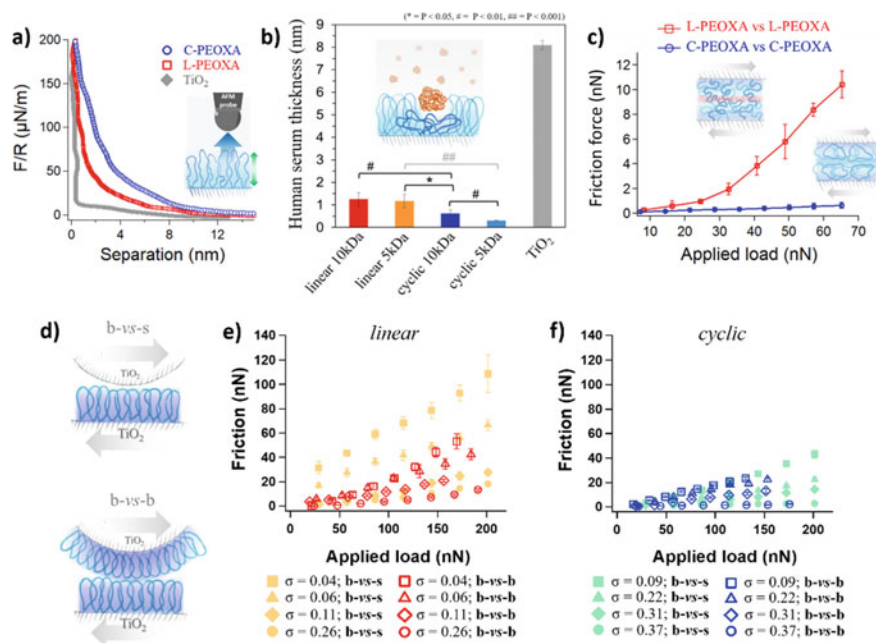
Our group initially investigated the assembly of linear and cyclic poly(2-ethyl-2-oxazoline) (PEOXA) adsorbates with  $M_w$  of 5 and 10 kDa ( $\text{Đ} = 1.1/1.3$ ), and including nitrodopamine (ND) anchors onto  $\text{TiO}_2$ -coated surfaces, generating linear and cyclic PEOXA brushes (L-PEOXA and C-PEOXA, respectively) [8–10]. A combination of variable-angle spectroscopic ellipsometry (VASE), quartz crystal microbalance with dissipation (QCM-D) and atomic force microscopy (AFM) highlighted the structural and interfacial characteristics of the different assemblies, and shed light on some fundamental topology effects distinguishing the properties of C-PEOXA brushes from those displayed by their linear counterparts.

C-PEOXA adsorbates featured smaller molecular dimensions compared to their L-PEOXA analogues of similar molar mass, and thus experienced a reduced steric hindrance during their assembly on  $\text{TiO}_2$  [8]. This phenomenon enabled the formation of significantly denser C-PEOXA brushes compared to L-PEOXA grafts, leading to an enhanced passivation and steric stabilization of the surface. An increment in steric repulsion toward compression, which was revealed by colloidal-probe AFM,



also translated into an augmented resistance of the functionalized surface toward unspecific adsorption of protein mixtures (Fig. 25.1a, b).

The nanotribological properties of topologically different PEOXA brushes were subsequently investigated via lateral force microscopy (LFM), by sliding L- and C-PEOXA brushes against identical brush countersurfaces, and simultaneously recording friction force-*vs*-applied load ( $F_fL$ ) profiles (Fig. 25.1c). Relevantly, the coefficient of friction ( $\mu$ ) measured in aqueous medium for cyclic brushes was one order of magnitude lower than that obtained by shearing the corresponding linear PEOXA grafts, and it was included between 0.005 and 0.007. The extremely lubricious character of C-PEOXA brushes was a rather surprising result, as PEOXA is an amphiphilic polymer for which water is not an athermal solvent [12]. Nevertheless, C-PEOXA brushes present values of  $\mu$  close to those recorded for very hydrophilic and



**Fig. 25.1** a Force-*vs*-separation approach profiles recorded on L-PEOXA and C-PEOXA films by AFM. Reproduced with permission from Morgese et al. [10]. copyright 2016 John Wiley and Sons. b Adsorption of full human serum on L- and C-PEOXA brushes estimated by VASE. Reproduced with permission from Divandari et al. [11]. Copyright 2017 American Chemical Society. c  $F_fL$  curves recorded with LFM by shearing L- and C-PEOXA brushes against identical brush countersurfaces. Reproduced with permission from Morgese et al. [10] copyright 2016 John Wiley and Sons. d The lubricious character of topologically different PEOXA brushes was studied by LFM, analyzing asymmetric (brush-*vs*-surface) and symmetric (brush-*vs*-brush) tribo-pairs. Reproduced with permission from Divandari et al. [12] Copyright 2018 American Chemical Society.  $F_fL$  curves recorded on e L-PEOXA brushes and f C-PEOXA brushes by shearing symmetric and asymmetric tribo-pairs. Reproduced with permission from Divandari et al. [12] Copyright 2018 American Chemical Society

ionic linear polymer brushes, which can incorporate a significantly higher amount of water (fluid lubricant) in their structure [13–17]. The exceptional lubricity of cyclic brushes was thus primarily attributed to the absence of linear chain ends dangling at their interface, which prevented polymer interdigitation, and substantially reduced the dissipation of mechanical energy that is typically generated by collisions between polymer segments [8, 18].

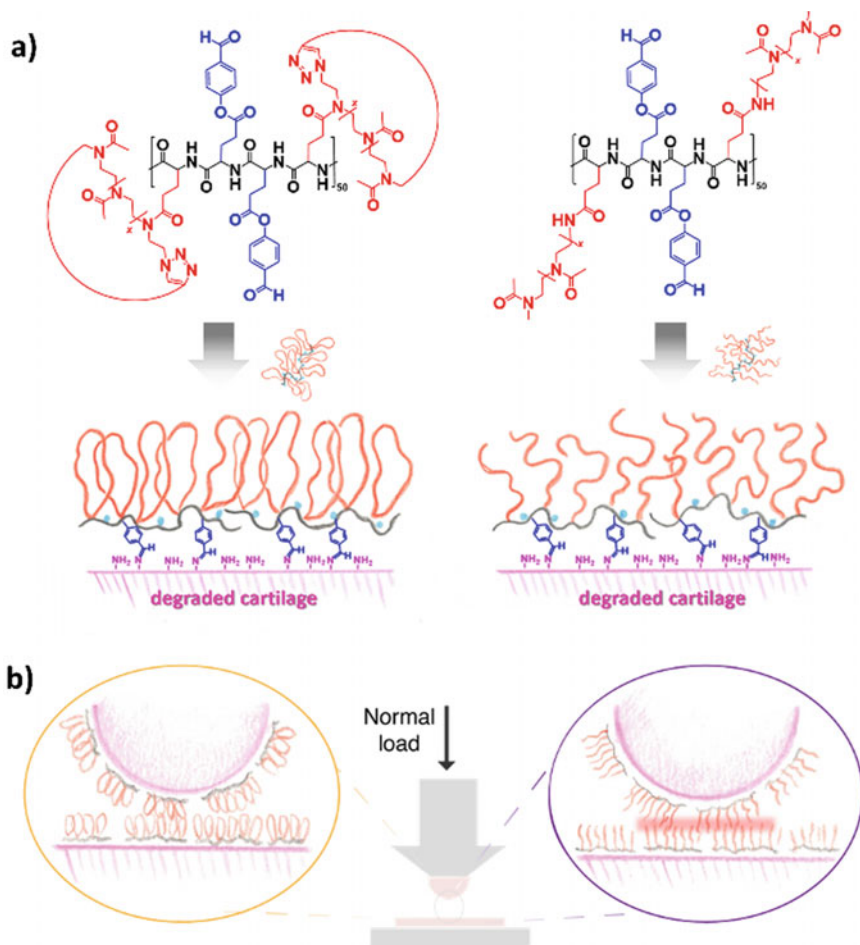
Hindrance of interpenetration between cyclic brushes was further emphasized by comparing  $F_fL$  profiles recorded on L- and C-PEOXA brushes ( $M_w = 10$  kDa,  $\bar{D} = 1.1/1.2$ ) presenting variable grafting densities ( $\sigma$ ), alternatively sliding them against identical brushes (brush-*vs*-brush) and bare  $TiO_2$  surfaces (brush-*vs*-surface) (Fig. 25.1d, f) [10]. Generally, friction progressively decreased with increasing  $\sigma$ , for brush-*vs*-brush as well as for brush-*vs*-surface tribo-pairs (Fig. 25.1f). However, the frictional properties of linear brushes were significantly influenced by the type of countersurface that was sheared against them, highlighting the contribution of brush interdigitation. Comparing  $F_fL$  profiles recorded on L-PEOXA brushes presenting the same value of  $\sigma$ , friction substantially decreased by replacing a bare  $TiO_2$ -coated countersurface with an identical linear brush (Fig. 25.1e).

This phenomenon was ascribed to excluded-volume effects that usually prevent the formation of an interpenetrated layer between oppositely sheared linear PEOXA grafts, and simultaneously cause a reduction in friction [19–22]. Interestingly, the clear increment in the slope of  $F_fL$  profiles recorded at normal loads higher than 100 nN suggested that interpenetration cannot be prevented when L-PEOXA brushes are highly compressed against identical linear grafts, leading to a consequent increment in mechanical energy dissipation and friction.

Conversely, the nanotribological behavior of C-PEOXA brushes was not influenced by the type of countersurface used to record  $F_fL$  curves (Fig. 25.1f), which nearly overlapped each other for each value of  $\sigma$ , suggesting that interdigitation between cyclic brushes basically did not contribute in determining mechanical-energy dissipation and thus friction. C-PEOXA grafts formed a molecularly smooth layer, which was significantly more lubricious than its linear-brush counterpart [10, 23].

Besides  $TiO_2$  substrates, which are of relevance for the fabrication of different medical devices and implants, cyclic PAOXA brush-forming adsorbates were additionally applied on cartilage with the aim of restoring its lubrication properties after degradation processes involved in osteoarthritis (OA), and to protect the tissue against enzymatic digestion correlated to this degenerative syndrome [24–29].

Cartilage-surface modifiers were based on graft copolymers including a poly(glutamic acid) (PGA) backbone, which was derivatised with cyclic poly(2-methyl-2-oxazoline) (PMOXA) side chains ( $M_w$  of  $\sim 8$  kDa,  $\bar{D} = 1.3$ ) and hydroxyl benzaldehyde (HBA) functions (Fig. 25.2a) [27]. The HBA groups can readily react with the amino groups of the collagen exposed at the tissue's interface after enzymatic degradation forming Schiff bases [30], while cyclic PMOXA segments extend from the cartilage surface generating a lubricious and passivating brush layer. Relevantly,



**Fig. 25.2** **a** Cartilage-surface modifiers were based on graft copolymers bearing topologically different PMOXA side chains and HBA groups, which binds to the tissue surface forming Schiff bases. **b** Experimental setup used to analyse the tribological properties of cartilage samples functionalized with PMOXA-based graft copolymers. **c** Values of  $\mu$  recorded by shearing cartilage samples functionalized with PMOXA-based graft copolymers presenting linear (*L*) and cyclic (*C*) side chains, and applying normal pressures of 0.5 (light grey), 0.7 (grey) and 0.9 (dark grey) MPa. The values of  $\mu$  recorded on untreated degraded cartilage (DC) and the native tissue (NC) are also reported. The density of PMOXA chains on PGA backbone (0.1, 0.3 and 0.6), were calculated as nPMOXA/glutamate units. \*\* $p < 0.05$ ; \* $p < 0.01$ ; † $p = 0.095$ . Reproduced with permission from Morgese et al. [27] copyright 2018 John Wiley and Sons

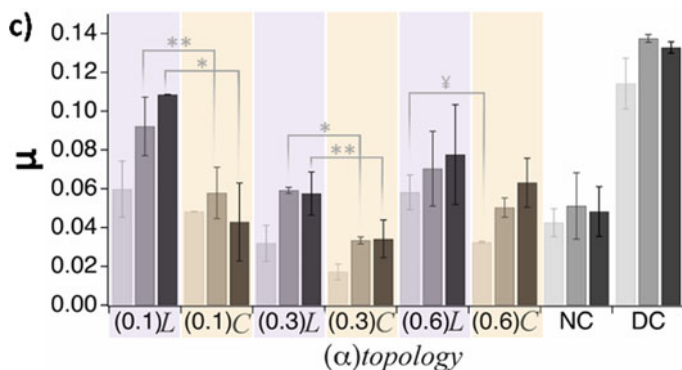


Fig. 25.2 (continued)

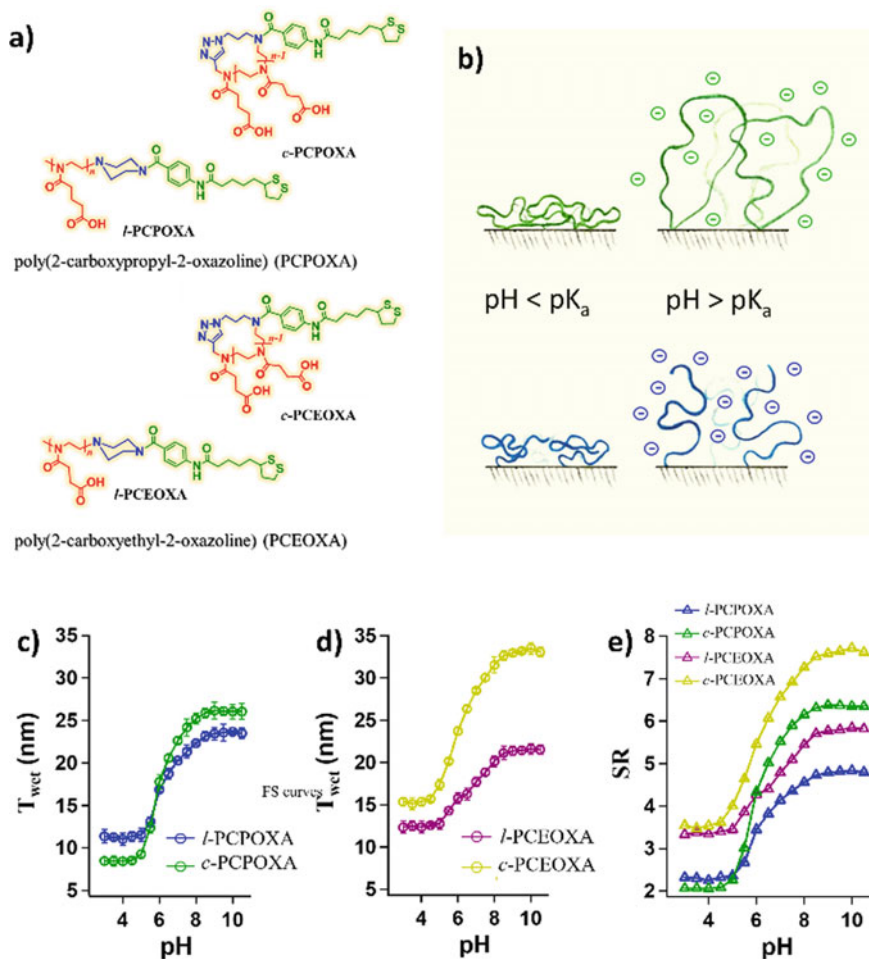
also on tissue substrates C-PMOXA brushes efficiently reduced friction, outperforming the lubricity of their linear PMOXA analogues, and in some cases matching the tribological properties of the healthy (not degraded) tissue (Fig. 25.2b-c).

In all these studies, intrinsic topology effects by chemically inert, cyclic macromolecules were demonstrated to be directly converted into a substantial modification of the interfacial physicochemical properties of brush assemblies on solid surfaces. However, the steric and conformational constraints introduced during cyclization additionally affect the characteristics of surface-grafted polymer assemblies when these feature a functional character.

This is the case of functional cyclic polymer brushes that respond to a chemical stimulus by a significant change in their properties or, alternatively, which are chemically designed to actively interact with proteins present in the medium.

Due to their constrained topology, cyclic polyacid brushes display an augmented expansion and increased hydration upon deprotonation and charging (above their  $pK_a$ ) when compared to their linear counterparts [31, 32]. This was demonstrated for poly(2-carboxypropyl-2-oxazoline) (PCPOXA) and poly(2-carboxyethyl-2-oxazoline) (PCEOXA) brushes immobilized on Au surfaces (Fig. 25.3a, b), which show a pH-responsive swelling behavior across  $pK_a$  values that were centered at pH  $\sim 6.5$ .

Upon ionization at relatively basic pH, the intramolecular steric constraints characterizing cyclic PCPOXA and PCEOXA brushes lead to enhanced electrostatic repulsion between charged polymer segments, and a simultaneous more marked expansion and a higher swelling ratio compared to their linear counterparts, as demonstrated by a combination of QCM-D and VASE (Fig. 25.3c-e) [32]. Simultaneously, the composition of polyacid brushes determines their hydration in both neutral and ionized forms, influencing their degree of swelling during pH-induced transition. In particular, across the entire pH range, PCEOXA brushes showed higher values of swelling ratio (SR, expressed as  $T_{wet}/T_{dry}$ ) compared to PCPOXA assemblies, most likely due to their more hydrophilic nature (Fig. 25.3e) [32].



**Fig. 25.3** **a** Chemical structures of PCPOXA and PCEOXA adsorbates. **b** Schematic depicting the pH-responsive swelling of linear and cyclic polyelectrolyte brushes. Wet thickness ( $T_{\text{wet}}$ ) of **c** PCPOXA and **d** PCEOXA brushes as a function of pH, measured by QCMD. **e** Swelling ratio (SR) corresponding to  $T_{\text{wet}}/T_{\text{dry}}$  as a function of pH for topologically different PCPOXA and PCEOXA brushes. Reproduced with permission from Trachsel et al. [32] copyright 2021 American Chemical Society

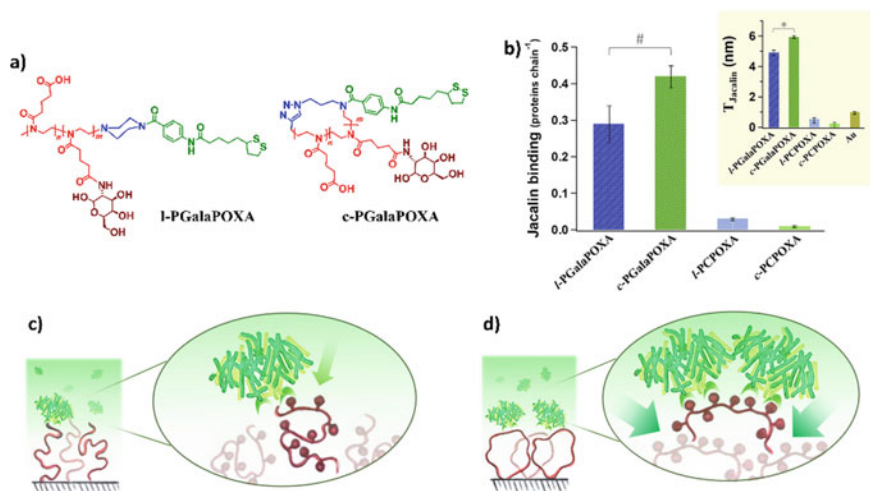
Hence, shifting the topology of grafted polyacids from linear to cyclic induces an amplification of pH-responsive properties, whereas the range of swelling within which the pH transition takes place is governed by the composition of the grafts.

Interestingly, when polyacid adsorbates were partially derivatised with sugar units, the subsequently generated brush assemblies showed a topology-dependent affinity toward proteins [31].

Generally, glycopolymers including multiple sugar functions strongly bind to lectins due to the cluster glycoside effect.<sup>33</sup> While a broad range of cell-adhesion and recognition processes involved in, e.g., cancer, inflammation, and infection, are regulated by the specific interaction between glycopolymers and lectins [33], the specific structure of carbohydrate-rich polymers determines the exposure and steric availability of carbohydrate ligands, thus in turn influencing protein-binding strength and kinetics [34–38].

This phenomenon becomes particularly evident by comparing the lectin-binding ability of topologically different glycopolymer brushes. Specifically, linear and cyclic PCPOXA adsorbates were modified by coupling galactosamine to their COOH side groups (Fig. 25.4a), yielding linear and cyclic poly(2-N-2-deoxy-D-galactopyranosecarboxamidepropyl-2-oxazoline) (l-PGalaPOXA and c-PGalaPOXA, respectively) with  $\sim 40$  mol % of sugar moieties distributed along the polymer backbones.

The intramolecular steric constraints within cyclic glycopolymer brushes determine an enhanced exposure of sugar functions, which are more favorably available as protein-binding sites with respect to analogous moieties along linear grafts. Especially concentrating on the interaction between topologically different PGalaPOXA



**Fig. 25.4** **a** Chemical structures of l- and c-PGalaPOXA adsorbates. **b** Jacalin binding (expressed as number of proteins chain<sup>-1</sup>) as measured by VASE on l- and c-PGalaPOXA. In the inset, the dry thickness of Jacalin layer ( $T_{\text{Jacalin}}$ ) formed on l- and c-PGalaPOXA brushes was reported. The corresponding l-PCPOXA and c-PCPOXA were applied as controls, together with bare Au surfaces. (\*  $p < 0.001$ ; #  $p < 0.05$ ). **c**, **d** The enhanced exposure of sugar functions on c-PGalaPOXA brushes determines a significant increment in protein-binding ability. Reproduced with permission from Trachsel et al. [31] copyright 2020 American Chemical Society

brushes and Jacalin—a tumor-specific lectin [39]—the unique accessibility of galactose functions along cyclic grafts leads to ~45% higher Jacalin-binding capacity with respect to that recorded on l-PGalaPOXA brushes of comparable composition and molar mass (Fig. 25.4b).

### 25.3 Cyclic Polymer Shells on Nanoparticles

The fabrication of cyclic polymer brushes on flat surfaces, and the characterization of their physicochemical properties demonstrated that polymer topology effects translate into surface assemblies with unique traits, such as improved steric stabilization and superlubricious behavior.

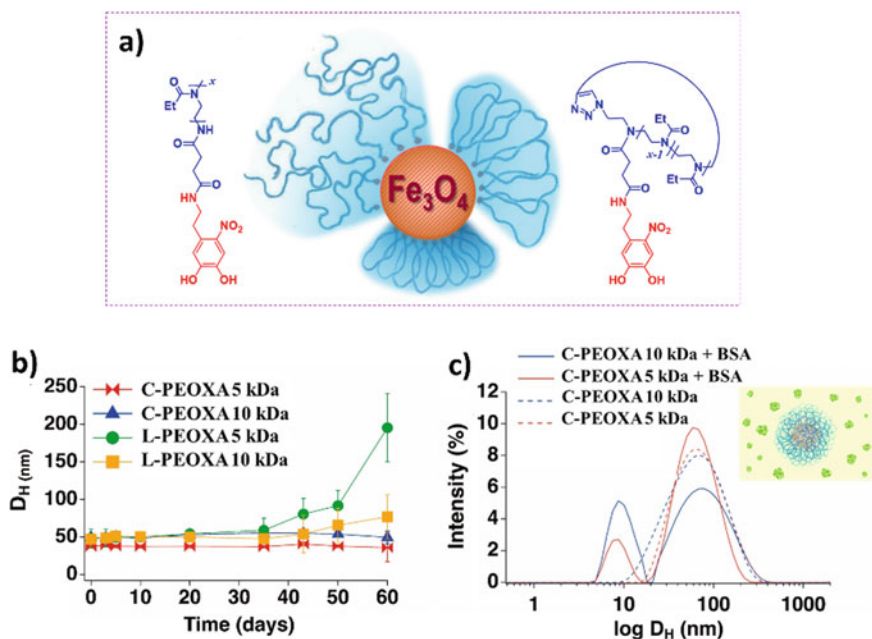
The distinctive structural properties of cyclic brushes are greatly emphasized if the grafting surface is constituted by an inorganic nanoparticle (NP), intrinsically characterized by an extremely high curvature.

This phenomenon was demonstrated for the first time by Morgese et al., who applied ND-bearing, cyclic PEOXA ligands for the functionalization of superparamagnetic  $\text{Fe}_3\text{O}_4$  NPs, and compared the properties of the obtained dispersions to those showed by linear PEOXA-stabilized NPs [40].

Due to the lower hydration volume and intrinsic viscosity of cyclic PEOXA, ultra-dense and highly compact brush shells are generated on the NPs. Namely, C-PEOXA adsorbates ( $M_w = 5$  and 10 kDa,  $\bar{D} = 1.1/1.3$ ) provided cyclic brush shells with  $\sigma$  included between 2.2 and 3.3 chains  $\text{nm}^{-2}$ , which are among the highest values ever obtained for polymer brush shells on NPs, and are ~80% higher than those generated by anchoring linear PEOXA analogues on the same NP cores (Fig. 25.5a). In addition, C-PEOXA brush shells are not only much denser but also significantly thinner than their linear brush counterparts.

C-PEOXA brush shells provide enhanced stability to the NP dispersions, which do not show any sign of aggregation for up to 2 months of incubation in phosphate buffer saline (PBS) (Fig. 25.5b), when subjected to ultracentrifugation or, alternatively, when strong magnetic fields are applied. The unique colloidal stability of C-PEOXA shell- $\text{Fe}_3\text{O}_4$  NPs is additionally preserved when their dispersions are subjected to thermal cycles reaching temperatures above PEOXA's lower critical solution temperature (LCST). In particular, above 60 °C core-cyclic brush shell NPs show a fully reversible collapse, while their linear brush-stabilized analogues irreversibly aggregate, due to an incomplete shielding of core-core interactions [40].

The efficient passivation and steric stabilization provided by ultra-dense, cyclic brush shells is finally tested within physiological solutions of bovine serum albumin (BSA). Remarkably, linear PEOXA shells on NPs cannot prevent the adsorption of the small serum proteins, despite they present  $\sigma$  values higher than 1 chain  $\text{nm}^{-2}$ . In contrast,  $\text{Fe}_3\text{O}_4$  NPs bearing cyclic PEOXA shells do not interact with BSA and show a completely unaltered colloidal stability (Fig. 25.5c).

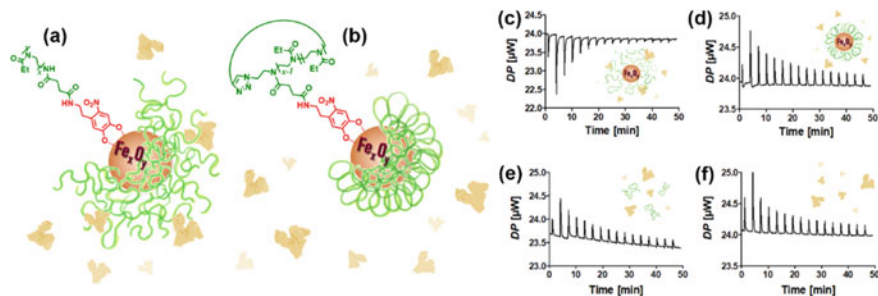


**Fig. 25.5** a Schematic depicting  $\text{Fe}_3\text{O}_4$  NPs functionalized with linear and cyclic ND-bearing PEOXA adsorbates. b Colloidal stability of L- and C-PEOXA shell- $\text{Fe}_3\text{O}_4$  NPs analyzed by dynamic light scattering (DLS) in phosphate buffer saline (PBS) solution. The values of  $D_H$  correspond to the average hydrodynamic diameters as number distribution, obtained over three replicates. c DLS profiles recorded for dispersions of C-PEOXA shell- $\text{Fe}_3\text{O}_4$  NPs (dashed profiles), and C-PEOXA shell- $\text{Fe}_3\text{O}_4$  NPs in the presence of BSA (solid profiles). The appearance of a signal at  $D_H \sim 10$  nm, and the constant values of  $D_H$  for C-PEOXA shell- $\text{Fe}_3\text{O}_4$  NPs indicate that BSA negligibly interacts with cyclic polymer shells. Reproduced with permission from Morgese et al. [40] copyright 2017 John Wiley and Sons

The inertness of C-PEOXA shell- $\text{Fe}_3\text{O}_4$  NPs toward serum proteins is further confirmed by isothermal titration calorimetry (ITC), which demonstrated a quantitative suppression of interaction with human serum albumin (HSA) (Fig. 25.6) [41].

Besides PAOXAs, Aboudzadeh et al. recently proposed an effective route to synthesize cyclic poly(ethylene glycol) (PEG) adsorbates featuring thiol functions, which can assemble onto Au surfaces forming dense cyclic PEG brushes [42]. When cyclic PEG ligands with  $M_w$  ranging from 2 to 11 kDa were assembled on Au NPs polymer brush shells providing enhanced colloidal stability with respect to linear PEG brush analogues were obtained [43]. These further studies enlarged the library of cyclic adsorbates for the generation of core-polymer shell NPs with potential biomedical applications, confirming the influence of ligand topology on the properties of the obtained colloidal dispersions.





**Fig. 25.6** **a, b**  $\text{Fe}_3\text{O}_4$  NPs bearing cyclic PEOXA shells quantitatively prevent association with HSA. **c** The values of differential power (DP) recorded after each HSA injection in dispersions of L-PEOXA shell- $\text{Fe}_3\text{O}_4$  NPs indicate a non-negligible interaction with the protein, as evidenced by the progressive appearance of exothermic injection peaks. **b** In contrast, addition of HSA to dispersions of C-PEOXA shell- $\text{Fe}_3\text{O}_4$  NPs generated only endothermic peaks, which were very similar to those recorded by injecting the protein to a solution of “free” polymer (**e**), or to pure 4-(2-hydroxyethyl)-1-piperazineethanesulfonic acid (HEPES) buffer (**f**). Reproduced with permission from Schroffenegger et al. [41] copyright 2020 American Chemical Society

## 25.4 Conclusions

An increasing number of studies are suggesting that shifting the topology of polymer surface modifiers from linear to cyclic can alter a large variety of technologically relevant interfacial properties when coatings, surfactants, and shells for NPs are fabricated.

The intrinsic topology effects characterizing cyclic polymer adsorbates can realistically enable not only the generation of biopassive assemblies, but also stimuli- and bio-responsive interfaces on multi-dimensional substrates (both macroscopic surfaces as well as high-aspect ratio nanomaterials). The augmented effective intramolecular repulsion between polymer segments within cyclic macromolecules does not only determine a higher excluded-volume effect and enhanced solvation [44], but it additionally leads to an increment in electrostatic repulsive forces when the polymers are ionized, and provides an increased exposure of functional groups enabling a more efficient binding of biological entities.

On the one hand, the amplified responsiveness of cyclic polyelectrolyte brushes broadens the tuning potential for interfacial physicochemical on “smart” surfaces, providing a new molecular design for responsive materials. On the other hand, the increased availability of functions on cyclic brush-bearing surfaces indicates that an enhancement in reactivity toward biological entities can be generalized to different polymer chemistries. If this hypothesis was validated, cyclic polymers could be applied as synthetic supports for biological recognition, improving the performance of nanomedical devices and biosensors. More generally, this concept could provide a new design paradigm to increment the reactivity of biointerfaces, which can supramolecularly or covalently associate with biological components present in the surrounding medium.

In summary, even though synthetic challenges and scalability in the preparation of cyclic macromolecules are still restricting their widespread application in the formulation of synthetic materials, the advantages gained in their application on surfaces are becoming increasingly evident. On flat surfaces and NPs the presence of a grafting surface acting as boundary seems further amplifying polymer topology-related effects, providing coatings with properties that largely surpass the performance of linear polymer-based analogues.

## References

1. M. Duval, P. Lutz, C. Strazielle, *Makromol. Chem. Rapid* **6**, 71 (1985)
2. J. Roovers, *J. Polym. Sci. Pol. Phys.* **23**, 1117 (1985)
3. G. Hadziioannou, P.M. Cotts, G. Tenbrinke, C.C. Han, P. Lutz, C. Strazielle, P. Rempp, A.J. Kovacs, *Macromolecules* **20**, 493 (1987)
4. S.S. Jang, T. Cagin, W.A. Goddard, *J. Chem. Phys.* **119**, 1843 (2003)
5. E.A. Dimarzio, C.M. Guttman, *Macromolecules* **20**, 1403 (1987)
6. S.J. Clarson, J.A. Semlyen, *Polymer* **27**, 1633 (1986)
7. S.J. Clarson, J.A. Semlyen, K. Dodgson, *Polymer* **32**, 2823 (1991)
8. G. Morgese, M. Trachsel, M. Romio, M. Divandari, S.N. Ramakrishna, E.M. Benetti, *Angew. Chem. Int. Edit.* **55**, 15583 (2016)
9. M. Divandari, G. Morgese, L. Trachsel, M. Romio, E.S. Dehghani, J.G. Rosenboom, C. Paradisi, M. Zenobi-Wong, S.N. Ramakrishna, E.M. Benetti, *Macromolecules* **50**, 7760 (2017)
10. M. Divandari, L. Trachsel, W.Q. Yan, J.G. Rosenboom, N.D. Spencer, M. Zenobi-Wong, G. Morgese, S.N. Ramakrishna, E.M. Benetti, *ACS Macro. Lett.* **7**, 1455 (2018)
11. W.Q. Yan, M. Divandari, J.G. Rosenboom, S.N. Ramakrishna, L. Trachsel, N.D. Spencer, G. Morgese, E.M. Benetti, *Polym. Chem.* **9**, 2580 (2018)
12. B. Verbraeken, B.D. Monnery, K. Lava, R. Hoogenboom, *Eur. Polym. J.* **88**, 451 (2017)
13. U. Raviv, S. Giasson, N. Kampf, J.F. Gohy, R. Jerome, J. Klein, *Nature* **425**, 163 (2003)
14. R. Heeb, R.M. Bielecki, S. Lee, N.D. Spencer, *Macromolecules* **42**, 9124 (2009)
15. E.S. Dehghani, V.V. Naik, J. Mandal, N.D. Spencer, E.M. Benetti, *Macromolecules* **50**, 2495 (2017)
16. E.S. Dehghani, S.N. Ramakrishna, N.D. Spencer, E.M. Benetti, *Macromolecules* **50**, 2932 (2017)
17. A. Li, N. Ramakrishna Shivaprakash, C. Nalam Prathima, M. Benetti Edmondo, D. Spencer Nicholas, *Adv. Mater. Interfaces* **1**, 1300007 (2014)
18. E. Eiser, J. Klein, T.A. Witten, L.J. Fetters, *Phys. Rev. Lett.* **82**, 5076 (1999)
19. J. Klein, Y. Kamiyama, H. Yoshizawa, J.N. Israelachvili, G.H. Fredrickson, P. Pincus, L.J. Fetters, *Macromolecules* **26**, 5552 (1993)
20. J. Klein, E. Kumacheva, D. Mahalu, D. Perahia, L.J. Fetters, *Nature* **370**, 634 (1994)
21. J. Klein, *Annu. Rev. Mater. Sci.* **26**, 581 (1996)
22. T. Kreer, M.H. Muser, K. Binder, J. Klein, *Langmuir* **17**, 7804 (2001)
23. M. Divandari, G. Morgese, S.N. Ramakrishna, E.M. Benetti, *Eur. Polym. J.* **110**, 301 (2019)
24. G. Morgese, B. Verbraeken, S.N. Ramakrishna, Y. Gombert, E. Cavalli, J.-G. Rosenboom, M. Zenobi-Wong, N.D. Spencer, R. Hoogenboom, E.M. Benetti, *Angew. Chem. Int. Edit.* **57**, 11667 (2018)
25. G. Morgese, E. Cavalli, M. Müller, M. Zenobi-Wong, E.M. Benetti, *ACS Nano* **11**, 2794 (2017)
26. G. Morgese, E.M. Benetti, M. Zenobi-Wong, *Adv. Health. Mater.* **7**, 1701463 (2018)
27. G. Morgese, E. Cavalli, J.G. Rosenboom, M. Zenobi-Wong, E.M. Benetti, *Angew. Chem. Int. Edit* **57**, 1621 (2018)

28. G. Morgese, S.N. Ramakrishna, R. Simic, M. Zenobi-Wong, E.M. Benetti, *Biomacromol* **19**, 680 (2018)
29. S.N. Ramakrishna, G. Morgese, M. Zenobi-Wong, E.M. Benetti, *Macromolecules* **52**, 1632 (2019)
30. G. Morgese, E. Cavalli, M. Muller, M. Zenobi-Wong, E.M. Benetti, *ACS Nano* **11**, 2794 (2017)
31. L. Trachsel, M. Romio, B. Grob, M. Zenobi-Wong, N.D. Spencer, S.N. Ramakrishna, E.M. Benetti, *ACS Nano* **14**, 10054 (2020)
32. L. Trachsel, S.N. Ramakrishna, M. Romio, N.D. Spencer, E.M. Benetti, *ACS Macro Lett.* **10**, 90 (2021)
33. J.J. Lundquist, E.J. Toone, *Chem. Rev.* **102**, 555 (2002)
34. C.R. Becer, M.I. Gibson, J. Geng, R. Ilyas, R. Wallis, D.A. Mitchell, D.M. Haddleton, *J. Am. Chem. Soc.* **132**, 15130 (2010)
35. Q. Zhang, L. Su, J. Collins, G.S. Chen, R. Wallis, D.A. Mitchell, D.M. Haddleton, C.R. Becer, *J. Am. Chem. Soc.* **136**, 4325 (2014)
36. Y. Chen, G.J. Chen, M.H. Stenzel, *Macromolecules* **43**, 8109 (2010)
37. Y. Chen, M.S. Lord, A. Piloni, M.H. Stenzel, *Macromolecules* **48**, 346 (2015)
38. C. Fasting, C.A. Schalley, M. Weber, O. Seitz, S. Hecht, B. Kokschi, J. Dornedde, C. Graf, E.W. Knapp, R. Haag, *Angew. Chem. Int. Edit* **51**, 10472 (2012)
39. M.V.K. Sastry, P. Banarjee, S.R. Patanjali, M.J. Swamy, G.V. Swarnalatha, A. Surolia, *J. Biol. Chem.* **261**, 1726 (1986)
40. G. Morgese, B.S. Shaghasemi, V. Causin, M. Zenobi-Wong, S.N. Ramakrishna, E. Reimhult, E.M. Benetti, *Angew. Chem. Int. Edit* **56**, 4507 (2017)
41. M. Schroffenegger, N.S. Leitner, G. Morgese, S.N. Ramakrishna, M. Willinger, E.M. Benetti, E. Reimhult, *ACS Nano* **14**, 12708 (2020)
42. M.A. Aboudzadeh, M. Dolz, X. Monnier, E. G. de San Roman, D. Cangialosi, M. Grzelczak, F. Barroso-Bujans, *Polym Chem.* **10**, 6495 (2019)
43. M.A. Aboudzadeh, A. Iturrospe, A. Arbe, M. Grzelczak, F. Barroso-Bujans, *ACS Macro Lett.* **9**, 1604 (2020)
44. M.D. Hossain, J.C. Reid, D.R. Lu, Z.F. Jia, D.J. Searles, M.J. Monteiro, *Biomacromol* **19**, 616 (2018)

# Chapter 26

## Morphological Significances of Cyclic Polymers in Solution and Solid State



Brian J. Ree, Takuya Isono, and Toshifumi Satoh

Cyclic polymers, defined by the absence of chain ends, exhibit different physical properties compared to their linear analogues of same chemical composition and molecular weight. Such set of attributes solely stems from the looped, endless nature of main chain enabling a unique chain conformation of its own. Specifically, the implications of cyclic topology are intrinsic consequences of morphological features, and, therefore, the subject of cyclic polymer morphology is crucial to understand the behaviors of these intricate materials from a wider perspective. Thus far, there have been various investigations on the morphological features of various cyclic homopolymers and block copolymers. This chapter will outline the progress of morphological investigations in three categories, cyclic polymers in solution, cyclic polymers in bulk, and cyclic polymers in thin films, and conclude with a brief summary.

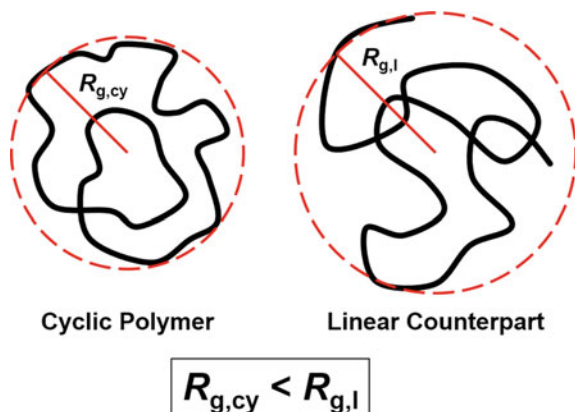
### 26.1 Introduction

Molecular topology, which defines the shape and spatial features of the main chain of a polymer, is a crucial aspect of polymer science due to its impact upon the physical properties of polymers [1–5]. Among many different types of polymer topology, cyclic topology is a classic example that well demonstrates the impact of topological influence by enabling a higher thermal stability, a higher glass transition temperature, a higher melting temperature, a lower viscosity, a shorter radius of gyration, and a smaller hydrodynamic volume than linear counterpart with the identical molecular weight [2, 6–10]. Another physical aspect often investigated with respect to cyclic polymers is their morphology, including self-assembly behavior,

---

B. J. Ree · T. Isono · T. Satoh (✉)  
Faculty of Engineering, Hokkaido University, Sapporo 060-8628, Japan  
e-mail: [satoh@eng.hokudai.ac.jp](mailto:satoh@eng.hokudai.ac.jp)

**Fig. 26.1** Schematic representation of chain conformations of cyclic and linear iterations of a flexible Gaussian polymer



in solution and solid state. It is no surprise that the absence of chain ends in cyclic polymers fundamentally facilitates a different set of chain conformation and arrangement compared to conventional linear counterparts (Fig. 26.1). With many studies reporting efficient and well-controlled strategies to synthesize cyclic polymers [6–9, 11–26], one may expect the morphological behaviors of cyclic polymers to be well investigated and documented. Ironically, the current state of literature regarding the understanding of the morphological aspect of cyclic polymers remains at a developing stage. More specifically, the number of morphological investigation of cyclic polymers are vastly outnumbered by the synthetic studies. In addition, among the morphological investigations, there are only a handful of reports that go beyond simply observing the type of morphology and determine the domain spacing ( $d$ -spacing) to provide detailed discussions into the fundamental aspects. Furthermore, the explicit correlation between polymer morphology and other physical properties necessitates a thorough comprehension of this matter for discussing and exploring the tangible limits of the proposed potentials of cyclic polymers. It is, therefore, necessary to examine and address the topological influence of cyclic polymers on their morphological structures based on fundamental basis.

From a perspective considering the detailed aspects of morphological characterization methods, however, the shortage of investigations on cyclic polymer morphology requires an in-depth consideration and discussion going beyond the number of publications. This particular subject of consideration is a technical challenge that must be appropriately addressed to succeed in characterizing morphological structures of cyclic polymers. With the dimensions of the morphologies of cyclic polymers, as well as most polymers in general, belonging in the nanometer realm, characterization is faced with difficulty regarding accuracy and precision via conventional methods such as transmission electron microscopy (TEM) and atomic force microscopy (AFM). Despite having the benefit of direct observation of polymer structure in real space, there are numerous innate disadvantages of microscopy specifically for polymers [26–29]. The alternative method is X-ray scattering, which offers

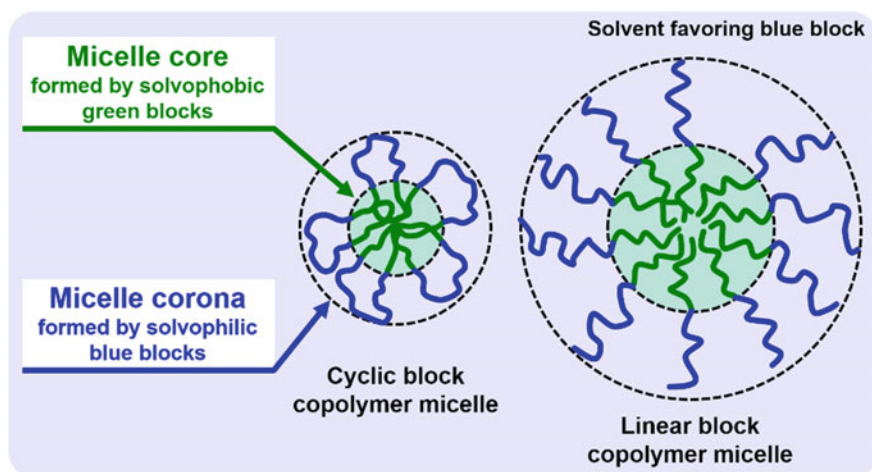
higher levels of accuracy and precision than microscopy. But, it is also facing challenges with the fact that the raw data collected through this method is in the reciprocal space unlike the real space microscopy images. Thusly, the retrieval of real space information, such as the morphological type and the dimensions of morphological features, from raw scattering data requires a rigorous analysis based on extensive knowledge in the theories and principles of scattering. Hence, the accessibility of this technique is relatively more limited than microscopy. As a third alternative that supplements the two aforementioned experimental methods, theoretical simulations are available for deriving predictions regarding the morphological behavior of cyclic polymers. Given the macromolecular characteristic of polymers, however, simulating polymers is a highly complex matter when compared to the conventional theoretical studies that model small molecules from atomistic perspective. It also must be noted that the number of theoretical studies on cyclic polymer morphology is even fewer than the experimental reports. Although the further technical aspects of microscopy, scattering, and theoretical simulations are beyond the scope of our discussion within this chapter, the aforementioned challenges regarding morphological investigation of cyclic polymer urge for more research effort and innovative strides for continuing the advancement of cyclic polymer research.

For the rest of this chapter, morphological investigations on cyclic polymers from the literature is reviewed. The intention behind this chapter is to provide a summary of the current progress in comprehending the morphologies of cyclic polymers as well as establish a grounded foundation for future research input. The contents of morphology of cyclic polymers are organized into the following order: cyclic polymers in solution, cyclic polymers in bulk, and cyclic polymers in nanoscale film.

## 26.2 Morphology of Cyclic Polymers in Solution

In this particular section, literature investigating the micellization of cyclic block copolymers in solution is discussed. Polymer micelles are phase separated structures assembled through the aggregation of amphiphilic cyclic block copolymers in a certain solvent environment where the solvophobic blocks form the micelle core and solvophilic blocks form the micelle corona (Fig. 26.2). Because cyclic topology is known to enable a smaller hydrodynamic size than that of linear topology, the resulting micelle dimensions of cyclic block copolymers are expected to be smaller than their linear counterparts of identical molecular weights. For their ability to form compact micelles, cyclic block copolymers are often discussed with the consideration of potential nanotechnological applications in photonics, drug delivery systems, cosmetics, and so on.

Classical aspects of micelle characterization include the shape of micelle, which generally ranges from globular (i.e., spherical and ellipsoidal), cylindrical, toroidal, to vesicular shapes. Once the micelle shape is determined, the dimensions of the



**Fig. 26.2** Schematic representation of globular micelles formed by linear and cyclic block copolymers

self-assembled structure such as radius and length are characterized. Additionally, the critical micelle concentration (CMC) is another important aspect of this subject as it determines the minimum threshold polymer concentration where the micelle is formed. Furthermore, aggregation number defines the number of copolymer chains in a single micelle. There are several reports that characterize these structural parameters of micelles based on experimental TEM studies [1, 30, 31] with complementary AFM and dynamic light scattering (DLS) measurements. However, the conclusions of these studies differ from each other as one study reports a pair of linear and cyclic block copolymers based on poly (butyl acrylate) (PBA) and poly (ethylene oxide) (PEO) to form micelles with same hydrodynamic radius in water [1], whereas another reporting a cyclic polystyrene-*block*-polyisoprene (PS-*b*-PI) forming large vesicles and networks consisting of cylindrical micelles as opposed to the conventional globular micelles formed by its linear analogue in *n*-decane [30]. A pair of studies on cyclic PS-*b*-PIs have also explored the effects of blending minor portions of linear PS homopolymer [31] and the linear diblock copolymer [32] on the micellization of cyclic block copolymer. Interestingly, drastic effects such as the transition from cylindrical to vesicular micelles upon the addition of PS homopolymers [31], and the favorable formation of globular micelles when blended with linear counterpart were observed for cyclic PS-*b*-PI in heptane [32]. This particular pair of studies also demonstrate the impact brought by the interaction between different topologies as well as denoting possible consequences arising from any non-cyclic impurities that may be present in a sample of cyclic polymers. Another study reports a series of linear and cyclic block copolymers based on poly (acrylic acid) (PAA) and poly(3-methylpentamethylene-4,4'-bibenzoate) (PBB) to form a variety of cylindrical micelles, globular micelles, and vesicles with a large size distribution in water [33]. Interestingly, a light scattering based study of a series of linear,

triblock and cyclic block copolymers of PEO and poly (butylene oxide) (PBO) have found the cyclic block copolymer to form micelles with a radius approximately half of linear counterpart's micelles [34]. There is also a couple of theoretical studies that attempted to make predictions on the micelle size and CMC between linear and cyclic block copolymers, in which the theoretical cyclic ABC triblock copolymer forms smaller micelles than its linear iteration [35], and cyclic diblock copolymer exhibiting a higher CMC than its linear analogue [36]. Thusly, these studies have demonstrated the drastically different morphological behavior of cyclic block copolymers. However, the morphological aspects discussed in the aforementioned reports do not cover the topological impact of cyclic block copolymers on their micellization in a comprehensive manner.

In effort to investigate the details of topological impact on micellization of cyclic block copolymers in a more rigorous manner, several reports based on small-angle X-ray scattering (SAXS) have been carried out. SAXS studies of cyclic block copolymer micelles began with the effort of analyzing the form factors of linear and cyclic PS-*b*-PI micelles with complementary small-angle neutron scattering (SANS), TEM, and DLS [37, 38]. Micelles of cyclic PS-*b*-PI were reported to form larger micelles than linear PS-*b*-PI in a polar solvent (*N,N*-dimethylformamide) and nonpolar solvents (decane and heptane). Interestingly, another study reported the unimolecular micellar morphology of linear and cyclic graft copolymers based on polycarbonate backbone and poly(*N*-acryloylmorpholine) [39], in which the cyclic graft copolymer formed a larger unimolecular micelle. Furthermore, a SANS based study reported the formation of cylindrical micelles by cyclic peptide-based block copolymers [40]. While these reports have successfully characterized the general micellar morphologies of linear and cyclic PS-*b*-PIs, the retrieval of specific structural parameters such as micelle core radius, micelle corona thickness, core-corona interface thickness, and radial density distribution was first demonstrated by a study regarding a pair of cyclic PBA-*b*-PEO diblock copolymer and linear PBA-*b*-PEO-*b*-PBA triblock copolymer [41]. This particular study successfully reported numerous structural parameters only by the means of quantitatively analyzing the X-ray scattering data via modeling, and demonstrated the subtle advantages of cyclic diblock copolymer over the linear triblock copolymer with regards to the fundamental chain packing behavior correlated to structural stability of micelles. Following this report, several reports have expanded upon the utilization of modeling approach with more intricate models in quantitatively analyzing SAXS profiles of various cyclic block copolymer micelles [42–44]. One study has characterized the micellization behavior of the cyclic and tadpole iterations of block copolymer based on poly (*n*-decyl glycidyl ether-*block*-2-(2-(2-methoxyethoxy)ethoxy)ethyl glycidyl ether) (PDGE-*b*-PTEGGE) [42]. The inclusion of both cyclic and tadpole counterparts have successfully demonstrated the structural advantages brought by the absence of chain end in the micelle's core and corona. Specifically, the inclusion of cyclic topology in the solvophilic blocks forming micelle corona have been identified to prevent the secondary micellar aggregation. The micelle corona stabilization effect from cyclic topology was also demonstrated by another study based on cyclic and linear PBA-*b*-PEO block copolymer [44].



The conclusions of quantitative SAXS studies collectively support the notion that the cyclic topology enables compact micelle dimensions as well as increased structural stability.

### 26.3 Morphology of Cyclic Polymers in Bulk State

Methods of morphological characterization in solid state do not differ too much from that of solution state. In fact, the characterization methods are still limited to TEM and X-ray scattering for the most. Differential scanning calorimetry (DSC) is at times incorporated as a complementary technique in characterizing the crystallinity and phase transition behaviors. In bulk state, phase separation could occur in both homopolymers and block copolymers. In the case of homopolymers, semi-crystalline characteristic can induce the phase separation between the crystalline and amorphous domains. Poly( $\epsilon$ -caprolactone) (PCL) is a classic example of a semi-crystalline polymer that forms a lamellar structure based on its crystalline and amorphous layers (Fig. 26.3). Thus far, there are three X-ray scattering based studies regarding cyclic and linear PCLs in bulk state [45–47]. For high molecular weight PCLs with  $M_n$  (number-average molecular weight) values ranging from 75,000 to 140,000  $\text{kg mol}^{-1}$ , cyclic topology does not impact the lamellar structure,  $d$ -spacing, and crystallinity [45]. As for cyclic PCLs with relatively lower molecular weight  $M_n$  values 6,200–15,200  $\text{kg mol}^{-1}$ , the crystallinity and relative thickness of crystalline layer against the amorphous layer within the phase separated lamellae increased when compared to linear PCLs of same molecular weight [46, 47]. Thusly, the topological impact of cyclic polymers does show dependency on molecular weight but the threshold molecular weight of PCL where the topological influence takes place

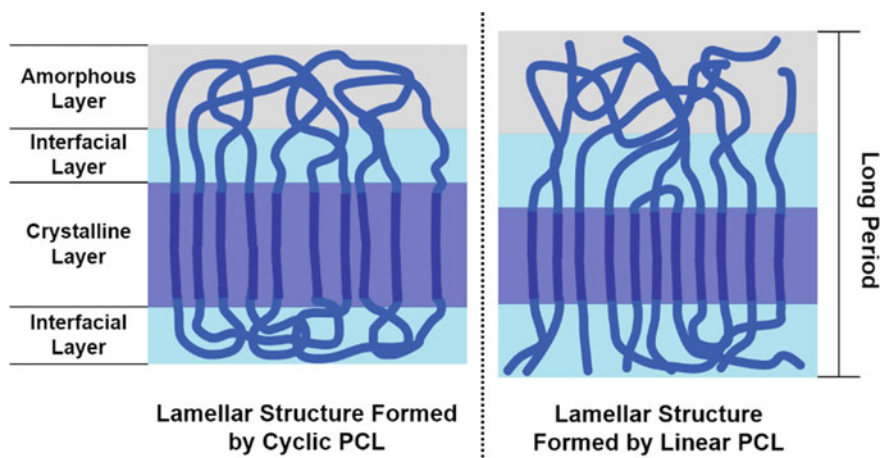


Fig. 26.3 Schematic representation of lamellar structures formed by linear and cyclic PCLs

has not been investigated. In addition, detailed morphological aspects of lamellar structure formed by cyclic PCL such as crystalline layer thickness, amorphous layer thickness, crystalline-amorphous interface thickness, and structural order, have not been characterized as of yet.

As for the investigation of phase separation behavior of cyclic block copolymers, there are a dozen of studies where half of them are experimental and the other half are theoretical. The experimental studies are all based on cyclic block copolymers with both blocks being soft, flexible segments: PS-*b*-PI [48–50], PAA-*b*-PBB [33], poly(styrene-*block*-dimethylsiloxane) [51], poly(styrene-*block*-2-vinylpyridine) [51], poly(styrene-*block*-butadiene) (PS-*b*-PBD) [52], and PEO-*b*-PBO [53]. Various types of morphologies were achieved with cyclic block copolymers such as lamellar [33, 48, 49, 51–53], hexagonally packed cylindrical [33, 49, 52], spherical [49, 52], and gyroid [52] structures. In general, the consensus of these studies is that cyclic topology causes block copolymers to form the same type of structure as their linear counterpart with a 5%–16% shorter *d*-spacing [33, 48, 49, 51]. However, there are some reports with controversial results where block copolymer systems based on PS-*b*-PI [50] and PS-*b*-PBD [52] exhibit different type of morphology between the linear and cyclic block copolymers. In addition, a few studies has demonstrated a 30% *d*-spacing reduction with cyclic PS-*b*-PI [50], as well as 38% *d*-spacing reduction with cyclic PEO-*b*-PBO [53] which are far greater than the other experimental reports. Although all experimental reports agree with the notion that cyclic topology is a key factor in reducing *d*-spacing as a consequence of reduced chain dimensions, the extent of *d*-spacing reduction generally remains unanswered. What is of further interest is the fact that the experimental demonstration of 30% to 38% *d*-spacing reduction [50, 53] agrees with the theoretically predicted *d*-spacing reduction of 30% to 37% [54–59]. There is a caveat to this comparison, however, as the experimentally achieved 30% *d*-spacing reduction [50] also involved a difference in the morphological type; linear PS-*b*-PI achieved cylindrical structure whereas cyclic PS-*b*-PI achieved spherical structure. This behavior disagrees with the theoretical studies, which they reinforce the notion that the cyclic and linear block copolymers should form the same morphological type [54–59]. As for the study reporting 38% *d*-spacing reduction [53], same lamellar structure were observed for both linear and cyclic PEO-*b*-PBO, thereby being the only study to agree with the theoretical studies.

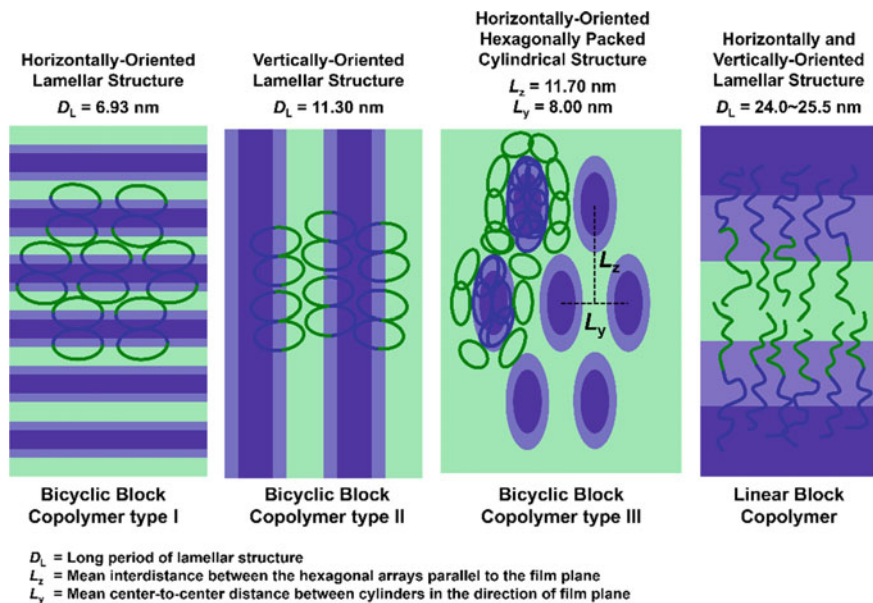
Overall, the experimental and theoretical investigations on the phase separation behaviors of cyclic copolymers in bulk state have demonstrated a variety of morphological types and the reduction of *d*-spacing when compared to the linear counterparts. However, the intricate details regarding the correlation between cyclic topology and bulk morphology such as the subtle differences in interface thickness between the two phases (between crystalline and amorphous, or of different blocks), structural ordering, and the driving force behind the transition in the type of morphology remain largely unexplored.

## 26.4 Morphology of Cyclic Polymers in Thin Films

Morphological behaviors of polymers in thin films differ from the bulk state due to the following factor: geometrical confinement effect. In bulk state, a polymer chain is free to take advantage of the dimensional freedom in all radial directions regarding its chain conformation. In thin film, chain conformation is confronted with a restriction, or a loss of a degree of freedom, in the direction of the film thickness. Consequently, this confinement effect alters the arrangement of polymer chains to accommodate the restrictive dimension in film thickness and result in their respective morphologies in thin films. Hence, one could easily suspect the correlation between this unique aspect of polymer thin films and cyclic topology is indeed, to say the least, intriguing. However, there are only four reports in the literature that investigated the thin film morphologies of cyclic polymers [60–63].

Half of the aforementioned reports are the only reports investigating the effect of cyclic topology on homopolymers in the form of PCL [60, 61]. Both studies utilized synchrotron grazing-incidence X-ray scattering (GIXS) method complemented with DSC to extensively characterize the thin film morphology of cyclic and linear PCLs in conjunction to their phase transition characteristics. It is reported that cyclic PCLs demonstrated thicker crystalline layer within the achieved lamellar structures as well as higher crystallinity than the linear counterparts. These behaviors of cyclic PCLs align with bulk state investigations (Fig. 26.3) [46, 47]. Additionally, the quantitative characterization of GIXS measurements has also unveiled the fact that, for PCL, cyclic topology greatly reduces the thickness of amorphous layer and increases the interface layer when compared to the linear topology [60]. It is also reported that cyclic topology increases the ordering of lamellar structure as well as the lamellar orientation with respect to the film substrate [61]. These insights inform that cyclic topology is indeed an advantageous factor for promoting PCL crystallization and lamellar formation under geometrical confinement. This unique insights regarding PCLs must be explored and tested for other semi-crystalline homopolymers in thin films.

The remaining two reports investigate the thin film morphologies of systems based on poly(styrene-*block*-ethylene oxide) (PS-*b*-PEO) [62], and PDGE-*b*-PTEGGE [63]. The former report, which utilized GIXS and AFM, has shown that cyclic PS-*b*-PEO achieves the same cylindrical structure as the linear counterpart but with a 25% shorter *d*-spacing [62]. The extent of morphological characterization was only limited to the identification of morphological type and *d*-spacing, however. The case of latter report regarding PDGE-*b*-PTEGGE based block copolymers, which utilized quantitative analysis of GIXS measurements, has demonstrated astounding 51.3%–72.8% *d*-spacing reduction, highly improved structural ordering and orientation, as well as confirming different morphological types compared to linear block copolymer (Fig. 26.4) [63]. It must be noted, however, that these block copolymers possessed bicyclic topology rather than the conventional cyclic topology.



**Fig. 26.4** Schematic representation of lamellar and cylindrical structures formed by bicyclic and linear PDGE-*b*-PTEGGE block copolymers in thin films

Thin film morphology remains as the least explored aspect of cyclic polymers and is in need of more input from both the experimental and theoretical investigations. The three reports mentioned in this section demonstrate the clear differences in the behavior of cyclic and linear polymers in thin film. In addition, the aforementioned study on bicyclic block copolymers [63] further demonstrate that there are unknown territories regarding the correlation between polymer morphology and complex variations of cyclic topologies.

## 26.5 Concluding Remarks

The current state of the morphological characterization of cyclic polymers in solution, bulk, and thin films has achieved important progress in comprehending the complex characteristics brought by cyclic topology. Notably, cyclic topology promotes the formation of more compact structures for both homopolymers and block copolymers. The dimensional reduction could also occur with a transition of the type of morphology. These experimental and theoretical conclusions denote cyclic topology as a powerful tool for altering and fine-tuning the chain conformation behavior of polymers. The extent of topological influence from cyclic topology to polymer morphology, and further implications related to physical properties is, however, under

investigation at primary stages. Moreover, the lack of variety in the chemical compositions and types of homopolymers and block copolymers also leave more research effort to be invested. Thorough comprehension of the correlation between cyclic topology and morphology remains an urgent challenge that must be addressed in order to continue and realize the development of cyclic polymers and related potential applications.

## References

1. S. Honda, T. Yamamoto, Y. Tezuka, *J. Am. Chem. Soc.* **132**, 10251–10253 (2010)
2. B.A. Laurent, S.M. Grayson, *Chem. Soc. Rev.* **38**, 2202–2213 (2009)
3. J. Cooke, K. Viras, G.-E. Yu, T. Sun, T. Yonemitsu, A.J. Ryan, C. Price, C. Booth, *Macromolecules* **31**, 3030–3039 (1998)
4. M.A. Cortez, W.T. Godbey, Y. Fang, M.E. Payne, B.J. Cafferty, K.A. Kosakowska, S.M. Grayson, *J. Am. Chem. Soc.* **137**, 6541–6549 (2015)
5. T. Yamamoto, Y. Tezuka, *Soft Matter* **11**, 7458–7468 (2015)
6. J.A. Semlyen (ed.), *Cyclic Polymers*, 2nd edn. (Kluwer Academic Publishers, Dordrecht, Netherlands, 2002)
7. H.R. Kricheldorf, *J. Polym. Sci. Part A: Polym. Chem.* **48**, 251–284 (2010)
8. Z. Jia, M.J. Monteiro, *J. Polym. Sci. Part A: Polym. Chem.* **50**, 2085–2097 (2012)
9. L. Xiang, W. Ryu, H. Kim, M. Ree, *Polymers* **10**, 577 (2018)
10. B.H. Zimm, W.H. Stockmayer, *J. Chem. Phys.* **17**, 1301–1314 (1949)
11. K. Dodgson, J.A. Semlyen, *Polymer* **18**, 1265–1268 (1977)
12. G. Hild, A. Kohler, P. Rempp, *Eur. Polym. J.* **16**, 525–527 (1980)
13. J. Roovers, P.M. Toporowski, *Macromolecules* **16**, 843–849 (1983)
14. H.R. Kricheldorf, S.-R. Lee, N. Schittenhelm, *Macromol. Chem. Phys.* **199**, 273–282 (1998)
15. H.R. Kricheldorf, S. Eggerstedt, *Macromol. Chem. Phys.* **199**, 283–290 (1998)
16. N. Hadjichristidis, M. Pitsikalis, S. Pispas, H. Iatrou, *Chem. Rev.* **101**, 3747–3792 (2001)
17. Y. Tezuka, R. Komiyama, *Macromolecules* **35**, 8667–8669 (2002)
18. B.A. Laurent, S.M. Grayson, *J. Am. Chem. Soc.* **128**, 4238–4239 (2006)
19. S. Hayashi, K. Adachi, Y. Tezuka, *Polym. J.* **40**, 572–576 (2008)
20. H. Durmaz, A. Dag, G. Hizal, U. Tunca, *J. Polym. Sci. Part A: Polym. Chem.* **48**, 5083–5091 (2010)
21. A.F. Voter, E.S. Tillman, *Macromolecules* **43**, 10304–10310 (2010)
22. B. Liu, H. Wang, L. Zhang, G. Yang, X. Liu, I. Kim, *Polym. Chem.* **4**, 2428–2431 (2013)
23. D. Lu, Z. Jia, M.J. Monteiro, *Polym. Chem.* **4**, 2080–2089 (2013)
24. S. Long, Q. Tang, Y. Wua, L. Wang, K. Zhang, Y. Chen, *React. Funct. Polym.* **80**, 15–20 (2014)
25. T. Ogawa, K. Nakazono, D. Aoki, S. Uchida, T. Takata, *ACS Macro Lett.* **4**, 343–347 (2015)
26. J.H. Butler, D.C. Joy, G.F. Bradley, S.J. Krause, *Polymers* **36**, 1781–1790 (1995)
27. D.J. Smith, *Mater. Today* **11**, 30–38 (2008)
28. M.R. Libera, R.F. Egerton, *Polym. Rev.* **50**, 321–339 (2010)
29. H. Aoki, *Microscopy* **66**, 223–233 (2017)
30. J.-L. Putaux, E. Minatti, C. Lefebvre, R. Borsali, M. Schappacher, A. Deffieux, *Faraday Discuss.* **128**, 163–178 (2005).
31. N. Ouarti, P. Viville, R. Lazzaroni, E. Minatti, M. Schappacher, A. Deffieux, R. Borsali, *Langmuir* **21**, 1180–1186 (2005)
32. N. Ouarti, P. Viville, R. Lazzaroni, E. Minatti, M. Schappacher, A. Deffieux, J.-L. Putaux, R. Borsali, *Langmuir* **21**, 9085–9090 (2005)
33. S. Honda, M. Koga, M. Tokita, T. Yamamoto, Y. Tezuka, *Polym. Chem.* **6**, 4167–4176 (2015)
34. G.-E. Yu, Z. Yang, D. Attwood, C. Price, C. Booth, *Macromolecules* **29**, 8479–8486 (1996)

35. Y. Zhao, Y.-T. Liu, Z.-Y. Lu, C.-C. Sun, *Polymer* **49**, 4899–4909 (2008)
36. Y.-L. Lin, M.-Z. Wu, Y.-J. Sheng, H.-K. Tsao, *J. Chem. Phys.* **136**, 104905 (2012)
37. E. Minatti, R. Borsali, M. Schappacher, A. Deffieux, V. Soldi, T. Narayanan, J.-L. Putaux, *Macromol. Rapid Commun.* **23**, 978–982 (2002)
38. E. Di Cola, C. Lefebvre, A. Deffieux, T. Narayanan, R. Borsali, *Soft Matter* **5**, 1081–1090 (2009)
39. R.J. Williams, A. Pitto-Barry, N. Kirby, A.P. Dove, R.K. O'Reilly, *Macromolecules* **49**, 2802–2813 (2016)
40. J. Yang, J.-I. Song, Q. Song, J.Y. Rho, E.D.H. Mansfield, S.C.L. Hall, M. Sambrook, F. Huang, S. Perrier, *Angew. Chem. Int. Ed.* **59**, 8860–8863 (2020)
41. K. Heo, Y.Y. Kim, Y. Kitazawa, M. Kim, K.S. Jin, T. Yamamoto, M. Ree, *ACS Macro Lett.* **3**, 233–239 (2014)
42. B.J. Ree, Y. Satoh, K.S. Jin, T. Isono, W.J. Kim, T. Kakuchi, T. Satoh, M. Ree, *NPG Asia Mater.* **9**, e453 (2017)
43. B.J. Ree, J. Lee, Y. Satoh, K. Kwon, T. Isono, T. Satoh, M. Ree, *Polymers* **10**, 1347 (2019)
44. B.J. Ree, T. Satoh, T. Yamamoto, *Polymers* **11**, 163 (2019)
45. E.J. Shin, W. Jeong, H.A. Brown, B.J. Koo, J.L. Hedrick, R.M. Waymouth, *Macromolecules* **44**, 2773–2779 (2011)
46. Y. Mato, K. Honda, K. Tajima, T. Yamamoto, T. Isono, T. Satoh, *Chem. Sci.* **10**, 440–446 (2019)
47. Y. Mato, K. Honda, B.J. Ree, K. Tajima, T. Yamamoto, T. Deguchi, T. Isono, T. Satoh, *Comm. Chem.* **3**, 97 (2020)
48. K. Ishizu, A. Ichimura, *Polymer* **39**, 6555–6558 (1998)
49. A. Takano, O. Kadoi, K. Hirahara, S. Kawahara, Y. Isono, J. Suzuki, Y. Matsushita, *Macromolecules* **36**, 3045–3050 (2003)
50. S. Lecommandoux, R. Borsali, M. Schappacher, A. Deffieux, T. Narayanan, C. Rochas, *Macromolecules* **37**, 1843–1848 (2004)
51. R.L. Lescanec, D.A. Hajduk, G.Y. Kim, Y. Gan, R. Yin, S.M. Gruner, T.E. Hogen-Esch, E.L. Thomas, *Macromolecules* **28**, 3485–3489 (1995)
52. Y. Zhu, S.P. Gido, *Macromolecules* **36**, 148–152 (2003)
53. J.F. Marko, *Macromolecules* **26**, 1442–1444 (1993)
54. A.J. Ryan, S.-M. Mai, J.P.A. Fairclough, I.W. Hamley, C. Booth, *Phys. Chem. Chem. Phys.* **3**, 2961–2971 (2001)
55. W.H. Jo, S.S. Jang, *J. Chem. Phys.* **111**, 1712–1720 (1999)
56. H.-J. Qian, Z.-Y. Lu, L.-J. Chen, Z.-S. Li, C.-C. Sun, *Macromolecules* **38**, 1395–1401 (2005)
57. G. Zhang, Z. Fan, Y. Yang, F. Qiu, *J. Chem. Phys.* **135**, 174902 (2011)
58. L. He, Z. Chen, R. Zhang, L. Zhang, Z. Jiang, *J. Chem. Phys.* **138**, 094907 (2013)
59. A.D. Goodson, J.E. Troxler, M.S. Rick, H.S. Ashbaugh, J.N.L. Albert, *Macromolecules* **52**, 9389–9397 (2019)
60. L. Xiang, W. Ryu, J. Kim, M. Ree, *Polym. Chem.* **11**, 4630–4638 (2020)
61. B.J. Ree, Y. Mato, L. Xiang, J. Kim, T. Isono, T. Satoh, *Polym. Chem.* (2021). <https://doi.org/10.1039/D0PY01567A>
62. J.E. Poelma, K. Ono, D. Miyajima, T. Aida, K. Satoh, C.J. Hawker, *ACS Nano* **6**, 10845–10854 (2012)
63. B.J. Ree, Y. Satoh, T. Isono, T. Satoh, *Nano Lett.* **9**, 6520–6525 (2020)

# Chapter 27

## Transforming Cyclic/Linear Polymer Topologies: Emerging Techniques and Opportunities



Satoshi Honda and Minami Oka

In this chapter, we describe linear–cyclic topological transformation, involving the cleavage/reformation of covalent bonds based on dynamic covalent chemistry. We first briefly present reaction designs for topological transformation and then introduce particular examples of linear–cyclic topological transformation. Finally, dynamic functions based on topological transformations including linear–cyclic topological transformation are discussed.

### 27.1 Introduction

Many of us first encountered structural formulas of polymers in high school chemistry. They were expressed simply by enclosing the repeating unit of the structure within parentheses, leaving no room for us to think about the structure outside the parentheses. However, the topology of polymers, or the connectivity of the main chains, such as branched and cyclic structures, is characterized by the structure outside the parentheses. Nevertheless, it had long been assumed that the physical properties of polymers are governed by the structure inside the parentheses, such as the functional group of the side chain and stereoregularity, because the structure outside the parentheses makes up only a small part of the entire polymer chain. However, with the development of organic/polymer synthesis allowing precise manipulation of polymer topology, the difference in topology alone leads to different physical properties, even in polymers with the same chemical composition and molecular weight. This also applies to cyclic polymers with intramolecularly linked ends outside the parentheses. Cyclic polymers have been shown to self-assemble to form a molecular assembly, amplifying the difference in the physical properties of

---

S. Honda (✉) · M. Oka  
The University of Tokyo, 3-8-1 Komaba, Meguro-ku, Tokyo 153-8902, Japan  
e-mail: [c-honda@mail.ecc.u-tokyo.ac.jp](mailto:c-honda@mail.ecc.u-tokyo.ac.jp)

each polymer and exhibiting properties different from those of a molecular assembly formed by linear polymers. However, most studies conducted thus far only compared the physical properties of polymers with different topologies, and we are now entering an era in which polymer functions may be dynamically manipulated by recombining polymer topologies on demand.

The transformations of linear–star [1], linear–cyclic [2–4], and star–network [5] topologies have been reported as typical polymer topological transformations. The transformations of these polymer topologies typically involve the cleavage or reformation of covalent or noncovalent bonds, and the chemical species that enable dynamic bond formation play a key role in each case. In this chapter, we introduce the linear–cyclic topological transformation, involving the cleavage/reformation of covalent bonds (also called dynamic covalent bonds [6–8]) by using relevant examples of polymer topological transformations.

## 27.2 Reaction Design for Topological Transformation

Topological transformation of polymers is realized through functional groups that can reversibly cleave certain bonds in the main or side chains and is characterized by different main-chain connectivities, depending on the cleaved or reformed state of the molecular chain. Covalent bonds, generally strong, are not in a dissociation equilibrium state in a normal environment. For the application of chemical stimulation for the reversible cleavage of molecular chains, which requires the use of reagents, numerous bond cleavage/reformation reactions and topological transformations have been reported. However, this section focuses on the reactions that can reversibly cleave only certain bonds by physical stimulation, such as thermal, light, or mechanical stimulation, and does not discuss chemical stimulation.

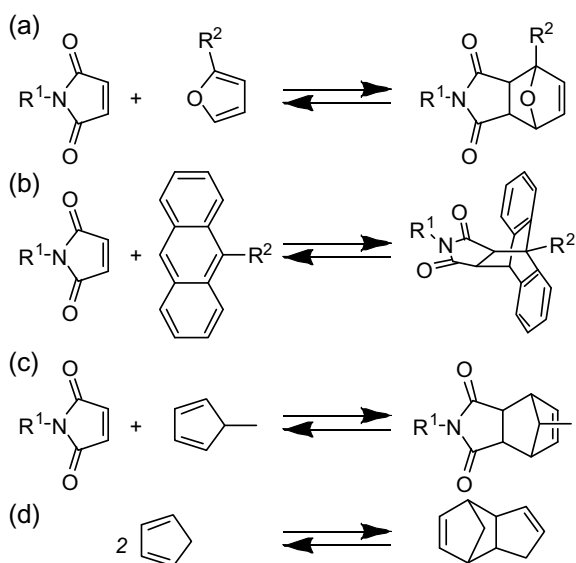
### 27.2.1 *Reversible Cycloaddition Reaction*

Atomic groups that dissociate/reform by thermal or light stimulation have been used for dynamic recombination of polymer topologies. The Diels–Alder and retro-Diels–Alder reactions are typical reversible reactions caused by thermal stimulation, and the reactions between maleimide and furan [9, 10], maleimide and anthracene [11, 12], and maleimide and fulvene [13, 14], in addition to the reversible dimerization reaction of cyclopentadiene [15, 16], have long been reported and applied for fabricating polymer materials (Fig. 27.1) [17, 18].

Many of the molecular species involved in reversible dimerization reactions by light stimulation, such as cinnamate [19–21], stilbene [22, 23], thymine [24–26], coumarin [27], and anthracene [28, 29], have also been actively introduced into polymer materials (Fig. 27.2).



**Fig. 27.1** Diels–Alder and retro-Diels–Alder reactions between **a** maleimide and furan, **b** maleimide and anthracene, **c** maleimide and fulvalene, and **d** cyclopentadienes

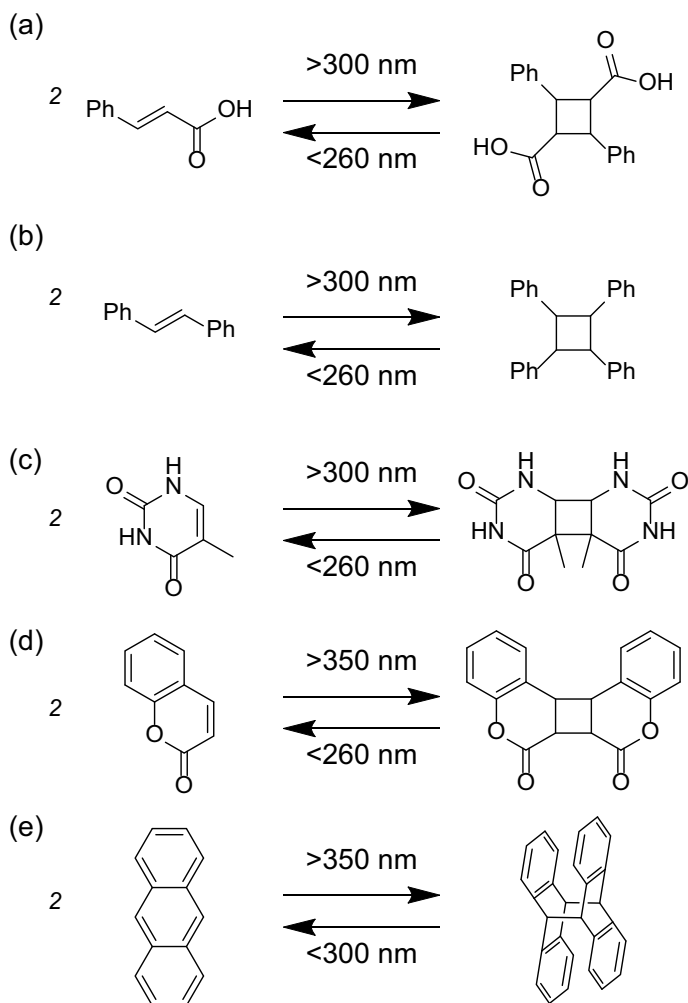


For example, Zheng et al. reported the star–network topological transformation by UV irradiation of eight-arm star-shaped poly (ethylene oxide) (PEO) with anthracene end groups (PEO-anthracene) (Fig. 27.3) [30]. The study showed that the aqueous solution of water-soluble PEO-anthracene cast into a glass cell formed a network upon UV irradiation at 365 nm, swelling to form a transparent gel sheet. Moreover, UV irradiation at 254 nm cleaved the dimerized anthracene motifs, increasing the size of the network and the degree of swelling. Because the photodimerization of anthracene is reversibly influenced by altering the wavelength of irradiated light, this phenomenon can be regarded as a star–network reversible topological transformation.

A linear–network topological transformation by light irradiation of linear polysiloxane containing coumarin side chains has been reported (Fig. 27.4) [31–33]. In this study, because the linear polysiloxane with coumarin side chains formed a network of noncovalent bonds via  $\pi$ – $\pi$  interactions even in the absence of dimerized coumarin, the change in viscoelasticity due to the recombination of polymer topologies was not significantly large at room temperature. In contrast, light irradiation of the linear polysiloxane with coumarin side chains after heating to a molten state cause a considerable change in viscoelasticity.

### 27.2.2 Cyclization by Stable Radicals

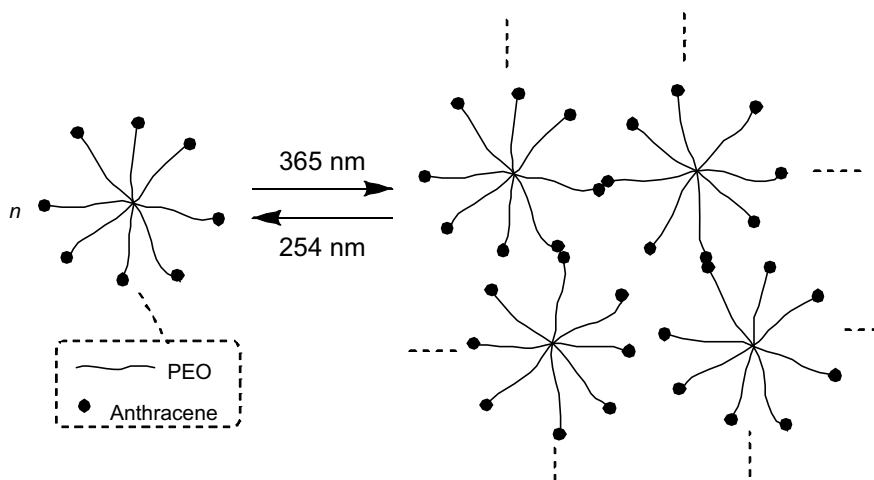
One of the dissociation/reformation reactions is the reversible radical reaction. While radical reactions can be applied to high-speed topological transformations by utilizing highly reactive radicals, reaction selectivity and controllability have been proven as



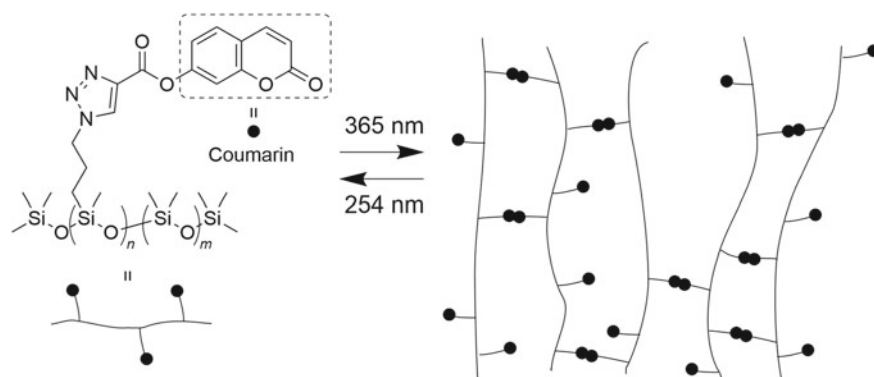
**Fig. 27.2** Reversible photodimerization reactions between **a** cinnamic acid, **b** stilbene, **c** thymine, **d** coumarin, and **e** anthracene

challenging. Polymer topological transformation using radical reactions includes the recombination of connectivities using the chain transfer reaction of thiyl radicals [34]. The chain transfer reaction proceeded by introducing allyl sulfide, which can reversibly dissociate/reform, into a polymer main chain and generating radicals by light irradiation, resulting in the recombination of the connectivities at the allyl sulfide motif (Fig. 27.5).

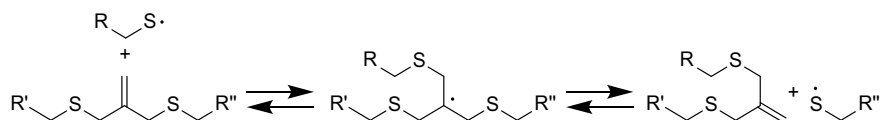
In contrast, some radical species reversibly dimerize. A classic example of famous radical species is the triphenylmethyl radical, which is at equilibrium with its dimer [35]. While the triphenylmethyl radical has low dimerization selectivity and an



**Fig. 27.3** Photoreversible sol-gel transition based on star-network topological transformation of aqueous PEO mixture

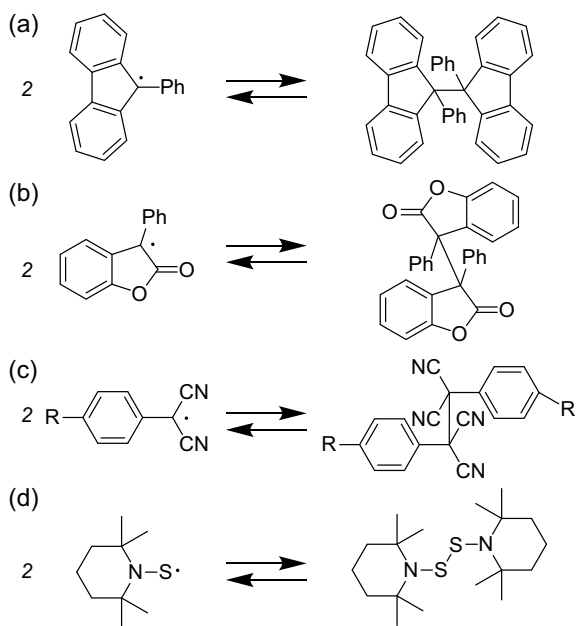


**Fig. 27.4** Photoreversible crosslinking reaction of linear polysiloxanes containing coumarin side chains



**Fig. 27.5** Alteration of the network topology by chain transfer reaction of thiyl radicals

**Fig. 27.6** Reversible dimerizations of **a** 9-phenylfluorenyl, **b** arylbenzofuranone, **c** dicyanomethylphenyl, and **d** thionitroxide radicals

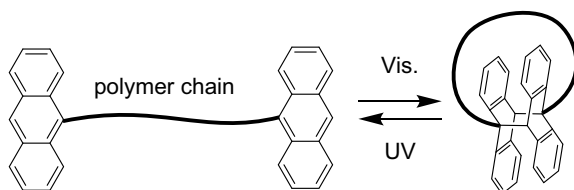


inevitable drawback of irreversible side reactions, continuous effort in the related field discovered various radical species that allow selective reversible dimerization reactions [36]. Representative examples include fluorenyl [37, 38], arylbenzofuranone [39–41], dicyanomethylphenyl [39, 42, 43], thionitroxide [44–46], and triphenylimidazolyl radicals [47–49]. Although many of these are reaction systems that achieve bonding/dissociation equilibrium by external stimulation, some radical species, such as the arylbenzofuranone radical, are in at bonding/dissociation equilibrium even at room temperature. In addition, the stability and reactivity of radical species can be modified by changing their substituent groups. However, most of these radical species were accidentally discovered and it has been difficult to design rationally. Nevertheless, these radical species, despite being stable radicals, can be utilized for topological transformations with properties different from those of cycloaddition reactions, such as enabling high-speed reactions unique to highly reactive radical species (Fig. 27.6).

### 27.3 Linear–Cyclic Topological Transformations Based on Cycloaddition Reactions

The Diels–Alder reaction is a cycloaddition reaction that has long been used for cyclic polymer synthesis [50]. It is used for linear–cyclic topological transformations because the reverse reaction, the retro-Diels–Alder reaction, occurs when the

**Fig. 27.7** Linear–cyclic topological transformation by reversible dimerization of anthracene end groups under dilution

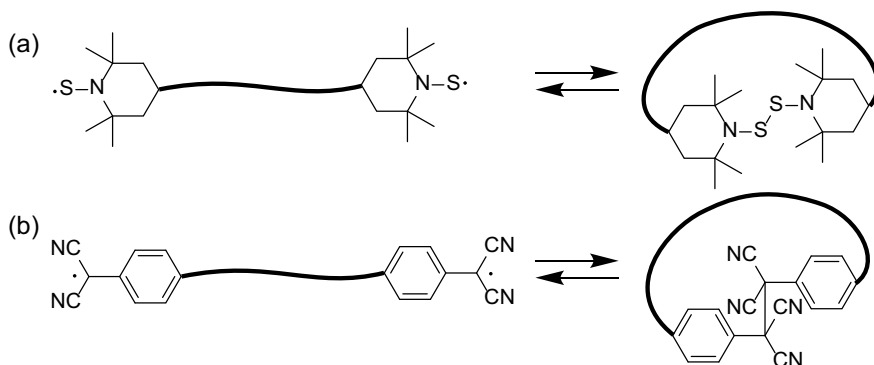


precursor diene and/or dienophile is stable. In 1999, Shiomi et al. synthesized a cyclic poly (methyl methacrylate) (PMMA) through cycloaddition, in which a linear PMMA, with maleimidyl and pentadienyl end groups, was cyclized by the Diels–Alder reaction [51]. Importantly, the cyclization lowered the glass transition temperature ( $T_g$ ) of PMMA by more than 40 °C. Since then, various cyclic polymer syntheses through cycloaddition have been reported, including the Diels–Alder cyclization of a linear polymer with maleimide and either furan [52], anthracene [53], or cyclopentadiene [54] as end groups. Although there were few cases explicitly focusing on the reversibility or retro-Diels–Alder reaction, Zhang et al. reported linear–cyclic topological transformations could occur by the Diels–Alder reaction, as well as the subsequent retro-Diels–Alder reaction, of a linear polymer with furan and maleimide as end groups [52].

In contrast, the extensively studied reversible photodimerization reaction systems have been effectively exploited to linear–cyclic topological transformations. One early work is based on the reversible photodimerization of anthracene reported by Tung et al. [55]. Subsequently, this reversible photodimerization system (Fig. 27.7) has been widely investigated, following the papers by Desvergne et al. [56] and Tung et al. [57]. An interesting case was published by Harada et al. in 2003 on the reversible intramolecular cyclization of cyclodextrin-encapsulated PEO with anthracene end groups, which is considered as the pioneering research that combined topological transformations with supramolecular chemistry [58]. On the other hand, the simple linear–cyclic topological transformations by this approach have been receiving attention continuously; recent reports, published more than 20 years from the aforementioned pioneering works, include works by Kim et al. in 2015 on a polyester system [59] and by Yamamoto et al. on a system using PEO and polytetrahydrofuran [60]. More recently, Barner-Kowollik et al. reported a linear–cyclic topological transformation based on reversible photodimerization of styrylpyrene [61]. As the variation of substitution groups with cinnamate, stilbene, thymine, coumarin, and anthracene allows the tuning of responsivity, continuous studies in the related field will lead to the birth of various linear–cyclic topological transformations.

## 27.4 Linear–Cyclic Topological Transformations Based on Radical Reactions

In reality, the number of radical species that enable reversible bonding is low compared to those undergo reversible cycloaddition reactions; thus, radical species is not widely exploited to linear–cyclic topological transformations. Yet, the number of reports has gradually increased along with the progress in organic and polymerization reactions. In 1996, Hawker et al. reported the cross-reactivity of 2,2,6,6-tetramethylpiperidine-1-oxyl (TEMPO) in nitroxide-mediated polymerization, which suggested the applicability of stable radicals for polymer reactions [62]. This concept of cross-reactivity was applied to the end-group transformation of a linear polymer by Zavarine et al. [63], where the reaction was achieved by the reversible generation of radicals by TEMPO at a temperature of 125 °C. And the concept was extended to reorganization of various polymer topologies [64], including reversible radical ring-crossover polymerization reported by Otsuka et al. [65]. They also reported a linear–cyclic topological transformation based on the dimerization of 2,2,6,6-tetramethylpiperidine-1-sulfanyl, a sulfur-containing analog of TEMPO (Fig. 27.8a) [66–68]. Moreover, there have recently been cases in which linear–cyclic topological transformation is achieved by a small molecule, with a dicyanomethylphenyl radical introduced at both ends of an alkyl linker (Fig. 27.8b) [69]. In this area, classical stable radical species have been utilized for linear–cyclic topological transformation, yet explorations for a novel stable radical species would readily be extended to further intriguing linear–cyclic topological transformation systems in the future.



**Fig. 27.8** Linear–cyclic topological transformations by **a** thionitroxide and **b** dicyanomethylphenyl radicals

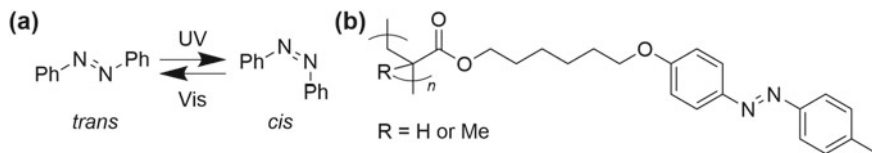
## 27.5 Creation of Dynamic Functions Based on Topological Transformations

As shown above, various linear–cyclic topological transformations caused by physical stimulation have been reported to date. However, this methodology has not been industrialized, to the best of our knowledge. Hence, development of practical functional materials based on linear–cyclic topological transformations should hold the key for next-generation innovation in material development, considering the research demands of achieving practical functions by harmonization of the linear–cyclic topological transformation reaction characteristics, the main chain polymer properties, and potential applications. In this section, we introduce recent developments in the application of topological transformations to development of materials exhibiting dramatic shift in their properties.

### 27.5.1 *Development of Polymers that Control Viscoelasticity with Recombination of Network–Star–8-Shaped Topology*

In the world of fiction, such as science fiction movies and manga, we often see characters who can change their appearance at will. In materials science, this ability can be described as a function of “free viscoelasticity control over a part of or entire substance.” Recently, the number of studies on controlling the viscoelasticity of a substance by light stimulation has increased rapidly, turning the events in the world of fiction into a possible reality. Unlike thermal stimulation, which tends to be transmitted over a wide or entire area of a substance, light stimulation has spatiotemporal locality. Therefore, it is studied as an unconventional method of controlling/processing substance morphology and for its application in adhesive preparation.

The sol–gel transformation has been known as the phenomenon of fluidization and non-fluidization of a solvent-containing mixture by external stimulation. However, gel materials have a drawback in that their properties change with the evaporation of their solvent component, and use of a substance in which fluidity can be changed even without a solvent component is necessary. In 1990, however, Koshihara et al. discovered a phenomenon known as the light-induced phase transition, in which the phase transition of a substance is caused by light stimulation in the absence of a solvent component [70]. In recent years, molecules that crystallize and melt through light-induced phase transitions, reported by several research groups, have attracted attention [71, 72]. These molecules contain multiple azobenzene moieties with steric conformational changes between the *trans* and *cis* isomers by photoisomerization (Fig. 27.9a). With their azobenzene moieties in the *trans* conformation, these molecules are easily arranged and crystallized because of their planar steric structure. In contrast, with their azobenzene moieties in the *cis* conformation, these



**Fig. 27.9** **a** Photoisomerization of azobenzene and **b** an example of an azobenzene side-chain polymer

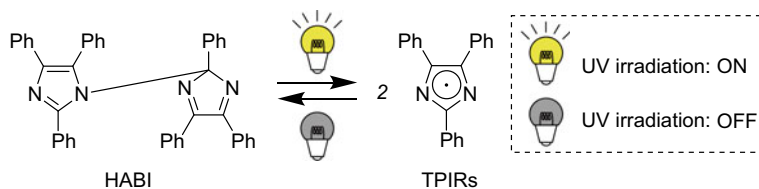
molecules melt as they do not easily arrange because of their bent steric structure. As the light-induced phase transition does not require a solvent component, unlike the gel materials, no changes in the properties of these molecules are caused by solvent evaporation and it is environmentally safe. However, because these low molecular weight substances are generally obtained as crystals, liquids, or a mixture thereof, they are ineffective for controlling viscoelasticity. In contrast, polymers inherently exhibit viscoelasticity because of entanglement of the molecular chains, which may be easily controlled by thermal stimulation. The discovery of polymer materials in which viscoelasticity can be modified only by light stimulation will be a breakthrough.

The change in viscoelasticity upon light stimulation of a polymer with an azobenzene side chain has been recently reported (Fig. 27.9b) [73]. The  $T_g$  of this polymer is higher than room temperature when the azobenzene side chain is in the *trans* conformation and lower than room temperature when it is photoisomerized to the *cis* isomer, demonstrating that viscoelasticity can be controlled without requiring a solvent component. However, the change in viscoelasticity exhibited by this polymer is based on the photoisomerization of the azobenzene side chain, limiting further side-chain functionalization.

Furthermore, silicone materials, commonly found in our daily lives, have the properties of either a solid or liquid. Silicone materials are used as silicone oil and grease because of their fluidity, while their crosslinked product, known as silicone rubber, lacks fluidity. In addition, various functional groups can be introduced into the polysiloxane side chain. If the polysiloxane topology can be reversibly transformed, it is possible to create a functional substance that exhibits a drastic change in viscoelasticity, while leaving room for the modification of the side chains. Based on this idea, Honda et al. developed poly (dimethyl siloxane) (PDMS) functionalized with hexaarylimidazole (HABI). The HABI can be synthesized by one-step simple oxidation of 2,4,5-triphenylimidazole (lophine) into triphenylimidazolyl radical (TPIR) and its selective dimerization. Upon UV irradiation, the bond between the two imidazole rings of HABI is cleaved to form a pair of triphenylimidazolyl radicals (TPIRs), and the termination of UV irradiation results in the rebonding of the TPIR pairs, returning to HABI (Fig. 27.10) [47].

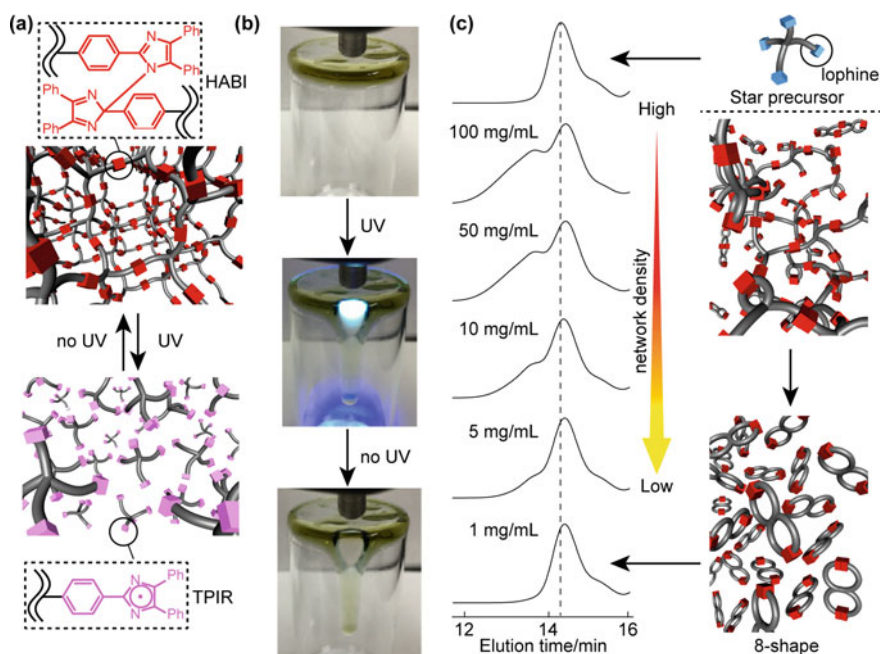
The TPIR is stable in the presence of oxygen [48], and the bond formed at the time of TPIR rebonding by the termination of UV irradiation is either a C–C, C–N, or N–N bond, leading to the formation of six isomers of HABI [74]. The rate of the TPIR-formation reaction associated with light irradiation of HABI is only 80 fs [75], and





**Fig. 27.10** Photocleavage of HABI into TPIRs and their rebonding into HABI by terminating photoirradiation

the reaction is stable in the presence of oxygen despite the radical product formed. Furthermore, there is the potential for introducing substituent groups onto HABI, and functionalization by these HABI motifs is expected in the future. In fact, Honda et al. have succeeded at the network–star topological transformation of PDMS based on the photoreaction of HABI (Fig. 27.11a) [76]. In response to light stimulation, network PDMS linked by HABI exhibited a large change in physical properties; the irradiated area fluidized and flowed (Fig. 27.11b, top and middle). This change



**Fig. 27.11** **a** Conceptual illustration of network–star topological transformation based on the photocleavage of HABI into the pair of TPIRs and their selective recoupling into HABI. **b** Photographs of network PDMS on a vial before (top), during (middle), and after (bottom) UV irradiation. **c** GPC traces of the products after UV irradiation to THF dispersions (1–100 mg/ml) of network PBA (left) and conceptual illustration of the topologies of product polymers (right). Reproduced from [76] (CC BY)

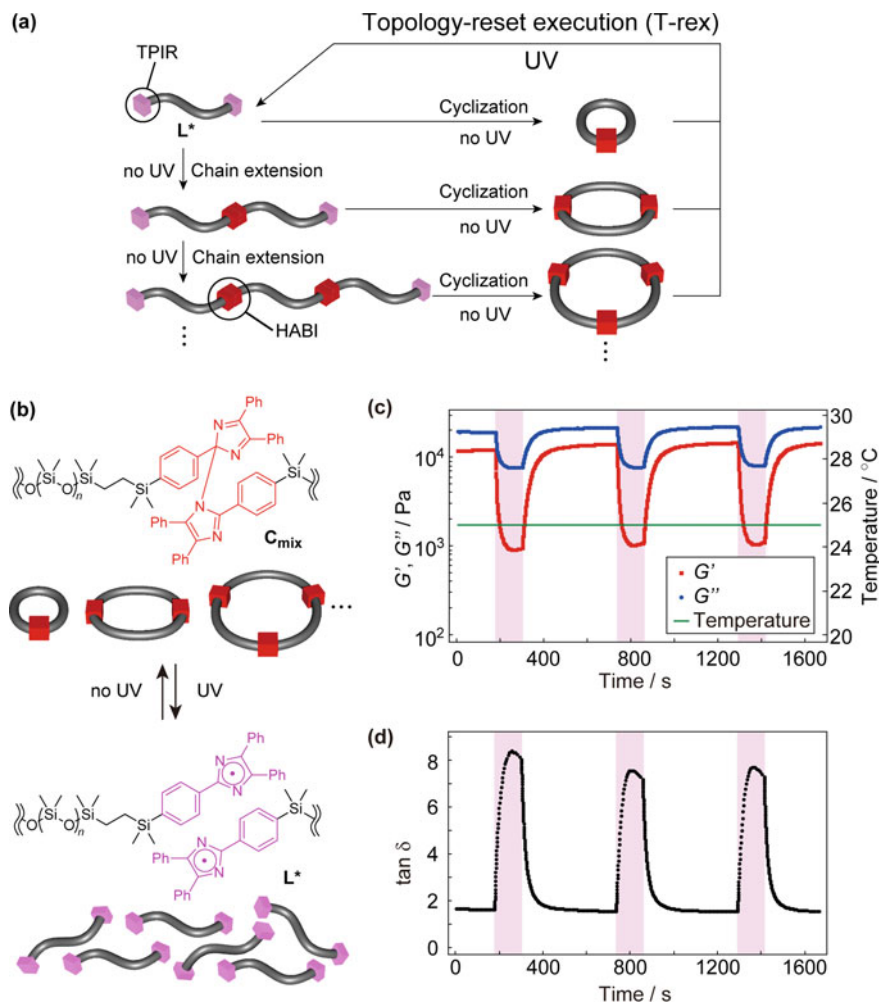
corresponds to the formation of a fluid-star-PDMS with TPIR end groups, due to the cleavage of the network by UV<sub>365</sub> irradiation (Fig. 27.11a). In addition, the network was regenerated upon the termination of UV<sub>365</sub> irradiation due to the rebonding between TPIRs leading to the loss of fluidity (Fig. 27.11b, bottom). This type of topological transformation that does not require a solvent has practical advantages.

In a solvent, however, this photoreaction is expected to change the proportion of products formed by the intermolecular and intramolecular reactions, and with sufficient dilution, the intramolecular reaction would first occur, producing 8-shaped polymers. Therefore, network poly (butyl acrylate) (PBA), with a uniform molecular weight, having HABI in the molecular chain, was synthesized and a mixture of network PBA and THF in various ratios was analyzed by SEC after light irradiation (Fig. 27.11c). As the mixing ratio of the network PBA decreased, the network PBA dissolved, rather than swelled, and a further decrease in the network PBA concentration resulted in the formation of 8-shaped PBA (Fig. 27.11c, bottom). Therefore, the essence of this system was a network–star–8-shaped topological transformation, including a ring-containing 8-shaped topology.

The ability to transform the topology of a material, even if the composition remains the same, would diversify its provisional forms. For example, the non-fluid network polymer packaged without any change in its topology is a solid. In contrast, the fluid 8-shaped polymer is a liquid, but can be used as a non-fluid network polymer if irradiated with UV light.

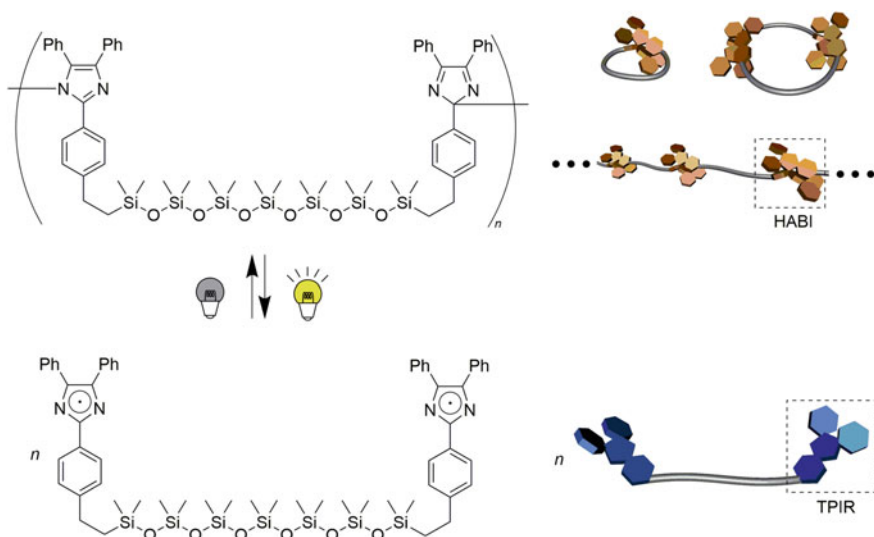
### ***27.5.2 Development of Silicone Materials with Physical Properties Changed by Recombination of Cyclic–Linear Topology***

Topological transformation based on the photoreaction of HABI is achieved by the most basic cyclic–linear topological transformation. Considering the process of HABI formation by linear polymers with TPIR end groups ( $L^*$ ) in a conceptual diagram, the intermolecular cyclization reaction produces cyclic polymers, while the intermolecular chain extension reaction produces a linear polymer with a longer chain (Fig. 27.12a). Eventually, this process depletes available TPIR end groups entirely to produce a mixture of cyclic polymers ( $C_{\text{mix}}$ ) with various ring sizes. Irradiation of the produced  $C_{\text{mix}}$  with UV light will reset the polymers to  $L^*$ , which is the minimum structural unit of the polymer (Fig. 27.12a). Honda et al. denoted such a topological operation as a topology-reset execution (T-rer) [77]. Cyclic PDMS ( $C_{\text{mix}}$ ) with HABI in its synthesized molecular chain is a liquid polymer with fluidity, suggesting that fluidity control can be achieved with a cyclic–linear topological transformation while maintaining the liquid state (Fig. 27.12b). Such materials are important in their applications for oil and grease that require viscosity adjustment. In general, liquids have the relationship of loss modulus ( $G''$ ) > storage modulus ( $G'$ ), which was also



**Fig. 27.12** **a** Conceptual diagram of T-rex. The rectangular solids at the ends of a linear polymer represent the TPIRs, and the cubes that are twice the size of the TPIRs represent HABI. **b** Photo-triggered T-rex for PMDS with HABI in the chains. Time course measurements of **c**  $G'$ ,  $G''$ , and **d**  $\tan \delta (G''/G')$  associated with the ON–OFF cycle of UV irradiation of  $C_{mix}$ . The shaded areas represent the presence of UV radiation. Reproduced from [77] with permission from Wiley–VCH

exhibited by  $C_{mix}$  (Fig. 27.12c). In addition, the time course of  $G'$  and  $G''$  in the ON–OFF cycle of UV irradiation showed a sharp decrease in  $G'$  and  $G''$  associated with UV irradiation (Fig. 27.12c). In particular, the level of  $G'$  decreased to less than 1/10 of that observed prior to UV irradiation. The relationship of  $G'' > G'$  did not change before or after UV irradiation, indicating that the fluid state was maintained. Within a few minutes after the termination of UV irradiation, both  $G'$  and  $G''$  returned to the level observed prior to irradiation, and these changes could be induced repeatedly. In



**Fig. 27.13** Topological transformation between cyclic PDMSs with HABIs in the chains and monodispersed linear oligosiloxanes with TPIR end groups upon ON–OFF cycle of photoirradiation. Reproduced from [78] with permission from Elsevier B.V

this study, loss tangent ( $\tan \delta = G''/G'$ ), which represents the contribution of elasticity and viscosity, increased from approximately 2 prior to UV irradiation to approximately 8 during UV irradiation, despite the decrease in both  $G'$  and  $G''$  (Fig. 27.12d). This is a dynamic substance that changes from a sticky to smooth liquid instantaneously by UV irradiation and returns to the sticky liquid soon after UV irradiation is terminated. Oka et al. recently reported a cyclic–linear topological transformation of PDMS with monodispersed linear oligosiloxane precursors with TPIR end groups (Fig. 27.13) [78]. Because a short molecular chain increases the contribution of TPIR or HABI in the molecular chain, both the cyclic and linear PDMS are powdery solids. However, the molecular weight changed upon light irradiation, while the solid state was maintained. Interestingly, this report shows the recombination of intermolecular and intramolecular bonds because the flexible siloxane chain has mobility, despite behaving like a solid in its macro physical properties.

## References

1. D. Aoki, S. Uchida, T. Takata, *Angew. Chem. Int. Ed.* **54**, 6770 (2015)
2. T. Ogawa, N. Usuki, K. Nakazono, Y. Koyama, T. Takata, *Chem. Commun.* **51**, 5606 (2015)
3. T. Ogawa, K. Nakazono, D. Aoki, S. Uchida, T. Takata, *ACS Macro Lett.* **4**, 343 (2015)
4. S. Valentina, T. Ogawa, K. Nakazono, D. Aoki, T. Takata, *Chem. Eur. J.* **22**, 8759 (2016)
5. S. Telitel, Y. Amamoto, J. Poly, F. Morlet-Savary, O. Soppera, J. Lalevée, K. Matyjaszewski, *Polym. Chem.* **5**, 921 (2014)

6. S.J. Rowan, S.J. Cantrill, G.R.L. Cousins, J.K.M. Sanders, J.F. Stoddart, *Angew. Chem. Int. Ed.* **41**, 898 (2002)
7. R.J. Wojtecki, M.A. Meador, S.J. Rowan, *Nat Mater* **10**, 14 (2011)
8. T. Maeda, H. Otsuka, A. Takahara, *Prog. Polym. Sci.* **34**, 581 (2009)
9. X. Chen, M.A. Dam, K. Ono, A. Mal, H. Shen, S.R. Nutt, K. Sheran, F. Wudl, *Science* **295**, 1698 (2002)
10. A. Sanyal, *Macromol. Chem. Phys.* **211**, 1417 (2010)
11. N. Yoshie, S. Saito, N. Oya, *Polymer* **52**, 6074 (2011)
12. J.R. Jones, C.L. Liotta, D.M. Collard, D.A. Schiraldi, *Macromolecules* **32**, 5786 (1999)
13. İ Sevim, W.M. Pankau, G. von Kiedrowski, *Chem. Eur. J.* **26**, 9032 (2020)
14. V. Ondrus, L. Fisera, K. Polborn, P. Ertl, N. Prónayová, *Monatshefte für Chemie/Chem. Monthly* **126**, 961 (1995)
15. M. Miura, F. Akutsu, T. Usui, Y. Ikebukuro, K. Nagakubo, *Die Makromolekulare Chemie* **186**, 473 (1985)
16. J.C. Salamone, Y. Chung, S.B. Clough, A.C. Watterson, *J. Polym. Sci., Part A: Polym. Chem.* **26**, 2923 (1988)
17. A.M. Peterson, G.R. Palmese, Reversible Diels–alder cycloaddition for the design of multi-functional network polymers, in *Click Chemistry for Biotechnology and Materials Science* (2009), <https://doi.org/10.1002/9780470748862.ch9>, pp. 195
18. Y.-L. Liu, T.-W. Chuo, *Polym. Chem.* **4**, 2194 (2013)
19. W.G. Kim, *J. Appl. Polym. Sci.* **107**, 3615 (2008)
20. D. Tunc, C. Le Coz, M. Alexandre, P. Desbois, P. Lecomte, S. Carlotti, *Macromolecules* **47**, 8247 (2014)
21. K.M. Gattás-Asfura, E. Weisman, F.M. Andreopoulos, M. Micic, B. Muller, S. Sirpal, S.M. Pham, R.M. Leblanc, *Biomacromol* **6**, 1503 (2005)
22. A.P. Somlai, R.A. Cozad, K.A. Page, H.R. Williams, D. Creed, C.E. Hoyle, *Photochem. Photobiol. Sci.* **7**, 578 (2008)
23. M. Schraub, H. Gray, N. Hampp, *Macromolecules* **44**, 8755 (2011)
24. M.J. Moghaddam, K. Kanbara, S. Hozumi, Y. Inaki, K. Takemoto, *Polym. J.* **22**, 369 (1990)
25. M. J. Moghaddam, S. Hozumi, Y. Inaki, K. Takemoto, *J. Polym. Sci. Part A: Polym. Chem.* **26**, 3297 (1988)
26. N. Tohnai, T. Sugiki, E. Mochizuki, T. Wada, Y. Inaki, *J. Photopolym. Sci. Technol.* **7**, 91 (1994)
27. S.R. Trenor, T.E. Long, B.J. Love, *Macromol. Chem. Phys.* **205**, 715 (2004)
28. M. Jun, O. Yoshifumi, T. Katsuyuki, *Chem. Lett.* **35**, 80 (2006)
29. P. Froimowicz, H. Frey, K. Landfester, *Macromol. Rapid Commun.* **32**, 468 (2011)
30. Y. Zheng, M. Micic, S.V. Mello, M. Mabrouki, F.M. Andreopoulos, V. Konka, S.M. Pham, R.M. Leblanc, *Macromolecules* **35**, 5228 (2002)
31. A.S. Fawcett, M.A. Brook, *Macromolecules* **47**, 1656 (2014)
32. A.S. Fawcett, T.C. Hughes, L. Zepeda-Velazquez, M.A. Brook, *Macromolecules* **48**, 6499 (2015)
33. R. Jellali, M. Alexandre, C. Jérôme, *Polym. Chem.* **8**, 2499 (2017)
34. T.F. Scott, A.D. Schneider, W.D. Cook, C.N. Bowman, *Science* **308**, 1615 (2005)
35. H. Lankamp, W.T. Nauta, C. MacLean, *Tetrahedron Lett.* **9**, 249 (1968)
36. D. Sakamaki, S. Ghosh, S. Seki, *Mater. Chem. Front.* **3**, 2270 (2019)
37. Y. Tian, K. Uchida, H. Kurata, Y. Hirao, T. Nishiuchi, T. Kubo, *J. Am. Chem. Soc.* **136**, 12784 (2014)
38. H. Sakai, T. Sumi, D. Aoki, R. Goseki, H. Otsuka, *ACS Macro Lett.* **7**, 1359 (2018)
39. M. Frenette, C. Aliaga, E. Font-Sanchis, J.C. Scaiano, *Org. Lett.* **6**, 2579 (2004)
40. E.V. Bejan, E. Font-Sanchis, J.C. Scaiano, *Org. Lett.* **3**, 4059 (2001)
41. H. Oka, K. Imato, T. Sato, T. Ohishi, R. Goseki, H. Otsuka, *ACS Macro Lett.* **5**, 1124 (2016)
42. J.P. Peterson, M.R. Geraskina, R. Zhang, A.H. Winter, *J. Org. Chem.* **82**, 6497 (2017)
43. T. Kobashi, D. Sakamaki, S. Seki, *Angew. Chem. Int. Ed.* **55**, 8634 (2016)
44. J.E. Bennett, H. Sieper, P. Tavs, *Tetrahedron* **23**, 1697 (1967)

45. B. Maillard, K.U. Ingold, *J. Am. Chem. Soc.* **98**, 520 (1976)
46. W.C. Danen, D.D. Newkirk, *J. Am. Chem. Soc.* **98**, 516 (1976)
47. T. Hayashi, K. Maeda, *Bull. Chem. Soc. Jpn.* **33**, 565 (1960)
48. G.R. Coraor, L.A. Cescon, R. Dessauer, A.S. Deutsch, H.L. Jackson, A. MacLachlan, K. Marcali, E.M. Potrafke, R.E. Read, *J. Org. Chem.* **36**, 2267 (1971)
49. Y. Kishimoto, J. Abe, *J. Am. Chem. Soc.* **131**, 4227 (2009)
50. A. Gandini, *Prog. Polym. Sci.* **38**, 1 (2013)
51. T. Mizawa, K. Takenaka, T. Shiomi, *J. Polym. Sci. Part A: Polym. Chem.* **38**, 237 (2000)
52. Y. Li, Y. Zhou, Y. Zhou, Q. Yu, J. Zhu, N. Zhou, Z. Zhang, X. Zhu, *React. Funct. Polym.* **116**, 41 (2017)
53. H. Durmaz, A. Dag, G. Hizal, U. Tunca, *J. Polym. Sci. Part A: Polym. Chem.* **48**, 5083 (2010)
54. M. Glassner, J.P. Blinco, C. Barner-Kowollik, *Macromol. Rapid Commun.* **32**, 724 (2011)
55. C.-H. Tung, L.-Z. Wu, Z.-Y. Yuan, N. Su, *J. Am. Chem. Soc.* **120**, 11594 (1998)
56. G. McSkimming, J.H.R. Tucker, H. Bouas-Laurent, J.-P. Desvergne, *Angew. Chem. Int. Ed.* **39**, 2167 (2000)
57. M. Xu, L.-Z. Wu, L.-P. Zhang, C.-H. Tung, *Tetrahedron Lett.* **42**, 9249 (2001)
58. M. Okada, A. Harada, *Macromolecules* **36**, 9701 (2003)
59. H. Wang, L. Zhang, B. Liu, B. Han, Z. Duan, C. Qi, D.-W. Park, I. Kim, *Macromol. Rapid Commun.* **36**, 1646 (2015)
60. T. Yamamoto, S. Yagyu, Y. Tezuka, *J. Am. Chem. Soc.* **138**, 3904 (2016)
61. H. Frisch, K. Mundsinger, B.L.J. Poad, S.J. Blanksby, C. Barner-Kowollik, *Chem. Sci.* **11**, 2834 (2020)
62. C.J. Hawker, G.G. Barclay, J. Dao, *J. Am. Chem. Soc.* **118**, 11467 (1996)
63. N.J. Turro, G. Lem, I.S. Zavarine, *Macromolecules* **33**, 9782 (2000)
64. H. Otsuka, *Polym. J.* **45**, 879 (2013)
65. G. Yamaguchi, Y. Higaki, H. Otsuka, A. Takahara, *Macromolecules* **38**, 6316 (2005)
66. A. Takahashi, R. Goseki, H. Otsuka, *Angew. Chem. Int. Ed.* **56**, 2016 (2017)
67. R. Takashima, D. Aoki, H. Otsuka, *Macromolecules* **53**, 4670 (2020)
68. N. Tsurumi, R. Takashima, D. Aoki, S. Kuwata, H. Otsuka, *Angew. Chem. Int. Ed.* **59**, 4269 (2020)
69. R. Zhang, J.P. Peterson, L.J. Fischer, A. Ellern, A.H. Winter, *J. Am. Chem. Soc.* **140**, 14308 (2018)
70. S. Koshihara, Y. Tokura, T. Mitani, G. Saito, T. Koda, *Phys. Rev. B* **42**, 6853 (1990)
71. H. Akiyama, M. Yoshida, *Adv. Mater.* **24**, 2353 (2012)
72. M. Hoshino, E. Uchida, Y. Norikane, R. Azumi, S. Nozawa, A. Tomita, T. Sato, S. Adachi, S. Koshihara, *J. Am. Chem. Soc.* **136**, 9158 (2014)
73. H. Zhou, C. Xue, P. Weis, Y. Suzuki, S. Huang, K. Koynov, G.K. Auernhammer, R. Berger, H.-J. Butt, S. Wu, *Nat Chem* **9**, 145 (2017)
74. S. Delbaere, M. Orio, J. Berthet, M. Sliwa, S. Hatano, J. Abe, *Chem. Commun.* **49**, 5841 (2013)
75. Y. Satoh, Y. Ishibashi, S. Ito, Y. Nagasawa, H. Miyasaka, H. Chosrowjan, S. Taniguchi, N. Mataga, D. Kato, A. Kikuchi, J. Abe, *Chem. Phys. Lett.* **448**, 228 (2007)
76. S. Honda, T. Toyota, *Nat. Commun.* **8**, 502 (2017)
77. S. Honda, M. Oka, H. Takagi, T. Toyota, *Angew. Chem. Int. Ed.* **58**, 144 (2019)
78. M. Oka, S. Honda, *Reactive and functional polymers* **158**, 104800 (2021)